TARGETING TUBERCULOSIS BY MULTITARGET APPROACH: DESIGN, SYNTHESIS AND EVALUATION OF NOVEL HETEROCYCLIC COMPOUNDS

A Thesis submitted in partial fulfillment for the degree of

DOCTOR OF PHILOSOPHY

In the faculty of Pharmacy

GOA UNIVERSITY

By

VAIBHAV V. POTDAR

Goa College of Pharmacy, Government of Goa
Panaji-Goa

November 2024

DECLARATION

I, Mr.Vaibhav Vijaykumar Potdar, hereby declare that this thesis represents work which has been carried out by me and that it has not been submitted, either in part or full, to any other University or Institution for the award of any research degree.

Place: Panaji - Goa. Mr.Vaibhav Vijaykumar Potdar

Date: 11/11/2024 (M.Pharm in Pharmaceutical Chemistry)

CERTIFICATE

I hereby certify that the work was carried out under my supervision and may be placed for evaluation.

Dr. Arun Bhimrao Joshi
(Ph.D.inPharmaceutical
sciences) Professor and Head,
Department of Pharmacognosy,
Goa College of Pharmacy,
Government of Goa,Panjim-Goa,
403001.

ENDORSEMENT BY PRINCIPAL

I hereby declare that this Thesis entitled **"TARGETING TUBERCULOSIS BY MULTITARGET APPROACH: DESIGN, SYNTHESIS AND EVALUATION OF NOVEL HETEROCYCLIC COMPOUNDS"** is a bonafide and genuine research work carried out by ***Mr. Vaibhav V.Potdar*** under the guidance of ***Dr.Arun Bhimrao Joshi*** Professor and Head, Department of Pharmacognosy , Goa College of Pharmacy, Panaji-Goa.

Date:

Place: Panaji-Goa.

_____

Dr. Gopal Krishna Rao
Principal
Goa College of Pharmacy,
18th June Road
Panaji- Goa.

ACKNOWLEDGEMENT

या कुन्देन्दुतुषारहारधवला या शुभ्रवस्त्रावृता
या वीणावरदण्डमण्डितकरा या श्वेतपद्मासना |
या ब्रह्माच्युतशंकरप्रभृतिभिर्देवैः सदा वन्दिता
सा मां पातु सरस्वती भगवती निःशेषजाड्यापहा ||

With an attitude of gratitude and honor, I would like to take this opportunity to thank the people who provided assistance in various forms and opened their doors to me whenever I needed help in the course of my productive PhD research work. I have no qualms in believing that these are all heavenly beings, who at one time or another, whenever the situation demanded, were responsible for helping me overcome every obstacle that impeded my progress.

I would like to express my sincere gratitude to my esteemed guide, Dr. Arun Bhimrao Joshi, Professor and Head of the Department of Pharmacognosy at Goa College of Pharmacy. His invaluable supervision, support, encouragement, and mentorship throughout my PhD journey have been truly transformative. His vast knowledge, extensive experience, remarkable enthusiasm, and unwavering commitment have inspired me in both my academic research and daily life.

I acknowledge Dr. Gopal Krishna Rao, Principal of Goa College of Pharmacy, for his valuable advice and providing all the necessary resources to facilitate my research work effectively.

I express my heartfelt gratitude to Dr. Vivek Kamat, Director of the Directorate of Technical Education Goa, as well as to all the authorities of the Government of Goa for granting me the opportunity to enroll in the Ph.D. program.

I am eternally grateful to members of my Doctoral Research Committee, Dr. Sanjay Pai PN, Professor and Head of Department of Pharmaceutical Chemistry at Goa College of Pharmacy, and Dr. Srinivas Joshi, Professor and Head of Department of Pharmaceutical Chemistry, Soniya Education Trust's (SET) College of Pharmacy, Dharwad. Their constructive comments, insightful suggestions, critical analyses, and wise advice have been a tremendous help in enhancing my research activities

I express my earnest gratitude and appreciation to Dr. Anand A. Mahajan, Professor in Pharmaceutical Analysis at the Goa College of Pharmacy, Panaji for his assistance in the analysis of the spectral data. His wise counsel, priceless direction, encouragement, and commitment have played a major role in helping me undertake research work.

I am also sincerely thankful to Dr. Kishore Bhat from the Maratha Mandal Institute of Dental Sciences in Belagavi, and The Director Sophisticated Analytical Instrumentation Facility (SAIF) and the Central Instrumentation Laboratory at Punjab University for their invaluable assistance in providing the spectral data. Additionally, I extend my deep appreciation to Dr. Srinivas Joshi, Professor in the Department of Pharmaceutical Chemistry at SET College of Pharmacy, Dharwad, for his support in carrying out and analyzing the molecular docking studies.

I express my heartfelt appreciation to the Heads of Departments of Goa College of Pharmacy, Dr. M. P. Joshi, Department of Pharmacology, Late Dr. Prashant Bhide, Department of Pharmaceutics for providing me with the lab equipment and for their inspiration and moral support all through the journey.

Also, I thank Dr. Yogita Sardessai (Professor) Dr. Rupesh Shirodkar (Professor), Dr. Shailendra Gurav, (Professor), Dr. Raghuvir Pissurlenkar (Professor), Dr. Rajashree Gude (Associate Professor), Ms. Lorna Silveira (Associate Professor), Smt. Teja Walke (Associate Professor) and Dr. Titiksh Devale (Associate Professor), Dr. Bothiraja Chelimpalia (Associate Professor), Ms.Lilian Almeida(retired Associate Professor) , Mrs. M.H. S.Gudinho (retired Associate Professor), for their kindness ,support , assistance and direction when required.

I want to take this opportunity to thank Dr. Sanjay Pai P. N., Head of Department of Pharmaceutical Chemistry, Goa College of Pharmacy for granting me the freedom to pursue my Research activities with little interference to the operations of the department. I really value the assistance I received from Dr. Sachi Kudchadkar, Smt. Shailaja Mallya, Dr, Smt. Vedita Hegde Desai, Maithili Krishna Smt. Sweta Borkar, Smt. Seema Shet, Smt. Saba Jamadar Smt. Asmita Arondekar, Shri. Rohan Prabhu, Shri. Raveendra Hullolikar, Dr. Damita Cota, and who all encouraged me and gave me valuable advice throughout my research.

I extend special regards to Dr. Adison Fernandes, Mr. Vithal Bhandare Dr. Rahul Chodankar, Dr. Lisel Mendosa, Dr. Nutan Naik, Dr. Anant Bhandarkar for their support and suggestions during completion of work.

I am grateful to all the present and ex-support staff members (administration, laboratory, library, and housekeeping) of the Goa College of Pharmacy. I would also like to take this opportunity to thank Smt. Arlette Baretto, Shri. Sham, Smt. Shanti, Smt. Sweta Vaiganker, Shri. Anad Pednekar, Shri. Thomas Martin, Shri Ravindra Kholkar and other individuals to whom I sincerely appreciate and thanks for all the help and support they have given from time to time.

I would like to thanks the Ph. D. Research scholars, current, and previous students of M. Pharm research programs especially Miss. Florinda for all the help.

I wish to acknowledge the steadfast support extended to me by several persons, the administrative staff of the Registrar's office, the Assistant Registrar's office (PG), as well as the Librarian and library staff of Goa University.

Finding the right words to convey the extent of love and gratitude that I feel for my nuclear and extended family – father (Late Vijay Kumar), mother (Smt. Vanamala), wife (Leenta), son (Shrish), mother-in-law (Late Smt. Pushpalata) father-in-law (Mr. Balwantrao), brothers (Mr. Vinod & Pavan), sisters-in-law (Mrs. Sunita & Sneha), nephews (Vedant, Avdhut) niece (Vedika) who have always prayed for me and remembered me is quite impossible. I include them in the definition of myself and what identity is without them, is hard to comprehend. They provided me with a fair part of psychological support and optimistic strength and displayed a strong will that helped me in reaching the targets I had set for myself. They have been that underlying level of assistive understanding and support in my attempts for studies over the past several years, which are very, and greatly valued, and indeed, without which it would have been impossible to complete the studies.

I would like to express my thanks to all relatives and friends, well-wishers including Guru (Shri Pappaji Puranik and Dr. Rajendra Mule) for their constant encouragement, suggestions, and prayers.

Additionally, I convey my utmost appreciation to all those who have either directly or indirectly contributed to my research work and this thesis and seek pardon to those I have not been able to mention individually.

Date:

…...Mr. Vaibhav V. Potdar

Dedicated to

My Family

TABLE OF CONTENTS

ABSTRACT

A series of 6-substituted-2-chloroquinoline-3-carbaldehyde hydrazide ester derivatives (4a-4r) were synthesized and evaluated for their potential as anti-tubercular, antibacterial, and anticancer agents. The synthesis followed a three-step process, involving the formation of substituted 2-chloroquinoline-3-carbaldehyde using the Meth-Cohn reaction, hydrazone derivatives from quinoline aldehydes, and esterification with acyl chlorides. The reactions yielded compounds with favourable characteristics, including good yields (48-79%) and confirmed structural integrity through spectral analysis (IR, NMR spectroscopy and Mass spectrometry).

Biological evaluations revealed promising results, particularly in anti-TB and antibacterial activities. Compounds 4m and 4r exhibited significant anti-TB activity, with MIC values of 6.25 µg/ml, comparable to standard drugs. The structural features, such as halogen substitutions, likely enhanced their activity. However, cytotoxicity concerns arose, especially for compound 4r, which exhibited strong activity but also significant toxicity in the MTT assay. Other compounds, including 4n, 4o, 4p, and 4q, demonstrated good anti-TB activity with MIC values of 12.5 µg/ml, making them suitable candidates for further development.

Antibacterial evaluations demonstrated broad-spectrum activity. Compounds 4f and 4r were most effective against *Staphylococcus. aureus*, while compounds 4p and 4r showed strong efficacy against *Bacillus subtilis*, with MIC values as low as 0.8 µg/ml. Compounds 4r and 4o exhibited good activity against *Klebsiella pneumoniae* and *Escherichia. coli*, respectively, with MICs ranging from 6.25 to 12.5 µg/ml. The antibacterial activity was attributed to specific structural modifications like halogenation and ester linkages, improving bacterial membrane permeability and target interactions.

Cytotoxicity assays in A549 (cancer) and Vero (non-cancerous) cell lines using MTT assay revealed that some compounds, including 4m and 4r, had selective cytotoxicity towards cancer cells. While 4r displayed excellent anti-TB activity, its low IC_{50} in both cancerous and non-cancerous cells highlighted the need for further structural optimization to reduce toxicity while retaining therapeutic potential.

In silico docking studies with PanK and PyrG enzymes demonstrated strong binding affinities for compounds like 4k, 4o, 4l, and 4b. The inhibition of these enzymes suggests potential antimycobacterial effects through the disruption of key bacterial pathways, such as CoA biosynthesis and nucleotide metabolism. The docking results pointed to significant polar interactions and hydrogen bonding, for stable enzyme inhibition. This highlights their potential as antimycobacterial agents. The structural differences between bacterial and human enzymes offer the possibility of designing selective inhibitors that minimize off-target effects in human cells, enhancing the therapeutic index of these compounds.

ADME predictions indicated favourable pharmacokinetics, with high gastrointestinal absorption and no blood-brain barrier permeability. None of the compounds were substrates for P-glycoprotein, reducing the risk of efflux-mediated drug resistance. Additionally, while the solubility of the compounds was moderate to low, their favourable lipophilicity (Log Po/w values between 2.89 and 3.73) indicated good membrane permeability, which is essential for ensuring bioavailability. However, predicted interactions with multiple CYP enzymes suggested the possibility of drug-drug interactions, which may need consideration during further development.

The study highlights the potential of these quinoline derivatives, particularly 4r, 4n, 4o, and 4p, as candidates for treating drug-resistant TB and bacterial infections. Further research should focus on reducing cytotoxicity, exploring SAR, and improving formulation for clinical application.

LIST OF ABBREVIATIONS

^{13}C NMR	Carbon-13 (C13) nuclear magnetic resonance
^{1}H NMR	Proton nuclear magnetic resonance
3D QSAR	Three-Dimensional Quantitative Structure Activity Relationship
ADME	Absorption, Distribution, Metabolism, Excretion
AIDS	Acquired immunodeficiency syndrome
Ala	Alanine
Arg	Arginine
Asn	Asparagine
ASP	Aspartic acid
ATP	Adenosine triphosphate
CB1a	A novel anticancer peptide derived from natural antimicrobial peptide cecropin B
CDK-2	Cyclin dependent kinase 2
CDK-5	Cyclin-dependent kinase 5
Cdr1P	Candida albicans drug resistance protein 1
Cdr2P	Candida albicans drug resistance protein 2
CH3I	Iodoform
CHO-K1	A cell line isolated from the ovary of an adult, female Chinese hamster
CLSI	The Clinical & Laboratory Standards Institute
CO_2	Carbon dioxide
CTP	Cytidine triphosphate
CYP	Cytochrome P450
CYS	Cysteine

DABCO	1,4-diazabicyclo[2.2. 2]octane
DBU	1,8-Diazabicyclo[5.4. 0]undec-7-ene
DCFH-DA	2′− 7′- Dichlorodihydrofluorescein diacetate
DMF	Dimethylformamide
DPPH	2, 2-Diphenyl-1-picrylhydrazyl.
ESI-MS	Electrospray ionization mass spectrometry
FabH	Beta-ketoacyl-acyl carrier protein synthase III gene
FAS-II	Fatty acid synthase II
FTIR	Fourier Transform Infrared Spectroscopy
g	Grams
Gln	Glutamine
Glu	Glutamic acid
Gly	Glycine
GROMACS	GROningen MAchine for Chemical Simulations
gyrA	DNA gyrase subunits A
gyrB	DNA gyrase subunits B
HCl	Hydrochloric acid
HEPG2	Hepatoblastoma cell line
HEPG2A16 CELL	Human liver cells infected with Plasmodium falciparum sporozoites
HIS	Histidine
HIV	Human immunodeficiency virus
IC 50	Half-maximal inhibitory concentration
ILE	Isoleucine
IUPAC	International Union of Pure and Applied Chemistry.
KatG	Catalase-peroxidase
Ki	Inhibitor constant

KOH	Potassium Hydroxide
LC 50	Lethal Concentration 50
LC-MS	Liquid chromatography-mass spectrometry
LDH	Lactate dehydrogenase
Leu	Leucine
Lys	Lysine
M	Molar
m/z	Mass-to-charge ratio
MDA-MB-231	An epithelial, human breast cancer cell line
MLOGP	Rule-based Moriguchi Log P
mm	Millimeter
mM	Micrometer
MOE	Molecular Operating Environment
MTT	(3-(4, 5-dimethylthiazolyl-2)-2, 5-diphenyltetrazolium bromide)
MurD	UDP-N-acetylmuramoyl-l-alanine:d-glutamate ligase
Na_2SO_4	Sodium Sulphate
NaOH	Sodium hydroxide
nM	Nanometer
nm	Nano meter
nS	Nano seconds
PBS	Phosphate buffer saline
PEG-400	Polyethylene glycol-400
Phe	Phenylalanine
POCl3	Phosphoryl Chloride
Pro	Proline
rpoB	DNA-directed RNA polymerase subunit beta

SARS-COV-2	Severe acute respiratory syndrome corona virus 2
SER	Serine
t-BuOK	Potassium tert-butoxide
Thr	Threonine
µg/ml	Microgram per milliliter
µM	Micromole
UTP	Uridine triphosphate
Uv-Vis	Ultra violet -Visible spectroscopy
Val	Valine
VEGFER-2	Vascular endothelial growth factor receptor 2
WHO	World Health organization
WLOGP	Boiled egg plot, water partition coefficient
XLOGP3	Lipid-water partition coefficient calculation indicator.
Z/E	Zusammen /Entgegen
ZnO	Zinc oxide

LIST OF FIGURES

LIST OF TABLES

CHAPTER-I

INTRODUCTION

1: INTRODUCTION

1.1 Bacterial Infections and Antimicrobial Agents

Bacteria are a vast and diverse group of microorganisms, with a simple cell structure without a defined nucleus, and membrane-bound organelles. These microorganisms were discovered by Antony Van Leeuwenhoek in 1676 which play a critical role in various ecosystems, including the human body. Bacteria can be found in diverse environments, from the human gut to the mountains, the depths of the ocean and even in ice and rocks. Their resilience is largely attributed to their ability to form endospores, enabling them to survive in extreme conditions.

Bacteria are classified based on their response to oxygen into three categories [1-3]

- **Aerobic Bacteria**: These bacteria require oxygen for growth and survival.
- **Anaerobic Bacteria**: These bacteria cannot tolerate oxygen and thrive in oxygen-free environments.
- **Facultative Anaerobes**: These bacteria prefer oxygen but can survive without it.

In humans and animals, bacteria can be both beneficial and pathogenic. Pathogenic bacteria cause diseases by invading tissues and releasing toxins. While many compounds can effectively kill bacteria, they may be unsuitable for treating infections due to their toxicity to the host. The challenge lies in identifying compounds that selectively disrupt bacterial metabolic pathways without affecting the host's metabolic functions [3-4].

The discovery and development of antimicrobial agents have been pivotal in treating bacterial infections. Antimicrobials include antibiotics and synthetic antimicrobials, which can be bactericidal (killing bacteria) or bacteriostatic (inhibiting

bacterial growth). Antibiotics have been the cornerstone of bacterial infection treatment since penicillin was discovered by Alexander Fleming in 1928.

Antibiotic resistance has become major global health challenges in the 21st century. The misuse and overuse of antibiotics in humans, veterinary practice, and agricultural science have accelerated the emergence and spread of resistant bacteria. Antibiotic resistance develops when bacteria adapt and acquire the ability to withstand the effects of drugs that previously killed them or prevented their growth [5-6].

1.1.1 Mechanisms of Antibiotic Resistance

- **Enzymatic Degradation**: Bacteria generate enzymes like beta-lactamases which degrade antibiotics before they can exert their effects [7-8].
- **Efflux Pumps**: Certain bacteria have efflux pumps that remove antibiotics from the cell, preventing the drugs from reaching their intended targets [4].
- **Target Modification**: Bacteria can modify the target site of an antibiotic, reducing the drug's effectiveness [2].
- **Reduced Permeability**: Changes in bacterial cell wall or membrane structure can prevent antibiotics from entering the cell [1,9].

1.1.2 Key Resistant Pathogens

- **Methicillin-Resistant Staphylococcus aureus (MRSA)**: MRSA shows resistance to beta-lactam antibiotics and is a major contributor to hospital-acquired infections.
- **Vancomycin-Resistant Enterococci (VRE)**: VRE are resistant to vancomycin making infections difficult to treat.
- **Multidrug-Resistant Mycobacterium tuberculosis (MDR-TB)**: MDR-TB strains are found resistant to isoniazid and rifampicin, which are important anti-TB drugs.

In the last decade, the increase in antibiotic resistance has outpaced development of new antibacterial agents, leading to a global health crisis. The challenges associated with antibiotic resistance can be categorized as follows:

1. **Decline in Antibiotic Discovery and Development**

   The pharmaceutical industry has witnessed a significant decline in the discovery of new antibiotics. High cost and lengthy process of developing new drugs, coupled with low financial returns, have led many companies to abandon antibiotic research. As a result, the pipeline for new antibiotics has diminished, with few new drugs being introduced to the market [10].

2. **Spread of Resistant Bacteria**

   The spread of resistant bacteria across the globe has been exacerbated by increased international travel and trade, insufficient practices and efforts of infection control in healthcare system, and poor sanitation in many parts of the world. Resistant bacteria, once confined to specific regions or settings, are now prevalent globally, thus complicating the efforts to control their spread [5-6].

3. **Resistance in Gram-Negative Bacteria**

   Resistance is developed for gram-negative bacteria, such as *Escherichia coli* and *Klebsiella pneumoniae*, to nearly all available antibiotics, including carbapenems, which are often considered the last line of defence. These bacteria have become particularly problematic because they have multiple mechanisms of resistance and are associated with high death rates in infections [4].

4. **Inadequate Global Surveillance and Regulation**

   A lack of comprehensive global surveillance systems has hindered the ability to monitor the spread of resistance and respond effectively. Furthermore, varying regulations and enforcement of antibiotic use across countries have enabled continuous misuse of these drugs, particularly in agriculture and veterinary science, where antibiotics are often used as growth promoters [11-12].

5. **Public Health and Economic Impact**

   The economic strain of developing resistance is immense. Infections caused by resistant bacteria result in longer hospital waits, more rigorous care, and the need for costly drugs. It leads to significant strain on the healthcare industry, particularly in low- and middle-income countries. Public health impacts include increased morbidity and mortality from previously treatable infections, making resistance a critical threat to global health security [13-14].

6. **Challenges in Diagnostic Testing**

   Rapid and accurate diagnostic tests are required to identify infections and determine suitable antibiotic treatment. However, the development and implementation of such tests have lagged, leading to over-prescription and misuse of antibiotics [3].

7. **The Global One Health Approach**

   The One Health approach, which acknowledges the interconnection between human, animal, and environmental health, is crucial for tackling antibiotic resistance. However, coordinating efforts across these sectors remains a significant challenge. The widespread use of antibiotics in agriculture, particularly in production of farm animals, contributes to resistance that can spread to humans through food-chain, water, and the environment [7-8].

8. **Emergence of New Resistant Pathogens**

   In the last decade, new resistant pathogens have emerged, such as *Clostridium difficile* and *Neisseria gonorrhoeae*, which have developed resistance to almost all available treatments. These pathogens present new challenges for public health, as they are associated with severe infections and limited treatment options [15-16].

9. **Policy and Global Initiatives**

   World Health Organization (WHO) has developed action plans and initiatives to combat antibiotic resistance. However, the implementation of these policies varies across countries, and global coordination remains a challenge. While some progress

has been made, there is still a need for stronger global governance and cooperation to address the threat of resistance effectively [5-6].

Antibiotic resistance represents a significant challenge that has only intensified in the last 5-10 years. Addressing this issue requires a comprehensive approach, including the development of new antibiotics and antibacterial agents, global surveillance and improved diagnostic tools. As resistance continues to increase, the need for coordinated global efforts becomes more urgent to prevent a future where common infections could once again become fatal.

Mycobacterium tuberculosis is one of the prominent causes of death because of bacterial infections, second only to HIV/AIDS in terms of mortality from a single infectious agent. Despite advances in antimicrobial agents, TB remains a persistent global health problem. The bacteria's complex structure, including a lipid-rich cell wall, makes it highly resistant to many conventional antibiotics. This, coupled with the slow growth rate of the organism, complicates treatment and requires prolonged therapeutic regimens [3,17-18].

1.2 Management of Tuberculosis: A Sustained Challenge

Tuberculosis (TB) is a chronic infection caused by *M. tuberculosis*, which evolved over 10,000 years ago from a soil bacterium [19]. While it mainly affects the lungs, TB can involve other organ systems. TB gets transmitted through respiratory droplets when an infected person coughs or sneezes. Despite medical advancements, TB remains one of the leading causes of mortality worldwide, particularly in developing countries where poor nutrition, overcrowding, and inadequate sanitation contribute to its spread.

The TB Structural Genomics Consortium has made substantial strides in understanding the molecular biology of TB. The complete genome sequence of the *M.*

tuberculosis strain H37Rv has been determined, offering valuable insights into the bacterium's pathogenesis and potential drug targets [2]. However, despite these scientific advances, the co-infection of TB with HIV and the rise of multidrug-resistant TB (MDR-TB) and extensively drug-resistant TB (XDR-TB) complicate disease management [11-12].

The occurrence of TB is disproportionately high in developing nations, accounting for 95% of global cases. The disease has a particularly devastating impact on young women, with over a million new cases annually in this demographic [20]. In 2020 alone, an estimated 10 million people contracted TB, and the COVID-19 pandemic further disrupted healthcare services, leading to increased TB mortality for the first time in over a decade [5-6]. These challenges underscore the need for urgent, sustained global action.

The management of TB is further complicated by patient non-compliance, lengthy treatment durations, and occurrence of MDR-TB and XDR-TB. Simultaneous infection with HIV exacerbates these challenges by increasing vulnerability to active TB and progress of the disease [3]. The unique composition of cell wall of *M. tuberculosis* consisting of mycolic acids, arabinogalactan, and peptidoglycan forms a robust permeability barrier, protecting the bacterium from antibiotics and contributing to its persistence and resistance [1,21-22].

The persistence of *M. tuberculosis* within the host, often in a dormant state, poses a significant challenge for treatment. The bacterium’s ability to remain latent, protected by its cell wall, complicates efforts to fully eradicate the infection [9,23]. Mismanagement of TB treatment such as incomplete therapy or inadequate drug combinations has led to the rise of drug-resistant strains, further complicating control efforts and treatment outcomes [24].

Advances in molecular biology have provided valuable insights into *M. tuberculosis* through the sequencing of the strain H37Rv genome, revealing potential

drug targets [2]. However, the slow progress in TB treatment over the past three decades, compounded by the rise of MDR and XDR strains, highlights the need for new diagnostics and treatment protocols [25-26]. Scientists are exploring host-directed therapies to enhance the immune response against latent TB, potentially improving treatment outcomes [27].

Metabolic modulation has also shown potential in treating both active and latent TB infections. Targeting TB's latent phase could reactivate dormant bacteria, making them susceptible to conventional antibiotics and improving treatment efficacy. These approaches along with ongoing research into new therapeutic targets, are important in managing drug-resistant TB [27].

1.3 Chemotherapy for Tuberculosis

The introduction of chemotherapy marked a significant milestone in the treatment of TB. The discovery of streptomycin in the 1940s by Selman Waksman and his colleagues ushered in the era of anti-TB chemotherapy [28-29]. Streptomycin was the first antibiotic effective against TB, followed by the development of other drugs such as isoniazid and rifampicin. These drugs, along with pyrazinamide and ethambutol, form the backbone of the current first-line treatment regimen.

Chemotherapy for TB aims to achieve three primary goals

- **Kill Dividing Bacilli**: Drugs showing early bactericidal action swiftly decrease the bacterial load, leading to symptom relief and reduced transmission.
- **Kill Persisting Bacilli**: To prevent relapse and achieve a cure, drugs must have a sterilizing effect, killing dormant bacilli.
- **Prevent Emergence of Resistance**: Combination therapy is required to hinder the emergence of resistant strains [2,30].

Current TB chemotherapy relies on a combination of drugs administered over an extended period. First-line treatments include isoniazid, rifampicin, ethambutol, and pyrazinamide (Table 1.1). However, the rise of drug-resistant TB has forced the use of more toxic and less effective second-line treatments. Despite the development of new drugs like bedaquiline, delamanid, and pretomanid, ensuring widespread access to these therapies remains a challenge [31].

Table 1.1: Antitubercular Drugs Based on Mechanism of Action

Drug Class	Mechanism of Action
Isoniazid, Pyrazinamide, Ethionamide	Inhibitors of fatty acid biosynthesis
Ethambutol, D-Cycloserine	Inhibitors of arabinogalactan and peptidoglycan biosynthesis
Streptomycin, Kanamycin, Amikacin	Inhibitors of protein synthesis
Rifampin, Rifapentine, Fluoroquinolones	Inhibitors of DNA-based processes
p-Aminosalicylic acid	Inhibitors of dihydrofolate reductase

1.4 Limitation of Current Drug Therapy and the Need for New Drug Targets

Despite the availability of effective drugs, TB remains a significant public health challenge. Several factors contribute to the complexity of TB treatment:

- **Inadequate Host Defence Mechanisms**: The immune system often fails to completely eradicate *M. tuberculosis*, leading to persistent infections.
- **Metabolic Characteristics of *M. tuberculosis***: The bacterium's ability to enter a dormant state makes it resistant to many antibiotics, which typically target actively dividing cells [32]. Current drugs are not effective in targeting non-replicating bacteria, which are often responsible for relapses. There is a need for drugs that

can target both actively replicating and dormant bacteria to achieve treatment shortening and reduce resistance [33].

- **Rapid Development of Drug Resistance**: The increasing prevalence of MDR and XDR strains of *M. tuberculosis* has significantly impacted the effectiveness of current treatment regimens. The reliance on first-line drugs such as isoniazid and rifampicin are hindered by mutations in target enzymes, including *InhA* and *rpoB*, which lead to resistance [34]. These mutations reduce the drugs' effectiveness, prompting the search for new drug targets to inhibit bacterial growth through alternative mechanisms [7-8].

  Resistance mechanisms involve various molecular targets, such as mutations in the *katG*, *inhA*, and *rpoB* genes, which affect the efficacy of isoniazid and rifampicin. This growing resistance, including the occurrence of totally drug-resistant (TDR) strains, poses a critical challenge to existing treatments, underscoring the urgent need for new drug targets and therapies [4].

  The treatment of MDR-TB remains challenging due to the reliance on second-line drugs, which are often less potent and more toxic. Treatment outcomes for MDR-TB are generally poorer than those for drug-sensitive TB, emphasizing the need for new, effective drugs that can overcome resistance while minimizing toxicity [10]. Additionally, in patients with comorbidities such as cancer or those on immunosuppressive therapies, susceptibility to TB is increased, further complicating treatment regimens [13-14].

  Current treatment strategies face significant limitations in addressing MDR and XDR strains. These challenges are compounded by the long duration of therapy and the side effects associated with second-line drugs. Mutations in key enzymes like *InhA* and *katG*, which are targeted by first-line drugs, highlight the urgent need for new therapeutic approaches [35-36]. The rise of MDR and XDR-TB

underscores the limitations of existing therapies and calls for the development of novel drug targets and treatment strategies [37-38].

Mutations in the *gyrA* and *gyrB* genes contribute to fluoroquinolone resistance in *M. tuberculosis*, with some mutations conferring high-level resistance to later-generation fluoroquinolones such as moxifloxacin, a key drug for treating MDR-TB [15]. In this context, DNA gyrase and topoisomerase I inhibitors present promising alternatives for managing MDR and XDR TB [16].

- **Toxicity of Drugs**: Many anti-TB drugs have significant side effects, limiting their use, particularly in resource-limited settings [2,30].
- **Economic Barriers**: The high cost and long duration of TB treatment pose significant challenges, especially in underdeveloped regions [1,22].

  There is a persistent challenge in managing tuberculosis, particularly due to the long treatment durations required to eliminate *M. tuberculosis* completely. Even after culture negativity, discontinuation of therapy can lead to relapse. The emergence of MDR-TB and XDR-TB further complicates management efforts, underscoring the need for new therapeutic regimens that can shorten treatment duration [39].

These limitations underscore the need for new drug targets and therapies that can effectively combat *M. tuberculosis*, particularly resistant strains, with minimal side effects and shorter treatment durations.

1.5 Recent Advances in Chemotherapy of Tuberculosis

The WHO's "STOP TB" approach aimed to decrease deaths due to TB by 50% by 2015 and eliminate the disease as a public health threat by 2050. Recent advances in TB chemotherapy have focused on the development of new drugs and treatments to overcome drug resistance and reduce treatment duration [5].

1.5.1 Short Course Chemotherapy

The standard treatment for TB consists of a six-monthly treatment, which includes an intensive phase of two months with isoniazid, rifampin, and pyrazinamide, following that a continuation phase of four months with isoniazid and rifampin [3]. This regimen has been highly effective in treating drug-susceptible TB, but the rise of TB strains showing resistance to drugs has necessitated the development of new therapeutic strategies [32].

1.5.2 Current Drug Development Pipeline

Despite the challenges posed by drug-resistant strains, several promising compounds are in various stages of development. These include both novel drugs targeting specific pathways in *M. tuberculosis* and repurposed drugs originally developed for other diseases which have shown efficacy against TB [2,29,34].

New antitubercular drugs, including bedaquiline and delamanid, have been approved in last 50 years. Bedaquiline, a diarylquinoline, inhibits bacterial ATP synthase and shows significant activity against both drug-sensitive and drug-resistant TB. Delamanid, a nitroimidazole, targets cell-wall synthesis and has improved sputum-culture conversion in MDR-TB patients. Repurposed drugs, like linezolid and carbapenems, also show promise in treating MDR-TB [10,40]. Additionally, drugs like OPC-67683 and PA-824, which inhibit mycolic acid biosynthesis, are undergoing clinical trials to further bolster TB treatment options [7-8,41].

Newer developments in TB chemotherapy include targeting energy metabolism and cell-wall biosynthesis. Compounds such as TB47 and CPZEN-45 target the cytochrome bc1 complex and arabinogalactan biosynthesis, respectively, and show preclinical promise against both drug sensitive and resistant *M. tuberculosis* strains.

Novel drug delivery systems, such as aerosol combinations, are also being explored to improve treatment efficacy [42-43].

The use of prodrugs continues to gain attention. Isoniazid, ethionamide, and pyrazinamide are well-known examples that are bioactivated by *M. tuberculosis* enzymes. Newer prodrugs, like pretomanid and delamanid, which target mycolic acid biosynthesis, show strong activity against MDR and XDR-TB and have progressed into advanced clinical trials [44-45]. Prodrugs like these, activated by nitroreductases, demonstrate potent bactericidal effects against drug-resistant TB strains. In addition to new prodrugs, research has highlighted inhibitors targeting different metabolic pathways. Compounds like bedaquiline (which targets ATP synthase) and PA-824 (which inhibits mycolic acid synthesis) are making strides in combatting MDR and XDR TB [13-14,46-47]. The combination regimen BPaL (bedaquiline, pretomanid, and linezolid) has further shown significant success in treating MDR and XDR TB, significantly reducing treatment duration and improving outcomes [36,48]. The ongoing research is focused on combining these agents with traditional therapies to shorten treatment regimens and improve outcomes [37-38].

Additionally, enzyme inhibitors targeting menaquinone biosynthesis, such as MenA inhibitors, show potential in disrupting the bacterial electron transport chain, effectively reducing energy production in TB bacteria [49]. Combining these inhibitors with standard TB drugs may enhance bactericidal activity [50]. Advances in immunomodulatory therapies, aimed at boosting the host's immune response against *M. tuberculosis*, could further complement existing chemotherapies and lead to shorter treatment regimens and better outcomes for patients with drug-resistant TB [51].

1.6 Potential Targets for TB

The treatment of tuberculosis is complicated by the bacterium's unique cell envelope, which serves as a critical barrier to drug penetration. The mycobacterial cell wall consists of peptidoglycan, arabinogalactan, and mycolic acids, which are essential for its survival and virulence [9,23]. Recent research has focused on identifying novel drug targets within these biosynthetic pathways, as well as other critical cellular processes [32].

1.6.1 New Targets in TB Drug Development

As the global battle against TB intensifies, the rise of MDR-TB and XDR-TB has highlighted the pressing need for new therapeutic strategies. While traditional TB drugs have targeted established pathways within *M. tuberculosis*, the bacterium's ability to develop resistance has significantly reduced the efficacy of these treatments. Consequently, there is an increasing focus on identifying novel drug targets that can help overcome these challenges.

Advances in molecular biology, genomics, and bioinformatics have been instrumental in uncovering new targets for TB drug development. These emerging targets include essential enzymes and proteins involved in the bacterium's survival, replication, and virulence, which are distinct from those targeted by current therapies. By focusing on these unique components, researchers aim to develop drugs that are effective against drug-resistant strains, reduce treatment duration, and minimize side effects [2].

The pursuit of these new drug targets offers a promising path for next-generation TB therapies. Many of these targets, including those related to cell wall synthesis, protein processing, and stress survival mechanisms, are absent in humans, providing the dual advantage of enhanced specificity and reduced toxicity. As research continues to reveal the complexities of *M. tuberculosis* biology, identifying and validating these

targets will be crucial in combating one of the world's most long-lasting infectious diseases [1,32].

Below is a list of these crucial targets that are currently being explored for new anti-TB drug development

- **Polyketide Synthase 13 (Pks13):** Pks13 is a critical enzyme to maintain the integrity of the *M. tuberculosis* cell wall as it is required in the last step of mycolic acid biosynthesis [1,32].
- **Mycobacterial Membrane Protein Large 3 (MmpL3):** MmpL3 is involved in the transfer of mycolic acids across the bacterial membrane and cell wall integrity [2,9,23]. Recent research has further highlighted MmpL3 as a key component of the TB cell envelope, particularly as a transporter essential for trehalose monomycolate (TMM) export. Multitargeting approaches that inhibit MmpL3, along with other pathways, hold significant promise for overcoming drug resistance and reducing treatment duration [43,52].
- **Filamenting Temperature-Sensitive Mutant Z (FtsZ):** FtsZ is a key protein which is critical for Z-ring formation, and cell division in mycobacteria [9,32].
- **Caseinolytic Protease P1P2 Complex (ClpP1P2):** ClpP1P2 is involved in protein quality control, and crucial for degrading damaged proteins, especially under stress conditions [23,32].
- **Decaprenylphosphoryl-β-D-ribose Oxidase Complex (DprE1/DprE2):** These enzymes are essential for the formation of arabinogalactan, an important part of the bacterial cell wall [1-2,9,23]. Recent studies have shown that DprE1 inhibitors, such as benzothiazinones (BTZ-043), are currently under clinical investigation for their ability to disrupt cell wall integrity, offering promising new avenues for TB treatment [44-45,53].

- **Decaprenylphosphoryl-β-D-ribose 2'-epimerase:** This enzyme is crucial in the formation of the mycobacterial cell wall, and so is a highly vulnerable drug target, particularly for MDR and XDR *M. tuberculosis* strains [54].
- **Alanine Racemase:** This enzyme plays a vital role in peptidoglycan synthesis. Since it is not found in humans, it can be used as a specific target for anti-TB drugs [55-56].
- **Flavin-dependent Thymidylate Synthase (FDTS):** FDTS plays a crucial role in thymine biosynthesis, which is not found in humans, making it an important target for selective inhibition [57].
- **Methionine Aminopeptidases (MetAPs):** These enzymes are involved in protein processing in *M. tuberculosis* and are considered promising targets for anti-TB drugs due to their role in both replicating and non-replicating bacteria [58].
- **P-type ATPases:** Essential for ion transport and bacterial survival, particularly under stress, P-type ATPases represent attractive targets for new chemotherapeutic agents [59].
- **KasB:** KasB is a key enzyme in FAS-II pathway and involved in extension of fatty acid chains in mycolic acid biosynthesis, making it an essential target for anti-TB drugs [60].
- **Enoyl-Acyl Carrier Protein Reductase (InhA):** Inhibitors of InhA have shown significant antimycobacterial activity as the enzyme is required in mycolic acid synthesis [61]. Pyridomycin**,** a natural product targets InhA and is effective against isoniazid-resistant TB strains [62]. Recent studies have also highlighted its critical role in mycolic acid biosynthesis, making it a key target for anti-TB drug development, with ongoing research into compounds that can effectively inhibit InhA and disrupt cell wall integrity [44-45,53].

- **Pantothenate Synthetase (PS):** This enzyme catalyses the final step of pantothenate synthesis and is a promising target for antimycobacterial drug development [63].
- **PhoPR Two-Component System:** The PhoPR system regulates the genetic material necessary for virulence and lipid synthesis in *M. tuberculosis*. Disrupting this system can attenuate bacterial growth [21].
- **Serine/Threonine Protein Kinases (STPKs):** STPKs help *M. tuberculosis* survives within macrophages by modulating intracellular signaling pathways like MAPK. They play a crucial role in signal transduction and bacterial adaptation, and are attractive targets for drug development, in drug-resistant TB strains [64-65].
- **N-acetylglucosamine-1-phosphate uridyltransferase (GlmUMtb):** This enzyme is involved in the biosynthesis of the peptidoglycan layer in the mycobacterial cell wall. Inhibitors targeting GlmUMtb could disrupt cell wall synthesis, and so can be promising drug target for new TB treatments [66].
- **Mycolic Acid Transport Inhibitors:** Mycolic acids are important factors of the bacterial cell wall, and inhibiting their transport disrupts cell wall integrity, leading to bacterial death. The compounds tested have shown high efficacy even against drug-resistant strains, offering a new avenue for TB chemotherapy [67].
- **Peptide Deformylase (PDF) Inhibitors:** PDF inhibitors are a new class of anti-TB drugs. These inhibitors target a fundamental bacterial enzyme which is involved in deformylation of newly synthesized proteins, a key process for bacterial growth[68].
- **CTP synthase (PyrG) and Pantothenate kinase (PanK) Inhibitors:** Recent research has targeted the enzymes PyrG and PanK, which are crucial for the biosynthesis of nucleotides and coenzyme A, respectively. Inhibitors of these enzymes disrupt essential metabolic pathways in *M. tuberculosis*, halting bacterial growth. Novel compounds that inhibit both PyrG and PanK provide a

multitargeting strategy that enhances the efficacy of TB treatments and limits the emergence of drug resistance [69-70].

Research continues to uncover new drug targets for TB, focusing on mycobacterial cell wall synthesis and other critical pathways. Enzymes like MurA, MurB, and MurD ligases, along with mycolic acid and arabinogalactan biosynthesis, are promising targets due to their absence in humans [7-8,41]. Potentiators like clavulanic acid combined with meropenem have shown potential in enhancing drug efficacy by weakening the bacterial cell wall and improving permeability. Multitarget-directed ligands (MTDLs) such as SQ109 and TB47 are another promising approach, targeting multiple pathways simultaneously, including cell wall biosynthesis and the electron transport chain, to enhance treatment efficacy [71-72]. Mutations in key enzymes such as katG and rpoB are associated with resistance to isoniazid and rifampicin, respectively. The role of efflux pumps in development of resistance, particularly against bedaquiline, is also being investigated [4].

1.7 Need of the study

Despite advancements in TB treatment and the discovery of new drug targets, the rise of drug-resistant TB highlights the urgent need for novel therapeutic agents that can effectively combat *M. tuberculosis*. Traditional antibiotics are increasingly becoming ineffective, necessitating research into novel compounds with enhanced anti-TB activity and selectivity. Developing compounds that demonstrate both antibacterial potency and minimal toxicity to human cells is crucial, as effective treatment depends not only on pathogen eradication but also on safety for the host.

This study is particularly needed to explore new chemical scaffolds, such as 6-substituted-2-chloroquinoline-3-carbaldehyde hydrazide ester derivatives, which could offer potential anti-TB agents. Furthermore, understanding the pharmacokinetic behaviour of new compounds through predictive Absorption, Distribution, Metabolism and Excretion (ADME) properties is essential for evaluating their suitability as drug candidates. Investigating their interactions with specific TB enzymes, such as PanK and PyrG, provides critical insights into their mechanism of action and potential efficacy with multi-target approach. Conducting cytotoxicity studies is equally vital to ensure that the compounds exhibit selective toxicity against mycobacterial cells without harming human tissues, as an ideal anti-TB drug must balance potency with safety. This comprehensive approach aims to address the gaps in current TB treatment by identifying promising new candidates that could lead to shorter, more effective, and safer therapies.

CHAPTER-II

AIM AND OBJECTIVES

2: AIM AND OBJECTIVES

1. To synthesize novel quinoline-3-carbaldehydesby suitable methods and prepare novel quinoline-3-carbaldehydes analogues by altering at aldehyde functionary.
2. To confirm and characterize the synthesized compounds by IR, ^{1}H-NMR, ^{13}C-NMR and Mass Spectra.
3. To screen the prepared derivatives for their i*n-vitro* biological efficacy
   3.1. Anti-tubercular potential by MABA method.
   3.2. Antibacterial efficacy by serial dilution method
   3.3. Cytotoxicity studies using A549 and Vero cell line
4. To inhibitory potential of the synthesized derivatives on the potential targets, pantothenate Kinase (PanK) and CTP synthase (PyrG), through a rational approach using *in silico* tools, viz. docking, binding free energy calculations.
5. To assess the ADME properties and drug likeness potential of title compounds using *in silico* online chemoinformatic tool SwissADME.

CHAPTER-III
LITERATURE REVIEW

3: LITERATURE REVIEW

3.1 CHEMISTRY OF QUINOLINE

Quinolines are a significant class of heterocyclic aromatic compounds, characterized by a fused benzene and pyridine ring systems. This structural framework provides quinolines with a unique combination of chemical stability and reactivity, making them important in the development of various pharmacologically active molecules. The nitrogen atom within the quinoline ring influences its weakly basic nature, contributing to its interaction with other chemical species and its role in biological systems [73].

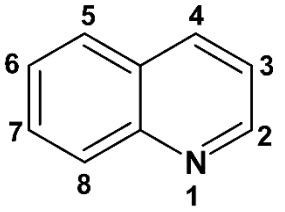

(1)

The aromatic nature of quinoline (1), resulting from its fused ring system, imparts considerable stability, enabling it to undergo a wide variety of substitution reactions. Quinoline's reactivity is largely affected by the electron distribution within its ring system. The nitrogen atom in the pyridine ring withdraws electron density, making certain positions on the benzene ring more reactive to electrophilic substitution. Specifically, the C-2, C-3, and C-4 positions are most susceptible to substitution reactions. Quinoline readily undergoes nitration, sulfonation, and halogenation reactions. These reactions typically occur at the C-2 and C-4 positions due to the electron-withdrawing nature of the nitrogen atom in the pyridine ring, which makes these positions more electron-rich and thus more reactive towards electrophiles [74-75].

The presence of the nitrogen atom also allows quinoline to participate in nucleophilic substitution reactions, although these are less common than electrophilic substitutions. Nucleophilic substitutions typically occur at the C-2 position, especially when an activating group is present [75]. It is weakly basic in nature due to the lone pair of electrons on the nitrogen atom. However, the basicity is less pronounced than in pyridine due to the electron-withdrawing effect of the adjacent benzene ring. Quinoline's aromaticity remains intact, as the nitrogen's lone pair does not participate in the aromatic π-system, preserving its aromatic character. The basicity of quinoline can be quantified by its pKa value, which is typically around 4.9, indicating that it is less basic than pyridine (pKa ~5.2) [76].

Quinoline is a polar compound, moderately soluble in organic solvents like ethanol and ether, and slightly soluble in water. Its solubility is influenced by the substituents attached to the quinoline ring, with electron-withdrawing groups decreasing solubility in nonpolar solvents. The chemical versatility has made quinoline a central scaffold in medicinal chemistry. The ability to synthesize a variety of derivatives through reactions such as the formation of quinoline-2-carbaldehyde (2), quinoline-3-carbaldehyde (3) and Schiff bases (4) has expanded the utility of quinolines in drug discovery [77-78].

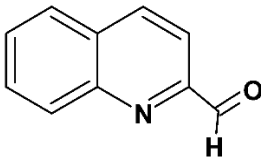

(2)

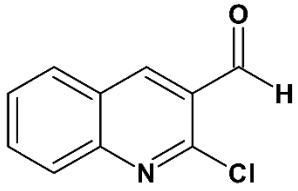

(3)

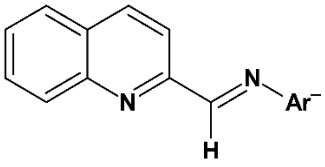

(4)

3.2 SYNTHESIS AND BIOLOGICAL ACTIVITIES OF QUINOLINE AND DERIVATIVES

Quinoline is a member of alkaloid family, widely recognized for its versatile biological activities. The presence of quinolines in nature, especially in various plant and microbial systems, further highlights their biological relevance. These naturally occurring quinolines often serve as defence mechanisms, exhibiting toxic properties against predators or pathogens. This natural occurrence, coupled with their synthetic versatility, positions quinolines as a critical focus in both organic and medicinal chemistry.

Heydari M *et al*. (2024) represented a significant advancement in the synthesis of 4H-pyrano[23-b] quinoline derivatives (5). The study utilized DABCO as a mediator for Knoevenagel condensation and heterocyclization under metal-free conditions, enabling a highly regioselective and efficient synthesis. The process was notable for its mild reaction conditions, excellent yields, and straightforward purification, making it appealing for large-scale synthesis and potential industrial applications. The eco-friendly nature of the protocol aligned with the growing demand for sustainable and green chemistry practices. Overall, this methodology presented a promising platform for the expedited synthesis of diverse O-heterocyclic compounds and offered valuable opportunities for further advancements in medicinal chemistry and drug development [79].

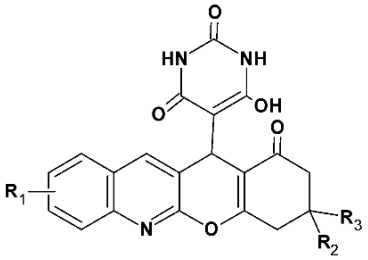

4a-l
(5)

Forozan R *et al.* (2023) explored the design and synthesis of a series of novel thioquinoline derivatives (6), bearing phenylacetamide, for evaluating their potential as α-glucosidase inhibitors. The synthesized compounds were extensively characterized using techniques such as FTIR, ^{1}H NMR, ^{13}C NMR, ESI-MS, and elemental analysis. Biological evaluation revealed that all derivatives exhibited significant α-glucosidase inhibitory activity, with IC_{50} values ranging from 14.0 to 373.85 μM, outperforming the standard drug acarbose. The most potent derivative, compound 9m (R-2,6-dimethylphenyl), showed competitive inhibition with a Ki value of 18.0 μM [80].

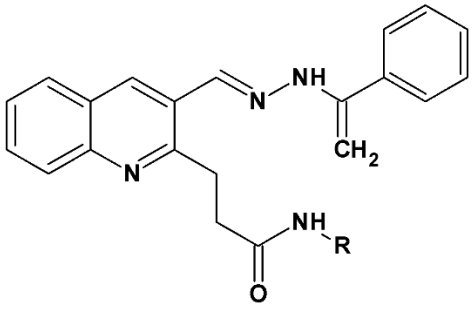

9a-p
(6)

Martins L M *et al.* (2022) discussed optimized reaction conditions for synthesizing 2,4-diaryl-quinoline derivatives (7) through a multicomponent reaction. The study utilized aniline derivatives, substituted phenylacetylene and phenylacetylenes as starting materials and varied the HCl solution (promotor) in low concentration, temperature, and reaction time to determine the best conditions. The optimal conditions were found to be a 0.5 M HCl solution under reflux for 72 hours. The study also proposed a mechanism for the multicomponent synthesis of quinoline derivatives catalysed by HCl, providing a detailed methodology for the efficient synthesis of these compounds [73].

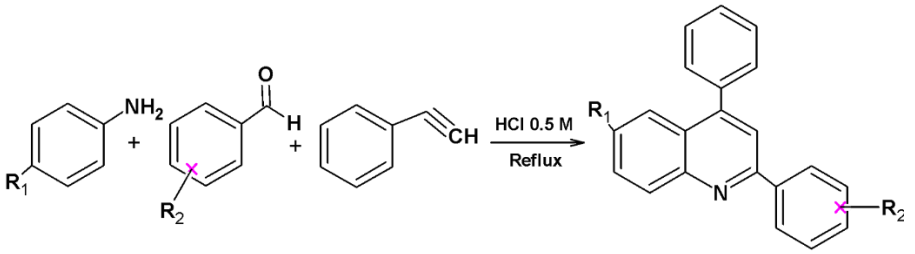

(**7**)

Elkaeed E B *et al*. (2022) synthesized a series of new quinoline and isatin derivatives as potential VEGFR-2 inhibitors using a multi-step synthetic pathway. The synthesized compounds were obtained in good yields (74-88%) and were characterized using IR, ^{1}H NMR, and ^{13}C NMR spectroscopy. The compounds were tested for their anti-proliferative activity against four cancer cell lines (*A549*, *Caco-2*, *HepG2*, and *MDA-MB-231*) using MTT assay. Compounds 13 and 14 (8) exhibited potent anti-cancer activity, with IC_{50} values of 9.3 µM and 5.7 µM, respectively, comparable to the reference drug doxorubicin (IC_{50} = 8.2 µM) against *Caco-2* cells. Compound 7 (8) exhibited significant anti-proliferative activity against *HepG2* (liver cancer) and *MDA-MB-231* (breast cancer) cell lines, with IC_{50} values of 12.5 µM and 10.8 µM, respectively. Both compounds also exhibited strong VEGFR-2 kinase inhibitory activity, with IC_{50} values of 69.11 nM and 85.89 nM, respectively [81].

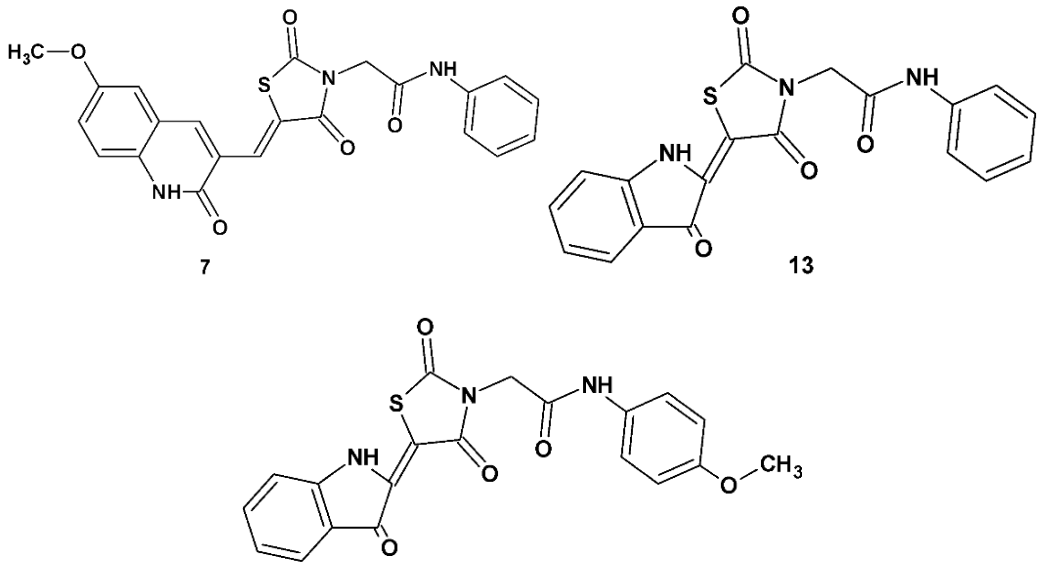

(**8**)

Murugan K *et al*. (2022) synthesized a 4,7-dichloroquinoline derivative (9) as potential insecticidal agent targeting the larval vectors of malaria (*Anopheles stephensi*) and dengue (*Aedes aegypti*). The synthesis involved the reaction of 4,7-dichloroquinoline with ethylene diamine to yield N^1-(7-chloroquinoline-4-yl) ethane-1,2-diamine. The final product was purified and characterized using techniques such as IR, ^{1}H NMR, ^{13}C NMR, mass spectrometry, and elemental analysis. The synthesized compound exhibited potent larvicidal and pupicidal activity, with LC_{50} values ranging from 4.408 µM/mL (first instar larvae) to 7.958 µM/mL (pupal stages) for *A. stephensi* and 5.016 µM/mL (first instar larvae) to 10.669 µM/mL (pupal stages) for *Aedes aegypti*. *In vitro* antiplasmodial studies demonstrated that the compound effectively inhibited the growth of *Plasmodium falciparum* (CQ-sensitive strain 3D7 and CQ-resistant strain INDO) with IC_{50} values of 6.7 nM and 8.5 nM, respectively, outperforming chloroquine (23 nM and 27.5 nM, respectively). Additionally, the

compound showed antiviral activity against dengue virus serotype 2 (DENV-2) and exhibited minimal toxicity to Vero cells at concentrations up to 100 µM/mL [82].

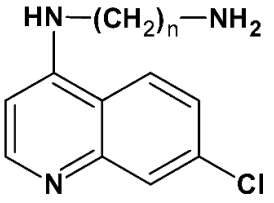

(**9**)

Zaib S *et al*. (2021) conducted a study to explore quinoline-thiosemicarbazone hybrids as potential therapeutics for Alzheimer's disease, focusing on their cholinesterase inhibitory activity. The synthesized compounds were evaluated using *in vitro* cholinesterase inhibition assays based on Ellman's method, with galantamine as a positive control. The lead compound, 5b (R_1= -OMe,R_2 = -H) (10), exhibited an IC_{50} value of 0.12 ± 0.02 µM against acetylcholinesterase (AChE), demonstrating 5-fold higher potency compared to the standard drug galantamine (IC_{50} = 0.62 ± 0.01 µM) [83].

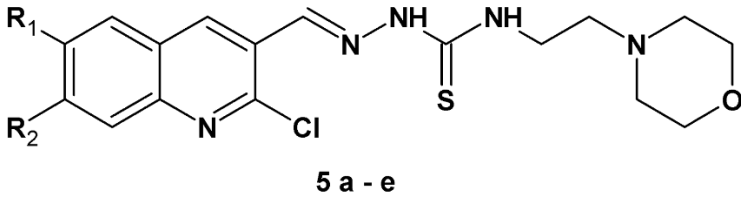

(**10**)

Pokalwar R U (2020) described a straightforward, solvent-free method for synthesizing new derivatives of dimethyl 1-(2-chloroquinolin-3-yl)-2,2-dicyanoethylphosphonate (11). The process involved Knoevenagel condensation of substituted 2-chloroquinoline-3-carbaldehydes and malononitrile with DBU catalyst,

yielding 2-((2-chloroquinolin-3-yl) methylene) malononitrile. Subsequent reactions with dimethyl phosphite using DBU at room temperature led to the formation of dimethyl (1-(2-chloroquinolin-3-yl)-2,2-dicyanoethyl) phosphonate derivatives. The synthesized compounds were characterized using IR, ^{1}H NMR, and Mass spectroscopy. The method was notable for its mild conditions, rapid reaction times, and high yields, presenting a valuable approach for synthesizing novel phosphonate derivatives [84].

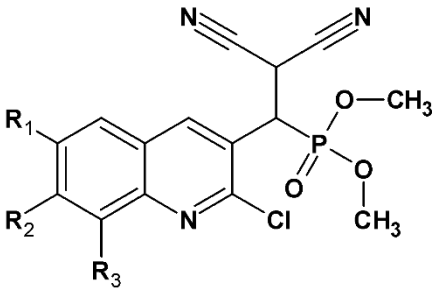

(11)

Kovalenko S M *et al.* (2020) investigated the synthesis of methyl 4-hydroxy-2-thioxo-1,2-dihydroquinoline-3-carboxylate derivatives (12) through alkylation using CH_3I generating a combinatorial library. The research highlighted the predominance of O-methylation over N-methylation, resulting in compounds like methyl 4-methoxy-2-(methylthio) quinoline-3-carboxylate and methyl 1-methyl-2-(methylthio)-4-oxo-1,4-dihydroquinoline-3-carboxylate. The structures were confirmed through elemental analysis, spectroscopy, LC/MS, and X-ray diffraction. The synthesized compounds were tested for anti-Hepatitis B Virus (HBV) activity using an *in vitro* model. At a 10 μM concentration, compound 4 showed the highest HBV replication inhibition of 83% with 91% cell survival, while compounds 6 and 3 showed 79% and 68% inhibition, respectively [85].

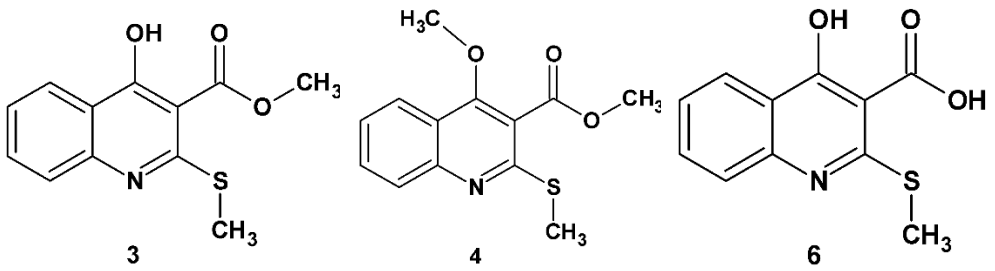

(12)

Tabassum R *et al.* (2020) reported a novel and efficient method for synthesizing functionalized 7-hydroxy-4-phenyl-1,2-dihydroquinoline derivatives (13). The protocol involved a one-pot, three-component reaction catalysed by ammonium acetate, leading to diverse quinoline derivatives with high yields. The synthesis was notable for its cost-effectiveness and atom economy, utilizing affordable reagents and catalysts under mild conditions. Structural analysis of the compounds was conducted using FTIR, ^{1}H NMR, and ^{13}C NMR spectroscopy, with MALDI-TOF-MS and EI mass spectrometry confirming the compound masses. This research introduced a streamlined and economically viable strategy for synthesizing quinoline derivatives [86].

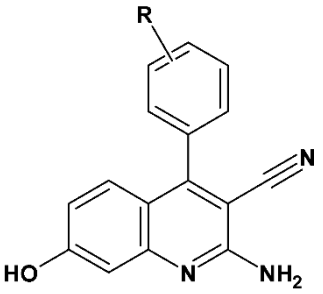

(13)

Chinh P T *et al*. (2020) synthesized a series of 2-carbaldehyde derivatives of quinoline and 1,4-dihydroquinoline (14) using the Vilsmeier-Haack reaction. The synthesis involved the reaction of various substituted anilines with ethyl acetoacetate

in the presence of $POCl_3$ and DMF as catalysts to form quinoline-2-carbaldehyde derivatives in good yields ranging from 68% to 75%. The structural identities of these compounds were confirmed through IR, ^1H NMR, and ^{13}C NMR spectroscopy [77].

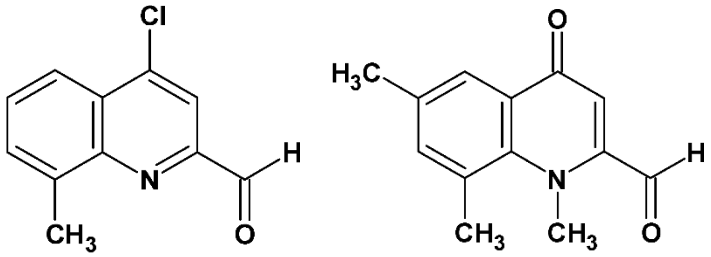

(**14**)

Rocha D H A *et al*. (2020) explored the synthesis of new heterocyclic scaffolds using chromene and quinoline-3-carbaldehydes as intermediates (15). These intermediates were efficiently synthesized using the Vilsmeier-Haack formylation reaction on flavanones and azaflavanones, yielding products with significant structural diversity. The synthesized quinoline derivatives were then employed in a series of reactions, including Wittig and cyclization reactions, to form various heterocyclic compounds such as (Z/E)-2-aryl-4-chloro-3-styryl-2H-chromenes, chromeno[3,4-c] quinolines, and styrylquinoline-1(2H)-carbaldehydes. This study highlighted the potential of chromene- and quinoline-3-carbaldehydes as versatile building blocks for constructing pharmacologically relevant heterocycles [87].

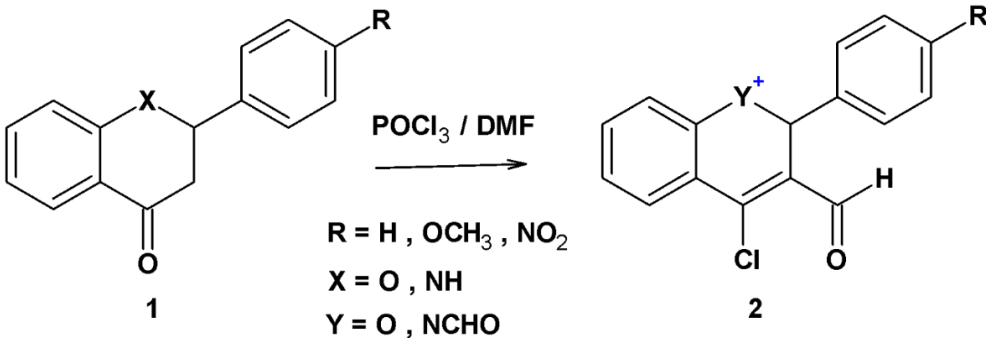

(**15**)

Farooq S *et al*. (2020) synthesized a series of tetrahydroquinoline derivatives (16) using a one-pot, three-component Mannich reaction involving formaldehyde, tetrahydroquinoline, and various amines under reflux conditions in ethanol. The products were characterized using IR, ^{1}H NMR, ^{13}C NMR, and mass spectrometry.
The synthesized compounds were evaluated for their biological activity, exhibiting significant antioxidant, anti-amylase, anti-cancer, and anti-inflammatory activities. Compound SF8 exhibited the highest antioxidant activity with an IC_{50} value of 29.19 µg/mL in the DPPH assay, surpassing the standard ascorbic acid. SF5 demonstrated maximum α-amylase enzyme inhibition (97.47% at 200 µg/mL). Cytotoxicity against Hep-2C cells was significant for SF8, with an IC_{50} value of 11.9 µM at 72 hours, comparable to cisplatin (IC_{50} = 14.6 µM). The *in vitro* nitric oxide assay identified SF13 as the most effective anti-inflammatory agent, scavenging 85% of nitric oxide at 50 µM concentration [88].

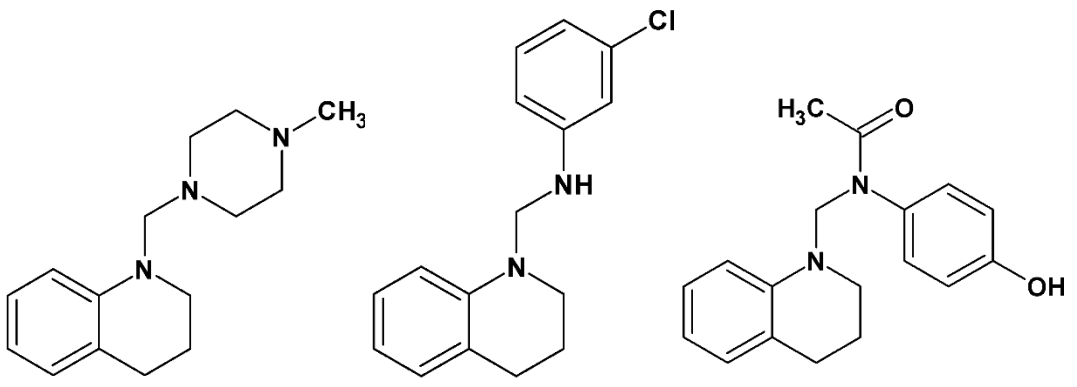

(16)

Moghaddam F M *et al*. (2019) reported a novel method for synthesizing indolo[3',2':5,6] thiopyrano[2,3-b]quinolines using 2-chloroquinoline-3-carbaldehydes and indoline-2-thione (17). The reaction proceeds via a one-pot, three-component condensation in the presence of ethanol and triethylamine as a base. The

method is highly efficient, producing the desired products in good yields (69-93%) under mild reaction conditions [89].

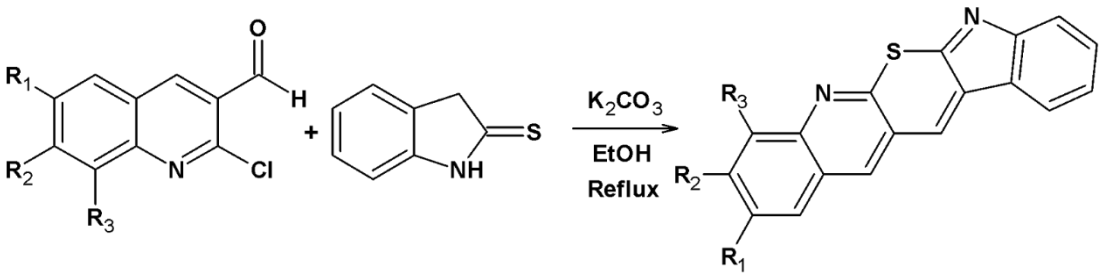

(**17**)

Hackler L Jr *et al*. (2019) synthesized enantiomers of an 8-hydroxyquinoline derivative (Q134) using an enantioselective method involving quinidine or quinine as a catalyst in the presence of formic acid. This synthesis yielded enantiomerically pure products, Q134R and Q134S (18), with yields of 14% and 33%, respectively, and an enantiomeric excess of 99%. The cytoprotective activity of these compounds was evaluated *in vitro*, where both enantiomers showed comparable and potent activity with IC_{50} values of 180 nM and 233 nM, respectively.

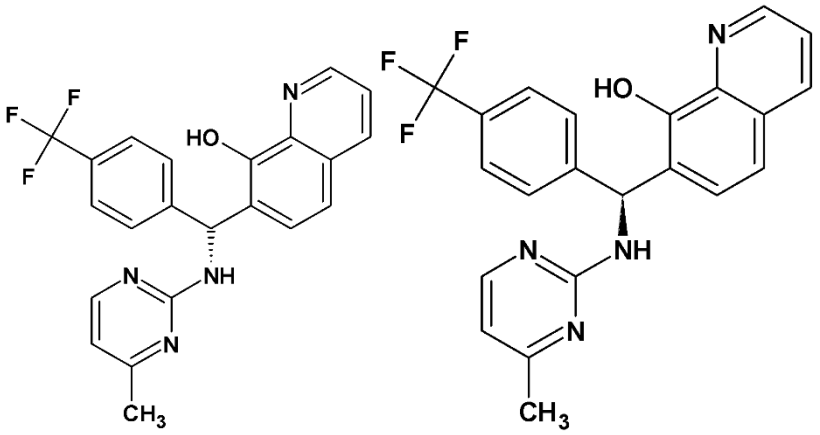

(**18**)

Further biological testing indicated that both Q134R and Q134S exhibited the ability to stabilize hypoxia-inducible factor-1 alpha (HIF1A) protein, suggesting a

potential role in neuroprotective applications, particularly for conditions like Alzheimer's disease [90].

Radini I A M *et al*. (2016) synthesized a series of novel quinoline derivatives (19) and evaluated their antimalarial activity against *P.falciparum*. The *in vitro* antimalarial assay was performed using a parasite inhibition assay to measure the compounds' effectiveness, with chloroquine (CQ) serving as the reference standard. The most active compounds, specifically 4b, 4g, 4i, and 12, exhibited IC_{50} values of 0.46, 0.30, 0.014, and 0.46 µg/mL, respectively, indicating potent antimalarial activity. Compound 4i (19) demonstrated the highest activity with an IC_{50} of 0.014 µg/mL, outperforming the reference standard CQ (IC_{50} = 0.49 µg/mL). These results suggest that the synthesized quinoline derivatives have potential antimalarial activity [91].

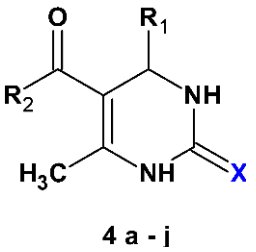

4 a - j

	R1	R2	X
4b	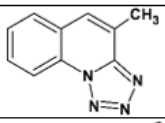	OEt	S
4g	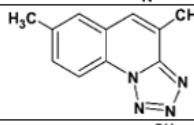	Me	S
4i	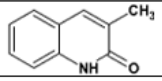	Me	S

(19)

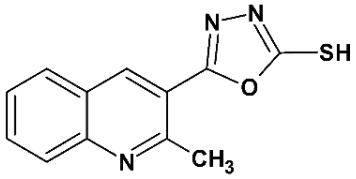

12

Puskullu M O *et al*. (2015) synthesized a series of quinoline-2-carbaldehyde hydrazone derivatives (20) as bioisosteric analogs of melatonin. The synthesis involved reacting quinoline-2-carboxaldehyde with various substituted hydrazine derivatives in ethanol, resulting in the formation of hydrazones with yields ranging from 33% to 78%. The products were purified via column chromatography and characterized using IR, ^{1}H NMR, ^{13}C NMR, and elemental analysis. The antioxidant activity of the synthesized compounds was determined using the DCFH-DA oxidation

method. Most of the compounds demonstrated significant antioxidant activity. The cytotoxicity was evaluated using MTT and LDH leakage assays in CHO-K1 cells. Most compounds induced membrane damage, but 3a (R_1-R_5 = -H) and 3m (R_1, R_3, R_5 = -H, R_2, R_4 - Cl) showed minimal cytotoxicity, indicating their potential as safer antioxidant agents [92].

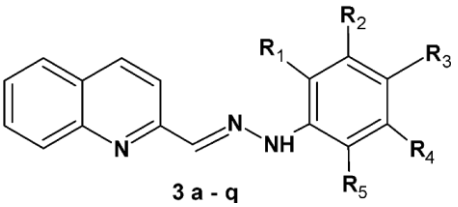

(**20**)

Pereira G R *et al*. (2013) synthesized 27 derivatives of 7-chloroquinolinotriazoles (21) using the copper-catalyzed azide-alkyne cycloaddition (CuAAC) click chemistry method, involving 4-azido-7-chloroquinoline and various alkynes. These compounds were evaluated for their antimalarial activity against *P. falciparum* (W2 strain) using the [3H]-hypoxanthine incorporation assay and for cytotoxicity against Hep G2A16 cells using the MTT assay. The results showed that all derivatives exhibited low cytotoxicity (CC_{50} (cytotoxic concentration for 50% inhibition) > 100 µM), while five derivatives demonstrated moderate antimalarial activity with IC_{50} values ranging from 9.6 to 40.9 µM. These findings prompted potential for further optimization and development of 7-chloroquinolinotriazoles as antimalarial agents [93].

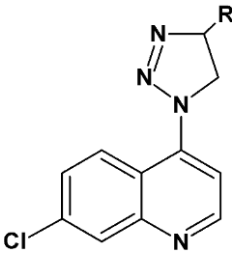

(**21**)

3.3 SYNTHESIS, ANTI-TB, ANTIMICROBIAL, AND CYTOTOXIC ACTIVITIES OF QUINOLINE AND DERIVATIVES

Quinolines play a pivotal role in hybrid molecule development, where their combination with other heterocyclic systems enhances biological activity. For instance, hybrid structures incorporating quinoline and benzimidazole moieties have demonstrated potent antifungal, and antimicrobial properties [94], underscoring the significance of quinoline in the design of multifunctional therapeutic agents. Schiff bases formed by the condensation of quinoline aldehydes with amines, have shown promising biological activities, along with antimicrobial and anticancer effects [78].

Suryanarayana K *et al.* (2023) focused on the design and synthesis of novel chloroquinoline-linked rhodanine derivatives containing a 1,2,3-triazole scaffold (22). The synthesis involved a multistep process starting with the formation of 6-chloroquinoline-2-carbaldehyde, followed by condensation with rhodanine and subsequent cyclization with various substituted azides to yield the target compounds. The synthesized compounds were characterized using ^{1}H NMR, ^{13}C NMR, and HR-MS. The anticancer activity of these compounds was evaluated against various cancer cell lines, including *MCF-7* (breast cancer), *HeLa* (cervical carcinoma), *HT-29* (colon cancer), and *Caco-2* (human epithelial). Among the synthesized derivatives, compound 10c (R= 4-Br) revealed the most potent anticancer activity, with IC_{50} values of 3.67 µM for MCF-7, 3.93 µM for *Caco-2*, 4.92 µM for *HeLa*, and 6.83 µM for *HT-29* [95].

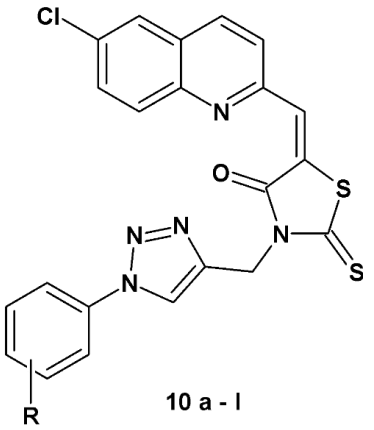

(**22**)

Shui H *et al.* (2022) reported synthesis of quinoline derivatives (23) using the acceptor less dehydrogenative coupling (ADC) reaction of 2-aminobenzyl alcohol and aryl secondary alcohols. The strong bases such as NaOH, KOH, or t-BuOK improved the chemo selectivity and yield of the reaction, with 1,4-dioxane identified as the most favourable solvent. The synthesized quinoline derivatives were evaluated for their antimicrobial activity using the broth microdilution method. This method determined the minimum inhibitory concentration (MIC) values against *Staphylococcus aureus* (Gram-positive), *E. coli* (Gram-negative), and *Candida albicans*. Notably, compounds 3ab (R_1= -H, R_2= 4-methoxyphenyl, R_3= methyl), 3ad (R_1= -H, R_2= 4-chlorophenyl, R_3= propyl), and 3ah (R_1= -H, R_2= phenyl, R_3= 2-furanomethyl) exhibited high antibacterial activity against *S. aureus*, with compound 3ad showing an MIC of 2 µg/mL, outperforming the standard drug norfloxacin. Compound 3ck demonstrated strong antifungal activity against *C. albicans* (MIC = 64 µg/mL). However, the compounds showed limited efficacy against *E. coli*. This study highlighted the potential of cyclometalated iridium-catalysed quinoline derivatives as promising antibacterial and antifungal agents [96].

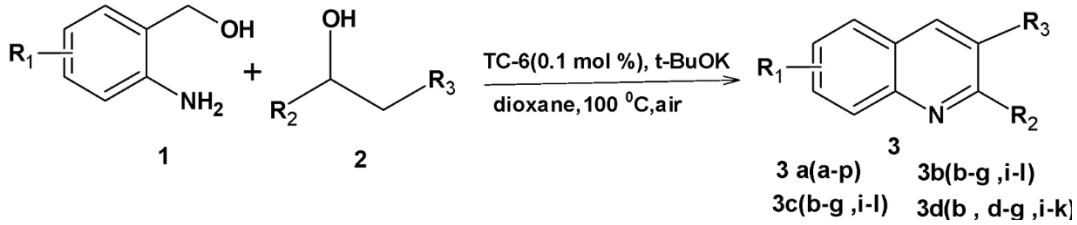

(**23**)

Nagamani M *et al.* (2022) explored the synthesis of quinoline-based 4-(methoxymethyl)-1,2,3-triazole derivatives (24) through a Vilsmeier-Haack reaction followed by a Huisgen 1,3-dipolar cycloaddition. The reaction involved 2-chloroquinoline-3-carbaldehyde, piperidine, and various aryl azides, in presence of DMF under microwave irradiation to yield the desired triazoles. The structures of these compounds were confirmed by spectral analysis (IR, ^{1}H NMR, and mass spectrometry). The synthesized compounds were tested for antibacterial activity using the agar well diffusion method against five Gram-positive (*M. tuberculosis*, *M. luteus*, MRSA, *Bacillus subtilis*, and *Bacillus cereus*) and five Gram-negative strains (*Pseudomonas aeruginosa*, *K. pneumoniae*, *E. coli*, *Proteus vulgaris*, and *Salmonella typhi*). The zones of inhibition were measured and compared with the standard antibiotic, gentamicin, to assess the antibacterial efficacy of each compound. The MIC values ranged from 50-150 µg/mL, indicating good antibacterial potential, especially against Gram-negative strains [97].

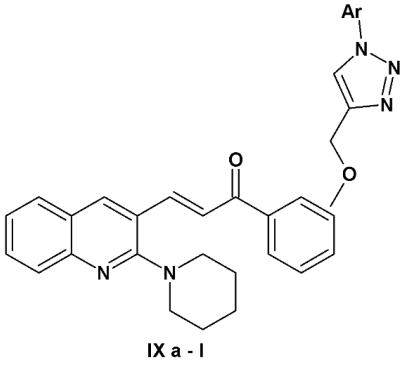

(**24**)

Fekadu G *et al.* (2022) focused on the synthesis of a series of 7-fluoroquinoline derivatives (25) through the Vilsmeier-Haack reaction, where 2-chloro-7-fluoroquinoline-3-carbaldehydes serve as the key intermediate. The chlorine atom in the fluoroquinoline was substituted with various nucleophiles, and the aldehyde group was further modified to yield carboxylic acid and imine derivatives. The synthesized compounds were characterized by NMR, FTIR, and mass spectrometry. The antibacterial activities of the compounds were evaluated using the disc diffusion method against strains such as *E. coli*, *P. aeruginosa*, *S. aureus*, and *Streptococcus pyogenes*, showing inhibition zones of 6.34 to 15.3 mm at 200 µg/mL [98].

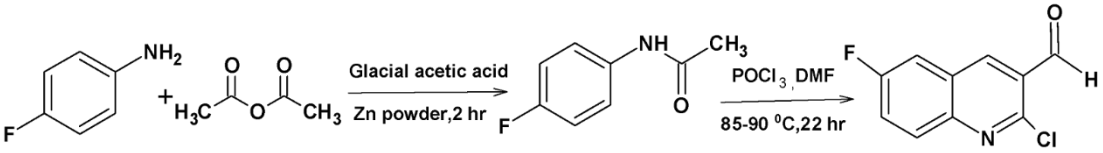

(**25**)

Lagdhir M *et al*. (2021) synthesized a series of quinoline hybrid derivatives (26) and evaluated their antimicrobial and antitubercular activities. The antibacterial and antifungal activities were assessed using the broth microdilution method against two gram-positive bacteria (*S. aureus* and *S. pyogenes*), two gram-negative bacteria (*E. coli* and *P. aeruginosa*), and three fungi (*Aspergillus clavatus*, *C. albicans*, and *Aspergillus niger*). Compound 6F (R- 2,4-$(OCH_3)_2$) demonstrated significant antibacterial activity with a MIC value of 62.5 µg/mL against *E. coli*. The antitubercular activity was tested against *M. tuberculosis* H37Rv, and compound 6G (R= 4-Cl) exhibited the highest potency with a MIC value of 50 µg/mL. The study highlights the potential of these quinoline derivatives for further antimicrobial and antitubercular studies [99].

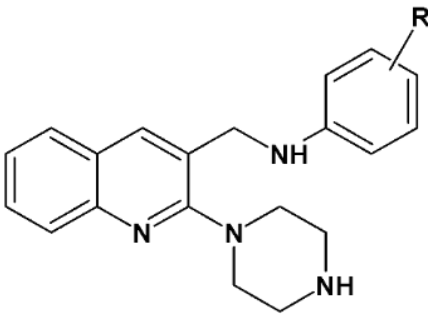

6 A-L

(26)

Zeleke D *et al*. (2021) synthesized a series of quinoline-stilbene derivatives using the Wittig reaction between substituted quinoline and benzyltriphenylphosphonium chloride, along with a novel pinacol derivative through the pinacolization of 2-methoxyquinoline-3-carbaldehyde using aluminum powder and potassium hydroxide. The structures of the synthesized compounds were confirmed using spectroscopic techniques (UV-Vis, FT-IR, and NMR). The synthesized compounds were evaluated for their antibacterial activity against two Gram-positive (*S. aureus*, *B. subtilis*) and two Gram-negative (*E. coli*, *Salmonella typhimurium*) bacteria using the paper disc diffusion method. Among the tested compounds, compound 19 (27) showed the highest antibacterial activity against *E. coli*, with an inhibition zone of 16.0 ± 0.82 mm at a concentration of 500 µg/mL, which was comparable to the standard drug ciprofloxacin (Zone of inhibition = 18.67 ± 0.47 mm) [100].

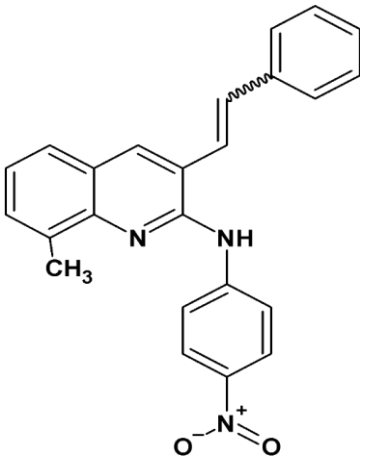

19

(**27**)

Guje P B *et al.* (2020) developed a novel and efficient method for synthesizing 3-(1H-benzo[d]imidazole-2-ylthio) methyl-2-chloroquinoline (28) using 2-chloroquinolin-3-carbaldehydes. Comprehensive characterization of the synthesized compounds was performed using IR, ^{1}H NMR spectroscopy, and Mass spectrometry. The antibacterial activity and antifungal activity against *C. Albicans*, *A. Niger*, and *A. Clavatus* of these compounds were investigated using Broth dilution technique. Compound 4e (R_1 and R_3= -H; R_2= methoxy) showed MIC values of 25, 100, 125 and 50 µg/ml against *S. aureus*, *E. coli*, *P. aeruginosa*, and *S. pyogenes* respectively when compared with standard Ciprofoxacin (MIC = 50, 25, 25, 50 µg/ml respectively). Additionally, compound 4e displayed antifungal activity with minimum fungicidal concentration of 500 µg/ml against *C. albicans, A. niger* and *A. clavatus* using Griseofulvin as the standard drug (MIC = 500, 100, 100 µg/ml) [101].

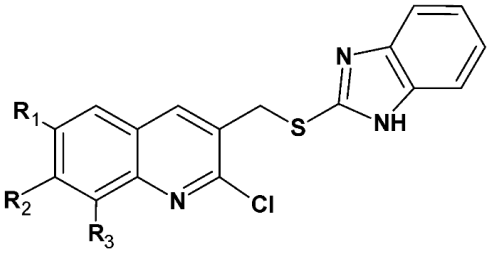

4 a-f

(28)

Cieslik W *et al*. (2020) synthesized a series of styrylquinolines (SQLs) to investigate their antifungal activity against *C. albicans*. The biological activity of these SQLs was tested against wild-type *C. albicans* and mutant strains with silenced efflux pumps (Cdr1p and Cdr2p). Among the synthesized compounds, SQL 3 (29) exhibited the strongest antifungal activity, especially against the cdr1Δ strain, with an MIC value of 3.29 mg/L. The study also demonstrated that SQL 3 showed a synergistic effect when combined with fluconazole (FIC ≤ 0.02), suggesting potent efflux pump inhibitor. The results indicated that styrylquinolines have promising antifungal properties, particularly in overcoming drug resistance in *C. albicans* [102].

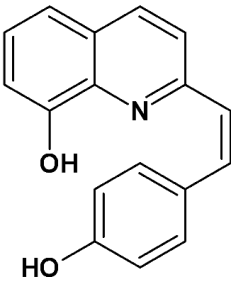

SQL3

(29)

Muthukumar K *et al*. (2019) synthesized a series of 2H-oxeto[2,3-b] quinolines (30) through a multi-step process involving the oxidation, reduction, and cyclization of 2-chloro-3-formyl quinolines. The biological activity of these compounds was assessed against seven bacterial strains including *S. aureus, B. subtilis, and S.*

pyogenes (Gram-positive) and *Salmonella typhi*, *E. coli*, *P. aeruginosa*, and *K. pneumoniae* (Gram-negative) using the agar well diffusion method. The results showed that compound 1e (R_1, R_3, R_4= -H; R_2= Cl) exhibited the most potent antibacterial activity with inhibition zones comparable to the standard drug ofloxacin, particularly against *S. aureus* and *S. typhi* [103].

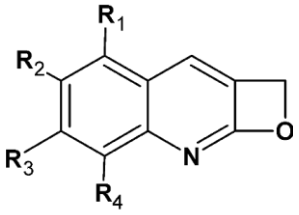

1 a-e

(**30**)

Krawczyk M *et al*. (2019) synthesized a series of 8-hydroxyquinoline glycoconjugates containing sulfur at the sugar anomeric position (31). The synthesis involved the introduction of a sulfur atom into the sugar molecule followed by a Cu(I)-catalyzed alkyne-azide cycloaddition (CuAAC) to connect the sugar derivatives to the quinoline moiety. The resulting compounds were confirmed using NMR spectroscopy and other analytical techniques. The biological activity of the synthesized compounds was evaluated using the MTT cytotoxicity assay on MCF-7 (breast cancer) and HCT-116 (colon cancer) cell lines. Among the tested glycoconjugates, the highest cytotoxic activity was observed against the MCF-7 cell line, displaying potential anticancer properties. The presence of copper ions enhanced the cytotoxic activity of these glycoconjugates, demonstrating their ability to form metal complexes, which is a crucial factor in their mechanism of action. The study suggested that these quinoline glycoconjugates have promising potential as targeted anticancer agents [104].

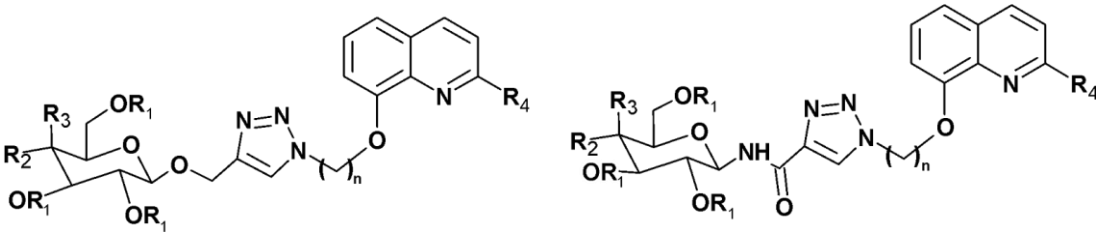

(31)

Beyzaei H *et al*. (2019) synthesized a series of 2-chloro-3-quinolinecarboxaldehyde Schiff bases (32) and evaluated for their antibacterial activity against six gram-positive (*Staphylococcus epidermidis*, *Rhodococcus equi*, *Enterococcus faecalis*, *S. aureus, B. subtilis subsp. spizizenii,* and *Streptococcus pneumoniae* and two gram-negative bacterial pathogens (*Shigella flexneri* and *Proteus vulgaris)*. The antibacterial efficacy was assessed using the disc diffusion, broth microdilution, and time-kill tests as per CLSI guidelines. The inhibition zone diameters (IZDs) ranged from 7.5 to 19.8 mm, with minimum inhibitory concentration (MIC) values between 256-2048 µg/mL, and minimum bactericidal concentration (MBC) values ranging from 512 to ≥2048 µg/mL. Compound 4c (Ar = Phenol) (32) displayed the most significant antibacterial activity, suggesting that modifications to the Schiff base structure could improve antimicrobial properties [78].

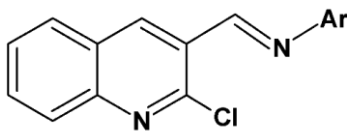

4 a-g

(32)

Aboelnaga A and EL-Sayed T H (2018) synthesized new 7-chloroquinoline derivatives using ultrasound irradiation via a click chemistry approach. The

synthesized derivatives were evaluated for their antimicrobial and anticancer activities. The anticancer activity was assessed against MCF-7 (breast cancer), HCT-116 (colon carcinoma), and HeLa (cervical carcinoma) cell lines. Compounds 3 and 9 (33) exhibited significant cytotoxic activity, particularly against the MCF-7 cell line, with IC_{50} values of 13.5 µM and 9.2 µM, respectively, indicating their potential as anticancer agents. In the antibacterial assays, the compounds demonstrated moderate to good inhibition against bacterial strains, with compound 7 (33) showing the highest activity against *E. coli* (MIC = 15 µg/mL) and *S. aureus* (MIC = 12.5 µg/mL). These findings suggest that the synthesized derivatives have potential applications as antibacterial and anticancer agents [105].

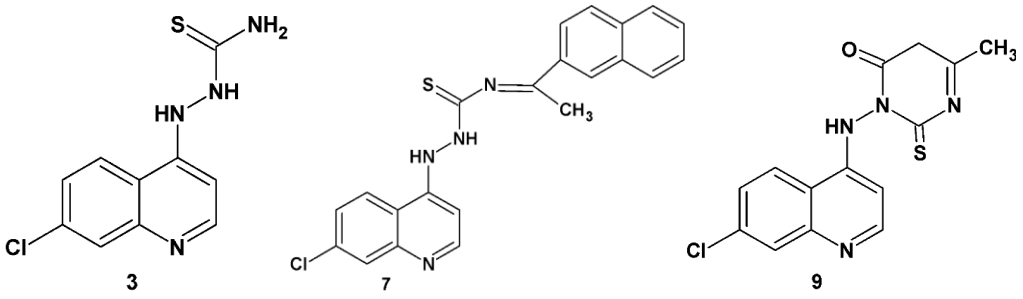

(33)

Korcz A *et al*. (2018) prepared a series of novel quinoline-3-carbaldehyde hydrazones (34) bearing either a 1,2,4-triazole or benzotriazole moiety. The biological activity of the synthesized compounds was evaluated against three human cancer cell lines: DAN-G (pancreatic cancer), LCLC-103H (large cell lung carcinoma), and SISO (cervical cancer) using a crystal violet microtiter plate assay. Among the tested compounds, those containing a benzotriazole moiety demonstrated enhanced cytostatic effects. The compound 5e (R= -H, R^1= 2-pyridyl) exhibited the most potent anticancer activity with IC_{50} values ranging from 1.23 to 1.49 µM against all cell lines. The study suggests that these benzotriazole-containing quinoline derivatives hold promising anticancer activity [106].

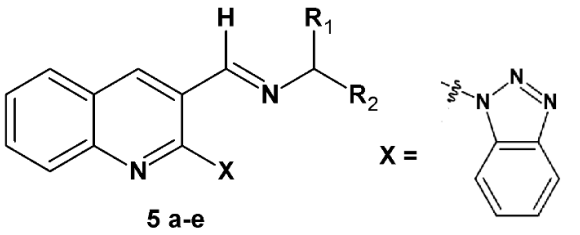

(**34**)

Mallandur B K *et al*. (2017) synthesized a series of Schiff bases derived from 2-chloroquinoline-3-carbaldehyde and its derivatives, incorporating 7-methyl-2-propyl-3H-benzoimidazole-5-carboxylic acid hydrazide (35). They were evaluated for antimicrobial activity against *E. coli*, *S. aureus*, *S. typhi*, and *C. albicans* using the disc diffusion and microbroth dilution methods. The results showed that compounds 3 and 4 exhibited moderate antibacterial activity against *E. coli* with inhibition zones of 16 mm and 15 mm, respectively. However, all compounds displayed decent antifungal activity against *C. albicans*, with inhibition zones of 15-17 mm. The minimum inhibitory concentration (MIC) values for compounds 3 and 4 were 25 µg/mL against *E. coli* and 12.5 µg/mL against *C. albicans*. This study suggested that the synthesized Schiff bases possess moderate antibacterial and antifungal properties, making them potential candidates for further antimicrobial research [94].

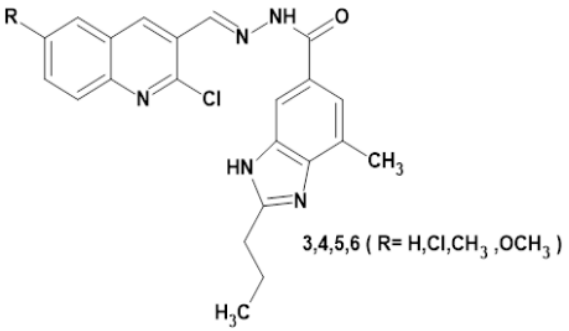

(**35**)

El-Gamal K M A *et al*. (2015) synthesized a series of novel quinoline derivatives (36) and evaluated their antimicrobial activity against various bacterial and fungal strains using the agar diffusion technique and determining the minimum inhibitory concentration (MIC) values. The compounds were tested against *S. pneumoniae*, *B. subtilis*, *P. aeruginosa*, and *E. coli*, as well as fungi such as *Aspergillus fumigatus* and *C. albicans*. Several compounds showed significant antibacterial activity, with MIC values ranging from 12.5 to 50 µg/mL, comparable to standard drugs like Ciprofloxacin, Ampicillin, and Gentamicin (MIC = 0.24 – 15.63 µg/mL). The antifungal activity was also notable, with MIC values ranging from 25 to 100 µg/mL, comparable to Amphotericin B (MIC = 19.7 – 28.7 µg/mL) [107].

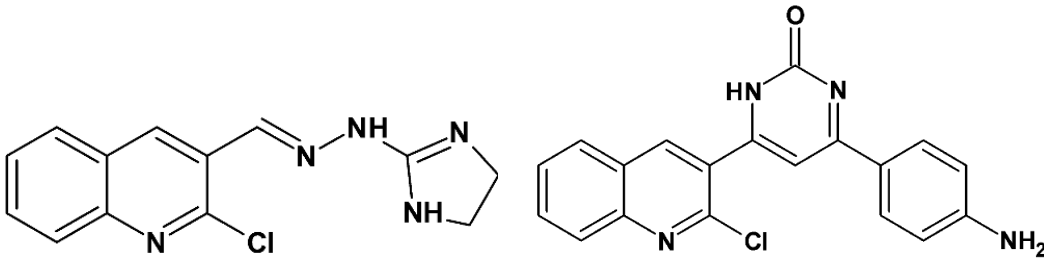

(**36**)

Miniyar P B *et al.* (2015) synthesized a series of 2-chloroquinoline-pyrazole derivatives (37) and evaluated their antimicrobial activity using the broth microdilution method. The compounds were tested against *S. aureus*, *B. subtilis*, *E. coli*, *A. fumigatus*, and *Penicillium notatum*. The compound MB-N (R= -NH_2, R_1= -H) demonstrated MIC values of 44 µg/mL against *B. subtilis*, and 46 µg/mL against *P. notatum*. Compound MB-A exhibited MIC of 43 µg/mL against *E. coli*. The study

indicated that these derivatives, particularly those with electron-donating substituents on the phenyl ring, possess significant antimicrobial potential [108].

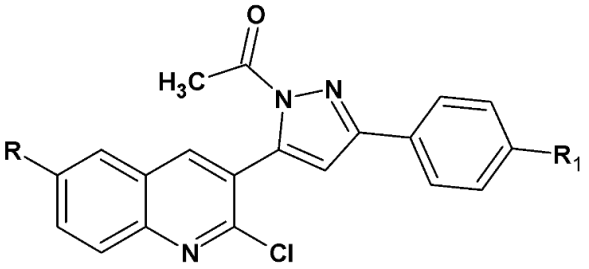

MB -A -MBBB
(37)

Mathew B *et al*. (2013) investigated the antitubercular activity of a novel quinoline derivative targeting the FtsZ protein in *M. tuberculosis* (Mtb). The compound's inhibitory activity against FtsZ was assessed using a polymerization assay, and its antibacterial efficacy was tested against Mtb H37Rv to determine the IC_{90} (concentration that inhibits 90% growth). The lead compound, 1 (38), exhibited an IC_{90} value of 20.4 µM against Mtb H37Rv and an FtsZ polymerization inhibition (ID_{50}) of 22.7 µM. Additionally, its cytotoxicity was tested on Vero cells, with a CC_{50} greater than 120 µM, indicating selectivity for the bacterial target. The study suggested the potential of quinoline derivatives as antitubercular agents targeting the FtsZ protein[109].

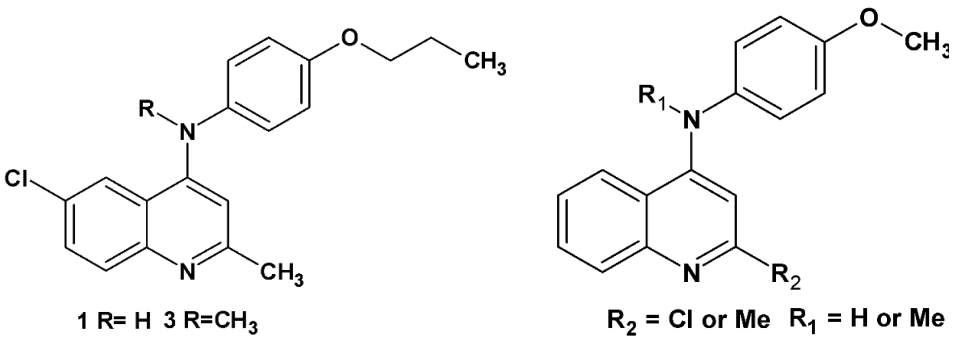

(**38**)

Thomas K D *et al*. (2011) synthesized three new series of 4-hydroxy-8-trifluoromethyl-quinoline derivatives through multi-step reactions (39). These compounds were evaluated for their antibacterial activity against five bacterial strains (*S. aureus*, *S. pyogenes*, *P. aeruginosa*, *K. pneumoniae*, and *E. coli*) using the broth microdilution method, which determined the MICs. The compounds were also tested for antimycobacterial activity against *M. tuberculosis* H37Rv, *M. smegmatis* (MC2), and *M. fortuitum* (ATCC 19542) using the BACTEC 460 TB radiometric system. The *in vitro* antibacterial study showed that compounds 5b, 5e, 5h, 5j, 6c, and 7c exhibited promising activity against all tested bacterial strains, with MIC values ranging from 0.1 to 1.6 µg/mL, indicating their potential as antibacterial and antitubercular agents [110].

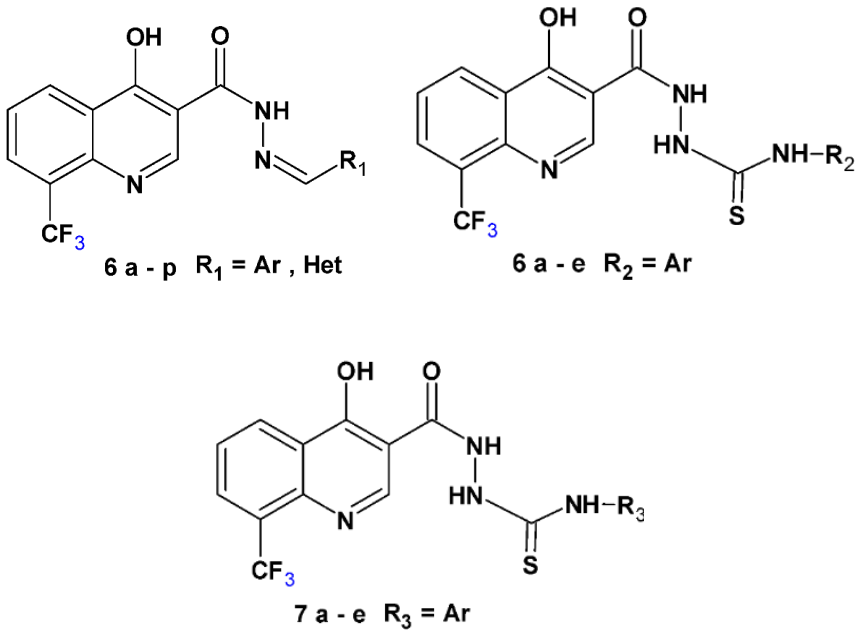

(**39**)

Kumar S *et al*. (2011) synthesized a series of secondary amines containing a 2-chloroquinoline lipophilic domain via nucleophilic substitution reactions, followed by N-methylation to obtain derivatives (40). The synthesized compounds were evaluated for their antifungal activity against strains such as *A. niger* MTCC 281, *Aspergillus flavus* MTCC 277, *Monascus purpureus* MTCC 369, and *Penicillium citrinum* NCIM 768 using the cup-plate method. The MIC values for the active compounds ranged from 25 to 100 µg/mL. Compounds of series 4-16 showed significant antifungal activity, while their N-methyl derivatives 20–25 demonstrated enhanced antifungal properties. Notably, compounds 24 (X= 3-Cl, 4-F) and 25 (X=3-Cl, 4-Cl) showed the

highest potency with MIC values of 25 µg/mL against all tested fungal strains, indicating their potential as effective antifungal agents [111].

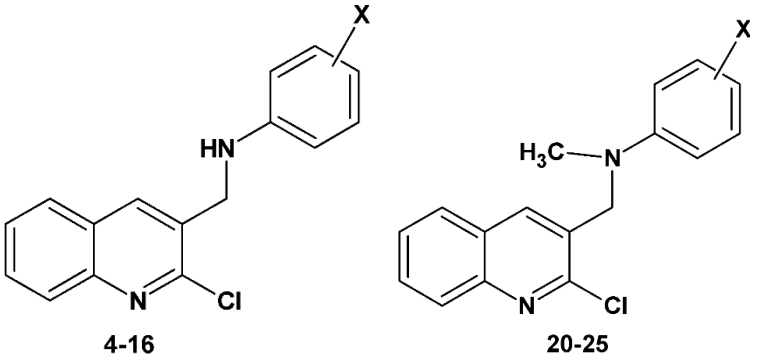

(**40**)

Reddy L V *et al*. (2011) presented a "green" synthesis of N-(quinoline-3-ylmethylene) benzohydrazide derivatives (41) using 2-chloroquinoline-3-carbaldehyde and various substituted hydrazides in PEG 400 as a solvent. The environmentally friendly PEG 400 was recovered and reused multiple times, maintaining effective product yields. Some of the synthesized compounds demonstrated significant cytotoxic activity against the human lung adenocarcinoma cell line (A549) *in vitro* MTT assay. The percentage of inhibition for each compound was tested at concentrations ranging from 1 to 25 µg/mL. Notably, compound 3c (41) exhibited the highest cytotoxicity with 89.32% inhibition at 25 µg/mL, while other compounds such as 3b, 3d, and 3h also showed strong activity. The study suggested that this class of hydrazide derivatives could be further explored for potential anticancer research [112].

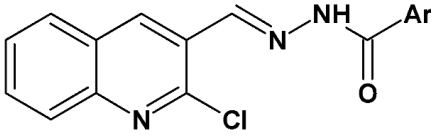

3 a-i

Derivative	Ar	Derivative	Ar
3b	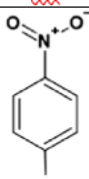	3d	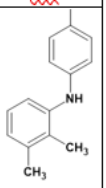
3c	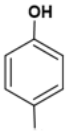	3h	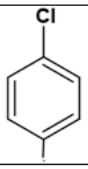

(**41**)

Eswaran S *et al*. (2010) synthesized four new series of quinoline derivatives (42) and evaluated their antibacterial and antituberculosis activities. The synthesized compounds were tested against pathogenic bacterial strains such as *E. coli*, *S. aureus*, *P. aeruginosa*, and *K. pneumoniae*, using a serial plate dilution method with ciprofloxacin as a standard. Additionally, their antituberculosis activity was tested against *M. tuberculosis* H37Rv and MDR-TB using the broth microdilution method with Resazurin as an indicator. Several hydrazone derivatives (e.g., compounds 4b, 4d, and 4s) showed significant antibacterial activity with a MIC value of 6.25 µg/mL, comparable to ciprofloxacin (MIC = 6.25 µg/mL). For antituberculosis activity, compounds 4k, 4s, and 7a (42) were highly potent, with a MIC of 3.12 µg/mL against *M. tuberculosis*, and showed better activity compared to standard drugs such as isoniazid (MIC = 1.5 µg/mL) and rifampicin (MIC = 0.5 µg/mL). The study concludes that these quinoline derivatives have potential antibacterial and antitubercular activity[113].

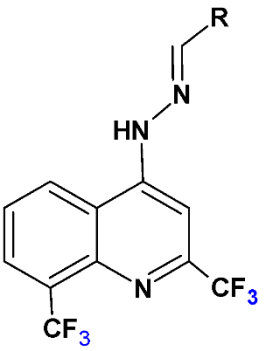

4 a-t

R = alkyl , aryl ,heteroary

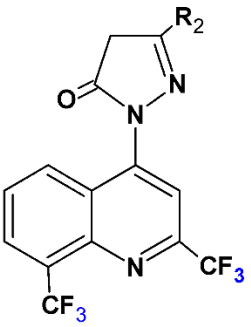

7 a-d

R_2 = alkyl , aryl

(42)

3.4 *IN SILICO* AND ADME STUDIES OF QUINOLINE AND DERIVATIVES

In silico studies, particularly molecular docking and molecular dynamics simulations, are frequently employed to explore the binding interactions of quinoline derivatives with their target proteins, enabling the identification of potential lead compounds with high binding affinity and specificity. Furthermore, ADME (Absorption, Distribution, Metabolism, and Excretion) studies provide crucial insights into the pharmacokinetic behaviour of quinoline derivatives, assessing their drug-likeness, oral bioavailability, metabolic stability, and potential toxicity. These studies collectively play a pivotal role in optimizing quinoline derivatives for drug development, ensuring that they possess the necessary properties for effective therapeutic applications.

El-Helw E A E *et al*. (2024) evaluated the binding affinity of the synthesized series of benzo[f]quinoline-based heterocyclic compounds against the CDK-5 enzyme. Among the synthesized compounds, pyrazolone derivative and cyanoethanohydrazone derivative exhibited the most potent antiproliferative efficacy, with binding energies of -6.6320 kcal/mol and -6.5696 kcal/mol, respectively, which were comparable to the co-crystallized ligand (EFP). The binding interactions revealed hydrogen bonding and hydrophobic interactions with key amino acids such as GLN 131, VAL 18, ALA 144, HIS 84, and LYS 89 of the CDK-5 enzyme (43). Additionally, ADME studies demonstrated favourable drug-likeness and oral bioavailability properties for these compounds, suggesting that they could be promising candidates for further optimization as chemotherapeutic agents [114].

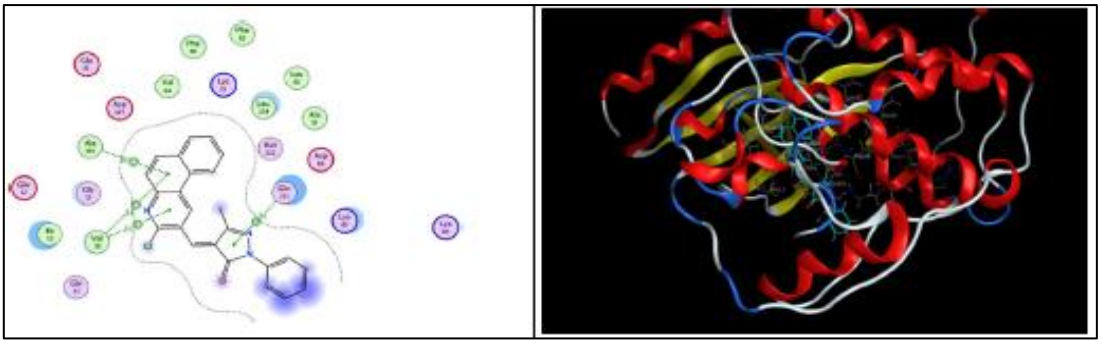

(**43**)

Muthiah G R P *et al*. (2024) designed and synthesized a series of quinoline derivatives containing substituted piperazine moieties (44) to explore their potential as anti-breast cancer agents targeting the Epidermal Growth Factor Receptor-Tyrosine Kinase (EGFR-TK). The synthesized compounds were evaluated for their binding affinity to the ATP binding site of EGFR through molecular docking studies, using the Glide module of the Schrödinger Suite. The docking analysis revealed that few compounds exhibited high docking and glide scores, indicating a strong binding affinity to EGFR. The interaction profiling showed that residues Lys745 and Asp855 played a significant role in hydrogen bonding with these compounds, while π-cation and π-π interactions were observed for few compounds with residues Phe723 and Lys745. Further, molecular dynamic simulation studies demonstrated that the EGFR-inhibitor complex remained stable throughout the simulation, indicating strong and stable interactions with the synthesized compounds [115].

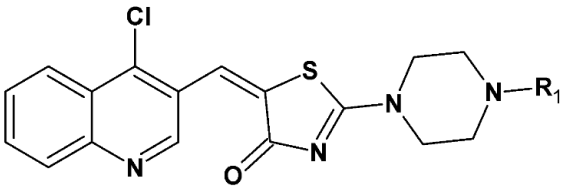

8 a-i

(**44**)

El-Mernissi R *et al*. (2023) conducted *in silico* studies to identify novel quinoline derivatives (45) as potential hepatocellular carcinoma (HCC) inhibitors targeting the colchicine binding site (CBS) of tubulin. The study involved 3D-QSAR analysis using Comparative Molecular Field Analysis (CoMFA) and Comparative Molecular Similarity Indices Analysis (CoMSIA) methods, which showed high predictive accuracy with R^2 values of 0.98 and Q^2 values of 0.68 and 0.57, respectively. The hydrophobic field was found to be the most significant contributor, accounting for 58% of the CoMSIA model's total contribution. Based on this analysis, three novel quinoline derivatives (Z1, Z2, and Z3) were proposed, with improved predicted activities over the existing compounds. Molecular docking studies demonstrated that these derivatives had favourable binding interactions with the CBS of tubulin. Additionally, the ADME analysis indicated that all proposed compounds had favourable pharmacokinetic properties. Molecular dynamics (MD) simulations further confirmed the stability of the Z2 and Z3 derivatives within the CBS, suggesting their potential as effective HCC inhibitors [116].

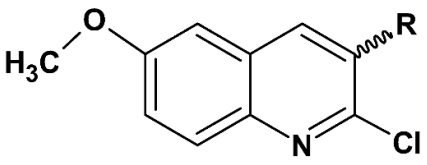

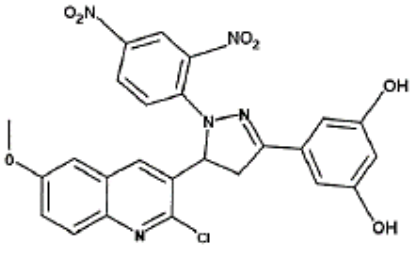

Z1

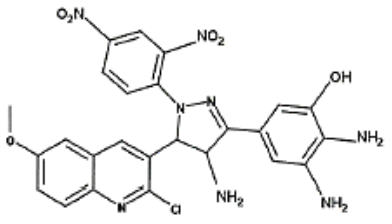

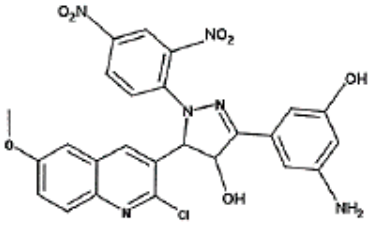

Z2 **Z3**

(45)

Suryanarayana K *et al*. (2023) performed molecular docking and modeling studies to evaluate the interaction of synthesized chloroquinoline-rhodanine-1,2,3-triazole hybrids (46) with the CDK2 enzyme (PDB: 1W98), a crucial target in cancer therapy. The docking results revealed that the most potent compound, 10c (R= 4-Br), exhibited a high binding affinity, with binding energies ranging from -7.37 to -8.21 kcal/mol. The compound formed key hydrogen bonds with amino acid residues Lys89, Glu81, and Leu83, indicating a stable interaction with the active site of CDK2. Additionally, hydrophobic interactions with residues such as Ile10, Phe80, and Leu134 contributed to the compound's strong binding. Molecular dynamics simulations further confirmed the stability of the 10c-CDK2 complex over a 50 ns period, with low root mean square deviation (RMSD) values, demonstrating the potential of these hybrids as effective CDK2 inhibitors in anticancer therapy [95].

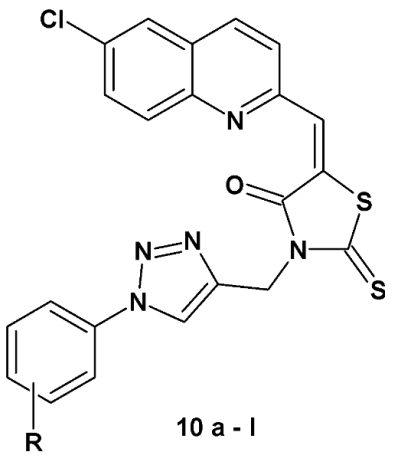

(**46**)

Sharma S (2023) conducted *in silico* molecular docking studies to evaluate the binding affinity of four synthesized 2H-thiopyrano[2,3-b]quinoline derivatives against the CB1a protein (PDB ID: 2IGR), a novel anticancer peptide derived from cecropin B. Molecular docking studies were performed using AutoDock Vina, and the results showed that the binding affinities of the compounds ranged from -5.3 to -6.1 kcal/mol. Key interactions included hydrogen bonding with amino acid residues such as GLU

A-9, PHE A-15, LYS A-16, and ILE A-8, indicating a stable interaction with the protein's active site (47). These findings suggest that the 2H-thiopyrano[2,3-b]quinoline derivatives have potential as anticancer agents [117].

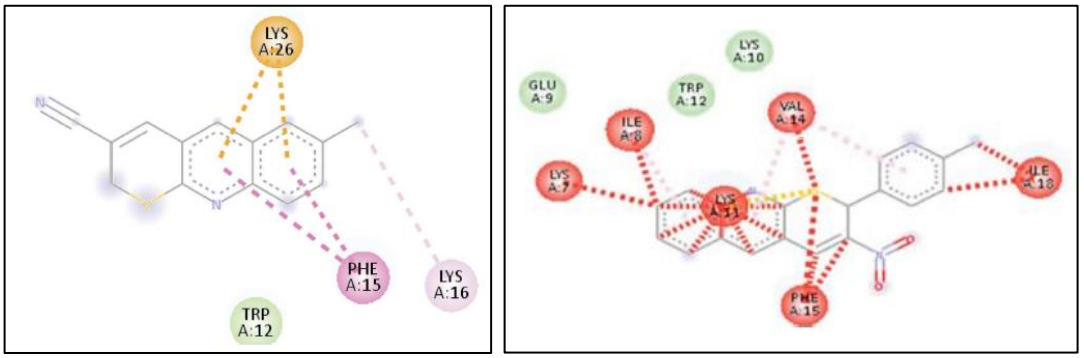

(**47**)

Hernández-Ayala L F *et al*. (2023) conducted a comprehensive study of 8356 quinoline derivatives designed using the CADMA-Chem protocol (48), evaluating their antioxidant and neuroprotective potential. The derivatives were screened based on bioavailability, toxicity, and manufacturability, resulting in 25 candidates. These selected compounds exhibited strong antioxidant activity, surpassing Trolox but not ascorbate in efficiency, as indicated by ionization potentials and bond dissociation energies. Molecular docking simulations revealed that several quinoline derivatives could inhibit enzymes such as catechol-O-methyltransferase (COMT), acetylcholinesterase (AChE) (48), and monoamine oxidase type B (MAO-B). Four derivatives were proposed as promising multifunctional antioxidants for neuroprotection against Alzheimer's and Parkinson's diseases, showing enhanced binding affinities compared to reference compounds [118].

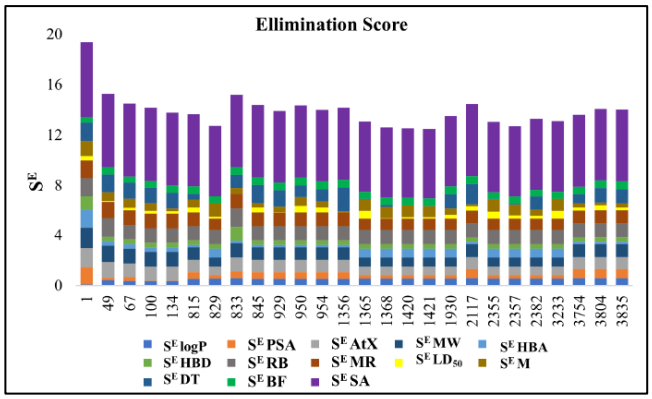

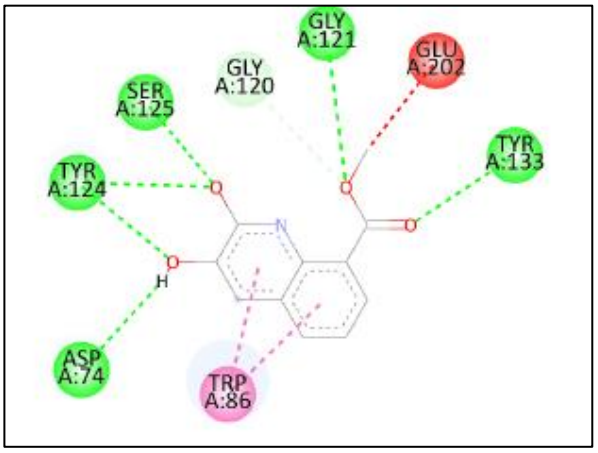

(**48**)

Nagamani M *et al*. (2022) conducted molecular docking studies to evaluate the binding potential of synthesized quinolone-based 4-(methoxymethyl)-1,2,3-triazole derivatives against the COVID-19 main protease (Mpro, PDB ID: 6LU7) using Autodock 4.2. The docking results revealed that the compounds demonstrated strong binding affinities, with binding energies ranging from -9.89 to -13.4 kcal/mol. Notably, compound IXf (Ar= 3-chlorophenyl), (49) featuring a chloro-substituted quinolone moiety, exhibited the highest binding affinity at -13.4 kcal/mol. This compound showed significant hydrogen bonding and hydrophobic interactions with key active site residues, particularly GLY143 and CYS145, which are crucial for the protease's

activity. These findings indicate that the quinolone-triazole hybrids have potential inhibitory effects on the SARS-CoV-2 Mpro enzyme, suggesting their potential as promising antiviral agents against COVID-19 [97].

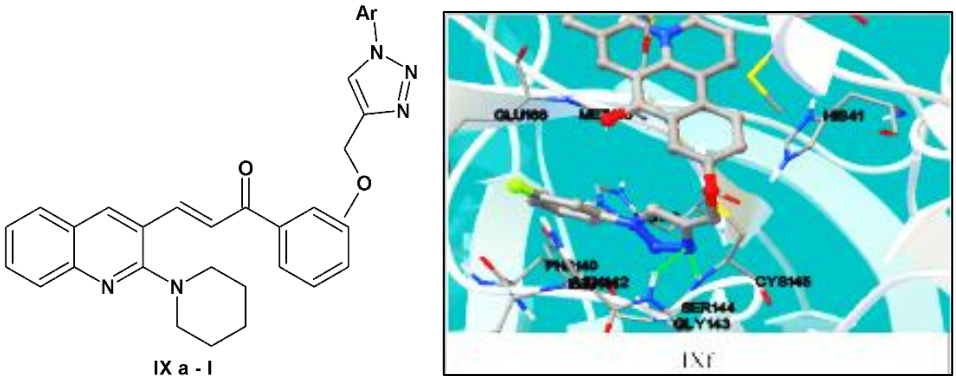

(**49**)

Fekadu G *et al*. (2022) performed *in silico* molecular docking studies using AutoDock Vina to assess the binding affinities of the synthesized fluoroquinoline derivatives (50) against *E. coli* DNA Gyrase B (PDB ID: 6F86) and human topoisomerase IIα (PDB ID: 4FM9). The docking results revealed that these compounds exhibited binding affinities ranging from -6.1 to -7.2 kcal/mol against *E. coli* DNA Gyrase B and -6.8 to -7.4 kcal/mol against human topoisomerase IIα. Compounds showed comparable or even higher binding affinities than the standard drug ciprofloxacin, demonstrating potential as antibacterial agents. The key interactions involved hydrogen bonding with amino acid residues such as Asp-73, Gly-77, and Thr-165 in *E. coli* DNA gyrase B and Leu-705, Ile-577, and Pro-593 in human topoisomerase IIα. The pharmacokinetic properties of the synthesized compounds were analysed using SwissADME, revealing that all the compounds adhered to Lipinski's rule of five, indicating good oral bioavailability. The compounds demonstrated favourable properties such as high gastrointestinal absorption, moderate

water solubility, and no violations of drug-likeness criteria, suggesting their suitability for further development as potential antibacterial or anticancer agents [98].

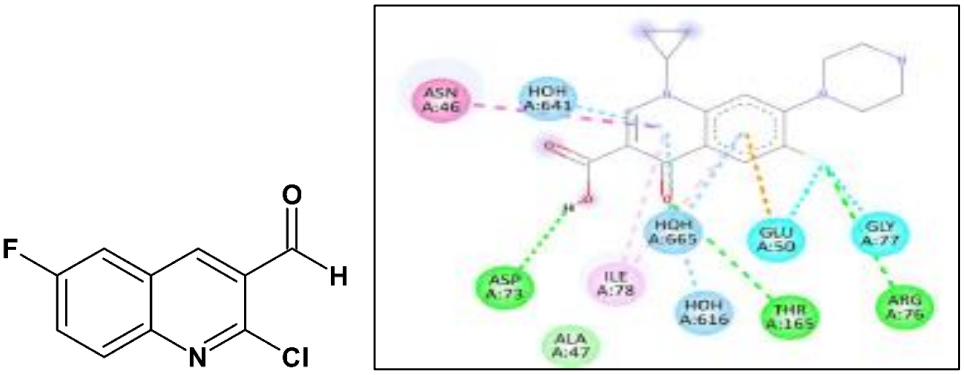

(**50**)

Samupindi T L *et al*. (2022) conducted comprehensive *in silico* studies on 4-aminoquinoline derivatives (51) to explore their potential as anti-tubercular agents. A pharmacophore modeling and 3D-QSAR (Quantitative Structure-Activity Relationship) analysis were carried out using the Schrödinger Phase module to identify key structural features contributing to anti-TB activity. The top pharmacophore hypothesis was a five-point model featuring one hydrogen bond acceptor, one hydrogen bond donor, two hydrophobic regions, and one aromatic ring.

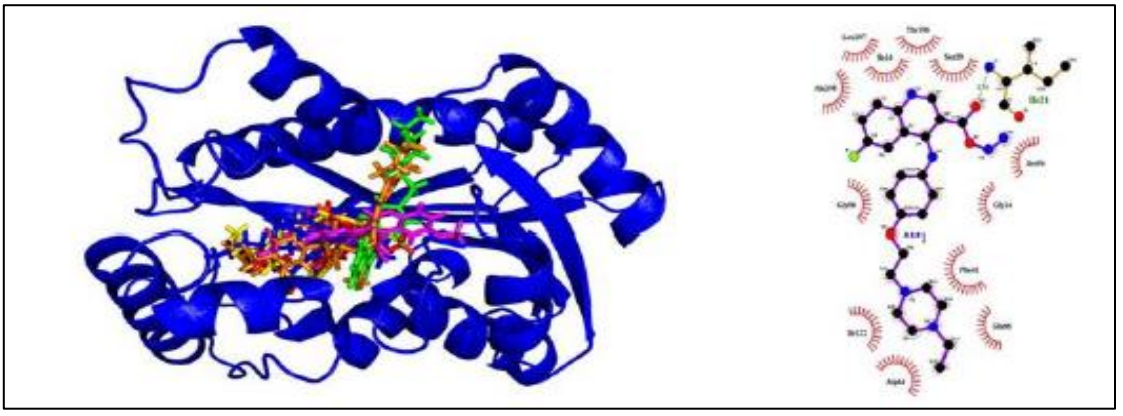

(**51**)

This hypothesis demonstrated a high regression coefficient ($R^2 = 0.9604$) and a cross-validation coefficient ($Q^2 = 0.7885$), indicating good predictive accuracy. Molecular docking studies were performed using the Surflex docking program to evaluate the binding affinities of these derivatives with the enoyl-acyl carrier protein reductase enzyme (EACP) (PDB ID: 1ZID). Compounds exhibited strong docking scores, with the compound forming three hydrogen bonds with ILE15 and SER94 residues (51). Molecular dynamics (MD) simulations using the GROMACS package confirmed the stability of the ligand-enzyme complexes, suggesting the potential of these derivatives as potent inhibitors of *M. tuberculosis* [119].

Zeleke D *et al*. (2021) studied molecular docking and *in silico* analysis to assess the binding affinities of the synthesized quinoline-stilbene and pinacol derivatives against bacterial DNA gyrase B (PDB ID: 1KZN) and human peroxiredoxin-5 (PDB ID: 1HD2), both crucial targets in antibacterial and antioxidant drug development. The docking simulations, performed using AutoDock Vina, revealed that compound 19 had the highest binding affinity with DNA gyrase B (52), with a binding energy of -8.5 kcal/mol, indicating strong interactions through hydrogen bonding with key residues such as Asp81 and Gly85. Similarly, the pinacol derivative showed significant binding affinity towards human peroxiredoxin-5 with a binding energy of -7.8 kcal/mol. Additionally, *in silico* ADME predictions using SwissADME indicated favourable pharmacokinetic properties, including high gastrointestinal absorption and drug-likeness, suggesting the synthesized compounds to be effective antibacterial and antioxidant agents [100].

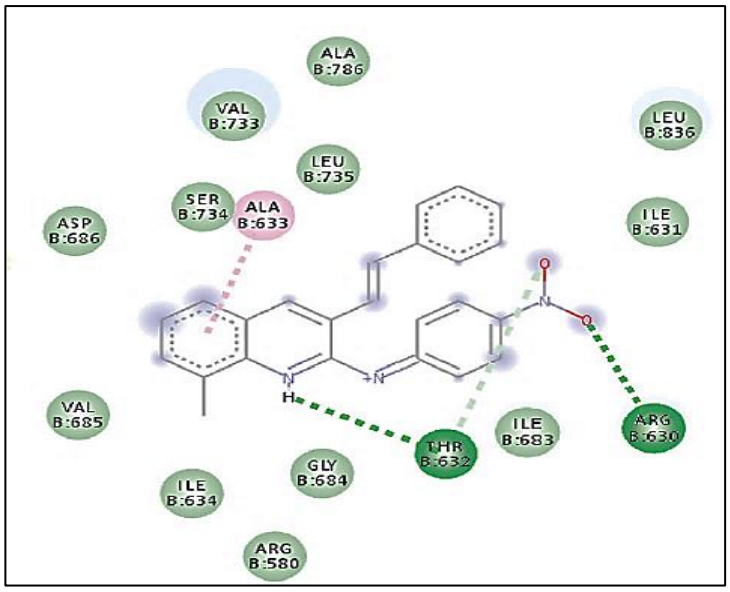

(**52**)

El-Shershaby M H *et al*. (2021) conducted *in silico* studies to evaluate the binding affinity of novel quinoline derivatives as dual inhibitors of DNA gyrase and dihydrofolate reductase (DHFR), which are essential enzymes for bacterial and fungal growth. Molecular docking studies were performed using MOE software, targeting *E. coli* DNA gyrase (PDB ID: 4DUH) and *A.flavus* DHFR (PDB ID: 6DTC). The compounds exhibited strong binding affinities, with the most potent derivatives showing binding energies ranging from -10.29 to -12.23 kcal/mol. The quinoline derivatives displayed multiple hydrogen bonding interactions with key active site residues, such as Arg76 and Arg136 in DNA gyrase and Ser69 in DHFR (53). These interactions, along with hydrophobic interactions, indicate that the quinoline derivatives have significant potential as antimicrobial agents targeting these enzymes[120].

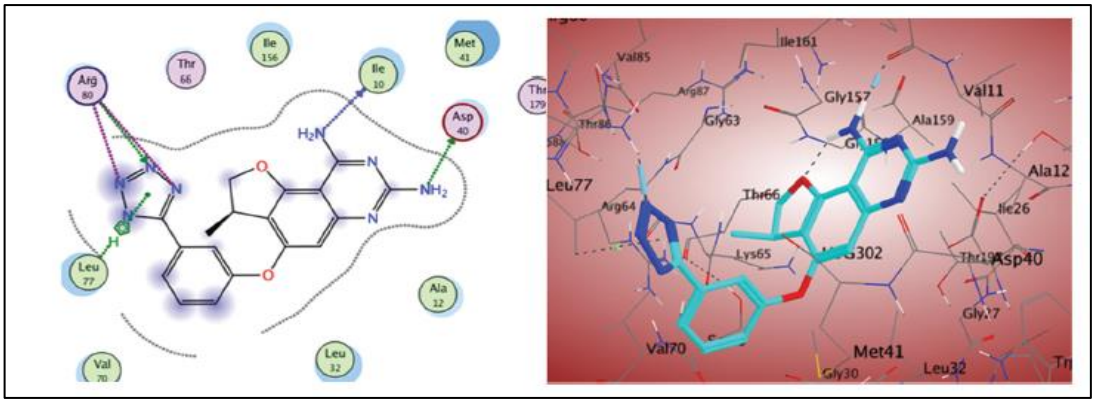

(**53**)

Guje P B *et al*. (2020) performed molecular docking studies for a series of novel 3-((1H-benzo[d]imidazol-2-ylthio) methyl)-2-chloroquinoline derivatives using the AutoDock Vina program to evaluate the binding affinity of these derivatives against the MurD ligase enzyme, a key enzyme involved in bacterial cell wall biosynthesis. The docking results showed that compounds 4e and 4f had the highest binding affinities with binding energies of -5.78 kcal/mol and -5.66 kcal/mol, respectively, indicating strong interactions with the active site residues of MurD ligase, including LEU13, ARG37, SER71, PRO72, GLY73, and ASN138. Compound 4e, featuring a methoxy substitution at the seventh position of the quinoline ring, formed hydrogen bonds with the ASN138 residue through its methoxy oxygen atom, and the sulfur atom of the 2-chloroquinoline interacted with the SER71 residue (54). These findings suggest that the synthesized quinoline derivatives, exhibited promising potential as antibacterial agents targeting bacterial MurD ligase [101].

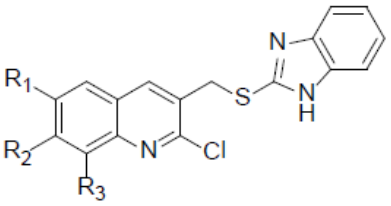

4a-f

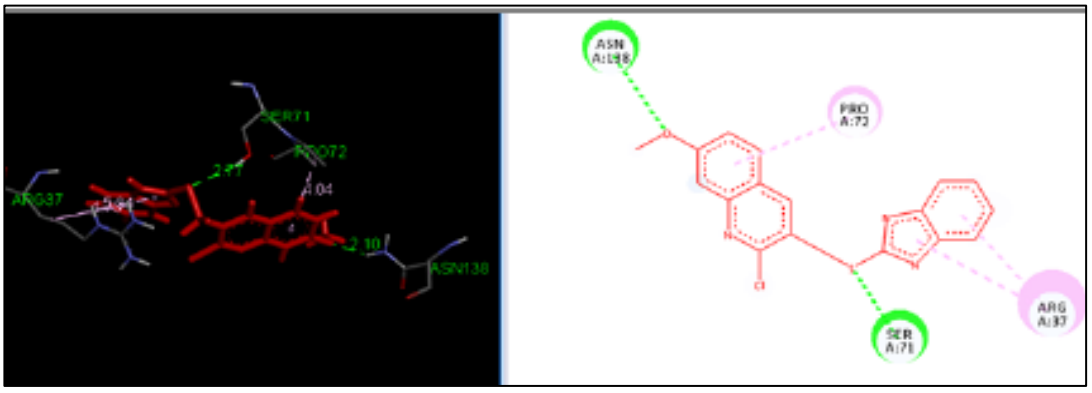

(**54**)

Celik I *et al*. (2020) analysed *in silico* molecular docking studies to investigate the potential interaction of the synthesized quinoline-2-carbaldehyde hydrazone derivatives with the bacterial enzyme FabH (β-ketoacyl-acyl carrier protein synthase III) from *Enterococcus faecalis*, a critical enzyme in the fatty acid biosynthesis pathway. The docking analysis was conducted using AutoDock Vina software, and the results demonstrated that several of the synthesized derivatives showed strong binding affinities towards the active site of FabH, with docking scores ranging between -6.2 to -7.8 kcal/mol. Multiple hydrogen bonds and hydrophobic interactions with key active site residues, such as Cys112, His244, and Phe391 were observed (55). The binding mode suggested that these compounds could effectively inhibit the enzyme's activity, potentially contributing to their antibacterial effect. Furthermore, ADME analysis using SwissADME showed that the compounds had favourable pharmacokinetic

properties, including good oral bioavailability, low toxicity, and adherence to Lipinski's rule of five, suggesting that these derivatives are promising candidates for further development as antimicrobial agents [121].

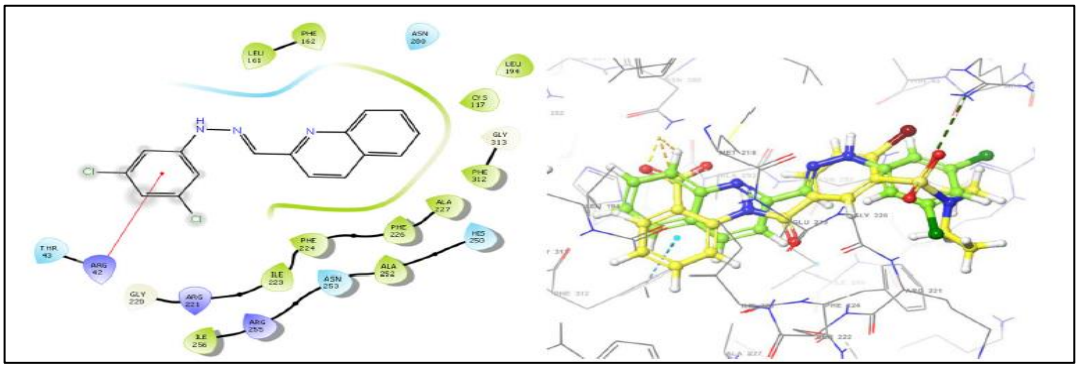

(55)

El-Gamal K M A *et al*. (2015) conducted molecular docking studies on a series of quinoline derivatives to evaluate their interactions with bacterial topoisomerase II DNA gyrase (PDB code: 4BUL). The docking studies revealed that the selected compounds exhibited good binding energies, ranging from –15.60 to –33.11 kcal/mol. Notably, compound 14 (56) formed two hydrogen bonds with key amino acid residues Asp 1083 and Ser 1084, while compounds 22 and 10 (56) formed single hydrogen bonds with Asp 1083, similar to the reference drug ciprofloxacin. These interactions suggest that the quinoline derivatives have a strong potential for further development as antimicrobial agents targeting bacterial topoisomerase II [107].

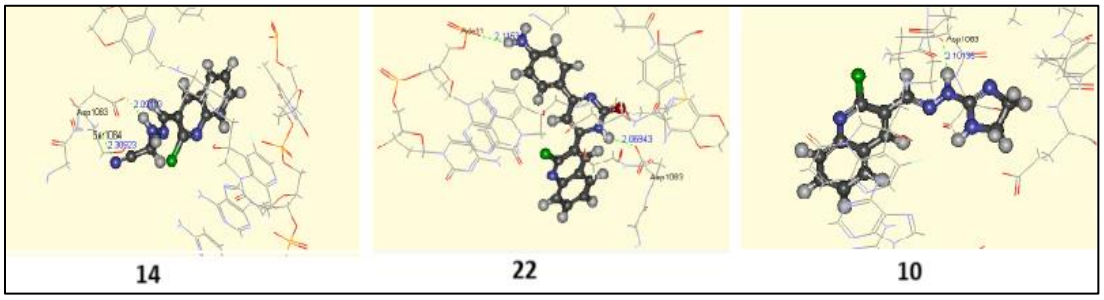

(56)

CHAPTER-IV
MATERIALS AND METHODS

4: MATERIALS AND METHODS

4.1 SYNTHESIS OF 6-SUBSTITUTED-2-CHLOROQUINOLINE-3-CARBALDEHYDE HYDRAZIDEESTER DERIVATIVES

In our research facility, ester derivatives of chloroquinoline-hydrazide hybrid molecules were prepared in three steps reported in literature.

4.1.1 Chemicals

Analytical-grade chemicals and reagents utilized in the synthesis were procured from suppliers such as Alfa Aesar, S.D. Fine-Chem, and Spectrochem Limited.

4.1.2 Instruments and Techniques

The melting points (M.P.) of the synthesized molecules were recorded using an open capillary tube with an electrical melting-point instrument and are reported without correction. The progress of synthesis reactions and product formation were monitored through thin-layer chromatography (TLC) using silica gelG plates (0.5 mm thickness), with spots detected under ultraviolet light and iodine vapor. Recrystallization with appropriate organic solvents was employed to purify all synthesized compounds.

Infrared (IR) spectra were obtained with an FT/IR-4100 spectrometer using potassium bromide (KBr) pellet method. The mass spectra were recorded using a Bruker ESI-MS instrument. For NMR analysis, ^{1}H NMR spectra were acquired in deuterated chloroform ($CDCl_3$) and dimethyl sulfoxide (DMSO) using Bruker 500 MHz spectrometer with tetramethylsilane (TMS) as the internal standard. ^{13}C NMR spectra were obtained in DMSO using a Bruker Avance Neo 500 MHz spectrometer, with chemical shift values (δ) reported in parts per million (ppm).

4.1.3 General procedures for synthesis of 6-substituted-2-chloroquinoline-3-carbaldehyde hydrazide ester derivatives

4.1.3.1 General procedure for synthesis of 6-substituted-2-chloroquinoline-3-carbaldehyde derivatives (2a, 2d, 2g, 2j, 2m, 2p)[111]

Dimethylformamide (9.13 g, 9.6 ml, 0. 125 mol) was cooled to 0 °C in a flask equipped with a drying tube. Phosphoryl chloride (53.7 g, 32.2 ml, 0.35 mol) was then carefully introduced one drop at a time with stirring. Subsequently, the substituted acetanilide (0. 05 mol) was added into the mixture. After a 5-minute interval, the reaction mixture was subjected to reflux heating for a suitable period (6-17 hours) at a temperature range of 70-80 °C.Upon completion of the reaction, the mixture was allowed to cool to ambient temperature and then transferred into 200-300 ml of ice-cold water. The resulting crude product was collected by filtration, dried, and subsequently purified through recrystallization using ethyl acetate. The scheme of the synthesis is presented in figure 4.1. The purified products (2a, 2d, 2g, 2j, 2m and 2p) were stored at room temperature in a tightly closed glass container. Physicochemical properties like melting point, colour, appearance, and TLC retention factor of these compounds were reported. The synthesized molecules were characterized for structural confirmation using analytical techniques such as FTIR, NMR spectroscopy and mass spectrometry.

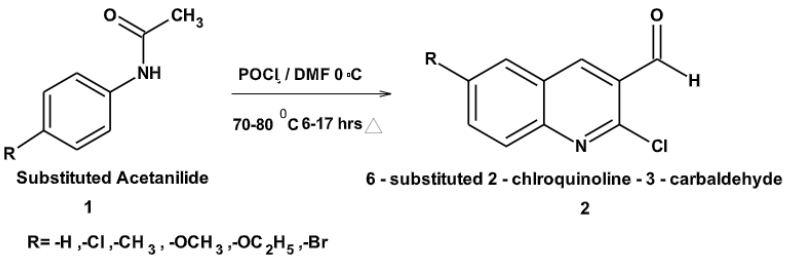

Figure4.1: Scheme for synthesis of 6-substituted-2-chloroquinoline-3-carbaldehyde derivatives (2) from substituted acetanilide (1)

4.1.3.2 General procedure for synthesis of 6-substituted-2-chloroquinoline-3-carbaldehyde hydrazide derivatives (3a, 3d, 3g, 3j, 3m, 3p)[122]

A mixture comprising 6-substituted 2-chloroquinoline-3-carbaldehyde (compounds 2a, 2d, 2g, 2j, 2m, 2p) (1 mmol) and 4-hydroxybenzoic acid hydrazide (1.1 mmol) dissolved in absolute ethanol (20 ml) was stirred at room temperature for 1-5 hours. Two drops of hydrochloric acid were then added in the mixture as the catalyst. After completion, the reaction mixture is quenched with dilute sodium bicarbonate ($NaHCO_3$) solution in water. The resulting precipitate is filtered, washed with 20 ml of water, and then recrystallized using ethanol. The scheme of the synthesis is presented in figure 4.2. The purified products (3a, 3d, 3g, 3j, 3m and 3p) were stored at room temperature in a tightly closed glass container. Physicochemical properties like melting point, colour, appearance and TLC retention factor of these compounds were reported. The synthesized molecules were characterized for structural confirmation using analytical techniques such as FTIR, NMR spectroscopy and mass spectrometry.

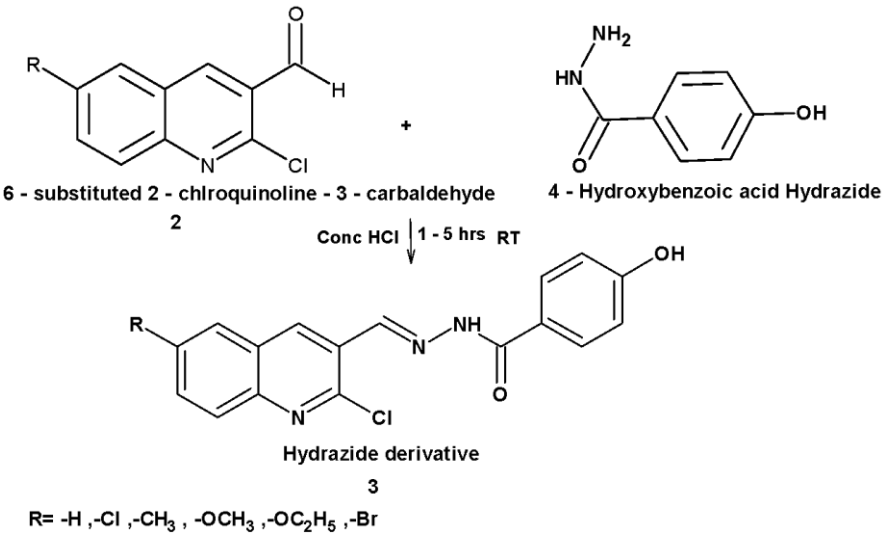

Figure4.2: Scheme for synthesis of 6-substituted-2-chloroquinoline-3-carbaldehyde hydrazide derivatives (3) from 6-substituted-2-chloroquinoline-3-carbaldehyde derivatives (2)

4.1.3.3 General procedure for synthesis of Ester derivatives of 6-substituted-2-chloroquinoline-3-carbaldehyde hydrazide (4a-4r)[123]

To a mixture comprising 6-substituted-2-chloroquinoline-3-carbaldehyde hydrazide (compounds 3a, 3d,3g,3j,3m,3p)(10 mmol) and ZnO (10 mol%), acyl chloride (12 mmol) was added while stirring at room temperature. The progress of reaction was checked using TLC. Once the reaction was complete, the mixture was treated with two fractions each of 5 ml ethyl acetate (EtOAc). It was then filtered to remove ZnO. The ethyl acetate phase was washed successively with 10% $NaHCO_3$ solution followed by water. It was passed through sodium sulphate for drying and the solvent was evaporated to obtain the product. Alternatively, the product could be isolated by adding 10% $NaHCO_3$ solution and water, separating the organic layer, and drying it over Na_2SO_4. The scheme of the synthesis is presented in figure 4.3. The purified products (4a-4r) were stored at room temperature in a tightly closed glass container. Physicochemical properties like melting point, colour, appearance and TLC retention factor of these compounds were reported. The synthesized molecules were characterized for structural confirmation using analytical techniques such as FTIR, NMR spectroscopy and mass spectrometry.

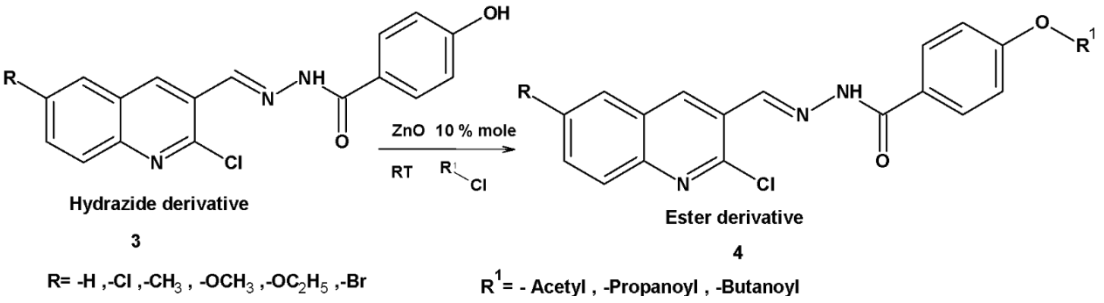

Figure4.3: Scheme for synthesis of 6-substituted-2-chloroquinoline-3-carbaldehyde hydrazide ester derivatives (4) from 6-substituted-2-chloroquinoline-3-carbaldehyde hydrazide derivatives (3)

4.2 BIOACTIVITY SCREENINGOF 6-SUBSTITUTED-2-CHLOROQUINOLINE-3-CARBALDEHYDEHYDRAZIDEESTER DERIVATIVES

4.2.1 *In vitro* Anti-Tubercular activity assessment using Microplate Alamar Blue assay

The anti-mycobacterial activity of the compounds against *M. tuberculosis* was assessed using the Microplate Alamar Blue assay (MABA)[124-125]. This colorimetry method is used to access cell proliferation. It is based on the reduction of the blue, non-fluorescent resazurin dye to a pink, fluorescent resorufin product by metabolically active cells, making it a sensitive and reliable indicator for evaluating antimicrobial activity.

4.2.1.1 Microorganism and method

The *M. Tuberculosis* strain (H37RV, ATCC No. 27294) was utilized for this assay. Standards including Isoniazid, Ethambutol, Pyrazinamide, Rifampicin, and Streptomycin were used for comparison purposes. Alamar Blue solution was prepared with Alamar Blue reagentin 10% aqueous Tween 80 solution which acts as non-ionic surfactant and emulsifier. *M. Tuberculosis* cells were allowed to grow in Middlebrook 7H9 broth along with suitable additives.

4.2.1.2 Assessment of anti-TB activity

First, 200µl of sterile deionized water was dispensed into outer wells of a sterile 96-well plate. Subsequently, 100 µl of Middlebrook 7H9 broth was added to every well of the 96-well plate. The standardized suspension of *M. Tuberculosis* was then appropriately added to get the required inoculum size in each well.

Serial dilutions of the synthesized molecules were directly prepared on the plate. The compounds were tested for concentrations ranging from 100 to 0.2 µg/ml. A set of established antitubercular drugs were used as positive control. The plates were covered with the lid and sealed with parafilm tape. The microwell plates were incubated at 37ºC for five days. Following this, 25µl of solution of Alamar Blue reagent and 10% Tween 80 (1:1) was dispensed in every microwell. The plates were re-incubated for further24 hours. A blue colour in a well solution indicated the absence of bacterial growth, whereas a pink coloured microwell solution signified growing bacteria. The MIC was determined as the lowest concentration of test substance that inhibited the colour change from blue to pink. The MIC of synthesized compounds were compared with those of the controls to evaluate their anti-TB activity[124].

4.2.2 *In vitro* Antibacterial activity assessment using Broth Microdilution method

The antibacterial activity of synthesized compounds (4a-4r) was assessed *in vitro* using the broth microdilution method following established protocol[126].

4.2.2.1 Microorganism and method

Standard gram-positive strains of *S. aureus* (ATCC 12598), *B.subtilis* (ATCC 6633), and gram-negative strains of *K.pneumoniae* (ATCC 29665) and *E. coli* (ATCC 25922) were used in the study. Nine dilutions of each drug were done with thioglycolate broth for MIC calculation.

4.2.2.2 Assessment of Antibacterial activity

Initially, 20 µL of the solution of synthesized molecules (test compound solution) was added to 380 µL of broth in a primary tube, ensuring an appropriate concentration for the subsequent dilution process. For the serial dilution, 200 µL of broth solution was added in the subsequent9 tubes. From the primary tube, 200 µL of

the test compound solution was transferred to the first tube having 200 µL of broth solution, achieving 10^{-1} dilution. This process was systematically repeated to achieve serial dilutions up to 10^{-9} for each compound. This resulted in final concentrations ranging from 100 to 0.2 µg/ml of synthesized molecules for which antibacterial activity was carried out. To prepare the inoculum, 5 µL from the stock cultures of the bacterial strains, was transferred into 2 mL of broth. Subsequently, 200 µL of this bacterial culture suspension was introduced into each of the serially diluted tubes.

All the tubes were then incubated in an anaerobic jar at 37°C for 48–72 hours. Post-incubation, each tube was observed for turbidity, indicating bacterial growth. Ciprofloxacin was used as the standard reference drug. The MIC values were calculated to determine the antibacterial potential of the synthesized molecules, where lower MIC values indicated greater antibacterial potency.

4.2.3 *In vitro* Cytotoxicity screening using MTT assay

The MTT assay is a commonly employed method for evaluating cell viability, proliferation and cytotoxicity of compounds. The cytotoxic activity of synthesized compounds (4a, 4c, 4d, 4l, 4m and 4r) possessing remarkable anti-TB activity was measured using this assay method following established protocols[127-129]to assess the cell viability.

4.2.3.1 Materials and cell lines

Cell line used: Vero and A549 cell lines

Dulbecco`s Modified Eagle Media (DMEM) with low glucose (Gibco, Invitrogen), Fetal bovine serum (FBS) (Gibco, Invitrogen), Antibiotic – Antifungal 100X solution (Thermo fisher Scientific) and MTT (5mg/ml) in phosphate-buffered saline (PBS) solution were used in the study. Untreated cells with media were used as the negative control.

4.2.3.2 Assessment of cytotoxic activity using A549 cell lines

The A549 cells were seeded in a 96 microwell flat bottom plate at an appropriate density and kept at 37ºC in 95% humidity and 5% CO_2 overnight. Following incubation, various concentrations (100, 50, 25, 12.5, 6.25, and 3.125 µg/mL) of the synthesized molecules (4a, 4c, 4d, 4l, 4m and 4r)were added to the wells and incubated for an additional 48 hours under the same conditions to allow for interaction between the test compounds and the cells. A microscopic analysis was carried out using Olympus Inverted microscope at 20x magnification to observe morphological changes in the cells on the exposure of various concentrations of synthesized compounds and positive control. Following the incubation, the medium was carefully aspirated, and the microwells were washed with sterile PBS two times to remove any residual compounds. Subsequently, 20 µL of the MTT solution (5 mg/mL in PBS) was added to all the microwells and the plate was re-incubated at 37ºC for 4 hours to assist the formation of formazan by metabolically active cells.

After this, 100 µL of DMSO was added to all the wells to ensure complete dissolution of formazan crystals, along with gentle shaking. The absorbance was recorded at the wavelength of 570 nm using the microplate reader. The absorbance of test solutions was directly proportional to viable cells, with higher absorbance indicating increased cellular activity. Doxorubicin was used as positive control. All the measurements were taken three times, and the IC_{50} values for cytotoxic activity were expressed as a % of cell viability relative to untreated control cells.

Formula for calculation:

$$\text{Surviving cells (\%)} = \frac{\text{Mean OD of test compound}}{\text{Mean OD of Negative control}} \times 100$$

4.2.3.3 Assessment of cytotoxic activity using Vero cell lines

The cell viability and therefore the cytotoxic activity of synthesized molecules (4a, 4c, 4d, 4l, 4m and 4r) was determined using Vero cell line with similar methodology as mentioned in section 4.2.3.2. Doxorubicin was used as positive control. All the measurements were taken three times, and the IC_{50} values for cytotoxic activity were expressed as a % of cell viability relative to untreated control cells. A microscopic analysis was carried out using Olympus Inverted microscope at 20x magnification to observe morphological changes in the cells 48 h after the exposure to various concentrations of synthesized compounds and positive control.

4.3 MOLECULAR DOCKING STUDY OF 6-SUBSTITUTED-2-CHLOROQUINOLINE-3-CARBALDEHYDE HYDRAZIDE ESTER DERIVATIVES

Molecular docking studies were performed to elucidate the binding interactions of the synthesized compounds (4a-4r) with Pantothenate kinase (MtPanK) and CTP synthase PyrG from *M. tuberculosis*, thereby providing critical insights for subsequent structural optimization[130-131].

4.3.1 Software used in the study

- SKETCH module, SYBYL software suite (Tripos Inc., St. Louis, USA)
- Surflex-Dock, Sybyl-X 2.0

4.3.2 Methodology

4.3.2.1 Docking study of synthesized molecules 4a-4r with MtPanK

The crystal structure of MtPanK in complex with GDP and phosphopantothenate (PDB ID: 3AEZ, resolution 2.20 Å, obtained via X-ray diffraction) was retrieved from the Protein Data Bank (PDB) (http://www.rcsb.org/pdb). Prior to docking, the crystal structure of protein was prepared by removing all crystallographic water molecules, followed by the addition of polar hydrogen atoms, and assignment of Gasteiger-Hückel charges to ensure accurate electrostatic interactions.

The three-dimensional structures of the ligand molecules were generated using the SKETCH module integrated within the SYBYL software suite (Tripos Inc., St. Louis, USA). The generated ligands underwent energy minimization using the Tripos force field. The Gasteiger-Hückel charges were assigned to the ligands to achieve the most stable conformation.

Molecular docking was conducted using the Surflex-Dock module, interfaced with Sybyl-X 2.0, to predict the optimal binding conformation of the ligands within

the active site of MtPanK. The docking parameters, including the protomol generation, docking precision, and scoring functions, were set to their default values as recommended by the software, ensuring consistent and reproducible results.

4.3.2.2 Docking study of synthesized molecules 4a-4r with MtPyrG

The crystal structure of the *M. tuberculosis* CTP synthase PyrG in complex with two UTP molecules (PDB ID 4ZDJ, 1.99 Å X-ray Diffraction) was extracted from the Protein Data Bank (PDB) (http://www.rcsb.org/pdb). The methodology as mentioned in section 4.3.2.1 was followed for this docking study.

4.3.3 Scoring and Visualization of Docking results

The docking poses generated by Surflex-Dock were evaluated using the Surflex-Dock scoring function. The top-ranked poses for each compound were selected based on their highest docking scores for further analysis. Individual contributions of H-bonding, hydrophobic interactions, and van der Waals forces to the docking score, were analysed to understand the nature of the interactions between the ligand and the protein active site. The top-ranked docking poses were visualized to examine the binding orientation of the ligands within the active site. Important interactions such as hydrogen bonds, hydrophobic contacts, and π-π stacking were identified and illustrated. The ligand interactions within the binding pocket of MtPanK and PyrG were assessed in detail, and the amino acid residues involved in the interaction were noted. The docking poses of the synthesized compounds were evaluated and assessed with the binding mode of the co-crystallized ligand of protein crystal structures, PDB ID 3AEZ and 4ZDJ.

4.4 PREDICTION OF ADME PROPERTIES OF 6-SUBSTITUTED-2-CHLOROQUINOLINE-3-CARBALDEHYDE HYDRAZIDE ESTER DERIVATIVES

The pharmacokinetic properties of the synthesized compounds (4a-4r) were evaluated using SwissADME, an online computational tool specifically designed for predicting ADME (Absorption, Distribution, Metabolism, and Excretion) parameters[132-133].

4.4.1 Software used in the study

- SwissADME, Swiss Institute of Bioinformatics (SIB)(SwissADME)

4.4.2 Methodology

The assessment of ADME properties of synthesized molecules included an evaluation of the compounds' drug-likeness, guided by Lipinski's Rule of Five, which predicts the oral bioavailability of chemical molecules.

The canonical Simplified Molecular-Input Line-Entry System (SMILES) notations were generated for the structures of synthesized compounds, designated as 4a to 4r. These SMILES representations were then submitted to the SwissADME platform, enabling the *in-silico* prediction of key physicochemical properties, Lipophilicity, Solubility, Pharmacokinetics, Drug likeness, and Medicinal Chemistry parameters. The ADME properties of synthesized molecules (4a to 4r) were then examined by using visual tools and relationship analysis.

This approach facilitated a comprehensive analysis of the compounds' drug-like properties and provided valuable insights into their suitability as potential drug candidates, based on parameters that influence bioavailability, metabolism, and overall pharmacokinetic behaviour.

CHAPTER-V

RESULTS AND DISCUSSIONS

5: RESULTS AND DISCUSSION

5.1 SYNTHESISOF ESTER DERIVATIVES OF 6-SUBSTITUTED-2-CHLOROQUINOLINE-3-CARBALDEHYDE HYDRAZIDE

5.1.1 Synthesis of 6-substituted-2-chloroquinoline-3-carbaldehyde derivatives (2a, 2d, 2g, 2j, 2m, 2p)

The synthesis of 6-substituted-2-chloroquinoline-3-carbaldehyde derivatives is an established method used to prepare quinoline-based compounds, which are known for their wide range of biological activities. In this study, substituted acetanilide were used as starting materials to prepare these derivatives (2a, 2d, 2g, 2j, 2m, 2p) via a Meth-Cohn quinoline synthesis as shown in the scheme(Figure 5.1). The procedure for synthesis is detailed in methodology section4.1.3.

The Meth-Cohn quinoline synthesis is a notable method used to prepare quinoline derivatives using the Vilsmeier-Haack reagent. The method is especially useful for introducing specific substituents at the 2- and 3-positions of the quinoline ring, such as chlorine and formyl groupsrespectively[134].

This reaction involves the use of phosphorus oxychloride ($POCl_3$) as the chlorinating agent and dimethylformamide (DMF) as the formylating reagent, which is carried out at a controlled temperature of 70–80°C.

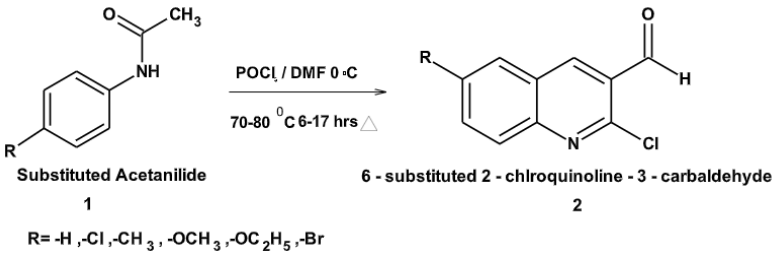

Figure 5.1: Scheme for synthesis of 6-substituted-2-chloroquinoline-3-carbaldehyde derivatives from substituted acetanilide using Vilsmeier Haack reagent

The choice of reaction conditions ensures the selective formation of the 3-carbaldehyde functionality on the quinoline ring while introducing diverse substitutions at the 6-position. This synthetic route offers a reliable and efficient pathway to develop quinoline derivatives with potential applications in drug discovery and medicinal chemistry.

5.1.1.1 Reaction mechanism

Step 1: The Meth-Cohn synthesisinvolvesgeneration of Vilsmeier-Haack reagent in the first step. The mechanism involves the generation of a reactive formylating agent from a combination of phosphorus oxychloride ($POCl_3$) and a formamide, usually dimethylformamide (DMF).The reaction begins with the nucleophilic attack of DMF on $POCl_3$, which leads to the formation of the Vilsmeier reagent, a chloroiminium ion (Figure 5.2)[135].The key structure of the Vilsmeier reagent is $[ClCH=N(CH_3)_2]^+$. The Vilsmeier complex is an electrophilic agent that initiates the reaction.

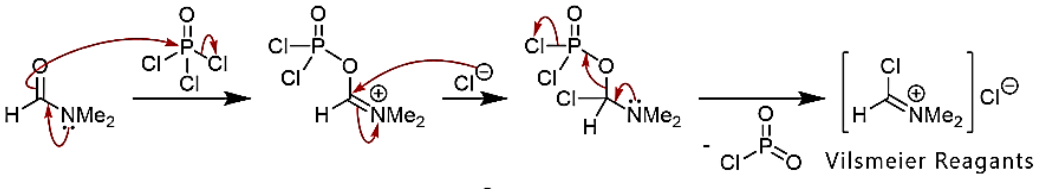

Figure 5.2: Mechanism for formation of Vilsmeier reagent from phosphorus oxychloride and dimethylformamide

Step 2: The acetanilide reacts with the Vilsmeier reagent, forming an imidoyl chloride intermediate.This intermediate undergoes tautomerism to form enamine intermediate (Figure 5.3).

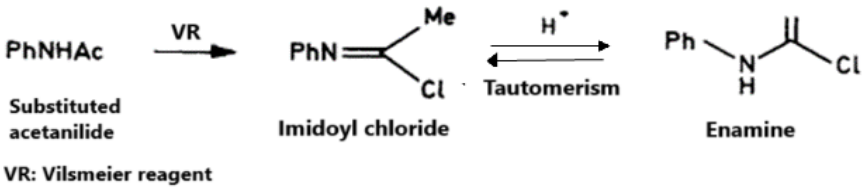

Figure 5.3: Scheme for formation of Enamine from Imidoyl chloride on tautomerism during Meth Cohn synthesis of substituted quinolines in presence of Vilsmeierreagent[134]

Step 3: The enamine is further di-formylated at its β-position, setting up the structure for subsequent cyclization.

Step 4: The di-formylated intermediate undergoes cyclization, where the nucleophilic aromatic ring attacks the formyl group, leading to the formation of the quinoline ring. This step generates a 2-chloroquinoline-3-carbaldehyde structure.

The reaction is typically carried out at moderate temperatures (70–80°C), which allows for the formation of the quinoline ring without decomposition of intermediates. The overall mechanism is represented in Figure 5.4[136]. The Meth-Cohn method is highly selective for introducing chlorine at the 2-position and a formyl group at the 3-position, making it a valuable tool in the synthesis of substituted quinolines. The reaction proceeds under relatively mild conditions, minimizing side reactions and improving yields.

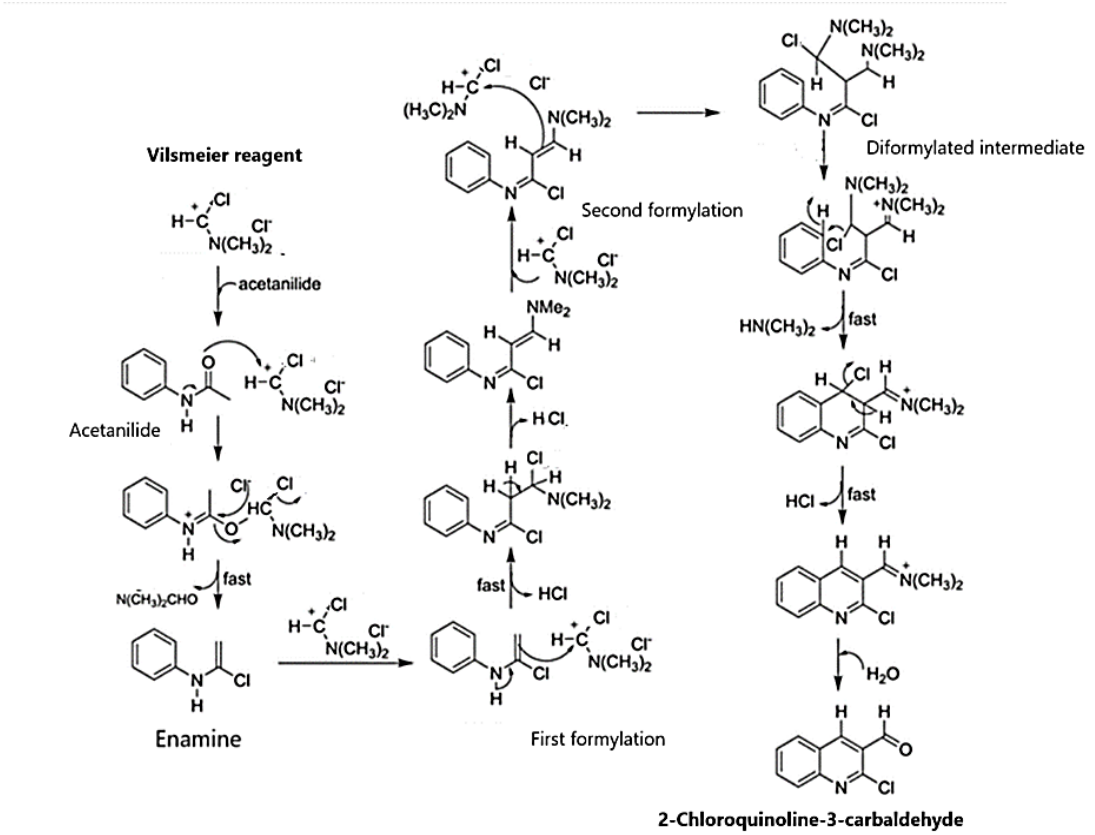

Figure 5.4: Mechanism for formation of 2-chloroquinoline-3-carbaldehyde from acetanilide in presence of Vilsmeierreagent[136]

5.1.1.2 Physicochemical properties of synthesized compounds (2a, 2d, 2g, 2j, 2m, 2p)

The physicochemical properties including melting point and TLC Rf values of synthesized 6-substituted-2-chloroquinoline-3-carbaldehyde derivatives 2a, 2d, 2g, 2j, 2m, 2p were determined and listed in the Table 5.1.

Table 5.1: Physicochemical properties of synthesized compounds - 2a, 2d, 2g, 2j, 2mand 2p

Sr. No.	Starting material	Product	Yield (%)	M.P. # (°C)	TLC R_f *
1	Acetanilide	2a	75	147-149	0.70
2	4-Chloroacetanilide	2d	55	190-191	0.68
3	4-Methylacetanilide	2g	65	120-121	0.61
4	4-Methoxyacetanilide	2j	55	167-169	0.62
5	4-Ethoxyacetanilide	2m	75	162-163	0.63
6	4-Bromoacetanilide	2p	78	184-186	0.60

***** TLC Retention factor (R_f)calculated using mobile phase: n-Hexane: Ethyl Acetate (3:7)
# M.P.: Melting point range

The percentage yields of the reactions were calculated and found to be in the range of 55% to 78%, reflecting the moderate to good efficiency of the synthetic route employed. The molecular characteristics, such as molecular formula, molecular weight, and physical appearance (colour and texture) of the products were represented in Table 5.2.

Table 5.2: Molecular characteristics of synthesized compounds - 2a, 2d, 2g, 2j, 2m and 2p

Product	IUPAC Nomenclature	Molecular formula	Mol. weight	Physical Appearance
2a	2-Chloroquinoline-3-carbaldehyde	$C_{10}H_6ClNO$	191.61	Light Yellow solid
2d	2,6-dichloroquinoline-3-carbaldehyde	$C_{10}H_5Cl_2NO$	226.05	Light Yellow solid
2g	2-Chloro-6-methylquinoline-3-carbaldehyde	$C_{11}H_8ClNO$	205.64	Yellow solid
2j	2-Chloro-6-Methoxy-quinoline-3-carbaldehyde	$C_{11}H_8ClNO_2$	221.64	Yellow solid
2m	2-Chloro-6-ethoxyquinoline-3-carbaldehyde	$C_{12}H_{10}ClNO_2$	235.66	Yellow solid
2p	6-Bromo-2-chloroquinoline-3-carbaldehyde	$C_{10}H_5BrClNO$	270.51	Yellow solid

5.1.1.3 Spectral data characterization of synthesized compounds (2a, 2d, 2g, 2j, 2m, 2p)

The synthesized compounds 2a, 2d, 2g, 2j, 2m and 2p were characterized using various spectroscopic techniques to confirm their structures and assess the presence of key functional groups as shown in Table 5.3.

Table 5.3: Spectral characterization of synthesized compounds 2a, 2d, 2g, 2j, 2m and 2p

Sr. No.	Product	Spectral characterizationof synthesized compounds 2a, 2d, 2g, 2j, 2m and 2p
1	2a	**IR (KBR, υ cm^{-1})**: 2867 (C-H Aldehyde), 1685 (C=O str), 1450-1600 (C-C Aromatic str) **^{1}H NMR (500 MHz, Chloroform-d)**: δ 10.53 (s, 1H), 7.3-8.7 (Aromatic H)
2	2d	**IR (KBR, υ cm^{-1})**: 2888 (C-H Aldehyde str), 1686 (C=O str), 1483-1614 (C-C Aromatic str)

Sr. No.	Product	Spectral characterizationof synthesized compounds 2a, 2d, 2g, 2j, 2m and 2p
		^{1}H NMR (500 MHz, Chloroform-d): δ 10.55 (s, 1H), 7.2-8.6 (Aromatic H)
3	2g	**IR (KBR, υ cm^{-1})**: 2874 (C-H Aldehyde str), 1690 (C=O str), 1580 (C=N str) 1452-1624 (C-C Aromatic str), 820 (C-Cl str) **^{1}H NMR (500 MHz, Chloroform-d)**: δ 10.30 (s, 1H), 7.2-8.6 (Aromatic H), 2.38 (s, 3H) **^{13}C NMR (500 MHz, DMSO-d$_6$)**: δ 21.29, 126.69, 126.80, 127.12, 127.48, 130.62, 134.48, 136.38, 147.65, 149.28, 189.28 **ESI-MS (m/z)**: 206.13 $(M+H)^+$
4	2j	**IR (KBR, υ cm^{-1})**: 2928 (C-H Aldehyde str), 1681 (C=O str), 1450-1649 (C-C Aromatic str), 1384 (C=N str), 861 (C-Cl str) **^{1}H NMR (500 MHz, Chloroform-d)**: δ 10.38 (s, 1H), 7.32-8.47 (Aromatic H), 2.48 (s, 3H) **^{13}C NMR (500 MHz, DMSO-d$_6$)**: δ 32.20, 55.34, 106.39, 122.89, 126.34, 129.03, 138.23, 145.67, 147.71, 158.53, 189.29 **ESI-MS (m/z)**: 222.06 $(M+H)^+$
5	2m	**IR (KBR, υ cm^{-1})**: 2850 (C-H Aldehyde str), 1690 (C=O str), 1450-1649 (C-C Aromatic), 1590 (C=N str), 720 (C-Cl str) **^{1}H NMR (500 MHz, Chloroform-d)**: δ 9.73 (s, 1H), 7.24-7.90 (Aromatic, 4H), 4.06 (q, 2H) 1.34 (t, 3H) **^{13}C NMR (500 MHz, DMSO-d$_6$)**: δ 14.7, 64.2, 106.4, 121.2, 126.3, 127.6, 130.9, 138.5, 146.5, 147.6, 156.2, 189.3
6	2p	**IR (KBR, υ cm^{-1})**: 2800 (C-H Aldehyde str), 1590 (C=O str), 1350-1480 (C-C Aromatic str), 1520(C=N str), 750 (C-Cl str), 700 (C-Br str) **^{1}H NMR (500 MHz, Chloroform-d)**: δ 9.86 (s, 1H), 8.14-9.04 (Aromatic, 4H) **^{13}C NMR (500 MHz, DMSO-d$_6$)**: δ 120.1, 126.3, 128.1, 129.6, 131.1, 132.7, 138.5, 146.5, 147.6, 189.3

The IR spectrum of 2-chloroquinoline-3-carbaldehyde (2a) showed absorption at 2867 cm^{-1} corresponding to the stretching vibration of the C-H bond in the aldehyde functional group. A strong absorption at 1685 cm^{-1} was indicative of the C=O stretching vibration from the formyl group (-CHO) present at the 3-position of the quinoline ring. Additionally, the presence of the aromatic quinoline system was confirmed by a series of absorption bands in the range of 1450–1600 cm^{-1}, corresponding to the C=C stretching vibrations of the aromatic ring. The ^1H NMR spectrum (500 MHz, $CDCl_3$) of 2a displayed the key signals like a singlet at δ 10.53 ppm corresponding to the proton of the aldehyde group (-CHO) at the 3-position and complex multiplet between δ 7.3 and 8.7 ppm, which was consistent with the aromatic protons of the quinoline ring system. The protons in positions 5 and 8 on the quinoline ring showed doublets at δ 8.05 and δ 7.95 whereas triplet at δ 7.85 and δ 7.65 correspond to the protons in positions 6 and 7 on the quinoline ring.

The IR spectrum of 2,6-dichloroquinoline-3-carbaldehyde (2d) showed peaks to confirm presence of C-H bond (2888 cm^{-1}) in the aldehyde group, C=O stretching vibration (1686 cm^{-1}) of the aldehyde functional group and C=C stretching vibrations (1483–1614 cm^{-1}) in the aromatic system. The ^1H NMR spectrum (500 MHz, $CDCl_3$) of molecule 2d confirmed presence of aldehyde proton (a singlet at δ 10.55 ppm), and aromatic protons of the quinoline system (δ 7.2 and 8.6 ppm). The proton at position 5 and 8 on the quinoline ring showed doublets at δ 7.95 and 8.02. A doublet of doublets at δ 7.88 corresponds to the proton at position 7 on the quinoline ring.

The spectral characterization of 2-chloro-6-methylquinoline-3-carbaldehyde (2g) was confirmed by various techniques. The IR spectrum showed key bands at 2874 cm^{-1} (C-H aldehyde), 1690 cm^{-1} (C=O stretching, Aldehyde), 1580 cm^{-1} (C=N stretching, Quinoline ring), and 820 cm^{-1} (C-Cl stretching). In the ^1H NMR spectrum, a singlet at δ 10.30 ppm corresponded to the aldehyde proton, aromatic

protons were observed between δ 7.2–8.6 ppm, and a singlet at δ 2.38 ppm was attributed to the methyl group at the 6-position. The ^{13}C NMR spectrum exhibited a signal at δ 21.29 ppm for the methyl carbon, while the aromatic and quinoline carbons appeared between δ 126.69–136.38 ppm, with the C=N and C-Cl carbons at δ 147.65 and 149.28 ppm. The aldehyde carbon was observed at δ 189.28 ppm. The molecular ion peak at m/z 206.13 $(M+H)^+$ in the mass spectrum confirmed the molecular weight of the compound.

The spectral characterization of 2-chloro-6-methoxyquinoline-3-carbaldehyde (2j) was confirmed by techniques like IR, ^1H NMR and ^{13}C NMR spectroscopy. The IR spectrum showed significant absorption bands at 2928 cm^{-1} for the aldehyde C-H stretching, 1681 cm^{-1} for the C=O stretching, 1450–1649 cm^{-1} for aromatic C=C stretching, 1384 cm^{-1} for C=N stretching, and 861 cm^{-1} for the C-Cl bond. The ^1H NMR spectrum exhibited a singlet at δ 10.38 ppm for the aldehyde proton, a multiplet between δ 7.32–8.47 ppm for the aromatic protons, and a singlet at δ 3.84 ppm corresponding to the methoxy group ($-OCH_3$). The ^{13}C NMR data showed signals at δ 55.34 ppm for the methoxy carbon, δ 106.39–138.23 ppm for the aromatic carbons, δ 147.71 ppm for the C-Cl carbon, δ 158.53 ppm for the C=N carbon, and δ 189.29 ppm for the carbonyl carbon (C=O). The mass spectrum displayed a molecular ion peak at m/z 222.06 $(M+H)^+$, confirming the molecular weight of the compound.

The spectral characterization of 2-chloro-6-ethoxyquinoline-3-carbaldehyde (2m) confirmed the structure of the compound. The IR spectrum showed characteristic absorption bands at 2850 cm^{-1} for aldehyde C-H stretching, 1690 cm^{-1} for C=O stretching, 1450–1649 cm^{-1} for aromatic C=C stretching, 1590 cm^{-1} for C=N stretching, and 720 cm^{-1} for C-Cl stretching. In the ^1H NMR spectrum, the aldehyde proton appeared as a singlet at δ 9.73 ppm, the aromatic protons were seen as a multiplet between δ 7.24–7.90 ppm, the ethoxy group ($-OCH_2CH_3$) was

represented by a multiplet at δ 4.06 ppm for the methylene protons and a triplet at δ 1.34 ppm for the methyl protons. The ^{13}C NMR spectrum showed a signal at δ 14.7 ppm for the ethyl group's methyl carbon, δ 64.2 ppm for the methylene carbon, δ 106.4–138.5 ppm for the aromatic carbons, δ 146.5 and 147.6 ppm for the C=N and C-Cl carbons, δ 156.2 ppm for the quinoline nitrogen-carbon, and δ 189.3 ppm for the aldehyde carbon.

The spectral characterization of 6-bromo-2-chloroquinoline-3-carbaldehyde (2p) confirmed the structure of the compound. The IR spectrum showed key absorption bands at 2800 cm^{-1} for aldehyde C-H stretching, 1590 cm^{-1} for C=O stretching, 1350–1480 cm^{-1} for aromatic C=C stretching, 1520 cm^{-1} for C=N stretching, 750 cm^{-1} for C-Cl stretching, and 700 cm^{-1} for C-Br stretching. In the ^{1}H NMR spectrum, the aldehyde proton appeared as a singlet at δ 9.86 ppm, and the aromatic protons were observed as a multiplet between δ 8.14–9.04 ppm. The ^{13}C NMR spectrum showed signals in the range of δ 120.1–138.5 ppm for the aromatic carbons, with δ 146.5 and 147.6 ppm assigned to the C=N and C-Cl carbons, and δ 189.3 ppm corresponding to the aldehyde carbon.

5.1.2 Synthesis of 6-substituted-2-chloroquinoline-3-carbaldehyde hydrazide derivatives (3a, 3d, 3g, 3j, 3m, 3p)

The formation of 6-substituted-2-chloroquinoline-3-carbaldehyde hydrazide derivatives is a key transformation in organic synthesis, particularly in medicinal chemistry for developing compounds with potential pharmacological activities such as antimicrobial, antitubercular, and anticancer activities. The reaction involves the condensation of an aldehyde with a hydrazide, leading to the formation of hydrazone derivatives (Figure 5.5).

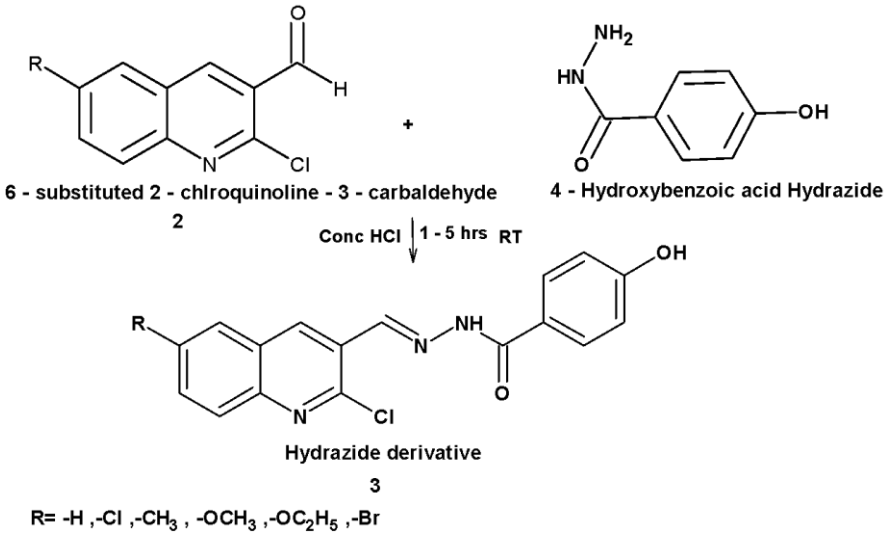

Figure 5.5: Scheme for synthesis of 6-substituted-2-chloroquinoline-3-carbaldehyde hydrazide-hydrazonederivatives

5.1.2.1 Reaction mechanism

The reaction is a condensation reaction between the aldehyde group of 6-substituted-2-chloroquinoline-3-carbaldehyde and the hydrazide group of 4-hydroxybenzoic acid hydrazide, resulting in the formation of hydrazone (-C=N-NH-) as shown in Figure 5.6. The reaction is typically catalysed by acidic conditions (e.g. concentrated HCl)[137].

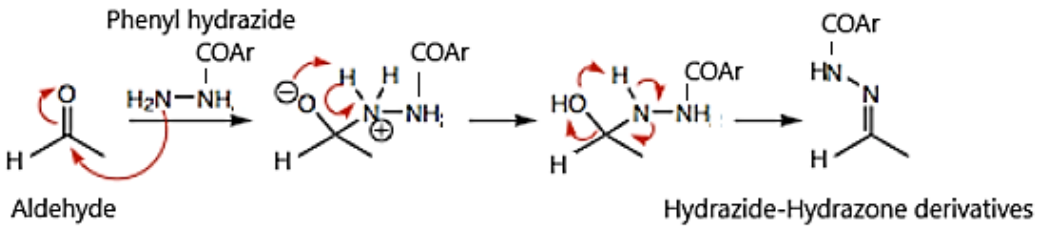

Figure 5.6: Mechanism for formation of hydrazide-hydrazone derivatives from substituted aldehyde with substituted hydrazide[138]

5.1.2.2 Physicochemical properties of synthesized compounds (3a, 3d, 3g, 3j, 3m, 3p)

The physicochemical properties including melting point and TLC Rf values of synthesized 6-substituted-2-chloroquinoline-3-carbaldehyde hydrazide derivatives 3a, 3d, 3g, 3j, 3m, 3p were determined and listed in the Table 5.4.

Table 5.4: Physicochemical properties of synthesized compounds - 3a, 3d, 3g, 3j, 3m and 3p

Sr. No.	Starting material	Product	Yield (%)	M.P. (°C)	TLC R_f *
1	2a	3a	40	210-213	0.75
2	2d	3d	42	230-232	0.70
3	2g	3g	32	167-168	0.70
4	2j	3j	40	276-278	0.72
5	2m	3m	65	210-213	0.68
6	2p	3p	60	220-222	0.59

***** TLC Retention factor (R_f) calculated using mobile phase: n-Hexane: Ethyl Acetate (3:7)
# M.P.: Melting point range

The percentage yields of the reactions were calculated and found to be in the range of 32% to 65%, reflecting the moderate efficiency of the synthetic route employed. The molecular characteristics, such as molecular formula, molecular

weight, and physical appearance (colour and texture) of the products were represented in Table 5.5.

Table 5.5: Molecular characteristics of synthesized compounds 3a, 3d, 3g, 3j, 3m and 3p

Product	IUPAC Nomenclature	Molecular formula	Mol. weight	Physical Appearance
3a	N'-[(2-chloroquinolin-3-yl) methylidene]-4-hydroxybenzohydrazide	$C_{17}H_{12}ClN_3O_2$	325.75	Light Yellow solid
3d	N'-[(2,6-dichloroquinolin-3-yl) methylidene]-4-hydroxybenzohydrazide	$C_{17}H_{11}Cl_2N_3O_2$	360.19	Yellow solid
3g	N'-[(2-chloro-6-methylquinolin-3-yl) methylidene]-4-hydroxybenzohydrazide	$C_{18}H_{14}ClN_3O_2$	339.77	Yellow solid
3j	N'-[(2-chloro-6-methoxyquinolin-3-yl) methylidene]-4-hydroxybenzohydrazide	$C_{18}H_{14}ClN_3O_3$	355.77	Yellow solid
3m	N'-[2-chloro-6-ethoxyquinolin-3-yl) methylidene]-4-hydroxybenzohydrazide	$C_{19}H_{16}ClN_3O_3$	369.80	Yellow solid
3p	N'-[6-bromo-2-chloroquinolin-3-yl) methylidene]-4-hydroxybenzohydrazide	$C_{17}H_{11}BrClN_3O_2$	404.64	Yellow solid

5.1.2.3 Spectral data characterization of synthesized compounds (3a, 3d, 3g, 3j, 3m, 3p)

The synthesized compounds 3a, 3d, 3g, 3j, 3m, and 3p were characterized using various spectroscopic techniques to confirm presence of key functional groups and their structures (Table 5.6).

Table 5.6: Spectral characterization of synthesized compounds 3a, 3d, 3g, 3j, 3m and 3p

Sr. No.	Product	Spectral Characterization
1	3a	**IR (KBR, υ cm^{-1})**: 3414 (O-H str), 1613 (C=O str),1507(C-C Aromatic str) **^{1}H NMR (500 MHz, Chloroform-d)**: δ 10.31(s, 1H,), 8.89 (s, 1H,),6.90-7.94 (Aromatic H)
2	3d	**IR (KBR, υ cm^{-1})**: 3434 (O-H str), 1614 (C=O str), 1371-1466 (C-C Aromatic str) **^{1}H NMR (500 MHz, Chloroform-d)**: δ 11.30(s,1H,), 8.65 (s, 1H,),6.90-7.94 (Aromatic H)
3	3g	**IR (KBR, υ cm^{-1})**: 3431 (O-H str), 1631 (C=O str), 1382 (C=N str), 1458-1515 (C-C Aromatic str), 847 (C-Cl str) **^{1}H NMR (500 MHz, Chloroform-d)**: δ 10.38 (s, 1H), 8.48 (s, 1H), 7.4-8.6 (Aromatic H), 3.8 (s, 3H) **^{13}C NMR (500 MHz, DMSO-d_6)**: δ 21.29 (-CH_3quinoline), 115.63 (C_3/C_5-phenyl), 126.42 (C_2/C_6-phenyl), 126.69 (C_3-quinoline), 126.79 (C_5-quinoline), 127.03 (C_8-quinoline), 127.46 (C_7-quinoline), 129.69 (C_{4a}-quinoline), 130.20 (C_4-quinoline), 130.60 (C_6-quinoline), 134.42 (C_1-phenyl), 142.24 (C_{8a}-quinoline), 146.95 (C_2-quinoline), 147.76 (C_4-phenyl), 160.46 (-C=N benzo hydrazide), 162.61 (-C=O benzohydrazide) **ESI-MS (m/z)**: 340.09 $(M+H)^+$
4	3j	**IR (KBR, υ cm^{-1})**: 3432 (O-H str), 1627 (C=O str), 1383-1452 (C-C Aromatic str), 1343 (C=N str), 832 (C-Cl str)

Sr. No.	Product	Spectral Characterization
		^{1}H NMR (500 MHz, Chloroform-d): δ 12.11 (s, 1H), 9.68 (s, 1H), 6.86-8.6 (Aromatic H), 3.88 (s, 3H) **^{13}C NMR (500 MHz, DMSO-d$_6$)**: δ 55.34, 107.34, 115.63, 122.90, 126.42, 126.92, 127.53, 129.02, 129.69, 129.87, 142.42, 145.35, 147.22, 158.53, 160.46, 162.61 **ESI-MS (m/z)**: 356.02 $(M+H)^+$
5	3m	**IR (KBR, υ cm^{-1})**: 3400 (O-H str), 1610 (C=O str), 1458-1500 (C-C Aromatic str), 1550 (C=N str), 780 (C-Cl str) **^{1}H NMR (500 MHz, Chloroform-d)**: δ 11.87 (s, 1H), 9.68 (s, 1 H), 8.98 (s, 1H), 6.88-7.85 (Aromatic, 8H), 4.06 (q, 2H), 1.34 (t, 3H) **^{13}C NMR (500 MHz, DMSO-d$_6$)**: δ 14.2, 64.3, 106.4, 115.7, 121.2, 124.5, 127.6, 128.1, 129.6, 130.9, 131.7, 146.5, 150.6, 156.2, 157.4, 164.7
6	3p	**IR (KBR, υ cm^{-1})**: 3470(O-H str), 1690(C=O str), 1458-1515 (C-C Aromatic), 1510(C=N str), 780 (C-Cl str), 700 (C-Br str) **^{1}H NMR (500 MHz, Chloroform-d)**: δ 12.04 (s, 1H), 9.68 (s, 1H), 9.04 (s, 1H), 8.14-8.39 (Aromatic, 8H) **^{13}C NMR (500 MHz, DMSO-d$_6$)**: δ 115.7, 120.1, 124.5, 128.0, 128.1, 129.6, 129.6, 131.1, 132.7, 146.5, 150.6, 157.4, 164.7

The spectral characterization of N'-[(2-chloroquinolin-3-yl)methylidene]-4-hydroxybenzohydrazide (3a) confirms the presence of key functional groups and the overall structure. In the IR spectrum, a broad absorption at 3414 cm^{-1} indicated the presence of an O-H group, while the strong band at 1613 cm^{-1} corresponded to C=O stretching, confirming the hydrazide moiety. The band at 1507 cm^{-1} was attributed to the aromatic C-C stretching. In the ^{1}H NMR spectrum, the singlet at δ 10.31 ppm represented the N-H proton of the hydrazide, while the singlet at δ 8.89 ppm corresponded to the O-H proton. The signals between δ 6.90 ppm and 7.94 ppm confirmed the presence of aromatic protons from both the quinoline and

hydroxybenzene rings. Triplet at δ 7.65 and 7.80 corresponded to the protons at positions 6 and 7on the quinoline ring. Doublet at δ 6.90 (2H) corresponded to protons at position 3 and 5 of benzene ring of the 4-hydroxyphenyl group whereas doublet at δ 7.9 corresponded to protons at position 2 and 6 of the same ring. Doublets at δ 7.95 and 8.15 corresponded to the protons at positions 5 and 8 on the quinoline ring.

The IR spectrum of N'-[(2,6-dichloroquinolin-3-yl) methylidene]-4-hydroxybenzohydrazide (3d) showed an absorption at 3434 cm^{-1}, corresponding to the O-H stretching vibration of the hydroxyl group. The band at 1614 cm^{-1} indicated the C=O stretching of the carbonyl group in the hydrazide moiety, while bands in the range of 1371–1466 cm^{-1} represented the C-C stretching vibrations from the aromatic rings. These bands confirmed the presence of the hydroxyl, carbonyl, and aromatic systems in the structure. In the ^{1}H NMR spectrum, a singlet at δ 11.30 ppm corresponded to the N-H proton of the hydrazide group, indicating its deshielded nature. The singlet at δ 8.65 ppm was assigned to the O-H proton from the hydroxyl group. The aromatic protons of the quinoline and benzene rings appeared as multiplets in the range of δ 6.90–7.94 ppm, confirming the aromaticity of the compound.

The spectral characterization of N'-[(2-chloro-6-methylquinolin-3-yl) methylidene]-4-hydroxybenzohydrazide (3g) confirmed its structure through IR, NMR spectroscopy, and mass spectrometry. The IR spectrum showed a broad absorption at 3431 cm^{-1} for the O-H stretch, 1631 cm^{-1} for the C=O stretch of the hydrazide, and 1382 cm^{-1} for the C=N stretch, while the 1458–1515 cm^{-1} range corresponded to aromatic C-C stretching and 847 cm^{-1} indicated the C-Cl bond. The ^{1}H NMR spectrum featured a singlet at δ 12.10 ppm for the N-H proton, δ 9.63 ppm for the O-H proton, multiplets between δ 7.4–8.6 ppm for the aromatic protons, and a singlet at δ 4.8 ppm for the methyl group. The ^{13}C NMR spectrum showed the

methyl carbon at δ 21.29 ppm, aromatic carbons between δ 115.63–146.95 ppm,C-Clappears at δ 146.95 ppm and C=N at δ 162.61 ppm, with the carbonyl carbon resonating at δ 160.46 ppm. The mass spectrum confirmed the molecular weight with a peak at m/z 340.09 $(M+H)^+$

The spectral characterization of N'-[(2-chloro-6-methoxyquinolin-3-yl) methylidene]-4-hydroxybenzohydrazide (3j) was carried out with IR, NMR spectroscopy, and mass spectrometry. In the IR spectrum, a broad absorption at 3432 cm^{-1} corresponded to the O-H stretching of the hydroxyl group, while the band at 1627 cm^{-1} indicated C=O stretching. Additional bands at 1383-1452 cm^{-1} were attributed to C-C aromatic stretching, and 1343 cm^{-1} corresponded to C=N stretching, with 832 cm^{-1} indicating the C-Cl bond. In the ^1H NMR spectrum, a singlet at δ 12.11 ppm corresponded to the N-H proton, while the singlet at δ 9.68 ppm was assigned to the O-H proton. The aromatic protons resonated between δ 6.86-8.6 ppm, and the methoxy group ($-OCH_3$) appeared as a singlet at δ 3.88 ppm. In the ^{13}C NMR spectrum, the signal at δ 55.34 ppm corresponded to the methoxy carbon, while signals between δ 107.34-145.35 ppm were attributed to the aromatic carbons. The signal for C-Cl appeared at δ 147.35 ppm and C-OR at δ 158.53 ppm The carbonyl carbon resonated at δ 162.61 ppm, with the C=N carbon at δ 160.46 ppm. The mass spectrum confirmed the molecular weight with a peak at m/z 356.02 $(M+H)^+$.

The IR spectrum of N'-[(2-chloro-6-ethoxyquinolin-3-yl) methylidene]-4-hydroxybenzohydrazide (3m) showed a broad absorption at 3400 cm^{-1} for the O-H stretching of the hydroxyl group. The strong absorption at 1610 cm^{-1} corresponded to C=O stretching of the hydrazide moiety, while the bands at 1458-1500 cm^{-1} were attributed to C-C aromatic stretching. A band at 1550 cm^{-1} indicated C=N stretching, and 780 cm^{-1} corresponded to the C-Cl stretching from the quinoline ring. In the ^1H NMR spectrum, a singlet at δ 11.87 ppm was attributed to the N-H proton of the

hydrazide group, while the O-H proton appeared at δ 9.68 ppm. The imine proton resonated at δ 8.98 ppm, and the aromatic protons appeared as multiplets between δ 6.88–7.85 ppm. The ethoxy group (-OCH_2CH_3) was identified by the signals at δ 4.06 ppm (methylene) and δ 1.34 ppm (methyl). In the ^{13}C NMR spectrum, the ethoxy methyl carbon resonated at δ 14.2 ppm, and the methylene carbon appeared at δ 64.3 ppm, while the aromatic carbons ranged from δ 106.4–131.7 ppm. The C-Cl carbon appeared at δ 146.5 ppm, the C=N carbon at δ 150.6 ppm, and the carbonyl carbon resonated downfield at δ 164.7 ppm.

The spectral characterization of N'-[(6-bromo-2-chloroquinolin-3-yl) methylidene]-4-hydroxybenzohydrazide (3p) was confirmed through IR, NMR, and ^{13}C NMR data. The IR spectrum exhibited a broad absorption at 3470 cm^{-1}, indicating O-H stretching of the hydroxyl group, while the strong absorption at 1690 cm^{-1} corresponded to C=O stretching of the hydrazide. Additional bands at 1458-1515 cm^{-1} were attributed to C-C aromatic stretching, 1510 cm^{-1} to C=N stretching, 780 cm^{-1} to C-Cl stretching, and 700 cm^{-1} to C-Br stretching. In the ^{1}H NMR spectrum, a singlet at δ 12.04 ppm corresponded to the NH proton, while the OH proton appeared at δ 9.68 ppm. The imine proton resonated at δ 9.04 ppm, and the aromatic protons appeared as multiplets between δ 8.14-8.39 ppm, confirming the aromaticity of the quinoline and benzene rings. The ^{13}C NMR spectrum showed signals for aromatic carbons between δ 115.7-132.7 ppm, with the C-Cl and C-Br carbons likely resonating around δ 146.5 ppm, the C=N carbon at δ 150.6 ppm,the C-O carbon attached to the hydroxyl group in the benzohydrazide at 157.4 ppm and the carbonyl carbon at δ 164.7 ppm.

5.1.3 Synthesis of Ester derivatives of 6-substituted-2-chloroquinoline-3-carbaldehyde hydrazide

Esterification of 6-substituted-2-chloroquinoline-3-carbaldehyde hydrazide derivatives(3a, 3d, 3g, 3j, 3m, 3p) was carried out using zinc oxide as the catalyst in presence of three acid chlorides (acetyl chloride, propanoyl chloride and butanoyl chloride) at room temperature (Figure 5.7) to prepare total 18 ester derivatives.

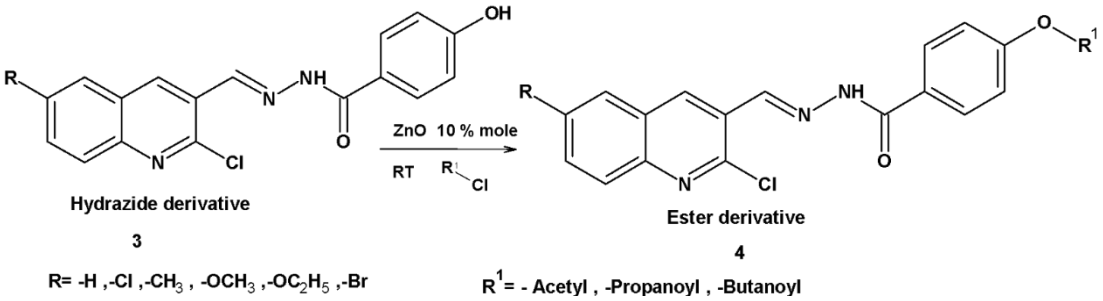

Figure 5.7: Scheme for synthesis of ester derivatives of 6-substituted-2-chloroquinoline-3-carbaldehyde hydrazide using zinc oxide as catalyst

5.1.3.1 Reaction mechanism

Zinc oxide (ZnO) acts as a heterogeneous Lewis acid catalyst in the acylation of phenols. Its role is to activate the acylating agent, typically an acyl chloride or anhydride, by coordinating with the carbonyl oxygen, making the carbonyl carbon more electrophilic. This enhances the nucleophilic attack of the phenolic oxygen on the acyl group, leading to the formation of an ester[139].

In a solvent-free process, ZnO facilitates the acylation at mild temperatures, making the reaction eco-friendly and reusable. Zinc oxide is especially effective in ensuring high selectivity for O-acylation over competitive reactions like C-acylation or Fries rearrangement.

5.1.3.2 Physicochemical properties of synthesized compounds(4a – 4r)

The physicochemical properties including melting point and TLC Rf values of synthesized 6-substituted-2-chloroquinoline-3-carbaldehyde hydrazide ester derivatives 4a-4r were determined and listed in the Table 5.7.

Table 5.7: Physicochemical properties of synthesized compounds 4a – 4r

Sr. No.	Starting material	Product	Yield (%)	M.P. (ºC)	TLC R_f *
1	3a	4a	62	217-218	0.61
2	3a	4b	65	208-211	0.68
3	3a	4c	50	219-220	0.73
4	3d	4d	56	216-217	0.62
5	3d	4e	52	211-212	0.73
6	3d	4f	48	215-217	0.58
7	3g	4g	60	251-252	0.62
8	3g	4h	62	268-269	0.71
9	3g	4i	53	275-276	0.61
10	3j	4j	70	280-281	0.60
11	3j	4k	65	235-236	0.70
12	3j	4l	70	270-271	0.63
13	3m	4m	61	273-274	0.66
14	3m	4n	75	287-289	0.71
15	3m	4o	78	301-303	0.57
16	3p	4p	63	308-310	0.71
17	3p	4q	79	322-324	0.63
18	3p	4r	69	336-337	0.73

***** TLC Retention factor (R_f) calculated using mobile phase: n-Hexane: Ethyl Acetate (3:7)

M.P.: Melting point range

The percentage yields of the reactions were calculated and found to be in the range of 48% to 79%, reflecting the moderate to good efficiency of the synthetic route employed. The molecular characteristics, such as molecular formula, molecular weight, and physical appearance (colour and texture) of the products were represented in Table 5.8.

Table 5.8: Molecular characteristics of synthesized compounds 4a – 4r

Product	IUPAC Nomenclature	Molecular formula	Mol. weight	Physical Appearance
4a	4-{2-2-[(2-chloroquinolin-3-yl) methylidene] hydrazine-1-carbonyl} phenyl acetate	$C_{19}H_{14}ClN_3O_3$	367.78	Light Yellow solid
4b	4-{2-2-[(2-chloroquinolin-3-yl) methylidene] hydrazine-1-carbonyl} phenyl propanoate	$C_{20}H_{16}ClN_3O_3$	381.81	Light Yellow solid
4c	4-{2-2-[(2-chloroquinolin-3-yl) methylidene] hydrazine-1-carbonyl} phenyl butanoate	$C_{21}H_{18}ClN_3O_3$	395.84	Yellow solid
4d	4-{2-2-[(2,6-dichloroquinolin-3-yl) methylidene] hydrazine-1-carbonyl} phenyl acetate	$C_{19}H_{13}Cl_2N_3O_3$	402.23	Yellow solid
4e	4-{2-2-[(2,6-dichloroquinolin-3-yl) methylidene] hydrazine-1-carbonyl} phenyl propanoate	$C_{20}H_{15}Cl_2N_3O_3$	416.25	Yellow solid

Product	IUPAC Nomenclature	Molecular formula	Mol. weight	Physical Appearance
4f	4-{2-2-[(2,6-dichloro quinolin-3-yl) methylidene] hydrazine-1-carbonyl} phenyl butanoate	$C_{21}H_{17}Cl_2N_3O_3$	430.28	Yellow solid
4g	4-{2-[(2-chloro-6-methyl quinolin-3-yl) methylidene] hydrazine carbonyl} phenyl acetate	$C_{20}H_{16}ClN_3O_3$	381.81	Yellow solid
4h	4-{2-[(2-chloro-6-methyl quinolin-3-yl) methylidene] hydrazine carbonyl} phenyl propionate	$C_{21}H_{18}ClN_3O_3$	395.84	Yellow solid
4i	4-{2-[(2-chloro-6-methyl quinolin-3-yl) methylidene] hydrazine carbonyl} phenyl butanoate	$C_{22}H_{20}ClN_3O_3$	409.87	Yellow solid
4j	4-{2-[(2-chloro-6-methoxy quinolin-3-yl) methylidene] hydrazine carbonyl} phenyl acetate	$C_{20}H_{16}ClN_3O_4$	397.81	Yellow solid
4k	4-{2-[(2-chloro-6-methoxy quinolin-3-yl) methylidene] hydrazine carbonyl} phenyl propionate	$C_{21}H_{18}ClN_3O_4$	411.84	Yellow solid
4l	4-{2-[(2-chloro-6-methoxy quinolin-3-yl) methylidene] hydrazine carbonyl} phenyl butanoate	$C_{22}H_{20}ClN_3O_4$	425.86	Yellow solid
4m	4-{2-2-[(2-chloro-6-ethoxy quinolin-3-yl) methylidene] hydrazine carbonyl} phenyl acetate	$C_{21}H_{18}ClN_3O_4$	411.84	Yellow solid

Product	IUPAC Nomenclature	Molecular formula	Mol. weight	Physical Appearance
4n	4-{2-2-[(2-chloro-6-ethoxyquinolin-3-yl) methylidene] hydrazinecarbonyl} phenylpropanoate	$C_{22}H_{20}ClN_3O_4$	425.86	Yellow solid
4o	4-{2-2-[(2-chloro-6-ethoxy quinolin-3-yl) methylidene] hydrazine carbonyl} phenyl butanoate	$C_{23}H_{22}ClN_3O_4$	439.89	Yellow solid
4p	4-{2-2-[(6-bromo-2-chloro quinolin-3-yl)methylidene] hydrazine carbonyl} phenyl acetate	$C_{19}H_{13}Br\ Cl\ N_3O_3$	446.68	Yellow solid
4q	4-{2-2-[(6-bromo-2-chloro quinolin-3-yl)methylidene]hydrazine carbonyl} phenyl propanoate	$C_{20}H_{15}Br\ Cl\ N_3O_3$	460.71	Yellow solid
4r	4-{2-2-[(6-bromo-2-chloro quinolin-3-yl)methylidene]hydrazine carbonyl} phenyl butanoate	$C_{21}H_{17}BrClN_3O_3$	474.73	Yellow solid

5.1.3.3 Spectral data characterization of synthesized compounds(4a-4r)

The synthesized compounds 4a-4r were characterized using various spectroscopic techniques to confirm their structures and assess the presence of key functional groups (Table 5.9).

Table 5.9: Spectral characterization of synthesized compounds 4a – 4r

Sr. No.	Product	Spectral Characterization of synthesized compounds 4a – 4r
1	4a	**IR (KBR, υ cm^{-1})**: 3288.03 (N-H str), 1649.8 (C=O str), 1610.27 (C=N str) **^{1}H NMR (500 MHz, Chloroform-d)**: δ 12.07 (s,1H), 7.69-8.59 (Aromatic H), 7.49 (m, CH=N), 2.28 (s, 3H) **ESI-MS (m/z)**: 368.10 $(M+H)^+$
2	4b	**IR (KBR, υ cm^{-1})**: 3285 (NH), 1815 (C=O), 1648(C=N) **^{1}H NMR (500 MHz, Chloroform-d)**: δ 12.07 (s,1H), 7.53-8.59 (Aromatic .H), 7.50 (m, CH=N), 2.40(q,2H) 1.19 (t, 3H) **ESI-MS (m/z)**: 382.08 $(M+H)^+$
3	4c	**IR (KBR, υ cm^{-1})**: 3250 (N-H str), 1748 (C=O str), 1634 (C=N str) **^{1}H NMR (500 MHz, Chloroform-d)**: δ 12.07 (s,1H), 7.69-8.59 (Aromatic H), 7.5 (m .CH=N), 2.5 (t,2H) ,1.7(m,2H) 0.94 (t, 3H) **ESI-MS (m/z)**: 396.01 $(M+H)^+$
4	4d	**IR (KBR, υ cm^{-1})**: 3250 (N-H str), 1650 (C=O str), 1600(C=N str) **^{1}H NMR (500 MHz, Chloroform-d)**: δ 12.07 (1H, N-H), 8.59 (s, NH) , 7.15-8.34 (Aromatic), 2.28 (s, 3H) **ESI-MS (m/z)**: 403.03 $(M+H)^+$
5	4e	**IR (KBR, υ cm^{-1})**: 3200 (N-H str), 1680 (C=O str), 1500-1600(C=N str) **^{1}H NMR (500 MHz, Chloroform-d)**: δ 12.07 (s,1H,), 8.59 (s, NH), 7.15-8.34 (Aromatic), 2.46-2.50(q, 2H),1.19 (t, 3H) **ESI-MS (m/z)**: 417.03 $(M+H)^+$

Sr. No.	Product	Spectral Characterization of synthesized compounds 4a – 4r
6	4f	**IR (KBR, υ cm^{-1})**: 3500 (N-H str), 1760 (C=O str), 1650(C=N str) **^{1}H NMR (500 MHz, Chloroform-d)**: δ 12.07 (s,1H), 8.59 (s, NH), 7.15-8.34 (Aromatic), 2.50(t,2H) ,1.70(m,2H) 0.94 (t, CH_3) **ESI-MS (m/z)**: 431.08 $(M+H)^+$
7	4g	**IR (KBR, υ cm^{-1})**: 3250(N-H str), 1620(C=O str), 1580(C=N str) **^{1}H NMR (500 MHz, Chloroform-d)**: δ 12.21(s, 1H), 8.56(s, 1H), 7.13-8.28(Aromatic), 2.38(s, 3H), 2.37(s, 3H) **^{13}C NMR (500 MHz, DMSO-d_6)**: δ 21.06(-CH_3 quinoline), 21.29(-CH_3 acetate ester), 122.52(C_3/C_5-phenyl), 126.69(C_2/C_6-phenyl), 126.76(C_3-quinoline), 126.79(C_5-quinoline), 127.03(C_8-quinoline), 127.46(C_7-quinoline), 129.92(C_{4a}-quinoline), 130.20(C_4-quinoline), 130.60(C_6-quinoline), 134.42(C_1-phenyl), 142.24(C_{8a}-quinoline), 146.95(C_2-quinoline), 147.76(C_4-phenyl), 153.34(-C=N benzo hydrazide), 162.61(-C=O benzo hydrazide), 169.22 (-C=O, acetate) **ESI-MS (m/z)**: 382.08 $(M+H)^+$
8	4h	**IR (KBR, υ cm^{-1})**: 3260 (N-H str), 1620 (C=O str), 1490 (C=N str) **^{1}H NMR (500 MHz, Chloroform-d)**: δ 12.12(s,1H),8.62(s,1H),7.18-8.55 (Aromatic), 2.72 (s,3H), 2.52 (q,2H), 1.38 (t,3H) **^{13}C NMR (500 MHz, DMSO-d_6)**: δ 9.08, 21.29, 27.45, 121.93, 126.69, 126.76, 126.79, 127.03, 127.46, 129.91, 130.20, 130.60, 134.42, 142.24, 146.95, 147.76, 153.85, 162.61, 172.53 **ESI-MS (m/z)**: 396.11. $(M+H)^+$
9	4i	**IR (KBR, υ cm^{-1})**: 3200(N-H str),1650(C=O str),1500(C=Nstr) **^{1}H NMR (500 MHz, Chloroform-d)**: δ 12.01(s,1H),8.68 (s,1H), 7.15-8.64 (Aromatic), 2.60 (s,3H), 2.49 (t,3H), 1.98 (m,2H), 0.93 (t,3H) **^{13}C NMR (500 MHz, DMSO-d_6)**: δ 13.65, 18.40, 21.29, 39.58, 121.93, 126.69, 126.76, 126.79, 127.03, 127.46, 129.91, 130.20,

Sr. No.	Product	Spectral Characterization of synthesized compounds 4a – 4r
		130.60, 134.42, 142.24, 146.95, 147.76, 153.21, 162.61, 171.94 **ESI-MS (m/z)**: 410.16. $(M+H)^+$
10	4j	**IR (KBR, υ cm^{-1})**: 3150(N-H str),1680(C=O str),1520(C=N str) **^{1}H NMR (500 MHz, Chloroform-d)**: δ 12.11 (s,1H), 8.68 (s,1H), 7.12-5.67 (Aromatic), 3.89 (s,3H), 2.38 (s,3H) **^{13}C NMR (500 MHz, DMSO-d_6)**: δ 21.06, 55.34, 107.34, 122.52, 122.90, 126.76, 126.92, 127.53, 129.02, 129.86, 129.92, 142.42, 145.35, 147.22, 153.34, 158.53, 162.61, 169.22 **ESI-MS (m/z)**: 398.08. $(M+H)^+$
11	4k	**IR (KBR, υ cm^{-1})**: 3210(N-H str), 1650(C=O str), 1550 (C=Nstr) **^{1}H NMR (500 MHz, Chloroform-d)**: δ 12.10(s,1H), 8.74(s,1H), 7.10-8.69 (Aromatic),3.92(s,3H),2.66(q,2H).1.28(t,3H) **^{13}C NMR (500 MHz, DMSO-d_6)**: δ 9.08, 27.45, 55.34, 107.34, 121.93, 122.90, 126.76, 126.92, 127.53, 129.02, 129.90, 129.91, 142.42, 145.35, 147.22, 153.85, 158.53, 162.61, 172.53 **ESI-MS (m/z)**: 412.07$(M+H)^+$
12	4l	**IR (KBR, υ cm^{-1})**: 3150 (N-H str), 1620 (C=O str), 1480(C=N str) **^{1}H NMR (500 MHz, Chloroform-d)**: δ 12.10 (s,1 H),8.69(s,1H),7.11-8.68 (Aromatic),3.86(s,3H), 2.59 (t, 2H), 1.78(m, 2H),1.18 (t,3H) **^{13}C NMR (500 MHz, DMSO-d_6)**: δ 13.65, 18.40, 36.20, 55.34, 107.34, 121.93, 122.90, 126.76, 126.92, 127.53, 129.02, 129.86, 129.91, 142.42, 145.35, 147.22, 153.21, 158.53, 162.61, 171.94 **ESI-MS (m/z)**: 426.14$(M+H)^+$
13	4m	**IR (KBR, υ cm^{-1})**: 3500 (N-H str), 1620 (C=O str), 1550 (C=N str) **^{1}H NMR (500 MHz, Chloroform-d)**: δ 10.87 (s, 1H), 8.98(s, 1H), 7.16-8.51 (Aromatic, 8H), 4.06 (m, 2H), 2.31(s, 3H), 1.34(s, 3H) **^{13}C NMR (500 MHz, DMSO-d_6)**: δ 9.1, 14.2, 27.8, 64.3, 106.4, 114.3, 121.2, 127.1, 128.9, 129.6, 130.9, 131.7, 146.5, 146.6, 150.5,

Sr. No.	Product	Spectral Characterization of synthesized compounds 4a – 4r
		150.6, 156.1. 164.6, 172.8 **ESI-MS (m/z)**: 412.48 (M+H
14	4n	**IR (KBR, υ cm^{-1})**: 3480 (N-H str), 1610 (C=O str), 1520 (C=N str) **^{1}H NMR (500 MHz, Chloroform-d)**: δ 12.06 (s, 1H), 8.98 (s, 1H), 7.16-8.51 (Aromatic, 8H), 4.07 (q, 2H), 2.61 (t, 2H), 1.34 (q, 2H),1.08 (t, 3H) **^{13}C NMR (500 MHz, DMSO-d_6)**: δ 9.3, 14.2, 27.8, 64.3, 106.8, 114.9, 121.1, 127.3, 128.8, 129.2, 130.5, 131.9, 146.5 ,146.6, 150.6,150.8, 156.3, 164.1 ,172.6 **ESI-MS (m/z)**:426.34 $(M+H)^+$
15	4o	**IR (KBR, υ cm^{-1})**: 3350 (N-H str), 1590 (C=O str), 1520 (C=N str) **^{1}H NMR (500 MHz, Chloroform-d)**: δ 12.17 (s, 1H), 8.98 (s, 1H), 7.16-8.50 (Aromatic, 8H), 4.06 (q, 2H), 2.59 (t, 3H), 1.51 (t, 2H),1.35 (m, 2H), 1.08 (t, 3H) **^{13}C NMR (500 MHz, DMSO-d_6)**: δ 9.1, 14.2, 27.8, 64.3, 106.4, 114.3, 121.2, 124.5, 127.1, 128.9, 129.6, 130.9, 131.7, 146.5, 146.5, 150.6, 150.6, 156.1, 164.6, 172.8 **ESI-MS (m/z)**:440.65 $(M+H)^+$
16	4p	**IR (KBR, υ cm^{-1})**: 3490 (N-H str), 1620 (C=O str), 1570 (C=N str) **^{1}H NMR (500 MHz, Chloroform-d)**: δ 12.04 (s, 1H), 9.04 (s, 1H), 7.51-8.39 (Aromatic, 8H), 2.59 (s, 3H) **^{13}C NMR (500 MHz, DMSO-d_6)**: δ 21.0, 114.3, 120.7, 124.1, 128.0-128.1, 129.5-129.7, 131.1, 132.7, 146.4-146.6, 150.5-150.7, 164.7, 169.1 **ESI-MS (m/z)**: 447.64 $(M+H)^+$
17	4q	**IR (KBR, υ cm^{-1})**: 3500 (N-H str), 1690 (C=O str), 1540 (C=N str) **^{1}H NMR (500 MHz, Chloroform-d)**: δ 12.28 (s, 1H), 9.04 (s, 1H), 7.51-8.39 (Aromatic, 8H), 2.61 (q, 2H), 1.28(t, 3H) **^{13}C NMR (500 MHz, DMSO-d_6)**: δ 27.8, 114.3, 120.1, 124.5,

Sr. No.	Product	Spectral Characterization of synthesized compounds 4a – 4r
		128.0-128.2 ,129.5-129.7, 131.1, 132.7, 146.4-146.6, 150.5-150.7, 164.7, 172.8 **ESI-MS (m/z)**: 461.48 $(M+H)^+$
18	4r	**IR (KBR, υ cm^{-1})**: 3350 (N-H str), 1650 (C=O str), 1490(C=N str) **^{1}H NMR (500 MHz, Chloroform-d)**: δ 12.22 (s,1H),9.04(s,1H),7.51-8.39 (Aromatic, 8H), 2.59 (t, 3H), 1.68(m, 2H),0.99 (t,2H) **^{13}C NMR (500 MHz, DMSO-d_6)**: δ 20.2, 114.3, 120.1, 124.5, 128.0-128.2, 129.5-129.7,131.1, 132.7, 146.4-146.6, 150.5-150.7, 164.7, 169.4 **ESI-MS (m/z)**: 475.84 $(M+H)^+$

The spectral characterization of4-{2-[(2-chloroquinolin-3-yl) methylidene] hydrazine-1-carbonyl} phenyl acetate (4a) confirmed its structure through IR, NMR spectroscopy, and mass spectrometry data. The IR spectrum showed an absorption at 3288.03 cm^{-1} corresponding to N-H stretching, while the band at 1649.8 cm^{-1} indicates C=O stretching, confirming the carbonyl groups in the structure. Additionally, the absorption at 1610.27 cm^{-1} was attributed to C=N stretching, representing the imine functionality. In the ^{1}H NMR spectrum, a singlet at δ 12.07 ppm corresponded to the N-H proton, while multiplets between δ 7.69-8.59 ppm represented the aromatic protons from both the quinoline and phenyl rings. A multiplet at δ 7.49 ppm was assigned to the CH=N proton, and a singlet at δ 2.28 ppm was attributed to the methyl protons of acetate group. The mass spectrum (ESI-MS) showed a molecular ion peak at m/z 368.10 $(M+H)^+$, confirming the molecular weight of the compound.

In the IR spectrum of 4-{2-[(2-chloroquinolin-3-yl)methylidene]hydrazine-1-carbonyl} phenyl propanoate (4b), an absorption at 3285 cm^{-1} corresponded to N-H stretching, while a strong band at 1815 cm^{-1} was attributed to C=O stretching, indicating the presence of a carbonyl group in the ester and hydrazine functionalities. The C=N stretching appeared at 1648 cm^{-1}, confirming the imine group. In the ^1H NMR spectrum, a singlet at δ 12.07 ppm corresponded to the N-H proton, while the aromatic protons were represented by multiplets between δ 7.53–8.59 ppm. The CH=N proton resonated at δ 7.50 ppm, and the triplet at δ 1.19 ppm corresponded to the methyl group (-CH_3) in the propanoate ester. The mass spectrum (ESI-MS) showed a molecular ion peak at m/z 382.08 $(M+H)^+$, confirming the molecular weight of the compound.

The spectral characterization of 4-{2-[(2-chloroquinolin-3-yl)methylidene]hydrazine-1-carbonyl} phenyl butanoate (4c) confirmed the structure through IR, NMR spectroscopy, and mass spectrometry data. The IR spectrum showed an absorption at 3250 cm^{-1} corresponding to N-H stretching, while the strong absorption at 1748 cm^{-1} indicated C=O stretching, confirming the presence of the ester carbonyl group. The band at 1634 cm^{-1} was attributed to C=N stretching, confirming the imine group in the molecule. In the ^1H NMR spectrum, a singlet at δ 12.07 ppm corresponded to the N-H proton, while the aromatic protons were represented by multiplets between δ 7.69–8.59 ppm. The CH=N proton resonated at δ 7.5 ppm, and a triplet at δ 0.94 ppm corresponded to the methyl group (-CH_3) in the butanoate ester. The mass spectrum (ESI-MS) showed a molecular ion peak at m/z 396.01 $(M+H)^+$, confirming the molecular weight of the compound.

The spectral characterization of 4-{2-[(2,6-dichloroquinolin-3-yl)methylidene]hydrazine-1-carbonyl} phenyl acetate (4d) was carried out using IR, NMR spectroscopy, and mass spectrometry data. In the IR spectrum, an absorption at 3250 cm^{-1} corresponded to N-H stretching, while the band at 1650 cm^{-1} indicated

C=O stretching, confirming the presence of the carbonyl group. The band at 1600 cm^{-1} was attributed to C=N stretching, which indicated the presence of the imine group. In the ^1H NMR spectrum, a singlet at δ 12.07 ppm corresponded to the N-H proton of the hydrazine moiety, and another singlet at δ 8.59 ppm corresponded to a second N-H proton, likely due to hydrogen bonding interactions. The aromatic protons were observed as multiplets between δ 7.15–8.34 ppm, and a singlet at δ 2.78 ppm corresponds to the methyl protons of the acetate group ($-CH_3$). The mass spectrum (ESI-MS) showed a molecular ion peak at m/z 403.03 (M+H)+, confirming the molecular weight of the compound.

The IR, NMR, and mass spectrometry data was used to confirm structure of 4-{2-[(2,6-dichloroquinolin-3-yl)methylidene]hydrazine-1-carbonyl}phenylpropanoate (4e). The IR spectrum showed an absorption at 3200 cm^{-1} for N-H stretching, while a strong band at 1680 cm^{-1} indicated C=O stretching, confirming the presence of a carbonyl group in the propanoate ester. The band between 1500-1600 cm^{-1} was attributed to C=N stretching, indicating the presence of the imine group.

In the ^1H NMR spectrum, a singlet at δ 12.07 ppm corresponded to the N-H proton, while another singlet at δ 8.59 ppm likely represented an additional N-H proton from the hydrazine moiety. The aromatic protons were observed as multiplets between δ 7.15-8.34 ppm. A quartet at δ 2.46-2.50 ppm corresponded to the methylene protons ($-CH_2-$) in the propanoate group, while a singlet at δ 1.19 ppm represented the methyl protons ($-CH_3$) of the propanoate ester. The mass spectrum (ESI-MS) showed a molecular ion peak at m/z 417.03 $(M+H)^+$, confirming the molecular weight of the compound.

The structure of molecule 4-{2-[(2,6-dichloroquinolin-3-yl)methylidene]hydrazine-1-carbonyl} phenyl butanoate (4f) was confirmed using IR, NMR spectroscopy, and mass spectrometry data. In the IR spectrum, a broad absorption at 3500 cm^{-1} corresponded to N-H stretching, while the strong band at

1760 cm^{-1} indicated C=O stretching, confirming the presence of the carbonyl group in the butanoate ester. The band at 1650 cm^{-1} was attributed to C=N stretching, indicating the imine group in the molecule.

In the ^{1}H NMR spectrum, a singlet at δ 12.07 ppm corresponded to the N-H proton of the hydrazine moiety, and another singlet at δ 8.59 ppm represented a second N-H proton. The aromatic protons were observed as multiplets between δ 7.15–8.34 ppm, confirming the presence of aromatic systems in the structure. Additionally, the triplet at δ 0.94 ppm corresponded to the methyl group ($-CH_3$) of the butanoate ester. The mass spectrum (ESI-MS) showed a molecular ion peak at m/z 431.08 $(M+H)^+$, confirming the molecular weight of the compound.

The spectral characterization of 4-{2-[(2-chloro-6-methylquinolin-3-yl)methylidene]hydrazine-1-carbonyl} phenyl acetate (4g) was confirmed through IR, NMR spectroscopy, and mass spectrometry data. In the IR spectrum, a broad absorption at 3250 cm^{-1} corresponded to N-H stretching, while the band at 1620 cm^{-1} indicated C=O stretching, confirming the presence of a carbonyl group. The C=N stretching was observed at 1580 cm^{-1}, confirming the imine group in the compound.

In the ^{1}H NMR spectrum, a singlet at δ 12.21 ppm was attributed to the N-H proton, another singlet at δ 8.56 ppm to an additional N-H proton, and aromatic protons were seen as multiplets between δ 7.13-8.28 ppm. Two singlets at δ 2.38 ppm corresponded to the methyl groups ($-CH_3$) of the acetate and methyl substituents on the quinoline ring. In the ^{13}C NMR spectrum, signals at δ 21.06 and 21.29 ppm corresponded to the methyl carbons, while aromatic carbons resonated between δ 122.52-147.76 ppm. The C=N carbon was observed at δ 153.34 ppm, and the carbonyl carbons appeared at δ 162.61 ppm (amide carbonyl) and 169.22 ppm (ester carbonyl). The mass spectrum (ESI-MS) showed a molecular ion peak at m/z 382.08 $(M+H)^+$, which confirmed the molecular weight of the compound.

The spectral characterization of 4-{2-[(2-chloro-6-methylquinolin-3-yl)methylidene]hydrazine-1-carbonyl} phenyl propionate (4h) was confirmed through IR, NMR spectroscopy, and mass spectrometry data. The IR spectrum showed a broad absorption at 3260 cm^{-1}, which corresponded to N-H stretching, while the band at 1620 cm^{-1} indicated C=O stretching, confirming the presence of a carbonyl group. The C=N stretching was observed at 1490 cm^{-1}, indicating the presence of an imine group.

In the ^{1}H NMR spectrum, a singlet at δ 12.12 ppm was attributed to the N-H proton, and another singlet at δ 8.62 ppm corresponded to the hydrazine proton. The aromatic protons were observed as multiplets between δ 7.18–8.55 ppm. Additional signals at δ 2.72 ppm and δ 2.52 ppm corresponded to the methyl and methylene protons of the propionate group, while a singlet at δ 1.38 ppm was attributed to the terminal methyl group (-CH_3) of the propionate ester. In the ^{13}C NMR spectrum, the methyl carbons were observed at δ 9.08 and 21.29 ppm, and the methylene carbon of the propionate group resonated at δ 27.45 ppm. The aromatic carbons of the quinoline and phenyl rings appeared between δ 121.93–147.76 ppm, and the C=N carbon was assigned to δ 153.85 ppm. The ester carbonyl appeared at δ 172.53 ppm, and the amide carbonyl appeared at δ 162.61 ppm. The mass spectrum (ESI-MS) showed a molecular ion peak at m/z 396.11 $(M+H)^{+}$, which confirmed the molecular weight of the compound.

The structure of 4-{2-[(2-chloro-6-methylquinolin-3-yl)methylidene]hydrazine-1-carbonyl} phenyl butanoate (4i) was confirmed through spectral characterization with IR, NMR spectroscopy, and mass spectrometry data. The IR spectrum displayed a broad absorption at 3200 cm^{-1} corresponding to N-H stretching, while the strong band at 1650 cm^{-1} indicated C=O stretching, confirming the presence of a carbonyl group. The C=N stretching appeared at 1500 cm^{-1}, confirming the imine group.

In the ^{1}H NMR spectrum, a singlet at δ 12.01 ppm was attributed to the NH proton, while another singlet at δ 8.68 ppm corresponded to the imine proton. Aromatic protons were observed as multiplets between δ 7.15–8.64 ppm. The signals at δ 2.60 ppm and δ 2.49 ppm corresponded to the protons of the butanoate side chain, while signals at δ 1.98 ppm and δ 0.93 ppm represented the methyl and methylene protons of the butanoate group. In the ^{13}C NMR spectrum, the ester carbonyl appeared at δ 171.94 ppm, while the amide carbonyl was observed at δ 162.61 ppm. The signals at δ 13.65 ppm, δ 18.40 ppm, and δ 21.29 ppm corresponded to the methyl and methylene carbons of the butanoate side chain. The aromatic carbons resonated between δ 121.93–147.76 ppm, and the C=N carbon was observed at δ 153.21 ppm. The mass spectrum (ESI-MS) showed a molecular ion peak at m/z 410.16 $(M+H)^{+}$, confirming the molecular weight of the compound.

The IR, NMR spectroscopy, and mass spectrometry data was used for spectral characterization of 4-{2-[(2-chloro-6-methoxyquinolin-3-yl)methylidene]hydrazine-1-carbonyl} phenyl acetate (4j). The IR spectrum showed a broad absorption at 3150 cm^{-1} corresponding to N-H stretching, while the strong absorption at 1680 cm^{-1} indicated C=O stretching, confirming the presence of a carbonyl group. The band at 1520 cm^{-1} was attributed to C=N stretching, indicating the presence of the imine group.

In the ^{1}H NMR spectrum, a singlet at δ 12.11 ppm was assigned to the N-H proton, and another singlet at δ 8.68 ppm corresponded to the imine proton. The aromatic protons were observed as multiplets between δ 7.12–8.67 ppm, while a singlet at δ 3.89 ppm represented the methoxy ($-OCH_3$) protons while singlet at δ 2.38 ppm corresponded to the methyl protons of the acetate group.In the ^{13}C NMR spectrum, the signals at δ 55.34 ppm corresponded to the methoxy carbon, while the signals at δ 21.06 ppm and δ 169.22 ppm were assigned to the methyl carbon and the ester carbonyl, respectively. The amide carbonyl appeared at δ 162.61 ppm, and the

aromatic carbons were observed between δ 107.34–147.22 ppm. The C=N carbon was assigned to δ 153.34 ppm, and the C-O methoxy carbon was observed at δ 158.53 ppm. The mass spectrum (ESI-MS) showed a molecular ion peak at m/z 398.08 $(M+H)^+$, confirming the molecular weight of the compound.

The spectral data of 4-{2-[(2-chloro-6-methoxyquinolin-3-yl)methylidene]hydrazine-1-carbonyl} phenyl propionate (4k) was used to confirm its structure with IR, NMR spectroscopy, and mass spectrometry. The IR spectrum showed a broad absorption at 3210 cm^{-1} corresponding to N-H stretching, while the strong absorption at 1650 cm^{-1} indicated C=O stretching, confirming the presence of a carbonyl group. The band at 1550 cm^{-1} was attributed to C=N stretching, confirming the imine group.

In the ^1H NMR spectrum, a singlet at δ 12.10 ppm was assigned to the N-H proton, and another singlet at δ 8.74 ppm corresponded to the imine proton. The aromatic protons were observed as multiplets between δ 7.10–8.69 ppm. A singlet at δ 3.92 ppm was attributed to the methoxy ($-OCH_3$) group, while a quartet at δ 2.66 ppm and a triplet at δ 1.28 ppm corresponded to the methylene and methyl protons of the propionate group, respectively.In the ^{13}C NMR spectrum, the signals at δ 9.08 ppm and δ 27.45 ppm were assigned to the methylene and methyl carbons of the propionate group, while the methoxy carbon resonated at δ 55.34 ppm. The aromatic carbons appeared between δ 107.34–147.22 ppm, and the C=N carbon was observed at δ 153.85 ppm. The ester carbonyl carbon was assigned to δ 172.53 ppm, and the amide carbonyl to δ 162.61 ppm. The mass spectrum (ESI-MS) showed a molecular ion peak at m/z 412.07 $(M+H)^+$, confirming the molecular weight of the compound.

The molecular structure of 4-{2-[(2-chloro-6-methoxyquinolin-3-yl) methylidene] hydrazine-1-carbonyl} phenyl butanoate (4l) was confirmed through spectral characterization with IR, NMR, and mass spectrometry data. The IR spectrum showed a broad absorption at 3150 cm^{-1} corresponding to N-H stretching,

while the band at 1620 cm^{-1} indicated C=O stretching, confirming the presence of the carbonyl group. The absorption at 1480 cm^{-1} was attributed to C=N stretching, confirming the imine group.

In the ^{1}H NMR spectrum, a singlet at δ 12.10 ppm corresponded to the N-H proton, while another singlet at δ 8.69 ppm was assigned to the imine proton. The aromatic protons appeared as multiplets between δ 7.11–8.68 ppm. A singlet at δ 3.86 ppm was assigned to the methoxy group ($-OCH_3$), while the triplet at δ 2.59 ppm, multiplet at δ 1.78 ppm, and singlet at δ 1.18 ppm corresponded to the methylene and methyl protons of the butanoate side chain.In the ^{13}C NMR spectrum, the signals at δ 13.65 ppm, δ 18.40 ppm, and δ 36.20 ppm were assigned to the methylene and methyl carbons of the butanoate chain. The methoxy carbon resonated at δ 55.34 ppm, while the aromatic carbons appeared between δ 107.34–147.22 ppm. The C=N carbon was observed at δ 153.21 ppm, with the ester carbonyl assigned to δ 171.94 ppm and the amide carbonyl at δ 162.61 ppm. The mass spectrum (ESI-MS) showed a molecular ion peak at m/z 426.14 $(M+H)^{+}$, confirming the molecular weight of the compound.

The spectral characterization of 4-{2-[(2-chloro-6-ethoxyquinolin-3-yl) methylidene] hydrazine-1-carbonyl} phenyl acetate (4m) was confirmed through IR, NMR, and mass spectrometry data. The IR spectrum displayed a broad absorption at 3500 cm^{-1}, corresponding to N-H stretching, while the strong band at 1620 cm^{-1} indicated C=O stretching, confirming the presence of the carbonyl group. The C=N stretching appeared at 1550 cm^{-1}, confirming the presence of the imine group.

In the ^{1}H NMR spectrum, a singlet at δ 11.87 ppm corresponded to the N-H proton, and another singlet at δ 8.98 ppm was assigned to the imine proton. The aromatic protons appeared as multiplets between δ 7.16–8.51 ppm, confirming the aromatic structure. The methylene protons of the ethoxy group resonated at δ 4.06 ppm, while the acetate methyl and ethyl protons appeared as singlets at δ 2.31 ppm

and δ 1.34 ppm, respectively.In the ^{13}C NMR spectrum, the signals at δ 9.1 ppm, δ 14.2 ppm, and δ 27.8 ppm were assigned to the ethyl and acetate carbons. The methylene carbon of the ethoxy group resonated at δ 64.3 ppm, while the aromatic carbons appeared between δ 106.4–131.7 ppm. The C=N carbon was observed at δ 150.5 ppm, the amide carbonyl carbon at δ 164.6 ppm, and the ester carbonyl carbon at δ 172.8 ppm. The mass spectrum (ESI-MS) showed molecular ion peak at 412.48 ($M+H^+$), confirming the molecular weight and formula.

The molecular structure of 4-{2-[(2-chloro-6-ethoxyquinolin-3-yl)methylidene]hydrazine-1-carbonyl}phenyl propanoate (4n) was confirmed using IR, NMR, and mass spectrometry data. The IR spectrum showed a broad absorption at 3480 cm^{-1} corresponding to N-H stretching, while a strong band at 1610 cm^{-1} indicated C=O stretching, confirming the presence of the carbonyl group. The C=N stretching was observed at 1520 cm^{-1}, indicating the imine group.

In the ^{1}H NMR spectrum, a singlet at δ 12.06 ppm corresponded to the N-H proton, and another singlet at δ 8.98 ppm was assigned to the imine proton. The aromatic protons were observed as multiplets between δ 7.16–8.51 ppm. The methylene protons of the ethoxy and propanoate groups resonated at δ 4.07 ppm and δ 2.61 ppm, while singlets at δ 1.34 ppm and δ 1.08 ppm were attributed to the methyl protons of the propanoate group. In the ^{13}C NMR spectrum, the signals at δ 9.3 ppm, δ 14.2 ppm, and δ 27.8 ppm were assigned to the methyl and methylene carbons of the propanoate side chain. The methylene carbon of the ethoxy group resonated at δ 64.3 ppm, while the aromatic carbons appeared between δ 106.8–131.9 ppm. The C=N carbon was observed at δ 150.6–150.8 ppm, and the amide carbonyl carbon at δ 164.1 ppm, with the ester carbonyl carbon at δ 172.6 ppm. The mass spectrum (ESI-MS) showed molecular ion peak at m/z 426.34 ($M+H^+$), confirming the molecular weight of the compound.

The spectral data of 4-{2-[(2-chloro-6-ethoxyquinolin-3-yl)methylidene]hydrazine-1-carbonyl} phenyl butanoate (4o) was used to confirm the structure of molecule using IR, NMR, and mass spectrometry. The IR spectrum showed a broad absorption at 3350 cm^{-1} corresponding to N-H stretching, while the strong absorption at 1590 cm^{-1} indicated C=O stretching, confirming the presence of a carbonyl group. The C=N stretching was observed at 1520 cm^{-1}, indicating the presence of an imine group.

In the ^{1}H NMR spectrum, a singlet at δ 12.17 ppm corresponded to the N-H proton, and another singlet at δ 8.98 ppm was assigned to the imine proton. The aromatic protons were observed as multiplets between δ 7.16–8.50 ppm, confirming the aromaticity of the molecule. The methylene protons of the ethoxy group resonated at δ 4.06 ppm, while the signals at δ 2.59 ppm, δ 1.51 ppm, δ 1.35 ppm, and δ 1.08 ppm corresponded to the methylene and methyl protons of the butanoate group.In the ^{13}C NMR spectrum, the signals at δ 9.1 ppm, δ 14.2 ppm, and δ 27.8 ppm were assigned to the methylene and methyl carbons of the butanoate group. The methylene carbon of the ethoxy group resonated at δ 64.3 ppm, while the aromatic carbons appeared between δ 106.4–131.7 ppm. The C=N carbon was observed at δ 150.6 ppm, while the amide carbonyl carbon appeared at δ 164.6 ppm, and the ester carbonyl carbon at δ 172.8 ppm. The mass spectrum (ESI-MS) showed molecular ion peak at m/z 440.65 ($M+H^{+}$), confirming the molecular weight of the compound.

The molecular structure of 4-{2-[(6-bromo-2-chloroquinolin-3-yl)methylidene]hydrazine-1-carbonyl} phenyl acetate (4p) was confirmed using IR, NMR, and mass spectrometry data. The IR spectrum displayed a broad absorption at 3490 cm^{-1}, corresponding to N-H stretching, while a strong band at 1620 cm^{-1} indicated C=O stretching, confirming the presence of a carbonyl group. The C=N stretching was observed at 1570 cm^{-1}, indicating the presence of an imine group.

In the ^{1}H NMR spectrum, a singlet at δ 12.04 ppm corresponded to the N-H proton, and another singlet at δ 9.04 ppm was assigned to the imine proton. The aromatic protons appeared as multiplets between δ 7.51–8.39 ppm, confirming the aromaticity of the compound. Additionally, a singlet at δ 2.59 ppm was attributed to the methyl protons of the acetate group. In the ^{13}C NMR spectrum, the signals at δ 21.0 ppm were assigned to the methyl carbon of the acetate group, while the aromatic carbons resonated between δ 114.3–132.7 ppm. The C=N carbon was observed at δ 150.5 ppm, and the amide carbonyl carbon appeared at δ 164.7 ppm, with the ester carbonyl carbon at δ 169.1 ppm. The mass spectrum (ESI-MS) showed molecular ion peak at m/z 447.64 ($M+H^{+}$), confirming the molecular weight of the compound.

The spectral characterization of 4-{2-2-[(6-bromo-2-chloroquinolin-3-yl)methylidene]hydrazine-1-carbonyl} phenyl propanoate (4q) was confirmed using IR, NMR, and mass spectrometry data. The IR spectrum showed a broad absorption at 3500 cm^{-1}, corresponding to N-H stretching, while the strong absorption at 1690 cm^{-1} indicated C=O stretching, confirming the presence of a carbonyl group. The C=N stretching appeared at 1540 cm^{-1}, confirming the imine group.

In the ^{1}H NMR spectrum, a singlet at δ 12.28 ppm corresponded to the N-H proton, and another singlet at δ 9.04 ppm was assigned to the imine proton. The aromatic protons were observed as multiplets between δ 7.51–8.39 ppm. Additionally, the methylene and methyl protons of the propanoate group resonated as a quartet at δ 2.61 ppm and a triplet at δ 1.28 ppm, respectively.In the ^{13}C NMR spectrum, the signals at δ 27.8 ppm were assigned to the methylene carbon of the propanoate group, while the aromatic carbons resonated between δ 114.3–132.7 ppm. The C=N carbon was observed at δ 150.5 ppm, the amide carbonyl carbon appeared at δ 164.7 ppm, and the ester carbonyl carbon was observed at δ 172.8

ppm. The mass spectrum (ESI-MS) showed molecular ion peaks at m/z 461.48 ($M+H^+$), confirming the molecular weight of the compound.

The spectral data of 4-{2-2-[(6-bromo-2-chloroquinolin-3-yl)methylidene]hydrazine-1-carbonyl} phenyl butanoate (4r) was used to confirm the molecular structure using IR, NMR, and mass spectrometry techniques. The IR spectrum showed a broad absorption at 3350 cm^{-1}, corresponding to N-H stretching, while a strong absorption at 1650 cm^{-1} indicated C=O stretching, confirming the presence of a carbonyl group. The C=N stretching was observed at 1490 cm^{-1}, confirming the imine group.

In the ^1H NMR spectrum, a singlet at δ 12.22 ppm corresponded to the N-H proton, and another singlet at δ 9.04 ppm was assigned to the imine proton. The aromatic protons were observed as multiplets between δ 7.51–8.39 ppm. The signals for the butanoate group included a triplet at δ 2.59 ppm for the methylene protons, a multiplet at δ 1.68 ppm for the methylene group, and a triplet at δ 0.99 ppm for the terminal methyl group. In the ^{13}C NMR spectrum, the signal at δ 20.2 ppm was assigned to the methylene carbon of the butanoate group. The aromatic carbons resonated between δ 114.3–132.7 ppm. The C=N carbon appeared at δ 150.5 ppm, the amide carbonyl carbon was observed at δ 164.7 ppm, and the ester carbonyl carbon was observed at δ 169.4 ppm. The mass spectrum (ESI-MS) showed molecular ion peak at m/z 475.84 ($M+H^+$), confirming the molecular weight of the compound.

5.2 BIOACTIVITY SCREENING OF ESTER DERIVATIVES OF 6-SUBSTITUTED-2-CHLOROQUINOLINE-3-CARBALDEHYDEHYDRAZIDE

5.2.1 *In vitro* Anti-Tubercular activity assessment using Microplate Alamar Blue assay

The Microplate Alamar Blue Assay (MABA) is a widely used method for assessing the viability and growth inhibition of *M. tuberculosis* and other microorganisms. It is based on the redox indicator and a non-fluorescent blue dye resazurin, which is metabolized by living cells into a fluorescent and colorimetric end product, resorufin (Figure 5.8). This transformation serves as an indicator of cellular metabolic activity and can be easily measured using a fluorescence or spectrophotometric plate reader.

In this assay, cells of *M.Tuberculosis*are incubated with test compounds in a 96-well microplate. After a defined incubation period, the Alamar Blue reagent (resazurin) is added to the wells. If the bacteria remain viable, they will reduce the resazurin into resorufin, leading to a colour change from blue to pink, which can be detected both visually and quantitatively using a plate reader. A lack of colour change indicates bacterial growth inhibition, reflecting the potency of compounds. The reduction of resazurin to resorufin is accompanied by a measurable shift in both absorbance and fluorescence. This can be quantified by measuring absorbance at 570 nm (reduced form) and 600 nm (oxidized form), or by measuring the fluorescent signal (excitation at 560 nm and emission at 590 nm)[140].

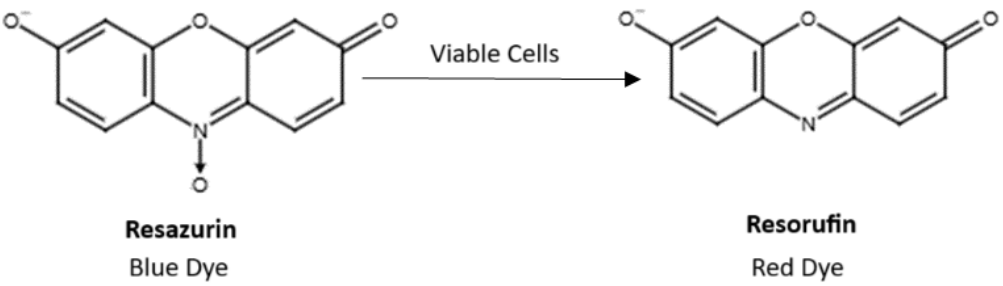

Figure 5.8: Conversion of Resazurin to Resorufin inMicroplate Alamar Blue assay method used for Anti-TB activity screening

The synthesized compounds 4a–4r were evaluated for their anti-tubercular activity against *M. tuberculosis* using the Alamar Blue Assay. The MIC values of the compounds were compared to standard anti-TB drugs such as Isoniazid, Ethambutol, Pyrazinamide, Rifampicin, and Streptomycin. The MIC values for the standard drugs ranged from 3.12 µg/ml (Rifampicin, Streptomycin) to 12.5 µg/ml (Pyrazinamide), serving as benchmarks for assessing the synthesized compounds (Figure 5.9).

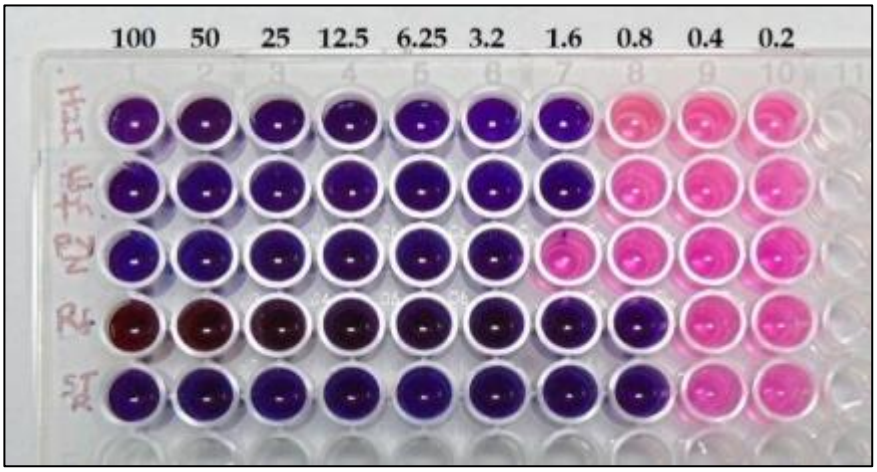

Figure 5.9: Microplate showing Alamar Blue assay results for antitubercular activity of standard Anti-TB drugs used as positive control; INH: Isoniazid, Eth: Ethambutol, Pyz: Pyrazinamide, Rf: Rifampicin, STR: Streptomycin (Blue colour: Sensitive / Anti-TB effect, Pink colour: Resistant/ No Anti-TB effect)

Table 5.10: Antitubercular activity assessment of positive control and synthesized molecules 4a – 4r using Microplate Alamar Blue assay method

Molecules	Concentration (µg/ml) of positive control and synthesized molecules 4a – 4r*							
	100	**50**	**25**	**12.5**	**6.25**	**3.12**	**1.6**	**0.8**
Isoniazid	S	S	S	S	S	R	R	R
Ethambutol	S	S	S	S	S	R	R	R
Pyrazinamide	S	S	S	S	R	R	R	R
Rifampicin	S	S	S	S	S	S	R	R
Streptomycin	S	S	S	S	S	S	R	R
4a	S	S	R	R	R	R	R	R
4b	S	R	R	R	R	R	R	R
4c	S	S	R	R	R	R	R	R
4d	S	S	R	R	R	R	R	R
4e	S	R	R	R	R	R	R	R
4f	S	R	R	R	R	R	R	R
4g	S	R	R	R	R	R	R	R
4h	S	R	R	R	R	R	R	R
4i	S	R	R	R	R	R	R	R
4j	S	R	R	R	R	R	R	R
4k	S	R	R	R	R	R	R	R
4l	S	S	R	R	R	R	R	R
4m	S	S	S	S	S	R	R	R
4n	S	S	S	S	R	R	R	R
4o	S	S	S	S	R	R	R	R
4p	S	S	S	S	R	R	R	R
4q	S	S	S	S	R	R	R	R
4r	S	S	S	S	S	R	R	R

* Coloured boxes represent MIC for positive control and test compounds

The synthesized compounds displayed a range of MIC values, with several showing promising anti-TB activity. Compounds 4m and 4r exhibited the highest potency, with MIC values of 6.25 µg/ml, comparable to Isoniazid and Ethambutol. Additionally, compounds 4n, 4o, 4p, and 4q showed moderate activity, with MIC values of 12.5 µg/ml,similar to Pyrazinamide. The results are presented in Figure 5.10 and Table 5.10. These findings indicate that specific structural modifications in the quinoline scaffold and ester linkage contribute to enhanced anti-tubercular activity.

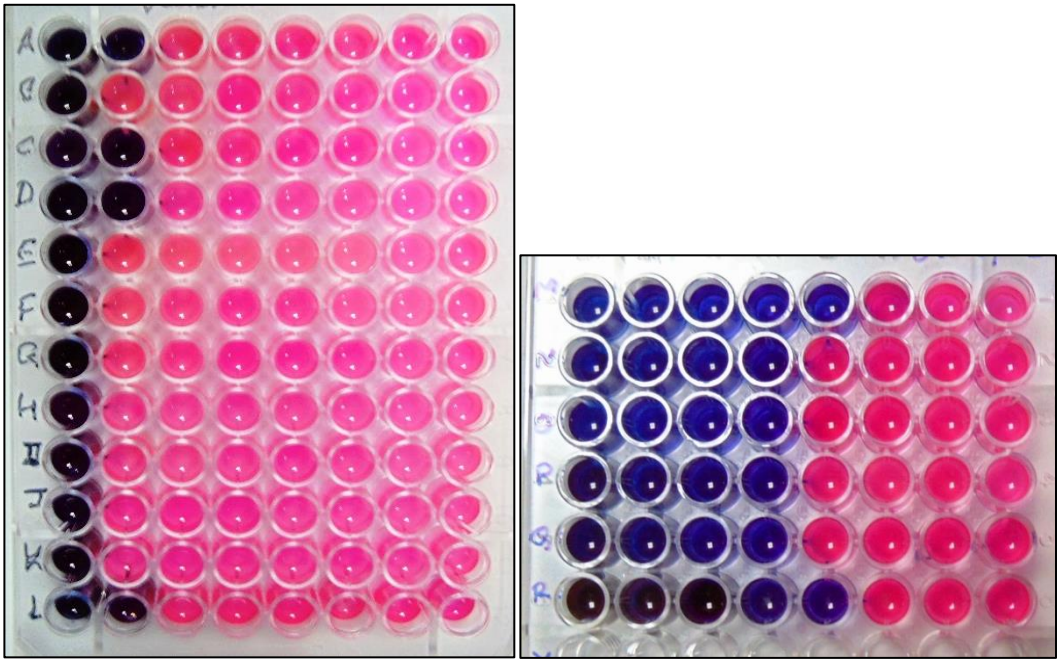

(i) **(ii)**

Figure 5.10: Microplate showing Alamar Blue assay results for antitubercular activity of synthesized molecules (i)4a – 4l and (ii)4m – 4r. Blue: Sensitive/Anti-TB effect, Pink: Resistant /No Anti-TB effect

SAR analysis revealed some key trends. Compounds 4a–4c, 4d–4f, 4g–4i, 4j–4l, 4m–4o, and 4p–4r share a common quinoline-based scaffold, differing in the carbon chain length of the ester linkages (acetate, propanoate, and butanoate).

Following are major observations related to chain length in the ester linkage -

1. Increasing the carbon chain length from acetate to propanoate resulted in reduced anti-TB activity. For example, compound 4a (acetate derivative) exhibited an MIC of 50 µg/ml, while compound 4b (propanoate derivative) showed lower activity, with an MIC of 100 µg/ml; compound 4e (propanoate derivative, MIC: 100 µg/ml) showed lower activity than 4d (acetate derivative, MIC: 50 µg/ml); compound 4m (acetate derivative, MIC: 6.25 µg/ml) showed higher activity than its propanoate derivative 4n with MIC value 12.5 µg/ml.
2. Increasing the carbon chain length from propanoate to butanoate resulted in increased anti-TB activity. For example, compound 4c (butanoate derivative, MIC: 50 µg/ml) showed higher activity than compound 4b (propanoate derivative, MIC: 100 µg/ml). Similar trend is seen for 4k (propanoate derivative, MIC: 100 µg/ml) to 4l (butanoate derivative, MIC: 50 µg/ml) and 4q (propanoate derivative, MIC: 12.5 µg/ml) to 4r (butanoate derivative, MIC: 6.25 µg/ml).

The comparative results of antitubercular activity of positive control and synthesized molecules are represented in Figure 5.11.

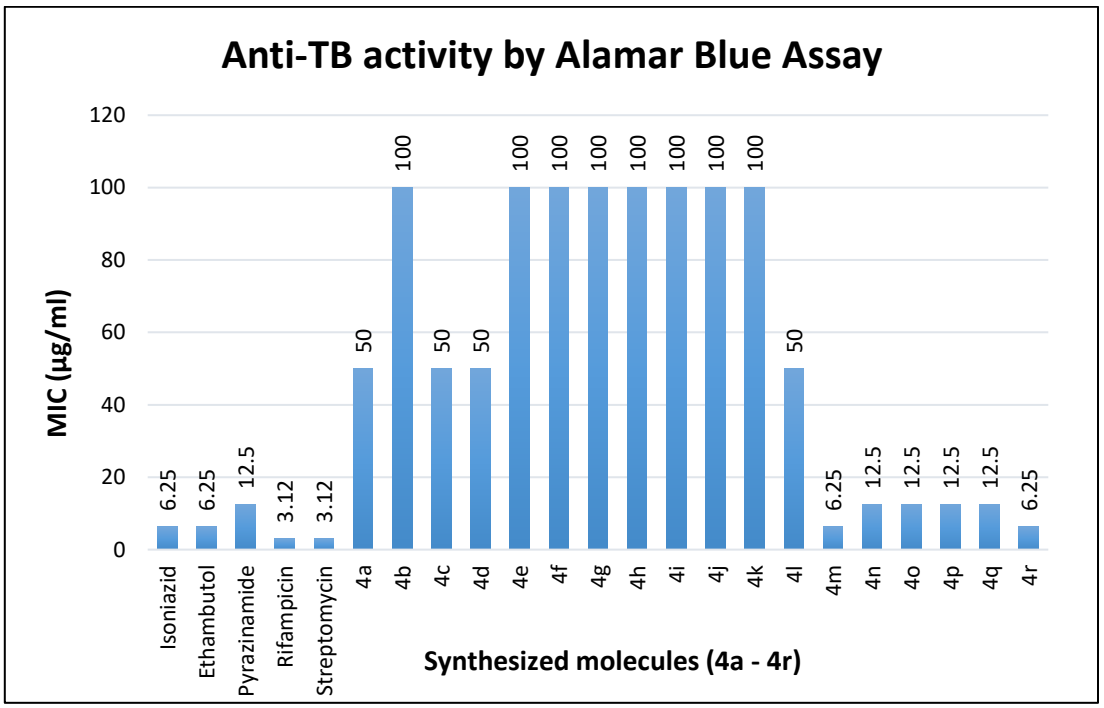

Figure 5.11: Comparison of MIC (µg/ml) values for antitubercular activity of positive control and synthesized molecules (4a – 4r)

Compounds 4m and 4r, both with MIC values of 6.25 µg/ml, were particularly notable. Compound 4m features a 2-chloro-6-ethoxy quinoline moiety with an acetate ester linkage, while compound 4r contains a 6-bromo-2-chloro quinoline moiety with a butanoate ester. These results suggest that variations in the ester linkage and substitutions on the quinoline ring can significantly enhance anti-TB activity.

5.2.2 *In vitro* Antibacterial activity assessment using Broth Microdilution method

The antibacterial activity of the synthesized compounds 4a-4r was determined using the broth microdilution assay, a standard method to assess the MIC of antimicrobial agents against bacteria. This method allows for the determination of the lowest concentration of a compound that inhibits visible bacterial growth in a liquid medium.

The broth microdilution method is based on the ability of a compound to inhibit bacterial growth in a nutrient broth medium. Bacterial cells are inoculated into a series of wells in a microtiter plate containing serial dilutions of the test compounds. After incubation, bacterial growth is assessed by turbidity, which indicates the presence of viable bacteria. The lowest concentration of the compound that prevents the visible turbidity in the wells is considered the MIC. The lower the MIC value, the more effective the compound is at inhibiting bacterial growth.

The synthesized compounds 4a–4r were evaluated for their antibacterial activity against both Gram-positive (*S. aureus*, *B. subtilis*) and Gram-negative (*K. pneumoniae*, *E. coli*) bacteria. Ciprofloxacin was used as the standard drug, with MIC values of 1.6 µg/ml (*S. aureus* and *K. pneumoniae*), 0.2 µg/ml (*B. subtilis*), and 1.6 µg/ml (*E. coli*). The MIC values for the synthesized molecules provide insight into their structure-activity relationships and overall efficacy against these bacterial strains.

5.2.2.1 Antibacterial activity of synthesized molecules 4a-4r against *S. aureus*

The MIC values against *S. aureus* ranged from 3.12 µg/ml to 25 µg/ml. Compound 4f and 4rshowed the most potent activity, with an MIC of 3.12 µg/ml, followed by compounds 4q, 4a, 4g and 4i, which exhibited MIC values of 6.25 µg/ml. These values, though higher than ciprofloxacin (1.6 µg/ml), indicated

reasonable antibacterial activity. The presence of halogen groups, especially in compound 4f (2,6-dichloro substitution), may have contributed to its enhanced activity. The remaining compounds, especially 4b, 4d, 4j, 4l, 4n, 4o and 4p, exhibited weaker activity, with MIC values of 25 µg/ml. The observations and results are presented in Figure 5.12 and Table 5.11. This suggests that certain structural features, such as the ester chain length or substitutions on the quinoline ring, may influence the effectiveness against *S. aureus*.

Table 5.11: Antibacterial activity assessment of positive control and synthesized molecules 4a – 4r against *S.Aureus*using Broth Microdilution method

Molecules	Concentration (µg/ml) of positive control and synthesized molecules 4a – 4r*									
	100	50	25	12.5	6.25	3.12	1.6	0.8	0.4	0.2
Ciprofloxacin	S	S	S	S	S	S	S	R	R	R
4a	S	S	S	S	S	R	R	R	R	R
4b	S	S	S	R	R	R	R	R	R	R
4c	S	S	S	S	R	R	R	R	R	R
4d	S	S	S	R	R	R	R	R	R	R
4e	S	S	S	S	R	R	R	R	R	R
4f	S	S	S	S	S	S	R	R	R	R
4g	S	S	S	S	S	R	R	R	R	R
4h	S	S	S	S	R	R	R	R	R	R
4i	S	S	S	S	S	R	R	R	R	R
4j	S	S	S	R	R	R	R	R	R	R
4k	S	S	S	S	R	R	R	R	R	R
4l	S	S	S	R	R	R	R	R	R	R
4m	S	S	S	S	R	R	R	R	R	R
4n	S	S	S	R	R	R	R	R	R	R
4o	S	S	S	R	R	R	R	R	R	R
4p	S	S	S	R	R	R	R	R	R	R

Molecules	Concentration (µg/ml) of positive control and synthesized molecules 4a – 4r*									
	100	**50**	**25**	**12.5**	**6.25**	**3.12**	**1.6**	**0.8**	**0.4**	**0.2**
4q	S	S	S	S	S	R	R	R	R	R
4r	S	S	S	S	S	S	R	R	R	R

* Coloured boxes represent MIC for positive control and test compounds. S: Sensitive (No turbidity = inhibition of microbial growth/Antibacterial effect),
R: Resistant (Presence of turbidity = Microbial growth/ No Antibacterial effect)

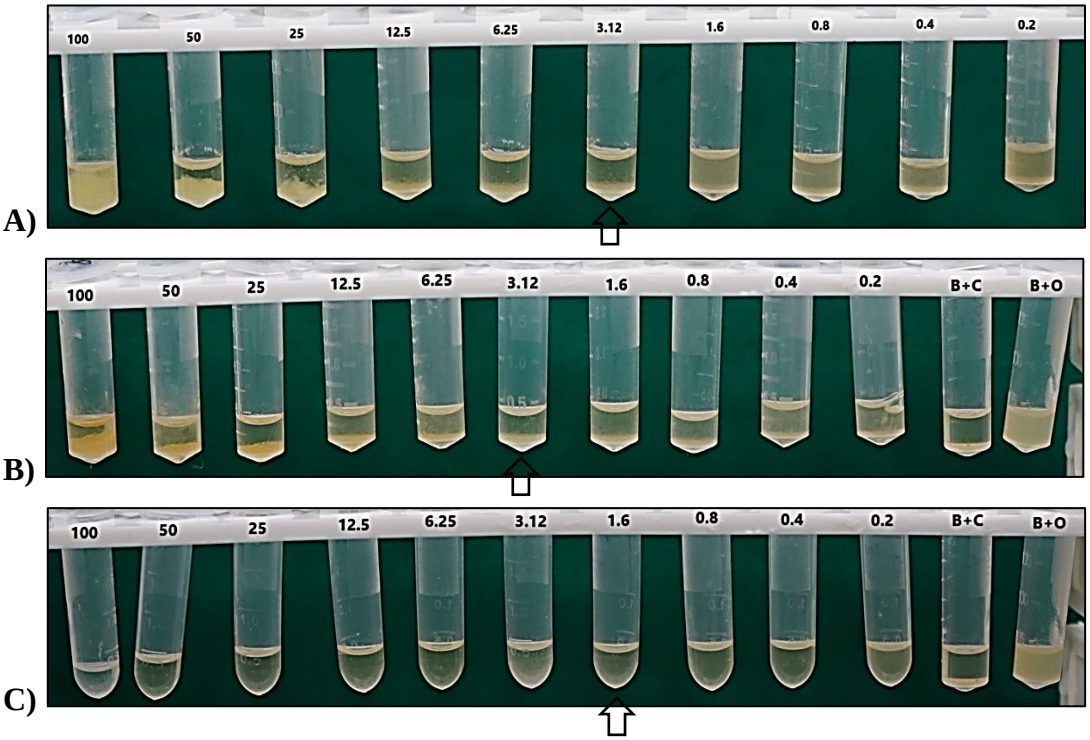

Figure 5.12: Assessment of antibacterial activity of synthesized molecules A) 4f, MIC = 3.12 µg/ml, B) 4r, MIC = 3.12 µg/mland C) positive control - Ciprofloxacin, MIC = 1.6 µg/ml against *S.Aureus*by observingturbidityin Broth microdilution method (B+C = Broth + control and B+O = Broth + Organism). Yellow coloured arrow indicates MIC for the positive control andsynthesized compounds

For *S. aureus*, the presence of two halogens in the quinoline structure along with ester linkage, appears to enhance antibacterial activity.For 2,6-dichloro

derivatives, i.e. 4d, 4e and 4f, compound 4f with longest ester linkage (butanoate ester) demonstrated the most potent activity against *S. aureus*, with MIC of 3.12 µg/ml, compared to 4d (acetate ester, MIC: 25 µg/ml) and 4e (propanoate ester, MIC: 12.5 µg/ml).

Similarly, among 2-chloro-6-bromo derivatives, i.e. 4p, 4q and 4r, compound 4r with butanoate ester linkage displayed strong antibacterial activity with MIC of 3.12 µg/ml (similar to 4f) compared to 4p (acetate ester, MIC: 25 µg/ml) and 4q (propanoate ester, MIC: 6.25 µg/ml). The comparative results of antibacterial activity of positive control and synthesized molecules are represented in Figure 5.13.

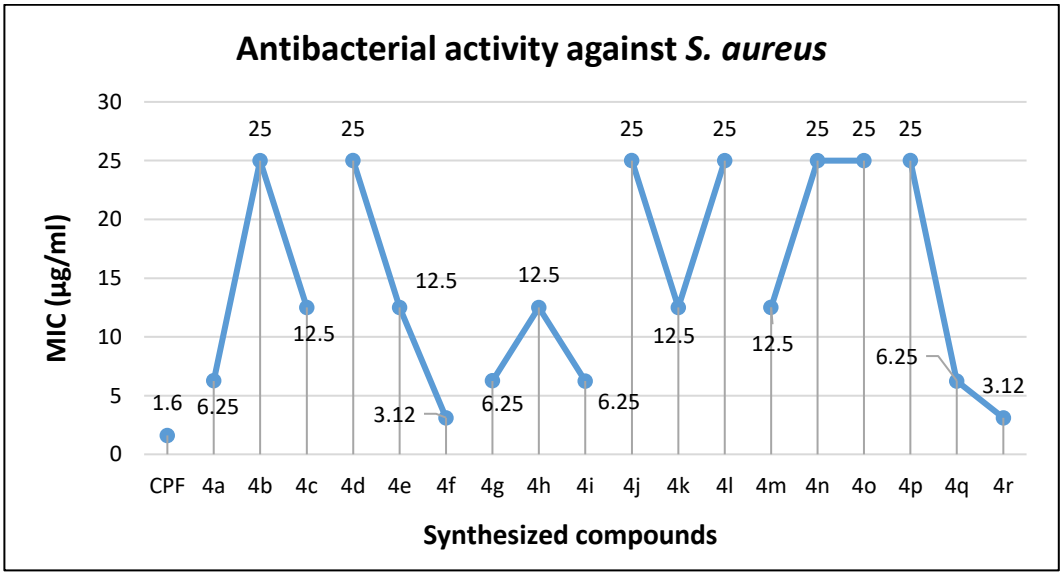

Figure 5.13: Comparison of MIC (µg/ml) values for antibacterial activity of positive control (CPF: Ciprofloxacin) and synthesized molecules (4a – 4r) against *S. aureus*

Compound 4a with 2-chloroquinoline moiety and acetate ester showed significant activity (MIC: 6.25 µg/ml). Increasing the length of ester linkage to propanoate (MIC: 25 µg/ml) and butanoate (MIC: 12.5 µg/ml) led to decrease in antibacterial activity.

5.2.2.2 Antibacterial activity of synthesized molecules 4a-4r against *B. subtilis*

Most of the synthesized compounds exhibited MIC values in the range of 0.8 – 12.5 µg/ml against *B. subtilis* compared to ciprofloxacin (0.2 µg/ml). However, compounds 4r and 4p displayed significant antibacterial activity, with MIC values of 1.6 µg/ml and 0.8 µg/ml, respectively. Compound 4n and 4o also showed good activity, with an MIC of 3.12 µg/ml. These results indicate that compounds with specific substitutions, such as 4r and 4p, could be potential leads for targeting Gram-positive bacteria like *B. subtilis*. In contrast, compounds like 4a, and 4b, which had MIC values of 25 µg/ml and 50 µg/ml, exhibited lower antibacterial activity. Theobservations and results are presented in Table 5.12 and Figure 5.14.

Table 5.12: Antibacterial activity assessment of positive control and synthesized molecules 4a – 4r against *B. subtilis* using Broth Microdilution method

Molecules	Concentration (µg/ml) of positive control and synthesized molecules 4a – 4r*									
	100	50	25	12.5	6.25	3.12	1.6	0.8	0.4	0.2
Ciprofloxacin	S	S	S	S	S	S	S	S	S	S
4a	S	S	S	R	R	R	R	R	R	R
4b	S	S	R	R	R	R	R	R	R	R
4c	S	S	S	S	R	R	R	R	R	R
4d	S	S	S	S	S	R	R	R	R	R
4e	S	S	S	S	R	R	R	R	R	R
4f	S	S	S	S	R	R	R	R	R	R
4g	S	S	S	S	S	R	R	R	R	R
4h	S	S	S	S	R	R	R	R	R	R
4i	S	S	S	S	R	R	R	R	R	R
4j	S	S	S	S	R	R	R	R	R	R
4k	S	S	S	S	R	R	R	R	R	R
4l	S	S	S	S	R	R	R	R	R	R
4m	S	S	S	S	R	R	R	R	R	R

Molecules	Concentration (µg/ml) of positive control and synthesized molecules 4a – 4r*									
	100	**50**	**25**	**12.5**	**6.25**	**3.12**	**1.6**	**0.8**	**0.4**	**0.2**
4n	S	S	S	S	S	S	R	R	R	R
4o	S	S	S	S	S	S	R	R	R	R
4p	S	S	S	S	S	S	S	S	R	R
4q	S	S	S	S	S	R	R	R	R	R
4r	S	S	S	S	S	S	S	R	R	R

* Coloured boxes represent MIC for positive control and test compounds. S: Sensitive (No turbidity = inhibition of microbial growth/Antibacterial effect), R: Resistant (Presence of turbidity = Microbial growth/ No Antibacterial effect)

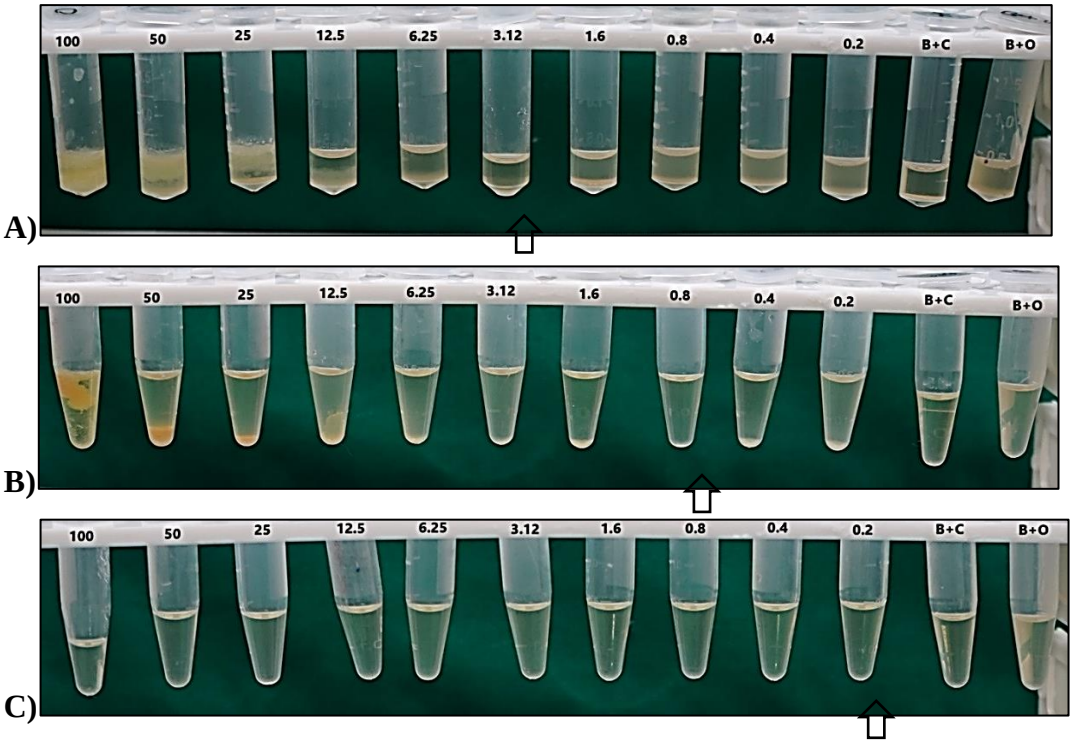

Figure 5.14: Assessment of antibacterial activity of synthesized molecules A) 4o, MIC = 3.12 µg/ml, B) 4p, MIC = 0.8 µg/ml and C) positive control - Ciprofloxacin, MIC = 0.2 µg/ml against *B. subtilis* by observing turbidity in Broth microdilution method (B+C = Broth + control and B+O = Broth + Organism). Yellow coloured arrow indicates MIC for the positive control and synthesized compound.

The synthesized molecules 4d (MIC: 6.25 µg/ml), 4e (MIC: 12.5 µg/ml) and 4f(MIC: 12.5 µg/ml) with 2,6-dichloro substitution on quinoline backbone, showed decrease in antibacterial activity against *B. subtilis* with increasing the ester linkage length. Similar effect was observed for the molecules with 2-chloro-6-methyl substitution on quinoline ring i.e. 4g (MIC: 6.25 µg/ml), 4h (MIC: 12.5 µg/ml) and 4i(MIC: 12.5 µg/ml). The comparative results of antibacterial activity of positive control and synthesized molecules are represented in Figure 5.15.

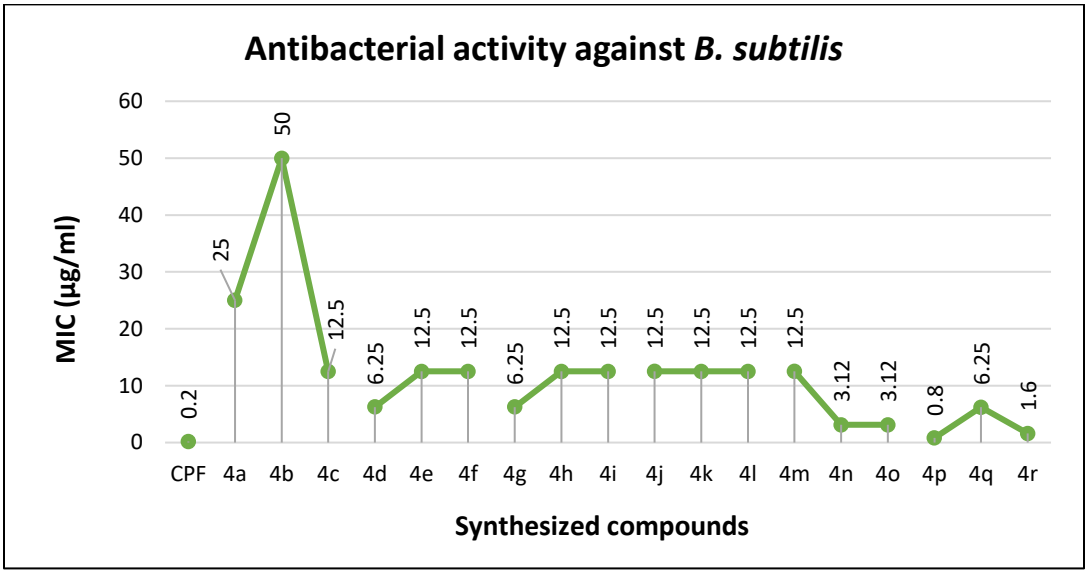

Figure 5.15: Comparison of MIC (µg/ml) values for antibacterial activity of positive control (CPF: Ciprofloxacin) and synthesized molecules (4a – 4r) against *B. subtilis*

The molecules with 2-chloro-6-ethoxy substitution on quinoline ring, i.e. 4m (acetate ester), 4n (propanoate ester) and 4o (butanoate ester), showed increased antibacterial activity with increasing the chain length from acetate (MIC: 12.5 µg/ml) to propanoate and butanoate (MIC: 3.12 µg/ml).

The molecules with 6-methoxy substitution,viz, 4j, 4k and 4l, did not show any change in antibacterial activity (MIC: 12.5 µg/ml) with change in ester linkage from acetate to butanoate.

5.2.2.3 Antibacterial activity of synthesized molecules 4a-4r against *K. pneumoniae*

The MIC values against *K. pneumoniae* ranged from 12.5 µg/ml to 50 µg/ml, with compound 4r exhibiting the lowest MIC of 12.5 µg/ml. The compounds like 4c, 4f, and 4r with butanoate ester linkage showed better activity than their corresponding acetate and propanoate ester derivatives. These results suggest that the variations in the ester group and quinoline ring play a role in inhibiting *K. pneumoniae*. Despite these results, none of the synthesized compounds were as potent as ciprofloxacin, which had an MIC of 1.6 µg/ml. The observations and results are presented in Table 5.13 and Figure 5.16.

Table 5.13: Antibacterial activity assessment of positivecontrol and synthesized molecules 4a – 4r against *K.Pneumoniae*using Broth Microdilution method

Molecules	Concentration (µg/ml) of positive control and synthesized molecules 4a – 4r*									
	100	**50**	**25**	**12.5**	**6.25**	**3.12**	**1.6**	**0.8**	**0.4**	**0.2**
Ciprofloxacin	S	S	S	S	S	S	S	R	R	R
4a	S	S	R	R	R	R	R	R	R	R
4b	S	S	R	R	R	R	R	R	R	R
4c	S	S	S	R	R	R	R	R	R	R
4d	S	S	R	R	R	R	R	R	R	R
4e	S	S	R	R	R	R	R	R	R	R

Molecules	Concentration (µg/ml) of positive control and synthesized molecules 4a – 4r*									
	100	**50**	**25**	**12.5**	**6.25**	**3.12**	**1.6**	**0.8**	**0.4**	**0.2**
4f	S	S	S	R	R	R	R	R	R	R
4g	S	S	R	R	R	R	R	R	R	R
4h	S	S	R	R	R	R	R	R	R	R
4i	S	S	R	R	R	R	R	R	R	R
4j	S	S	S	R	R	R	R	R	R	R
4k	S	S	S	R	R	R	R	R	R	R
4l	S	S	S	R	R	R	R	R	R	R
4m	S	S	S	R	R	R	R	R	R	R
4n	S	S	S	R	R	R	R	R	R	R
4o	S	S	R	R	R	R	R	R	R	R
4p	S	S	S	R	R	R	R	R	R	R
4q	S	S	S	R	R	R	R	R	R	R
4r	S	S	S	S	R	R	R	R	R	R

* Coloured boxes represent MIC for positive control and test compounds. S: Sensitive (No turbidity = inhibition of microbial growth/Antibacterial effect),
R: Resistant (Presence of turbidity = Microbial growth/ No Antibacterial effect)

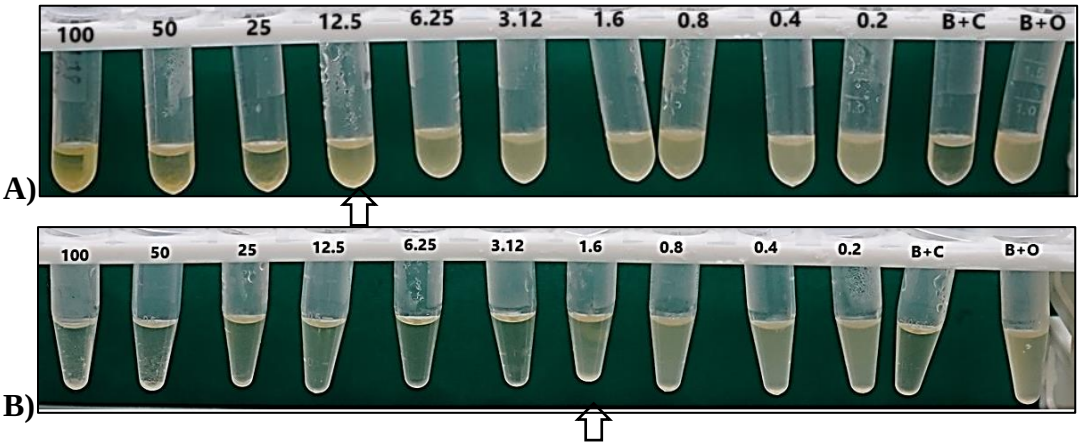

Figure 5.16: Assessment of antibacterial activity of synthesized molecules A) 4r, MIC = 12.5 µg/ml, and B) positivecontrol - Ciprofloxacin, MIC = 1.6 µg/ml

against *K. pneumoniae* by observing turbidity in Broth microdilution method (B+C = Broth + control and B+O = Broth + Organism). Yellow coloured arrow indicates MIC for the positive control and synthesized compound.

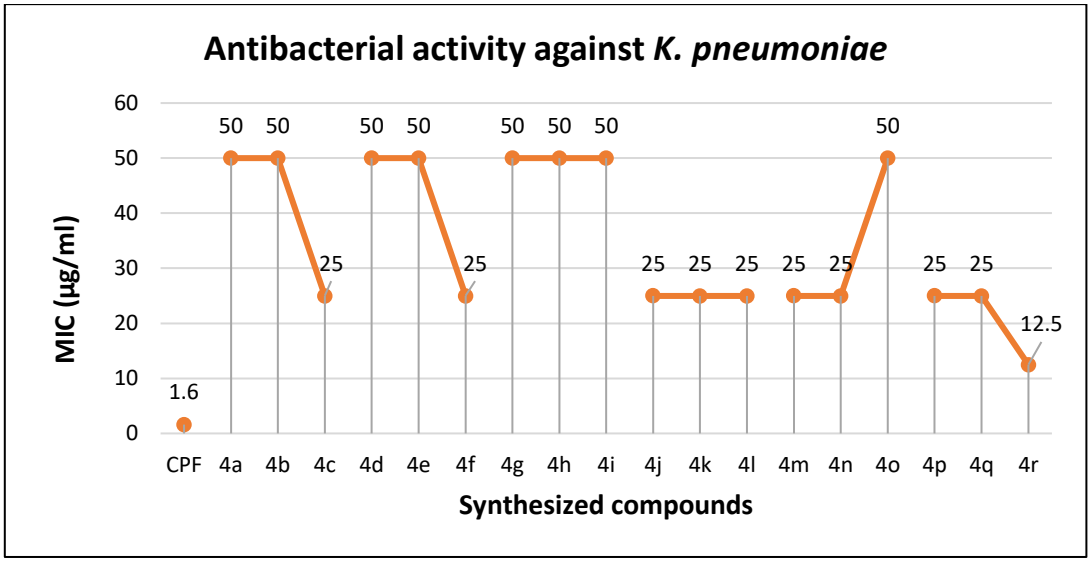

Figure 5.17: Comparison of MIC (µg/ml) values for antibacterial activity of positive control (CPF: Ciprofloxacin) and synthesized molecules (4a – 4r) against *K. pneumoniae*

Many compounds like 4g, 4h, 4i, 4j, 4k, 4l, 4m, and 4nshowed weak antibacterial activity with MIC values in the range of 25-50 µg/ml.No change in the activity was observed with change in length of ester linkage and substitution at 6^{th} position on quinoline ring. Compound 4o with butanoate ester showed loss of activity compared to its corresponding derivatives with acetate (4m) and propanoate (4n) linkage. The comparative results of antibacterial activity of positive control and synthesized molecules are represented in Figure 5.17.

5.2.2.4 Antibacterial activity of synthesized molecules 4a-4r against *E. coli*

Against *E. coli*, the MIC values ranged from 6.25 µg/ml to 100 µg/ml. Compound 4o demonstrated the highest potency, with an MIC of 6.25 µg/ml, followed by compounds 4n, 4r, and 4q, which exhibited MIC values of 12.5 µg/ml. This trend indicates that the butanoate derivatives (such as 4r) and ethoxy-substituted quinoline derivatives (like 4n and 4o) have a significant effect against Gram-negative bacteria like *E. coli*. However, compounds such as 4a, 4e, 4f, and 4g exhibited lower activity, with MIC values of 50–100 µg/ml. The observations and results are presented in Table 5.14 and Figure 5.18.

Table 5.14: Antibacterial activity assessment of positive control and synthesized molecules 4a – 4r against *E. coli* using Broth Microdilution method

Molecules	Concentration (µg/ml) of positive control and synthesized molecules 4a – 4r*									
	100	50	25	12.5	6.25	3.12	1.6	0.8	0.4	0.2
Ciprofloxacin	S	S	S	S	S	S	S	R	R	R
4a	S	S	R	R	R	R	R	R	R	R
4b	S	R	R	R	R	R	R	R	R	R
4c	S	S	R	R	R	R	R	R	R	R
4d	S	S	R	R	R	R	R	R	R	R
4e	S	R	R	R	R	R	R	R	R	R
4f	S	R	R	R	R	R	R	R	R	R
4g	S	R	R	R	R	R	R	R	R	R
4h	S	R	R	R	R	R	R	R	R	R
4i	S	R	R	R	R	R	R	R	R	R
4j	S	R	R	R	R	R	R	R	R	R
4k	S	R	R	R	R	R	R	R	R	R

Molecules	Concentration (µg/ml) of positive control and synthesized molecules 4a – 4r*									
	100	**50**	**25**	**12.5**	**6.25**	**3.12**	**1.6**	**0.8**	**0.4**	**0.2**
4l	S	R	R	R	R	R	R	R	R	R
4m	S	S	S	R	R	R	R	R	R	R
4n	S	S	S	S	R	R	R	R	R	R
4o	S	S	S	S	S	R	R	R	R	R
4p	S	S	S	R	R	R	R	R	R	R
4q	S	S	S	S	R	R	R	R	R	R
4r	S	S	S	S	R	R	R	R	R	R

* Coloured boxes represent MIC for positivecontrol and test compounds. S: Sensitive (No turbidity = inhibition of microbial growth/Antibacterial effect),
R: Resistant (Presence of turbidity = Microbial growth/ No Antibacterial effect)

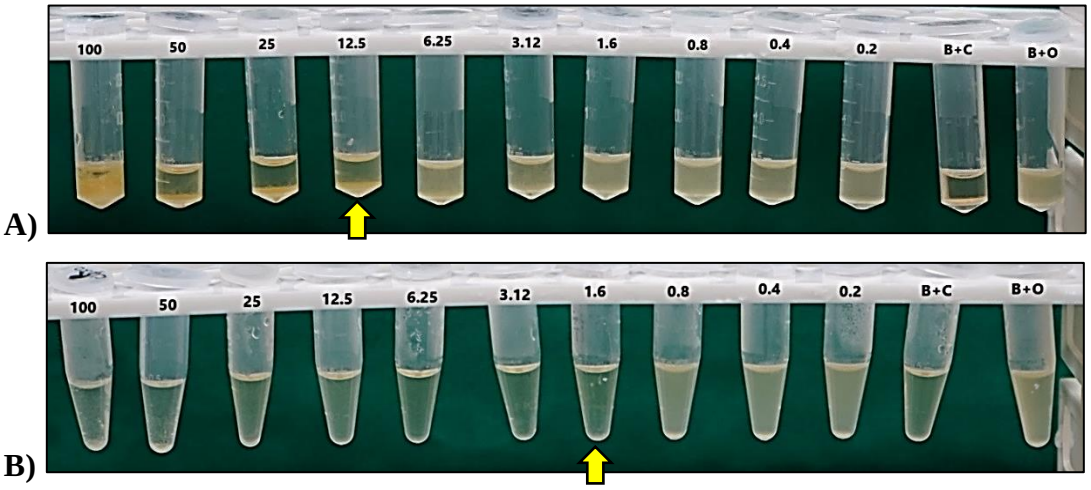

Figure 5.18: Assessment of Antibacterial activity of synthesized molecules A) 4q, MIC = 12.5 µg/ml, and B) positive control - Ciprofloxacin, MIC = 1.6 µg/ml against *E. Coli*by observing turbidity in Broth microdilution method (B+C = Broth + control and B+O = Broth + Organism). Yellow coloured arrow indicates MIC for the positive controland synthesized compound.

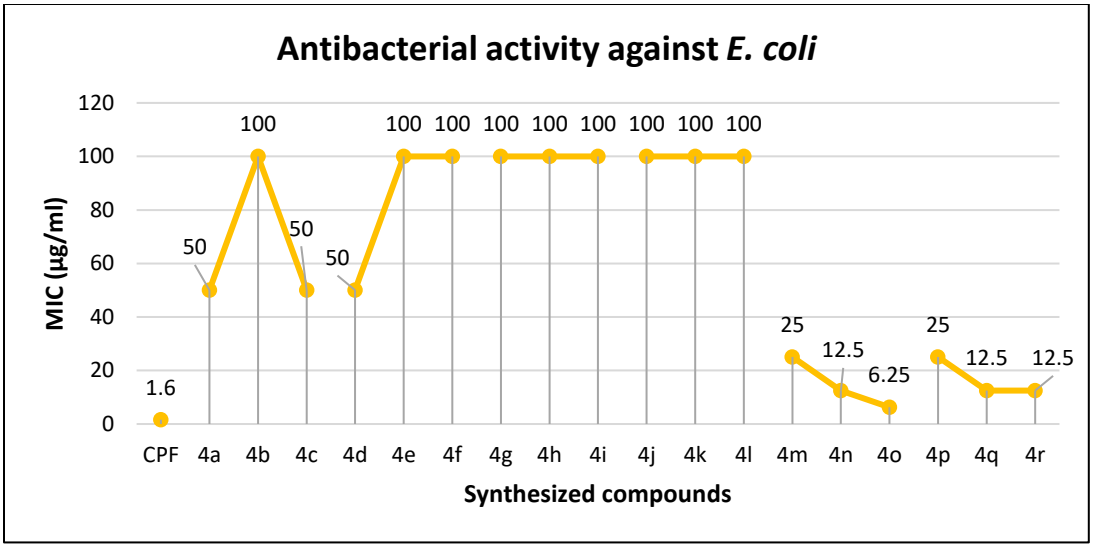

Figure 5.19: Comparison of MIC (µg/ml) values for antibacterial activity of positive control (CPF: Ciprofloxacin) and synthesized molecules (4a – 4r) against *E. coli*

The observed antibacterial activity trends provide valuable insights into the SAR of the synthesized compounds -

1. Compounds with the 6-bromo-2-chloro substitution (e.g., 4r and 4p) demonstrated enhanced activity against both Gram-positive and Gram-negative bacteria, highlighting the importance of halogen substitutions at specific positions on the quinoline ring for antibacterial potency.
2. The variation in ester chain length also played a critical role in antibacterial activity. For instance, compound 4r (butanoate derivative) exhibited potent activity against both *S. aureus* and *K. pneumoniae*, whereas compounds with shorter ester chains, such as 4a and 4b, generally displayed lower activity.

The comparative results of antibacterial activity of positive control and synthesized molecules are represented in Figure 5.19.

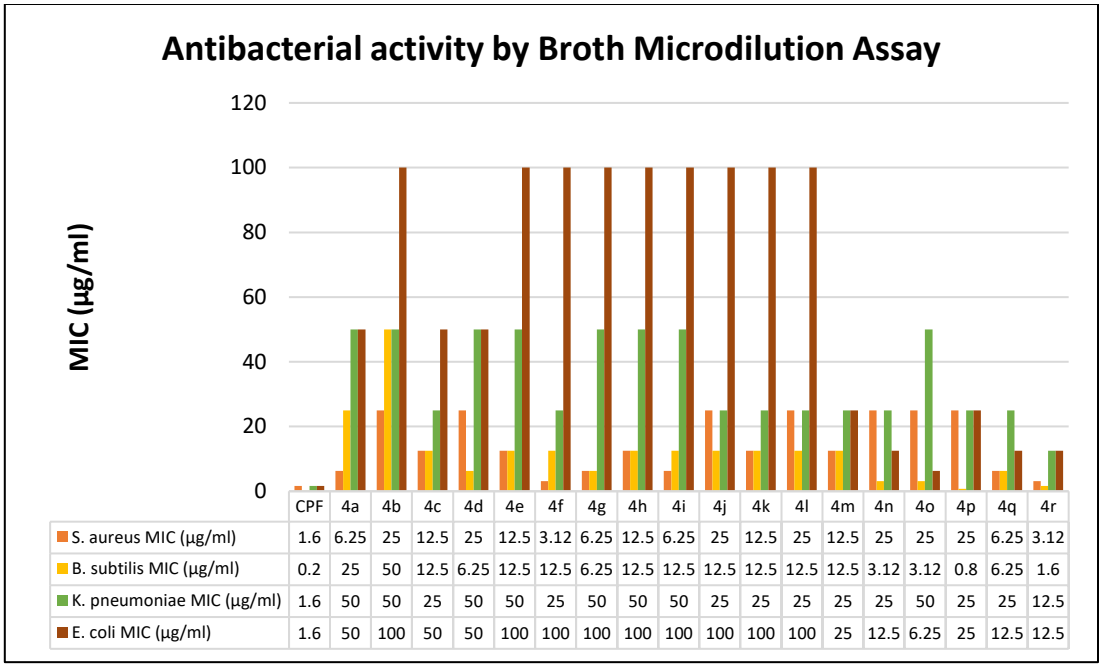

	CPF	4a	4b	4c	4d	4e	4f	4g	4h	4i	4j	4k	4l	4m	4n	4o	4p	4q	4r
S. aureus MIC (µg/ml)	1.6	6.25	25	12.5	25	12.5	3.12	6.25	12.5	6.25	25	12.5	25	12.5	25	25	25	6.25	3.12
B. subtilis MIC (µg/ml)	0.2	25	50	12.5	6.25	12.5	12.5	6.25	12.5	12.5	12.5	12.5	12.5	12.5	3.12	3.12	0.8	6.25	1.6
K. pneumoniae MIC (µg/ml)	1.6	50	50	25	50	50	25	50	50	50	25	25	25	25	25	50	25	25	12.5
E. coli MIC (µg/ml)	1.6	50	100	50	50	100	100	100	100	100	100	100	100	25	12.5	6.25	25	12.5	12.5

Figure 5.20: Overview of MIC (µg/ml) values for antibacterial activity of positive control (CPF: Ciprofloxacin) and synthesized molecules (4a – 4r) against *S. aureus, E. coli, K. pneumoniae* and*E. coli*

The synthesized quinoline derivatives exhibited varying degrees of antibacterial activity, with compounds like 4r, 4o, 4n, 4q, and 4f showing promising results against multiple bacterial strains (Figure 5.20). The differences in activity can be attributed to the structural variations in the ester linkage and substitutions on the quinoline ring, which significantly influence the potency against both Gram-positive and Gram-negative bacteria.

5.2.3 *In vitro* Cytotoxicity screening using MTT assay

The cytotoxicity of the synthesized compounds (4a, 4c, 4d, 4l, 4m and 4r) with significant Anti-TB and antibacterialactivity(against *S. aureus*, *B. subtilis*, *K. pneumoniae*, and *E. coli*) was evaluated using the MTT assay in two different cell lines: A549 (human lung carcinoma) and Vero (African green monkey kidney) cell lines.

The MTT assay is a colorimetric assay used to measure cell viability and cytotoxicity by evaluating the metabolic activity of living cells. The MTT assay relies on the ability of viable cells to reduce the yellow, water-soluble tetrazolium salt, MTT (3-(4,5-dimethylthiazol-2-yl)-2,5-diphenyl tetrazolium bromide), into insoluble purple formazan crystals. This reduction is mediated by mitochondrial enzymes (principally NAD(P)H-dependent oxidoreductases), which are only active in metabolically active (live) cells[140] (Figure 5.21).

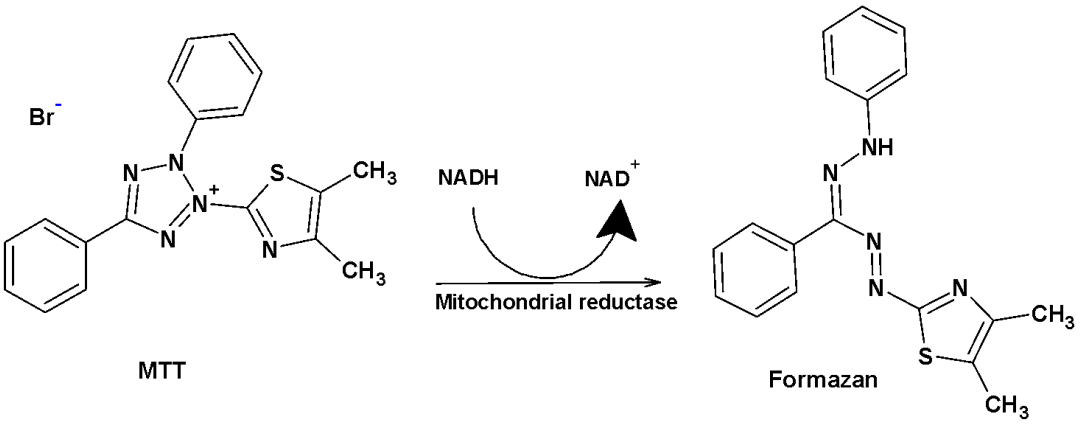

Figure 5.21: Chemical reaction involved in MTT assay for cell viability

Cells are seeded in a 96-well plate and treated with test compounds at varying concentrations. The plate is incubated for a specific time to allow the compound to exert its effects on cell viability. After incubation with the compounds, MTT reagent

is added to each well. Viable cells will reduce the MTT reagent to form purple formazan crystals, while non-viable cells will not. The plate is incubated for a few hours (typically 2–4 hours) to allow sufficient formazan crystal formation in the viable cells. After incubation, the formazan crystals are dissolved using a solubilizing agent, like DMSO or a similar reagent, to convert the insoluble crystals into a coloured solution. The absorbance of the solution is then measured at 570 nm using a microplate reader. The amount of formazan formed is directly proportional to the number of viable cells in each well. The optical density (OD) is recorded, and cell viability is quantified. Higher Absorbance indicates a higher number of viable cells, as more MTT has been reduced to formazan. Lower Absorbance suggests a reduction in cell viability, indicating cytotoxic effects of the tested compound.

Both *M. tuberculosis* and cancer cells rely on similar biological pathways for survival, growth, and proliferation. Many anti-TB drugs and compounds targeting specific bacterial enzymes, metabolic pathways, or DNA replication also affect rapidly dividing cells like cancer cells. For instance, drugs that interfere with nucleotide biosynthesis or inhibit enzymes critical for DNA replication in *M. tuberculosis* may also show cytotoxicity against cancer cells due to their ability to halt cell division. Many anti-TB drugs share common mechanisms such as induction of oxidative stress through generation of reactive oxygen species (ROS), tubulin polymerization, modulation of host immune response andregulation of cell cycle with anticancer drugs. Hence, it is important to study cytotoxicity of anti-TB drugs especially in normal cells[141-145].

In this study, the cytotoxic potential of the compounds was assessed to determine their selectivity and safety profile, providing insights into their therapeutic window and possible off-target effects. The results from both cell lines wereanalysed to compare cytotoxicity at concentrations relevant to their antimicrobial activity

5.2.3.1 Cytotoxicity assay with Lung Carcinoma A549 cell lines

A549 cells, derived from human lung carcinoma, are widely used in cytotoxicity assays due to their relevance in studying lung cancer cell viability. These cells provide a model to evaluate the potential cytotoxic effects of new compounds, particularly in the context of lung-related diseases such as tuberculosis (TB) and lung cancer.

There is growing interest in the relationship between *M. tuberculosis* infections and lung cancer, as chronic inflammation caused by TB has been associated with an increased risk of lung cancer development. Thus, testing compounds that demonstrate both anti-TB and anticancer activity in lung cells is significant, as they could offer dual therapeutic potential.

The results of cytotoxicity study at concentrations of 3.125, 6.25, 12.5, 25, 50 and 100 µg/ml along with IC_{50} values for the synthesized compounds in A549 cells were represented in Table 5.15, Table 5.16 and Figure 5.22 with a plot of cell viability % vs concentration of compounds in µg/ml. Doxorubicin was used as positive control and the cytotoxic effects are depicted in Table 5.17.

Table 5.15: Cytotoxic activity assessment of synthesized molecules 4a, 4c and 4d using MTT assay method (n=3) for A549 cell line

Concentration (µg/ml)	**Cell viability readings for A549 cell line at 570 nm**								
	4a			**4c**			**4d**		
100	40.47	40.63	40.39	11.03	11.19	10.95	14.03	14.52	14.27
50	61.39	60.99	61.23	40.71	40.79	40.63	41.28	40.79	41.20
25	65.04	65.37	65.21	69.34	69.42	69.26	63.75	63.50	63.67
12.5	74.45	74.29	74.37	73.48	73.72	73.64	77.86	77.94	78.02
6.25	83.62	84.02	83.86	85.89	85.40	85.48	88.24	88.00	88.16
3.125	94.73	94.81	94.16	89.94	89.62	89.78	90.02	90.43	90.27
Negative Control	100			100			100		
IC_{50} (µg/ml)	74.57			47.32			48.64		
Standard	0.07			0.06			0.04		

Concentration (µg/ml)	**Cell viability readings for A549 cell line at 570 nm**		
	4a	**4c**	**4d**
Deviation			

Table 5.16: Cytotoxic activity assessment of synthesized molecules 4l, 4m and 4r using MTT assay method (n=3) for A549 cell line

Concentration (µg/ml)	**Cell viability readings for A549 cell line at 570 nm**								
	4l			**4m**			**4r**		
100	36.42	36.09	36.33	40.79	40.47	40.63	33.58	33.82	33.74
50	54.18	54.42	54.34	51.42	51.74	51.58	55.64	55.80	55.72
25	68.05	68.05	68.21	76.40	76.32	76.56	65.61	65.29	65.45
12.5	69.51	69.67	69.59	81.35	81.75	81.59	68.13	68.37	68.29
6.25	73.88	74.05	74.13	84.35	84.43	84.51	77.78	77.70	77.62
3.125	89.46	90.92	89.54	96.19	96.59	96.43	85.40	84.27	85.24
Negative Control	100			100			100		
IC_{50} value (µg/ml)	65.71			72.97			62.94		
Standard Deviation	0.07			0.02			0.08		

Table 5.17: Cytotoxic activity assessment of positive control using MTT assay method (n=3) for A549 cell line

Concentration (µg/ml)	**Cell viability readings for A549 cell line at 570 nm (Doxorubicin)**		
100	11.13	11.38	11.13
50	29.16	29.28	29.16
25	35.17	35.29	35.17
12.5	45.14	45.27	45.14
6.25	47.95	48.08	47.95
3.125	49.10	49.23	49.42
Negative Control	100		
IC_{50} value (µg/ml)	2.15		
Standard Deviation	0.04		

Compounds 4m and 4r, which exhibited the highest anti-TB activity (MIC of 6.25 µg/ml), showed relatively low cytotoxicity in A549 cells, with IC_{50} values of

72.97 µg/ml and 62.94 µg/ml, respectively. This suggests a promising therapeutic window, where the compounds demonstrate selective toxicity toward *M. tuberculosis*without significantly harming human lung cells. Given the association between TB and lung cancer, compounds like 4m and 4r could potentially be explored for their dual role in targeting both TB and cancer cells, providing a unique advantage in regions with high TB prevalence and lung cancer co-morbidity.

Compound 4r showed potent antibacterial activity against *S. aureus* (MIC of 3.12 µg/ml), *B. subtilis* (MIC of 1.6 µg/ml), *K. pneumoniae* (MIC of 12.5 µg/ml), and *E. coli* (MIC of 12.5 µg/ml). Despite its broad-spectrum antibacterial activity, its relatively higher IC_{50} value in A549 cells (62.94 µg/ml) indicates that 4r might be a good candidate for further development, balancing its cytotoxic and antimicrobial profiles.

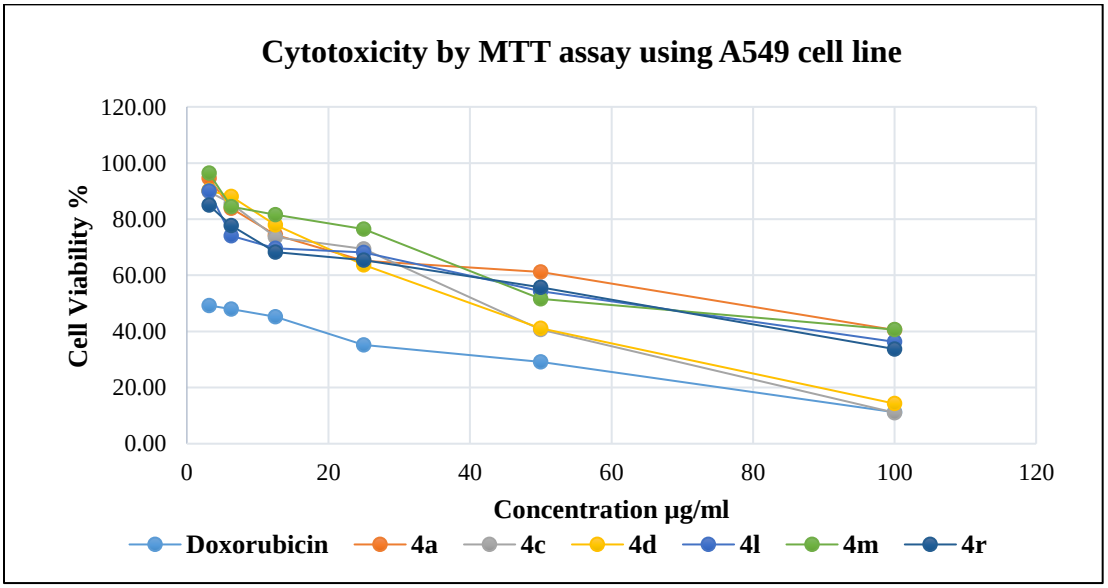

Figure 5.22: Cell viability (% relative to control) observed in MTT cytotoxicity assay using A549 cell line for six concentrations of synthesized molecules (4a, 4c, 4d. 4l, 4m and 4r) and positive control (Doxorubicin), n=3 and all the values are represented as ±SD

The molecules, 4c and 4d, exhibited stronger cytotoxicity in A549 cells, with IC_{50} values of 47.32 µg/ml and 48.64 µg/ml, respectively. Compound 4c showed moderate antibacterial activity against *S. aureus* (MIC of 12.5 µg/ml), *B. subtilis* (MIC of 12.5 µg/ml), *K. pneumoniae* (MIC of 25 µg/ml), and *E. coli* (MIC of 25 µg/ml), but its higher cytotoxicity in A549 cells may limit its therapeutic potential due to off-target effects.

Compound 4a showed an IC_{50} value of 74.57 µg/ml in A549 cells, indicating lower cytotoxicity compared to 4c and 4d. Its moderate antibacterial activity against *S. aureus* (MIC of 6.25 µg/ml) suggests that it could be further explored, especially if lower cytotoxicity is a priority in developing lung-targeted therapies.

To further assess the cytotoxicity of the synthesized compounds (4a, 4c, 4d, 4l, 4m, and 4r) on A549 cell line at concentrations of 3.125, 6.25, 12.5, 25, 50 and 100 µg/ml, microscopic observations were recorded before the addition of the MTT reagent. Microscopic analysis provides a qualitative view of cellular health and morphology in response to treatment, allowing for the early detection of cytotoxic effects such as cell rounding, detachment, and the presence of debris.

By comparing test compound treated cells with negative controls, this approach offers insights into the impact of each compound on cell viability and integrity, complementing the quantitative data obtained from the MTT assay. The results from the microscopic analysis are critical in understanding the morphological changes that occur before metabolic activity is measured via MTT reduction to formazan, helping to establish a clearer picture of the compound's cytotoxic potential at different concentrations.

The microscopic analysis of cytotoxic effects of synthesized compounds 4a, 4c, 4d, 4l, 4m, and 4r on A549 cell line at two concentrations 6.25 and 50 µg/ml is represented in the following section.

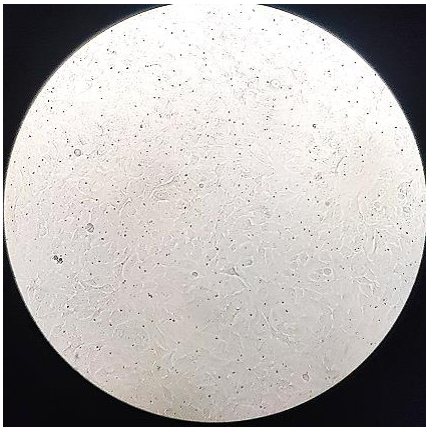

Figure 5.23: Microscopic analysis of A549 cells treated with negative control in MTT assay

The image of negative control (Figure 5.23)showed a relatively uniform distribution of cells across the field. It appeared that the cells were well-adhered to the plate and exhibited typical morphology for A549 cells, with elongated or irregular shapes, indicating a healthy culture before treatment. The cells appeared intact, with no visible signs of cell death or detachment, as expected in negative control. The cell membrane integrity looks preserved, and there are no significant clumps or signs of necrosis.

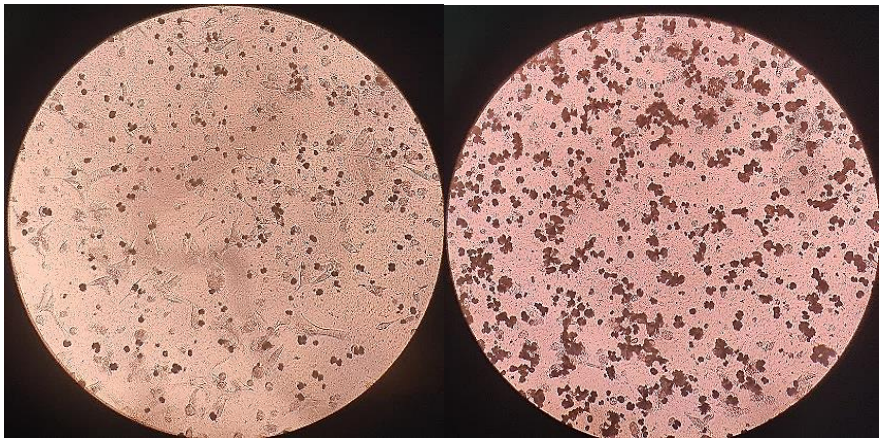

Figure 5.24: Microscopic analysis of A549 cells treated with synthesized compound 4a in MTT assay A) 6.25 µg/ml B) 50 µg/ml

The effects of compound 4a on A549 cells were captured in the images shown inFigure 5.24.At the concentration of 6.25 µg/ml of compound 4a, A549 cells largely retained their characteristic morphology, with most cells appearing elongated and well-adhered, similar to the negative control. The overall cell density was relatively high, and there was limited evidence of cell rounding or debris, indicating minimal cytotoxicity at this dose. In contrast, at the higher concentration of 50 µg/ml, significant morphological changes were observed. A large number of cells became rounded and detached, with a substantial reduction in cell density, suggesting a pronounced cytotoxic effect. Additionally, numerous cell aggregates and debris were visible, indicating increased cell death, likely due to necrosis or apoptosis. These findings demonstrate a clear concentration-dependent cytotoxic effect of compound 4a on A549 cells, with higher concentrations inducing greater cytotoxicity and lower concentrations showing comparatively minimal impact on cell viability.

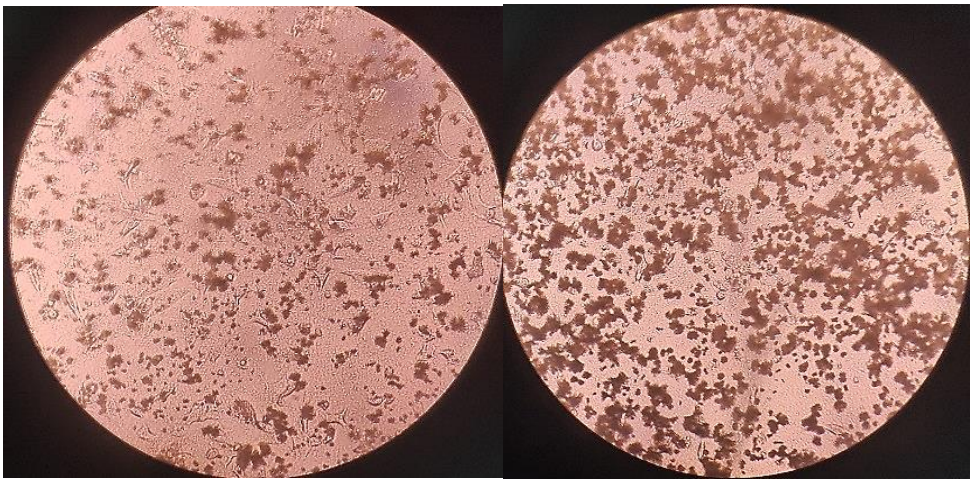

Figure 5.25: Microscopic analysis of A549 cells treated with synthesized compound 4c in MTT assay A) 6.25 µg/ml B) 50 µg/ml

TheFigure 5.25highlights effects of compound 4c on A549 cells at concentrations of 6.25 ppm and 50 ppm. At the lower concentration of 6.25 µg/ml, a significant portion of the cells maintained their typical elongated morphology,

indicating that the cytotoxic effects of the compound were not as pronounced. Some cells appear rounded and detached, but the overall cell density remains relatively high, suggesting that the majority of the cells remain viable at this concentration. In contrast, at 50 µg/ml, the cytotoxic effects were much more severe. Most cells are rounded and detached from the surface, with a notable reduction in cell adherence and an increase in cellular debris. The cell density is considerably lower than at 6.25 µg/ml, with widespread cell death evident across the field of view. These observations suggest that compound 4c exerts a concentration-dependent cytotoxic effect on A549 cells, with higher concentrations (50 µg/ml) leading to a significant loss of cell viability compared to the relatively minor effects observed at 6.25 µg/ml.

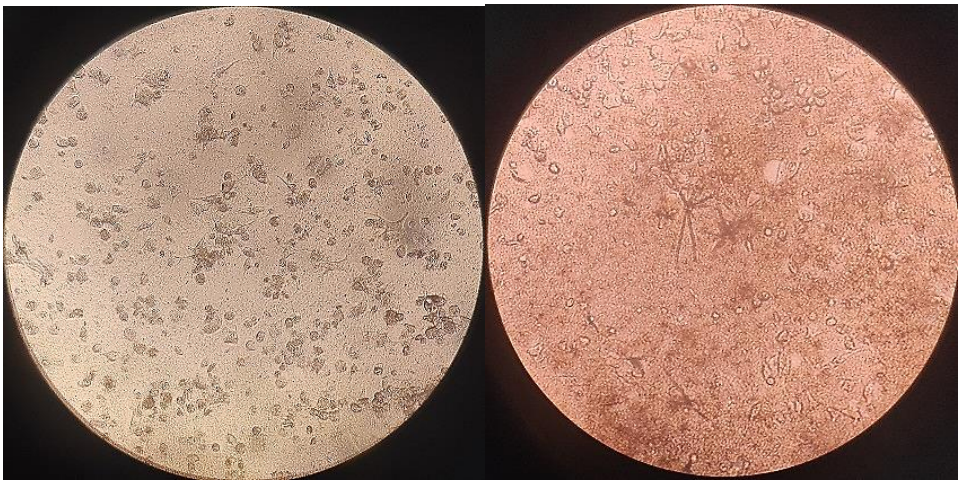

Figure 5.26: Microscopic analysis of A549 cells treated with synthesized compound 4d in MTT assay A) 6.25 µg/ml B) 50 µg/ml

The impact of compound 4d on A549 cells was evaluated at concentrations of 6.25 µg/ml and 50 µg/ml (Figure 5.26). At the lower concentration of 6.25 µg/ml, many cells retain their typical morphology, appearing elongated and attached to the surface. Although some cells exhibit signs of rounding and detachment, the overall cell density remains relatively high, indicating moderate cytotoxic effects. Most of the cells continue to appear healthy and viable, suggesting that 4d at this

concentration does not severely impair cell viability.At 50 µg/ml, the cytotoxicity is significantly more pronounced. Most cells are rounded, detached, and exhibit a loss of adherence, with a marked reduction in cell density. Additionally, a substantial amount of cellular debris is present, indicating widespread cell death. The difference between the two concentrations highlights a concentration-dependent response, where 50 µg/ml of compound 4d leads to extensive cytotoxicity in A549 cells, whereas 6.25 µg/ml has a relatively moderate effect.

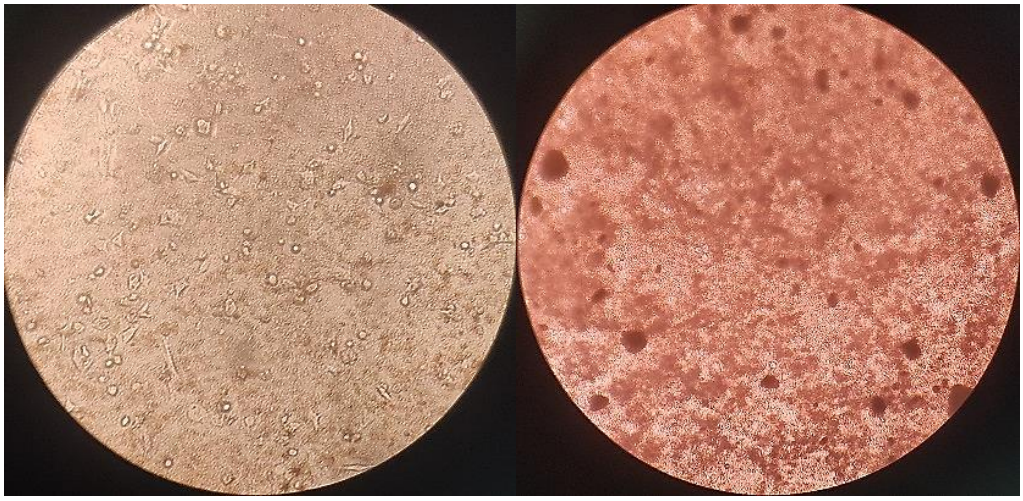

Figure 5.27: Microscopic analysis of A549 cells treated with synthesized compound 4l in MTT assay A) 6.25 µg/ml B) 50 µg/ml

Effects of compound 4l on A549 cells at 6.25 µg/ml and 50 µg/ml concentrations depicts its cytotoxic effects (Figure 5.27). At 6.25 µg/ml, the cells largely maintained their typical elongated and adherent morphology, with only a few showing signs of rounding or detachment. The overall cell density remains relatively high, indicating that compound 4l at this lower concentration does not exert significant cytotoxic effects on A549 cells. Most cells appear healthy and viable, suggesting minimal impairment of cell viability at this dose.In contrast, at 50 µg/ml, there is a marked decrease in cell density, with the majority of cells becoming

rounded and detached from the surface. The presence of cellular debris is widespread, indicating a high level of cell death. This concentration of compound 4l results in significant cytotoxicity, severely affecting cell morphology and survival. The pronounced difference between the two concentrations illustrates a strong concentration-dependent cytotoxic effect, where 50 µg/ml leads to extensive damage, while 6.25 µg/ml shows minimal impact on cell health.

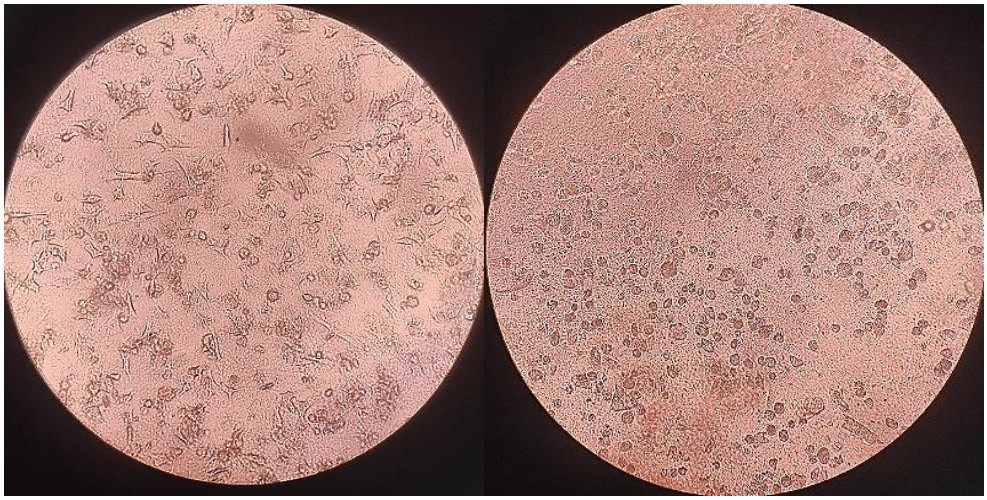

Figure 5.28: Microscopic analysis of A549 cells treated with synthesized compound 4m in MTT assay A) 6.25 µg/ml B) 50 µg/ml

The cytotoxic effects of compound 4m on A549 cells at concentrations of 6.25 µg/ml and 50 µg/ml are depicted in Figure 5.28. At 6.25 µg/ml, the cells retain a relatively healthy morphology, with the majority of them adhering to the surface and displaying elongated, spread-out shapes. Although a few cells exhibit rounding, the overall cell density remains high, indicating minimal cytotoxicity at this concentration. This suggests that compound 4m has a limited impact on cell viability at 6.25 µg/ml, allowing for the preservation of normal cellular functions.At the higher concentration of 50 µg/ml, however, there is a significant increase in the number of rounded, detached cells, and a notable reduction in cell density. Many

cells appear unhealthy, with widespread detachment from the surface, indicating that the cytotoxic effects are more severe at this concentration. The presence of cellular debris further suggests an elevated level of cell death. The difference between the two concentrations demonstrates a clear concentration-dependent response, with compound 4m showing strong cytotoxicity at 50 µg/ml while exerting minimal effects at 6.25 µg/ml.

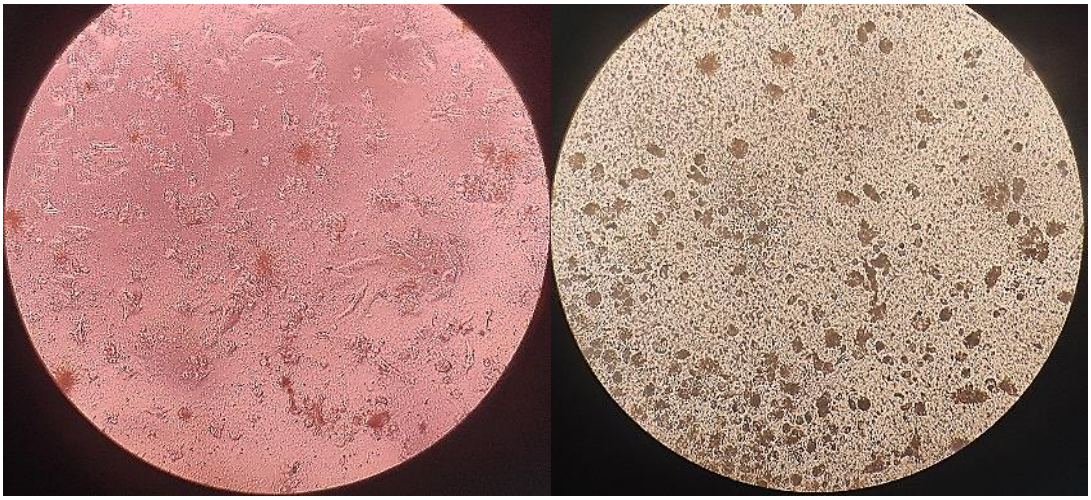

Figure 5.29: Microscopic analysis of A549 cells treated with synthesized compound 4r in MTT assay A) 6.25 µg/ml B) 50 µg/ml

The images in Figure 5.29 captured the cytotoxic effects of compound 4r on A549 cells at 6.25 µg/ml and 50 µg/ml concentrations. At 6.25 µg/ml, the cells exhibit considerable morphological changes, with a noticeable increase in cell rounding and detachment compared to the other compounds at the same concentration. Although some cells remain adherent, there is clear evidence of cytotoxicity at this concentration, with several cells losing their typical elongated shape. The overall cell density is reduced, suggesting that compound 4r is more cytotoxic even at a lower concentration compared to other compounds tested.At 50 µg/ml, the cytotoxicity is markedly severe. The majority of cells are rounded and

detached from the surface, with significant cellular debris present, indicating widespread cell death. The field shows a substantial reduction in viable, adherent cells, pointing to a high degree of cytotoxicity at this concentration. The pronounced difference between the 6.25 µg/ml and 50 µg/ml concentrations demonstrates a strong concentration-dependent cytotoxic effect for compound 4r, with severe effects observed even at the lower concentration.

Overall, compound 4r appears to be the most promising candidate, given its strong antibacterial and anti-TB activity, combined with a relatively high IC_{50} value in A549 cells, indicating a favourable therapeutic index. Given the potential correlation between TB infection and lung cancer development, compounds like 4r, which exhibit both anti-TB and moderate cytotoxicity in lung cancer cells, offer promising avenues for future research. Compounds 4m and 4a also show potential due to their lower cytotoxicity, though further optimization might be needed to enhance their antibacterial profiles. However, the overall effectiveness of the synthesized compounds is discussed after their effect on Vero cell lines is analysed.

5.2.3.2 Cytotoxicity assay with Vero cell lines

The cytotoxicity of the synthesized compounds (4a, 4c, 4d, 4l, 4m and 4r) was further evaluated using the MTT assay in Vero cell lines. Vero cells, derived from the kidney of the African green monkey, are commonly used in cytotoxicity assays to assess the impact of compounds on non-cancerous, and non-human mammalian cells. This cell line is a relevant model for assessing off-target toxicity, particularly for compounds intended for therapeutic use, as it provides an indication of the safety profile in non-lung tissues, such as kidney cells.

The results of cytotoxicity study at concentrations of 3.125, 6.25, 12.5, 25, 50 and 100 µg/mlalong with IC_{50} values for the synthesized compounds in Vero cells were represented in Table 5.18, Table 5.19 and Figure 5.30 with a plot of cell viability % vs concentration of compounds in µg/ml. Doxorubicin was used as positive control and the cytotoxic effects are mentioned in Table 5.20.

Table 5.18: Cytotoxic activity assessment of synthesized molecules 4a, 4c and 4d using MTT assay method (n=3) for Vero cell line

Concentration (µg/ml)	**Cell viability readings for Vero cell lineat 570 nm**								
	4a			**4c**			**4d**		
100	44.34	44.63	44.53	20.72	20.43	20.62	19.26	18.88	19.07
50	55.28	55.76	55.47	37.46	37.17	37.37	21.30	21.78	21.59
25	65.92	63.99	64.67	62.15	62.54	62.25	27.01	27.59	27.40
12.5	71.15	69.80	70.09	77.06	76.77	76.96	30.40	30.69	30.59
6.25	79.48	79.86	79.67	80.74	80.54	80.64	67.18	66.89	66.99
3.125	89.74	89.55	89.84	90.42	91.19	90.71	75.90	75.41	75.61
Negative Control	100			100			100		
IC_{50} value (µg/ml)	76.02			48.97			11.82		
Standard Deviation	0.07			0.06			0.06		

Table 5.19: Cytotoxic activity assessment of synthesized molecules 4l, 4m and 4r using MTT assay method (n=3) for Vero cell line

Concentration (µg/ml)	**Cell viability readings for Vero cell line at 570 nm**								
	4l			**4m**			**4r**		
100	42.11	42.30	42.21	43.85	44.05	43.95	21.78	21.01	20.43
50	53.73	53.34	53.44	53.73	53.24	53.53	34.46	34.27	34.37
25	58.18	58.47	58.37	71.06	71.35	71.06	38.82	38.53	38.33
12.5	64.09	63.79	63.99	83.16	82.58	82.87	42.30	42.50	42.21
6.25	75.99	75.80	75.90	92.26	92.84	92.35	48.11	48.50	48.31
3.125	81.03	80.93	81.22	96.71	96.81	96.61	60.60	60.12	60.31
Negative Control	100			100			100		
IC_{50} value (µg/ml)	68.26			76.41			4.56		
Standard Deviation	0.03			0.01			0.06		

Table 5.20: Cytotoxic activity assessment of positive control using MTT assay method (n=3) for Vero cell line

Concentration (µg/ml)	**Cell viability readings for Vero cell line at 570 nm (Doxorubicin)**		
100	13.50	13.16	13.27
50	38.67	38.33	38.56
25	40.96	40.62	40.73
12.5	42.68	42.91	42.79
6.25	46.00	46.34	46.11
3.125	48.28	47.94	48.17
Negative Control	100		
IC_{50} value (µg/ml)	2.41		
Standard Deviation	0.02		

Compound 4r exhibited the highest cytotoxicity in Vero cells, with an IC_{50} of 4.56 µg/ml. This finding is significant because 4r demonstrated potent anti-TB activity (MIC of 6.25 µg/ml) and antibacterial activity, particularly against *S. aureus* (MIC of 3.12 µg/ml) and *B. subtilis* (MIC of 1.6 µg/ml). However, the low IC_{50} value in Vero cells suggests that 4r may cause cytotoxicity at concentrations close to those required for its therapeutic effect, raising concerns about its potential toxicity in non-target cells, particularly in the kidneys. This warrants further investigation into its safety profile and possible modifications to reduce off-target effects.

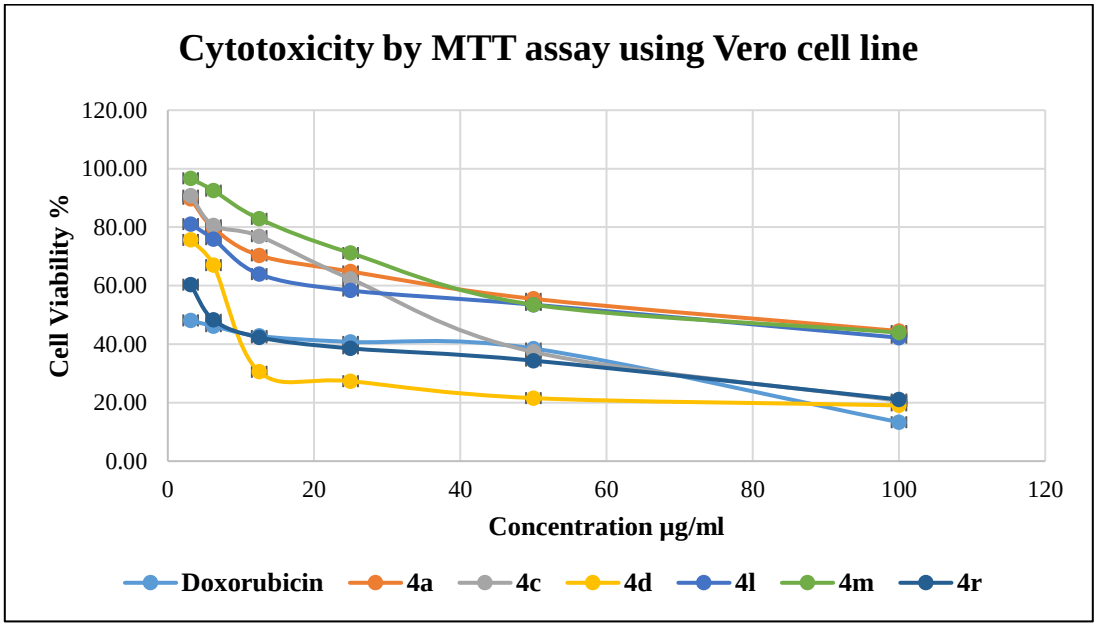

Figure 5.30: Cell viability (% relative to control) observed in MTT cytotoxicity assay using Vero cell line for six concentrations of synthesized molecules (4a, 4c, 4d. 4l, 4m and 4r) and positive control (Doxorubicin), n=3 and all the values are represented as ±SD

Compounds 4d and 4c also exhibited moderate cytotoxicity in Vero cells, with IC_{50} values of 11.82 µg/ml and 48.97 µg/ml, respectively. While compound 4d showed relatively low cytotoxicity in A549 cells, its higher cytotoxicity in Vero cells

suggests that this compound may have selective toxicity toward kidney cells. This poses a challenge in terms of balancing the therapeutic efficacy of 4d with its safety, especially given its promising antibacterial activity against *S. aureus* and *B. subtilis*.

On the other hand, compounds 4a, 4l, and 4m exhibited relatively low cytotoxicity in Vero cells, with IC_{50} values of 76.02 µg/ml, 68.26 µg/ml, and 76.41 µg/ml, respectively. These results are encouraging because both 4m and 4a demonstrated good antibacterial activity (MIC of 6.25 µg/ml for 4m and 6.25 µg/ml for 4a against *S. aureus*), while maintaining a favourable cytotoxicity profile in Vero cells. The higher IC_{50} values suggest a wider therapeutic window for these compounds, indicating they may be safer in non-lung tissues compared to compounds like 4r.

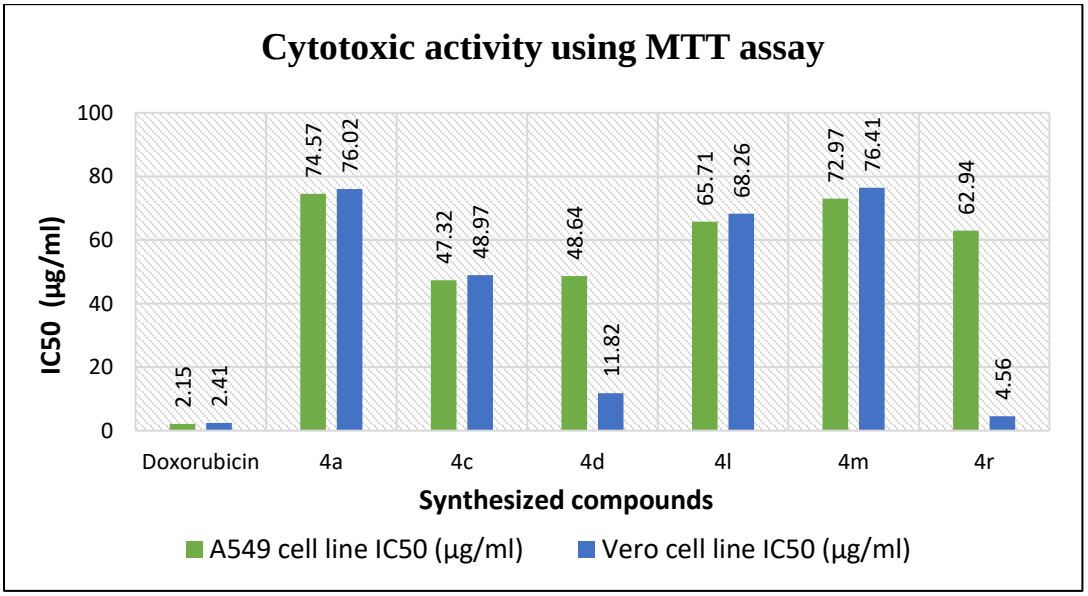

Figure 5.31: Cytotoxic activity (IC50 values) of synthesized molecules 4a, 4c, 4d, 4l, 4m and 4r using MTT assay with A549 and Vero cell lines

By comparing the results of the cytotoxic effects on Vero cells with the previously obtained results from A549 cells as shown in Figure 5.31, a clearer picture of selective toxicity of the compounds can be established.

The microscopic analysis of synthesized compounds 4a, 4c, 4d, 4l, 4m, and 4r on Vero cell line was carried outat concentrations of 3.125, 6.25, 12.5, 25, 50 and 100 µg/ml, where the observations were recorded before the addition of the MTT reagent.

The microscopic analysis of cytotoxic effects of synthesized compounds 4a, 4c, 4d, 4l, 4m, and 4r on Vero cell line at two concentrations 6.25 and 50 µg/ml is represented in the following section.

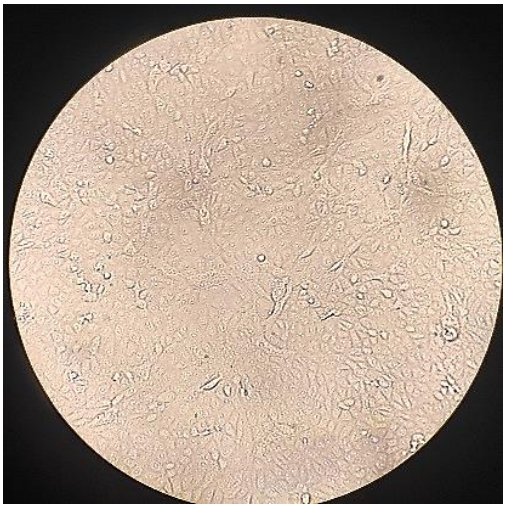

Figure 5.32: Microscopic analysis of Vero cells treated with negative control in MTT assay

The negative control image (Figure 5.32) shows healthy Vero cells with typical morphology. The cells appear elongated and spread out across the surface, with strong adherence and a high overall cell density. There is minimal evidence of cell rounding or detachment, indicating that the cells are in a healthy, viable state without any apparent cytotoxic effects. No significant cellular debris is visible, which further suggests the absence of stress or damage to the cells.

This control image establishes the expected morphology of Vero cells under normal, untreated conditions and will help in further interpreting the cytotoxic effects of the test compounds. When compared to the test compound images, this negative control serves as a baseline to highlight the cytotoxic effects of the compounds. In the treated samples, significant changes such as cell rounding, detachment, and reduced cell density indicate the cytotoxicity induced by the test compounds. The healthy, adherent state of the cells in the negative control highlights the contrast with these effects, underscoring the concentration-dependent impact of the compounds on cell viability.

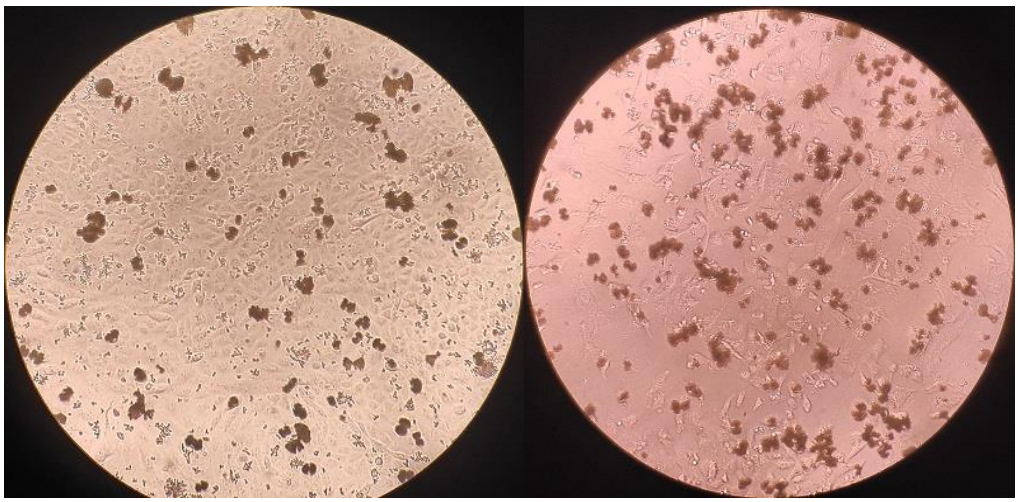

Figure 5.33: Microscopic analysis of Vero cells treated with synthesized compound 4a in MTT assay A) 6.25 µg/ml B) 50 µg/ml

The cytotoxic effects of compound 4a in Vero cells at concentrations of 6.25 µg/ml and 50 µg/ml were captured in Figure 5.33. At 6.25 µg/ml, many cells retain their typical elongated morphology, with a substantial portion of the cells remaining attached and displaying a healthy appearance. There is some rounding and detachment observed, but the overall cell density is relatively high, suggesting that

cytotoxicity at this concentration is minimal. Most cells appear to be viable, indicating that 4a exerts only a mild effect on Vero cells at this lower concentration.

At 50 µg/ml, the cytotoxicity becomes more pronounced. A larger number of cells exhibit signs of stress, with increased rounding and detachment from the surface. The presence of cellular debris is more evident, and the overall cell density is reduced compared to the 6.25 µg/ml concentration. This suggests that compound 4a induces a concentration-dependent cytotoxic effect in Vero cells, with higher concentrations resulting in more significant damage to cell viability and morphology.

Comparison with A549 Cells: Interestingly, compound 4a at 6.25 µg/ml exhibited similar minimal cytotoxic effects in both Vero and A549 cells, with relatively high cell viability in both cases. However, at 50 µg/ml, the A549 cells showed a slightly more pronounced cytotoxic response, with more extensive cell detachment and rounding compared to Vero cells. This suggests that A549 cells may be slightly more sensitive to the cytotoxic effects of 4a at higher concentrations.

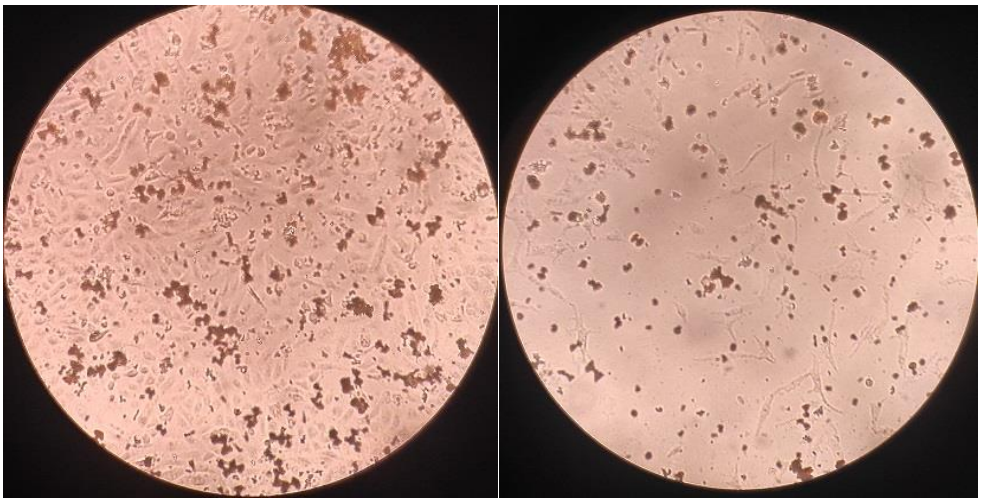

Figure 5.34: Microscopic analysis of Vero cells treated with synthesized compound 4c in MTT assay A) 6.25 µg/ml B) 50 µg/ml

The effects of compound 4c on Vero cells were analysed at 6.25 µg/ml and 50 µg/ml concentrations as depicted in Figure5.34. At 6.25 µg/ml, the cells generally retain their typical elongated and spread-out morphology, with many cells remaining adherent. Although there is some degree of rounding and detachment, the overall cell density remains relatively high, indicating that compound 4c exerts only mild cytotoxic effects at this concentration. The cells display characteristics similar to those observed in the lower concentration images for other compounds.

At 50 µg/ml, a more pronounced cytotoxic effect is observed. A larger number of cells show rounding and detachment, with many no longer adhering to the surface. Cellular debris is more prominent, and the overall cell density is significantly reduced compared to the 6.25 µg/ml concentration, indicating a substantial loss in cell viability. The differences between these two concentrations highlight the dose-dependent cytotoxicity of compound 4c on Vero cells.

Comparison with A549 Cells: The cytotoxicity profile of compound 4c on Vero cells follows a similar pattern to that observed in A549 cells, with lower concentrations (6.25 µg/ml) showing minimal effects and higher concentrations (50 µg/ml) leading to significant cell death. However, A549 cells showed slightly greater sensitivity to 4c at 50 µg/ml, with a more pronounced reduction in cell density and adherence compared to Vero cells. This indicates that while both cell types are affected by higher doses of 4c, A549 cells may be slightly more vulnerable to its cytotoxic effects.

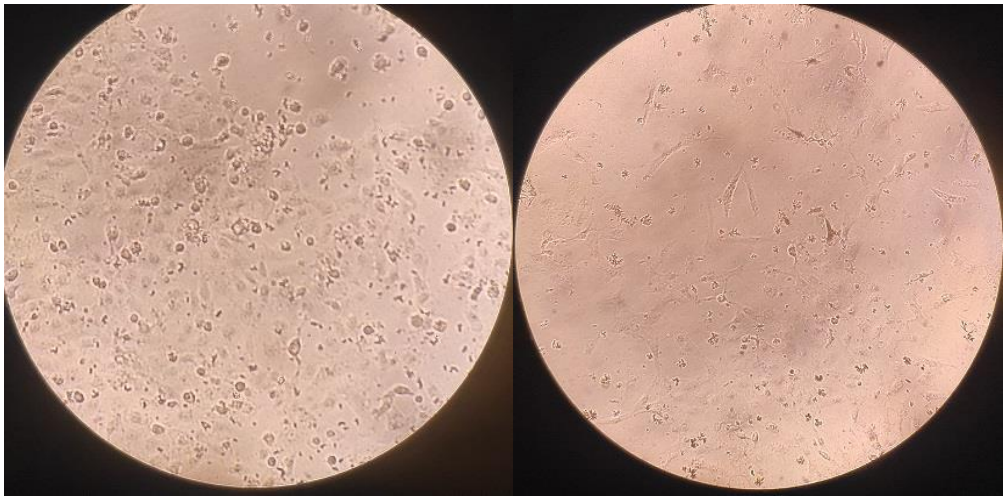

Figure 5.35: Microscopic analysis of Vero cells treated with synthesized compound 4d in MTT assay A) 6.25 µg/ml B) 50 µg/ml

Figure 5.35 captured cytotoxicity of compound 4d on Vero cells at 6.25 µg/ml and 50 µg/ml concentrations. At 6.25 µg/ml, most of the cells maintain their characteristic elongated and spread-out morphology, indicating that compound 4d induces minimal cytotoxic effects at this concentration. Although some cells show signs of rounding and detachment, the overall cell density remains relatively high, and cell viability appears largely preserved.

At 50 µg/ml, however, the cytotoxic effects become more evident. A significant number of cells are rounded and detached from the surface, with a reduction in cell density. The presence of cellular debris is also more pronounced, suggesting increased cell death at this higher concentration. The comparison between the two concentrations demonstrates a concentration-dependent cytotoxic response, with the higher concentration of 4d leading to much greater cellular stress and loss of viability.

Comparison with A549 Cells: The cytotoxic effects of compound 4d on Vero cells are consistent with the observations in A549 cells, with a more pronounced effect at

50 µg/ml. However, A549 cells appear to be more sensitive to compound 4d, as the cytotoxicity at 6.25 µg/ml was more pronounced in A549 cells than in Vero cells. This suggests that while 4d has cytotoxic effects on both cell types, Vero cells exhibit slightly greater resistance to the compound at lower concentrations.

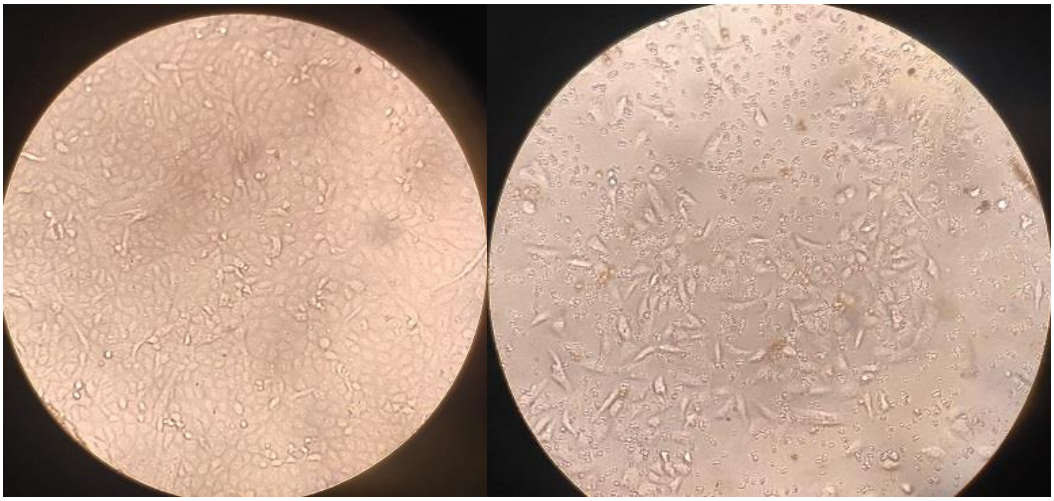

Figure 5.36: Microscopic analysis of Vero cells treated with synthesized compound 4l in MTT assay A) 6.25 µg/ml B) 50 µg/ml

The cytotoxic effects of compound 4l on Vero cells at 6.25 µg/ml and 50 µg/ml concentrations were determined as shown in Figure 5.36. At 6.25 µg/ml, most of the cells maintain a normal morphology, characterized by a high degree of adhesion and a spread-out, elongated structure. There is little evidence of cell rounding or detachment, and the overall cell density remains high, suggesting that compound 4l induces minimal cytotoxicity at this lower concentration.

At 50 µg/ml, a noticeable increase in cytotoxic effects is observed. Many cells show signs of rounding and detachment, with some areas displaying visible cellular debris, indicating higher levels of cell death. The overall cell density is reduced compared to the 6.25 µg/ml concentration, although some cells still retain their

normal elongated morphology. The difference between the two concentrations points to a dose-dependent cytotoxic effect of compound 4l, with significant damage to cell viability at the higher concentration.

Comparison with A549 Cells: Similar to the results in Vero cells, compound 4l exhibited concentration-dependent cytotoxicity in A549 cells. However, the A549 cells were slightly more sensitive to compound 4l at the higher concentration (50 µg/ml), where a more extensive reduction in cell viability and increased cellular debris were observed. This suggests that while 4l is cytotoxic to both Vero and A549 cells, its effects may be somewhat more pronounced in cancerous lung cells.

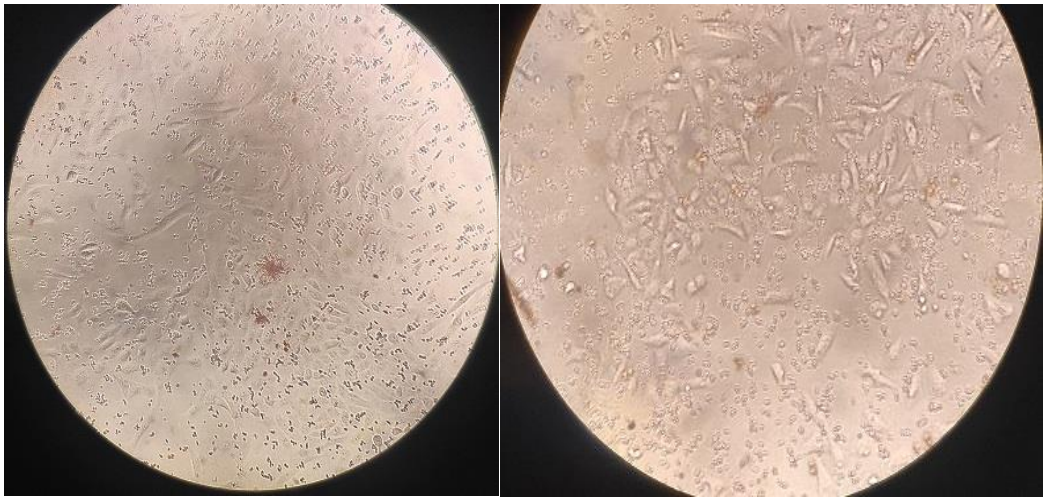

Figure 5.37: Microscopic analysis of Vero cells treated with synthesized compound 4m in MTT assay A) 6.25 µg/ml B) 50 µg/ml

The effects of compound 4m on Vero cells were assessed at concentrations of 6.25 µg/ml and 50 µg/ml as shown in Figure 5.37. At 6.25 µg/ml, most cells retain their typical elongated and spread-out morphology, indicating minimal cytotoxic effects. There is little evidence of cell rounding or detachment, and the cell density remains high, suggesting that compound 4m has a limited impact on Vero cells at

this lower concentration. This observation is consistent with relatively low cytotoxicity observed in other cell lines at this dose.

At 50 µg/ml, the cytotoxic effects are much more pronounced. A significant number of cells have become rounded and detached from the surface, and there is a noticeable decrease in cell density. Cellular debris is also visible, indicating a higher degree of cell death at this concentration. While some cells still maintain their normal morphology, the overall impact on cell viability is substantial, indicating a strong concentration-dependent cytotoxic response.

Comparison with A549 Cells: The cytotoxic profile of compound 4m in Vero cells aligns with its effects in A549 cells, where minimal impact was observed at 6.25 µg/ml but significant cytotoxicity occurred at 50 µg/ml. However, A549 cells appeared slightly more sensitive to the higher concentration of 4m, with a greater degree of rounding and detachment observed. This suggests that while 4m induces cytotoxicity in both Vero and A549 cells, the cancerous lung cells may be somewhat more susceptible to its effects.

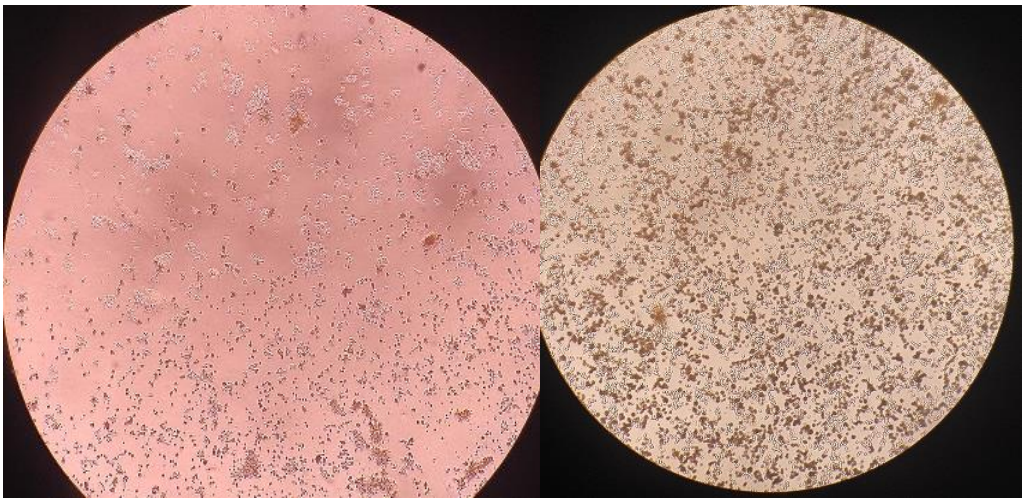

Figure 5.38: Microscopic analysis of Vero cells treated with synthesized compound 4r in MTT assay A) 6.25 µg/ml B) 50 µg/ml

The cytotoxicity of compound 4r on Vero cells was evaluated at 6.25 µg/ml and 50 µg/ml concentrations as depicted in Figure 5.38. At 6.25 µg/ml, the cells show significant cytotoxicity compared to the lower concentration images of other compounds. Many cells are rounded and detached, with cellular debris clearly visible throughout the field. The overall cell density is reduced, indicating that even at this lower concentration, compound 4r exerts a considerable cytotoxic effect on Vero cells.

At 50 µg/ml, the cytotoxic effects are even more pronounced. Most of the cells are detached or rounded, and a significant amount of cellular debris is present. The cell density is drastically reduced, and there is very little evidence of viable, adherent cells. This severe cytotoxicity at 50 µg/ml further confirms the strong concentration-dependent effect of compound 4r on cell viability, with notable damage observed even at lower doses.

Comparison with A549 Cells: Compound 4r exhibited similar strong cytotoxic effects in A549 cells at both concentrations, but the cytotoxicity appears to be slightly more pronounced in Vero cells. This suggests that Vero cells may be slightly more sensitive to compound 4r than A549 cells. The marked reduction in cell viability, even at 6.25 µg/ml, underscores the potent cytotoxicity of this compound in both cell types.

The results from the MTT assay on Vero cells highlight the importance of assessing cytotoxicity in multiple cell lines to obtain a comprehensive view of a compound's safety profile. The cytotoxicity evaluation of compounds 4a–4r in both Vero and A549 cell lines demonstrated concentration-dependent effects, with higher concentrations showing significant cell rounding, detachment, and reduced viability in both cell types.

While compound 4r remains a promising candidate due to its potent anti-TB and antibacterial activity, its high cytotoxicity in Vero cells suggests a need for caution. Compounds like 4m and 4a, which exhibit lower cytotoxicity in Vero cells and strong antimicrobial activity, could be considered more favourable for further development, especially if reduced off-target toxicity is prioritized.

5.3 MOLECULAR DOCKING STUDY OF ESTER DERIVATIVES OF 6-SUBSTITUTED-2-CHLOROQUINOLINE-3-CARBALDEHYDEHYDRAZIDE

5.3.1 Docking study of synthesized molecules 4a-4r with MtPanK

Molecular docking studies were conducted to explore the mechanism and detailed intermolecular interactions between the synthesized compounds (4a-4r) and Pantothenate kinase from *M. tuberculosis* (MtPanK), in complex with GDP and phosphopantothenate (PDB ID 3AEZ).

PanK is a conserved enzyme across a wide variety of bacterial species, including *M. tuberculosis*, and plays a role in the biosynthesis of coenzyme A (CoA), an essential cofactor for fatty acid metabolism, energy production, and other vital cellular processes. Inhibiting this enzyme disrupts CoA biosynthesis, leading to impaired bacterial energy metabolism, lipid biosynthesis, and overall cellular function, leading to bacteriostatic or bactericidal effects[146-147].

Targeting PanK presents an opportunity to broaden the antibacterial spectrum of the synthesized compounds, potentially affecting a wide range of bacterial species and offering a novel mechanism to combat resistant strains. Importantly, while PanK is essential in bacteria, its role in human cells is less critical due to differences in CoA biosynthesis pathways. This distinction allows for the design of compounds that selectively inhibit bacterial PanK, potentially reducing cytotoxicity in human cells and enhancing the therapeutic potential of the synthesized molecules[148-150].

Therefore, inhibiting PanK in *M. tuberculosis* and other bacteria can disrupt essential cellular functions, making it a promising target for antitubercular drug development, with the added advantage of reducing side effects through selective inhibition.

This study was performed using the Surflex-Dock module of the Sybyl-X 2.0 software. All synthesized molecules (4a-4r), as well as the native ligand of enzyme, were docked into the active site of the enzyme, as illustrated in Figure 5.39.

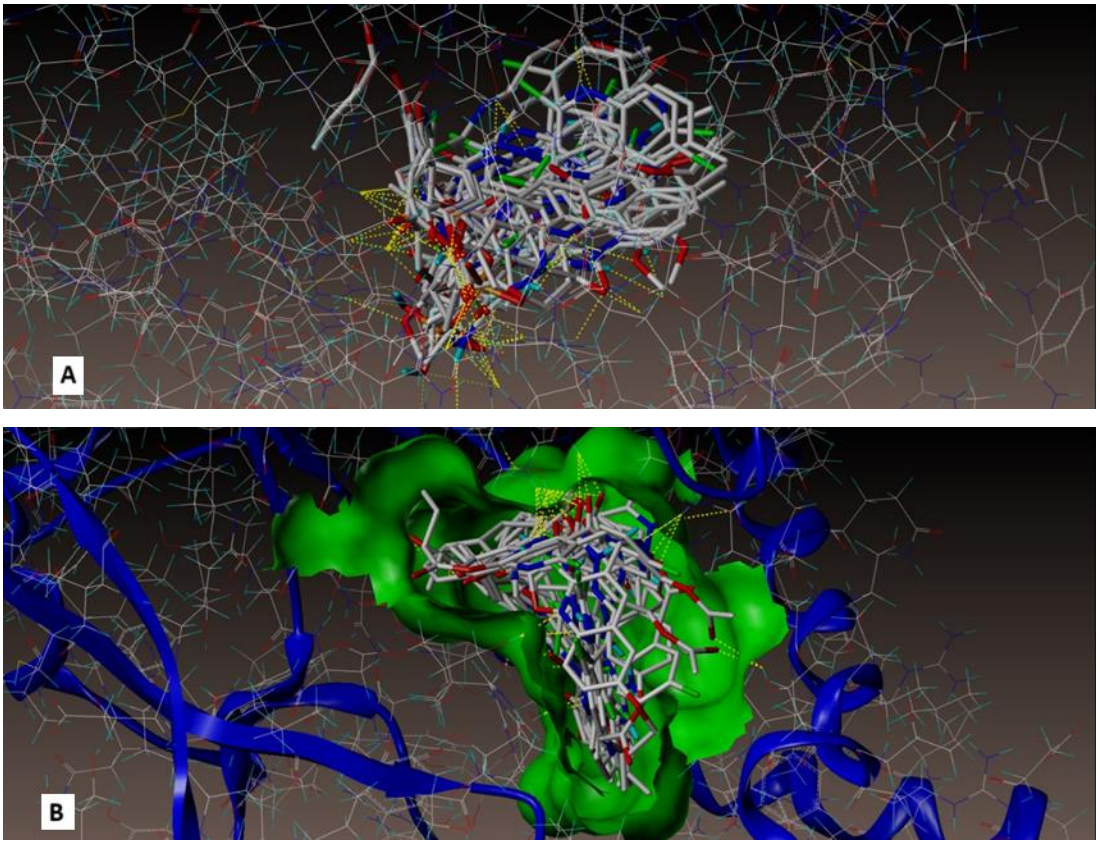

Figure 5.39: Docked view of synthesized compounds 4a-4r at the active site of the enzyme MtPanK (PDB ID: 3AEZ)

The predicted binding energies of the docked compounds are summarized in Table 5.21. Each score provided by the software is important to analyse the binding efficiency and potential biological activity of the synthesized compounds (4a-4r).

Table 5.21: Docking study results for synthesized molecules 4a – 4r withcrystal structure of proteinMtPanK (PDB ID 3AEZ)

Compounds	C Score[a]	Crash Score[b]	Polar Score[c]	D Score[d]	PMF Score[e]	G Score[f]	Chem Score[g]
4k	8.39	-1.20	3.85	-132.942	-67.279	-171.261	-31.078
3AEZ_ligand	8.24	-0.66	6.34	-107.242	-136.977	-251.349	-15.170
4o	7.27	-0.88	2.08	-131.799	-89.014	-165.104	-28.986
4l	7.01	-0.88	2.63	-97.918	-50.716	-184.109	-21.583
4h	6.84	-1.43	3.45	-116.733	-70.194	-158.839	-31.377
4i	6.58	-2.03	1.21	-130.415	-48.733	-231.741	-31.733
4e	6.45	-1.48	2.39	-117.828	-62.137	-211.944	-24.054
4a	6.45	-2.62	2.92	-128.695	-52.935	-237.306	-26.652
4q	6.37	-0.69	3.45	-109.235	-75.571	-128.828	-25.675
4g	6.28	-0.91	2.65	-119.521	-51.784	-166.629	-31.000
4n	6.25	-2.14	1.66	-132.615	-57.586	-226.000	-28.231
4j	6.13	-1.55	2.52	-120.416	-52.350	-186.816	-26.422
4b	6.04	-0.53	2.80	-103.058	-74.313	-114.608	-23.764
4r	5.82	-2.04	3.18	-116.871	-51.696	-175.129	-32.879
4c	5.60	-2.94	2.14	-134.672	-52.061	-202.950	-28.103
4m	5.40	-1.72	3.27	-93.294	-16.021	-139.686	-21.158
4f	5.16	-1.96	1.73	-103.963	-35.186	-195.993	-22.157
4d	5.06	-2.18	2.84	-95.802	-27.420	-173.741	-20.061
4p	4.78	-1.70	1.69	-123.191	-74.268	-198.273	-27.231

[a]CScore (Consensus Score) integratesnumber of popular scoring functions for ranking the affinity of ligands bound to the active site of a receptor and reports the output of total score.

[b] Crash-score reveals inappropriate penetration into the binding site. Crash scores close to 0 are favourable. Negative numbers indicate penetration.

[c] Polar score indicates the contribution of the polar interactions to the total score. The polar score may be useful for excluding docking results that make no hydrogen bonds.

[d]Dscore (Dock score) indicates charge and van der Waals interactions between the protein and ligand.
[e]PMFscore (Potential Mean Force) indicates the Helmholtz free energies of interactions for protein-ligand atom pairs (Potential of Mean Force, PMF).
[f]Gscore(Gibbs Free Energy) shows hydrogen bonding, complex (ligand-protein), and internal (ligand-ligand) energies.
[g] Chem-score points for H-bonding, lipophilic contact, and rotational entropy, alongwith an intercept term.

C Score

- This score represents the overall docking affinity of the ligand (compound) with the target. Higher values indicate better binding affinity.
- Compound 4k shows the highest C Score (8.39), indicating it may have the best binding affinity among the synthesized compounds, followed by 3AEZ_ligand (8.24), which is likely the reference or control ligand.

Crash Score

- The Crash Score represents how much the ligand geometry has been distorted during docking. Lower (or more negative) crash scores are better as they indicate minimal distortion, while high negative values can suggest unfavourable binding conformations.
- Compound 4a has a relatively high Crash Score (-2.62), indicating potential strain in its binding conformation. Compound 4b has the least crash (-0.53), suggesting a more stable pose.

Polar Score

- The Polar Score evaluates the polar interactions (such as hydrogen bonding) between the ligand and the target protein. Higher scores indicate more or stronger polar interactions.
- 3AEZ_ligand has the highest polar score (6.34), suggesting significant hydrogen bonding interactions, while compound 4k also has a high polar score (3.85), implying a reasonable number of polar interactions.

D Score

- This is a key score reflecting the energy associated with the binding interaction. More negative values indicate stronger binding.
- Compounds 4o (-131.799) and 4k (-132.942) have highly negative D Scores, indicating strong binding affinity with the target protein. Compound 4m shows the least negative D Score (-93.294), suggesting relatively weaker binding.

PMF Score

- The PMF score measures the potential interaction energy between the ligand and the protein. Similar to the D Score, more negative values suggest better interaction.
- 3AEZ_ligand (-136.977) and compound 4p (-74.268) have strong interaction energy. Compound 4m (-16.021) has the least negative PMF score, indicating weaker interactions.

G Score

- The G Score reflects the estimated free energy of binding. More negative values indicate more favourable binding.
- Compound 4i shows a very negative G Score (-231.741), suggesting strong binding, whereas compound 4m has a much less negative G Score (-139.686), indicating less favourable binding.

Chem Score

- This score accounts for the chemical nature of the interactions (e.g., electrostatic, van der Waals forces). It provides an additional perspective on binding affinity.
- Compound 4r has a relatively high Chem Score (-32.879), followed by compound 4k (-31.078), indicating favourable chemical interactions between these compounds and the target.

Compound 4k stands out with a high C Score, low Crash Score, and strong polar and D Scores, suggesting it could be one of the top candidates in terms of binding affinity and stability in the binding pocket. The control ligand (3AEZ_ligand) also performs well in many categories (high Polar Score and good PMF Score), which validates the docking process. Compounds 4o, 4k, and 4a showed strong binding based on their Dock Scores, and 4i has a highly negative G Score, indicating significant potential as an active compound. Compound 4m shows relatively weaker performance across multiple scores (e.g., D Score and PMF Score), indicating less favourable binding.

The interactions of compounds 4a-4r with MtPanKwere investigated to evaluate their binding affinity and interaction profile, which is pivotal for their efficacy as potential antitubercular agents. The ability of these molecules to interact with key active site residues and inhibit PanK could lead to the disruption of CoA biosynthesis, required for the survival and virulence of *M. tuberculosis*.

As depicted in Figure 5.40, compound 4kformed five hydrogen bonding interactions within the active site of the enzyme (PDB ID: 3AEZ). Two of these interactions involve the oxygen atoms of the 1-phenylpropionate moiety with the hydrogen atoms of ARG238 (O---H-ARG238, 1.99 Å; 2.49 Å). Additionally, the nitrogen atom of the imine group (CH=N) forms a hydrogen bond with GOL326 (N---H-GOL326, 2.42 Å), while the oxygen atom of the methoxy group at the 6^{th}position of the quinoline ring interacts with the hydrogen atom of PAZ314 (O---H-PAZ314, 1.83 Å). The remaining two hydrogen bonds originate from the oxygen atom of the C=O group in the 1-phenylpropionate moiety, interacting with ALA100 and ARG238 (O---H-ALA100, 1.96 Å; O---H-ARG238, 2.25 Å).

A)

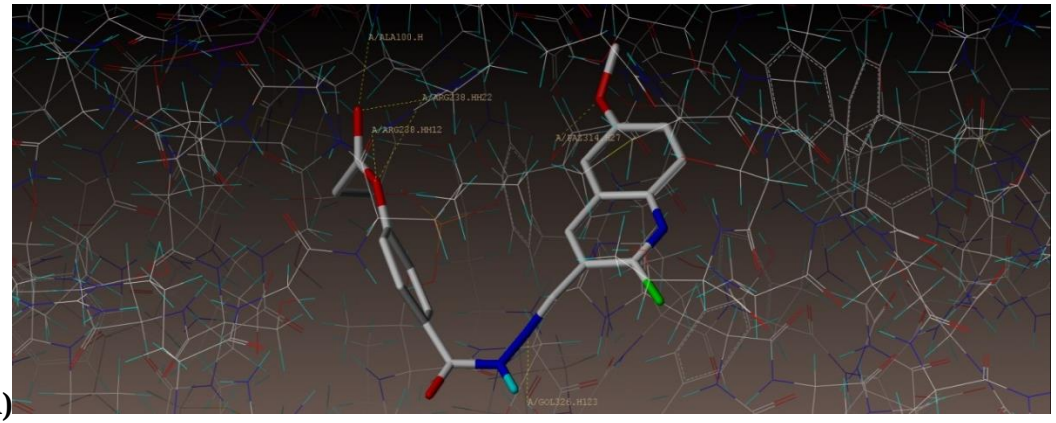

B)

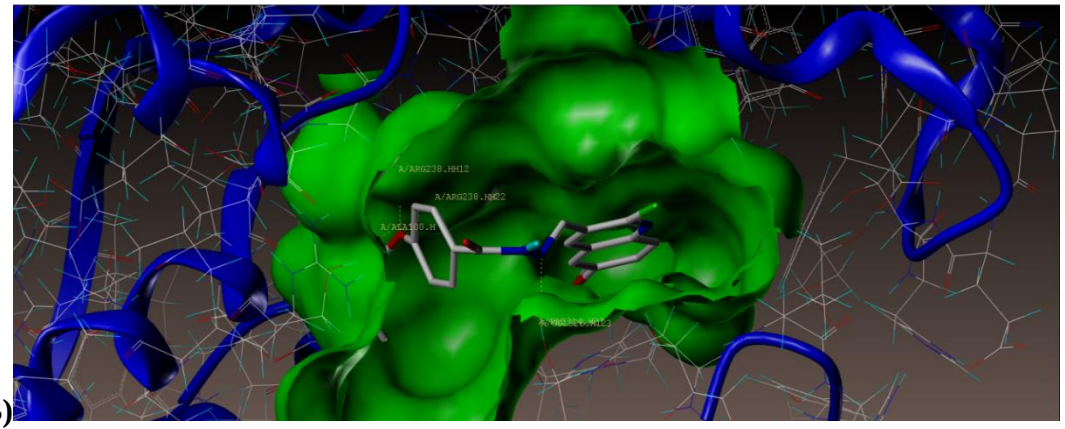

C)

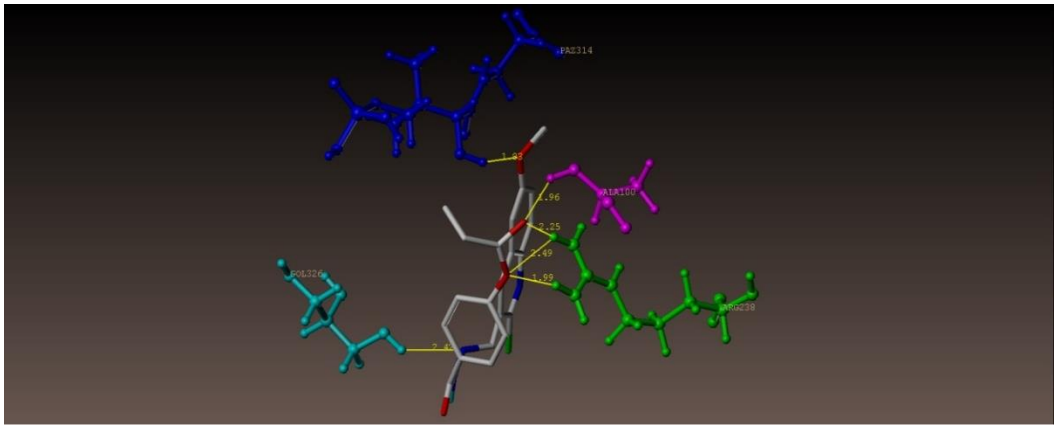

Figure 5.40: Docked view of compound 4k at the active site of the enzymeMtPanK PDB: 3AEZ A) Compound 4k in stick form at the active site of enzyme in wireframe form B) Compound 4k at the active site of enzyme in

ribbon form C) Ball and stick model of Compound 4k interacting with amino acids of enzyme

In a similar fashion, Figure 5.41 illustrates the interactions of compound 4o, which forms five hydrogen bonds within the active site. Two of these interactions are established between the oxygen atoms of the C=O group in the 1-phenylbutyrate moiety and the hydrogen atoms of PAZ314 and LYS103 (O---H-PAZ314, 1.98 Å; O---H-LYS103, 2.08 Å). The nitrogen atom of the imine group (CH=N) forms two additional interactions with ARG108 and SER104 (N---H-ARG108, 2.72 Å; N---H-SER104, 2.68 Å), while the nitrogen atom at the 1stposition of the quinoline ring interacts with GOL326 (O---H-GOL326, 2.77 Å). The final hydrogen bond arises from the oxygen atom of the 1-phenylbutyrate group interacting again with PAZ314 (O---H-PAZ314, 2.18 Å).

For comparison, Figure 5.42 shows the interactions of the 3AEZ reference ligand, which forms ten hydrogen bonding interactions within the enzyme's active site.

Figures 5.43 provides a visual representation of the hydrophobic and hydrophilic amino acids surrounding compounds 4k and 4o. The consensus docking scores for all the compounds range from 8.39 to 4.78, summarizing the collective forces of interaction between the ligands and the protein. Notably, the synthesized compounds demonstrated similar interactions with key amino acid residues (PAZ314, ARG238, ALA100, LYS103, and SER104) as those observed with the reference 3AEZ ligand. This suggests that the synthesized molecules preferentially bind to the protein with comparable or greater affinity than the 3AEZ ligand, as detailed in Table 5.21.

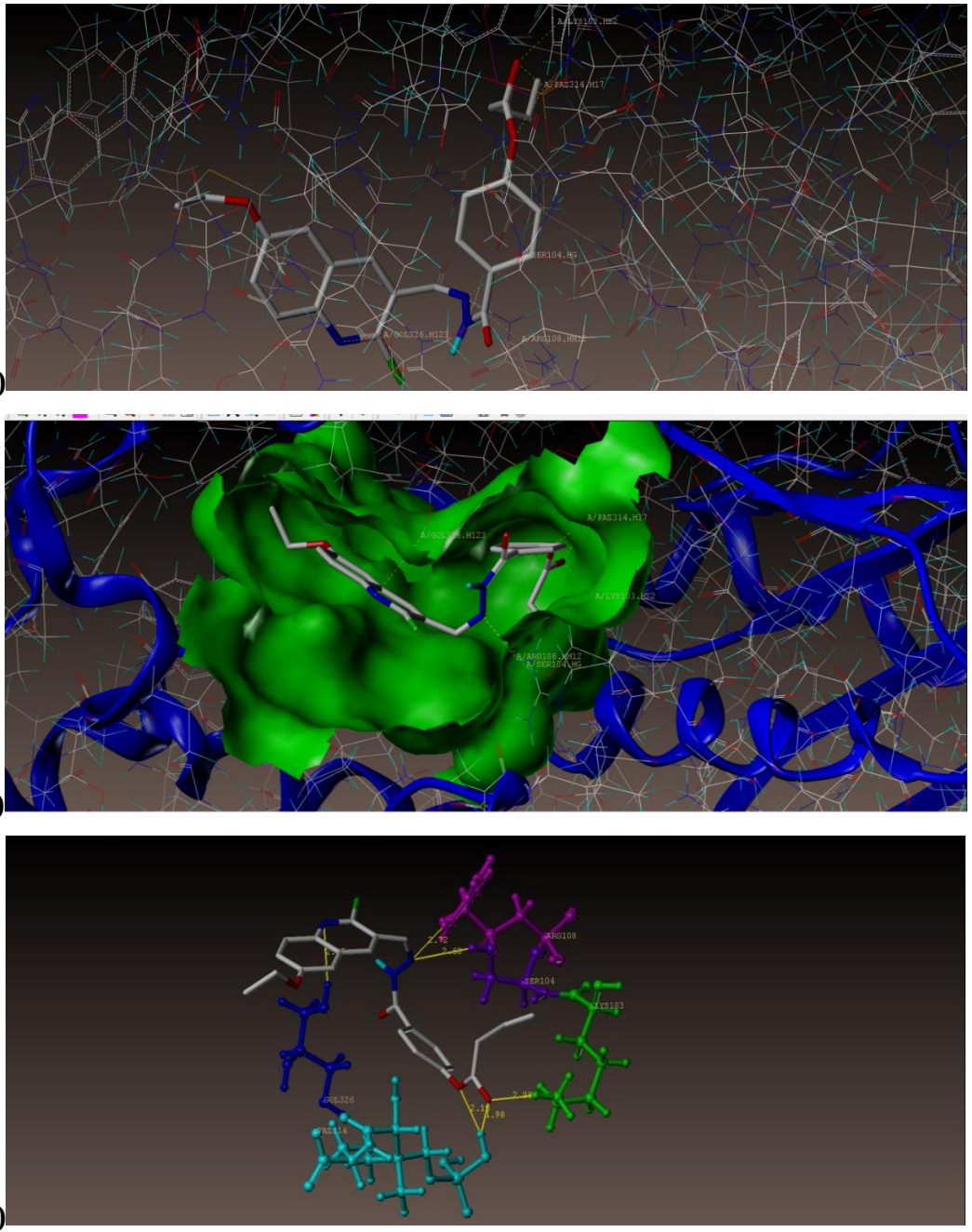

Figure 5.41: Docked view of compound 4o at the active site of the enzymeMtPanK(PDB: 3AEZ) A) Compound 4o in stick format the active site of enzyme in wireframe form B) Compound 4o at the active site of enzyme in

ribbon form C) Ball and stick model of Compound 4o interacting with amino acids of enzyme

A)

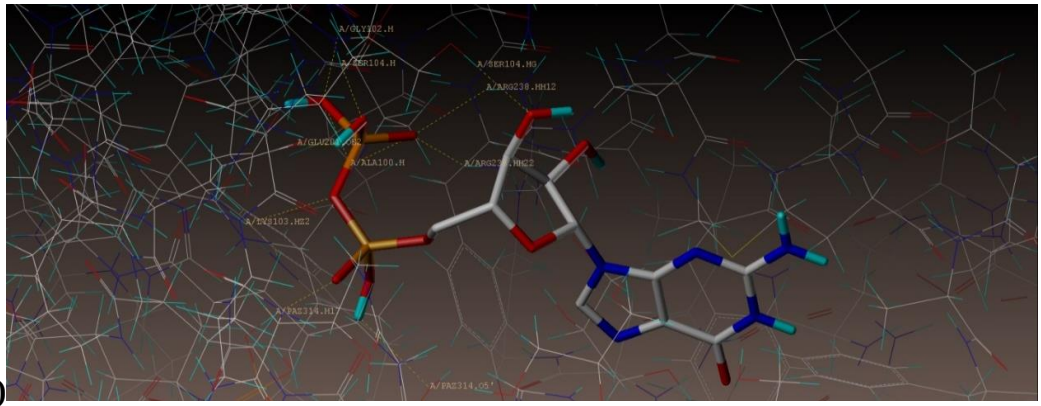

B)

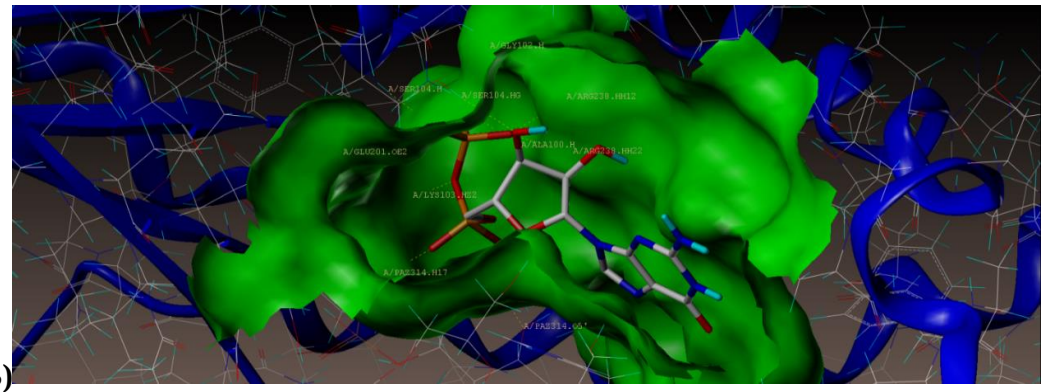

C)

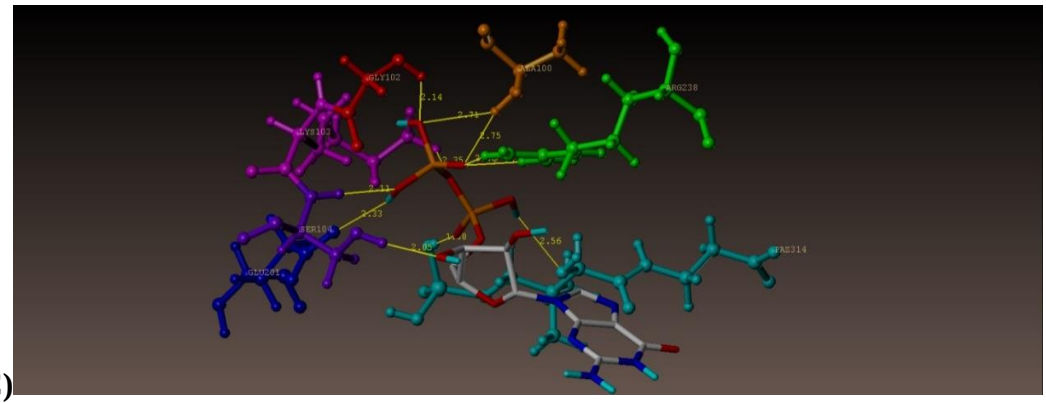

Figure 5.42: Docked view of 3AEZ_ligand at the active site of the enzyme MtPanK(PDB: 3AEZ) A) 3AEZ_ligand in stick form at the active site of enzyme in wireframe form B) 3AEZ_ligand at the active site of enzyme in ribbon form C) Ball and stick model of 3AEZ_ligand interacting with amino acids of enzyme

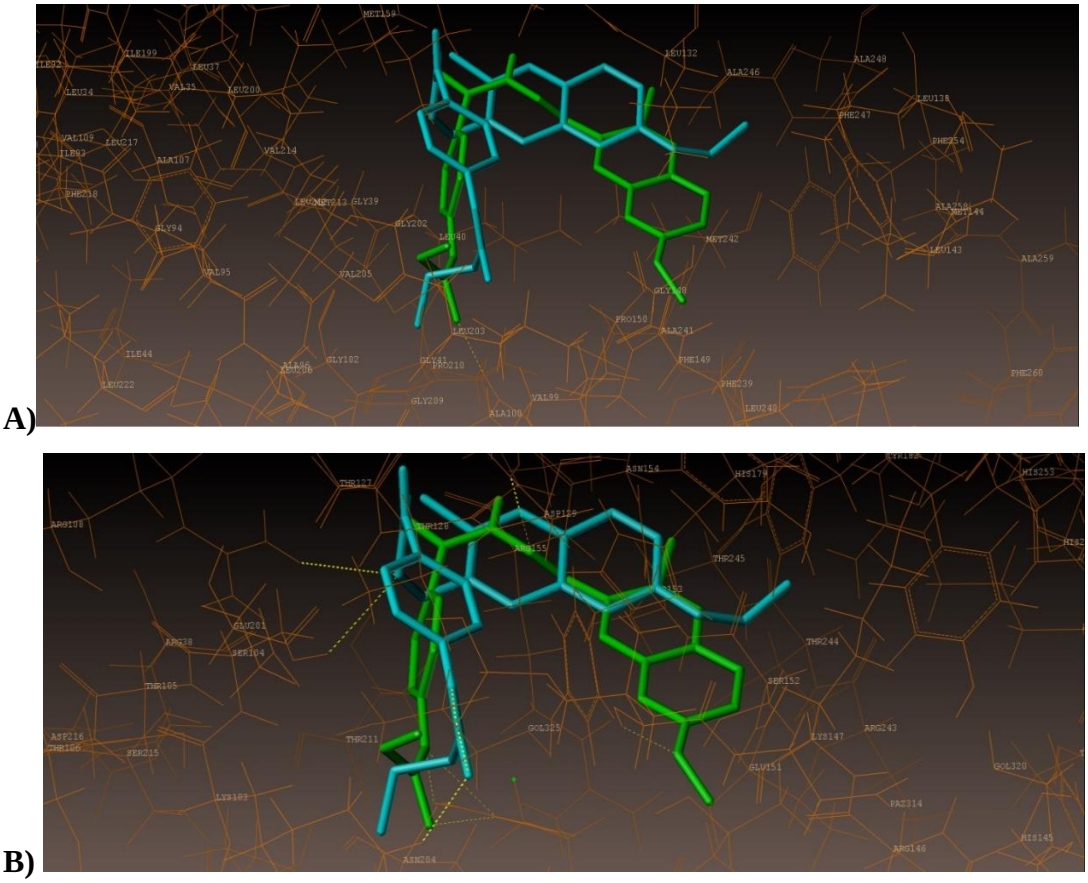

Figure 5.43: A) Hydrophobic amino acids surrounded to compounds 4k (green colour) and 4o (cyan colour). B) Hydrophilic amino acids surrounded to compounds 4k and 4o.

These findings highlighted the significance of MtPanK as a therapeutic target in antitubercular and antibacterial drug discovery. The favourable docking scores and interactions observed in this study suggest that the synthesized compounds are potential inhibitors of MtPanK, justifying further investigation in biological assays to confirm their efficacy in inhibiting the growth of *M. tuberculosis* and other pathogenic bacteria.

5.3.2 Docking study of synthesized molecules 4a-4r with CTP synthase MtPyrG

Molecular docking studies were conducted to explore the mechanism and detailed intermolecular interactions between the synthesized compounds and *M. tuberculosis* PyrG in complex with two UTP molecules (PDB ID 4ZDJ, 1.99 Å resolution, X-ray diffraction).

CTP synthase is a crucial enzyme involved in the conversion of UTP to CTP, a process essential for bacterial nucleic acid metabolism and viability. Inhibiting this enzyme disrupts nucleotide biosynthesis, impairing RNA and DNA replication, thereby bacterial growth and survival. This makes CTP synthase a promising target for developing antitubercular agents and broad-spectrum antibacterial therapies, particularly against drug-resistant strains[151].

In humans, CTP synthase exists in two isoforms (CTPS1 and CTPS2) that regulate cellular CTP levels for DNA and RNA synthesis, membrane lipid production, and cell division. However, structural differences between bacterial and human CTP synthase offer the potential to design selective inhibitors that specifically target bacterial enzymes, with no or minimum effects on human cells.

This docking study was carried out using the Surflex-Dock module of the Sybyl-X 2.0 software. The synthesized inhibitors 4a-4r, along with the reference ligand, were docked into the enzyme's active site, as illustrated in Figures 5.44.

A)

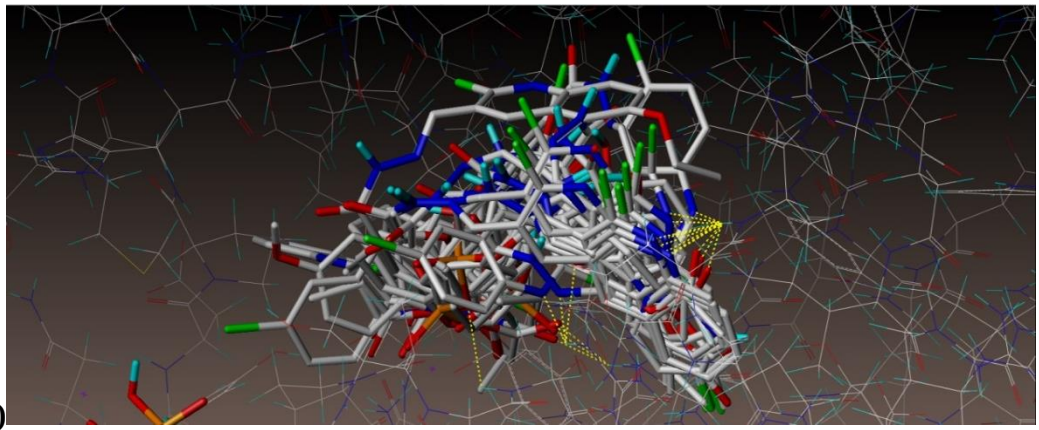

B)

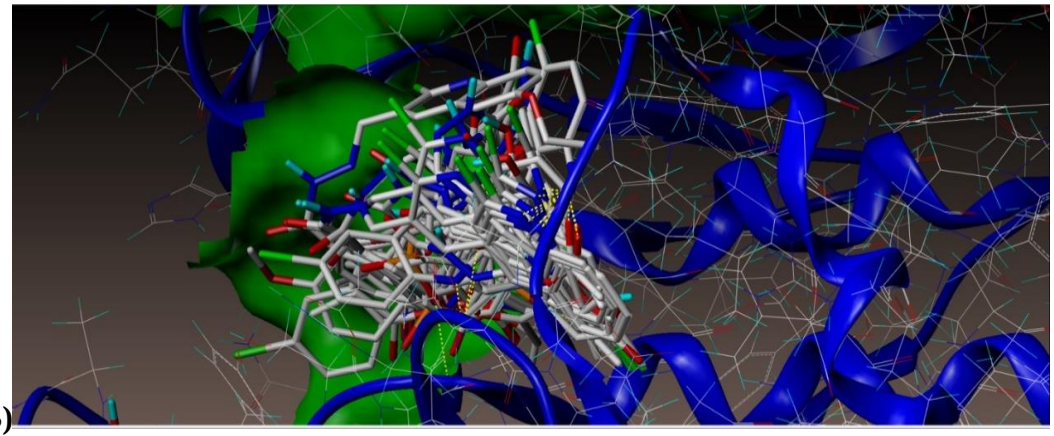

Figure 5.44: Docked view of the synthesized compounds 4a-4r at the active site of the enzyme CTP synthase PyrG (PDB ID: 4ZDJ)A) Molecules in Ball and stick model B) Molecules represented in ball and stick model with enzyme in ribbon form

The predicted binding energies of the docked compounds are presented in Table 5.22.

Table 5.22: Docking study results for synthesized molecules 4a – 4r with crystal structure of protein CTP synthase PyrG (PDB ID 4ZDJ)

Compounds	C Score[a]	Crash Score[b]	Polar Score[c]	D Score[d]	PMF Score[e]	G Score[f]	Chem Score[g]
4ZDJ_ligand	13.17	-2.53	12.94	-199.327	-113.793	-318.226	-13.778
4b	8.06	-1.46	5.63	-92.915	-0.188	-146.627	-32.070
4l	7.92	-1.11	4.51	-90.547	-4.571	-146.473	-26.176
4o	7.76	-1.38	4.54	-91.973	-7.810	-107.915	-26.666
4m	7.75	-1.56	2.31	-107.362	-33.063	-167.438	-24.736
4i	7.39	-1.35	3.22	-95.683	-18.230	-191.974	-28.053
4c	7.07	-2.24	5.05	-102.217	-10.613	-148.127	-31.553
4h	7.06	-1.59	3.31	-97.511	5.878	-164.133	-27.187
4f	6.86	-1.83	5.34	-103.516	-9.793	-148.626	-32.044
4a	6.62	-1.13	3.45	-92.408	-6.558	-134.844	-26.274
4k	6.43	-0.94	4.54	-80.983	-2.628	-122.332	-24.483
4q	6.40	-2.78	5.38	-107.055	6.202	-161.058	-31.751
4g	5.89	-1.23	3.68	-99.243	-26.490	-151.325	-26.377
4n	5.85	-0.79	4.49	-68.482	12.184	-84.134	-21.970
4r	5.51	-1.41	5.32	-85.964	-32.350	-98.979	-27.881
4e	5.40	-1.13	4.81	-88.484	-1.906	-129.441	-29.775
4d	5.40	-2.78	4.12	-114.733	2.376	-182.266	-30.652
4j	5.22	-0.70	3.26	-77.236	-7.395	-112.315	-20.636
4p	4.80	-0.55	3.32	-75.362	-11.580	-110.927	-21.606

[a]CScore (Consensus Score) integrates number of popular scoring functions for ranking the affinity of ligands bound to the active site of a receptor and reports the output of total score.

[b] Crash-score reveals inappropriate penetration into the binding site. Crash scores close to 0 are favourable. Negative numbers indicate penetration.

[c] Polar indicates the contribution of the polar interactions to the total score. The polar score may be useful for excluding docking results that make no hydrogen bonds.

[d] D-score indicates charge and van der Waals interactions between the protein and the ligand.

[e] PMF-score indicates the Helmholtz free energies of interactions for protein-ligand atom pairs (Potential of Mean Force, PMF).

[f] G-score shows hydrogen bonding, complex (ligand-protein), and internal (ligand-ligand) energies.

[g] Chem-score points for H-bonding, lipophilic contact, and rotational entropy, along with an intercept term.

- 4ZDJ_ligand has the highest C Score (13.17), indicating the best overall binding affinity. Among the synthesized compounds, 4b (8.06) and 4l (7.92) showed the strongest binding affinities.
- 4p has the least negative Crash Score (-0.55), indicating minimal distortion during docking and a stable binding conformation. 4d and 4q have more negative crash scores (-2.78), which may suggest less favourable binding poses.
- 4ZDJ_ligand stands out with a significantly high Polar Score (12.94), indicating strong polar interactions. Among the compounds, 4b (5.63) and 4q (5.38) showed notable polar interactions, confirming the presence of hydrogen bonding with the target protein.
- 4ZDJ_ligand exhibits the most favourable Docking Score (-199.327), indicating the strongest binding interaction. For the synthesized compounds, 4m (-107.362) and 4q (-107.055) showed strong binding, while 4n (-68.482) had the weakest binding interaction.
- 4n has a relatively high PMF Score (12.184), indicating weaker interactions. In contrast, 4ZDJ_ligand (-113.793) and 4r (-32.350) showed more favourable interaction energies.
- 4ZDJ_ligand again shows the best binding based on the most negative G Score (-318.226), indicating highly favourable binding. Among the synthesized compounds, 4i (-191.974) and 4d (-182.266) showed strong binding, while 4n (-84.134) and 4r (-98.979) exhibited weaker binding. 4b (-32.070), 4f (-32.044), and 4q (-31.751) had high Chem Scores, indicating favourable chemical interactions.
- 4ZDJ_ligand (-13.778) has a relatively lower Chem Score, suggesting that chemical interactions contributed less to its overall binding.

Among synthesized compounds, 4b, 4l, and 4m showed strong binding affinity across multiple scores. The molecules 4n and 4p demonstrated weaker binding and could be less promising for further investigation. Polar interactions and Docking Scores (D Score) suggested that 4b, 4l, and 4i could have strong potential as antibacterial agents based on their docking performance.

Thedocking poses of these molecules were visualized using the software and discussed in the following section.

As illustrated in Figure 5.45, compound 4b formed two hydrogen bonding interactions at the enzyme's active site (PDB ID: 4ZDJ). One of these interactions involved the nitrogen atom of the imine group (CH=N) forming a hydrogen bond with ARG223 (N---H-ARG223, 2.28 Å). The second hydrogen bond arose from the nitrogen atom at the 1stposition of the quinoline ring, which interacted with the hydrogen atom of ALA253 (N---H-ALA253, 2.61 Å).

As depicted in Figure5.46, compound 4lformed two hydrogen bonding interactions at the active site of the enzyme (PDB ID: 6M3M), among those an interaction was of oxygen atom of 1-phenyl acetate ring with hydrogen atom of LEU26 (O------H-LEU26, 2.01 Å), and remaining another hydrogen bonding interaction raised from the nitrogen atom which is present on the 1st position of quinoline ring with hydrogen atom of ALA253 (N-----H-ALA253, 2.02 Å).

As shown in the Figure 5.47, 4ZDJ_ligand formed four hydrogen bonding interactions at the active site of the enzyme (PDB ID: 4ZDJ).

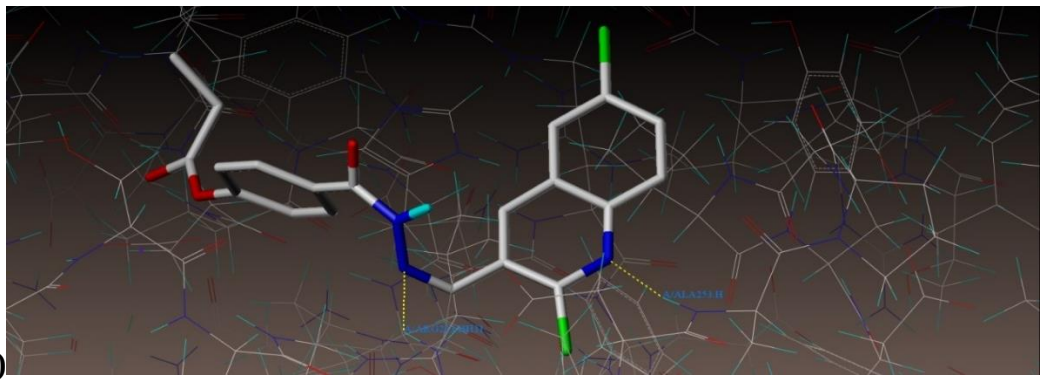

A)

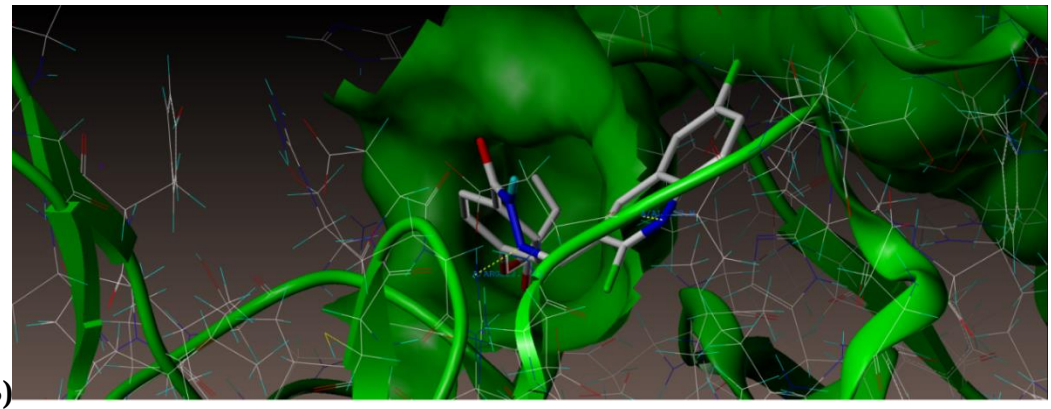

B)

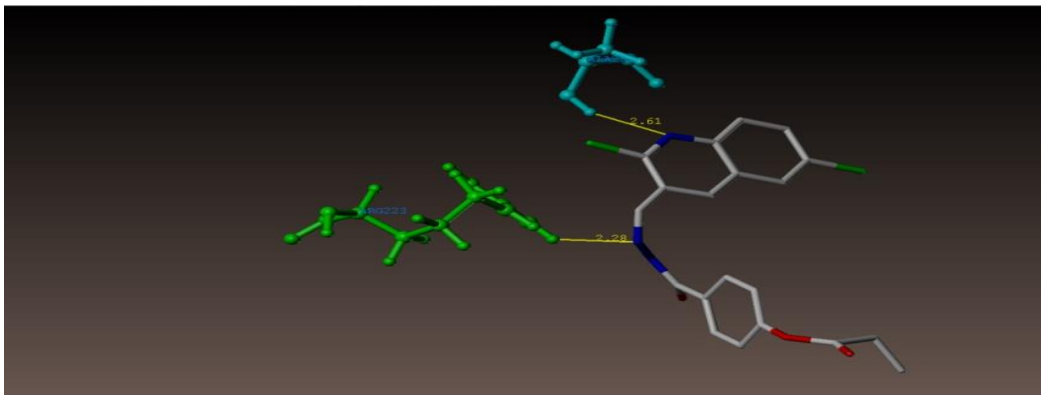

C)

Figure 5.45: Docked view of compound 4b at the active site of the enzyme CTP synthase PyrG (PDB: 4ZDJ) A) Compound 4b in stick model at the active site of enzyme in wireframe form B) Compound 4b in active site of enzyme in ribbon form C) Ball and stick model of compound 4b interacting with amino acids of enzyme

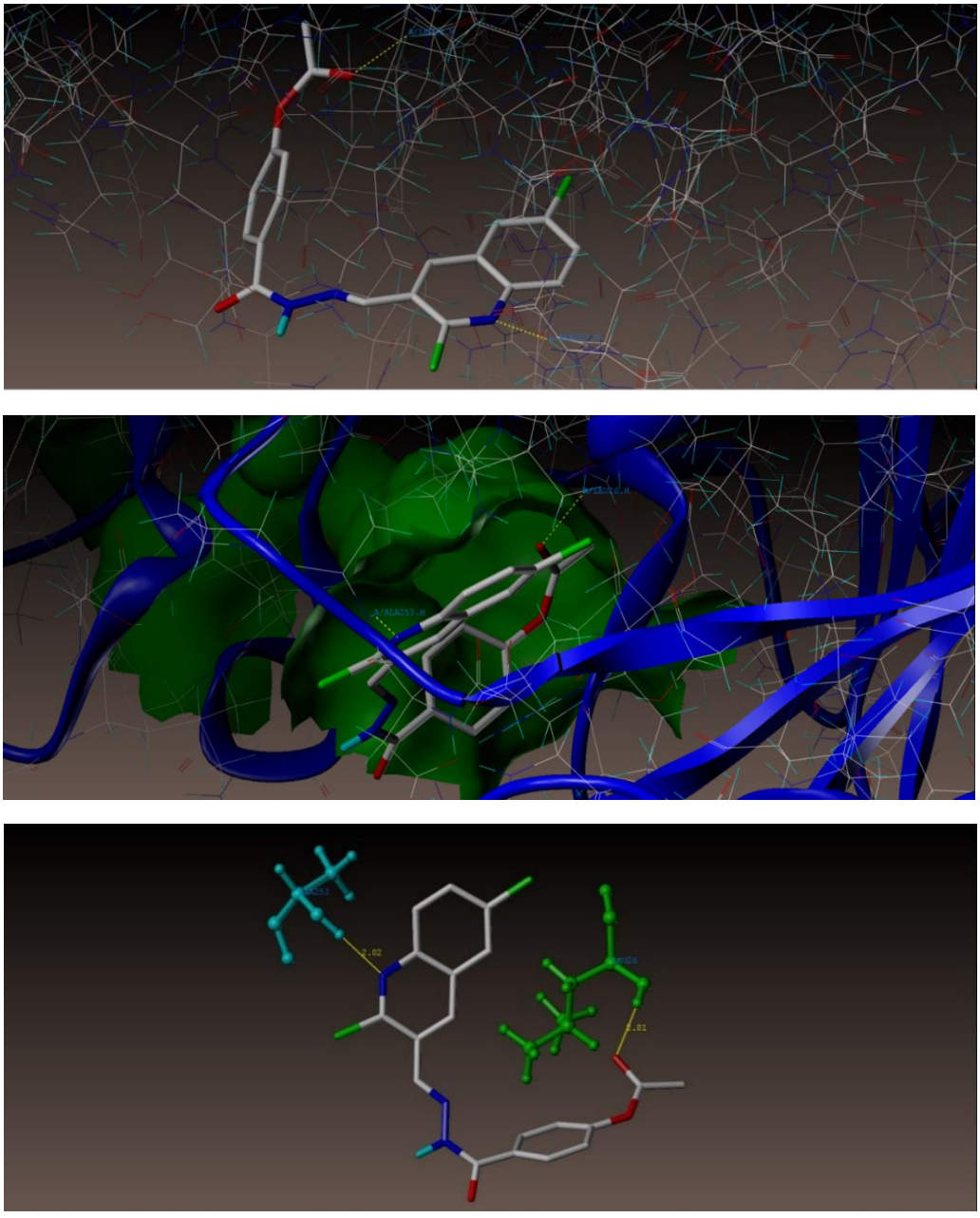

Figure 5.46: Docked view of compound 4l at the active site of the enzyme CTP synthase PyrG(PDB: 4ZDJ) A) Compound 4l in stick model at the active site of enzyme in wireframe form B) Compound 4l in active site of enzyme in ribbon

form C) Ball and stick model of compound 4l interacting with amino acids of enzyme

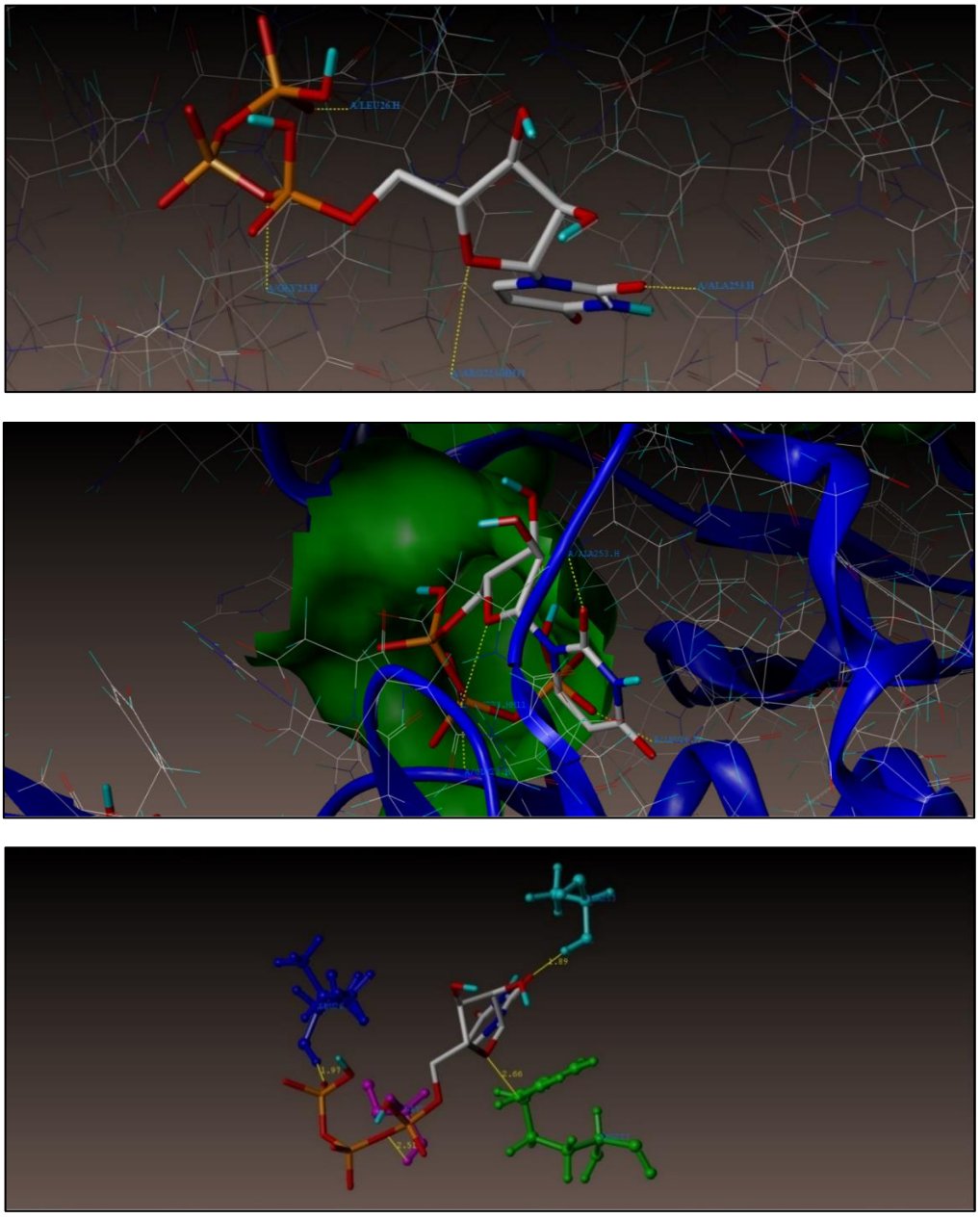

Figure 5.47: Docked view of 4ZDJ_ligand at the active site of the enzyme CTP synthase PyrG PDB: 4ZDJ A) 4ZDJ_ligand in stick model at the active site of enzyme in wireframe form B) 4ZDJ_ligand in active site of enzyme in ribbon

form C) Ball and stick model of 4ZDJ_ligand interacting with amino acids of enzyme

A)

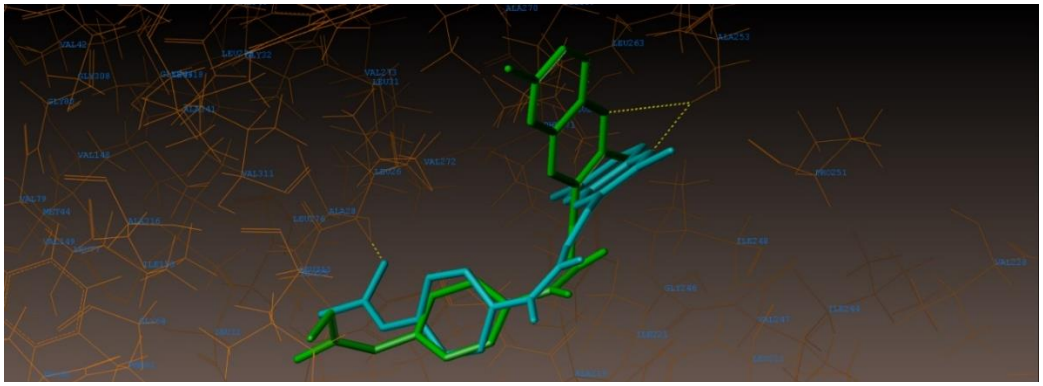

B)

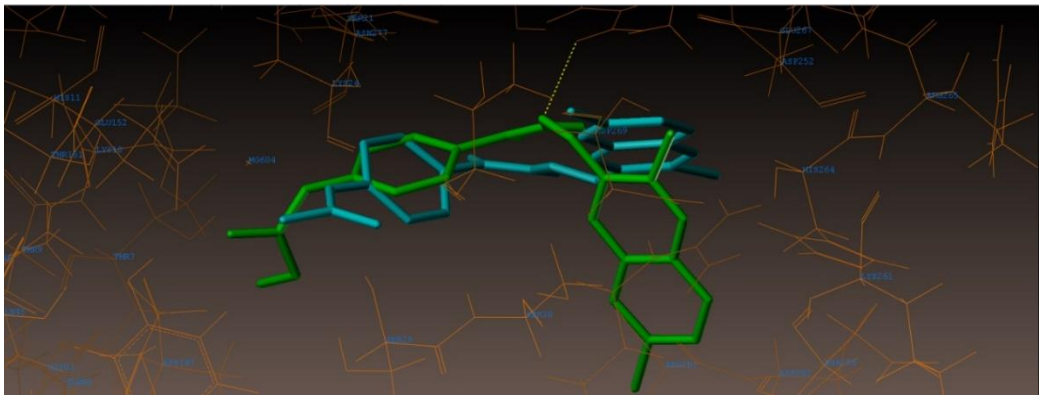

Figure 5.48: A) Hydrophobic amino acids surrounded to compounds 4b (green colour) and 4l (cyan colour). B) Hydrophilic amino acids surrounded to compounds 4b and 4l

Figure 5.48 represented interactions of hydrophobic and hydrophilic amino acids surrounding compounds4b and 4l.

All the compounds showed consensus score in the range 8.06-4.80, indicating the summary of all forces of interaction between ligands and the protein. The synthesized compounds showed same type of interactions with amino acid residues (LEU26, ALA253 and ARG223) as that of 4ZDJ_ligand. This indicated that molecules preferentially bind to protein in similar way as that of the 4ZDJ_ligand.

A multi-targeted approach to antitubercular therapy involving the simultaneous inhibition of PanK and PyrG presents a promising strategy to combat tuberculosis, especially in light of rising drug resistance. By inhibiting both PanK and PyrG, this approach disrupts essential metabolic and biosynthetic pathways in Mtb, potentially enhancing the bactericidal effect and minimizing the likelihood of resistance development compared to single targettreatments.By leveraging the interconnected nature of CoA and pyrimidine pathways, multi-target inhibitors not only weaken resilience of mycobacterium but may also improve treatment outcomes and help manage multidrug-resistant strains[152-154].

Molecules like 4k, 4o, 4l, and 4b have shown significant binding affinity across both docking results of Pank and PyrG, suggesting they could serve as dual-target inhibitors. This dual inhibition capability implies that these compounds might disrupt both CoA biosynthesis and nucleotide synthesis pathways, which are crucial for bacterial survival and proliferation. The ability of these molecules to bind effectively to both enzymes suggests thatthey possess structural features that allow them to accommodate the binding pockets of PanK and PyrG. High C Scores in both docking results indicate a favourable orientation and fit within the active site of each enzyme, likely due to adaptable polar and hydrophobic regions in the molecule. Compounds like 4k and 4b have shown high Polar Scores in both docking results, indicating formation of hydrogen bonds and polar interactions in active sites of both enzymes. Such interactions strengthen binding stability and suggest potential for effective inhibition.

5.4 PREDICTION OF ADME PROPERTIES OF 6-SUBSTITUTED-2-CHLOROQUINOLINE-3-CARBALDEHYDE HYDRAZIDE ESTER DERIVATIVES

In drug discovery and development, evaluating the ADME properties of novel compounds is critical for understanding their pharmacokinetic behaviour and potential efficacy as therapeutic agents. The prediction of ADME characteristics for synthesized molecules, 4a-4r, using SwissADME software, provides valuable insights into their drug-like properties, including bioavailability, permeability, metabolic stability and toxicity risks[155]. These predictions are pivotal in determining the suitability of these compounds for further development and optimizing their pharmacological profiles for better therapeutic outcomes.

Physicochemical properties of synthesized molecules 4a-4r were predicted as shown in Table 5.23. Table 5.24 and Table 5.25.

Table 5.23: Physicochemical properties predicted by SwissADME software for synthesized molecules 4a – 4f

Molecule	**4a**	**4b**	**4c**	**4d**	**4e**	**4f**
Physicochemical properties						
Molecular weight (g/mol)	416.26	381.81	395.84	402.23	416.26	430.28
Num. heavy atoms	28	27	28	27	28	29
Num. aromatic heavy atoms	16	16	16	16	16	16
Fraction Csp3	0.1	0.1	0.14	0.05	0.1	0.14
Num. rotatable bonds	7	7	8	6	7	8
Num. H-bond acceptors	5	5	5	5	5	5
Num. H-bond donors	1	1	1	1	1	1
Molar Refractivity	109.24	104.23	109.03	104.43	109.24	114.04
TPSA ($Å^2$)	80.65	80.65	80.65	80.65	80.65	80.65

Table 5.24: Physicochemical properties predicted by SwissADME software for synthesized molecules 4g – 4l

Molecule	**4g**	**4h**	**4i**	**4j**	**4k**	**4l**
Physicochemical properties						
Molecular weight (g/mol)	381.81	395.84	409.87	397.81	411.84	425.86
Num. heavy atoms	27	28	29	28	29	30
Num. aromatic heavy atoms	16	16	16	16	16	16
Fraction Csp3	0.1	0.14	0.18	0.1	0.14	0.18
Num. rotatable bonds	6	7	8	7	8	9
Num. H-bond acceptors	5	5	5	6	6	6
Num. H-bond donors	1	1	1	1	1	1
Molar Refractivity	104.39	109.19	114	105.91	110.72	115.53
TPSA (Å²)	80.65	80.65	80.65	89.88	89.88	89.88

Table 5.25: Physicochemical properties predicted by SwissADME software for synthesized molecules 4m – 4r

Molecule	**4m**	**4n**	**4o**	**4p**	**4q**	**4r**
Physicochemical properties						
Molecular weight (g/mol)	411.84	425.86	439.89	446.68	460.71	474.73
Num. heavy atoms	29	30	31	27	28	29
Num. aromatic heavy atoms	16	16	16	16	16	16
Fraction Csp3	0.14	0.18	0.22	0.05	0.1	0.14
Num. rotatable bonds	8	9	10	6	7	8
Num. H-bond acceptors	6	6	6	5	5	5
Num. H-bond donors	1	1	1	1	1	1
Molar Refractivity	110.72	115.53	120.33	107.12	111.93	116.73
TPSA (Å²)	89.88	89.88	89.88	80.65	80.65	80.65

The molecular weights of these compounds ranged from 381 to 474 g/mol, which is within the acceptable range for oral drug-like molecules, typically capped at

500 g/mol. This suggests that the molecules are likely to exhibit favourable absorption and distribution characteristics.

Topological Polar Surface Area (TPSA) values for these compounds ranged between 80.65 and 89.88 $Å^2$, representing moderate polar surface area. These values are below the threshold of 140 $Å^2$ for good oral absorption and below the 90 $Å^2$ threshold for penetration across the blood-brain barrier, suggesting good membrane permeability and oral bioavailability potential.The number of rotatable bonds varied from 6 to 10 across the series, providing an indication of molecular flexibility. A moderate number of rotatable bonds (usually fewer than 10) is desirable as it balances the molecule's flexibility without compromising on its bioavailability.

The Csp^3 fraction for the molecules ranged between 0.05 and 0.18, suggesting that these compounds are relatively flat with limited sp^3 hybridization. Decreased Csp^3 values indicate more planar structures, which may sometimes be associated with poor solubility and bioavailability.Butthe values in this low range do not pose a significant challenge to the compounds' drug-likeness.

The molar refractivity of these molecules was found within the range of 104 to 115, indicating their polarizability. These values are appropriate for drug-like molecules, balancing lipophilicity and molecular volume, thus influencing the molecules to permeate through membranes and interact with biological targets.

Lipophilicity related properties of synthesized molecules 4a-4r were predicted as shown in Table 5.26, Table 5.27 and Table 5.28.

Table 5.26: Lipophilicity related properties predicted by SwissADME software for synthesized molecules 4a – 4f

Molecule	**4a**	**4b**	**4c**	**4d**	**4e**	**4f**
Lipophilicity						
Log Po/w (iLOGP)	3.1	2.92	3.14	2.89	3.1	3.19
Log Po/w (XLOGP3)	4.91	4.28	4.64	4.44	4.91	5.27
Log Po/w (WLOGP)	4.62	3.97	4.36	4.23	4.62	5.01
Log Po/w (MLOGP)	3.49	3	3.22	3.27	3.49	3.71
Log Po/w (SILICOS-IT)	5.11	4.46	4.86	4.72	5.11	5.51
Consensus Log Po/w	4.25	3.73	4.04	3.91	4.25	4.54

Table 5.27: Lipophilicity related properties predicted by SwissADME software for synthesized molecules 4g – 4l

Molecule	**4g**	**4h**	**4i**	**4j**	**4k**	**4l**
Lipophilicity						
Log Po/w (iLOGP)	2.89	3.17	3.27	3.19	3.1	3.36
Log Po/w (XLOGP3)	4.18	4.65	5.01	3.78	4.25	4.61
Log Po/w (WLOGP)	3.89	4.28	4.67	3.59	3.98	4.37
Log Po/w (MLOGP)	3	3.22	3.44	2.47	2.69	2.91
Log Po/w (SILICOS-IT)	4.59	4.99	5.39	4.14	4.54	4.94
Consensus Log Po/w	3.71	4.06	4.36	3.43	3.71	4.04

Table 5.28: Lipophilicity related properties predicted by SwissADME software for synthesized molecules 4m – 4r

Molecule	**4m**	**4n**	**4o**	**4p**	**4q**	**4r**
Lipophilicity						
Log Po/w (iLOGP)	3.46	3.73	3.69	3	3.17	3.36
Log Po/w (XLOGP3)	4.15	4.62	4.98	4.5	4.97	5.33
Log Po/w (WLOGP)	3.98	4.37	4.76	4.34	4.73	5.12
Log Po/w (MLOGP)	2.69	2.91	3.12	3.38	3.6	3.81
Log Po/w (SILICOS-IT)	4.54	4.94	5.35	4.75	5.15	5.55
Consensus Log Po/w	3.76	4.11	4.38	4	4.32	4.63

The Log P (partition coefficient) is a measure of a molecule's hydrophobicity, which provides insight into its solubility and permeability. Different models in SwissADME use various algorithms to predict this value.

- **iLOGP** This model is based on a physics-informed method that estimates Log P by focusing on free energies of solvation in water and n-octanol. Lower iLOGP values indicate more hydrophilic molecules, while higher values suggest greater lipophilicity.
- **XLOGP3** This is a knowledge-based method that estimates Log P using atom contributions and correction factors. It's commonly used for molecules with complex structures like those in drug discovery. A higher XLOGP3 indicates a more lipophilic (hydrophobic) compound, favouring membrane permeability but potentially reducing water solubility.
- **WLOGP** This method relies on fragment-based contributions to calculate Log P. It often provides similar insights as XLOGP3 but may vary depending on how molecular fragments interact with different chemical environments.
- **MLOGP** This model is another fragment-based prediction method, but it uses specific molecular fragments to calculate Log P. Variations from WLOGP or XLOGP3 may arise due to differences in the fragment library and calculation methods.
- **SILICOS-IT** This method is a hybrid approach using 3D molecular structure and surface interactions to estimate Log P. It's useful for predicting behaviour in systems where molecular shape and solvation play a significant role.
- **Consensus Log Po/w** This value represents the average of the different Log P models. By combining the predictions, it provides a more balanced estimate of the molecule's lipophilicity.

The Log Po/w values for the synthesized molecules 4a-4r were predicted using various models in SwissADME software, showing the following ranges: iLOGP (2.89-3.73),XLOGP3 (3.7-5.3), WLOGP (3.59-5.12), MLOGP (2.69-3.81), SILICOS-IT (4.14-5.55), and Consensus Log Po/w (3.4-4.6). These values indicate that the molecules possess moderate to high lipophilicity. The iLOGP and MLOGP values suggest a somewhat balanced lipophilicity, potentially offering good membrane permeability and reasonable water solubility. In contrast, higher values from XLOGP3, WLOGP, and SILICOS-IT point towards strong lipophilicity, which favours membrane penetration but could limit solubility in aqueous environments. The Consensus Log Po/w (3.4-4.6) provides an overall assessment of moderate to high lipophilicity, which may be favourable for drug absorption, particularly for oral bioavailability, though care should be taken regarding solubility and distribution in biological systems.

Water solubility related properties of synthesized molecules 4a-4r were predicted as shown in Table 5.29, Table 5.30 and Table 5.31.

Table 5.29: Water solubility related properties predicted by SwissADME software for synthesized molecules 4a – 4f

Molecule	**4a**	**4b**	**4c**	**4d**	**4e**	**4f**
Water Solubility						
Log S (ESOL)	-5.47	-4.88	-5.11	-5.17	-5.47	-5.71
Solubility (mol/l) e-05	0.335	1.32	0.772	0.671	0.335	0.196
Class	Moderate soluble	Moderate soluble	Moderate soluble	Moderate soluble	Moderate soluble	Moderate soluble
Log S (Ali)	-6.34	-5.69	-6.06	-5.85	-6.34	-6.71
Solubility (mol/l) e-06	0.457	2.06	0.871	1.41	0.457	0.193
Class	Poorly	Moderate	Poorly	Moderate	Poorly	Poorly

Molecule	**4a**	**4b**	**4c**	**4d**	**4e**	**4f**
	soluble	soluble	soluble	soluble	soluble	soluble
Log S (SILICOS-IT)	-7.93	-7.34	-7.74	-7.54	-7.93	-8.32
Solubility (mol/l) e-08	1.17	4.52	1.82	2.88	1.17	0.474
Class	Poorly soluble	Poorly soluble	Poorly soluble	Poorly soluble	Poorly soluble	Poorly soluble

Table 5.30: Water solubility related properties predicted by SwissADME software for synthesized molecules 4g – 4l

Molecule	**4g**	**4h**	**4i**	**4j**	**4k**	**4l**
Water Solubility						
Log S (ESOL)	-4.88	-5.18	-5.42	-4.65	-4.95	-5.19
Solubility (mol/l) (e-05)	1.31	0.654	0.382	2.25	1.12	0.653
Class	Moderate soluble	Moderate soluble	Moderate soluble	Moderate soluble	Moderate soluble	Moderate soluble
Log S (Ali)	-5.58	-6.07	-6.44	-5.36	-5.85	-6.22
Solubility (mol/l) (e-06)	2.62	0.851	0.360	4.35	1.42	0.599
Class	Moderate soluble	Poorly soluble	Poorly soluble	Moderate soluble	Moderate soluble	Poorly soluble
Log S (SILICOS-IT)	-7.33	-7.72	-8.11	-7.05	-7.45	-7.84
Solubility (mol/l) (e-08)	4.70	1.90	0.769	8.81	3.56	1.45
Class	Poorly soluble	Poorly soluble	Poorly soluble	Poorly soluble	Poorly soluble	Poorly soluble

Table 5.31: Water solubility related properties predicted by SwissADME software for synthesized molecules 4m – 4r

Molecule	4m	4n	4o	4p	4q	4r
Water Solubility						
Log S (ESOL)	-4.89	-5.19	-5.43	-5.49	-5.79	-6.02
Solubility (mol/l) (e-06)	12.9	6.43	3.74	3.26	1.63	0.952
Class	Moderate soluble	Moderate soluble	Moderate soluble	Moderate soluble	Moderate soluble	Poorly soluble
Log S (Ali)	-5.75	-6.23	-6.61	-5.91	-6.4	-6.78
Solubility (mol/l) (e-06)	1.80	0.585	0.247	1.22	0.396	0.168
Class	Moderate soluble	Poorly soluble	Poorly soluble	Moderate soluble	Poorly soluble	Poorly soluble
Log S (SILICOS-IT)	-7.45	-7.84	-8.23	-7.73	-8.12	-8.52
Solubility (mol/l) (e-08)	3.56	1.45	0.587	1.85	0.750	0.305
Class	Poorly soluble	Poorly soluble	Poorly soluble	Poorly soluble	Poorly soluble	Poorly soluble

The Log S value refers to the solubility prediction of a molecule, typically expressed as the logarithm of the aqueous solubility (S). In drug design, understanding solubility is essential for predicting bioavailability.

- **Log S (ESOL)** The **ESOL** (Estimated Solubility) method is a simple, fragment-based model for predicting aqueous solubility based on molecular properties such as molecular weight, the number of rotatable bonds, and polar surface area. It gives a good balance between accuracy and computational efficiency, making it useful for quick solubility estimations.
- **Log S (Ali)** This model, developed by Ali et al., is also fragment-based but employs a different fragment library and algorithm compared to ESOL. It focuses more on accurately modelling the behaviour of functional groups and

their interactions in solution, providing another perspective on how the molecule might dissolve in water.

- **Log S (SILICOS-IT)** This model uses a combination of 3D molecular structures and fragment-based contributions to estimate solubility. It is particularly useful when considering the molecular shape and steric interactions in predicting solubility, offering a more structural-based approach compared to the purely fragment-based models.

The Log S values for the synthesized molecules 4a-4r were predicted using various models in SwissADME software. The ESOL method predicted most of the molecules to be moderately soluble except 4r. Moderate solubility suggests these molecules should dissolve reasonably well in aqueous environments, supporting better absorption and bioavailability.

The Ali model predicted the molecules to be poorly or moderately soluble. Poor solubility could potentially limit the molecules' absorption and distribution in biological systems, especially if administered orally.

The SILICOS-IT model predicted all the molecules to be poorly soluble, likely due to its emphasis on structural and steric properties. This implies that the compounds may face solubility challenges in dissolving in water, creating impact on their pharmacokinetic behaviour.

While the ESOL model suggests moderate solubility for most compounds, the Ali and SILICOS-IT models provide more cautious estimates, emphasizing the need to balance lipophilicity and solubility for optimal drug absorption and effectiveness.
The figure 5.49 shows corelation of three key properties of synthesized compounds: Molecular Weight, Log Po/w (iLOGP), and Log S (ESOL).

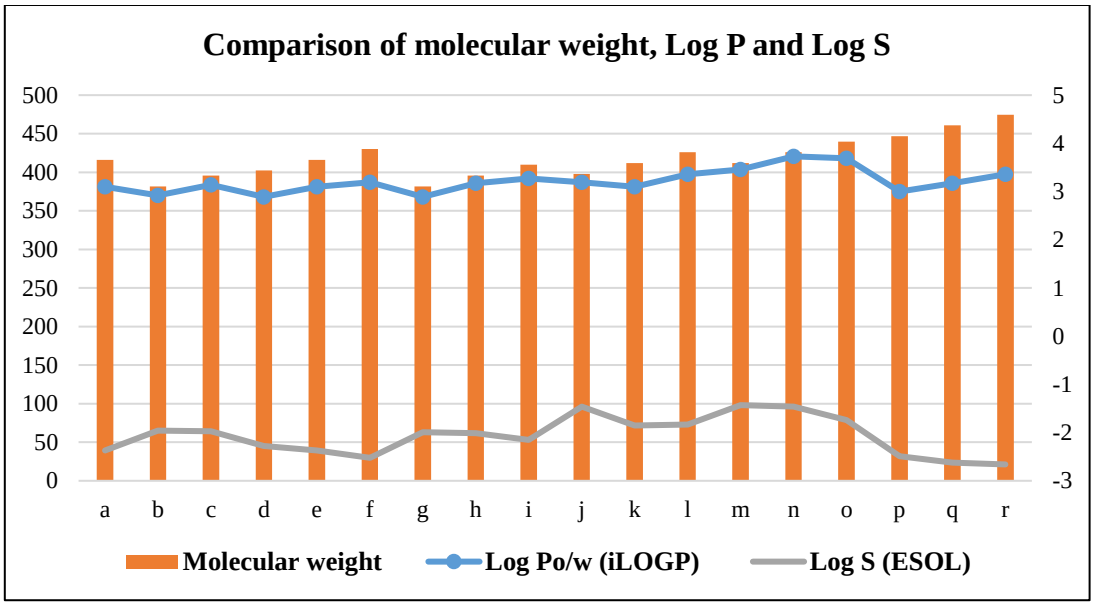

Figure 5.49: Correlationof three key properties of synthesized compounds 4a-4r – Molecular weight, Log P and Log S predicted using SwissADME software

The clustered column linechartin Figure 5.49 shows that all compounds have a similar molecular weight, moderate to high lipophilicity (favourable for permeability), but poor solubility, which could be a limiting factor for drug development. Efforts to improve the solubility of these compounds may be necessary without significantly impacting their lipophilicity and molecular weight.

Pharmacokinetics properties of synthesized molecules 4a-4r were predicted as shown in Table 5.32, Table 5.33 and Table 5.34.

Table 5.32: Pharmacokinetics properties predicted by SwissADME software for synthesized molecules 4a – 4f

Molecule	**4a**	**4b**	**4c**	**4d**	**4e**	**4f**
Pharmacokinetics						
GI absorption	High	High	High	High	High	High
BBB permeation	No	No	No	No	No	No
P-gp substrate	No	No	No	No	No	No
CYP1A2 inhibitor	Yes	Yes	Yes	Yes	Yes	Yes
CYP2C19 inhibitor	Yes	Yes	Yes	Yes	Yes	Yes
CYP2C9 inhibitor	Yes	Yes	Yes	Yes	Yes	Yes
CYP2D6 inhibitor	No	No	No	No	No	No
CYP3A4 inhibitor	Yes	Yes	Yes	No	Yes	Yes
Log Kp (skin permeation) cm/s	-5.35	-5.59	-5.42	-5.60	-5.35	-5.18

Table 5.33: Pharmacokinetics properties predicted by SwissADME software for synthesized molecules 4g – 4l

Molecule	**4g**	**4h**	**4i**	**4j**	**4k**	**4l**
Pharmacokinetics						
GI absorption	High	High	High	High	High	High
BBB permeation	No	No	No	No	No	No
P-gp substrate	No	No	No	No	No	No
CYP1A2 inhibitor	Yes	Yes	Yes	Yes	Yes	Yes
CYP2C19 inhibitor	Yes	Yes	Yes	Yes	Yes	Yes
CYP2C9 inhibitor	Yes	Yes	Yes	Yes	Yes	Yes
CYP2D6 inhibitor	No	No	No	No	No	No
CYP3A4 inhibitor	Yes	No	Yes	Yes	Yes	Yes
Log Kp (skin permeation) cm/s	-5.18	-5.66	-5.41	-5.24	-6.04	-5.79

Table 5.34: Pharmacokinetics properties predicted by SwissADME software for synthesized molecules 4m – 4r

Molecule	**4m**	**4n**	**4o**	**4p**	**4q**	**4r**
Pharmacokinetics						
GI absorption	High	High	High	High	High	High
BBB permeation	No	No	No	No	No	No

Molecule	**4m**	**4n**	**4o**	**4p**	**4q**	**4r**
P-gp substrate	No	No	No	No	No	No
CYP1A2 inhibitor	Yes	Yes	Yes	Yes	Yes	Yes
CYP2C19 inhibitor	Yes	Yes	Yes	Yes	Yes	Yes
CYP2C9 inhibitor	Yes	Yes	Yes	Yes	Yes	Yes
CYP2D6 inhibitor	No	No	No	No	No	No
CYP3A4 inhibitor	Yes	Yes	Yes	No	Yes	Yes
Log Kp (skin permeation) cm/s	-5.87	-5.62	-5.45	-5.83	-5.58	-5.41

High GI Absorption This indicates that the molecules are likely well-absorbed through the gastrointestinal tract, which is favourable for oral administration. High GI absorption typically suggests good oral bioavailability.

No BBB Permeation The lack of BBB permeation suggests that these molecules are unlikely to cross into the central nervous system (CNS). This could be advantageous for compounds where CNS side effects are undesirable, but limiting for those aimed at CNS targets.

No P-glycoprotein (P-gp) substrate Since these molecules are not substrates for P-glycoprotein, they are unlikely to be effluxed out of cells by this transporter, which is often a mechanism of drug resistance. This is a positive trait for maintaining drug levels inside target cells.

The molecules are likely inhibitors of the CYP1A2, CYP2C19 and CYP2C9 enzymes, which means they could interfere with the metabolism of drugs metabolized by these pathways, potentially leading to drug-drug interactions. Lack of inhibition for CYP2D6 means the compounds are unlikely to affect drugs metabolized by this enzyme. CYP3A4 is a major enzyme involved in drug metabolism, and if the compounds inhibit this enzyme, it could lead to significant drug-drug interactions. However, since there is variability in inhibition, some molecules may have different effects on CYP3A4 activity.

Log Kprefers to skin permeability. The values in the range of -5.18 to -6.04 suggest low skin permeability, meaning the compounds are unlikely to be absorbed effectively through the skin, which is important for determining the route of administration (e.g., oral rather than transdermal).

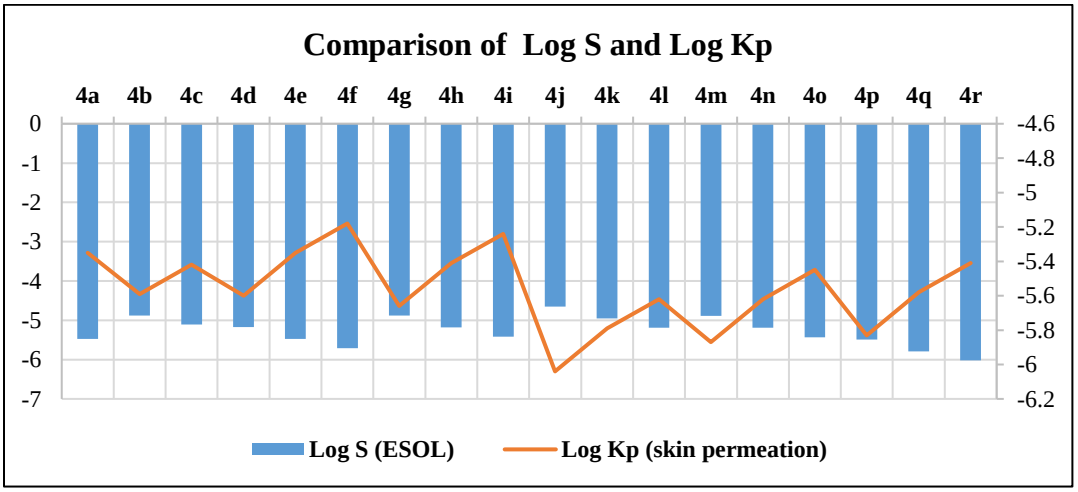

Figure 5.50: Comparison of Log S and Log Kp values of synthesized molecules 4a-4r predicted using SwissADME software

The chart in Figure 5.50shows that the synthesized compounds exhibit poor solubility (as indicated by low Log S values) and low skin permeability (based on Log Kp values). These characteristics suggest challenges for oral and transdermal delivery, and further modifications might be necessary to improve either solubility or skin permeation for drug formulation purposes.

Drug likeness related properties of synthesized molecules 4a-4r were predicted as shown in Table 5.35, Table 5.36 and Table 5.37.

Table 5.35: Drug likeness related properties predicted by SwissADME software for synthesized molecules 4a – 4f

Molecule	**4a**	**4b**	**4c**	**4d**	**4e**	**4f**
Drug likeness						
Ghose	Yes	Yes	Yes	Yes	Yes	Yes
Veber	Yes	Yes	Yes	Yes	Yes	Yes
Egan	Yes	Yes	Yes	Yes	Yes	Yes
Muegge	Yes	Yes	Yes	Yes	Yes	No*
Bioavailability Score	0.55	0.55	0.55	0.55	0.55	0.55

***** 1 violation: XLOGP3>5

Table 5.36: Drug likeness related properties predicted by SwissADME software for synthesized molecules 4g – 4l

Molecule	**4g**	**4h**	**4i**	**4j**	**4k**	**4l**
Drug likeness						
Ghose	Yes	Yes	Yes	Yes	Yes	Yes
Veber	Yes	Yes	Yes	Yes	Yes	Yes
Egan	Yes	Yes	Yes	Yes	Yes	Yes
Muegge	No	Yes	Yes	No*	Yes	Yes
Bioavailability Score	0.55	0.55	0.55	0.55	0.55	0.55

* 1 violation: XLOGP3>5

Table 5.37: Drug likeness related properties predicted by SwissADME software for synthesized molecules 4m – 4r

Molecule	**4m**	**4n**	**4o**	**4p**	**4q**	**4r**
Drug likeness						
Ghose	Yes	Yes	Yes	Yes	Yes	Yes
Veber	Yes	Yes	Yes	Yes	Yes	Yes
Egan	Yes	Yes	Yes	Yes	Yes	Yes
Muegge	Yes	Yes	Yes	Yes	Yes	No*
Bioavailability Score	0.55	0.55	0.55	0.55	0.55	0.55

* 1 violation: XLOGP3>5

The drug-likeness and related properties of the synthesized molecules based on the models and scores provided are highly favourable for drug development:

Drug-likeness Models Most of the molecules passed all major drug-likeness filters including Ghose, Veber, Egan, and Muegge. These filters evaluate various physicochemical properties such as molecular weight, hydrogen bond donors/acceptors, log P, polar surface area, and number of rotatable bonds. Passing these models suggests that most of the molecules are in accordance with the properties typically associated with orally active drugs.

Bioavailability ScoreA bioavailability score of 0.55 is indicative of moderate oral bioavailability. This score reflects the likelihood that the compounds will be well-absorbed when taken orally. The score is derived based on molecular properties like lipophilicity and size, which influence absorption.

In summary, these molecules exhibit good drug-likeness and reasonable oral bioavailability, making them promising candidates for further exploration in drug development.

Medicinal Chemistry related properties of synthesized molecules 4a-4r were predicted as shown in Table 5.38, Table 5.39 and Table 5.40.

Table 5.38: Medicinal Chemistry related properties predicted by SwissADME software for synthesized molecules 4a – 4f

Molecule	**4a**	**4b**	**4c**	**4d**	**4e**	**4f**
Medicinal Chemistry						
PAINS	0 alert	0 alert	0 alert	0 alert	0 alert	0 alert
Brenk	3 alerts	3 alerts	3 alerts	3 alerts	3 alerts	3 alerts
Lead likeness	No	No	No	No	No	No
Synthetic accessibility	2.79	2.78	2.9	2.69	2.79	2.91

Brenk Alerts: 2-halo_pyridine, imine_1, phenol ester
Lead likeness: MW>350, XLOGP3>3.5

Table 5.39: Medicinal Chemistry related properties predicted by SwissADME software for synthesized molecules 4g – 4l

Molecule	**4g**	**4h**	**4i**	**4j**	**4k**	**4l**
Medicinal Chemistry						
PAINS	0 alert	0 alert	0 alert	0 alert	0 alert	0 alert
Brenk	3 alerts	3 alerts	3 alerts	3 alerts	3 alerts	3 alerts
Lead likeness	No	No	No	No	No	No
Synthetic accessibility	2.79	2.89	3.01	2.83	2.93	3.05

Brenk Alerts: 2-halo_pyridine, imine_1, phenol_ester
Lead likeness: MW>350, XLOGP3>3.5

Table 5.40: Medicinal Chemistry related properties predicted by SwissADME software for synthesized molecules 4m – 4r

Molecule	**4m**	**4n**	**4o**	**4p**	**4q**	**4r**
Medicinal Chemistry						
PAINS	0 alert	0 alert	0 alert	0 alert	0 alert	0 alert
Brenk	3 alerts	3 alerts	3 alerts	3 alerts	3 alerts	3 alerts
Lead likeness	No	No	No	No	No	No
Synthetic accessibility	2.79	2.78	2.9	2.69	2.79	2.91

Brenk Alerts: 2-halo_pyridine, imine_1, phenol ester
Lead likeness: MW>350, XLOGP3>3.5

The medicinal chemistry-related properties of the synthesized molecules, based on the models and scores provided, offer key insights into their drug development potential

PAINS (Pan-Assay Interference Compounds) Zero Alerts indicates that none of the molecules show structural motifs commonly associated with assay interference, meaning they are less likely to give false-positive results in biological screening assays. This is a positive result, as PAINS compounds can often mislead during drug discovery by showing activity unrelated to the desired therapeutic effect.

Brenk Alerts Three Brenk alerts flag potential problematic substructures that might cause toxicity, instability, or other issues in drug development. Having 3 alerts means

there are certain structural features in the molecules that might need optimization to reduce potential safety risks or improve pharmacokinetic properties.

Lead Likeness The molecules did not meet the criteria for lead likeness, which generally involves smaller, simpler compounds that are ideal for further optimization in the lead discovery process. This suggests that the potent molecules may need some structural modification to serve as ideal lead compounds.

Synthetic Accessibility (2.69-3.05) This score indicates that the molecules are moderately easy to synthesize, with scores in the range suggesting they are not overly complex or difficult to produce. This is advantageous for scaling up synthesis in later stages of drug development.4e has the lowest synthetic accessibility score (around 2.6), indicating it may be the easiest to synthesize among the compounds.Compounds 4c, 4f, 4k, 4o and 4r showed the scores around 2.9. 4i and 4l have the highest scores (3.01 and 3.05 respectively) and may be challenging to synthesize in this series (Figure 5.51).

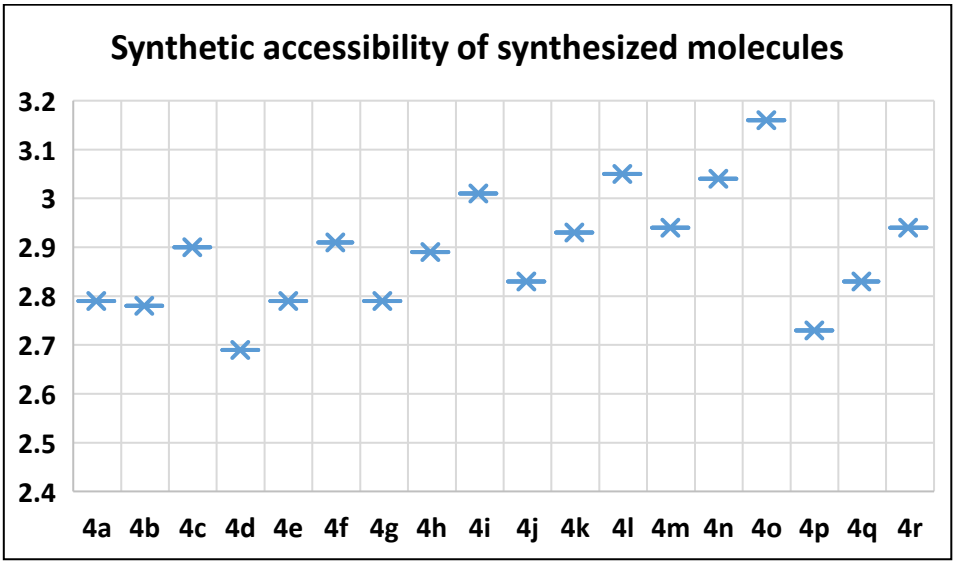

Figure 5.51: Comparison of synthetic accessibility of synthesized molecules (4a-4r) predicted using SwissADME software

The molecules have a clean profile with no PAINS alerts, but the Brenk alerts highlight potential areas for structural refinement. Although they are not classified as "lead-like," their moderate synthetic accessibility supports their feasibility for further optimization.

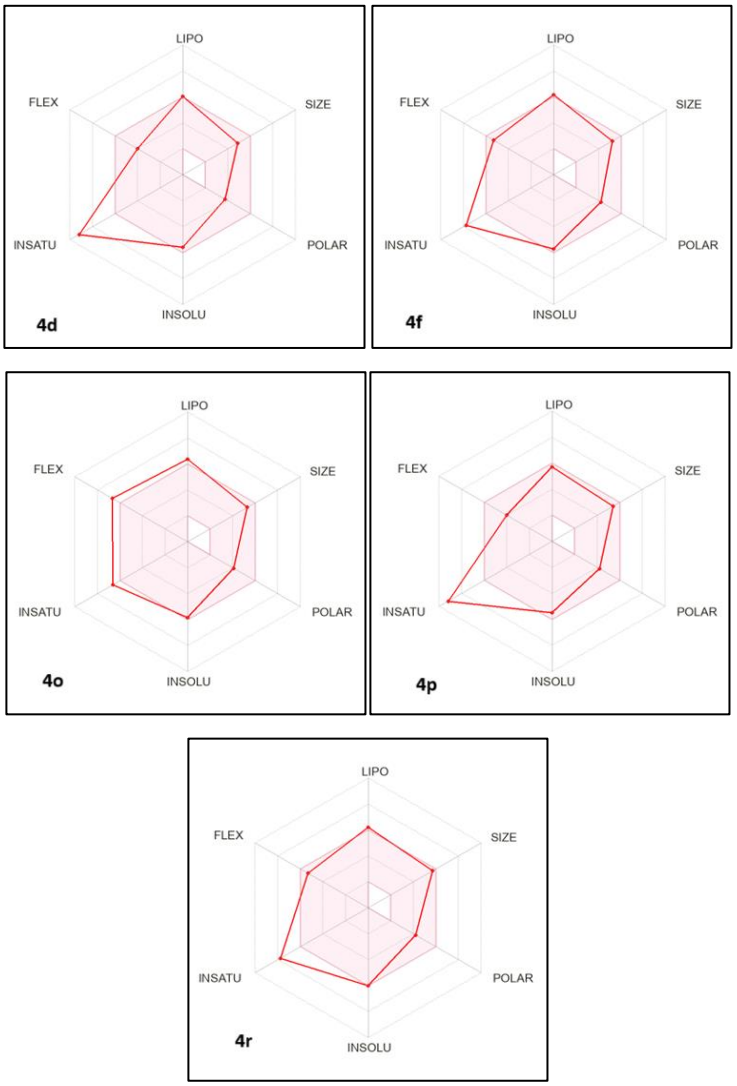

Figure 5.52: Bioavailability radar plots of synthesized compounds 4d, 4f, 4o, 4p and 4r obtained from SwissADME software (LIPO – Lipophilicity, SIZE - Molecular Weight, POLAR - Polarity, INSOLU – Insolubility, INSATU – Saturation, FLEX – Flexibility)

The Bioavailability Radar plots of few representative molecules 4d, 4f, 4o, 4p and 4r (Figure 5.52) obtained from SwissADME software wereanalysed. They provide a visual representation of six key physicochemical properties (LIPO – Lipophilicity, SIZE - Molecular Weight, POLAR - Polarity,INSOLU – Insolubility, INSATU – Saturation, FLEX – Flexibility) related to drug-likeness.

Compound 4d showed favourable lipophilicity, size, polarity, and flexibility, which are key factors for good bioavailability. However, the plot suggests potential issues with solubility (INSOLU) and saturation (INSATU), which might need optimization to improve its drug-likeness profile.

Compound 4f showed favourable properties in terms of lipophilicity, size, polarity, and flexibility, which support good bioavailability. However, the compound may have issues with solubility (poor) and saturation (high degree of unsaturation), affecting its absorption and distribution. These aspects may need optimization to improve the compound's overall drug-likeness profile.

Compound 4o showed promising characteristics in terms of lipophilicity, size, polarity, and flexibility, but solubility might require optimization to improve its drug-likeness and absorption.

Compound 4p demonstrated favourable properties in lipophilicity, size, polarity, and flexibility, making it promising in terms of oral bioavailability. However, poorsolubility and low saturation may pose challenges for drug-likeness and could require optimization for further development.

Compound 4r showed promising attributes in terms of lipophilicity, size, polarity, and flexibility, which support its potential as a drug-like compound. However, the poor solubility and low saturation may require attention for improving its overall pharmacokinetic properties.

5.5 SPECTRAL DATA OF SYNTHESIZED COMPOUNDS

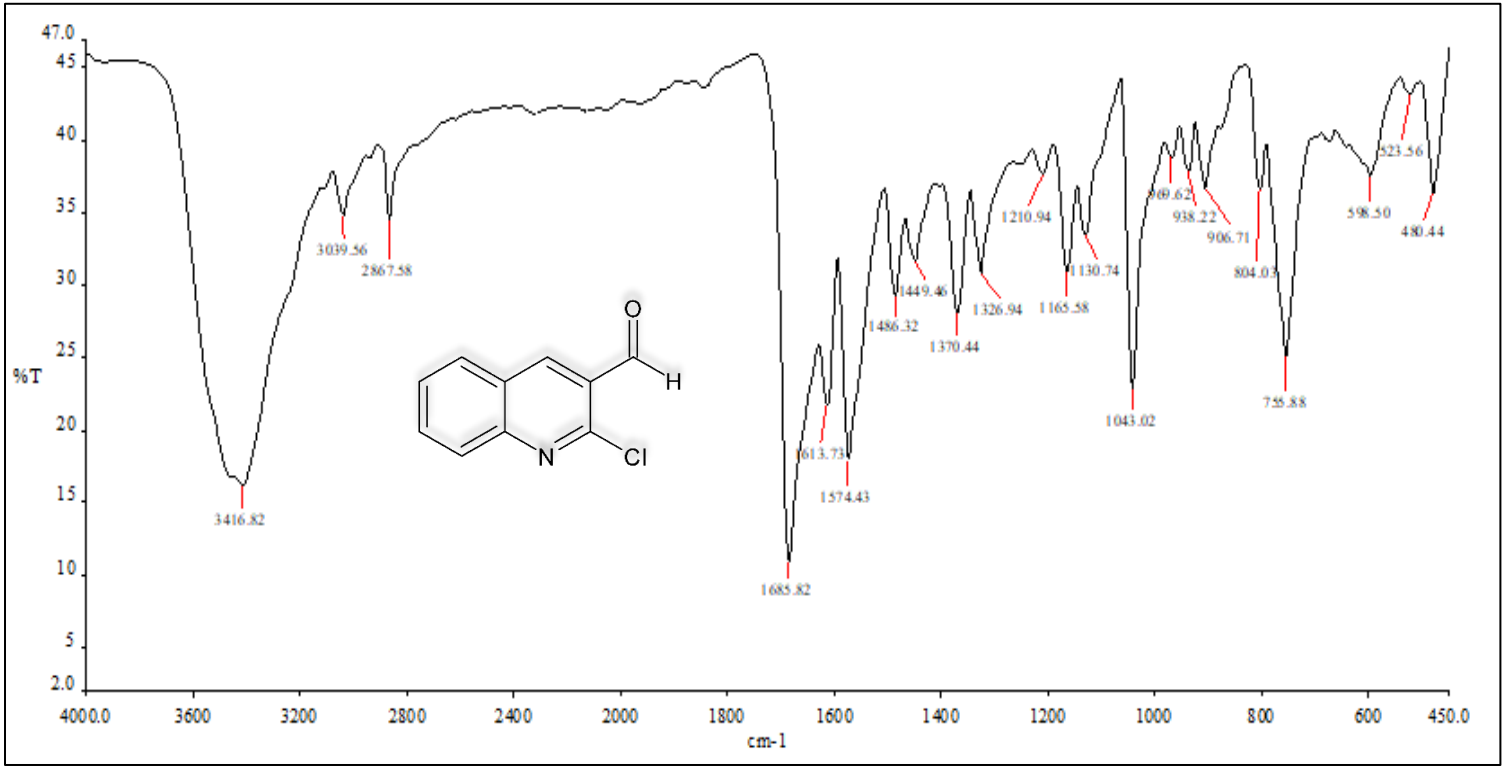

Figure 5.53: IR spectrum of 2-chloroquinoline-3-carbaldehyde (Compound 2a)

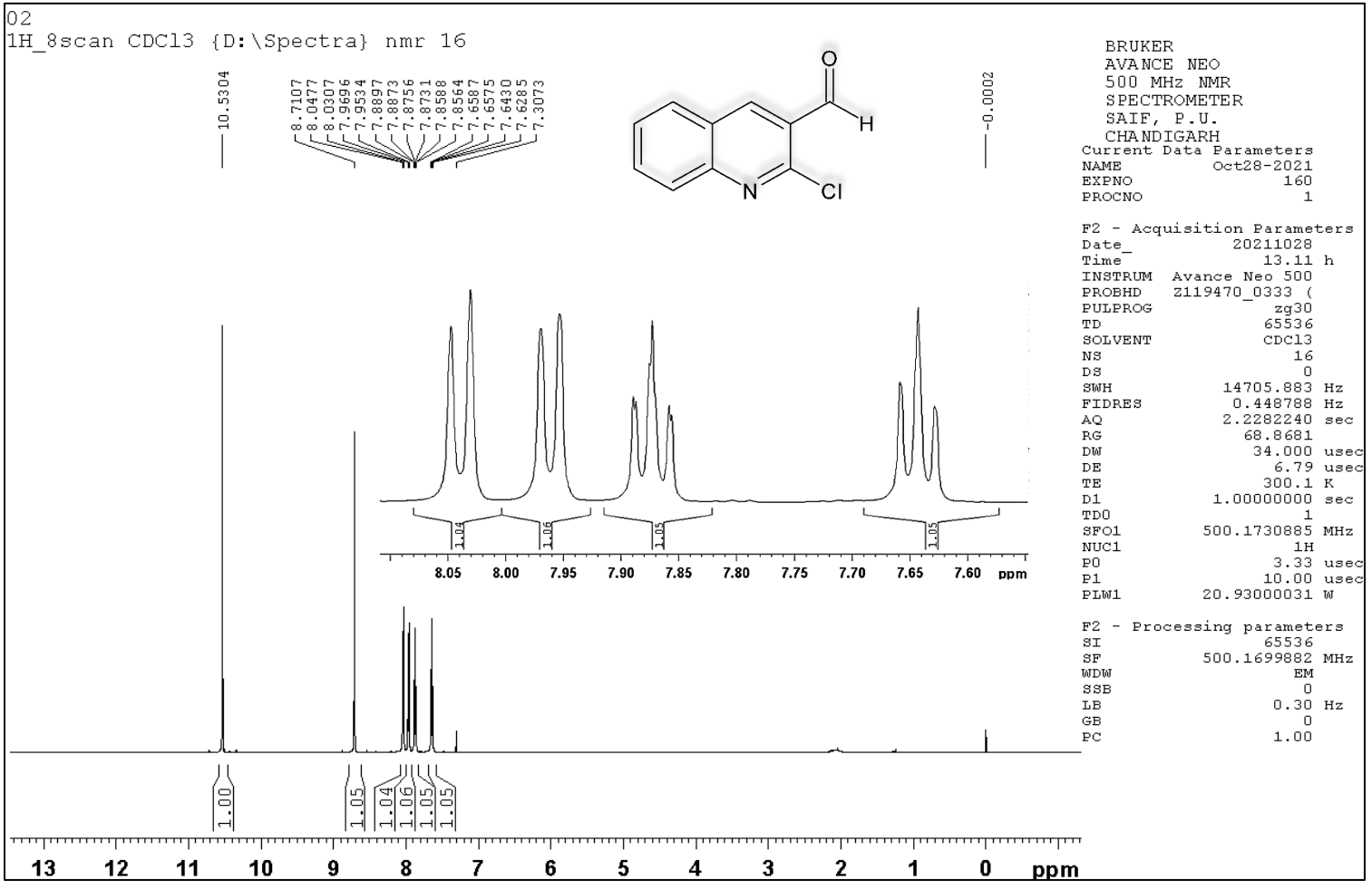

Figure 5.54: ^{1}H NMR spectrum of 2-chloroquinoline-3-carbaldehyde (Compound 2a)

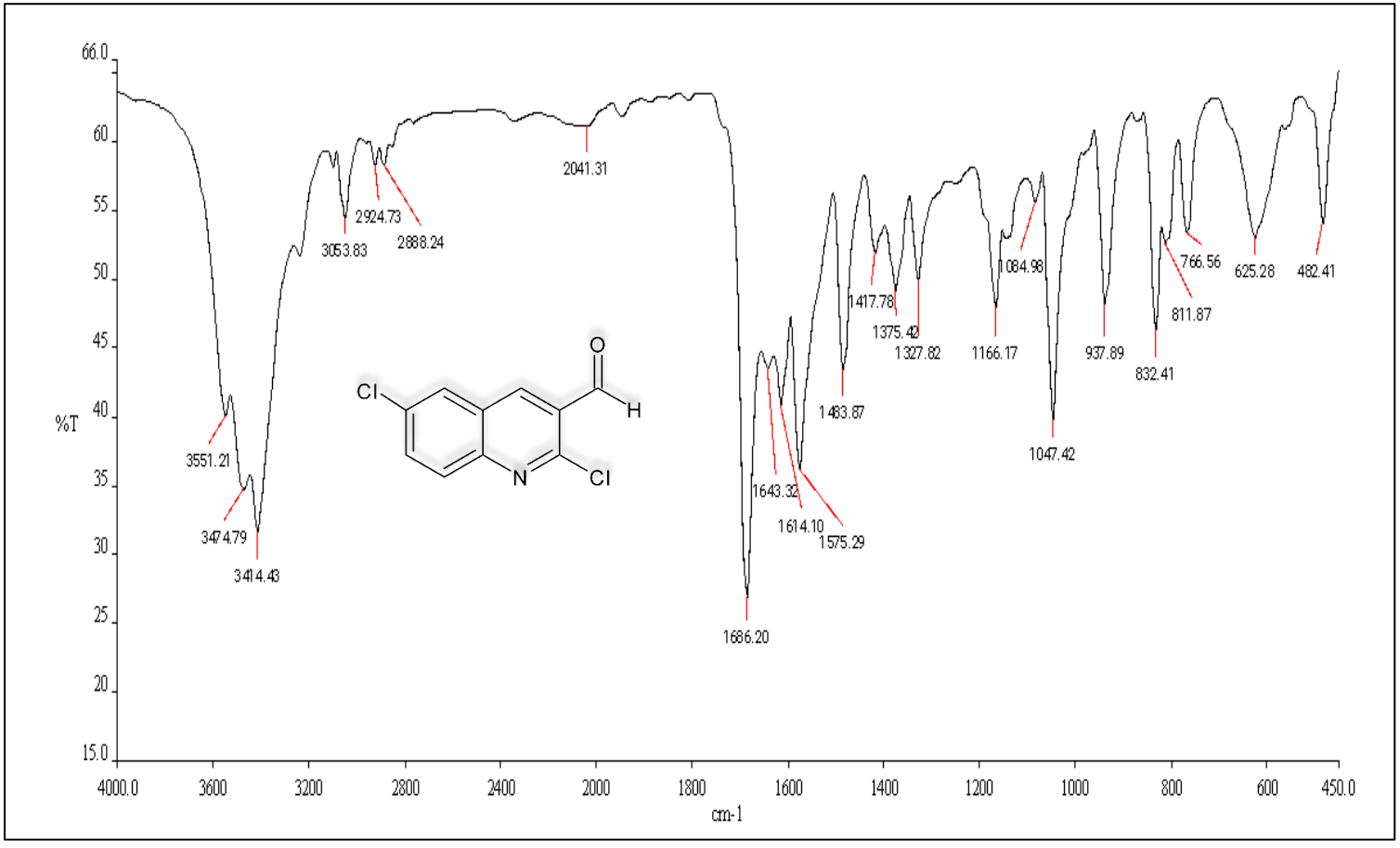

Figure 5.55: IR spectrum of 2,6-dichloroquinoline-3-carbaldehyde (Compound 2d)

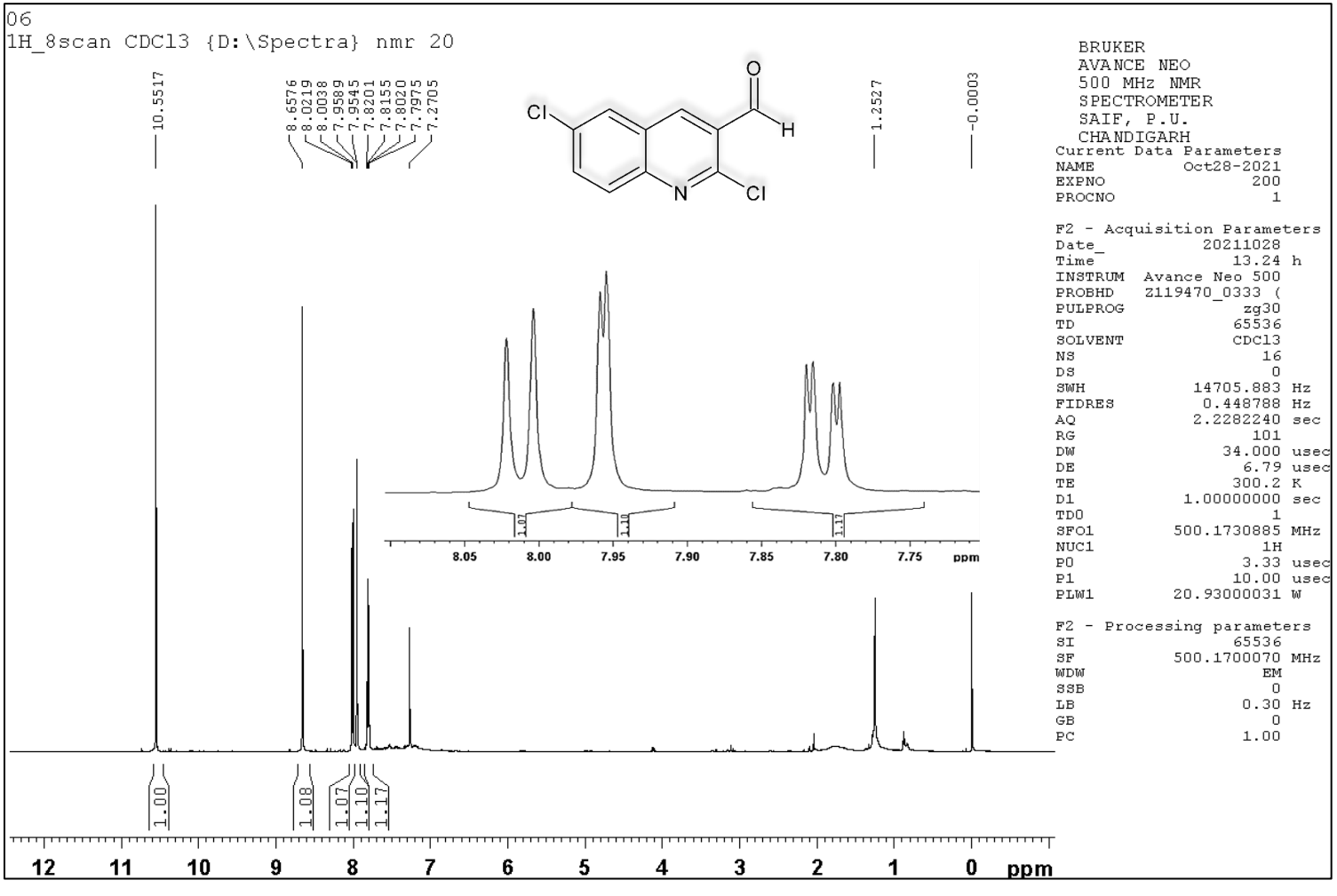

Figure 5.56: ^{1}H NMR spectrum of 2,6-dichloroquinoline-3-carbaldehyde (Compound 2d)

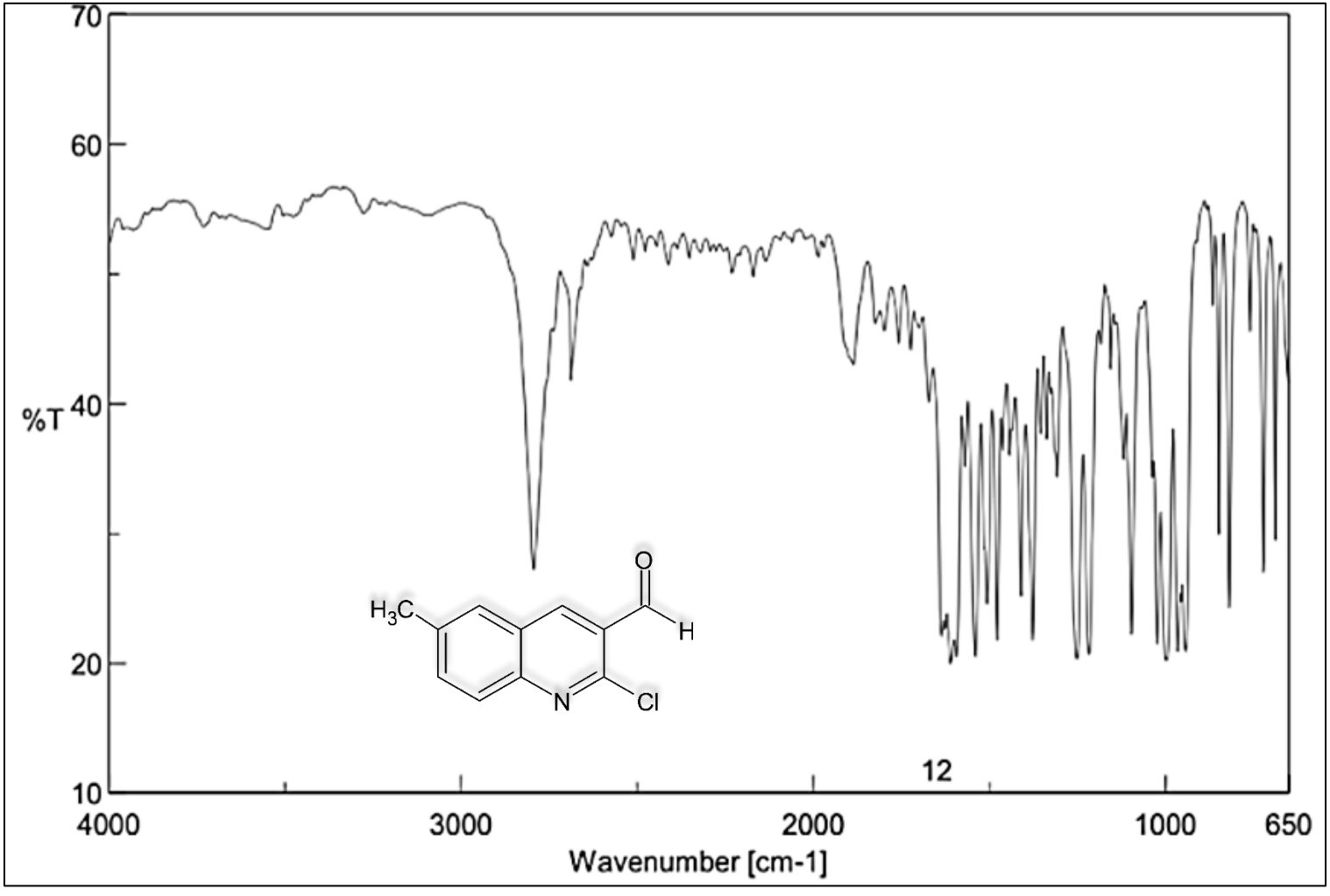

Figure 5.57: IR spectrum of 2-chloro-6-methylquinoline-3-carbaldehyde (Compound 2g)

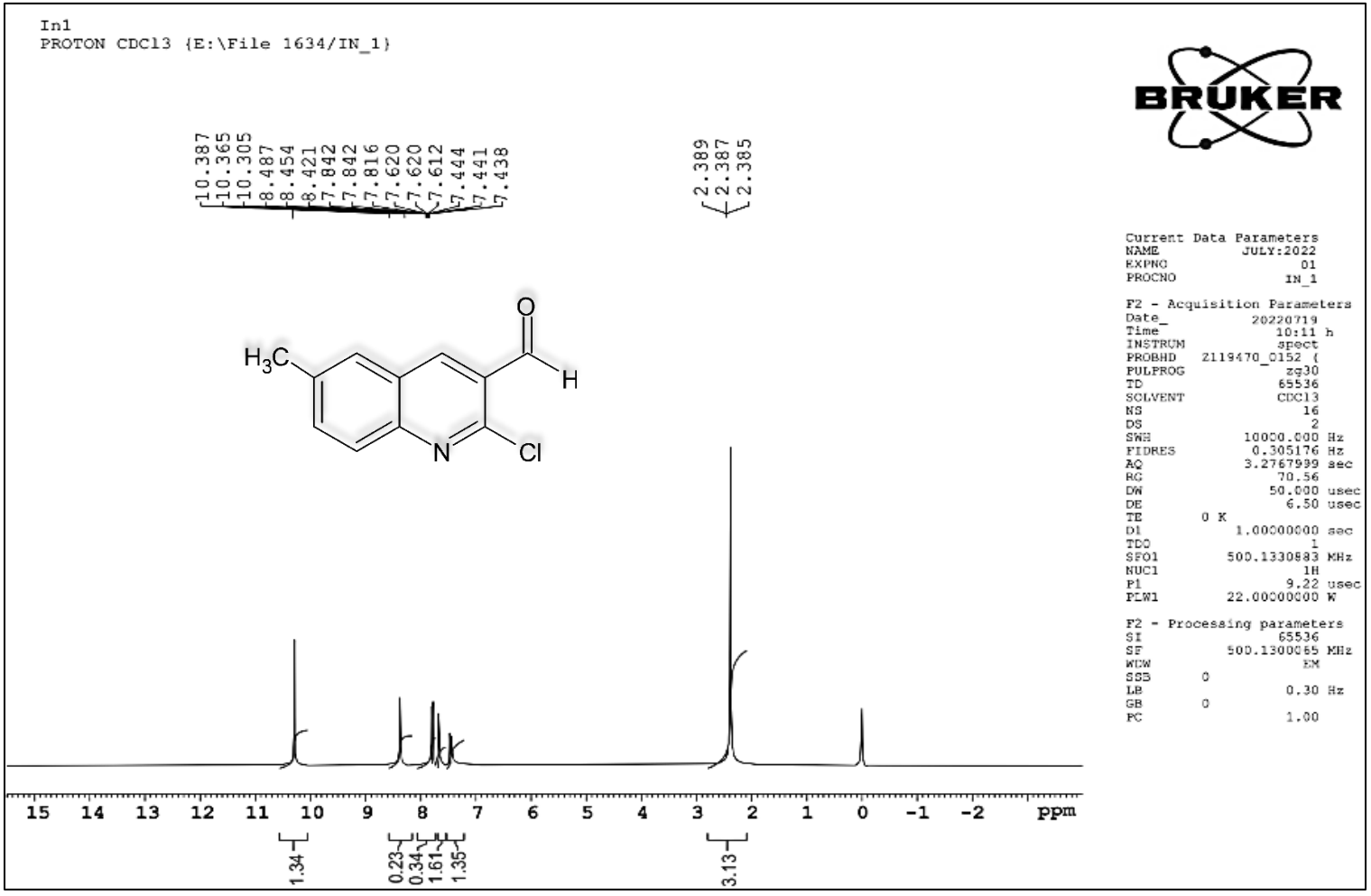

Figure 5.58: ^{1}H NMR spectrum of 2-chloro-6-methylquinoline-3-carbaldehyde (Compound 2g)

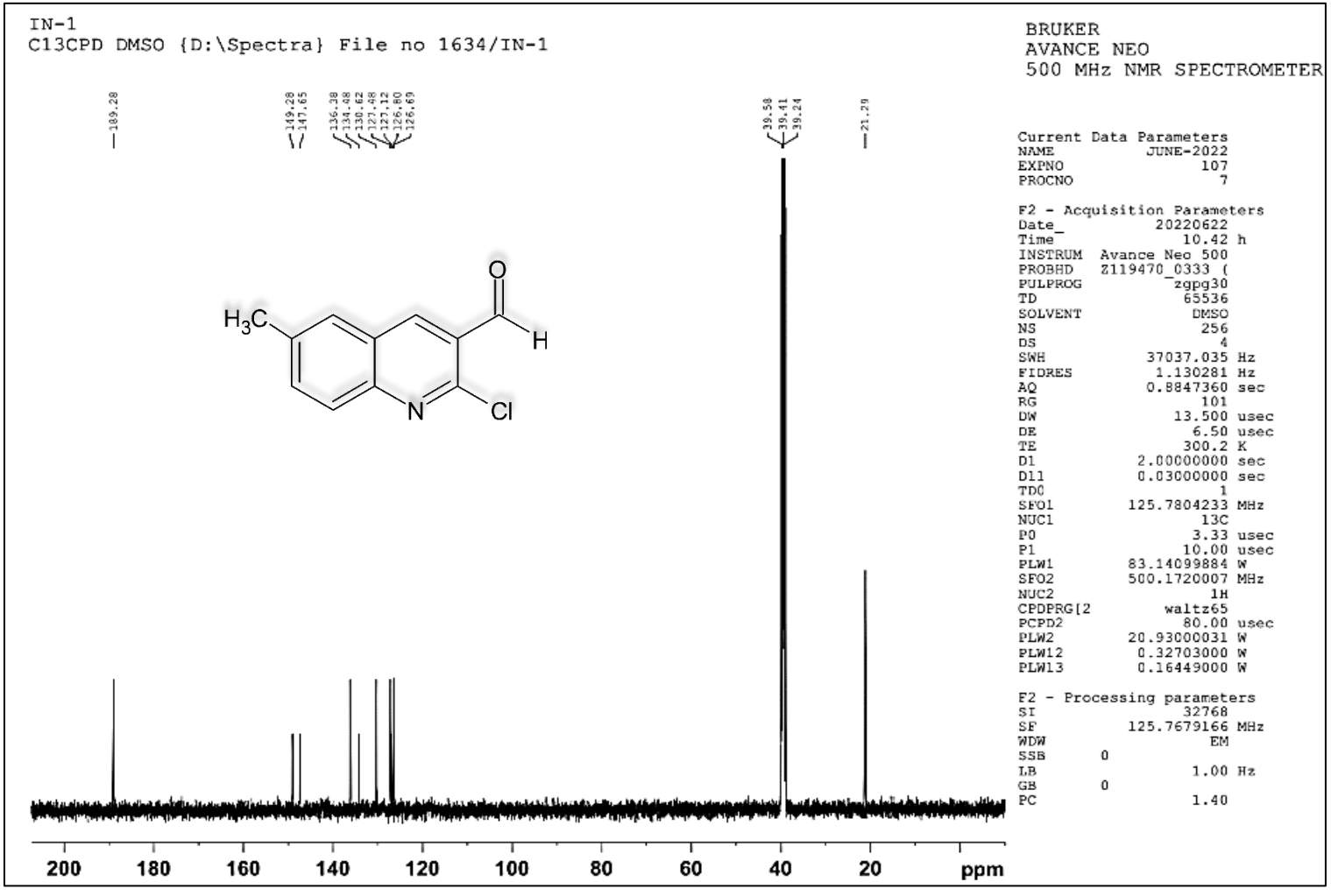

Figure 5.59: ^{13}C NMR spectrum of 2-chloro-6-methylquinoline-3-carbaldehyde (Compound 2g)

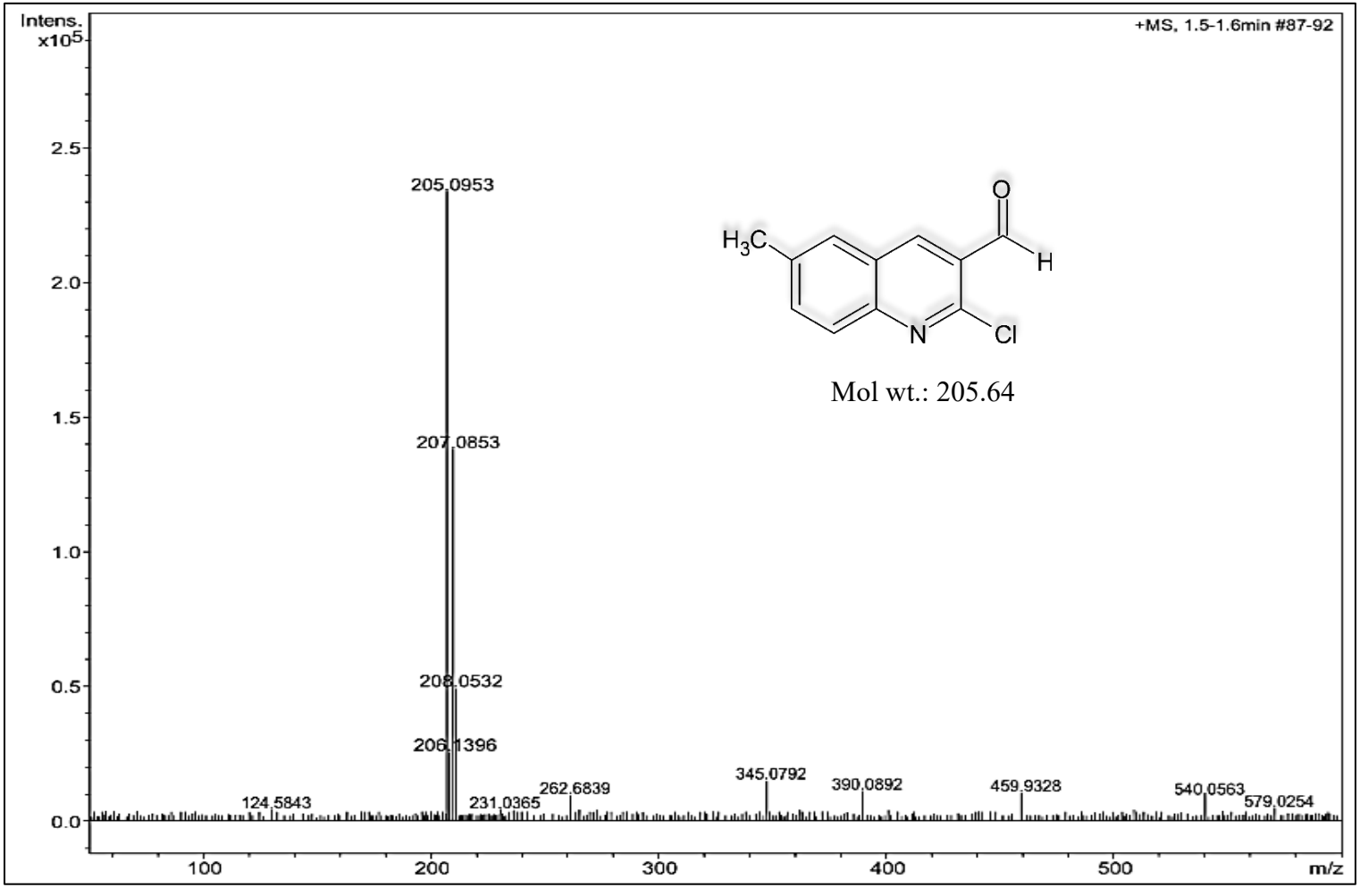

Figure 5.60: Mass spectrum of 2-chloro-6-methylquinoline-3-carbaldehyde (Compound 2g)

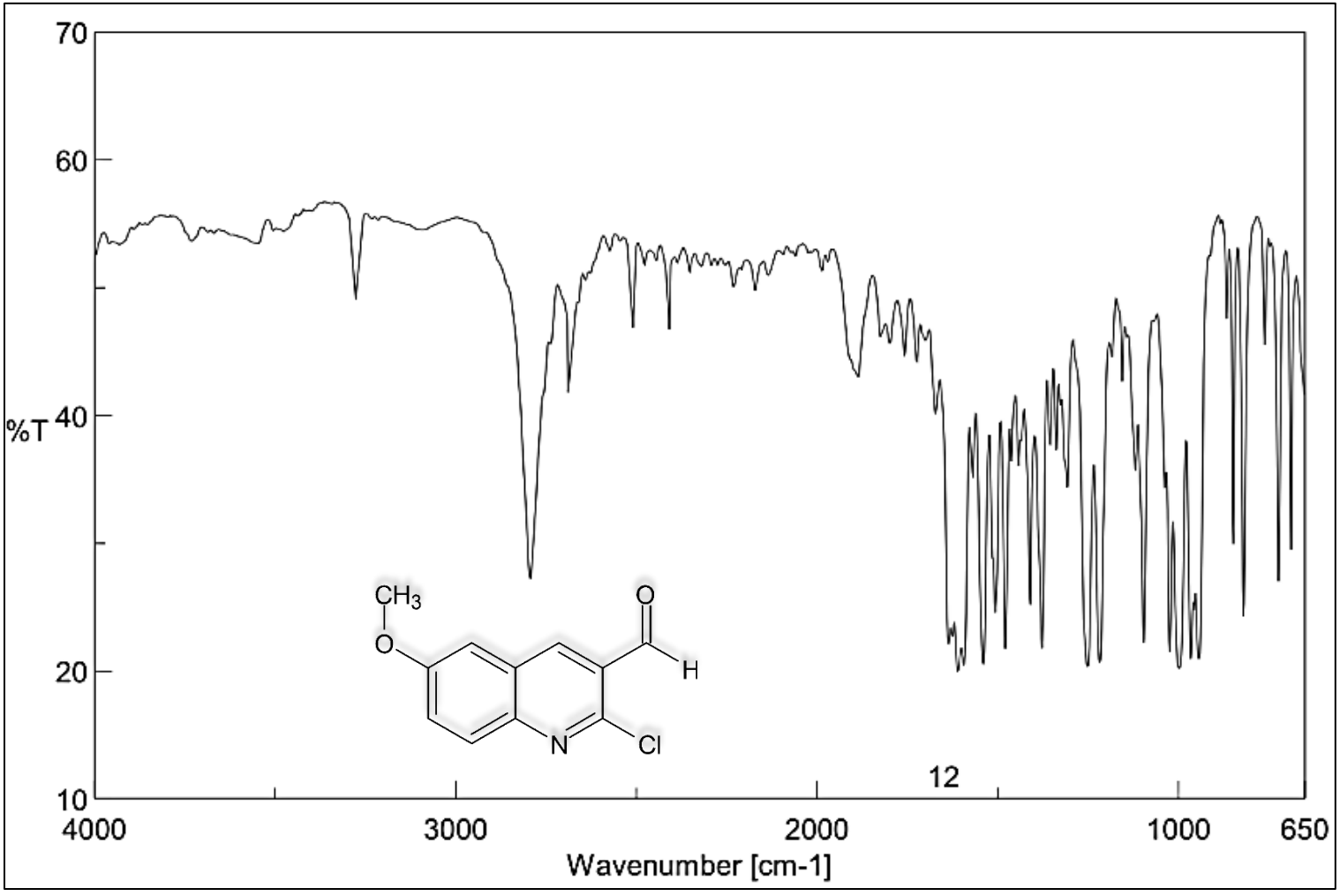

Figure 5.61: IR spectrum of 2-chloro-6-Methoxy-quinoline-3-carbaldehyde (Compound 2j)

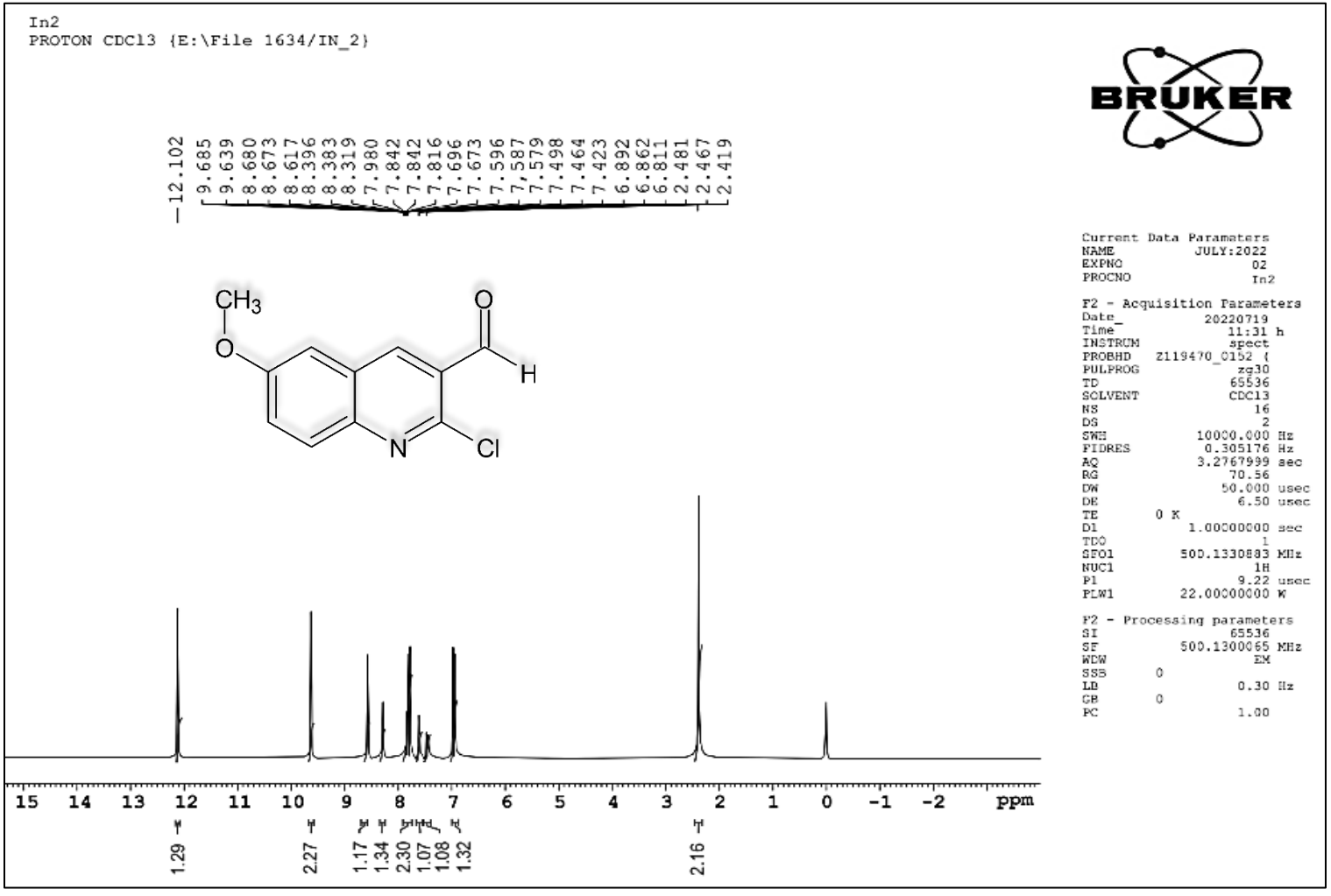

Figure 5.62: ^{1}H NMR spectrum of 2-chloro-6-Methoxy-quinoline-3-carbaldehyde (Compound 2j)

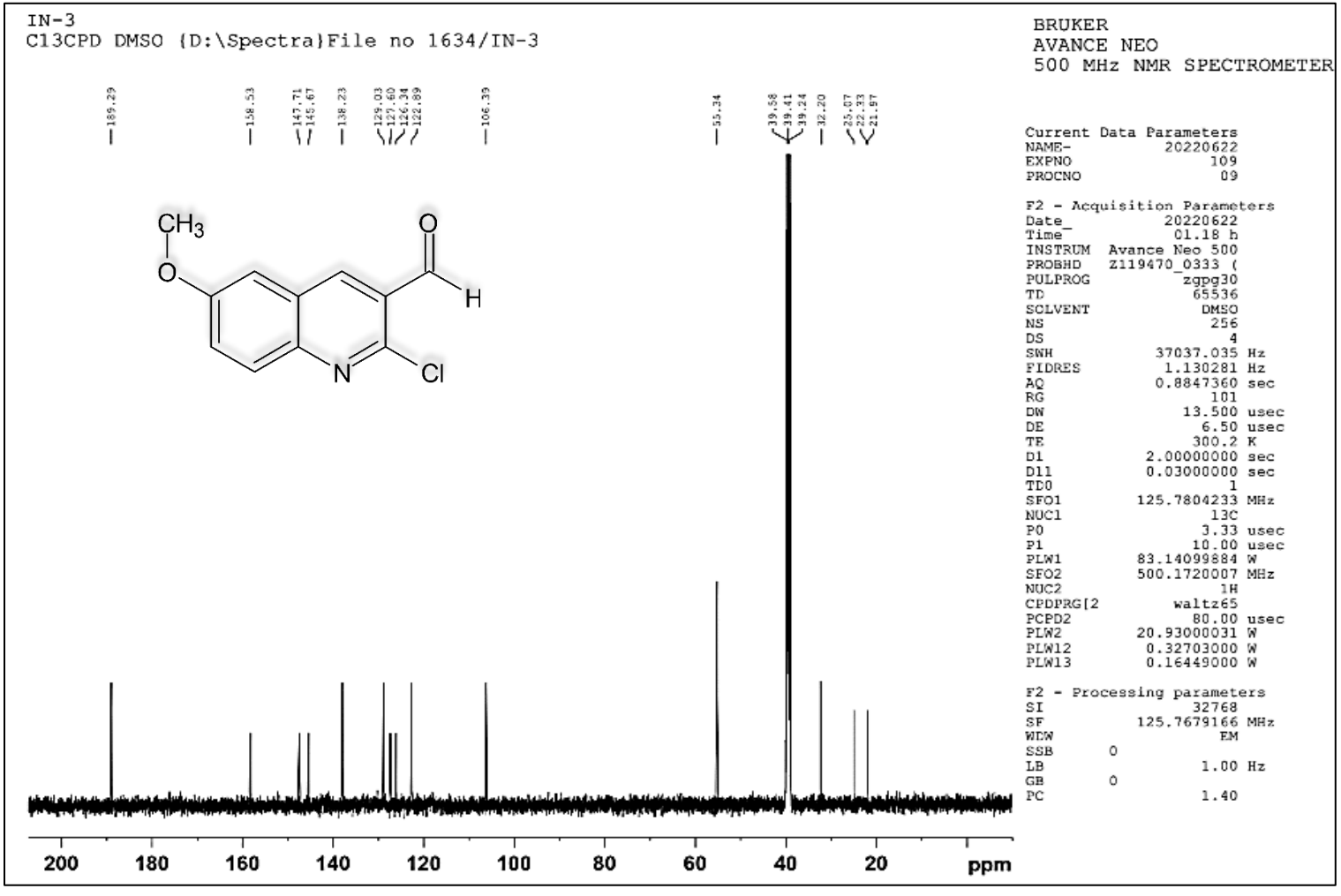

Figure 5.63: ^{13}C NMR spectrum of 2-chloro-6-Methoxy-quinoline-3-carbaldehyde (Compound 2j)

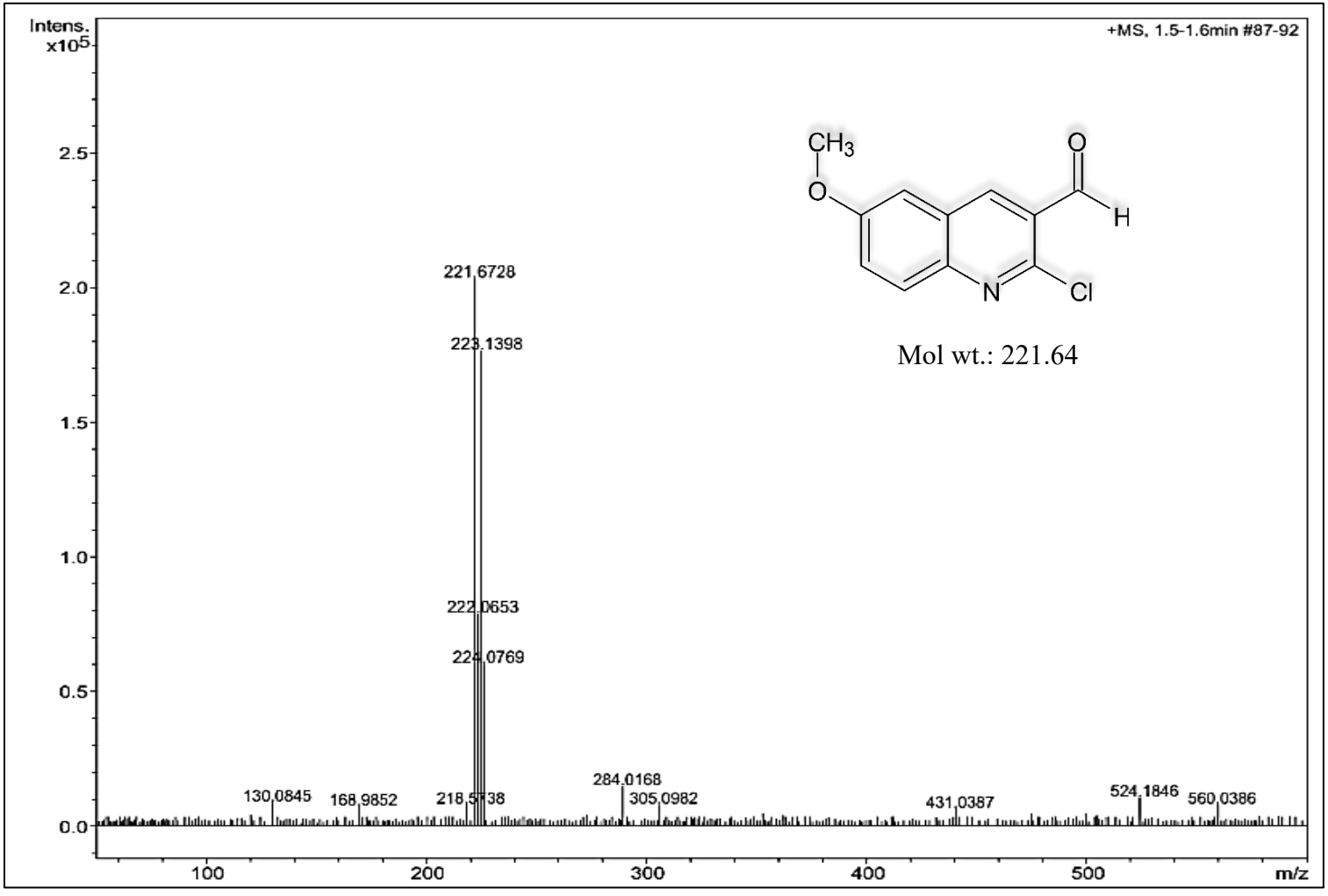

Figure 5.64: Mass spectrum of 2-chloro-6-Methoxy-quinoline-3-carbaldehyde (Compound 2j)

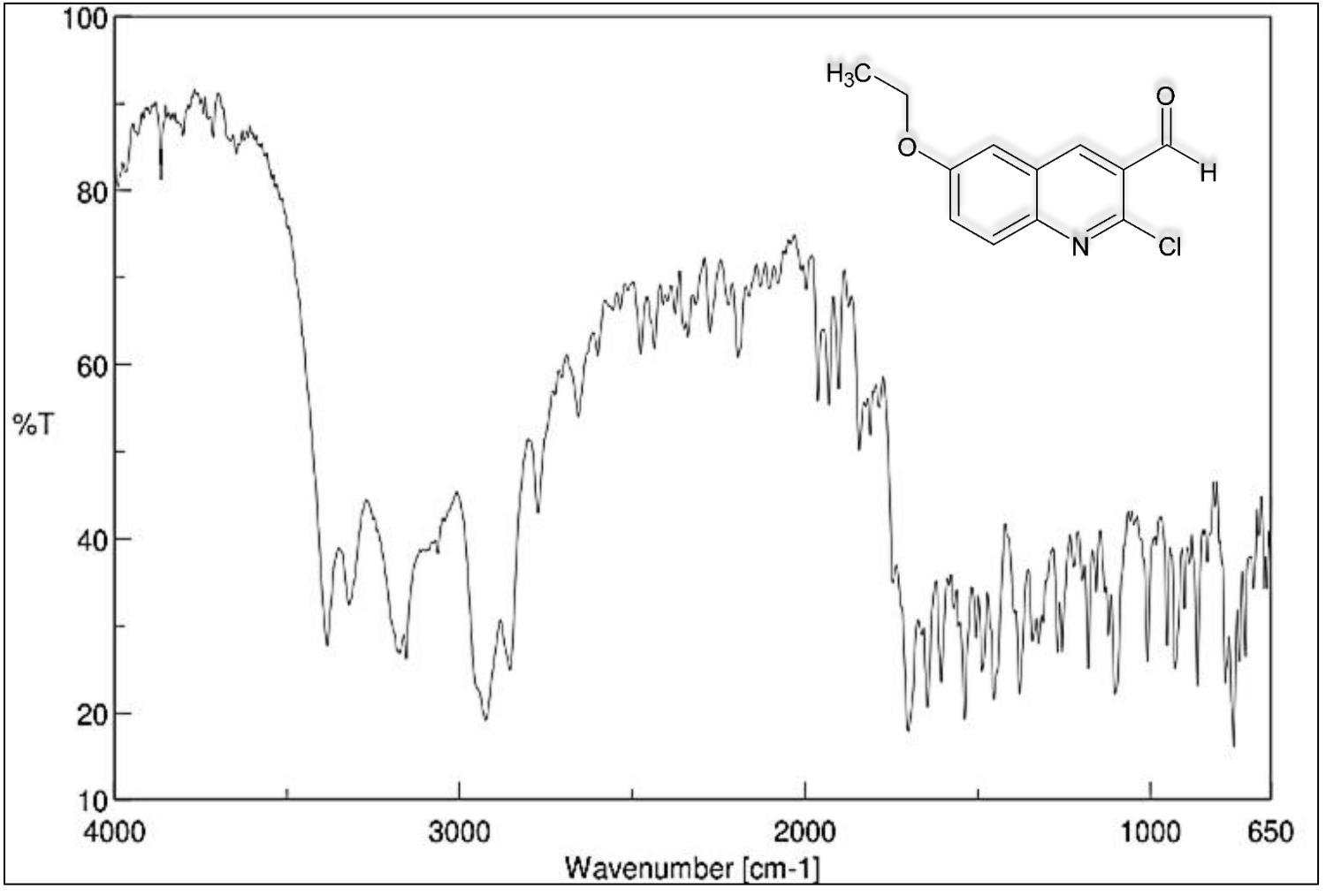

Figure 5.65: IR spectrum of 2-chloro-6-ehtoxyquinoline-3-carbaldehyde (Compound 2m)

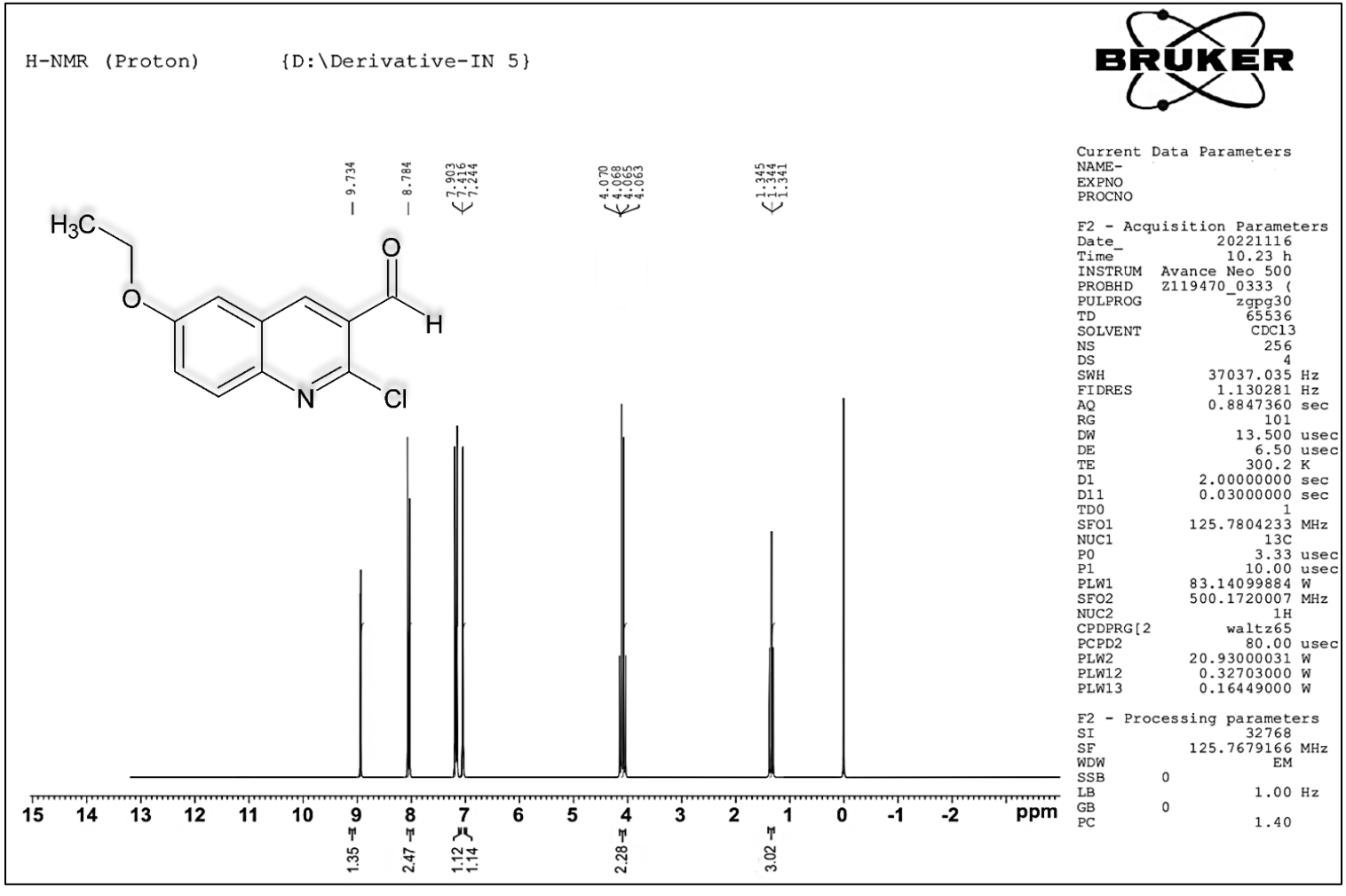

Figure 5.66: ^{1}H NMR spectrum of 2-chloro-6-ehtoxyquinoline-3-carbaldehyde (Compound 2m)

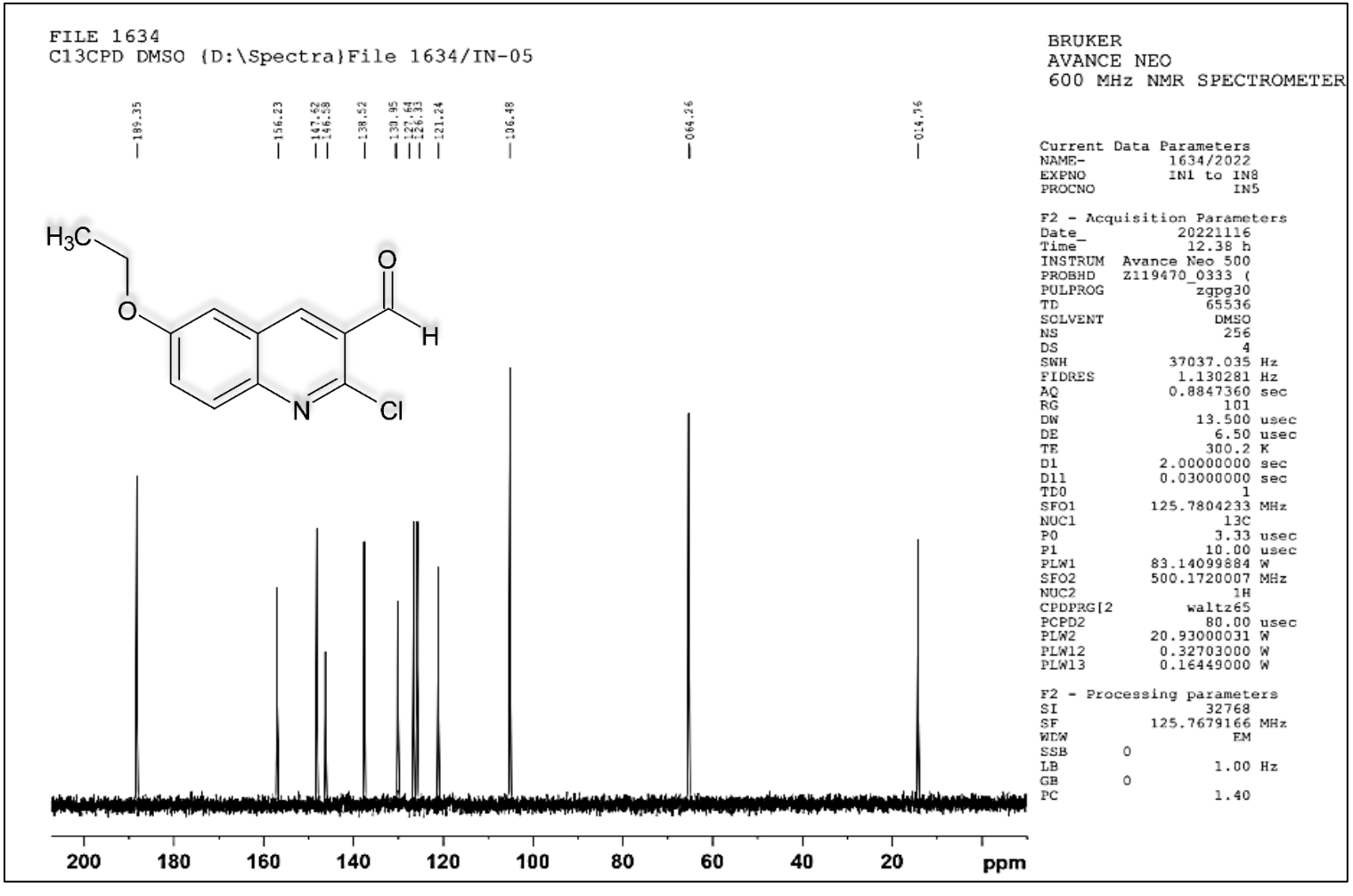

Figure 5.67: ^{13}C NMR spectrum of 2-chloro-6-ehtoxyquinoline-3-carbaldehyde (Compound 2m)

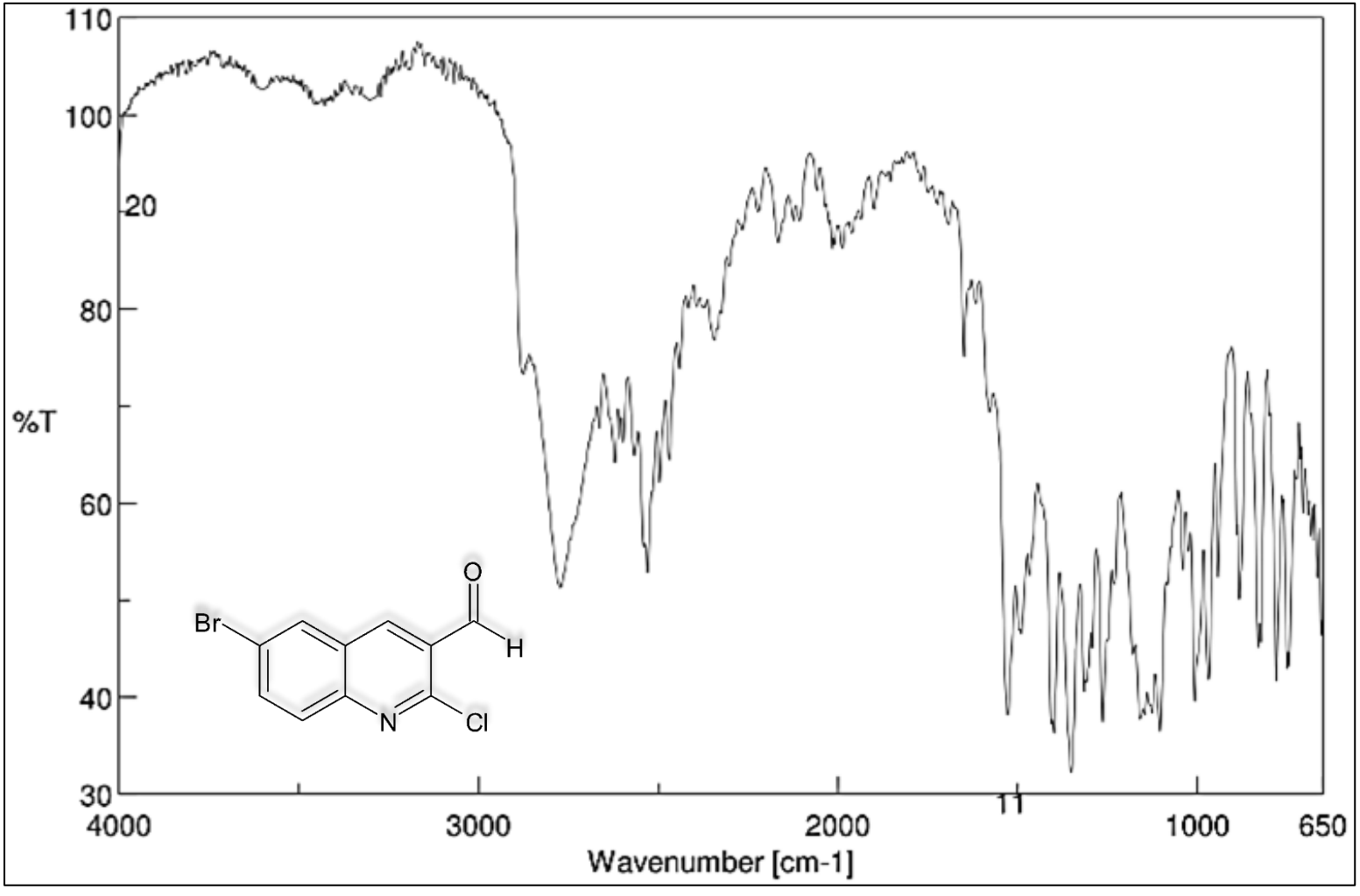

Figure 5.68: IR spectrum of 6-bromo-2-chloroquinoline-3-carbaldehyde (Compound 2p)

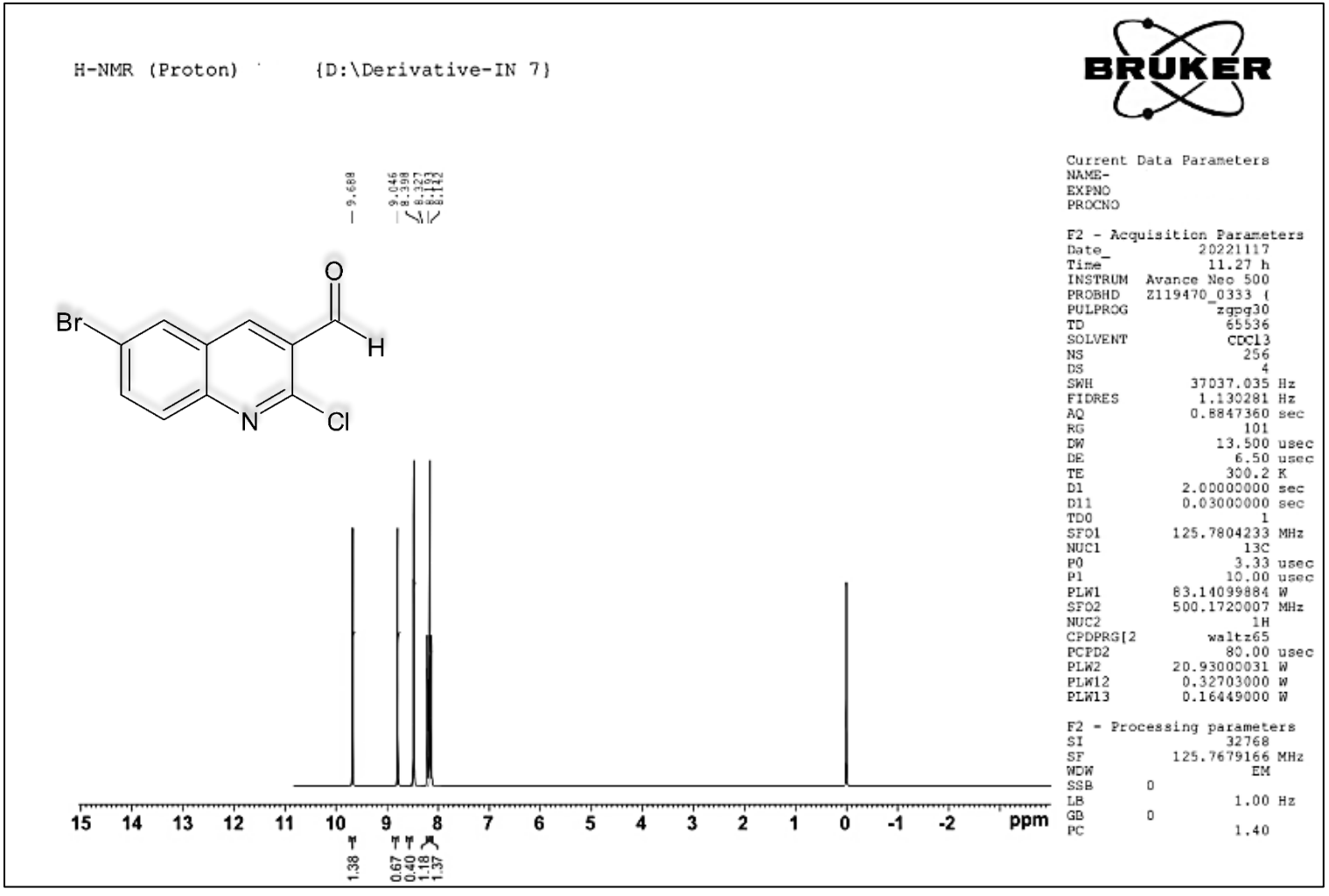

Figure 5.69: ^{1}H NMR spectrum of 6-bromo-2-chloroquinoline-3-carbaldehyde (Compound 2p)

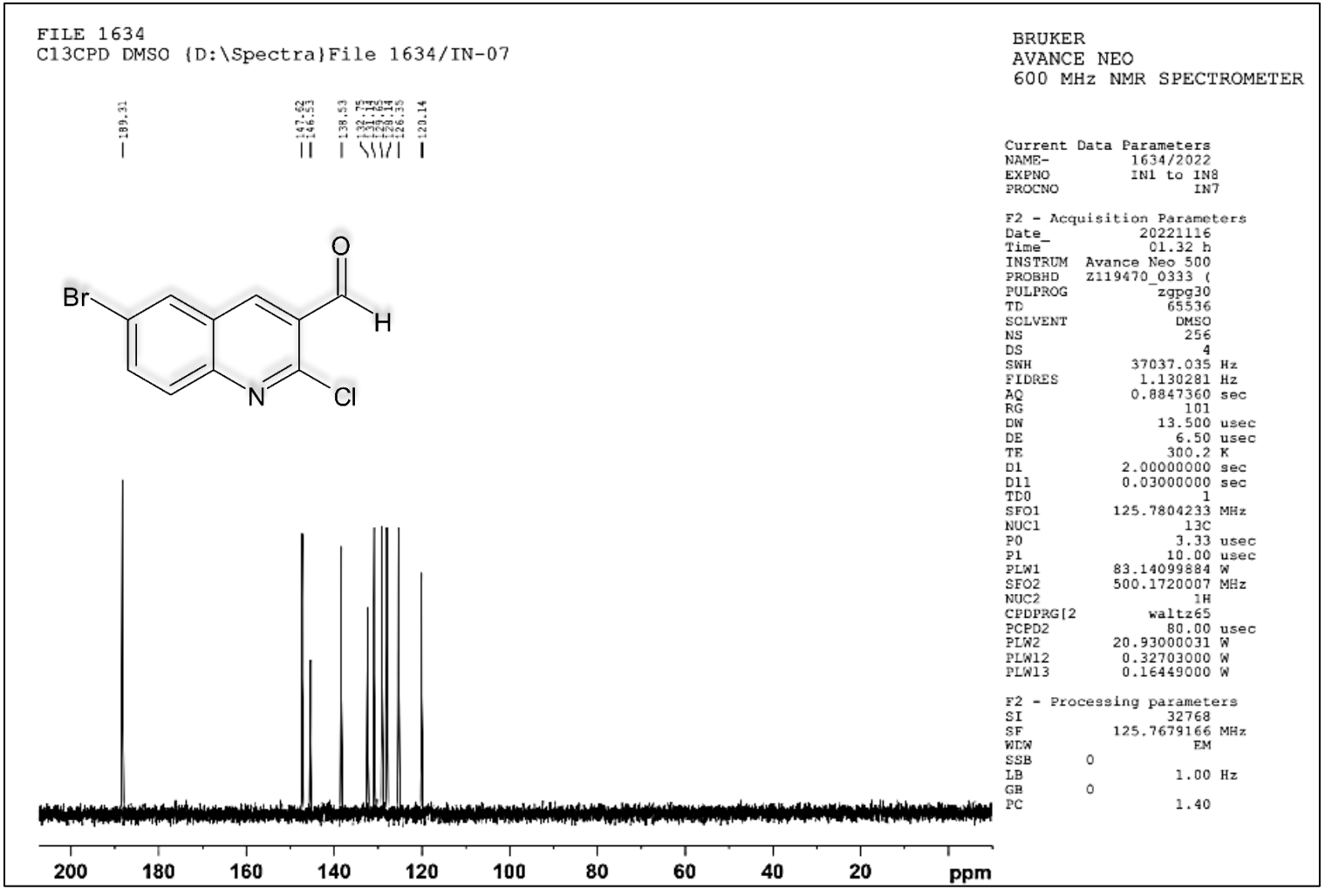

Figure 5.70: ^{13}C NMR spectrum of 6-bromo-2-chloroquinoline-3-carbaldehyde (Compound 2p)

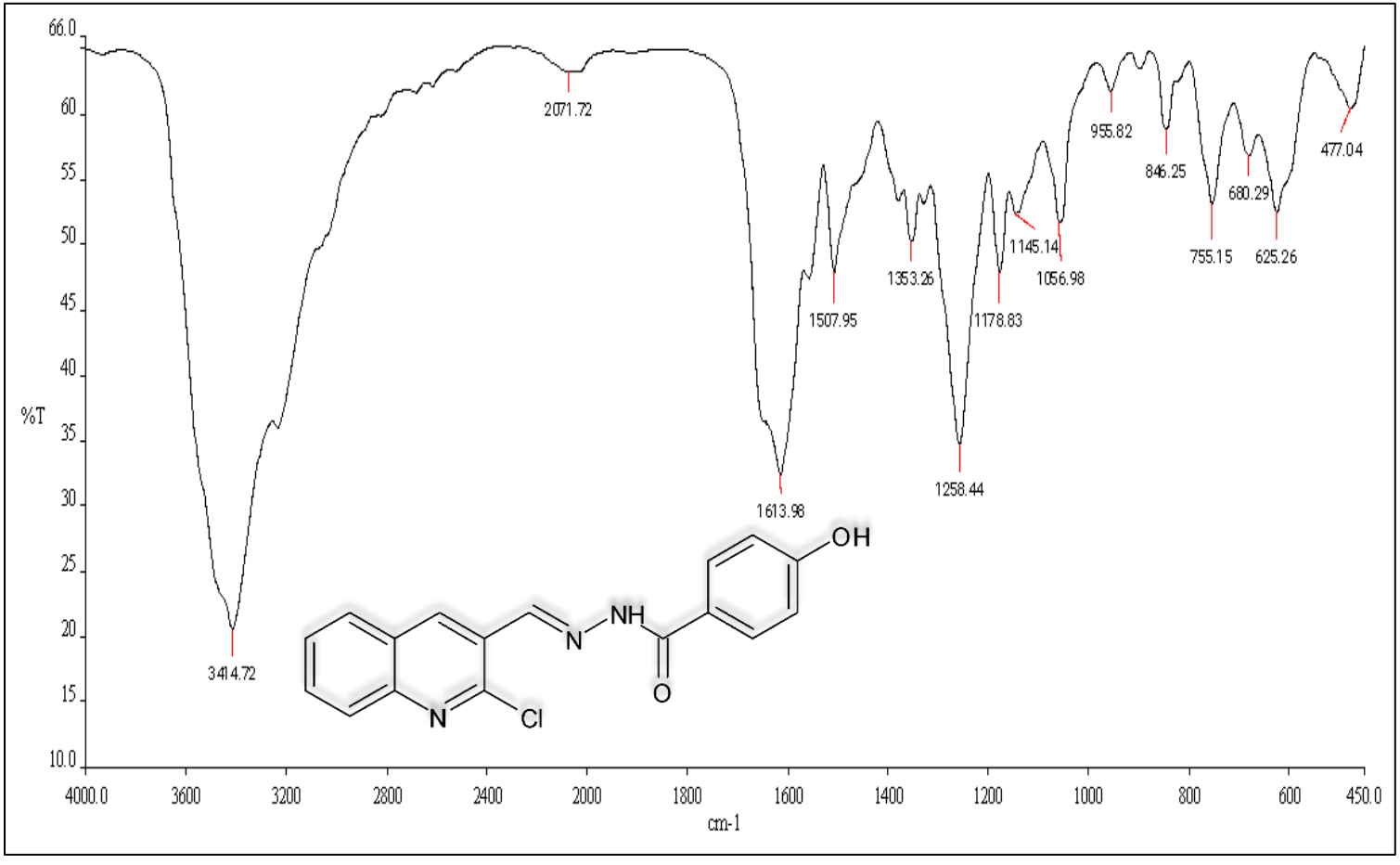

Figure 5.71: IR spectrum of N'-[(2-chloroquinolin-3-yl) methylidene]-4-hydroxybenzohydrazide (Compound 3a)

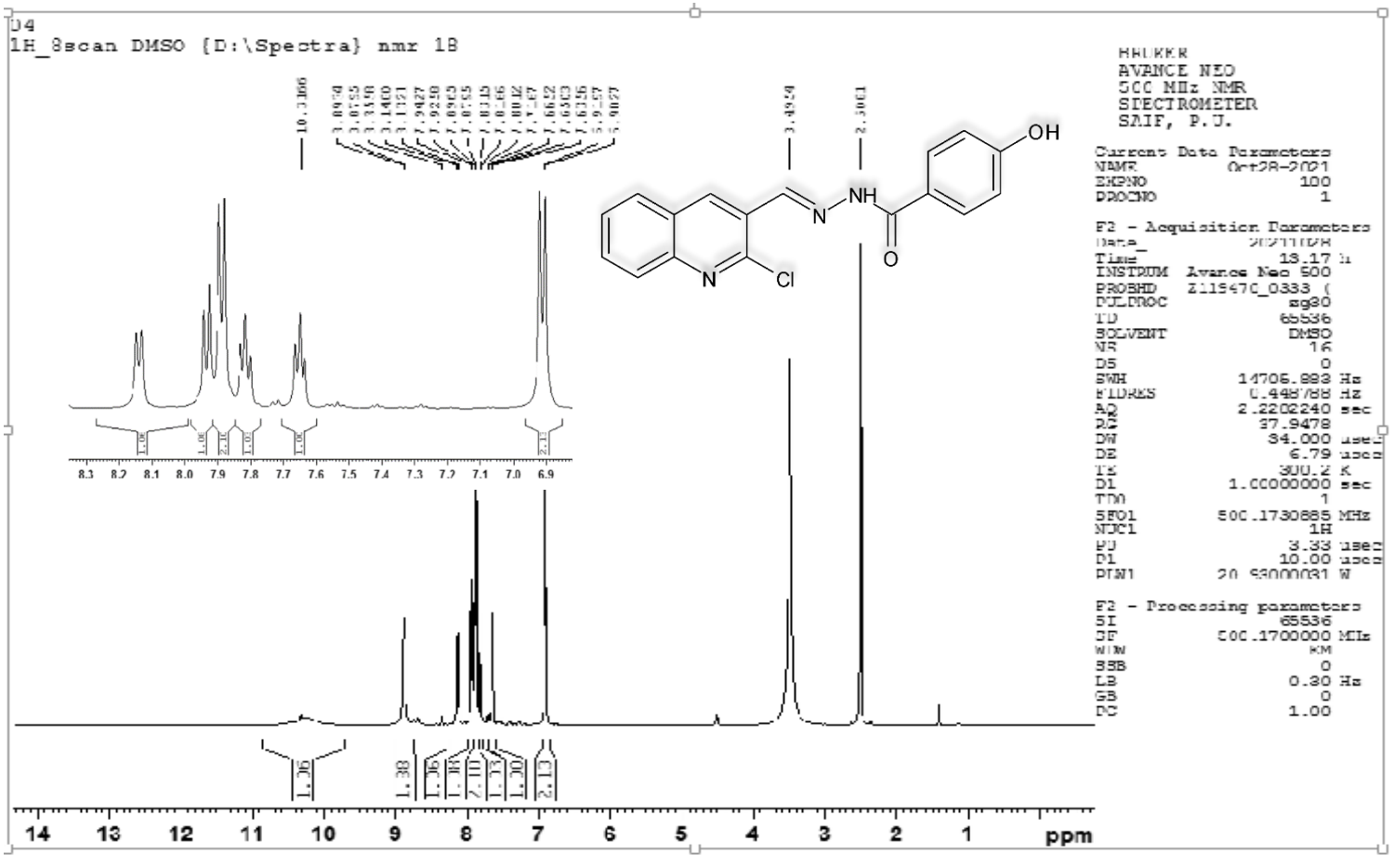

Figure 5.72: ^{1}H NMR spectrum of N'-[(2-chloroquinolin-3-yl) methylidene]-4-hydroxybenzohydrazide (Compound 3a)

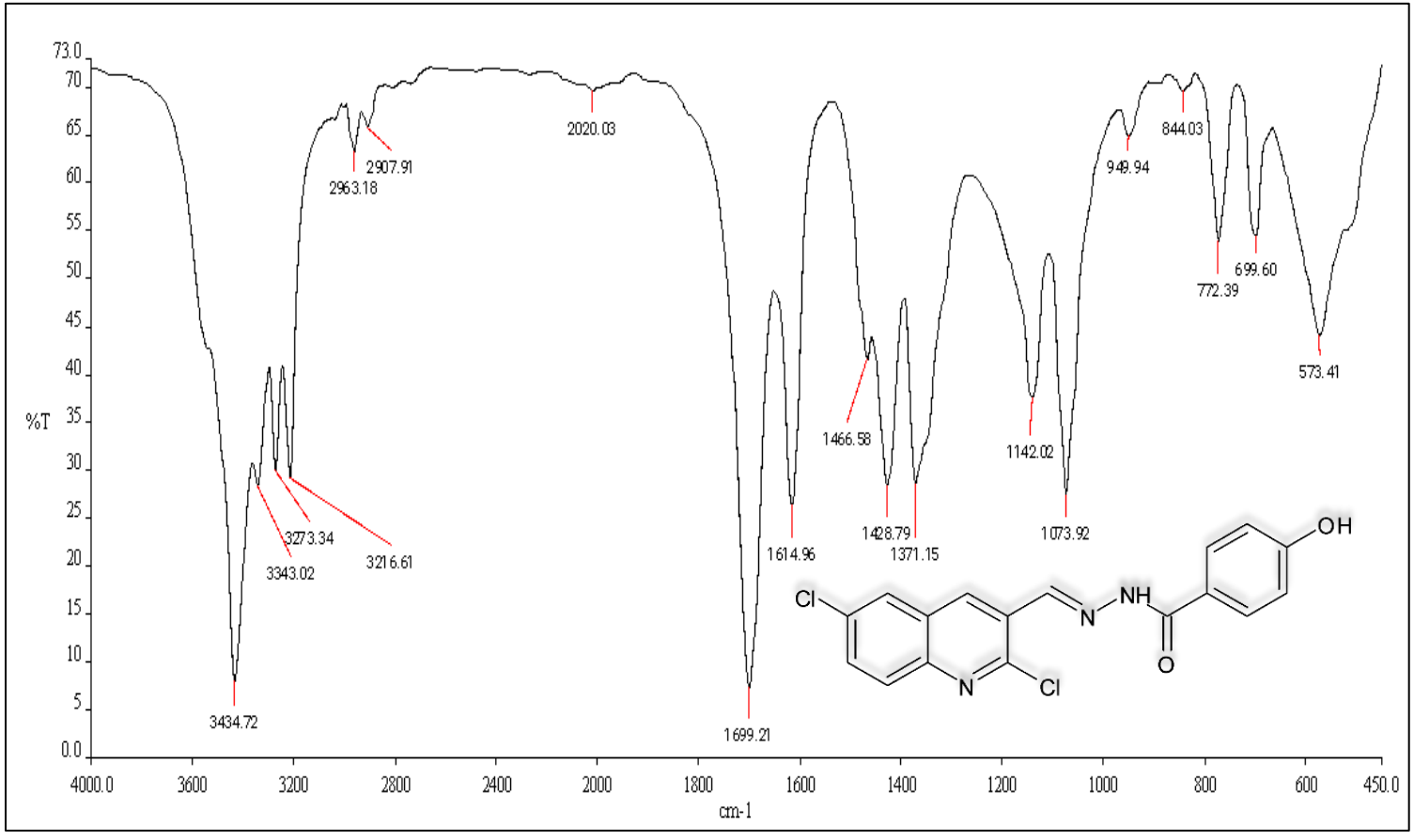

Figure 5.73: IR spectrum of N'-[(2,6-dichloroquinolin-3-yl) methylidene]-4-hydroxybenzohydrazide (Compound 3d)

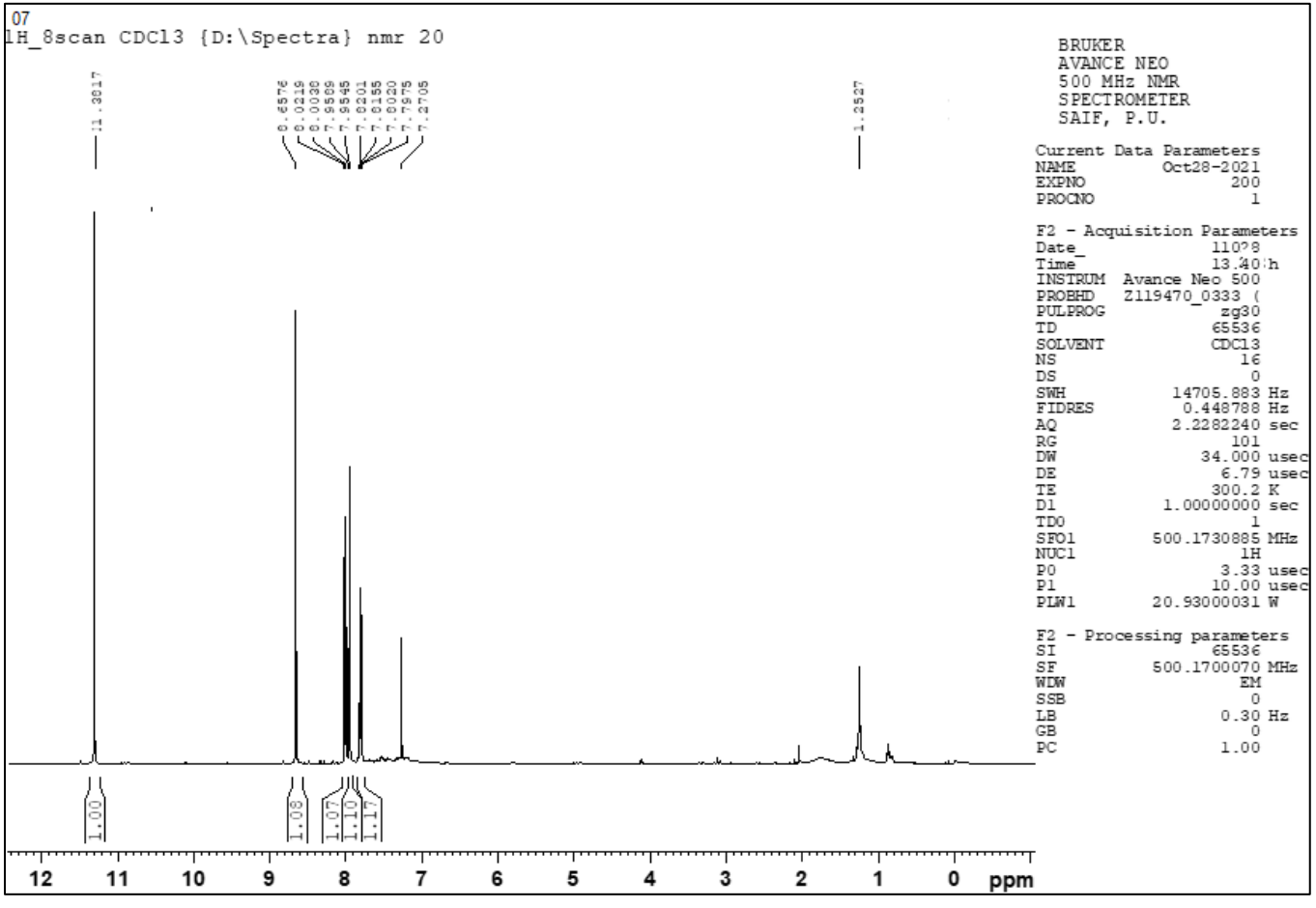

Figure 5.74: ^{1}H NMR spectrum of N'-[(2,6-dichloroquinolin-3-yl) methylidene]-4-hydroxybenzohydrazide (Compound 3d)

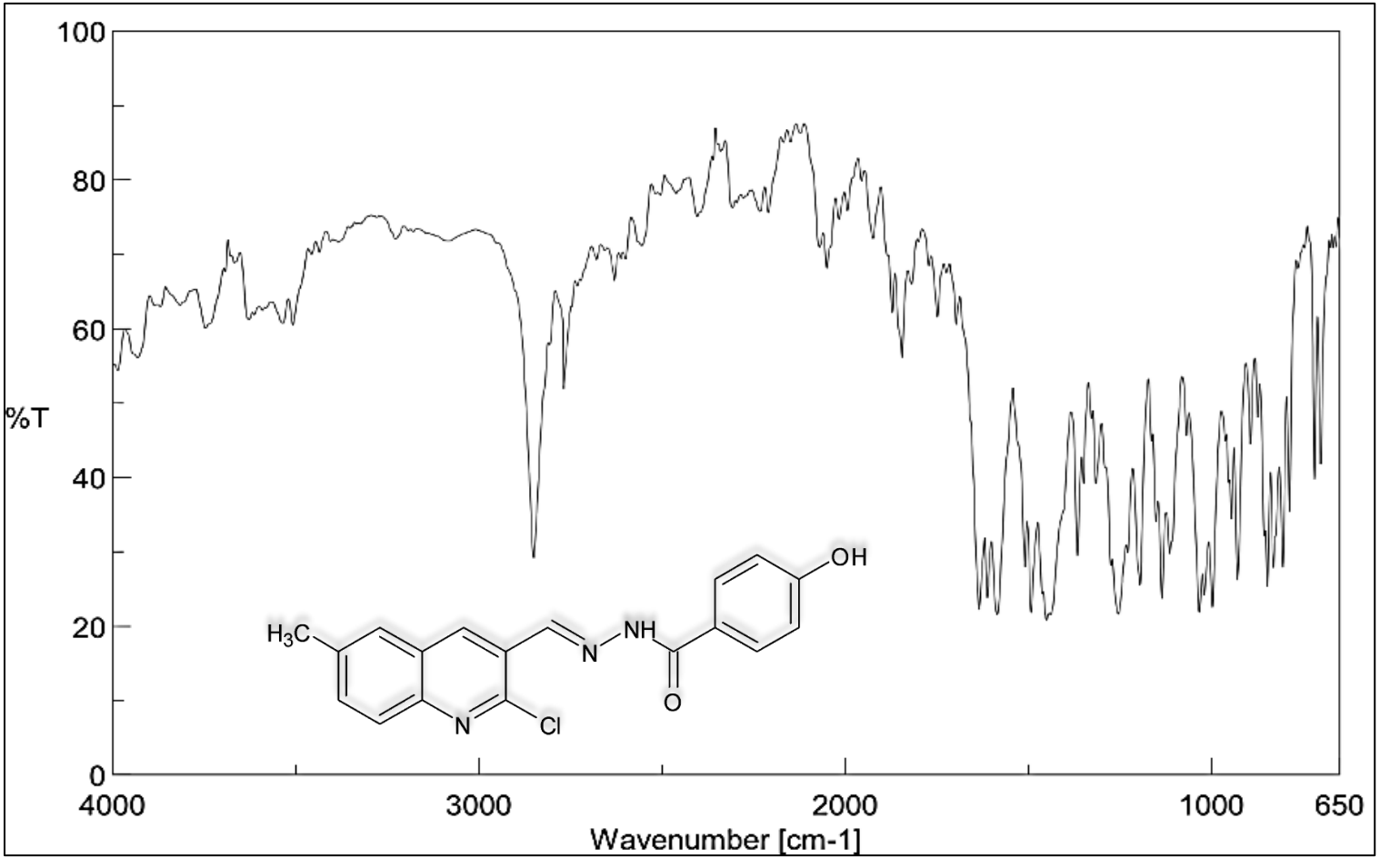

Figure 5.75: IR spectrum of N'-[(2-chloro-6-methylquinolin-3-yl) methylidene]-4-hydroxybenzohydrazide (Compound 3g)

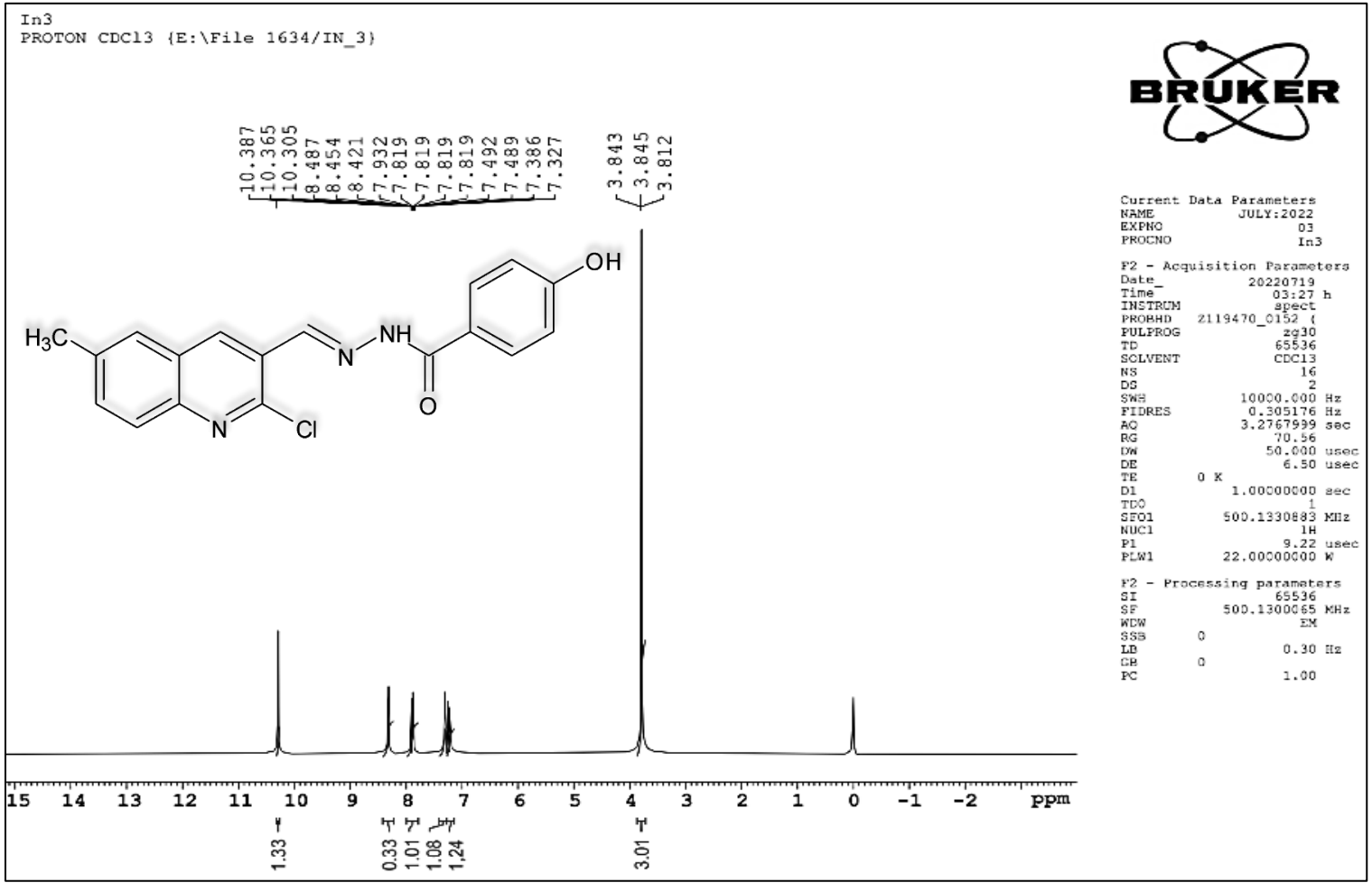

Figure 5.76: ^{1}H NMR spectrum of N'-[(2-chloro-6-methylquinolin-3-yl) methylidene]-4-hydroxybenzohydrazide (Compound 3g)

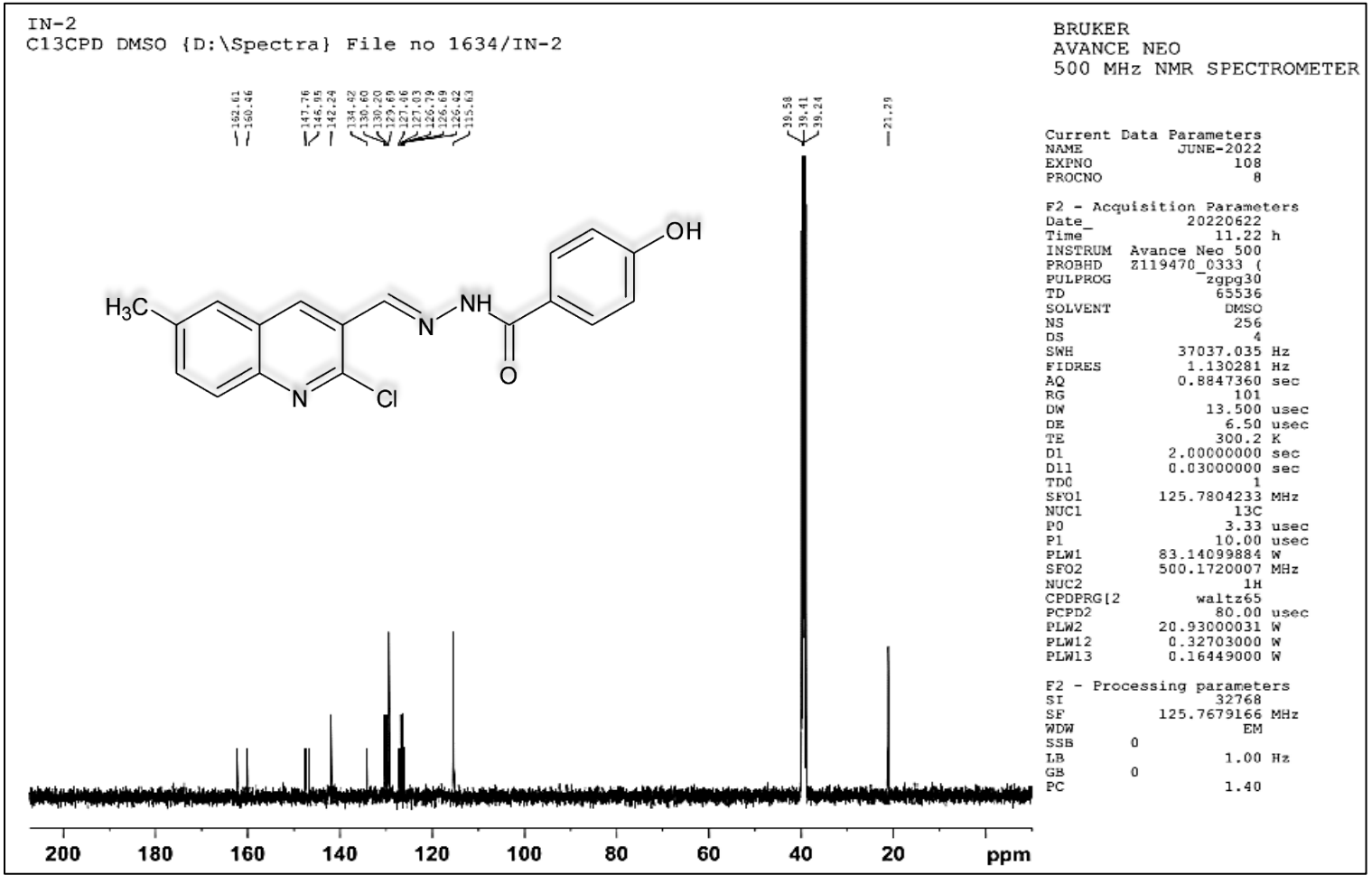

Figure 5.77: ^{13}C NMR spectrum of N'-[(2-chloro-6-methylquinolin-3-yl) methylidene]-4-hydroxybenzohydrazide (Compound 3g)

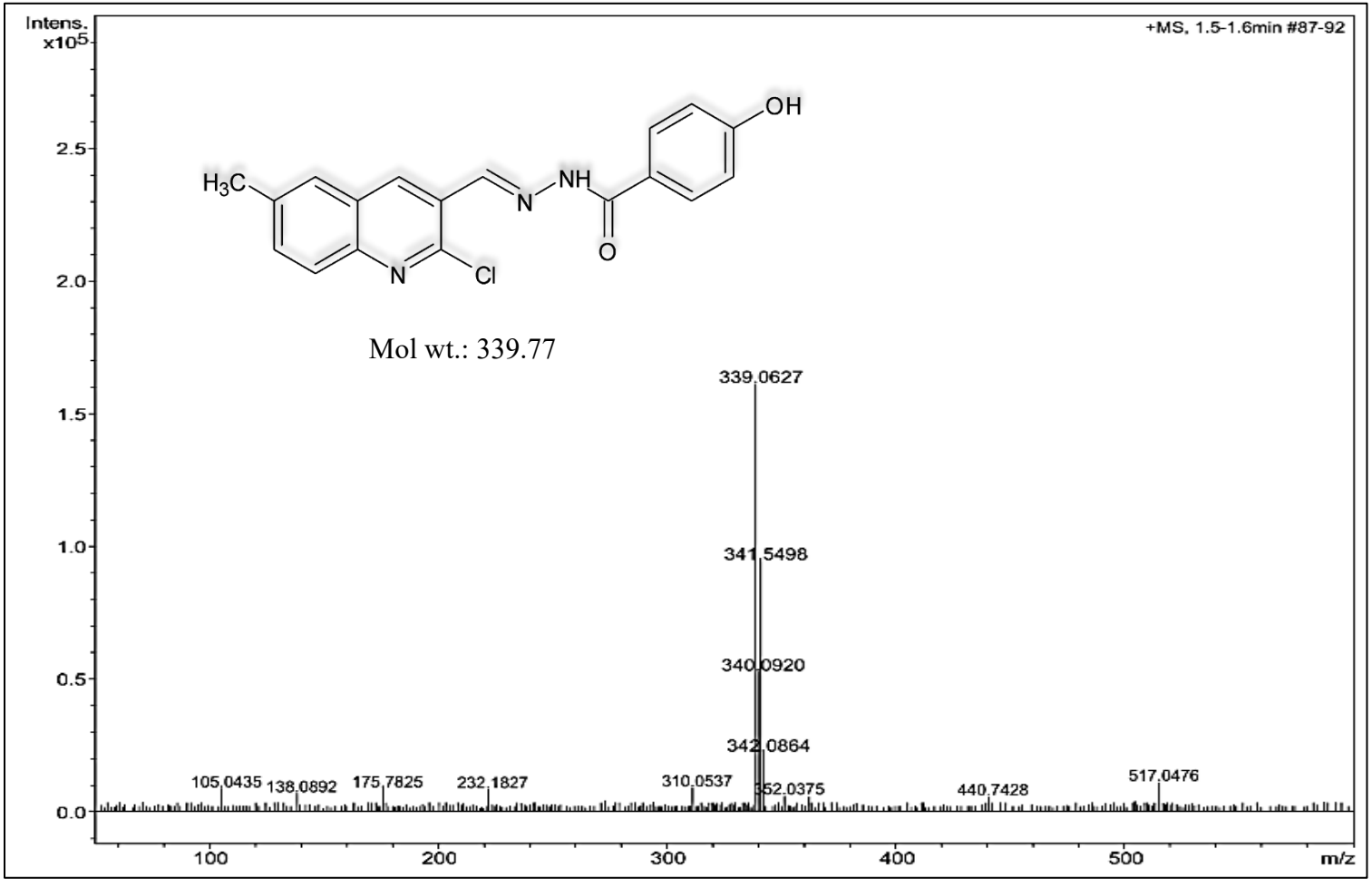

Figure 5.78: Mass spectrum of N'-[(2-chloro-6-methylquinolin-3-yl) methylidene]-4-hydroxybenzohydrazide (Compound 3g)

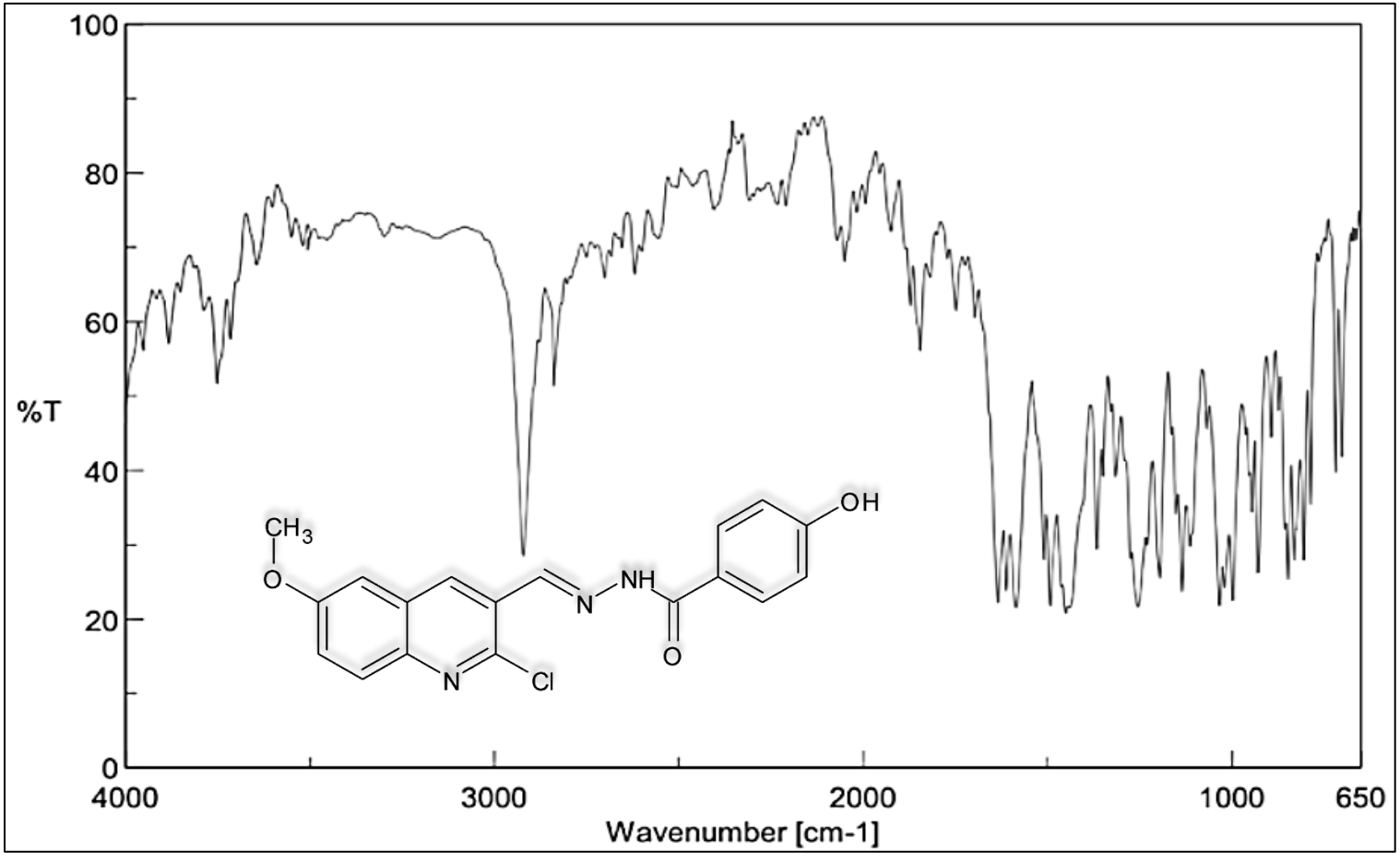

Figure 5.79: IR spectrum of N'-[(2-chloro-6-Methoxyquinolin-3-yl) methylidene]-4-hydroxybenzohydrazide (Compound 3j)

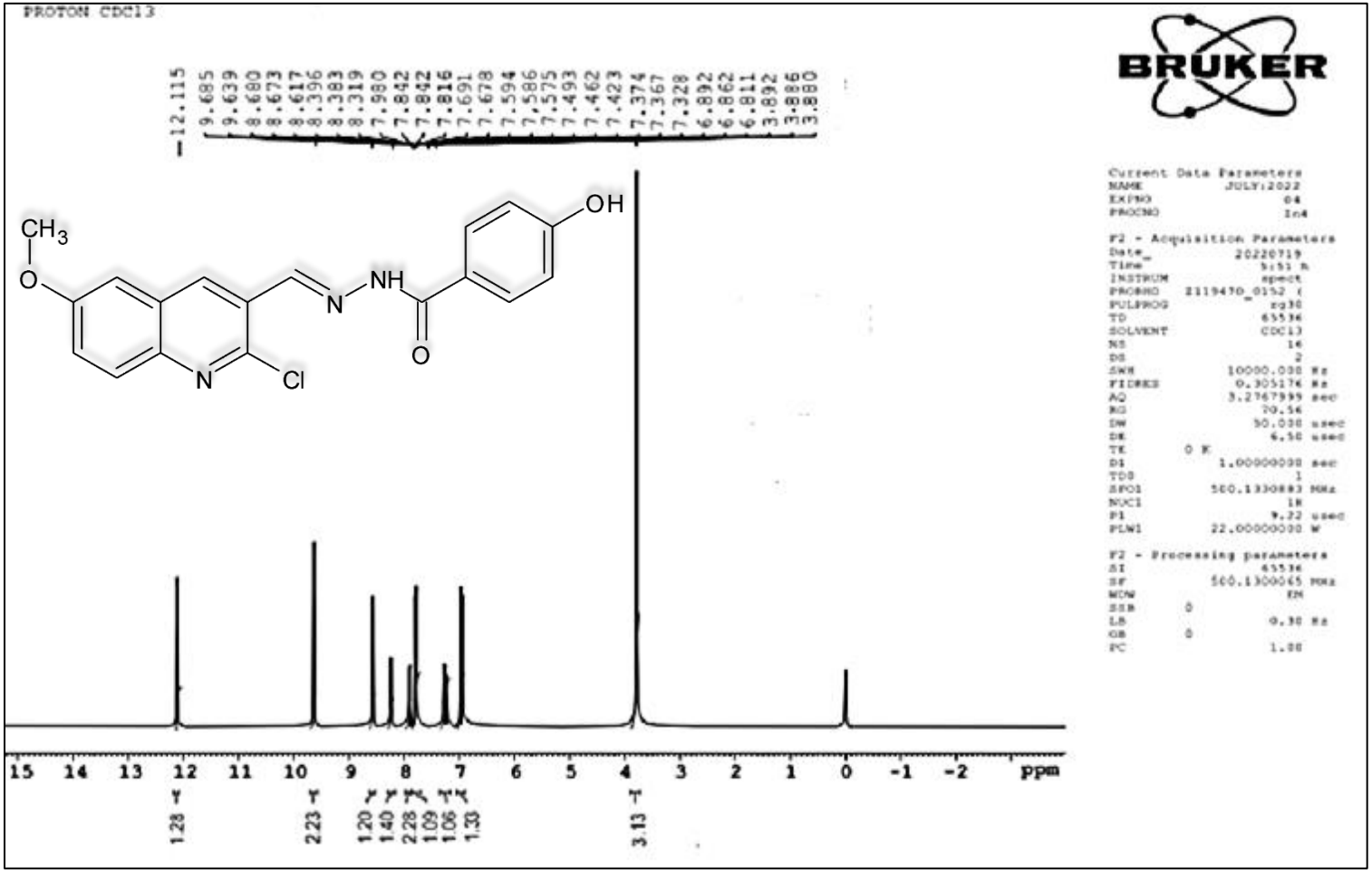

Figure 5.80: ^{1}H NMR spectrum of N'-[(2-chloro-6-Methoxyquinolin-3-yl) methylidene]-4-hydroxybenzohydrazide (Compound 3j)

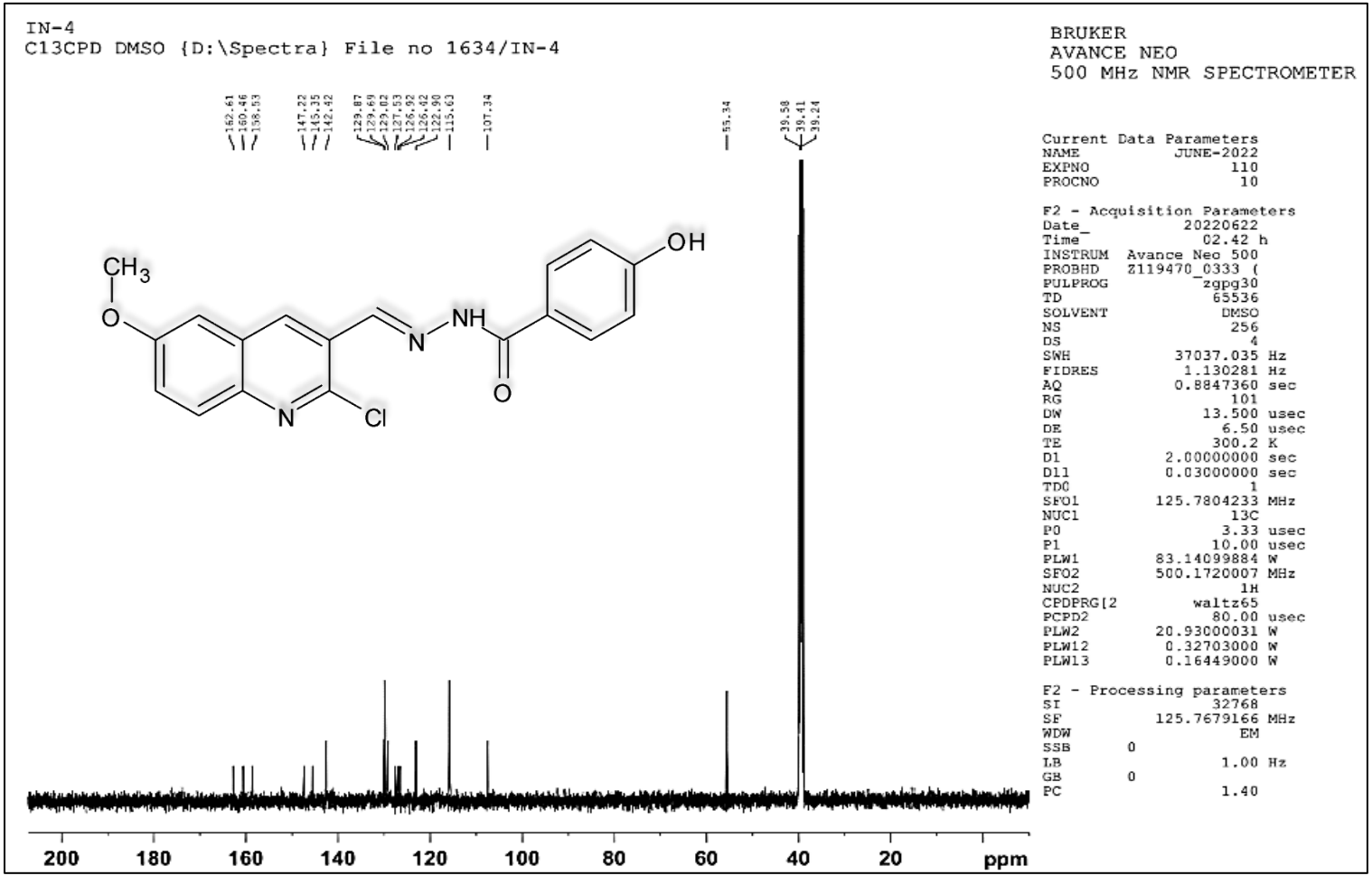

Figure 5.81: ^{13}C NMR spectrum of N'-[(2-chloro-6-Methoxyquinolin-3-yl) methylidene]-4-hydroxybenzohydrazide (Compound 3j)

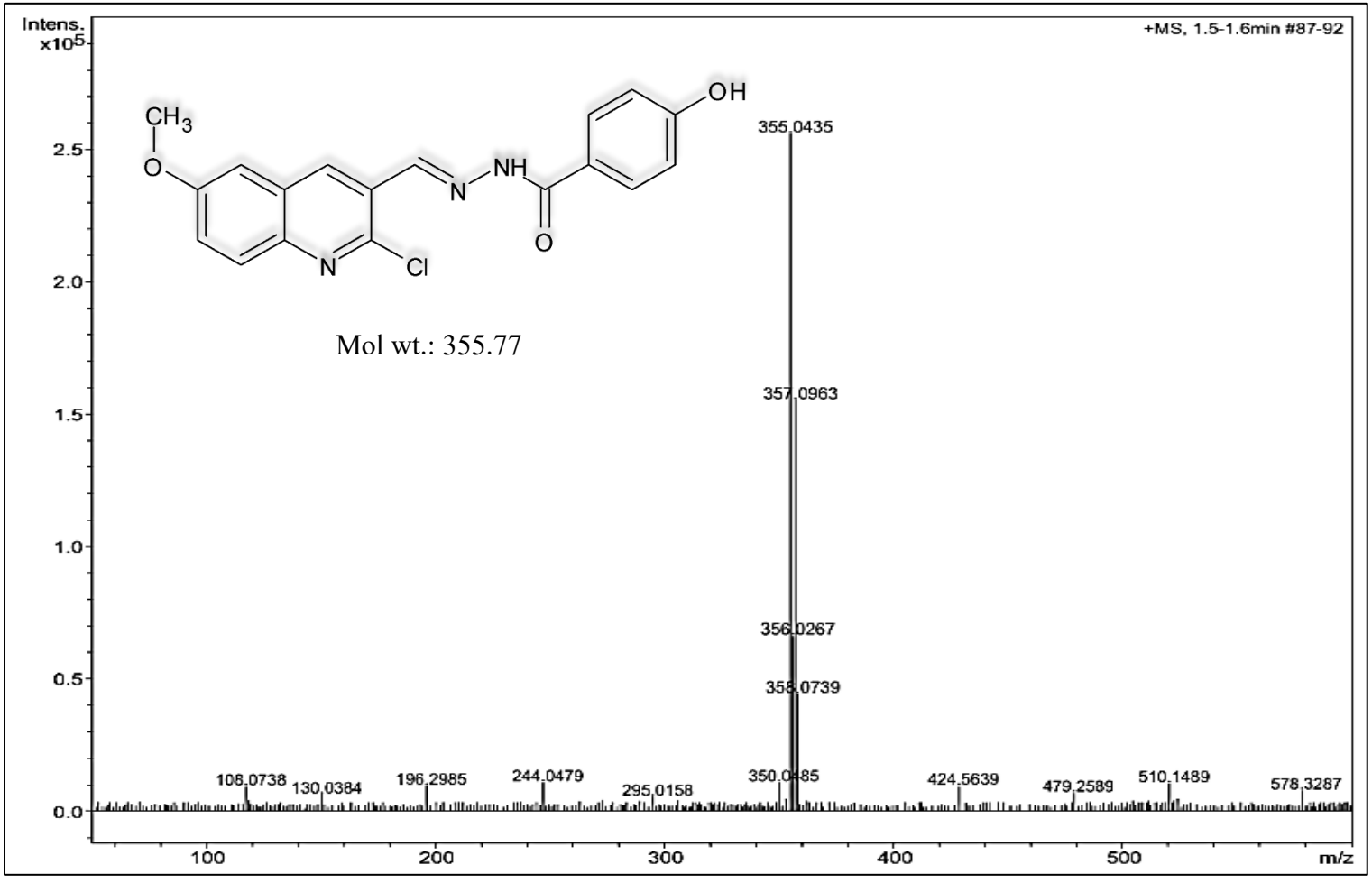

Figure 5.82: Mass spectrum of N'-[(2-chloro-6-Methoxyquinolin-3-yl) methylidene]-4-hydroxybenzohydrazide (Compound 3j)

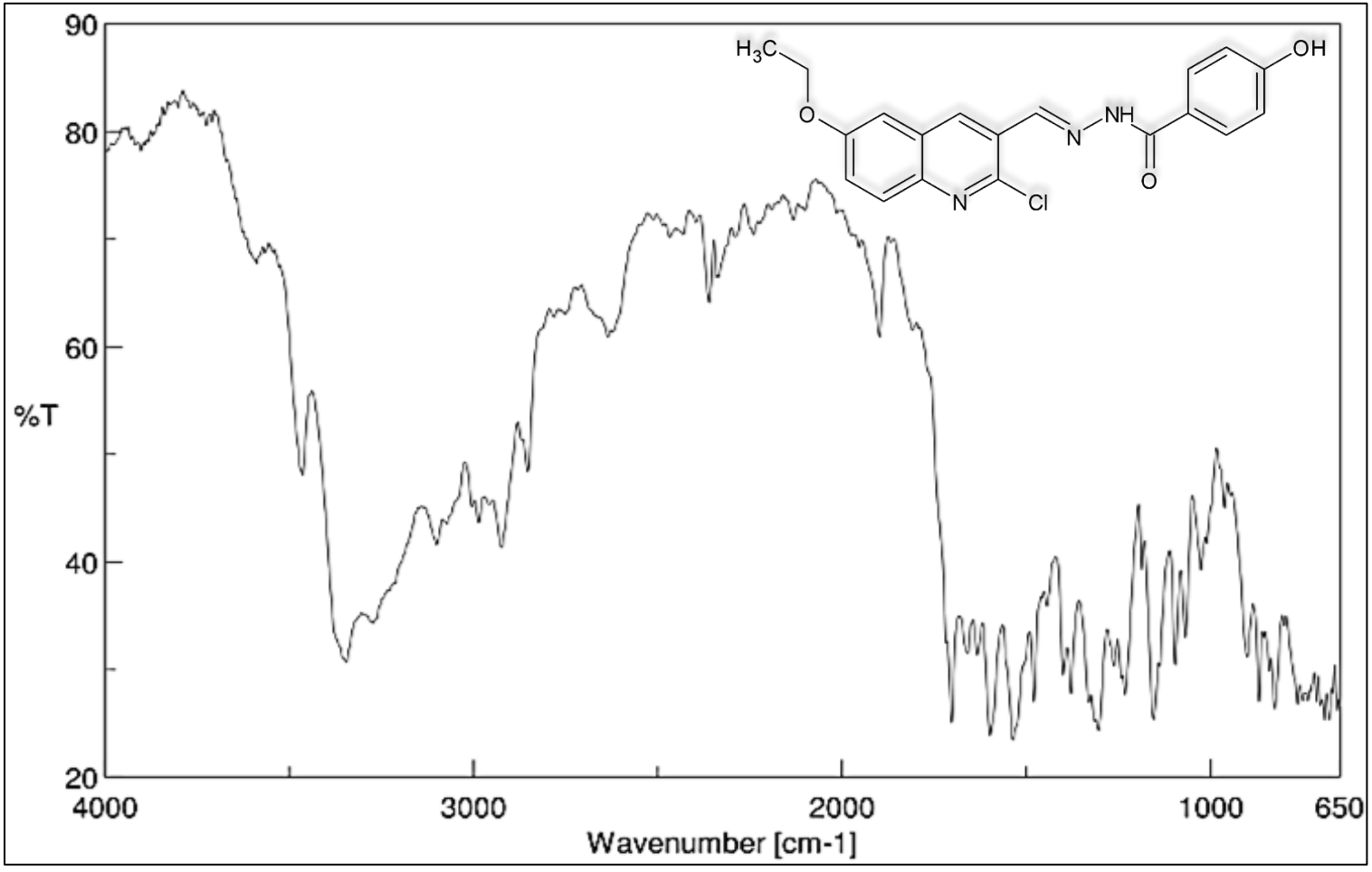

Figure 5.83: IR spectrum of N'-[2-chloro-6-ethoxyquinolin-3-yl) methylidene]-4-hydroxybenzohydrazide (Compound 3m)

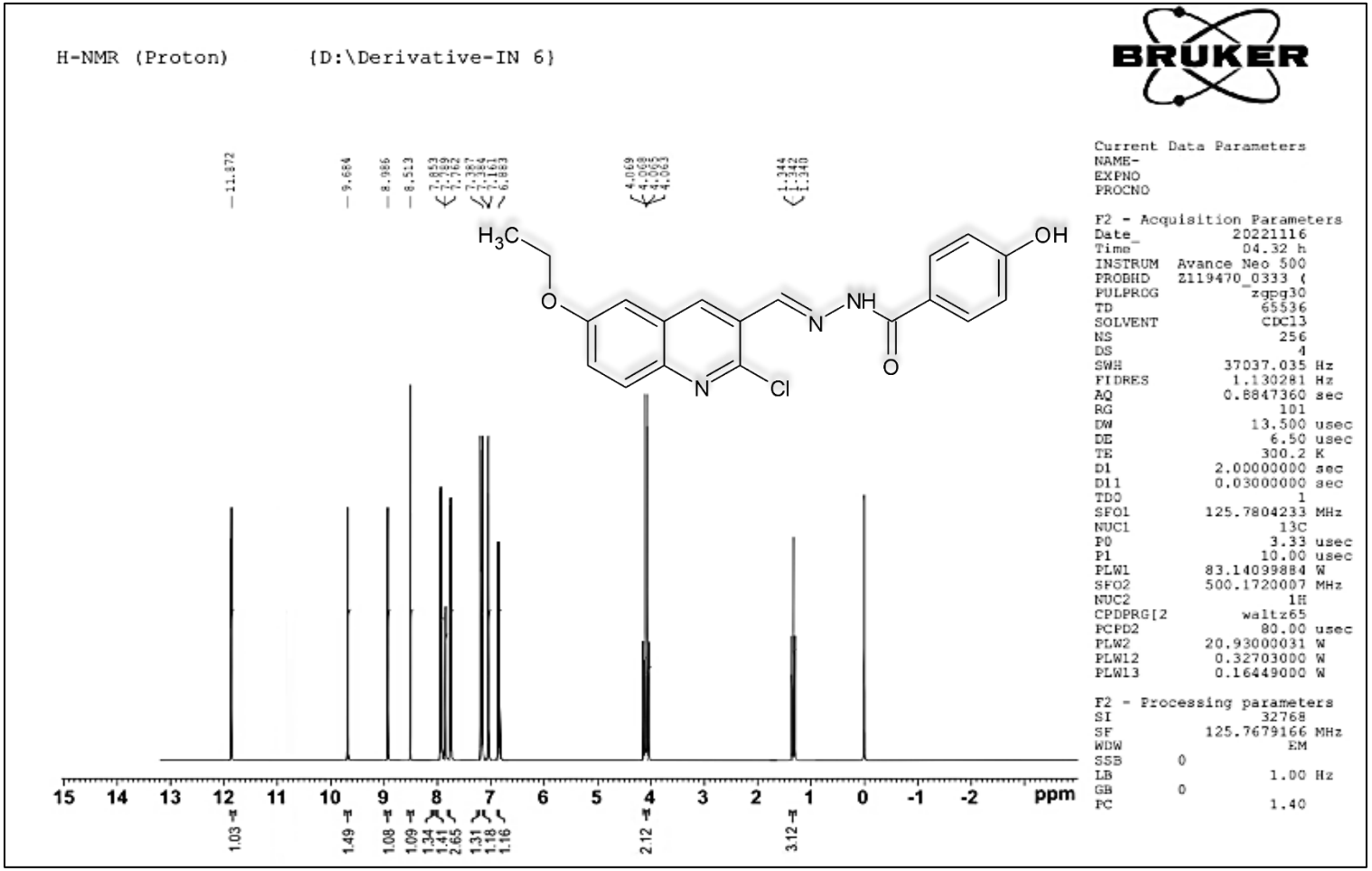

Figure 5.84: ^{1}H NMR spectrum of N'-[2-chloro-6-ethoxyquinolin-3-yl) methylidene]-4-hydroxybenzohydrazide (Compound 3m)

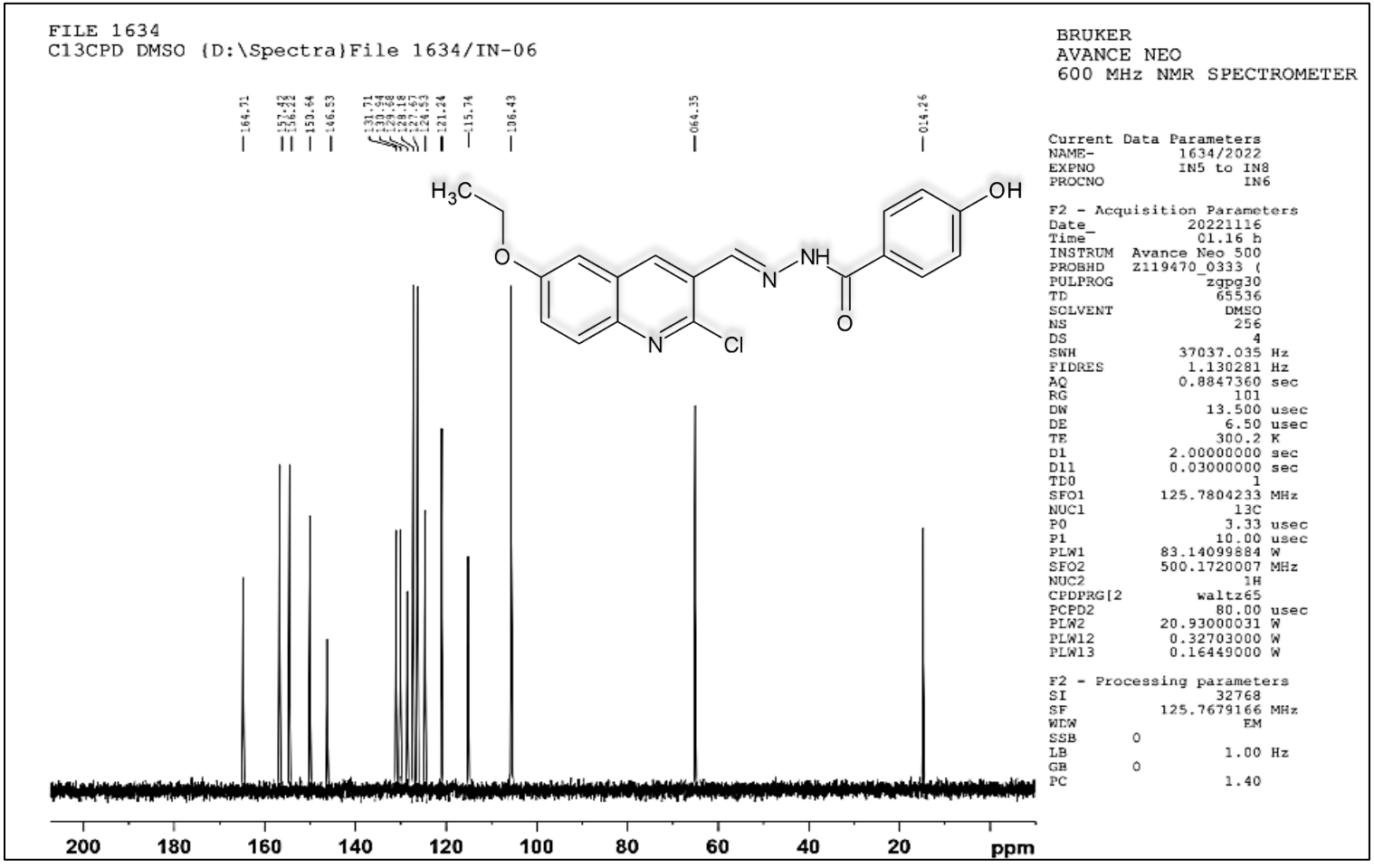

Figure 5.85: ^{13}C NMR spectrum of N'-[2-chloro-6-ethoxyquinolin-3-yl) methylidene]-4-hydroxybenzohydrazide (Compound 3m)

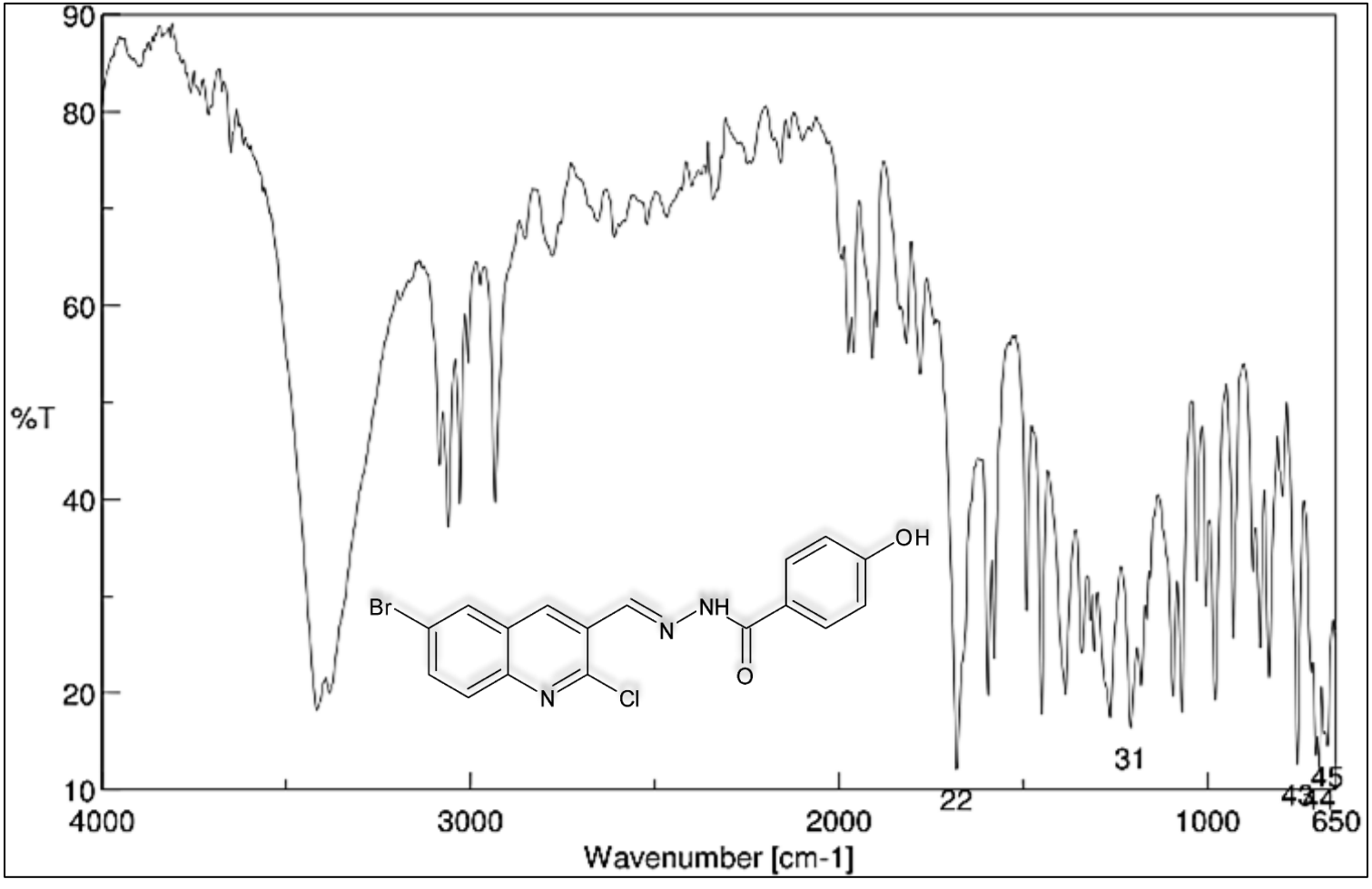

Figure 5.86: IR spectrum of N'-[6-bromo-2-chloroquinolin-3-yl) methylidene]-4-hydroxybenzohydrazide (Compound 3p)

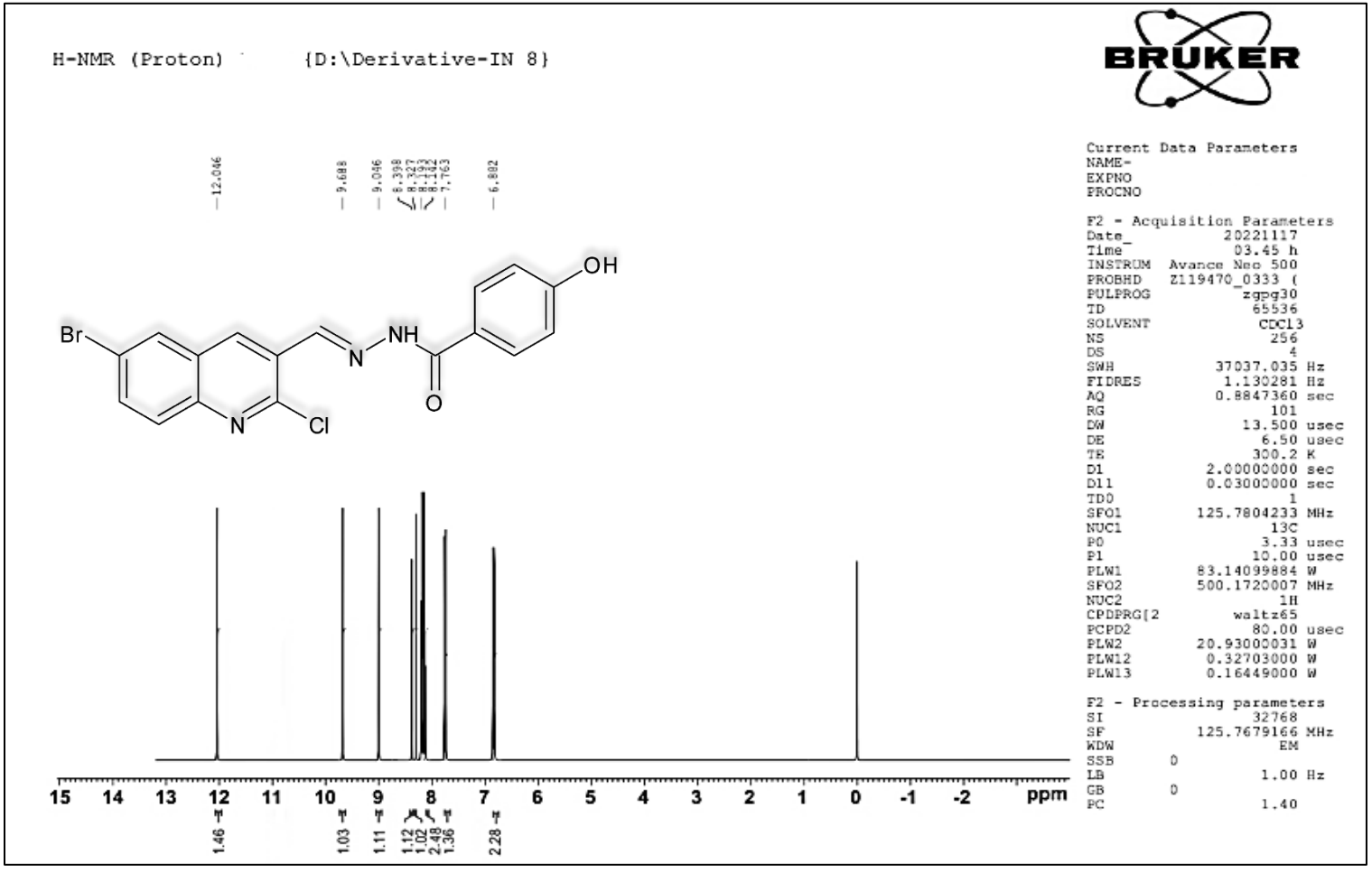

Figure 5.87: ^{1}H NMR spectrum of N'-[6-bromo-2-chloroquinolin-3-yl) methylidene]-4-hydroxybenzohydrazide (Compound 3p)

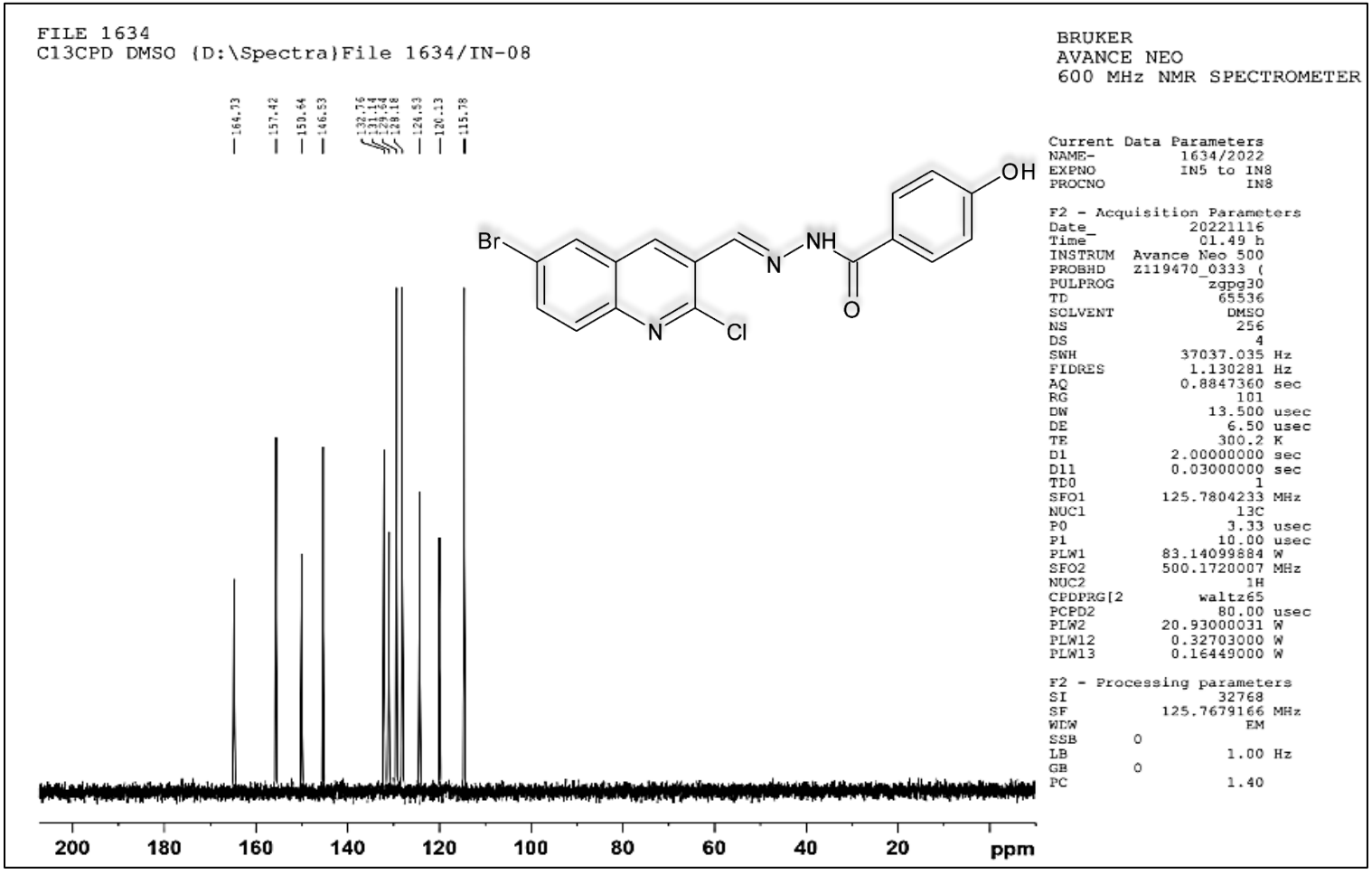

Figure 5.88: ^{13}C NMR spectrum of N'-[6-bromo-2-chloroquinolin-3-yl) methylidene]-4-hydroxybenzohydrazide (Compound 3p)

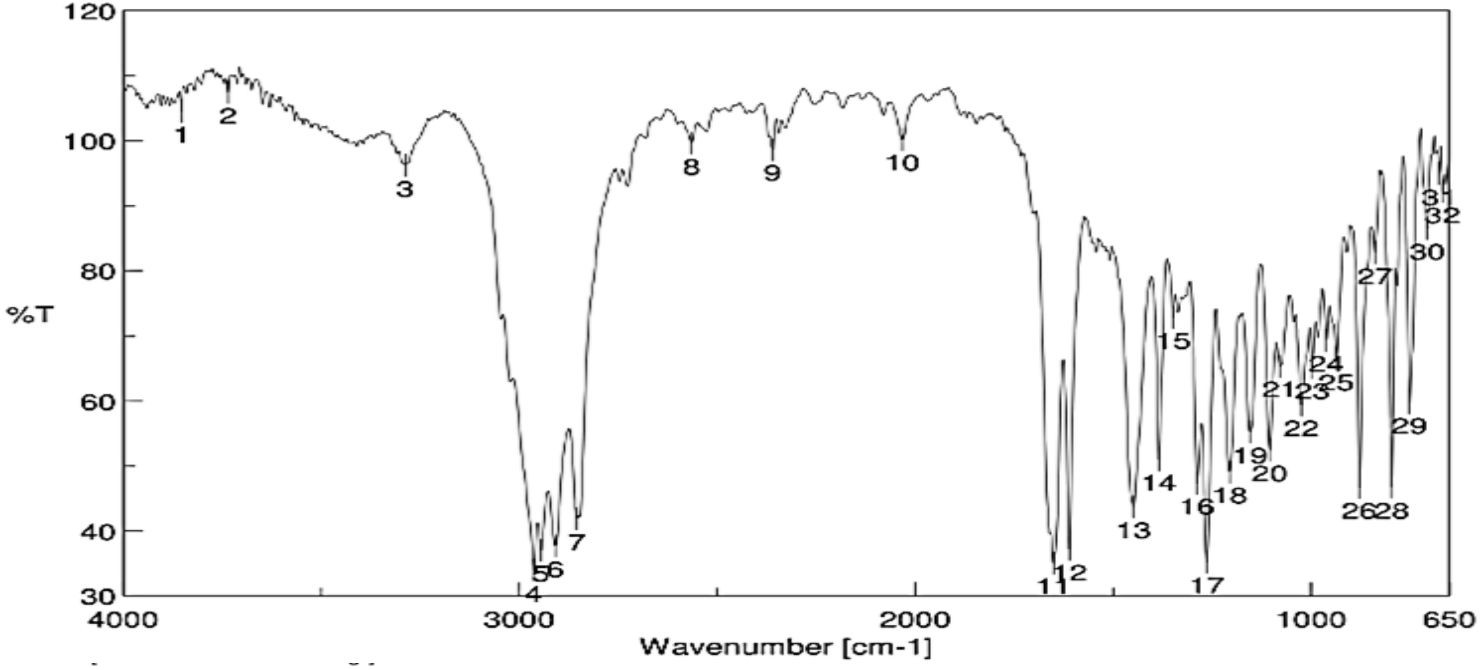

No.	Position	Intensity	No.	Position	Intensity
1	3853.08	104.422	2	3735.44	107.392
3	3288.04	96.2051	4	2963.09	33.8807
5	2944.77	36.9657	6	2908.13	37.6662
7	2854.13	41.8029	8	2564.86	99.59
9	2359.48	98.5585	10	2032.6	100.122
11	1649.8	35.0527	12	1610.27	37.1487
13	1447.31	43.6619	14	1383.68	50.9172
15	1348	72.7695	16	1287.25	47.3038
17	1263.15	35.145	18	1205.29	48.9995
19	1154.19	55.2027	20	1104.05	52.4195
21	1078.01	65.2779	22	1024.02	59.3509
23	996.053	65.1081	24	960.377	69.2606
25	936.271	66.4224	26	877.452	46.6234
27	838.883	82.7279	28	795.493	46.7
29	751.138	59.6987	30	705.819	86.4728
31	675.928	94.8964	32	667.25	92.1298

Figure 5.89: IR spectrum of 4-{2-2-[(2-chloroquinolin-3-yl) methylidene] hydrazine-1-carbonyl} phenyl acetate (Compound 4a)

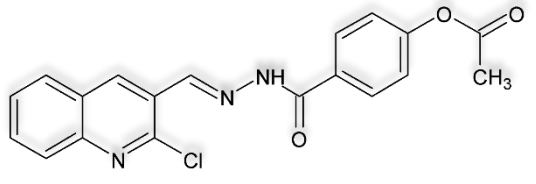

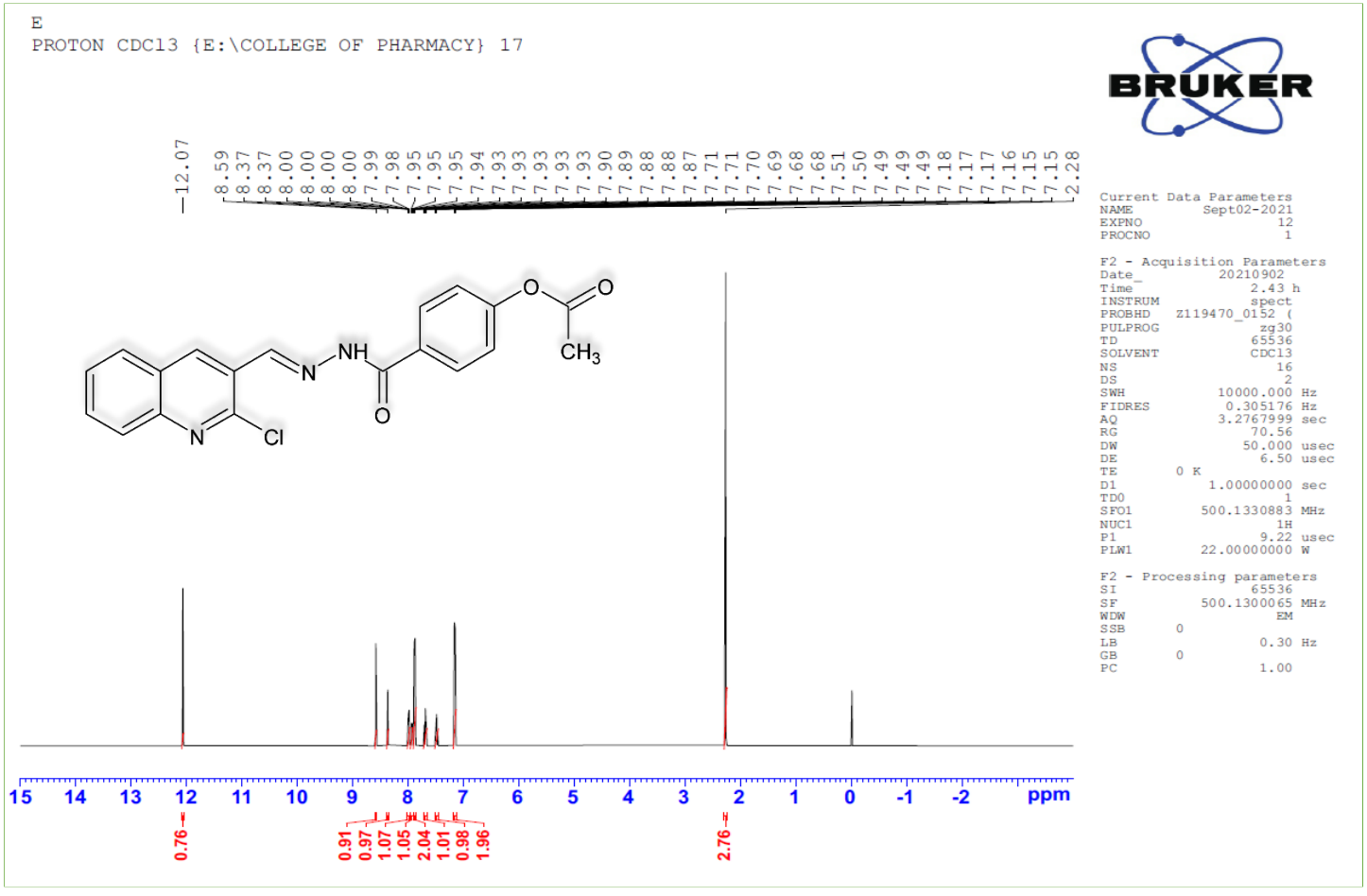

Figure 5.90: ^{1}H NMR spectrum of 4-{2-2-[(2-chloroquinolin-3-yl) methylidene] hydrazine-1-carbonyl} phenyl acetate (Compound 4a)

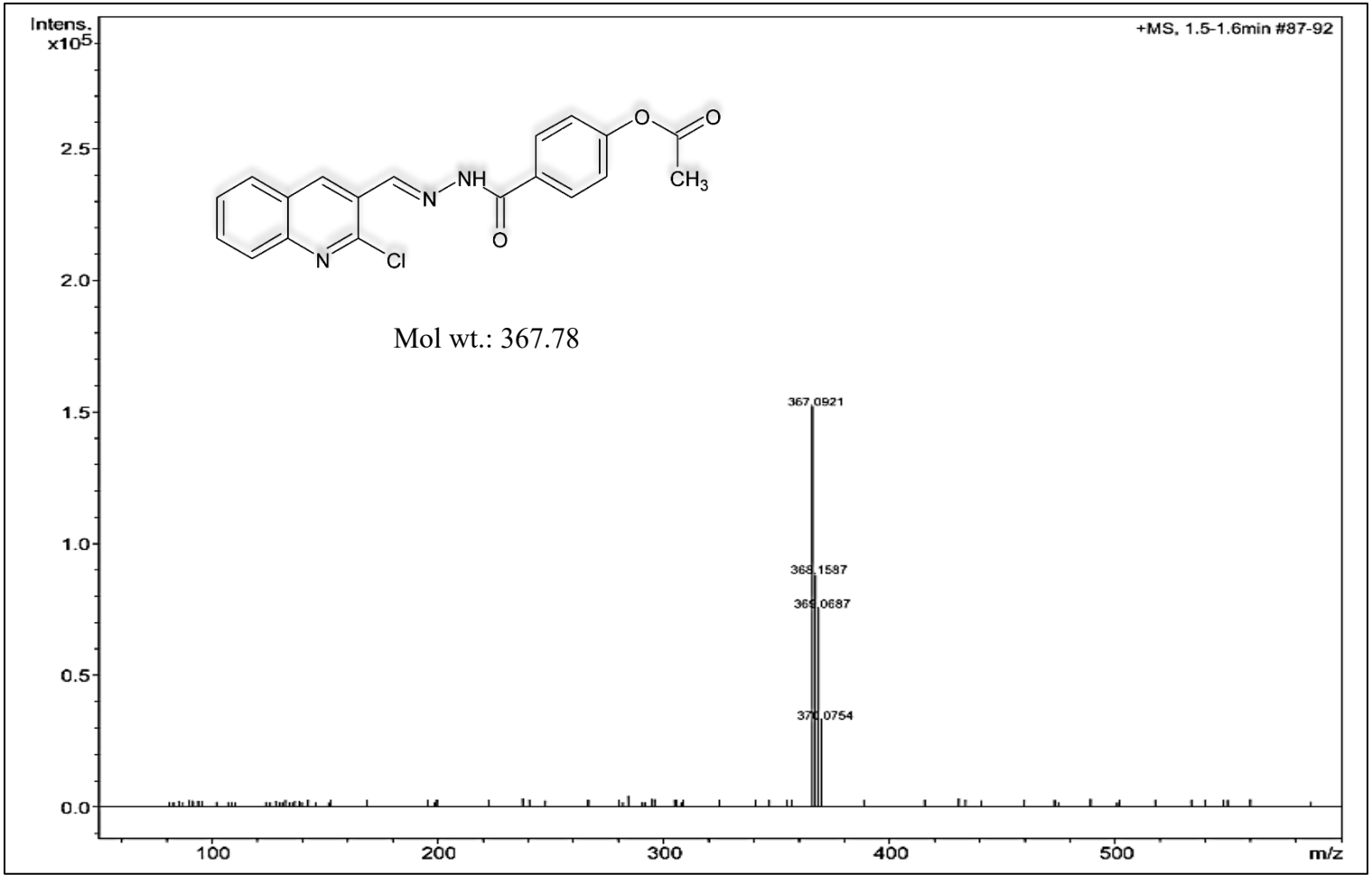

Figure 5.91: Mass spectrum of 4-{2-2-[(2-chloroquinolin-3-yl) methylidene] hydrazine-1-carbonyl} phenyl acetate (Compound 4a)

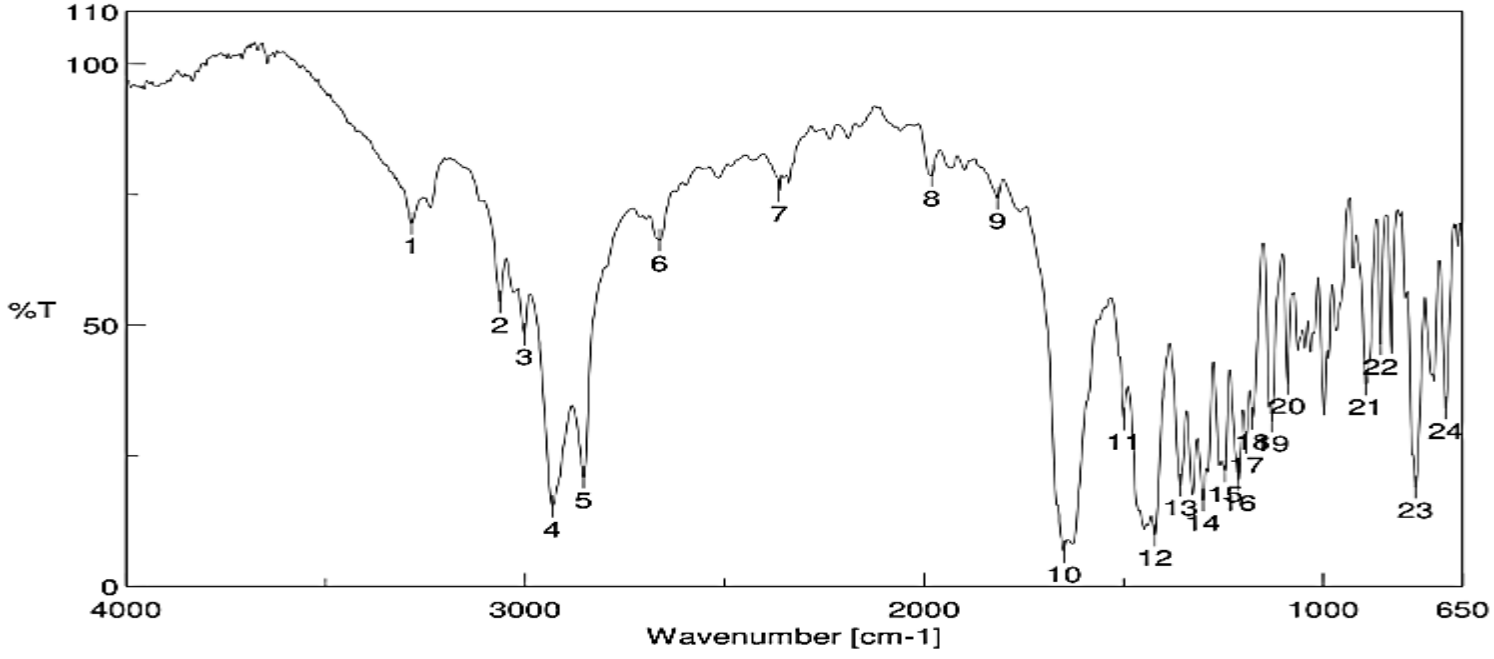

No.	Position	Intensity	No.	Position	Intensity
1	3285.14	69.4409	2	3062.41	54.4446
3	3001.66	48.1934	4	2931.27	15.3071
5	2853.17	20.8739	6	2663.21	66.2157
7	2363.34	75.6481	8	1981.5	78.536
9	1815.65	74.2315	10	1648.84	6.6676
11	1498.42	31.9772	12	1421.28	9.76042
13	1357.64	19.3957	14	1300.75	16.4653
15	1245.79	22.0312	16	1211.08	20.3028
17	1192.76	27.4977	18	1176.36	32.0699
19	1128.15	31.6393	20	1088.62	38.8093
21	892.88	38.667	22	855.275	46.3792
23	767.53	18.9688	24	692.32	34.1568

Figure 5.92: IR spectrum of 4-{2-2-[(2-chloroquinolin-3-yl) methylidene] hydrazine-1-carbonyl} phenyl propanoate (Compound 4b)

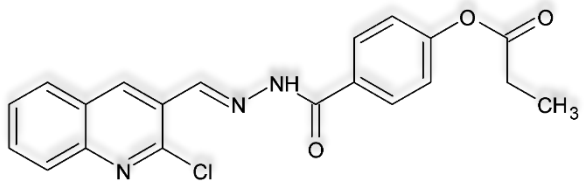

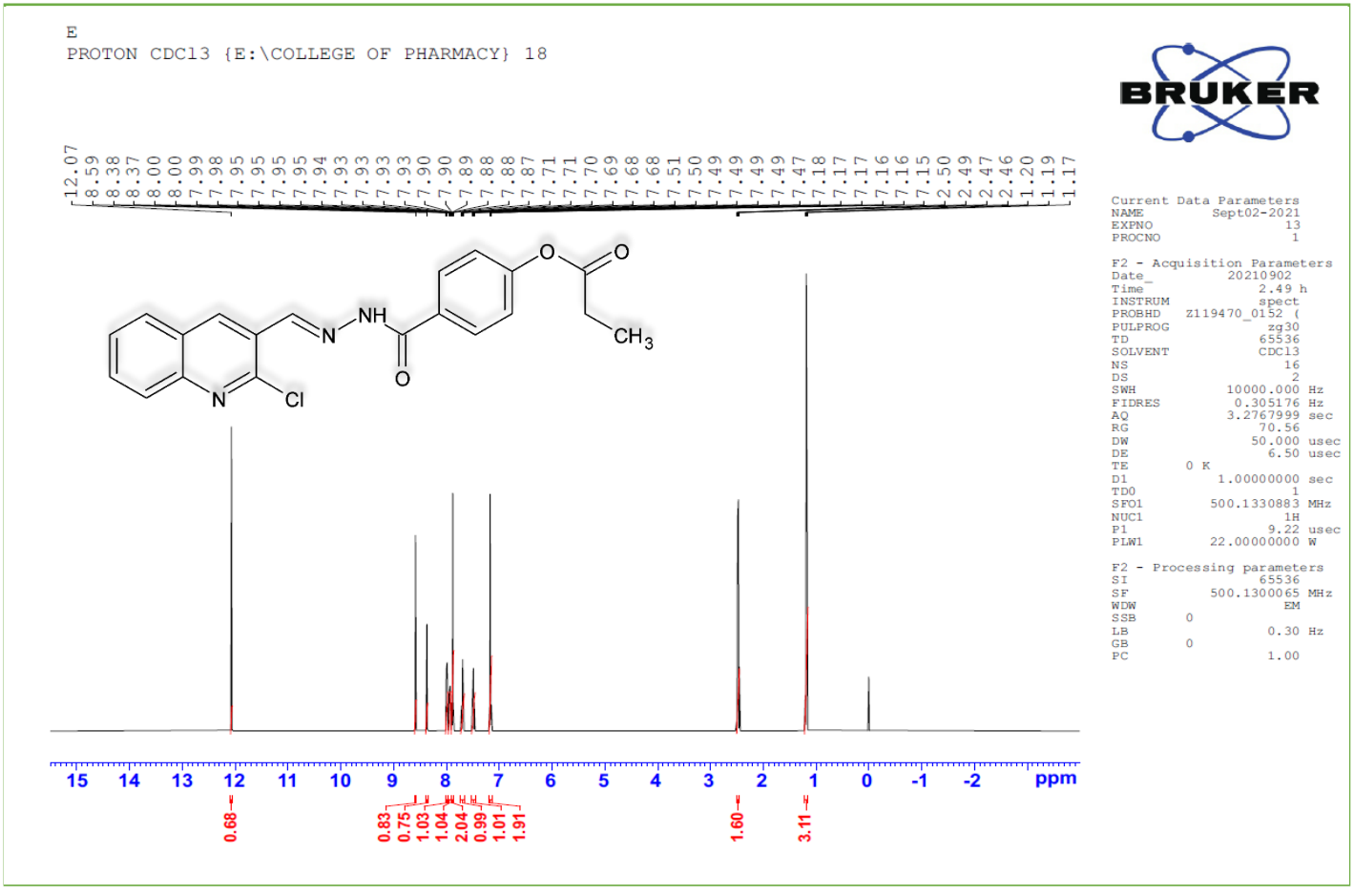

Figure 5.93: ^{1}H NMR spectrum of 4-{2-2-[(2-chloroquinolin-3-yl) methylidene] hydrazine-1-carbonyl} phenyl propanoate (Compound 4b)

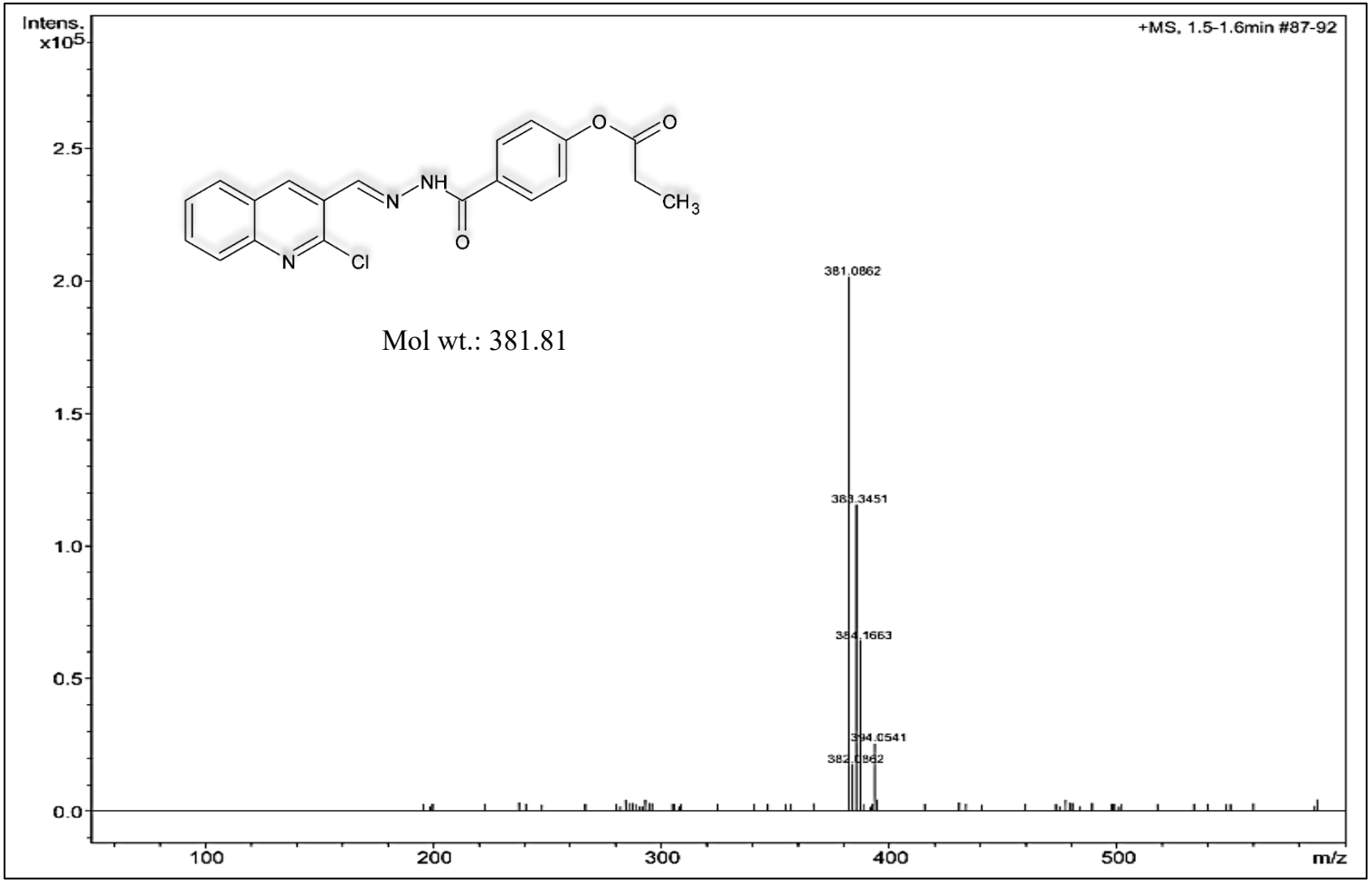

Figure 5.94: Mass spectrum of 4-{2-2-[(2-chloroquinolin-3-yl) methylidene] hydrazine-1-carbonyl} phenyl propanoate (Compound 4b)

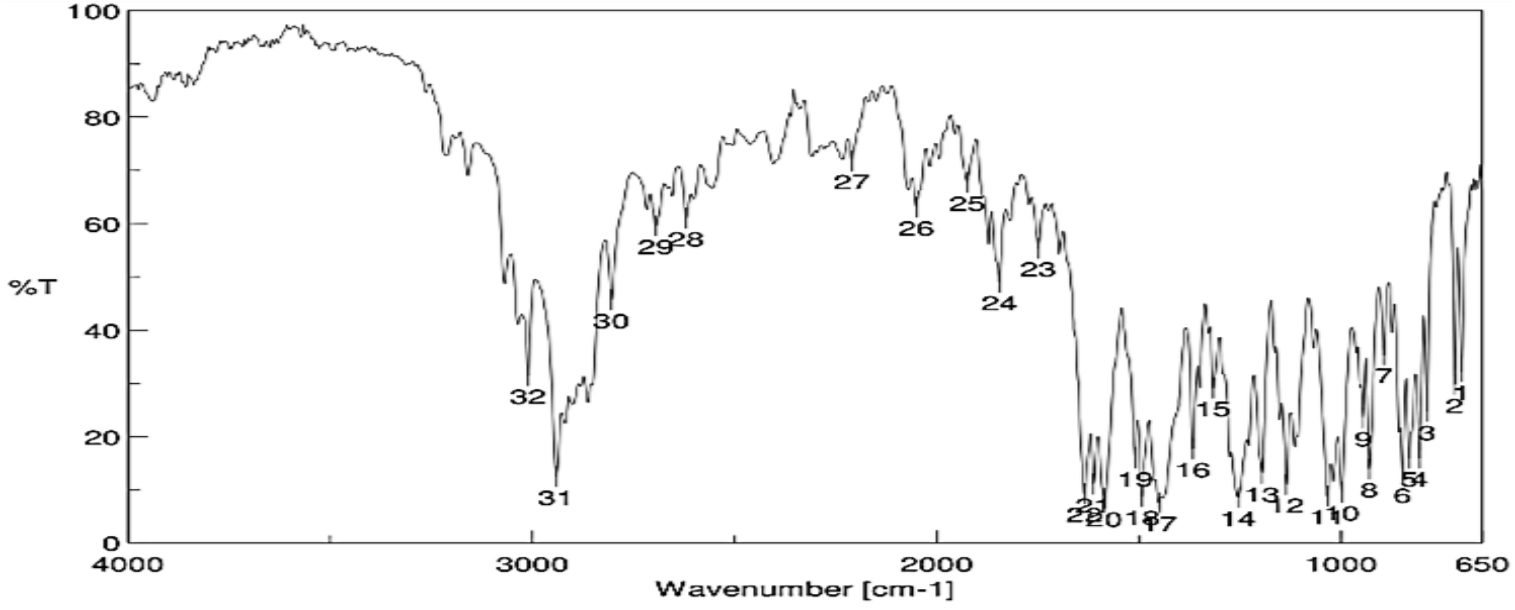

No.	Position	Intensity	No.	Position	Intensity
1	701.962	32.128	2	718.354	29.7057
3	786.815	24.6634	4	805.135	15.8826
5	831.169	15.8504	6	847.561	12.8439
7	893.844	35.2603	8	929.521	13.8463
9	944.949	23.4626	10	997.982	9.50854
11	1032.69	8.72431	12	1134.9	10.9335
13	1195.65	13.036	14	1254.47	8.49877
15	1316.18	29.0474	16	1366.32	17.6817
17	1449.24	7.49052	18	1491.67	8.71521
19	1509.03	15.923	20	1585.2	8.3717
21	1612.2	11.0111	22	1634.38	9.18073
23	1748.16	55.2897	24	1844.58	48.9863
25	1924.61	67.7423	26	2049.96	63.0372
27	2210.02	71.7839	28	2619.82	60.9864
29	2694.07	59.5443	30	2803.99	45.6003
31	2940.91	12.4405	32	3010.34	31.4023

Figure 5.95: IR spectrum of 4-{2-2-[(2-chloroquinolin-3-yl) methylidene] hydrazine-1-carbonyl} phenyl butanoate (Compound 4c)

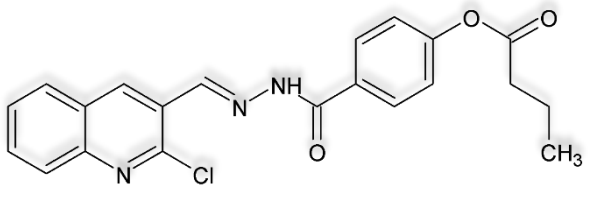

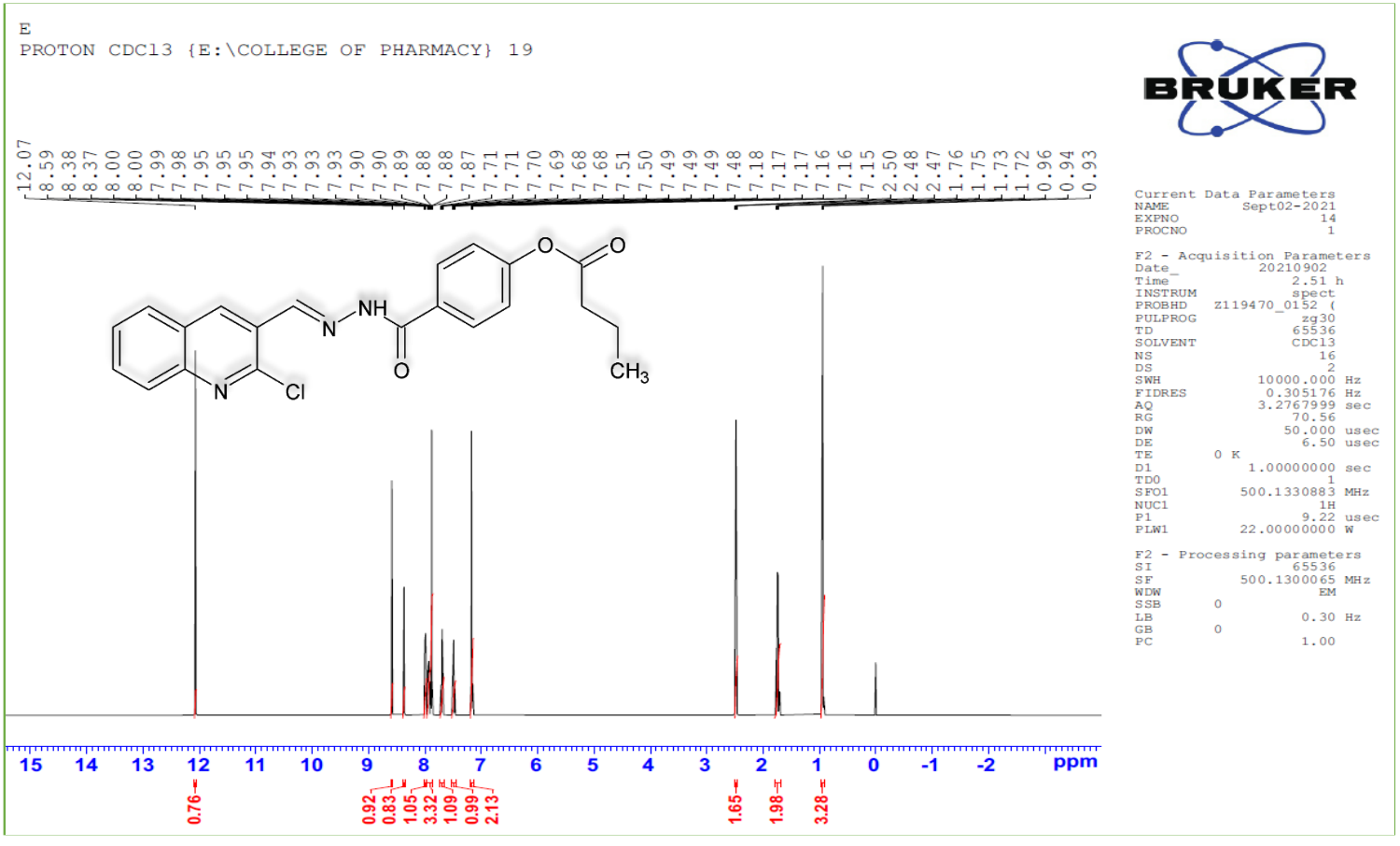

Figure 5.96: ^{1}H NMR spectrum of 4-{2-2-[(2-chloroquinolin-3-yl) methylidene] hydrazine-1-carbonyl} phenyl butanoate (Compound 4c)

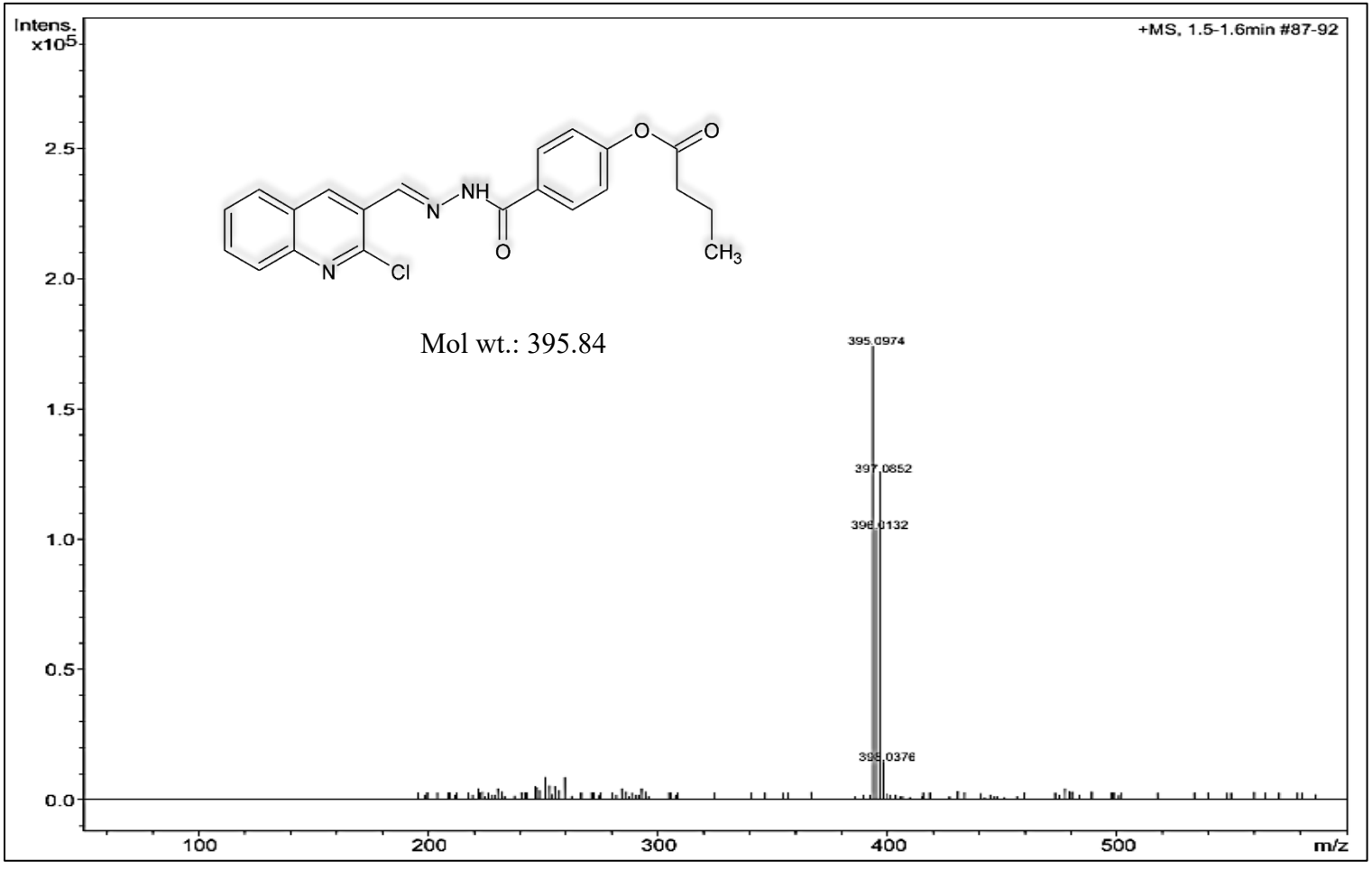

Figure 5.97: Mass spectrum of 4-{2-2-[(2-chloroquinolin-3-yl) methylidene] hydrazine-1-carbonyl} phenyl butanoate (Compound 4c)

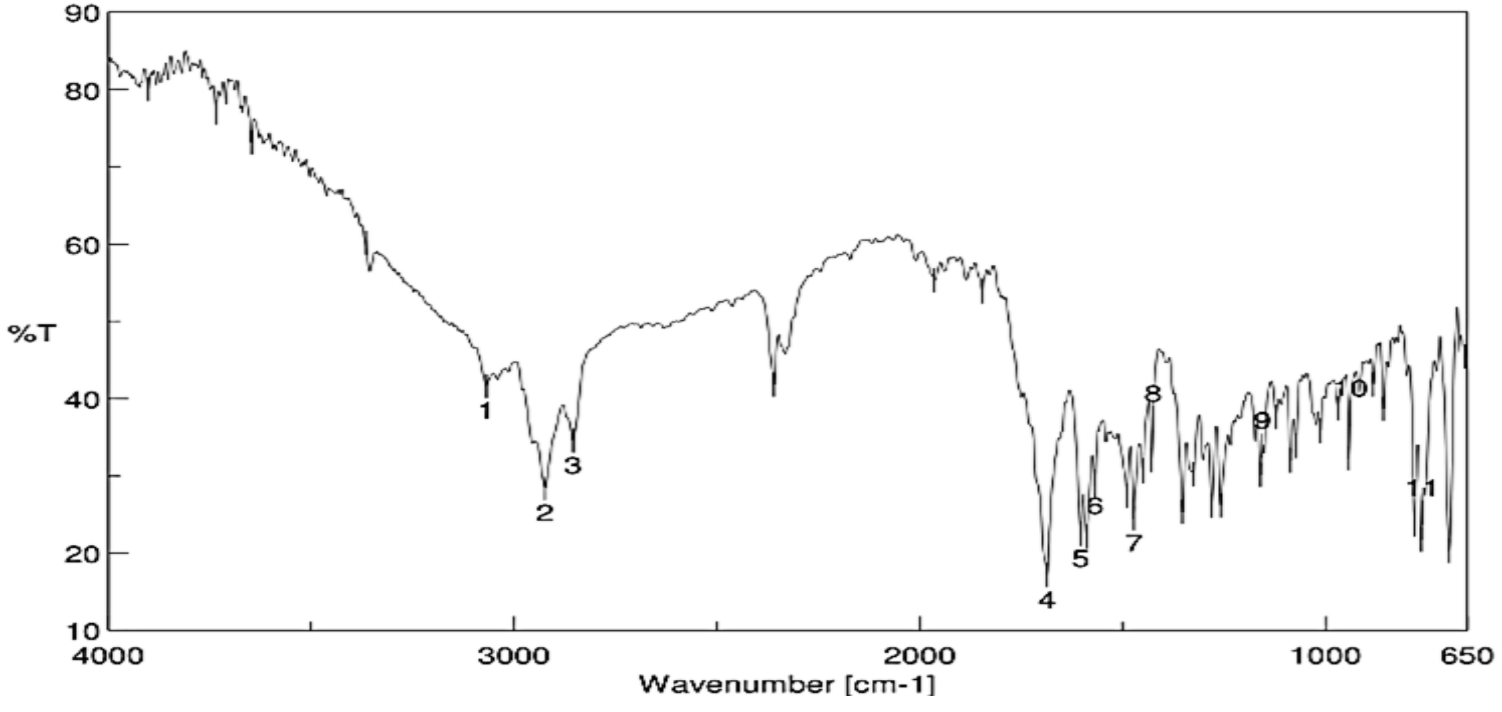

No.	Position	Intensity	No.	Position	Intensity
1	3068.19	41.6229	2	2924.52	28.4233
3	2854.13	34.5934	4	1686.44	17.1479
5	1603.52	22.4968	6	1567.84	29.2877
7	1472.38	24.4886	8	1424.17	37.3905
9	1155.15	33.9257	10	938.199	38.06
11	760.78	25.222			

Figure 5.98: IR spectrum of 4-{2-2-[(2,6-dichloroquinolin-3-yl) methylidene] hydrazine-1-carbonyl} phenyl acetate (Compound 4d)

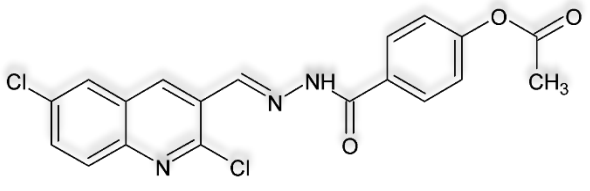

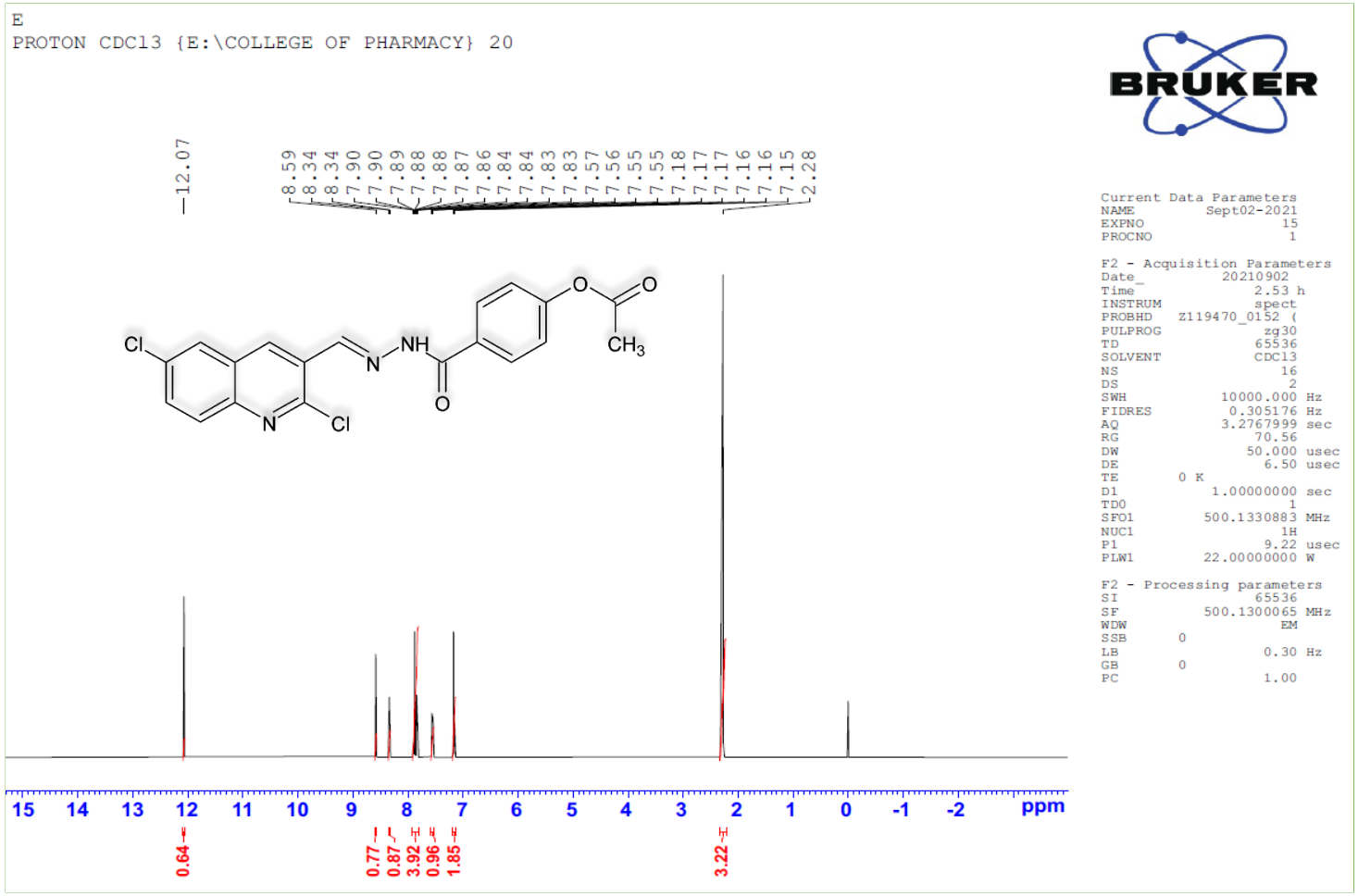

Figure 5.99: ^{1}H NMR spectrum of 4-{2-2-[(2,6-dichloroquinolin-3-yl) methylidene] hydrazine-1-carbonyl} phenyl acetate (Compound 4d)

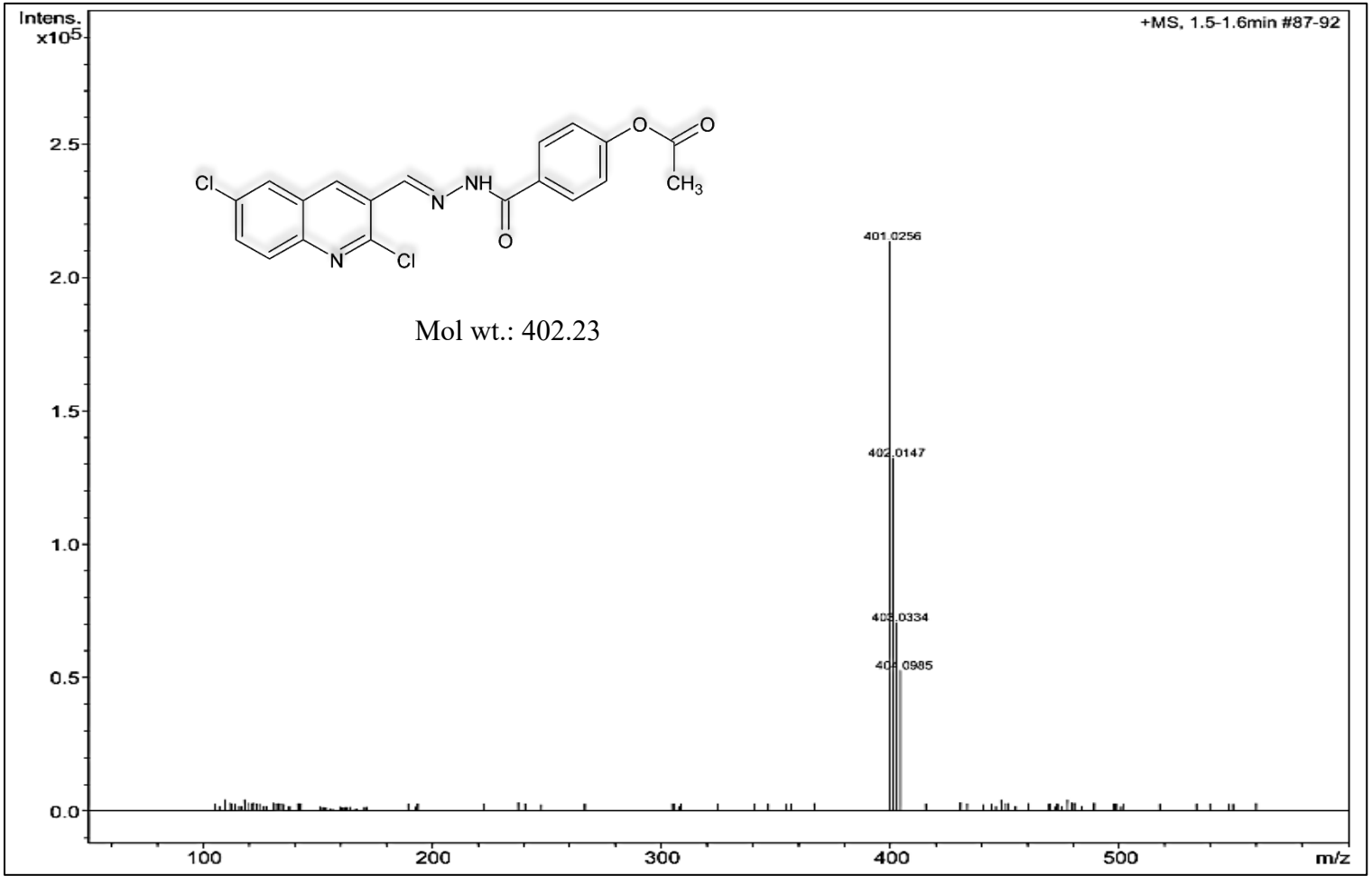

Figure 5.100: Mass spectrum of 4-{2-2-[(2,6-dichloroquinolin-3-yl) methylidene] hydrazine-1-carbonyl} phenyl acetate (Compound 4d)

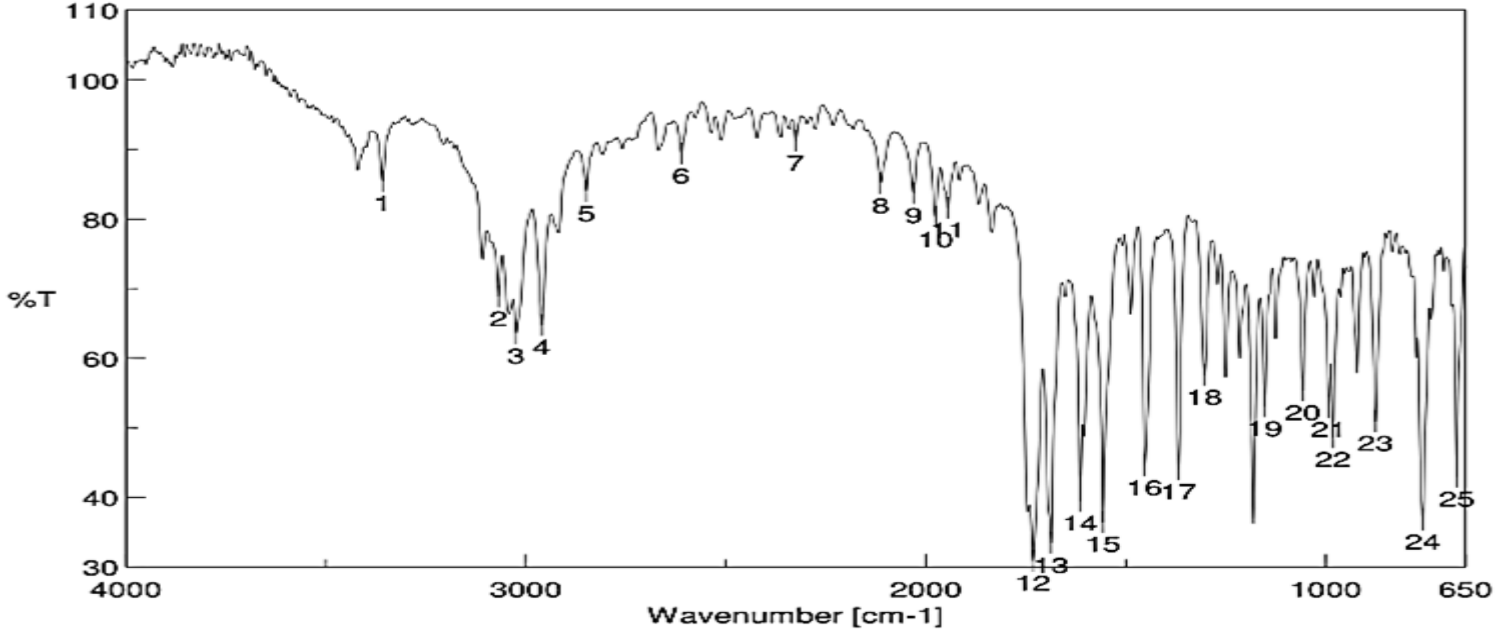

No.	Position	Intensity	No.	Position	Intensity
1	3358.43	85.3851	2	3068.19	68.8533
3	3024.8	63.5363	4	2959.23	64.7812
5	2848.35	83.976	6	2611.14	89.4404
7	2324.77	91.2043	8	2112.64	85.1296
9	2030.68	83.6997	10	1975.71	80.2651
11	1944.86	81.604	12	1731.76	30.8775
13	1686.44	33.502	14	1614.13	39.5197
15	1556.27	36.4486	16	1452.14	44.5983
17	1368.25	44.045	18	1303.64	57.5755
19	1153.22	53.0986	20	1056.8	55.3787
21	992.196	52.9466	22	980.625	48.6274
23	874.56	50.9214	24	756.923	36.7777
25	672.071	42.9764			

Figure 5.101: IR spectrum of 4-{2-2-[(2,6-dichloroquinolin-3-yl) methylidene] hydrazine-1-carbonyl} phenyl propanoate (Compound 4e)

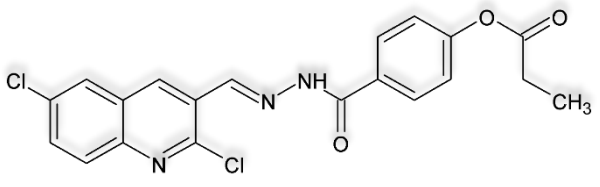

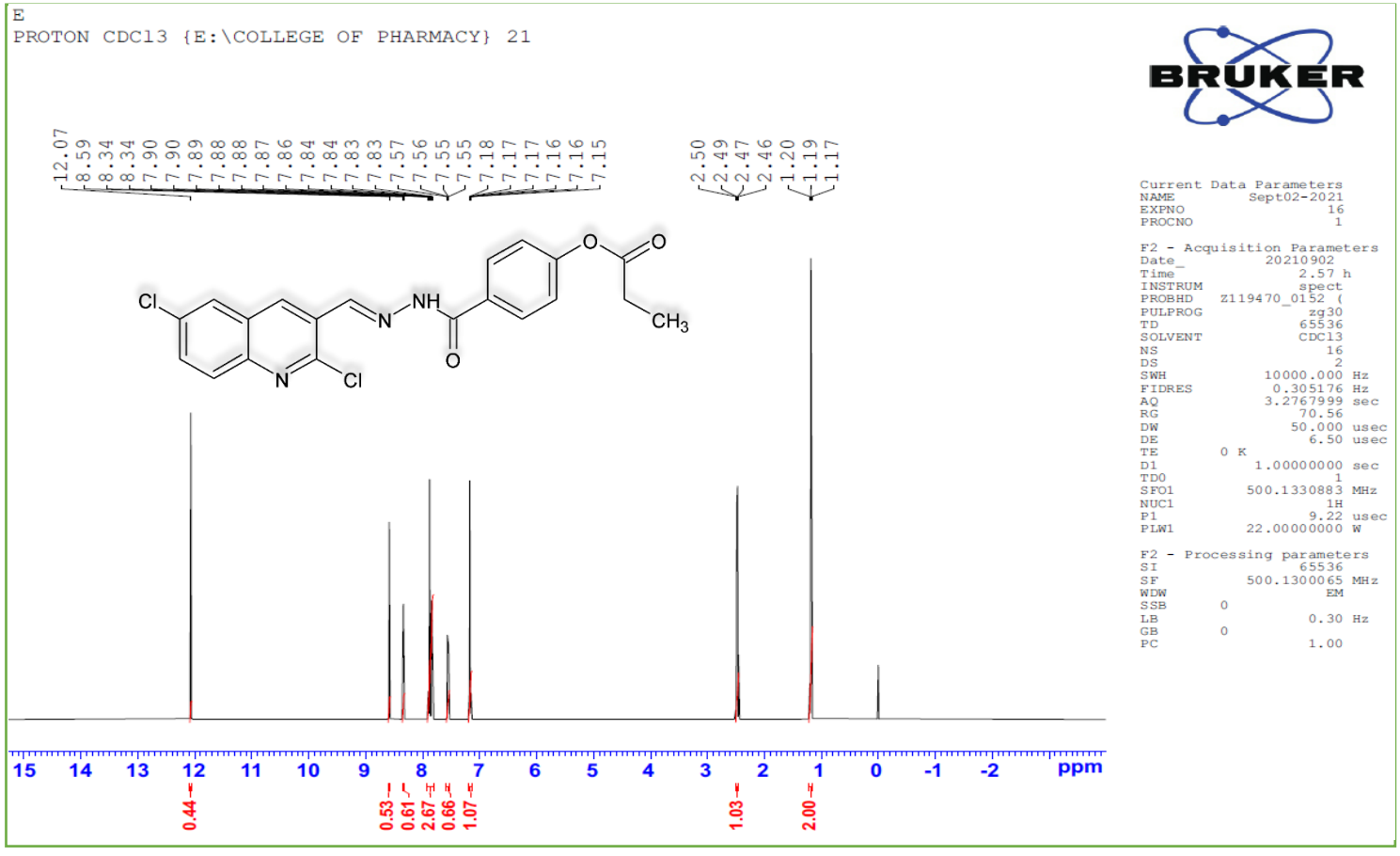

Figure 5.102: ^{1}H NMR spectrum of 4-{2-2-[(2,6-dichloroquinolin-3-yl) methylidene] hydrazine-1-carbonyl} phenyl propanoate (Compound 4e)

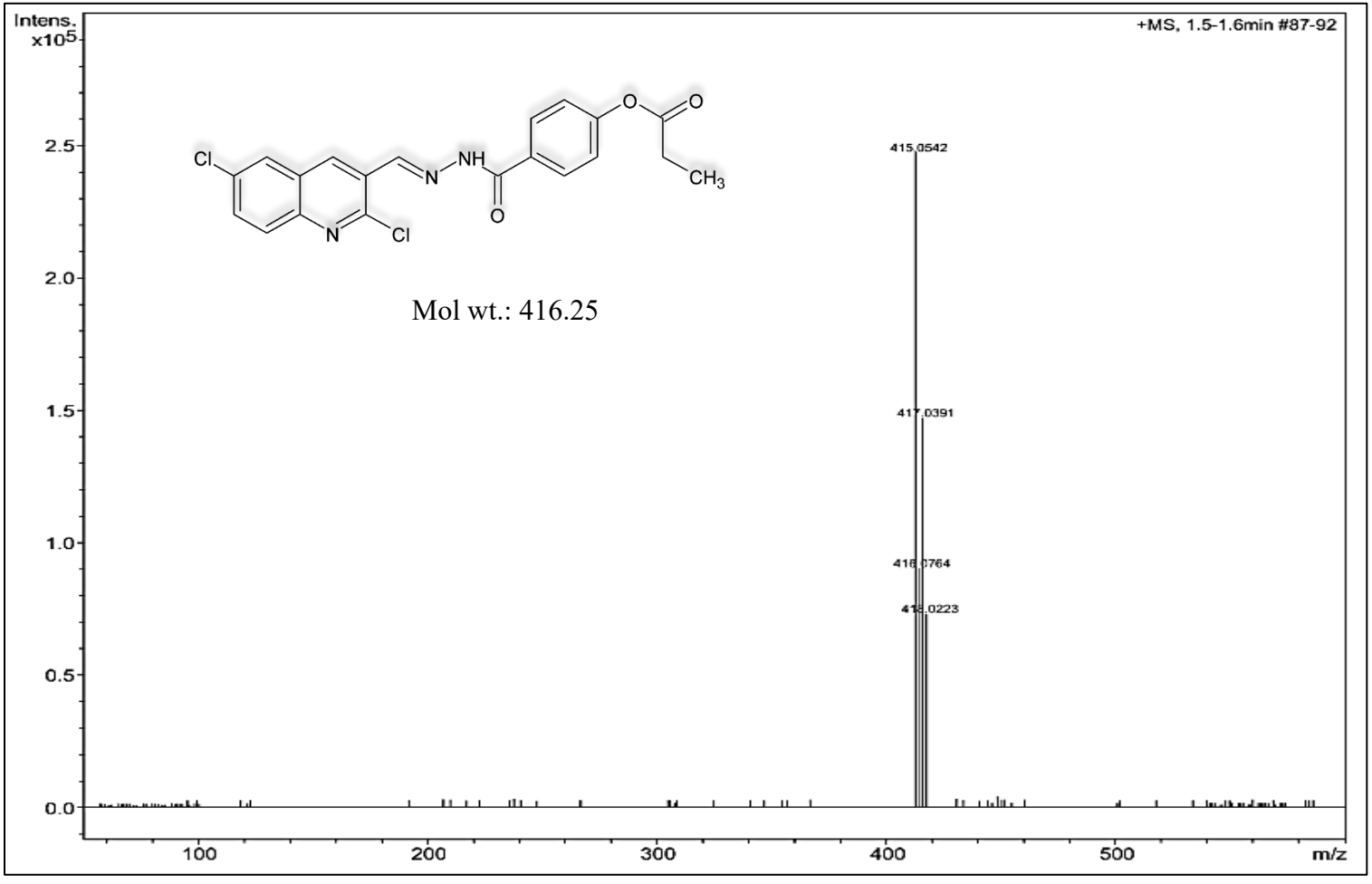

Figure 5.103: Mass spectrum of 4-{2-2-[(2,6-dichloroquinolin-3-yl) methylidene] hydrazine-1-carbonyl} phenyl propanoate (Compound 4e)

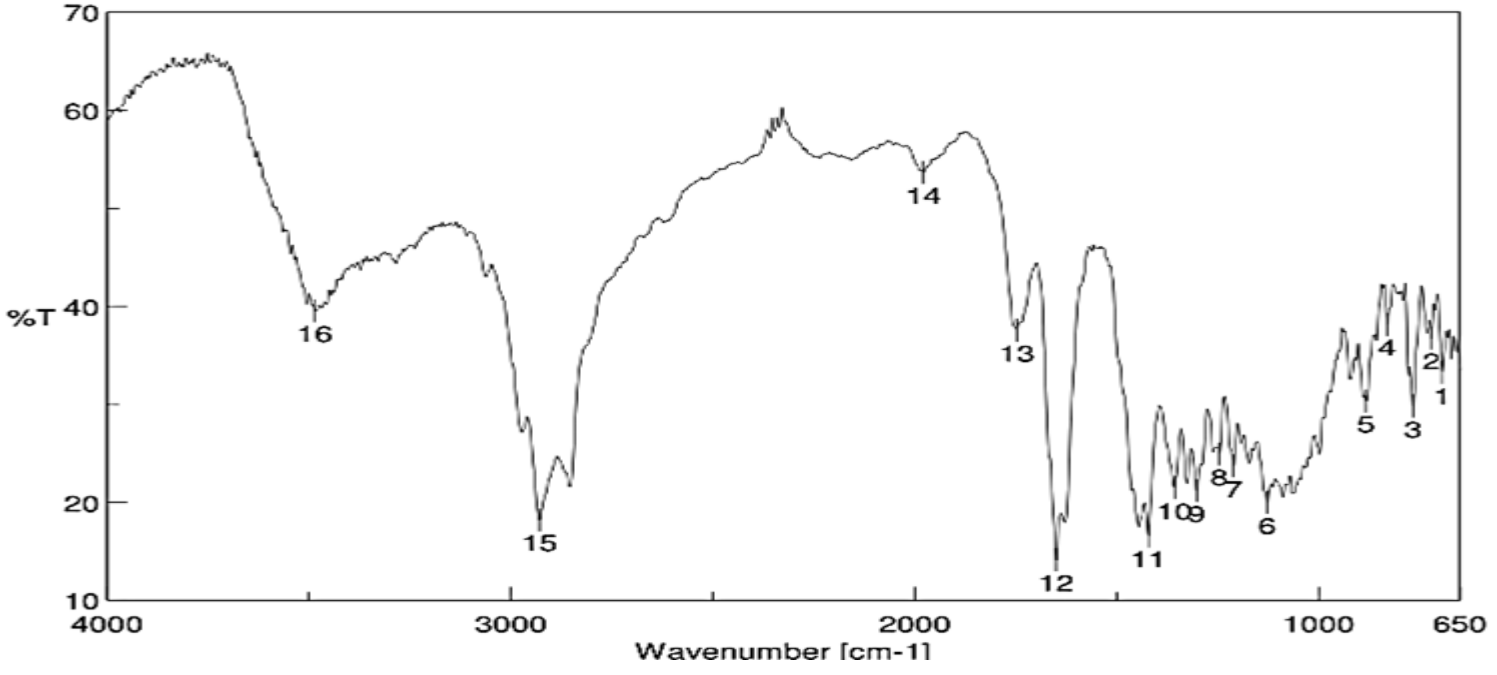

No.	Position	Intensity	No.	Position	Intensity
1	693.284	33.2473	2	720.282	36.7397
3	765.601	29.8143	4	830.205	38.1579
5	882.274	30.3077	6	1127.19	19.9657
7	1211.08	23.7038	8	1245.79	24.9269
9	1301.72	21.2104	10	1356.68	21.4852
11	1421.28	16.5474	12	1649.8	14.1127
13	1747.19	37.5409	14	1978.61	53.6403
15	2929.34	18.2267	16	3485.7	39.5494

Figure 5.104: IR spectrum of 4-{2-2-[(2,6-dichloro quinolin-3-yl) methylidene] hydrazine-1-carbonyl} phenyl butanoate (Compound 4f)

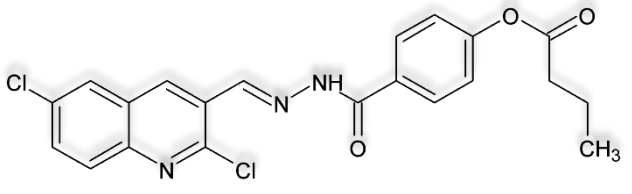

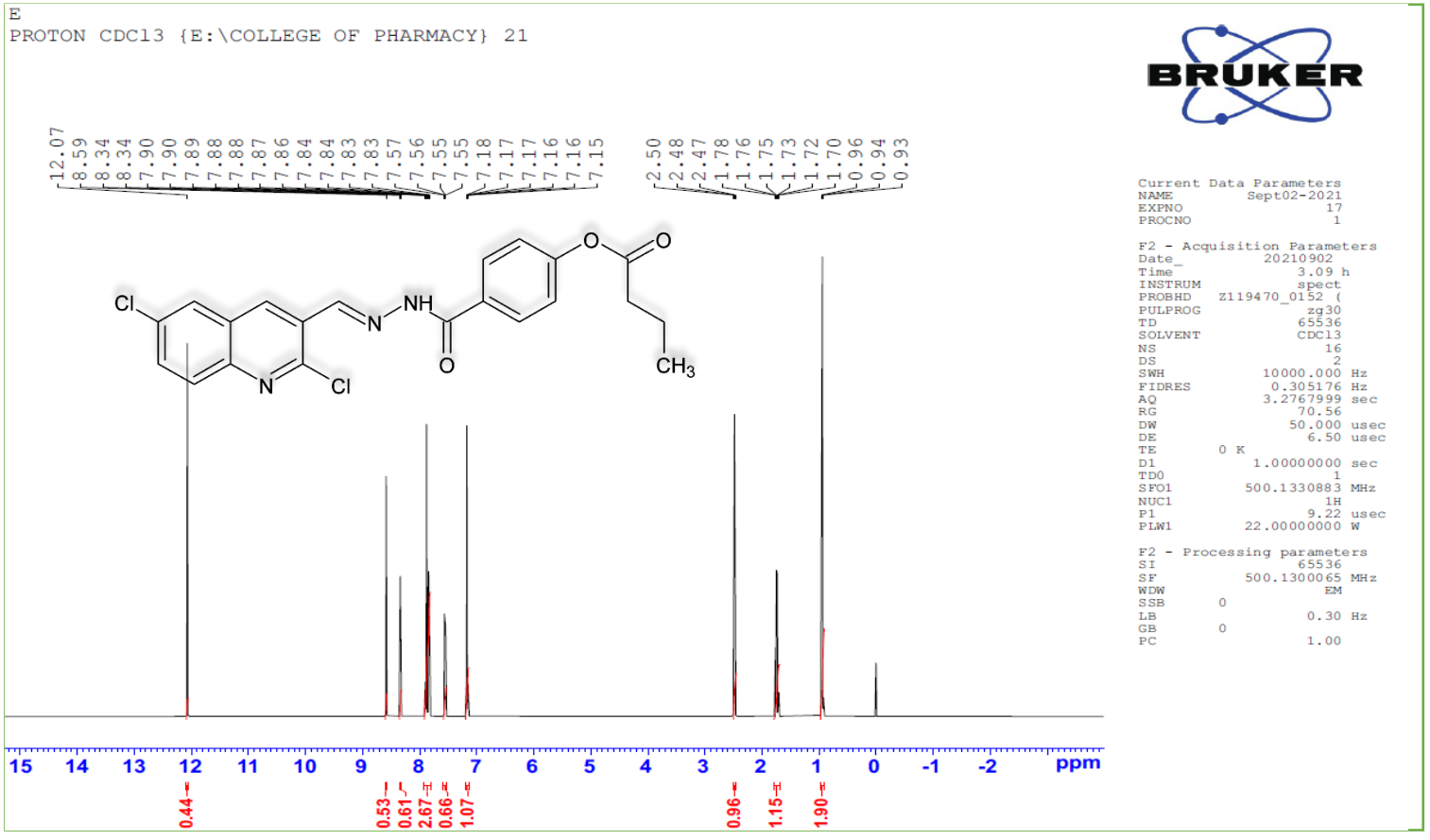

Figure 5.105: ^{1}H NMR spectrum of 4-{2-2-[(2,6-dichloro quinolin-3-yl) methylidene] hydrazine-1-carbonyl} phenyl butanoate (Compound 4f)

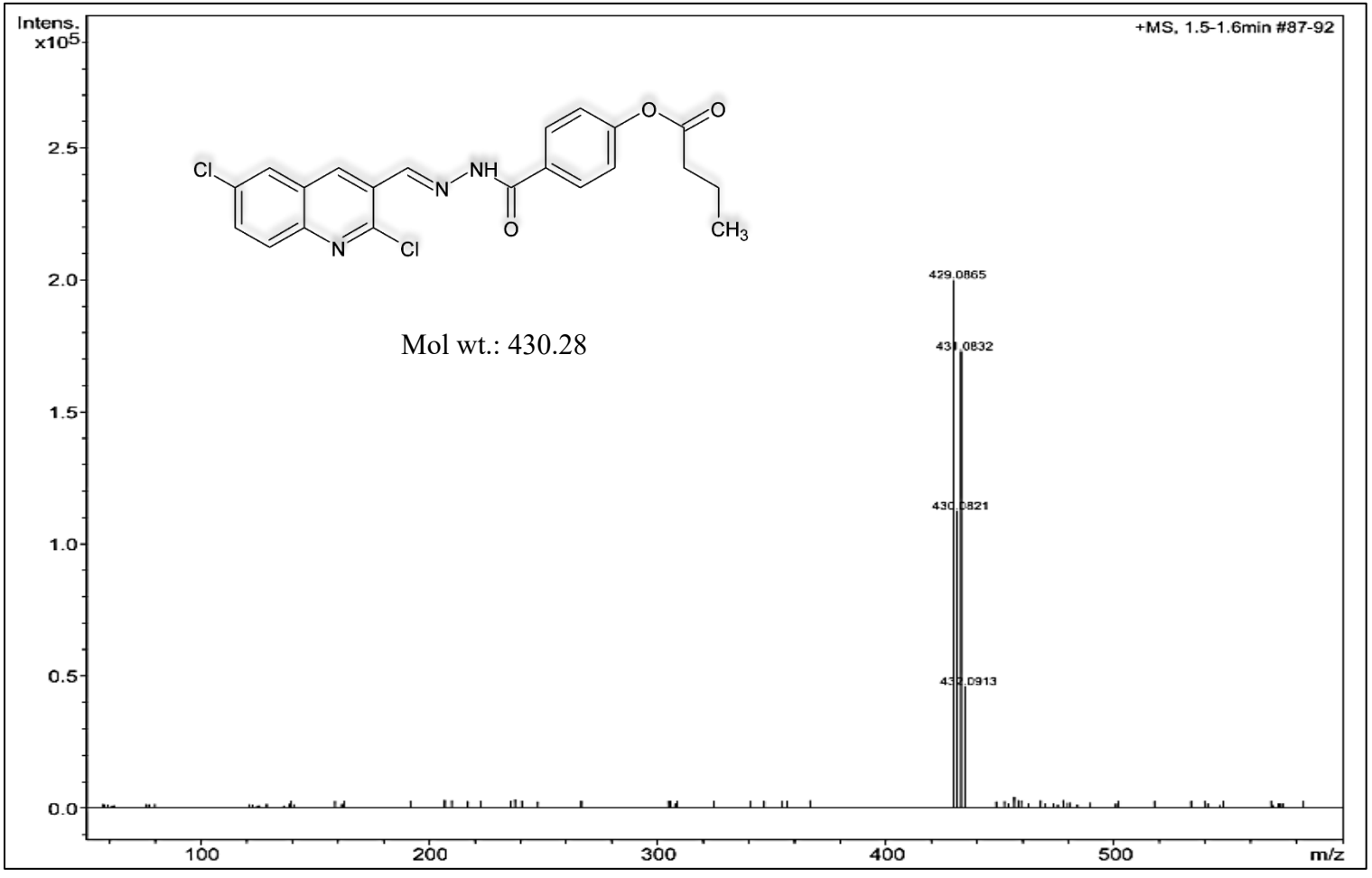

Figure 5.106: Mass spectrum of 4-{2-2-[(2,6-dichloroquinolin-3-yl) methylidene] hydrazine-1-carbonyl} phenyl butanoate (Compound 4f)

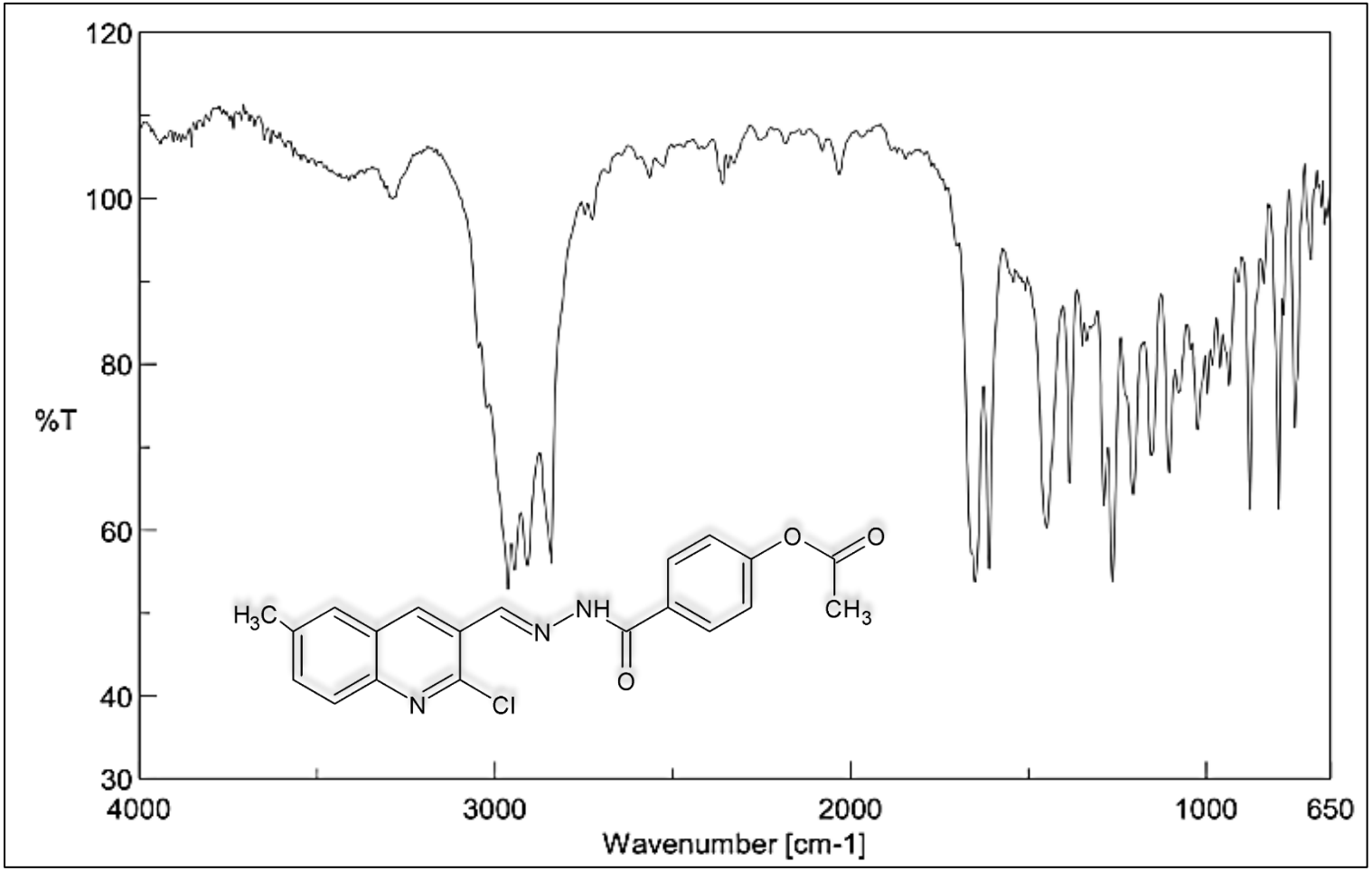

Figure 5.107: IR spectrum of 4-{2-[(2-chloro-6-methylquinolin-3-yl) methylidene] hydrazine carbonyl} phenyl acetate (Compound 4g)

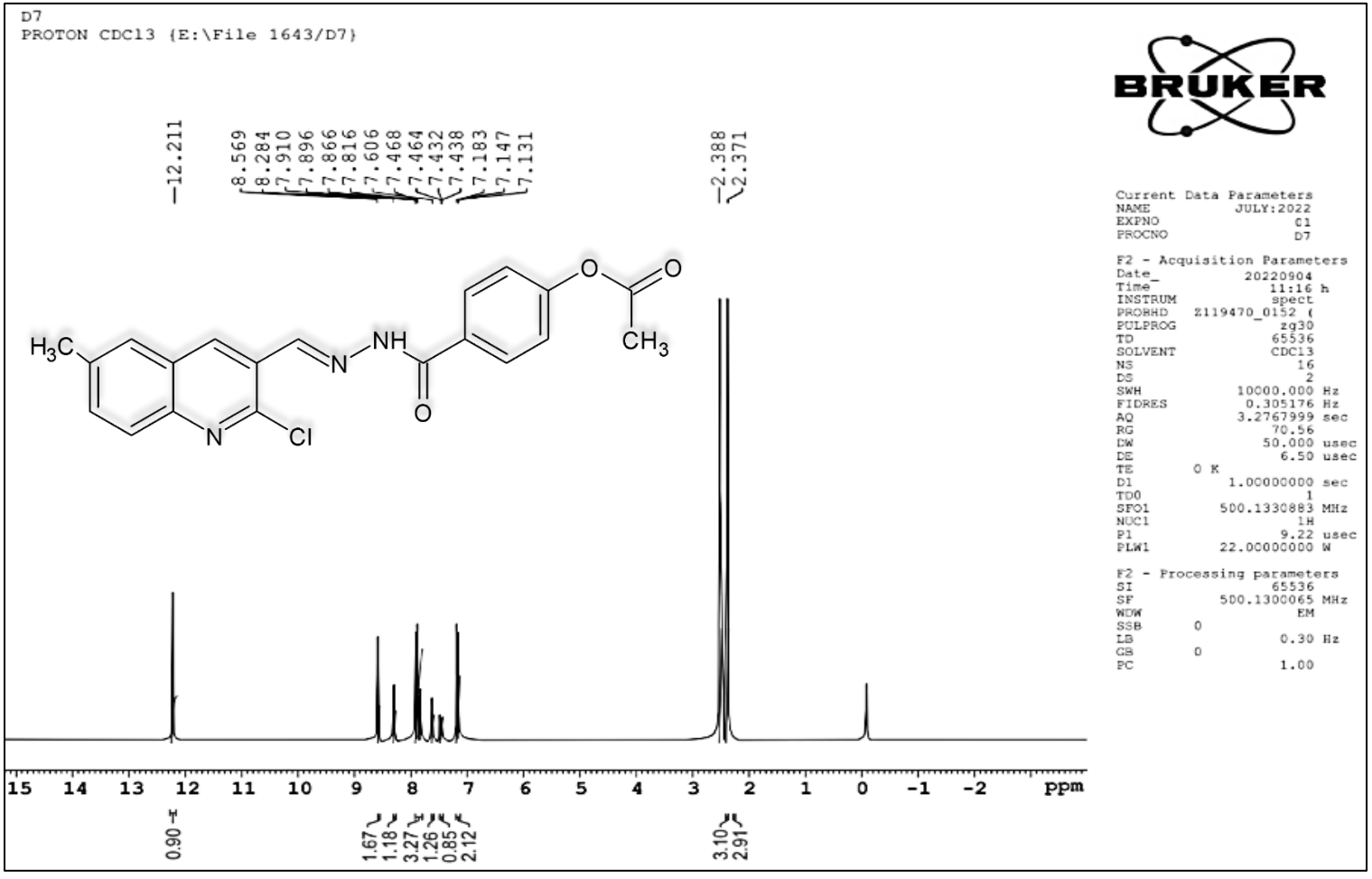

Figure 5.108: ^{1}H NMR spectrum of 4-{2-[(2-chloro-6-methylquinolin-3-yl) methylidene] hydrazine carbonyl} phenyl acetate (Compound 4g)

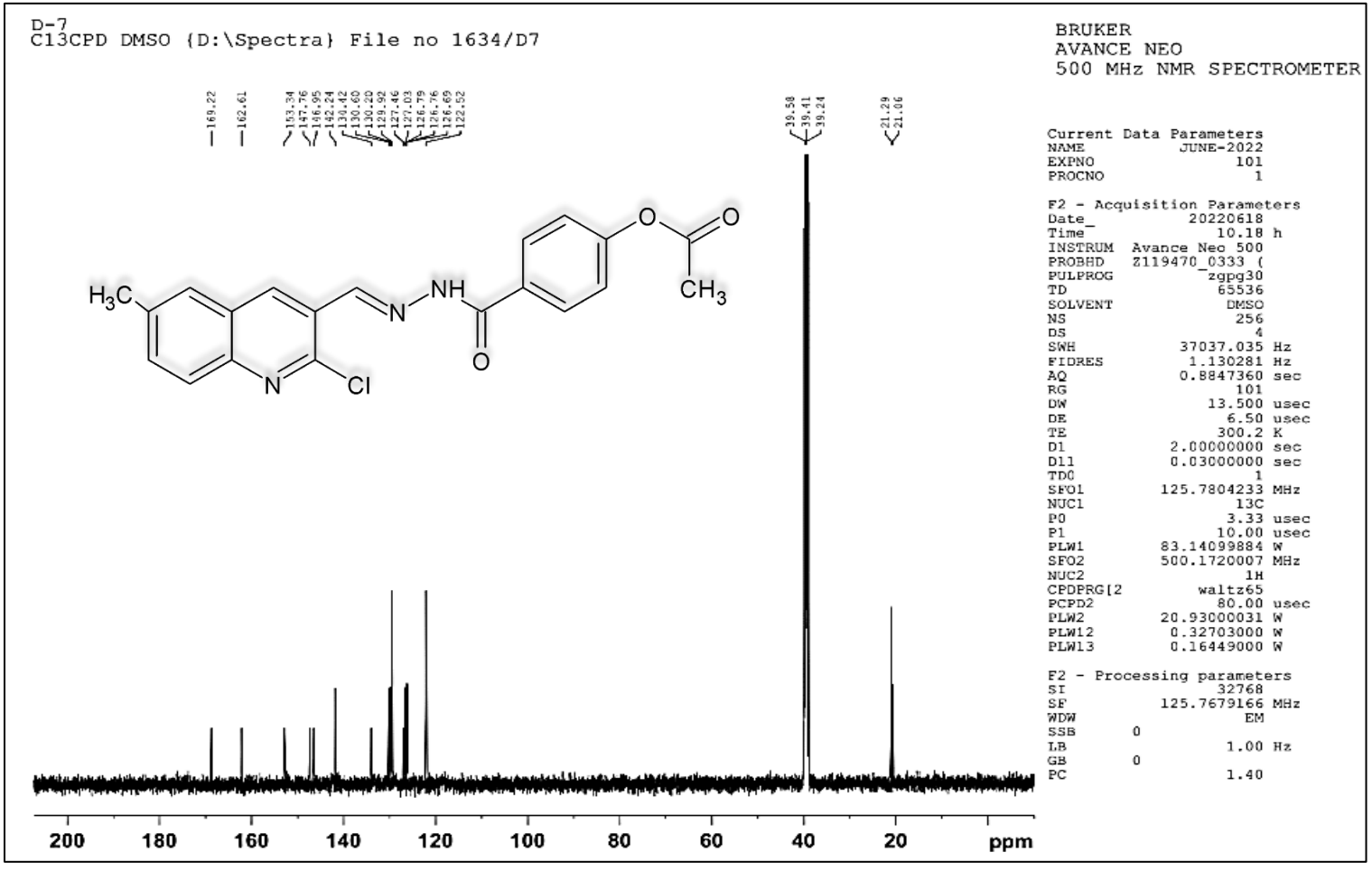

Figure 5.109: ^{13}C NMR spectrum of 4-{2-[(2-chloro-6-methylquinolin-3-yl) methylidene] hydrazine carbonyl} phenyl acetate (Compound 4g)

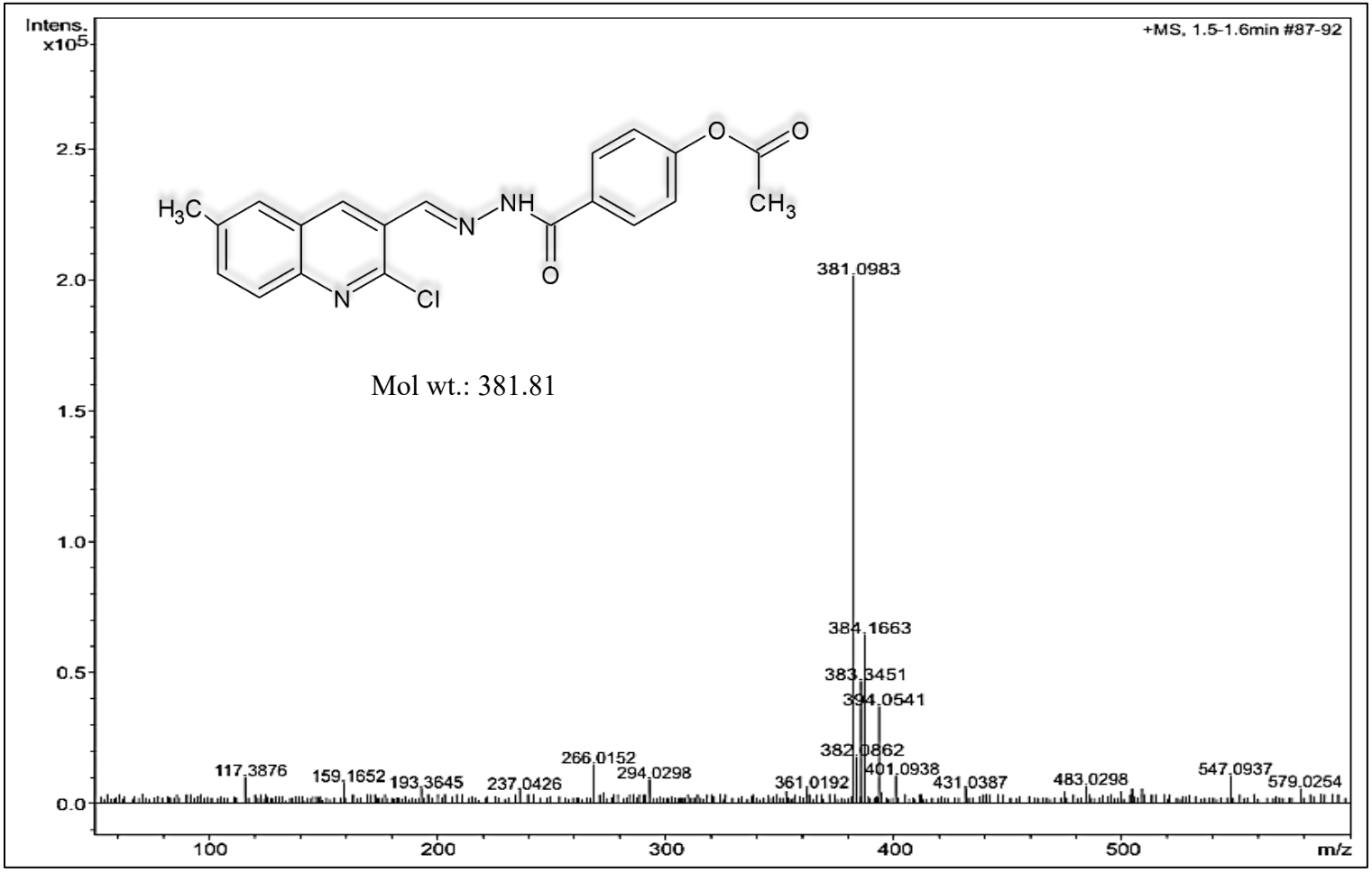

Figure 5.110: Mass spectrum of 4-{2-[(2-chloro-6-methylquinolin-3-yl) methylidene] hydrazine carbonyl} phenyl acetate (Compound 4g)

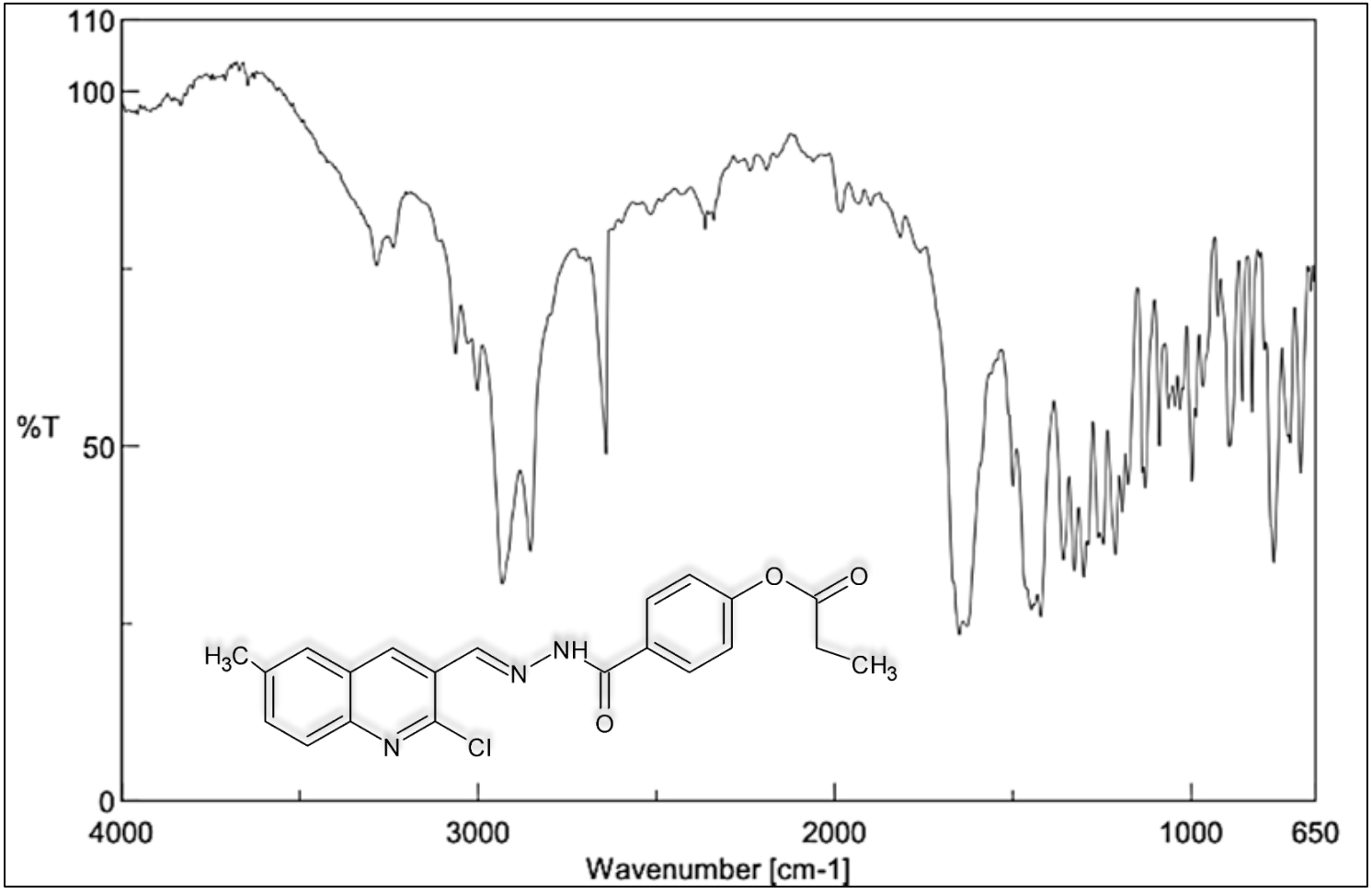

Figure 5.111: IR spectrum of 4-{2-[(2-chloro-6-methyl quinolin-3-yl) methylidene] hydrazine carbonyl} phenyl propionate (Compound 4h)

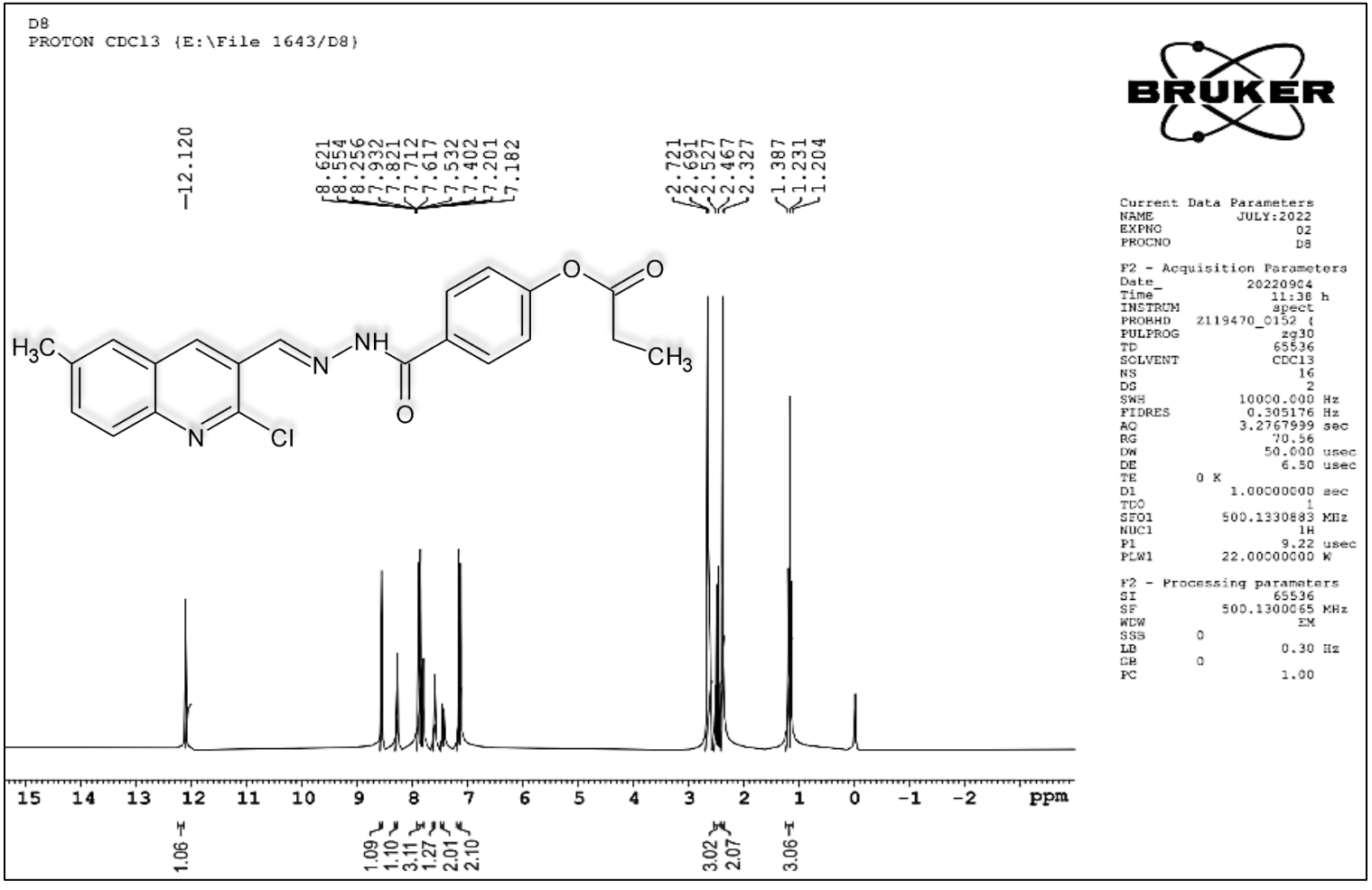

Figure 5.112: ^{1}H NMR spectrum of 4-{2-[(2-chloro-6-methyl quinolin-3-yl) methylidene] hydrazine carbonyl} phenyl propionate (Compound 4h)

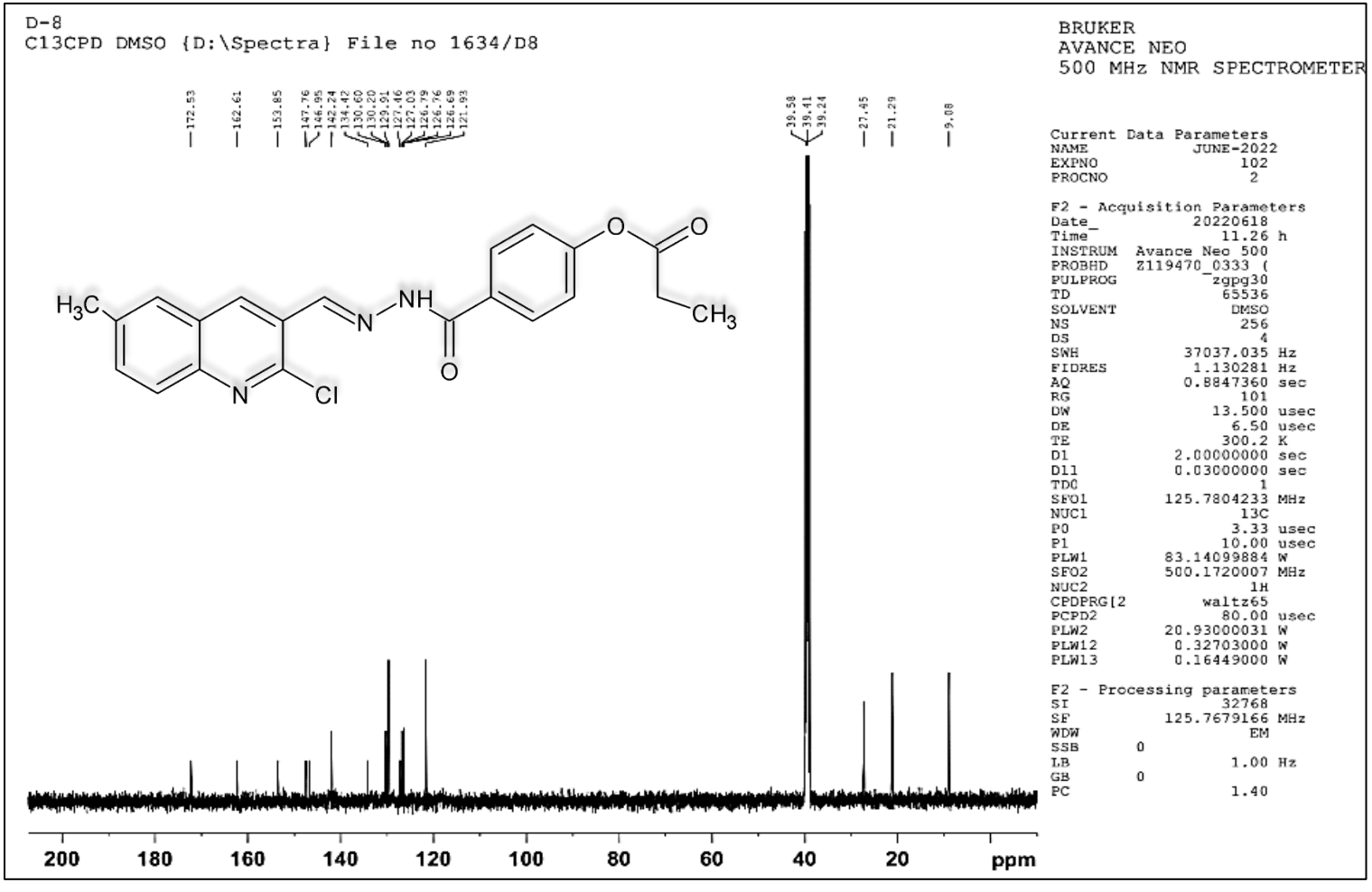

Figure 5.113: ^{13}C NMR spectrum of 4-{2-[(2-chloro-6-methyl quinolin-3-yl) methylidene] hydrazine carbonyl} phenyl propionate (Compound 4h)

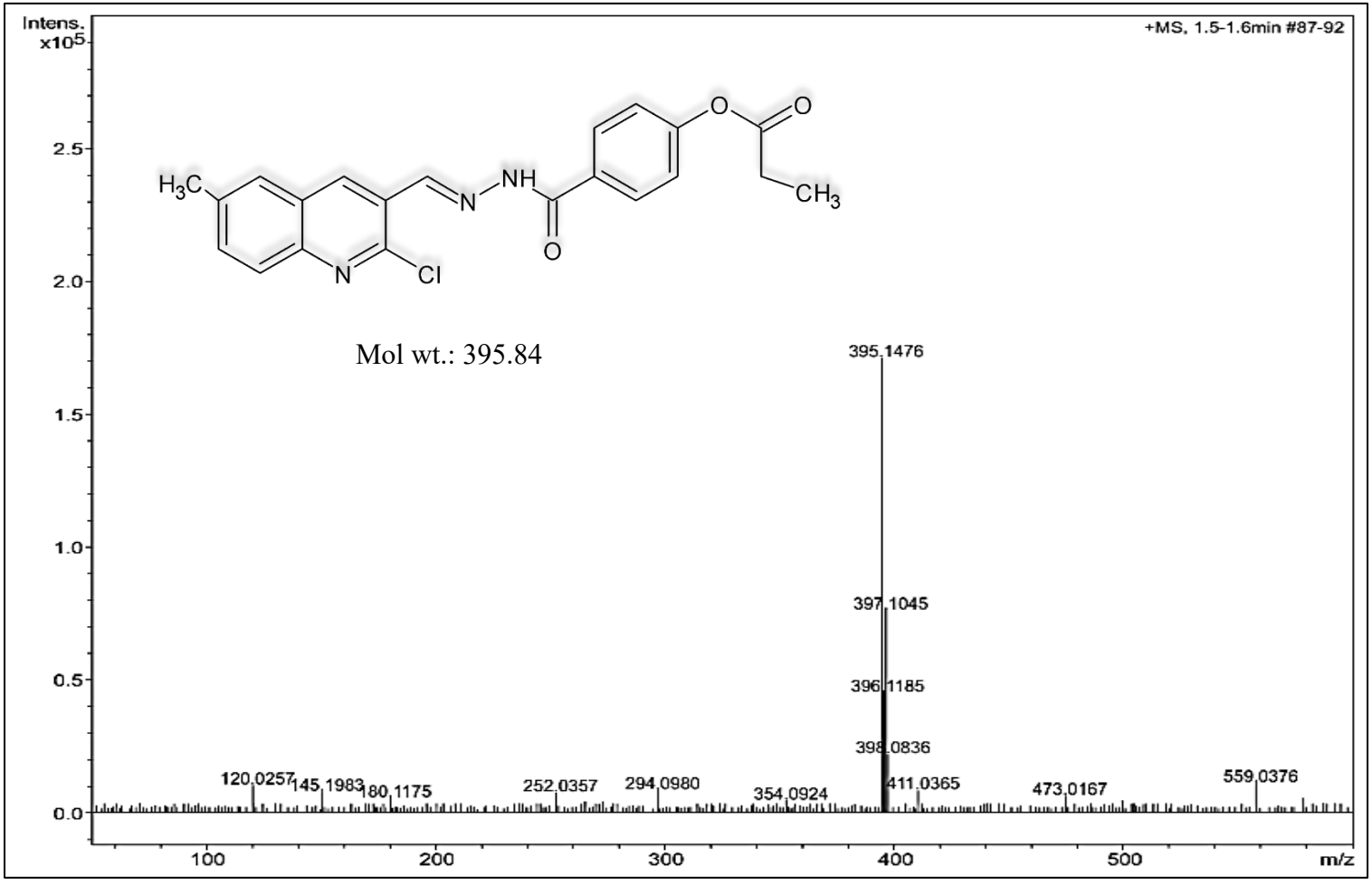

Figure 5.114: Mass spectrum of 4-{2-[(2-chloro-6-methyl quinolin-3-yl) methylidene] hydrazine carbonyl} phenyl propionate (Compound 4h)

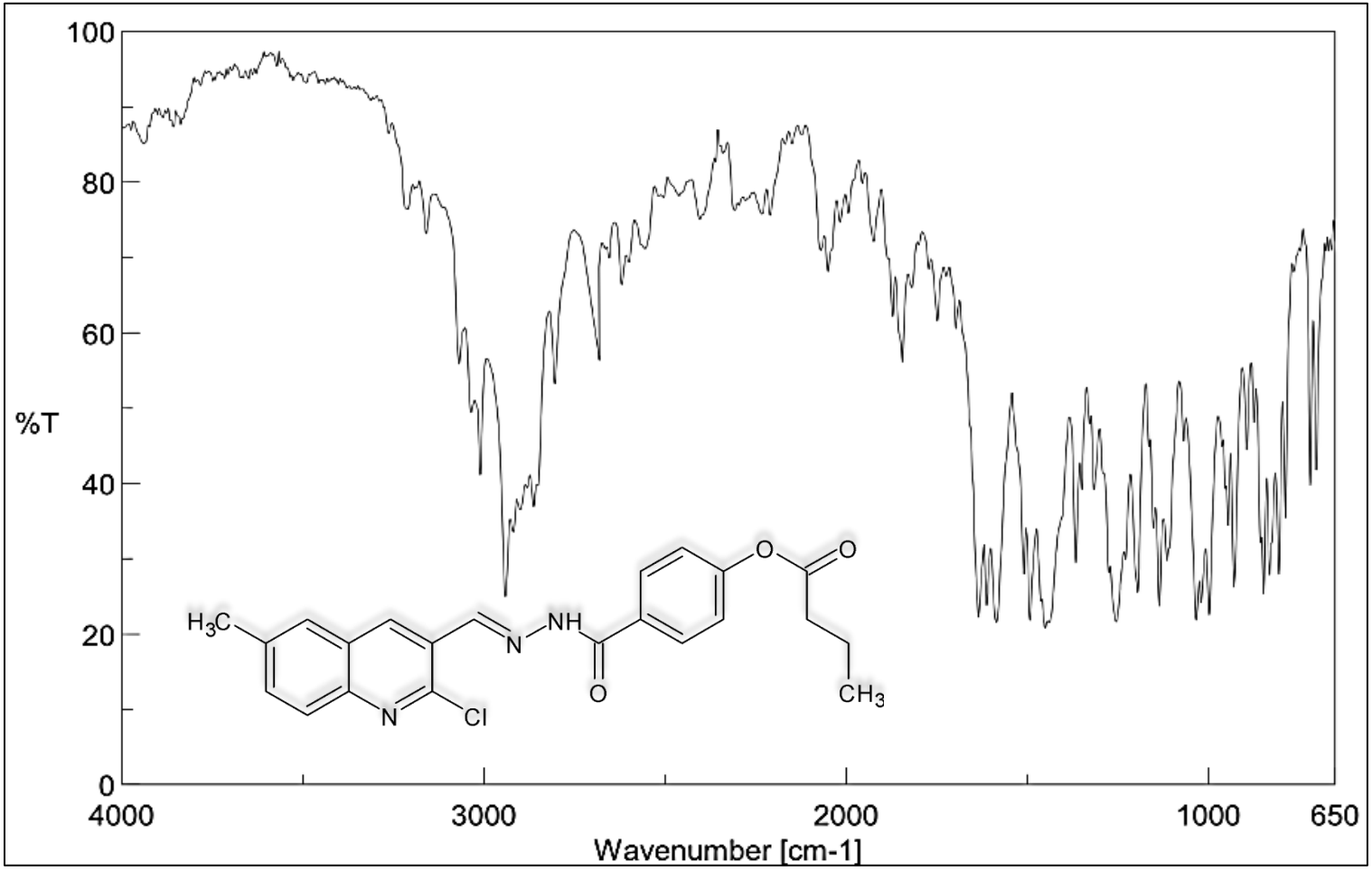

Figure 5.115: IR spectrum of 4-{2-[(2-chloro-6-methyl quinolin-3-yl) methylidene] hydrazine carbonyl} phenyl butanoate (Compound 4i)

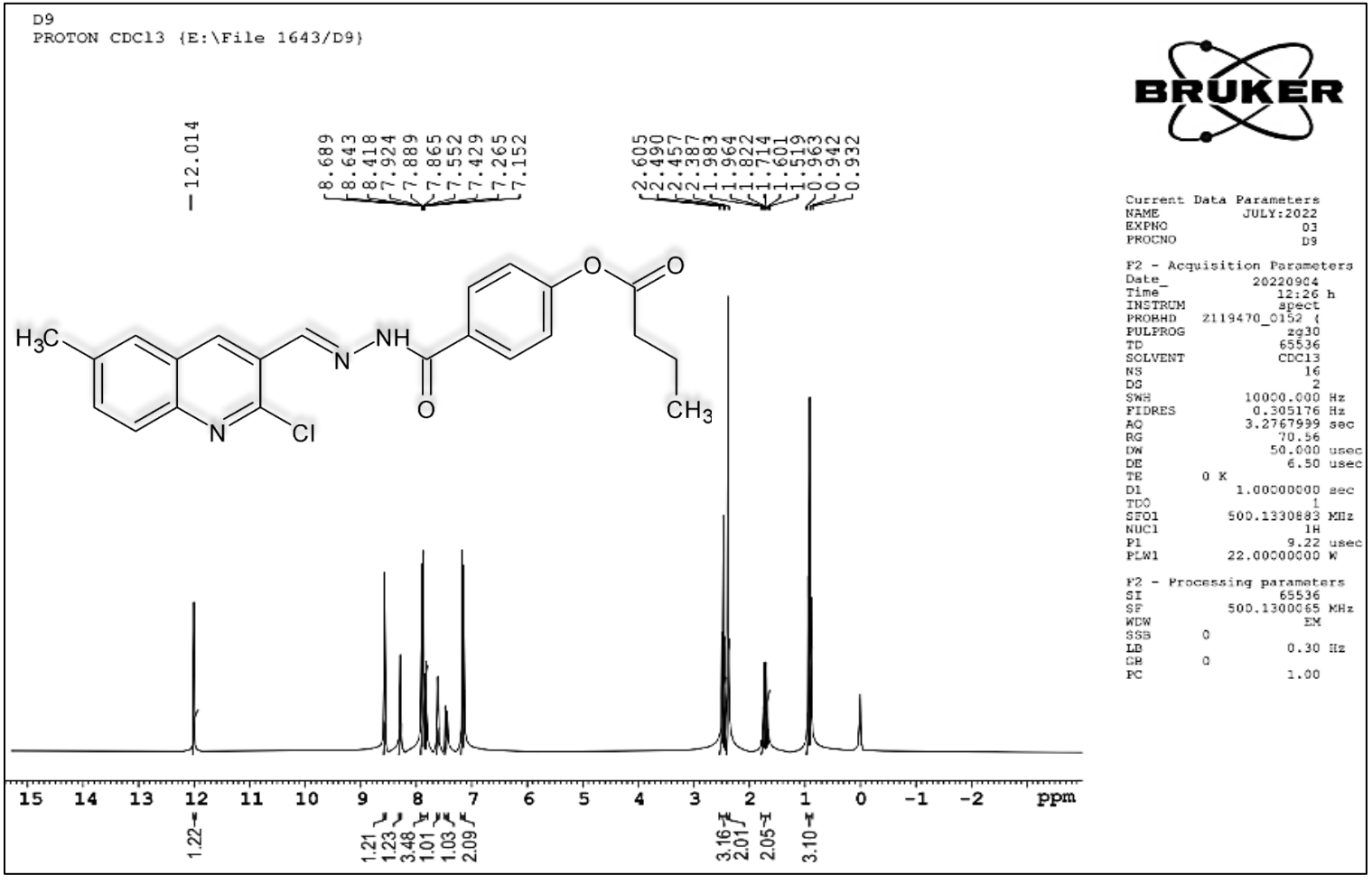

Figure 5.116: ^{1}H NMR spectrum of 4-{2-[(2-chloro-6-methyl quinolin-3-yl) methylidene] hydrazine carbonyl} phenyl butanoate (Compound 4i)

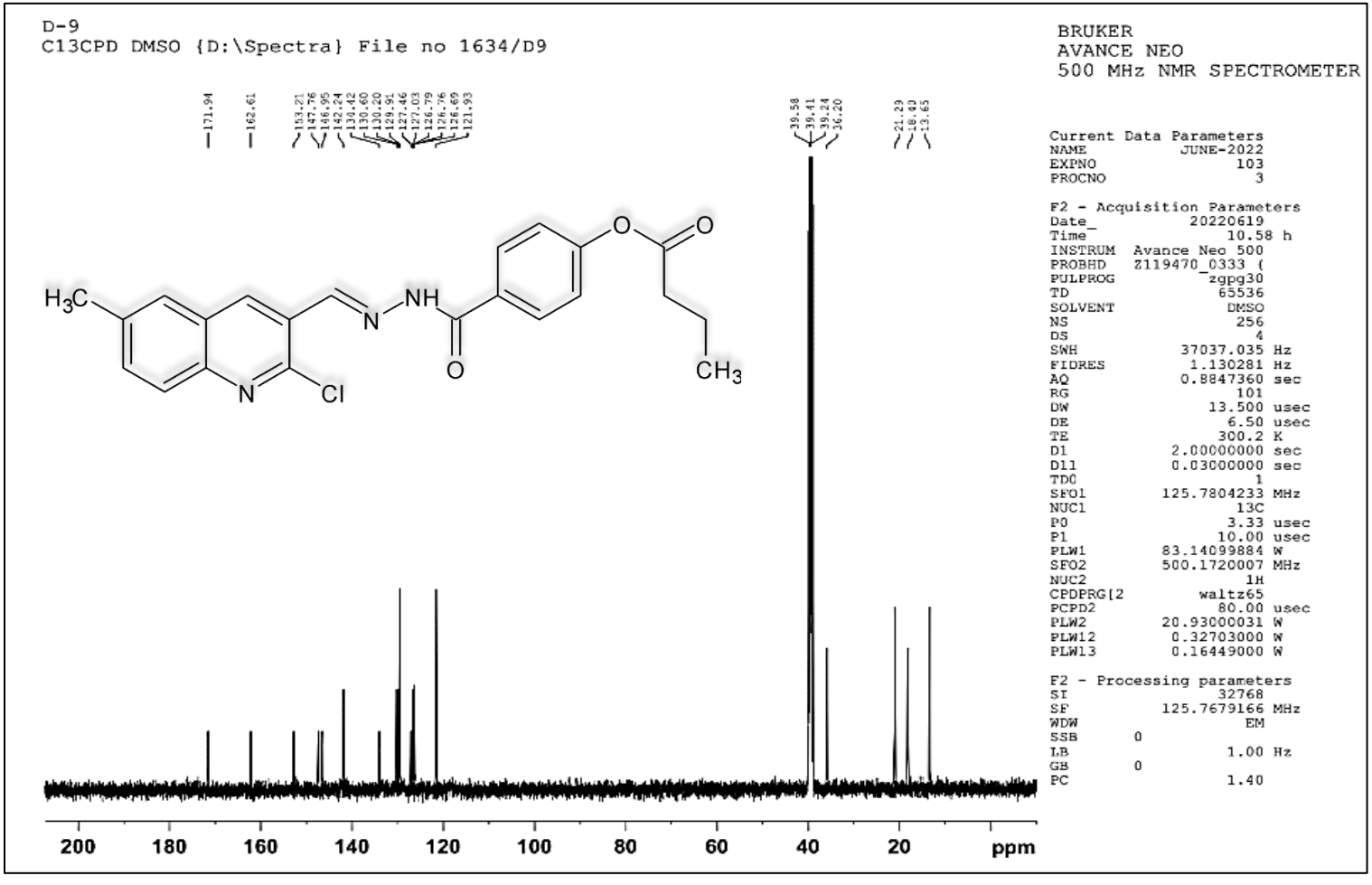

Figure 5.117: ^{13}C NMR spectrum of 4-{2-[(2-chloro-6-methyl quinolin-3-yl) methylidene] hydrazine carbonyl} phenyl butanoate (Compound 4i)

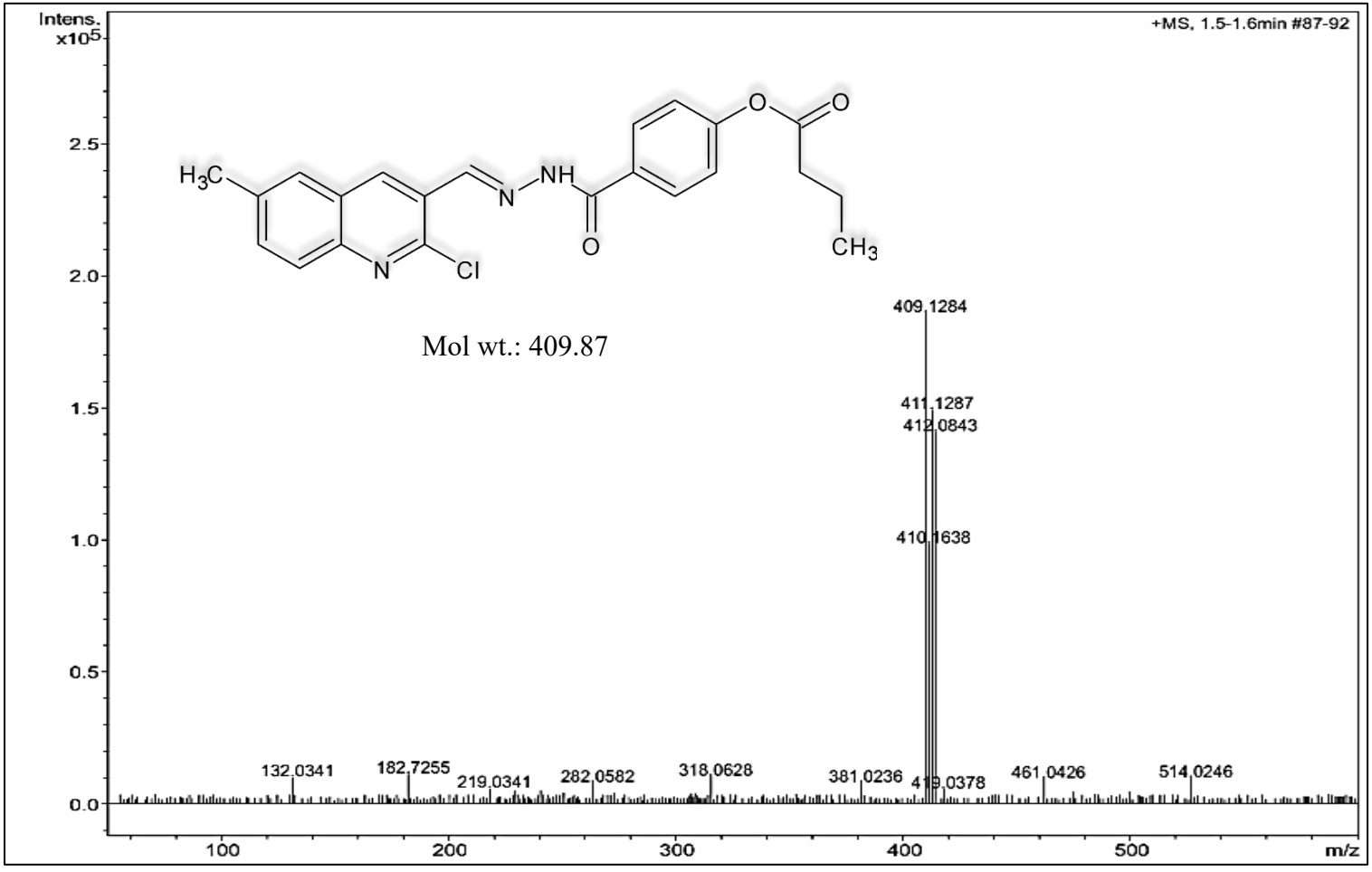

Figure 5.118: Mass spectrum of 4-{2-[(2-chloro-6-methyl quinolin-3-yl) methylidene] hydrazine carbonyl} phenyl butanoate (Compound 4i)

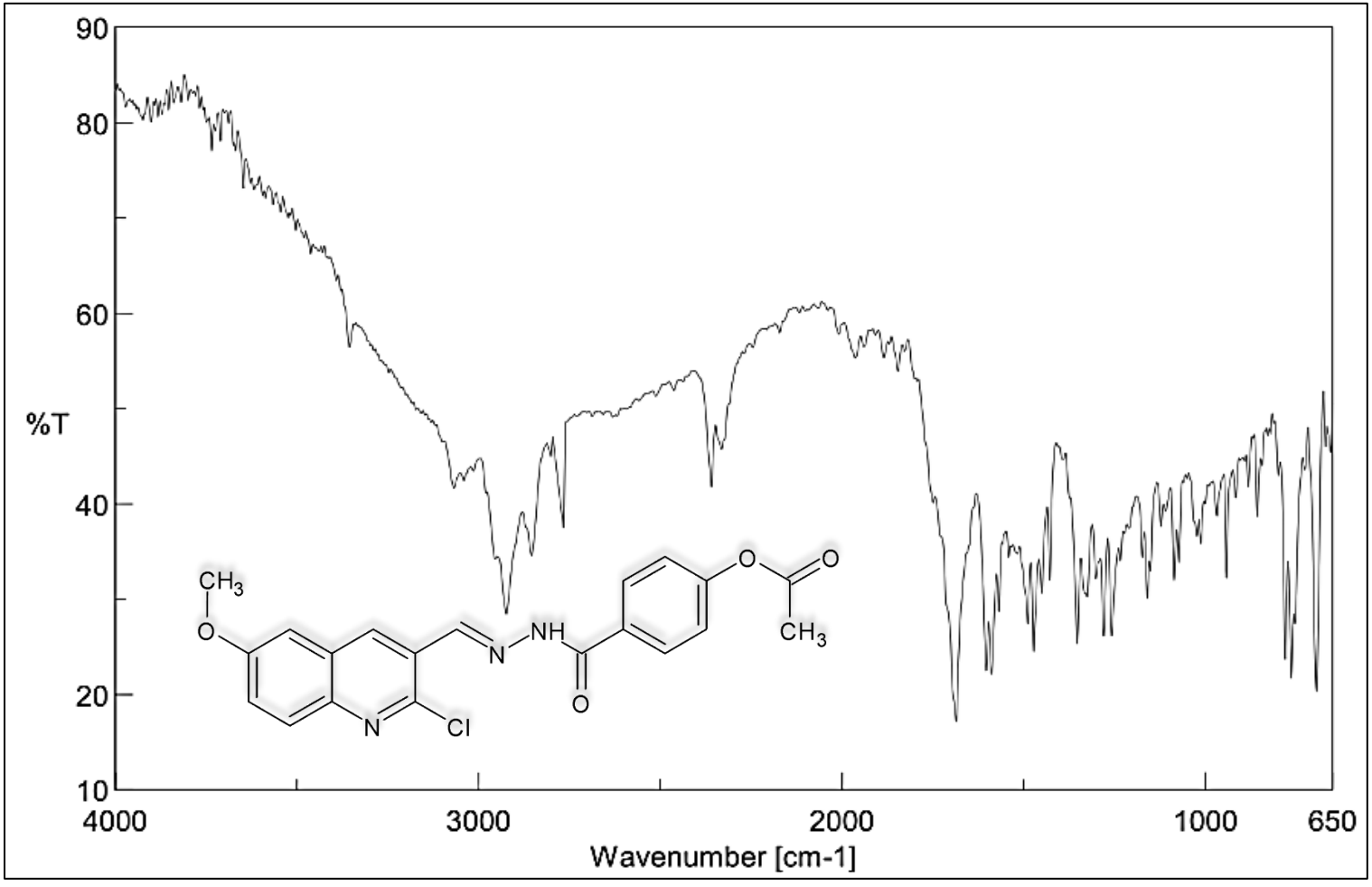

Figure 5.119: IR spectrum of 4-{2-[(2-chloro-6-methoxy quinolin-3-yl) methylidene] hydrazine carbonyl} phenyl acetate (Compound 4j)

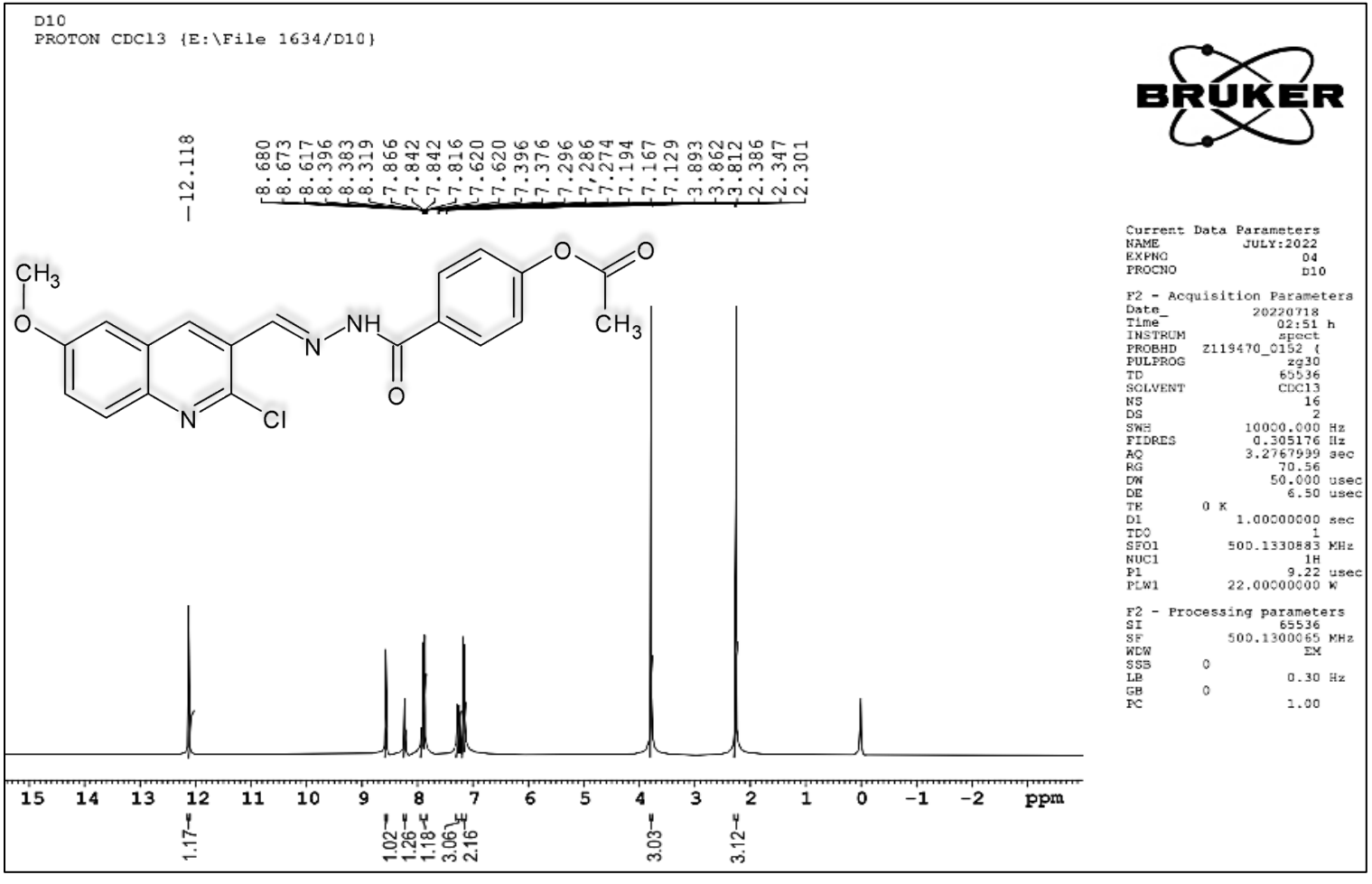

Figure 5.120: ^{1}H NMR spectrum of 4-{2-[(2-chloro-6-methoxy quinolin-3-yl) methylidene] hydrazine carbonyl} phenyl acetate (Compound 4j)

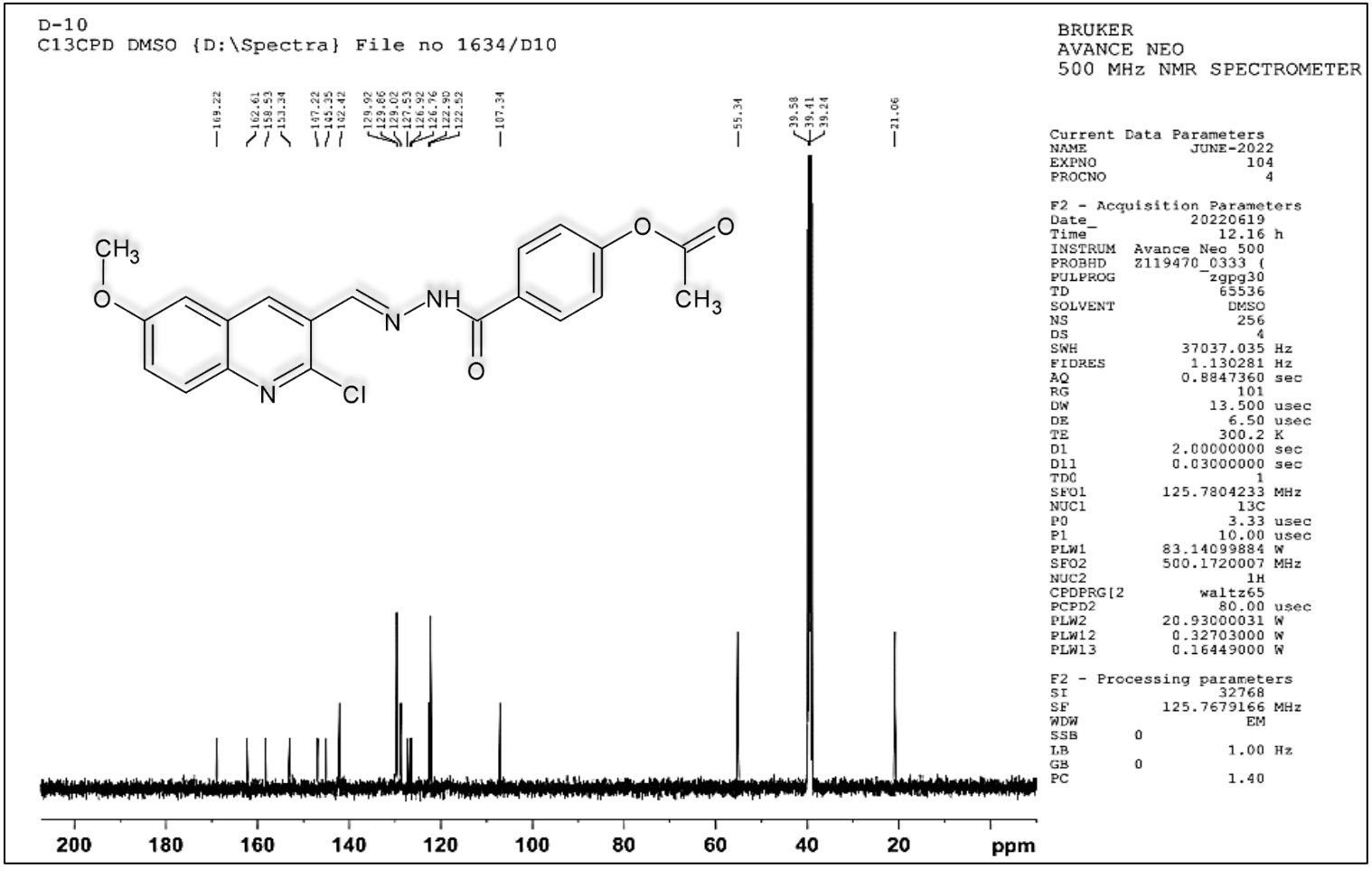

Figure 5.121: ^{13}C NMR spectrum of 4-{2-[(2-chloro-6-methoxy quinolin-3-yl) methylidene] hydrazine carbonyl} phenyl acetate (Compound 4j)

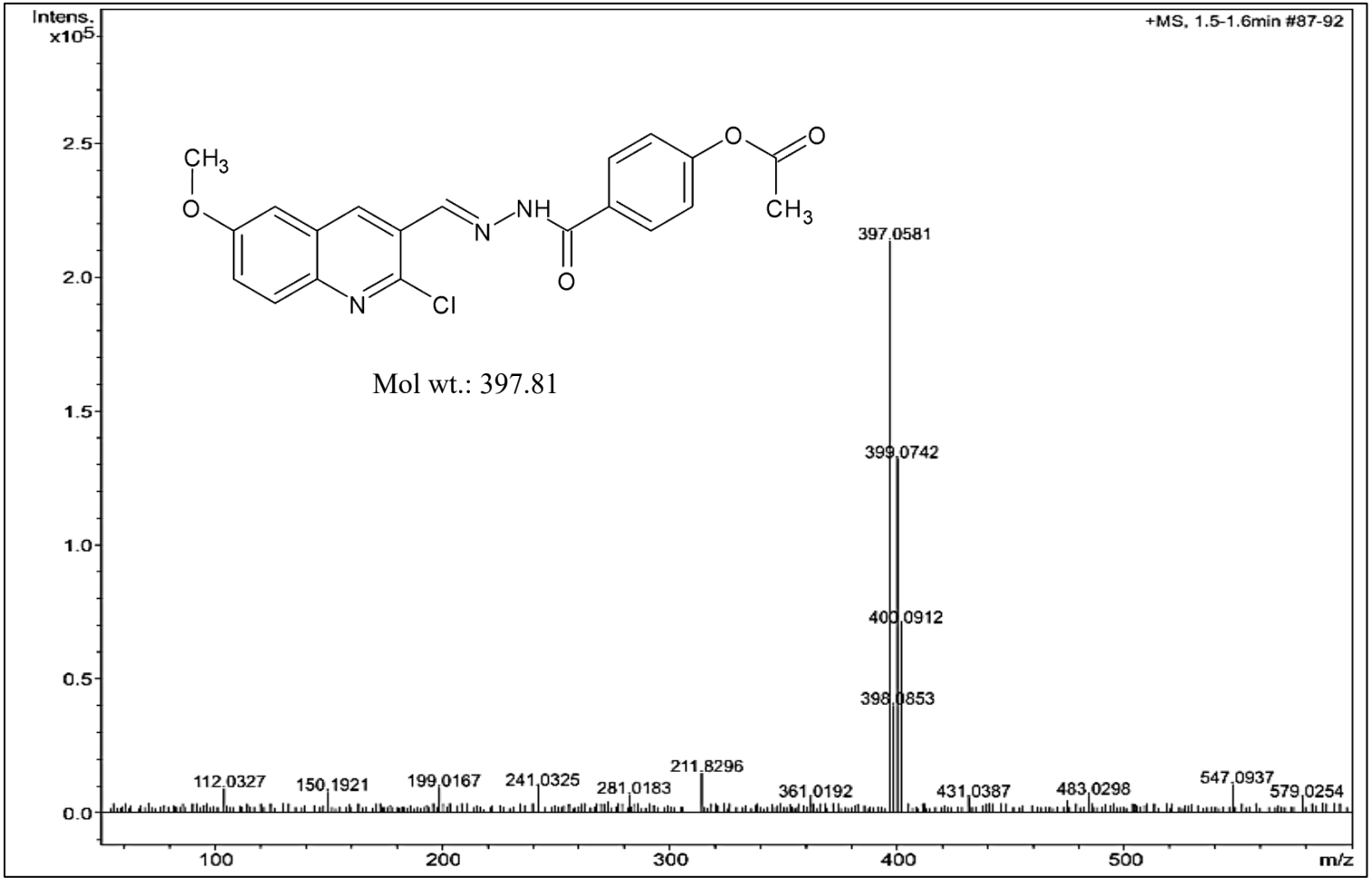

Figure 5.122: Mass spectrum of 4-{2-[(2-chloro-6-methoxy quinolin-3-yl) methylidene] hydrazine carbonyl} phenyl acetate (Compound 4j)

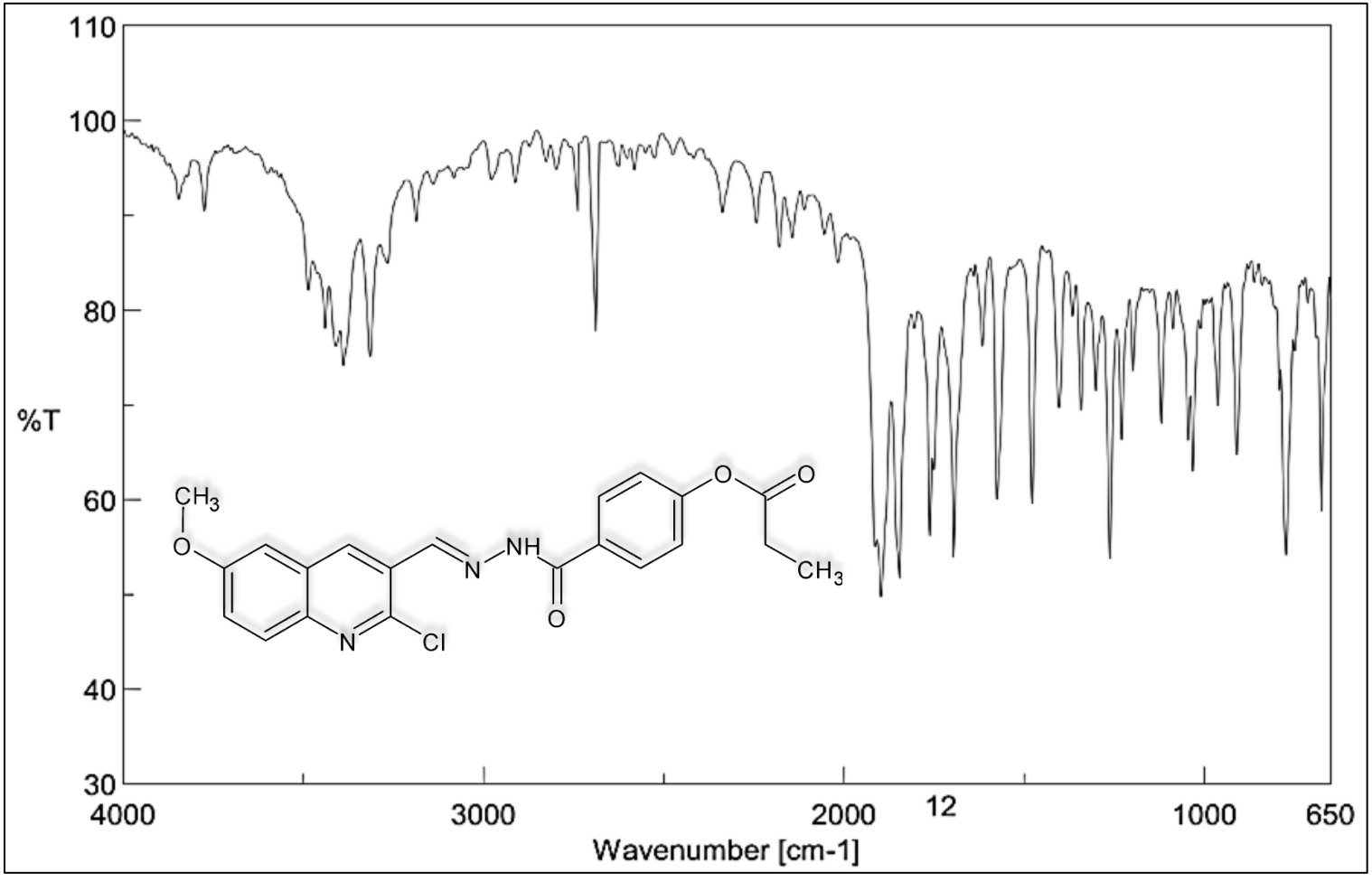

Figure 5.123: IR spectrum of 4-{2-[(2-chloro-6-methoxy quinolin-3-yl) methylidene] hydrazine carbonyl} phenyl propionate (Compound 4k)

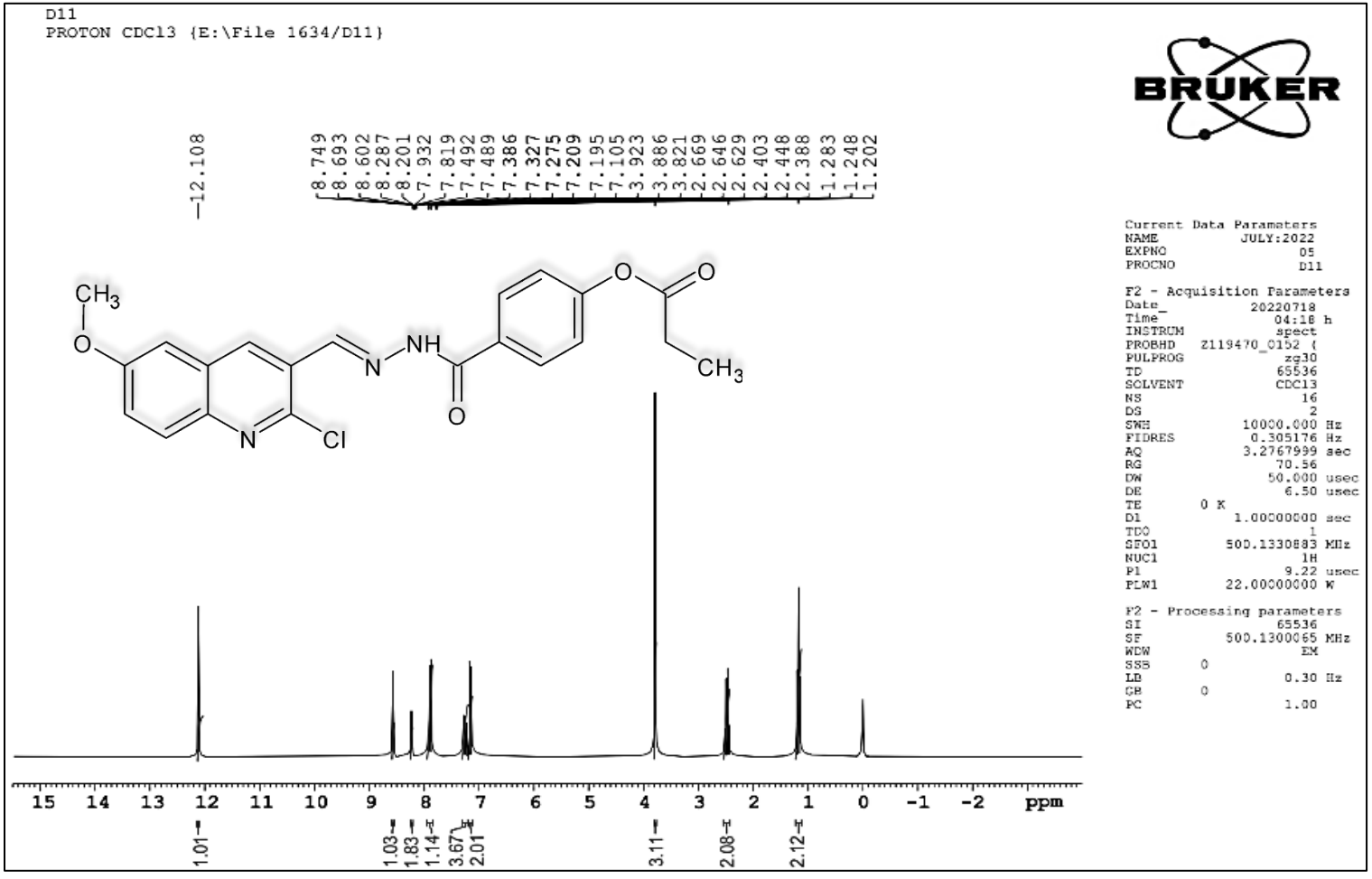

Figure 5.124: ^{1}H NMR spectrum of 4-{2-[(2-chloro-6-methoxy quinolin-3-yl) methylidene] hydrazine carbonyl} phenyl propionate (Compound 4k)

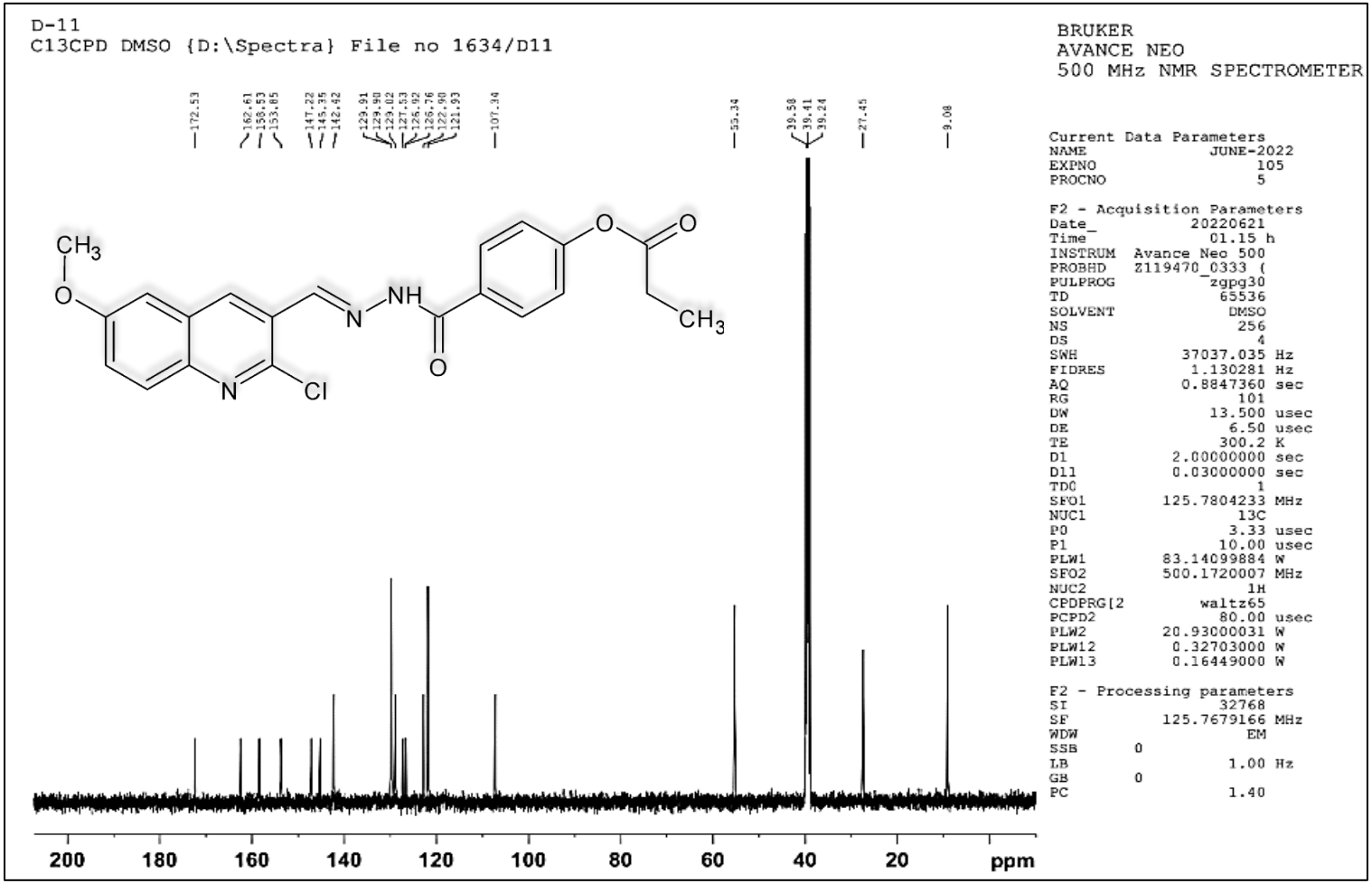

Figure 5.125: ^{13}C NMR spectrum of 4-{2-[(2-chloro-6-methoxy quinolin-3-yl) methylidene] hydrazine carbonyl} phenyl propionate (Compound 4k)

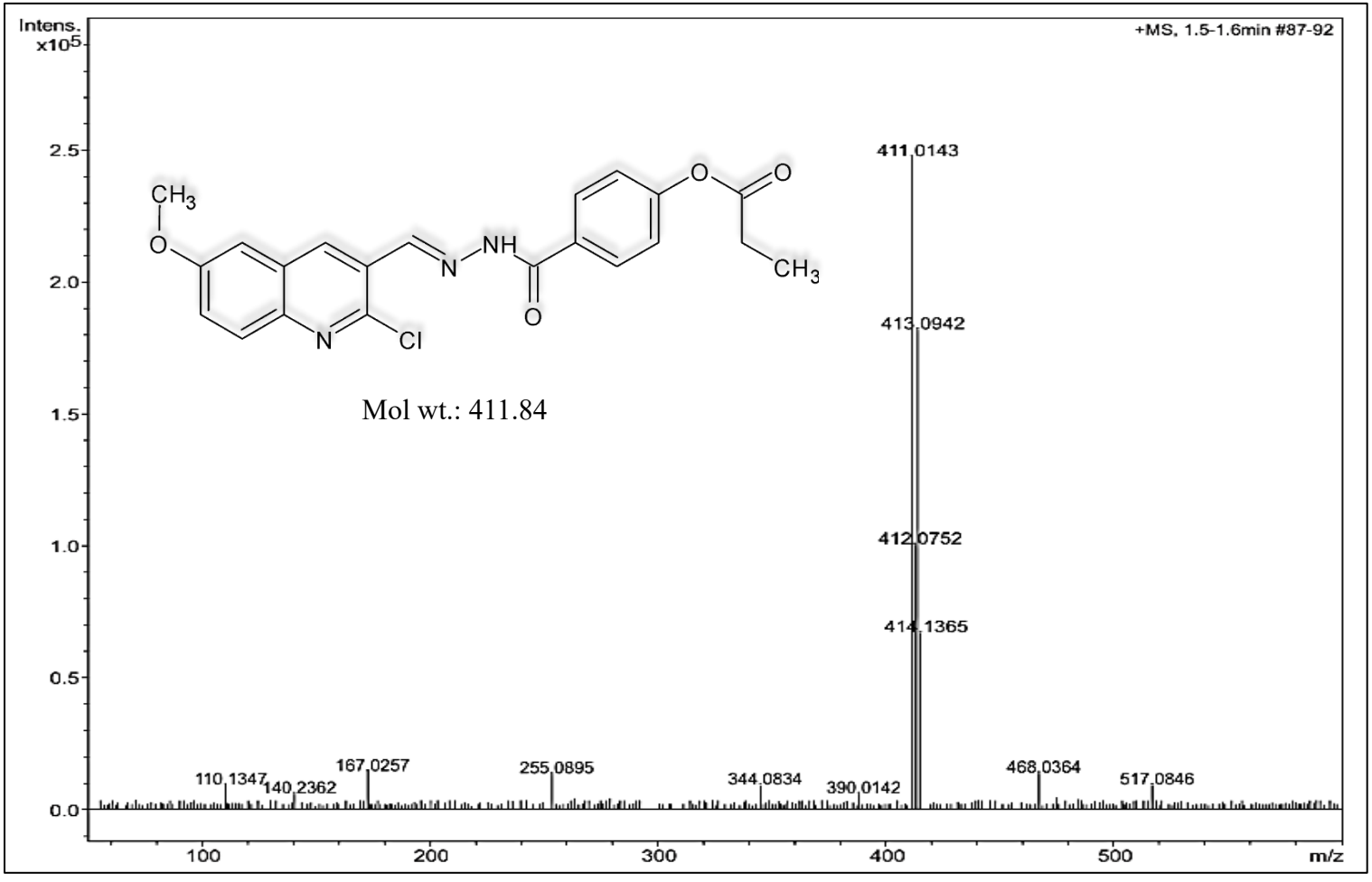

Figure 5.126: Mass spectrum of 4-{2-[(2-chloro-6-methoxy quinolin-3-yl) methylidene] hydrazine carbonyl} phenyl propionate (Compound 4k)

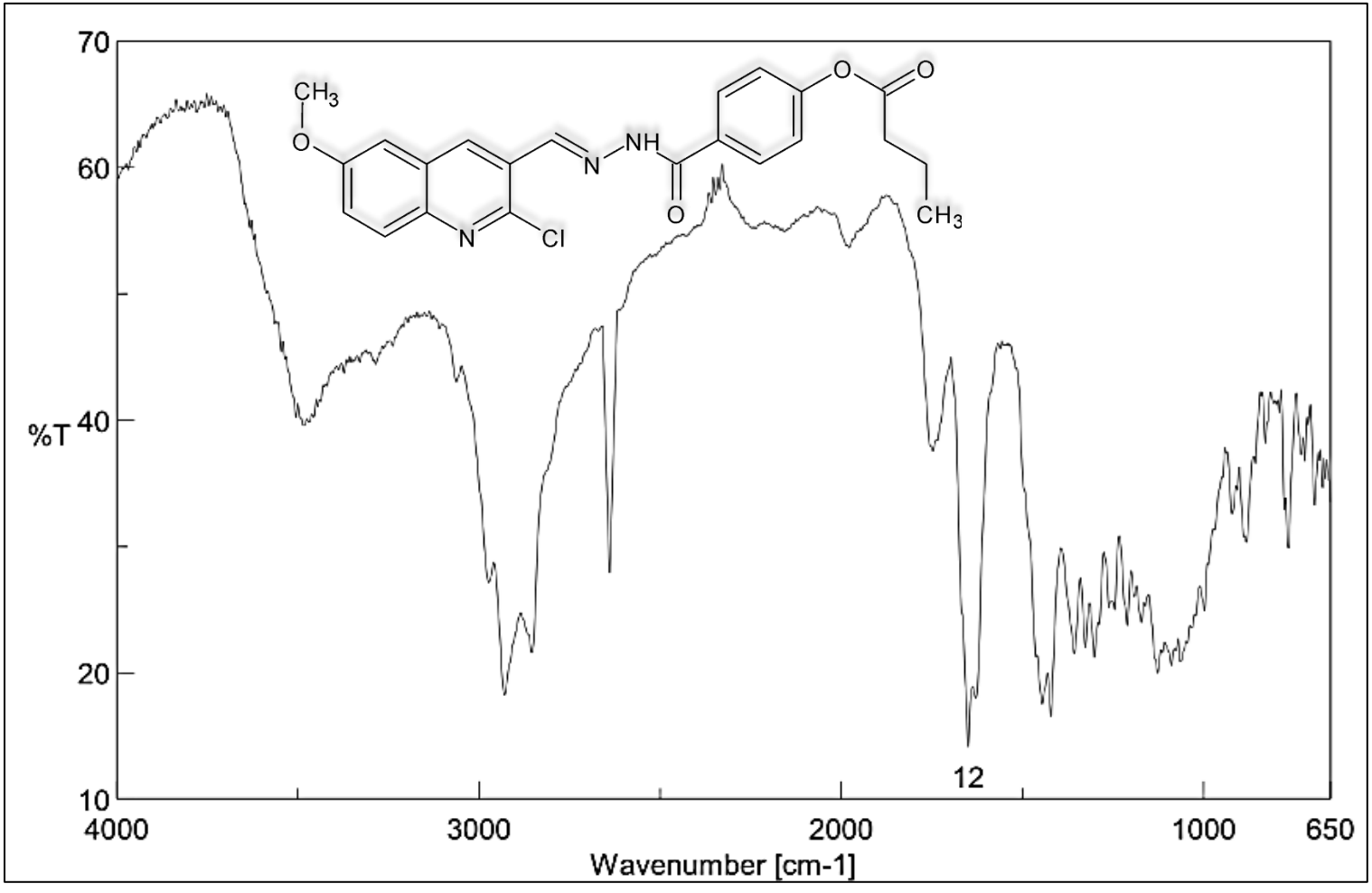

Figure 5.127: IR spectrum of 4-{2-[(2-chloro-6-methoxy quinolin-3-yl) methylidene] hydrazine carbonyl} phenyl butanoate (Compound 4l)

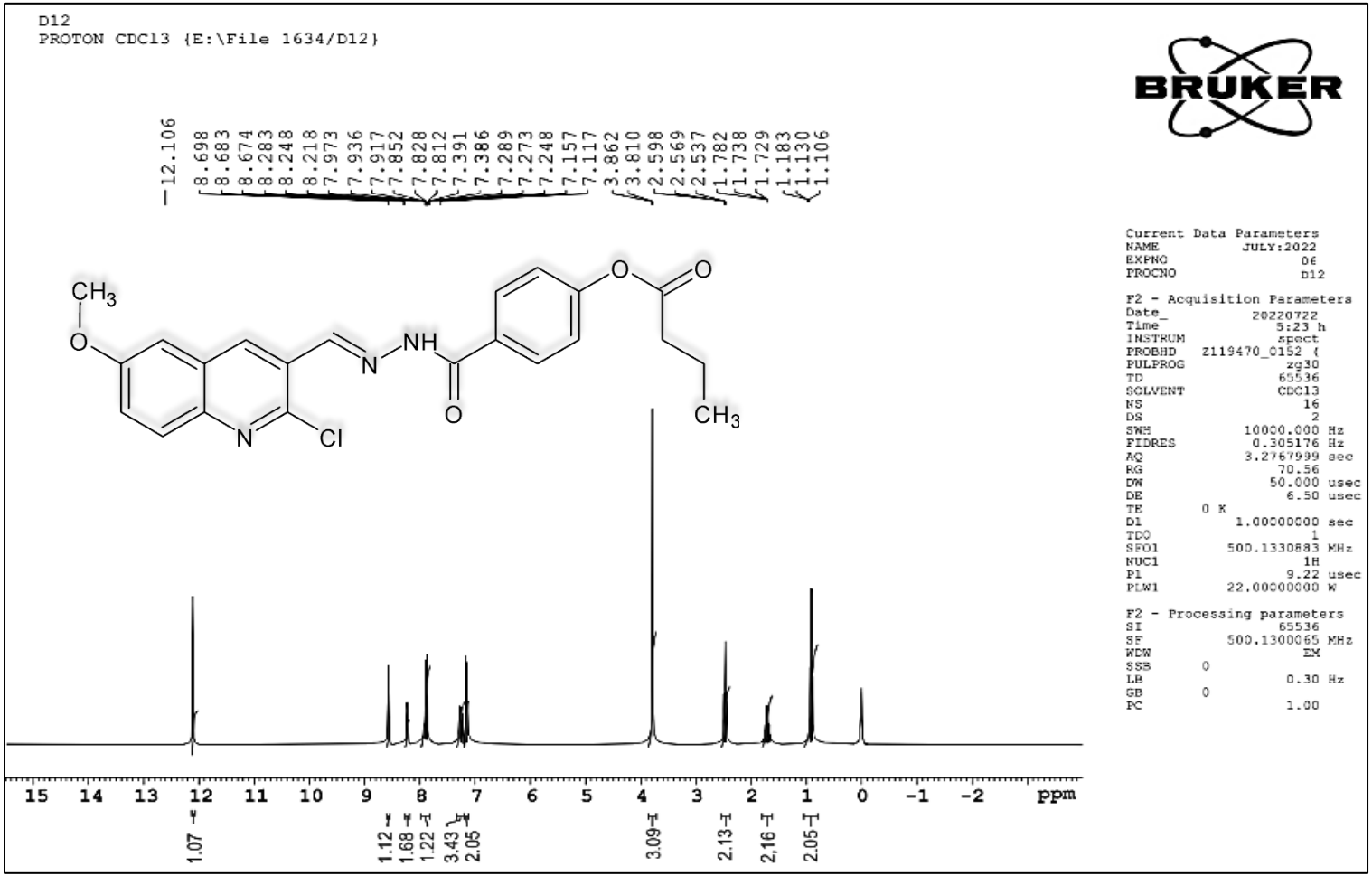

Figure 5.128: ^{1}H NMR spectrum of 4-{2-[(2-chloro-6-methoxy quinolin-3-yl) methylidene] hydrazine carbonyl} phenyl butanoate (Compound 4l)

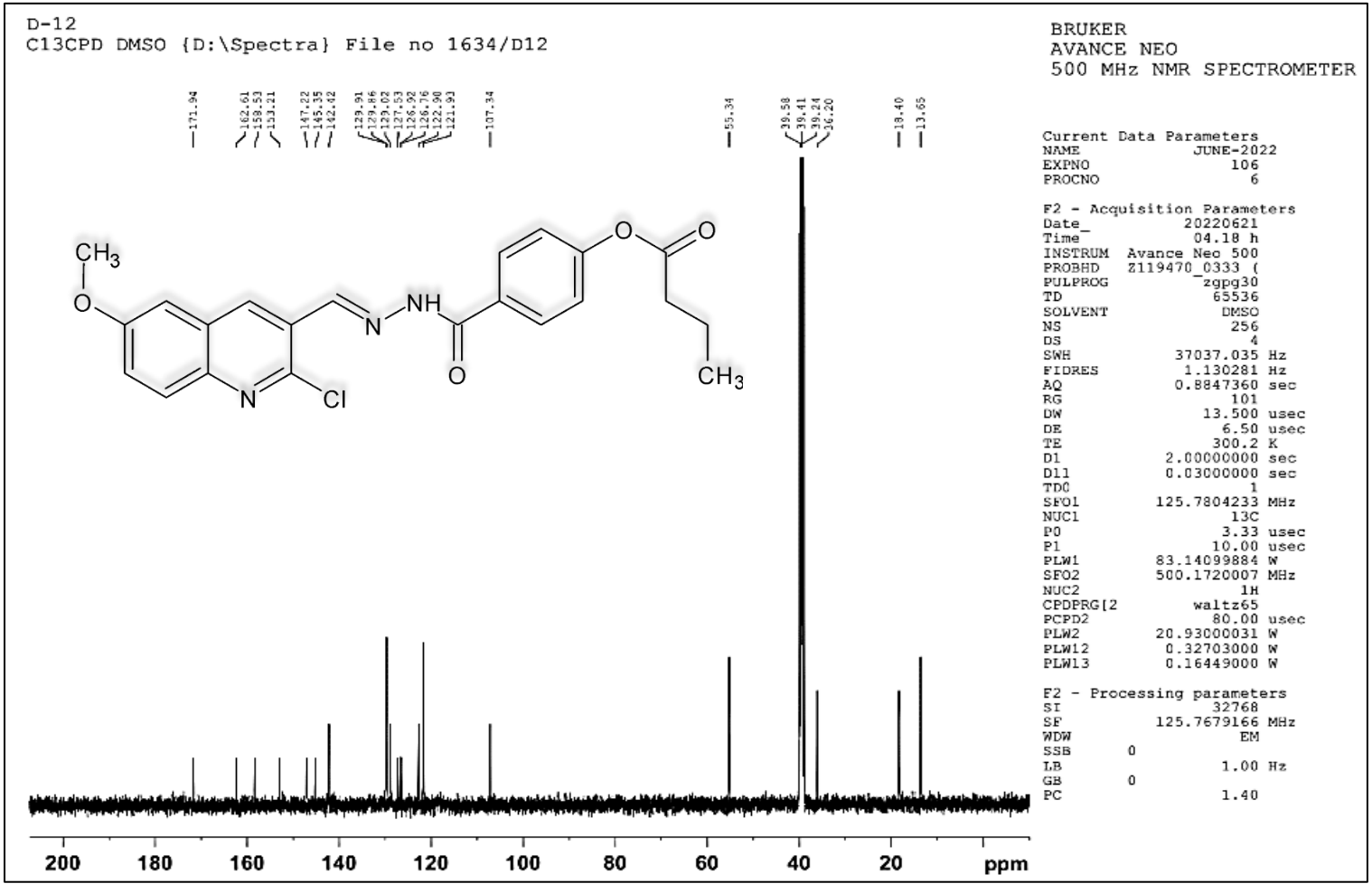

Figure 5.129: ^{13}C NMR spectrum of 4-{2-[(2-chloro-6-methoxy quinolin-3-yl) methylidene] hydrazine carbonyl} phenyl butanoate (Compound 4l)

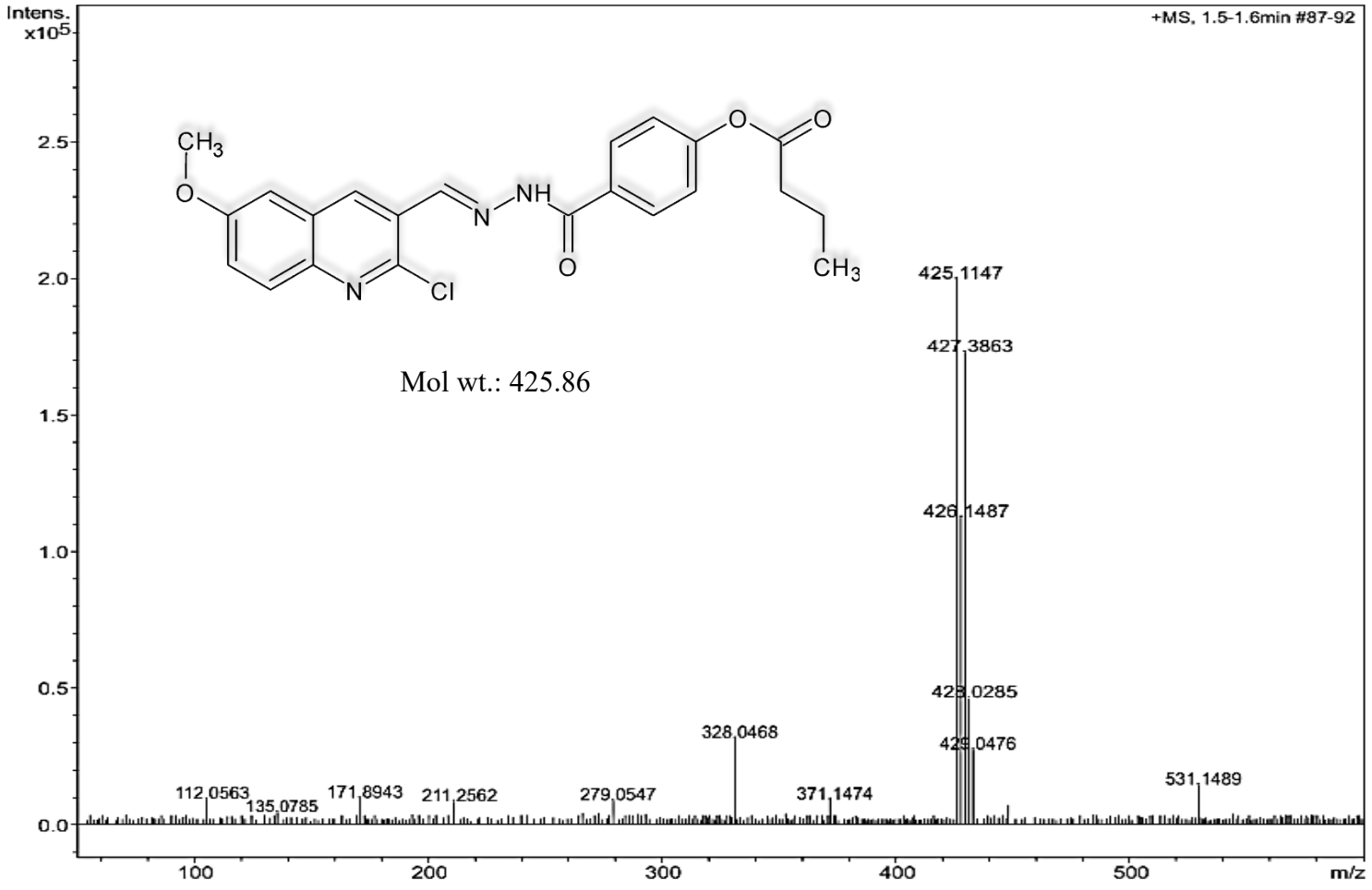

Figure 5.130: Mass spectrum of 4-{2-[(2-chloro-6-methoxy quinolin-3-yl) methylidene] hydrazine carbonyl} phenyl butanoate (Compound 4l)

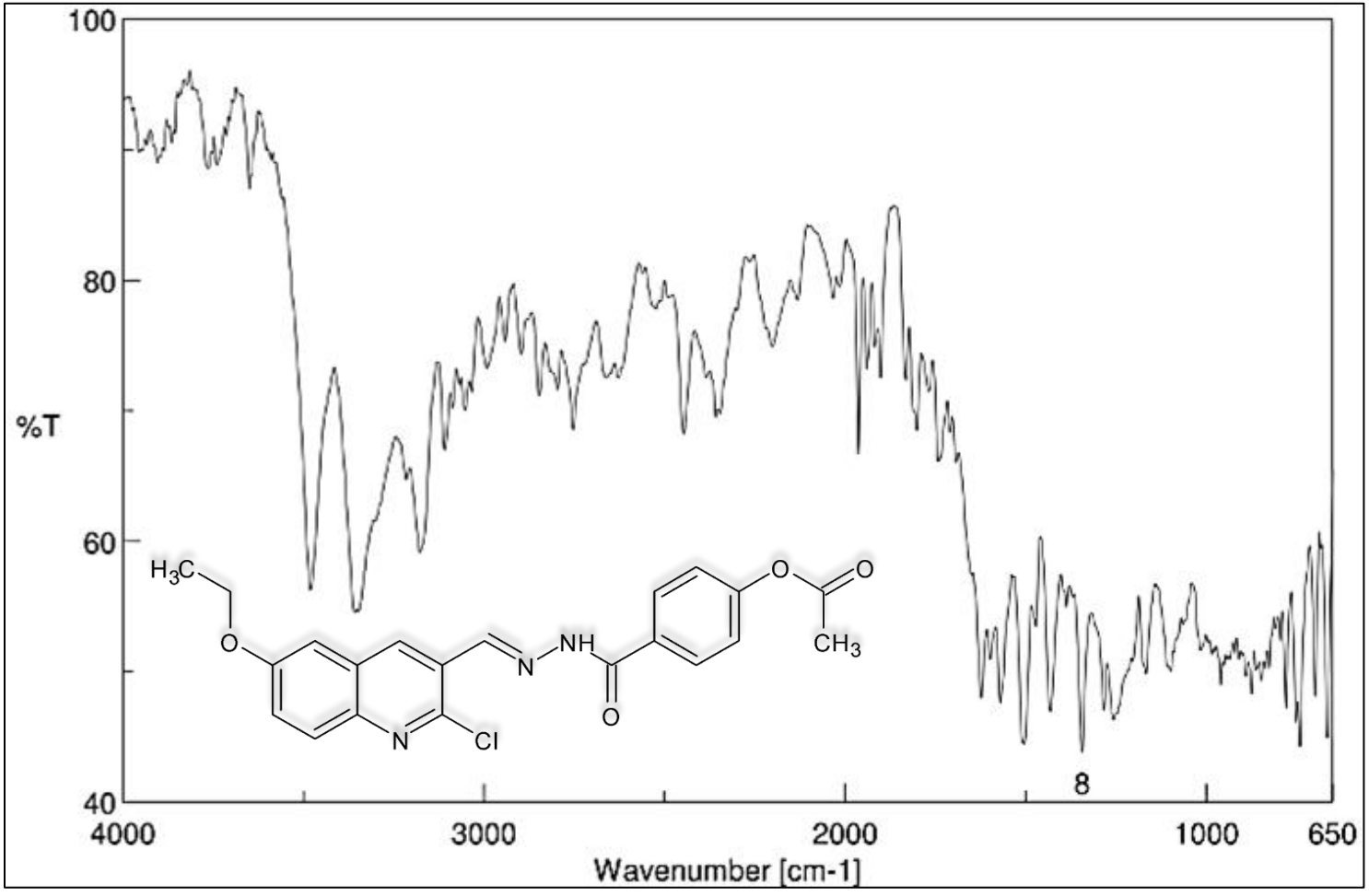

Figure 5.131: IR spectrum of 4-{2-2-[(2-chloro-6-ethoxy quinolin-3-yl) methylidene] hydrazine carbonyl} phenyl acetate (Compound 4m)

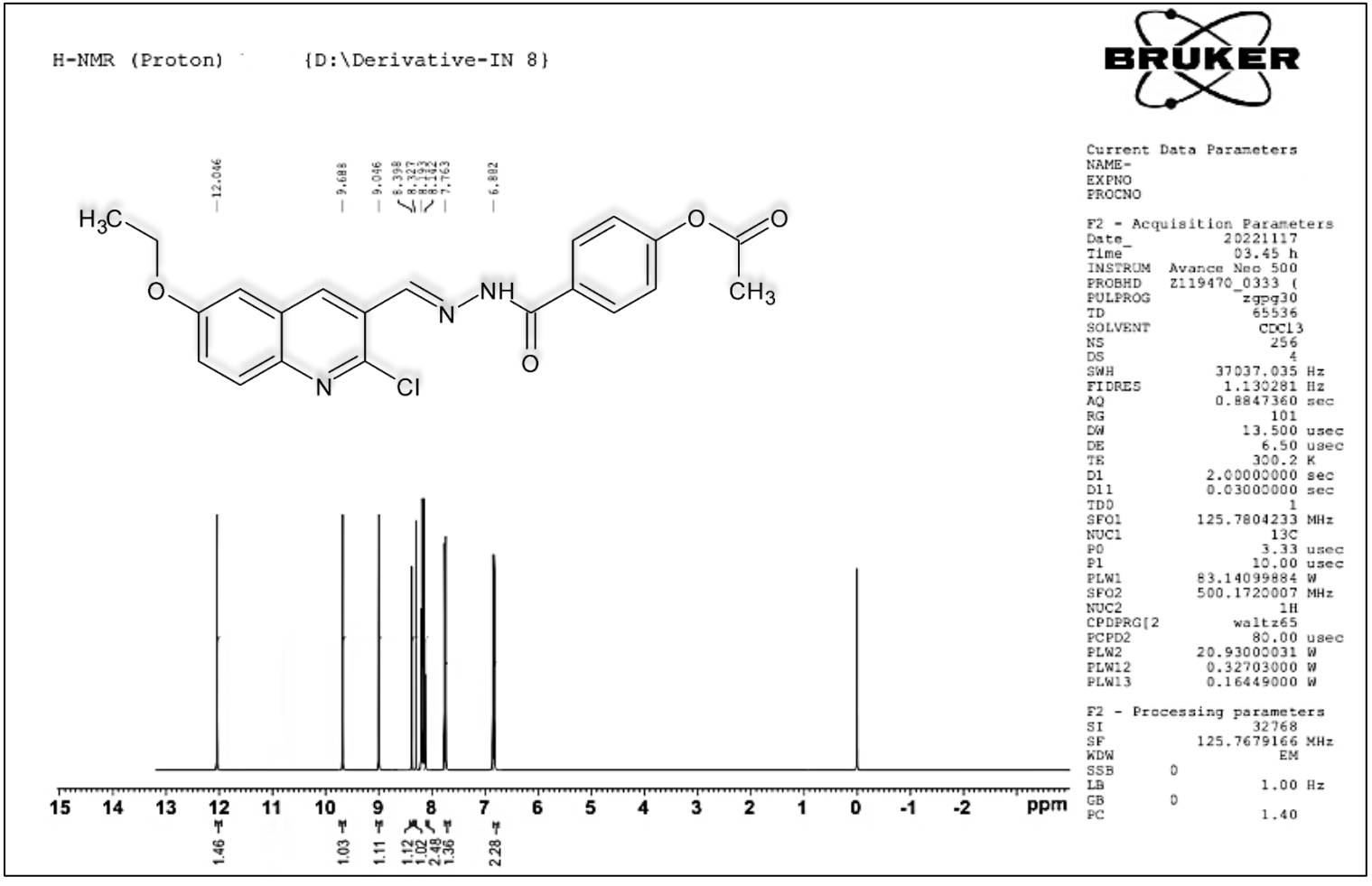

Figure 5.132: ^{1}H NMR spectrum of 4-{2-2-[(2-chloro-6-ethoxy quinolin-3-yl) methylidene] hydrazine carbonyl} phenyl acetate (Compound 4m)

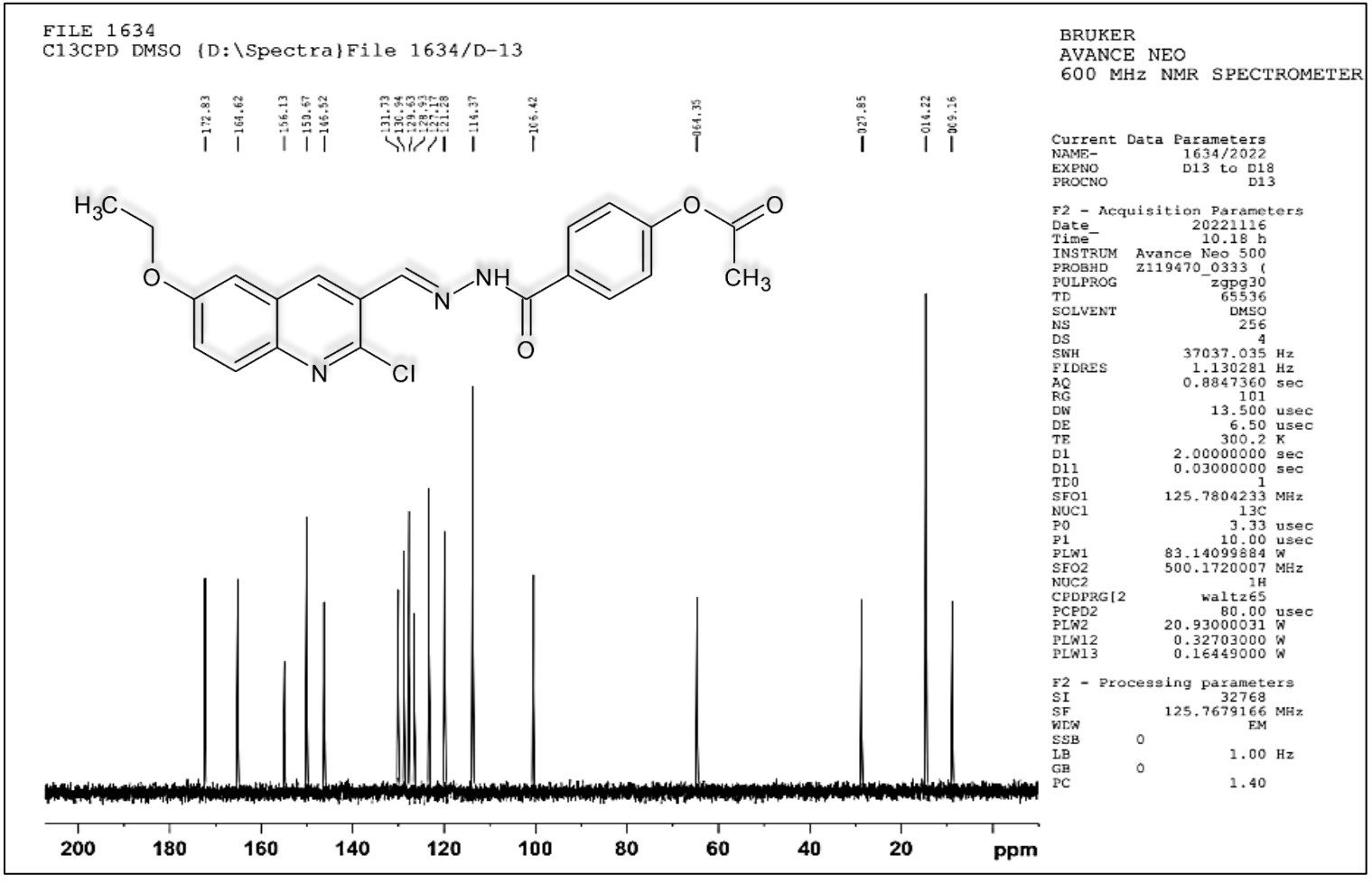

Figure 5.133: ^{13}C NMR spectrum of 4-{2-2-[(2-chloro-6-ethoxy quinolin-3-yl) methylidene] hydrazine carbonyl} phenyl acetate (Compound 4m)

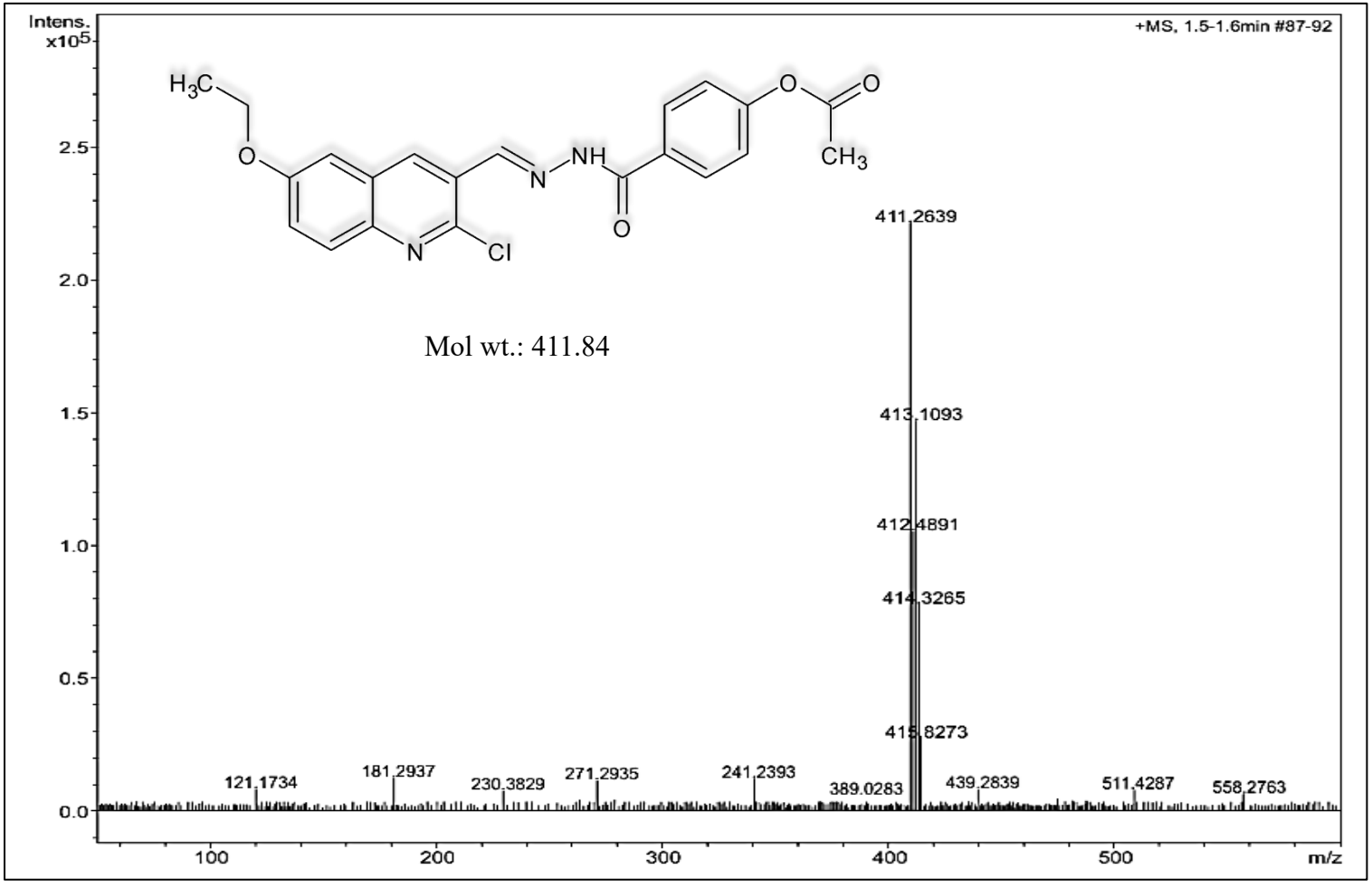

Figure 5.134: Mass spectrum of 4-{2-2-[(2-chloro-6-ethoxy quinolin-3-yl) methylidene] hydrazine carbonyl} phenyl acetate (Compound 4m)

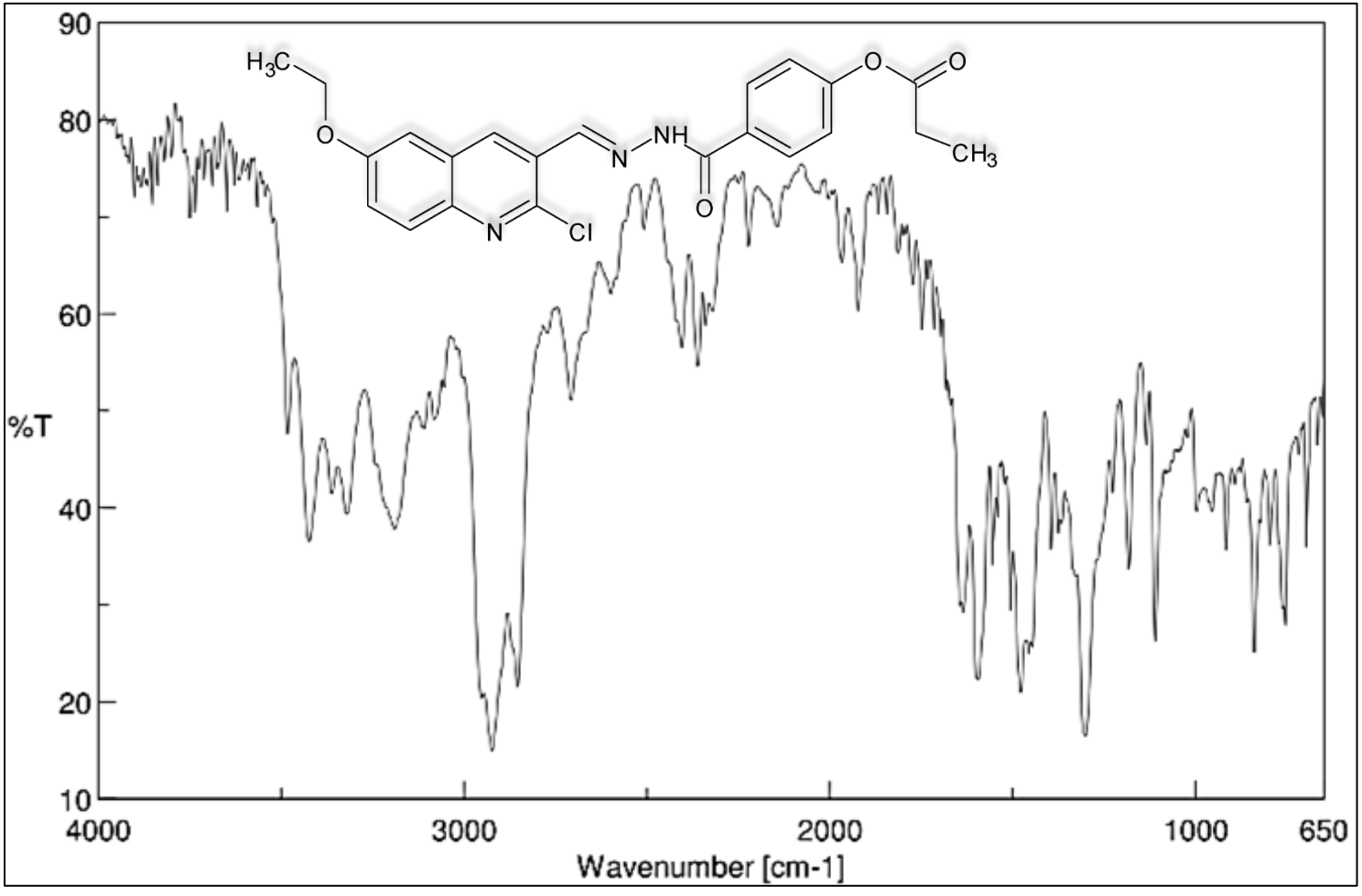

Figure 5.135: IR spectrum of 4-{2-2-[(2-chloro-6-ethoxyquinolin-3-yl) methylidene] hydrazine carbonyl} phenyl propanoate (Compound 4n)

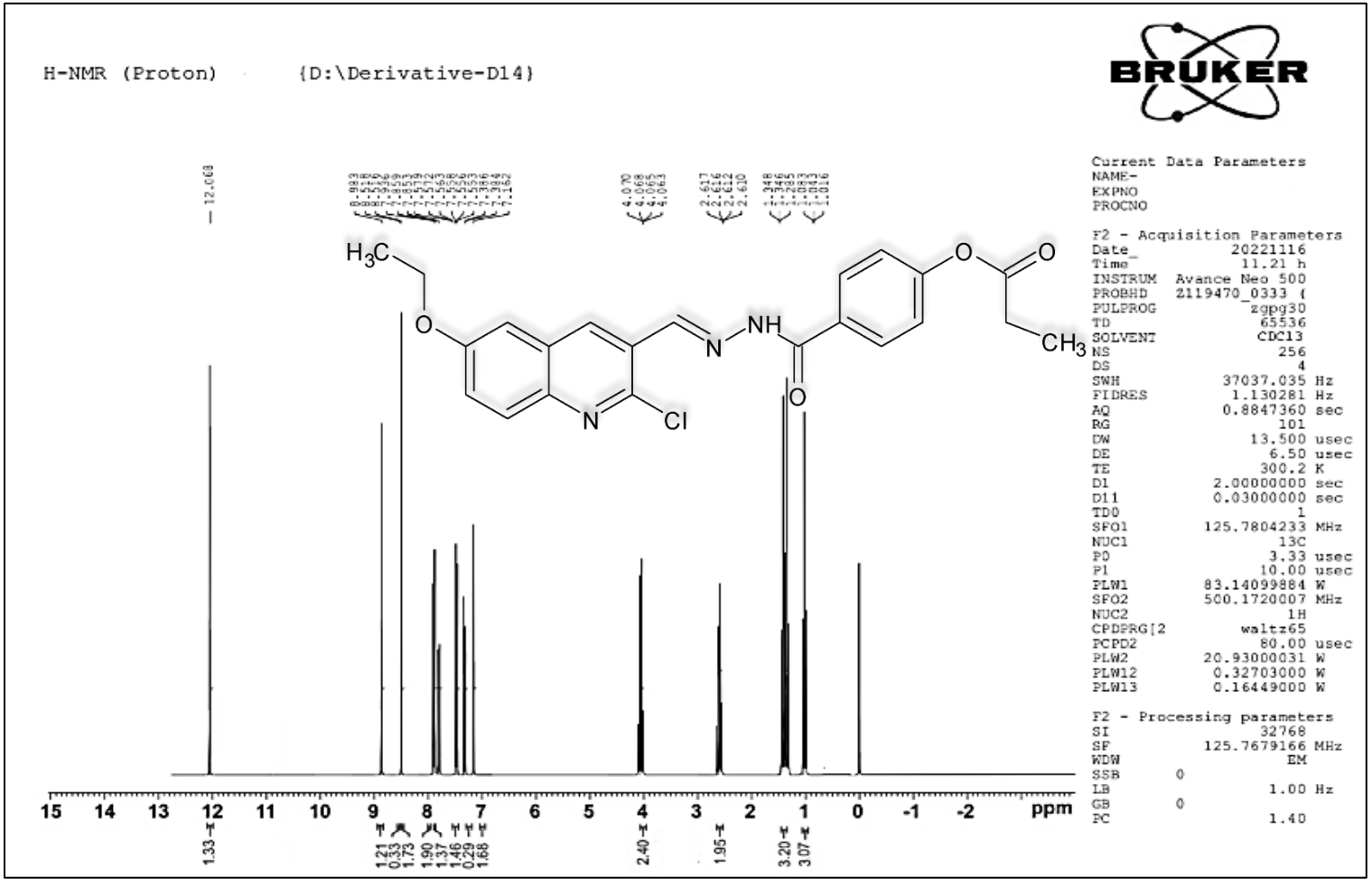

Figure 5.136: ^{1}H NMR spectrum of 4-{2-2-[(2-chloro-6-ethoxyquinolin-3-yl) methylidene] hydrazine carbonyl} phenyl propanoate (Compound 4n)

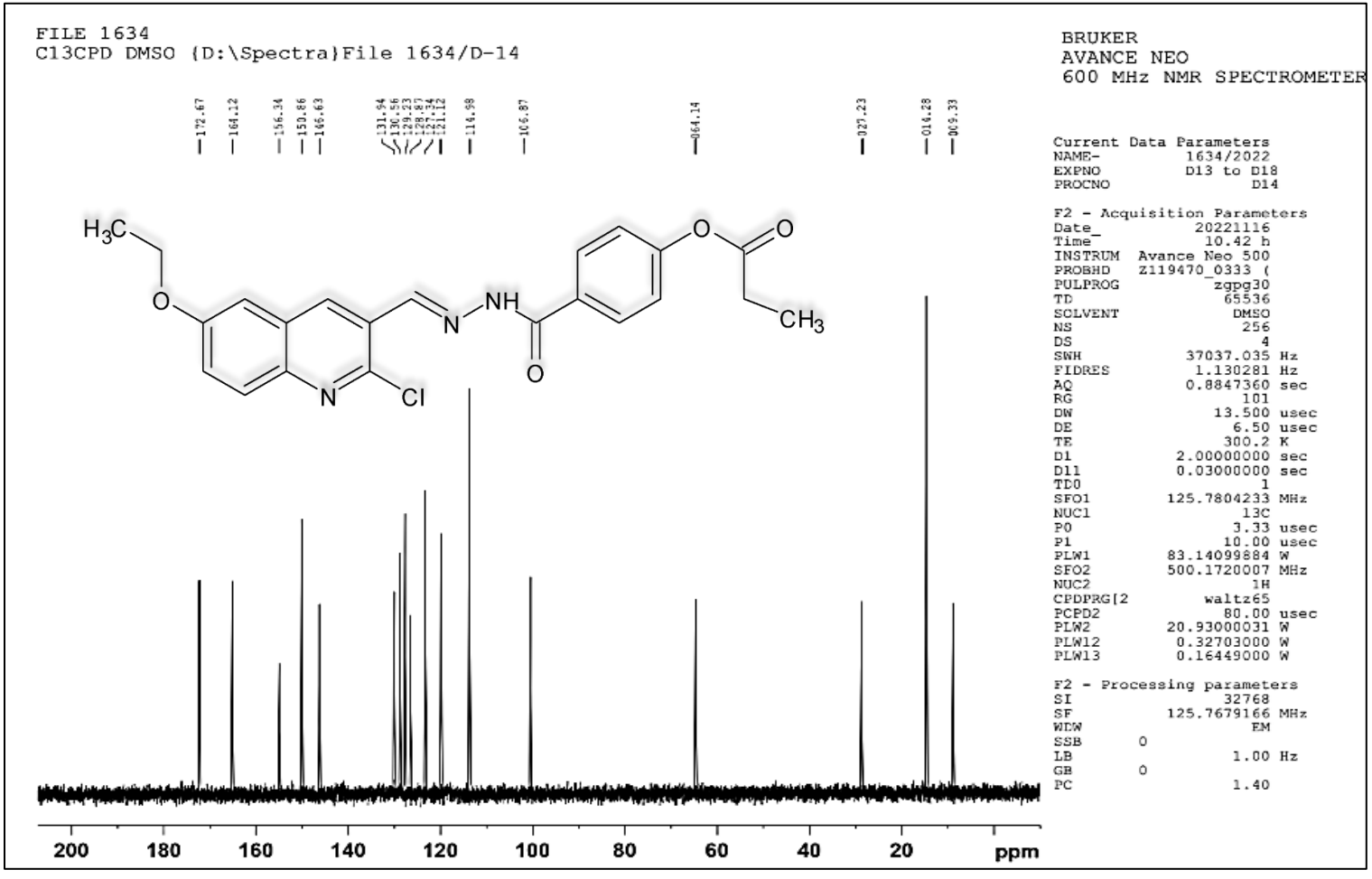

Figure 5.137: ^{13}C NMR spectrum of 4-{2-2-[(2-chloro-6-ethoxyquinolin-3-yl) methylidene] hydrazine carbonyl} phenyl propanoate (Compound 4n)

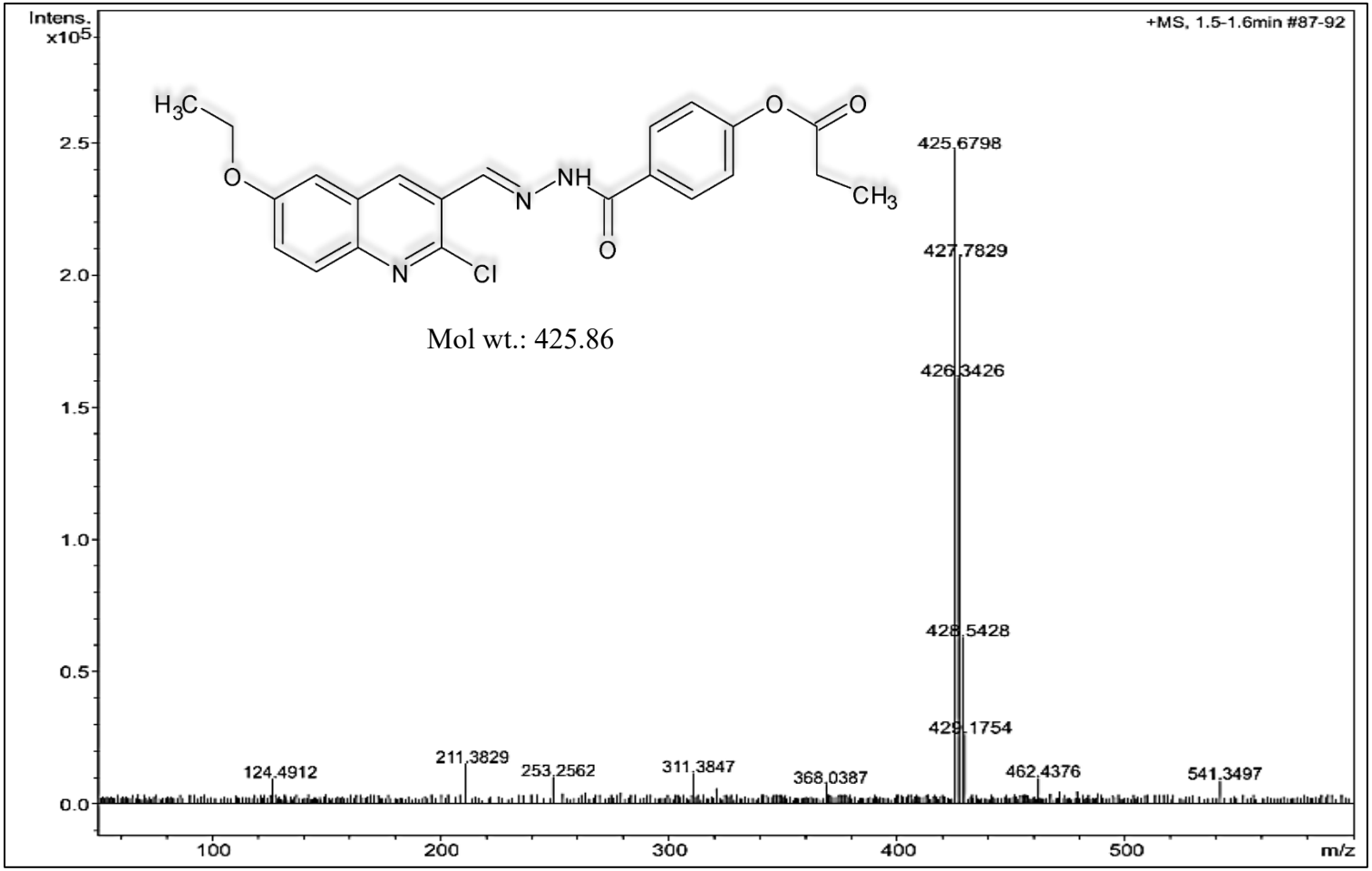

Figure 5.138: Mass spectrum of 4-{2-2-[(2-chloro-6-ethoxyquinolin-3-yl) methylidene] hydrazine carbonyl} phenyl propanoate (Compound 4n)

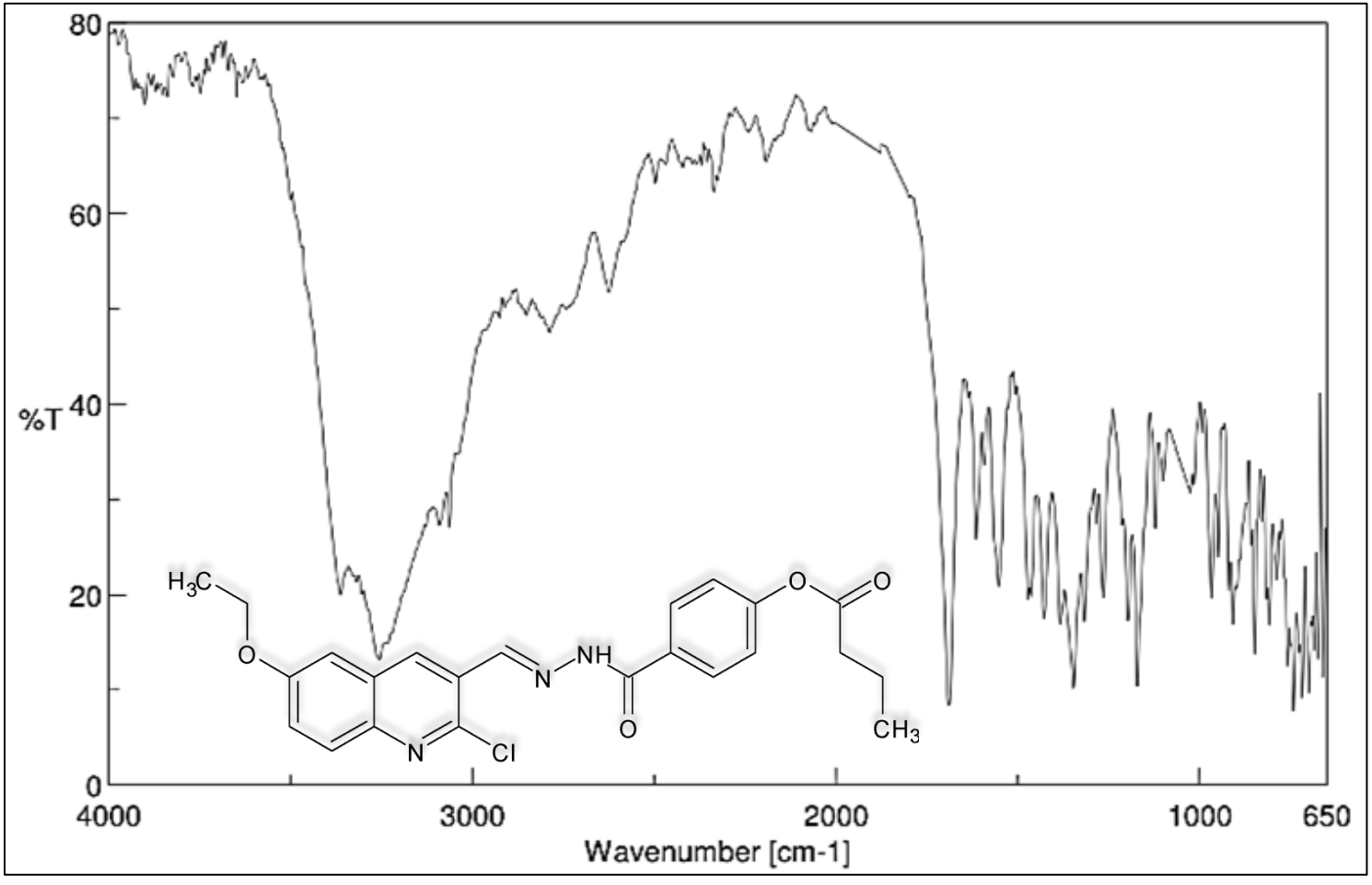

Figure 5.139: IR spectrum of 4-{2-2-[(2-chloro-6-ethoxy quinolin-3-yl) methylidene] hydrazine carbonyl} phenyl butanoate (Compound 4o)

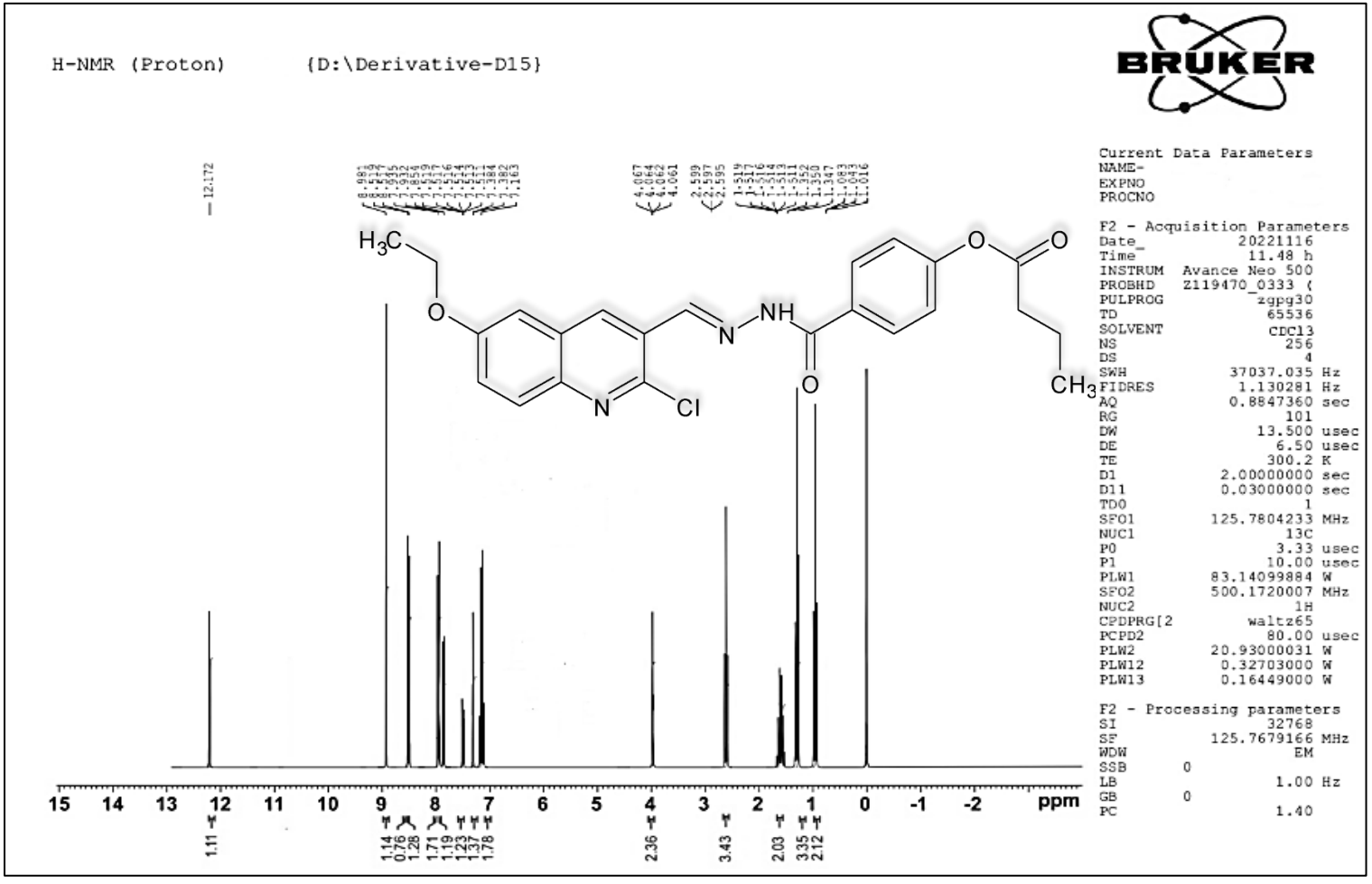

Figure 5.140: ^{1}H NMR spectrum of 4-{2-2-[(2-chloro-6-ethoxy quinolin-3-yl) methylidene] hydrazine carbonyl} phenyl butanoate (Compound 4o)

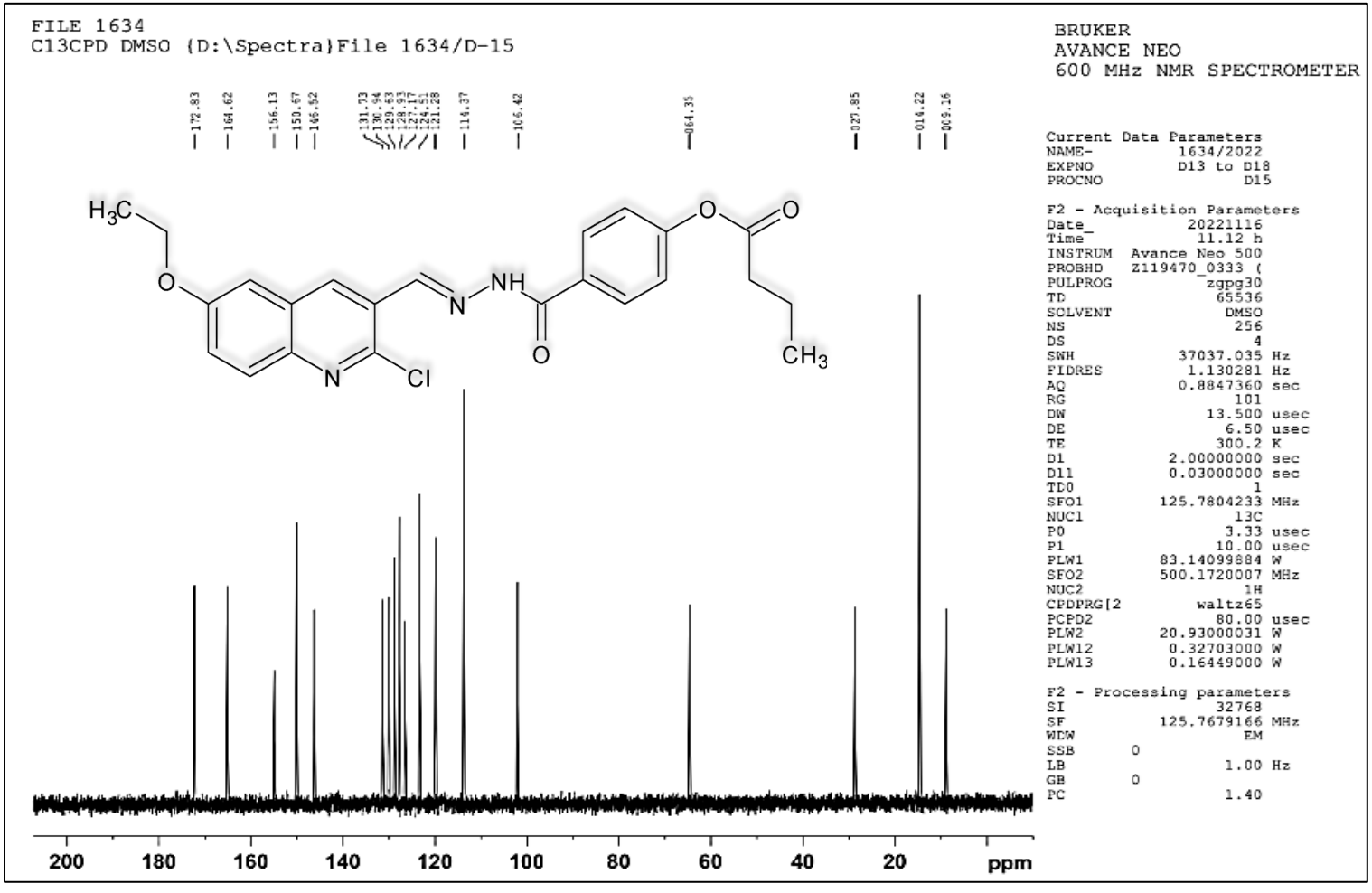

Figure 5.141: ^{13}C NMR spectrum of 4-{2-2-[(2-chloro-6-ethoxy quinolin-3-yl) methylidene] hydrazine carbonyl} phenyl butanoate (Compound 4o)

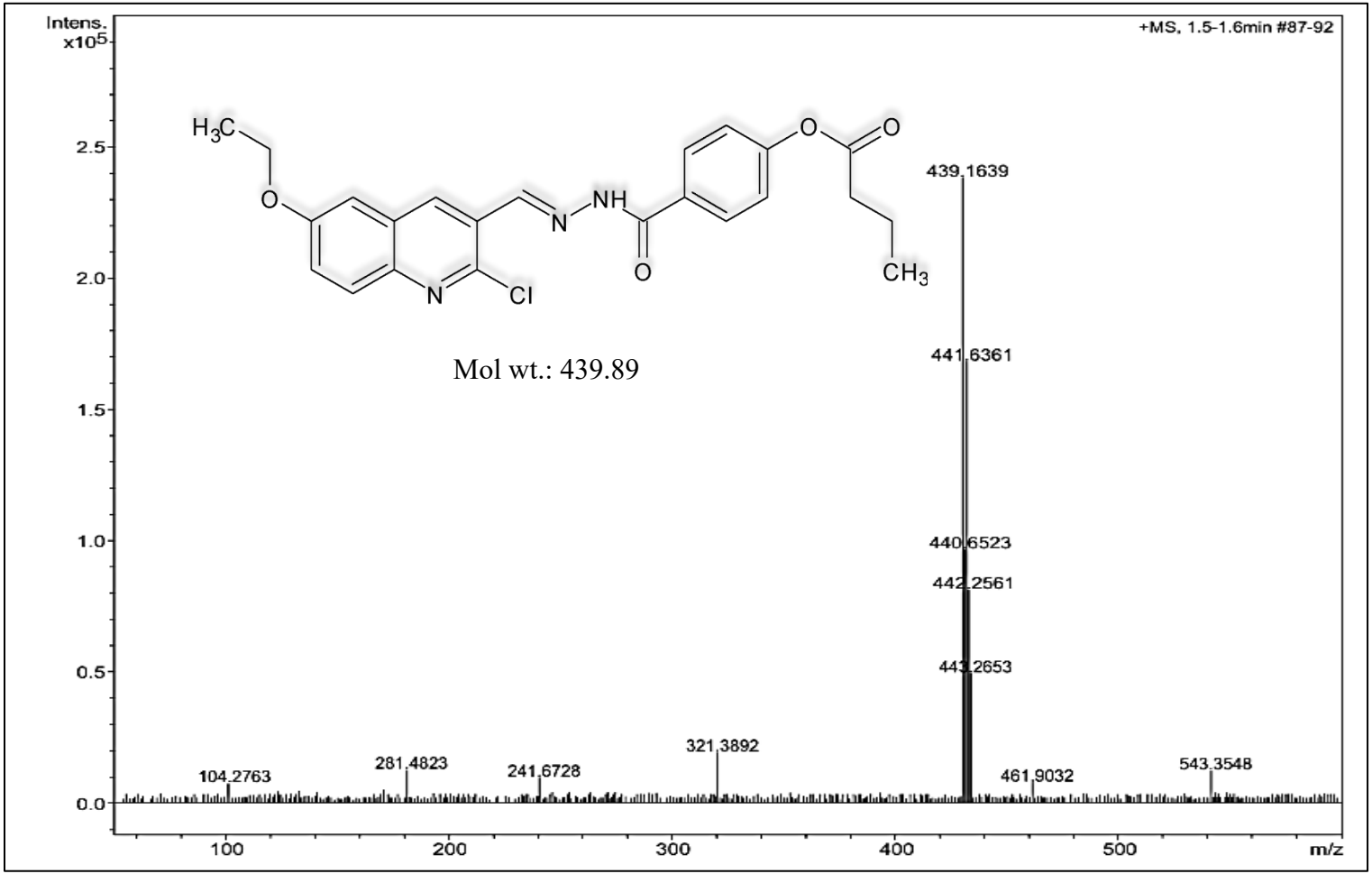

Figure 5.142: Mass spectrum of 4-{2-2-[(2-chloro-6-ethoxy quinolin-3-yl) methylidene] hydrazine carbonyl} phenyl butanoate (Compound 4o)

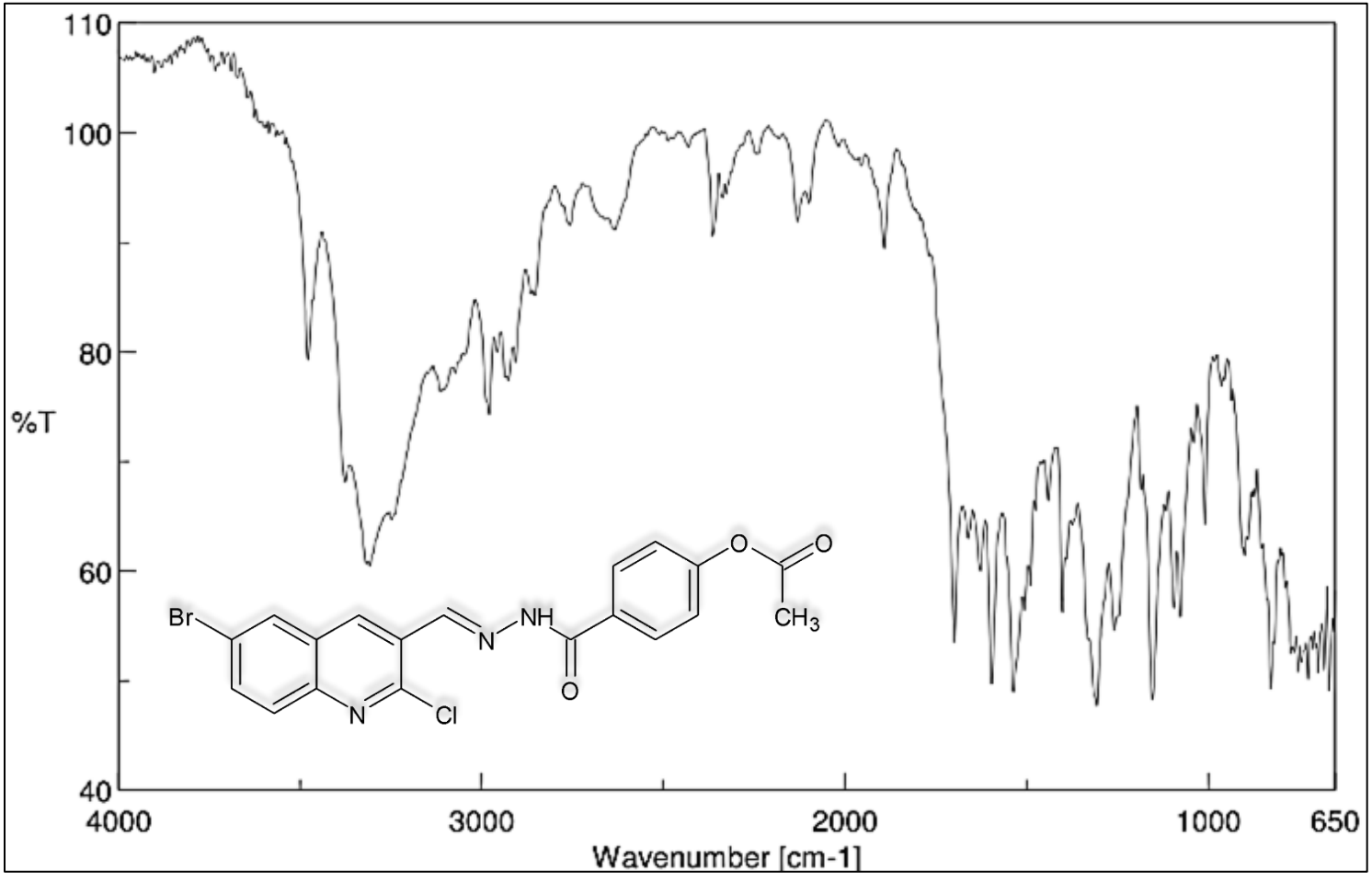

Figure 5.143: IR spectrum of 4-{2-2-[(6-bromo-2-chloro quinolin-3-yl)methylidene] hydrazine carbonyl} phenyl acetate (Compound 4p)

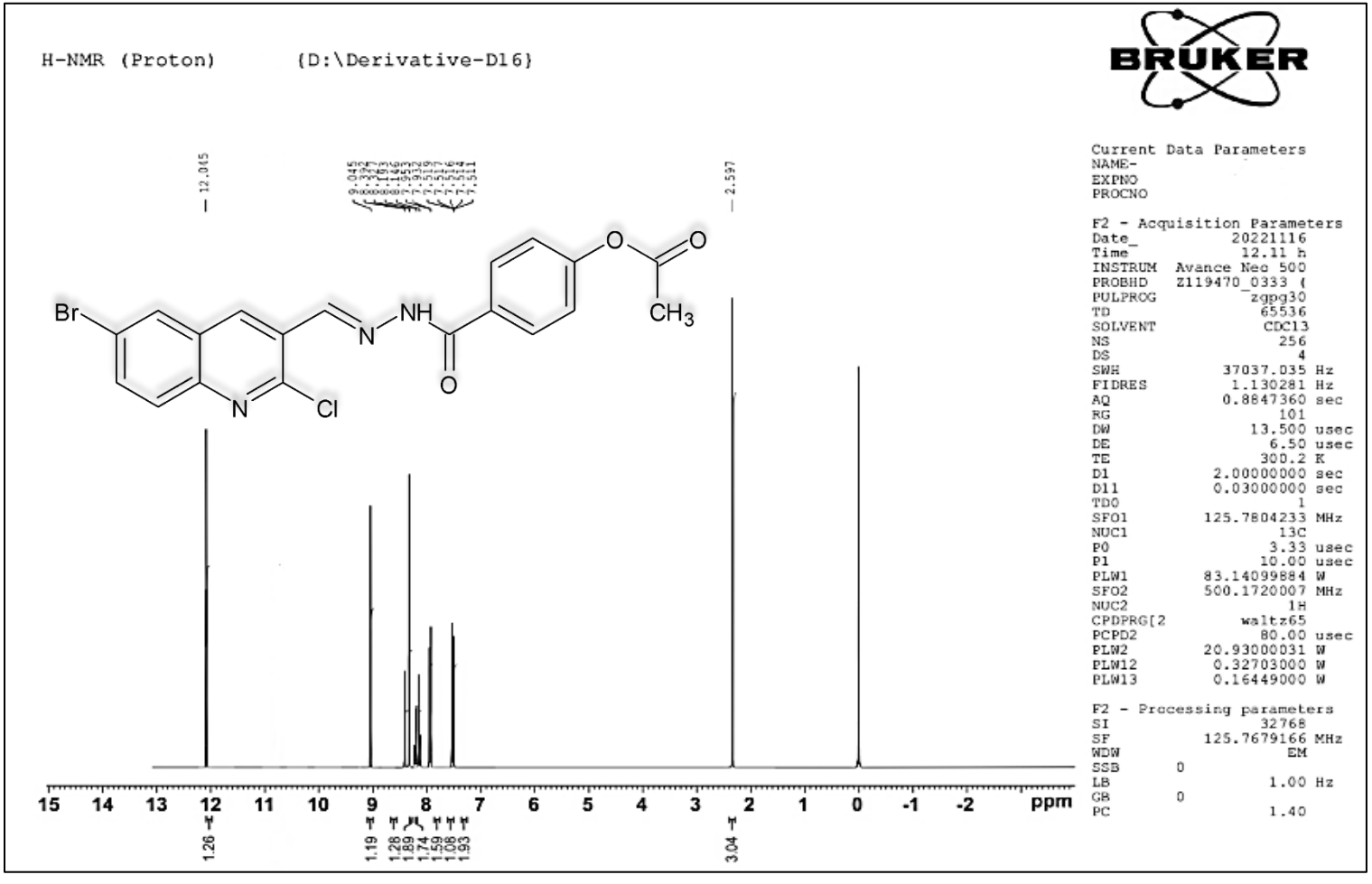

Figure 5.144: ^{1}H NMR spectrum of 4-{2-2-[(6-bromo-2-chloro quinolin-3-yl)methylidene] hydrazine carbonyl} phenyl acetate (Compound 4p)

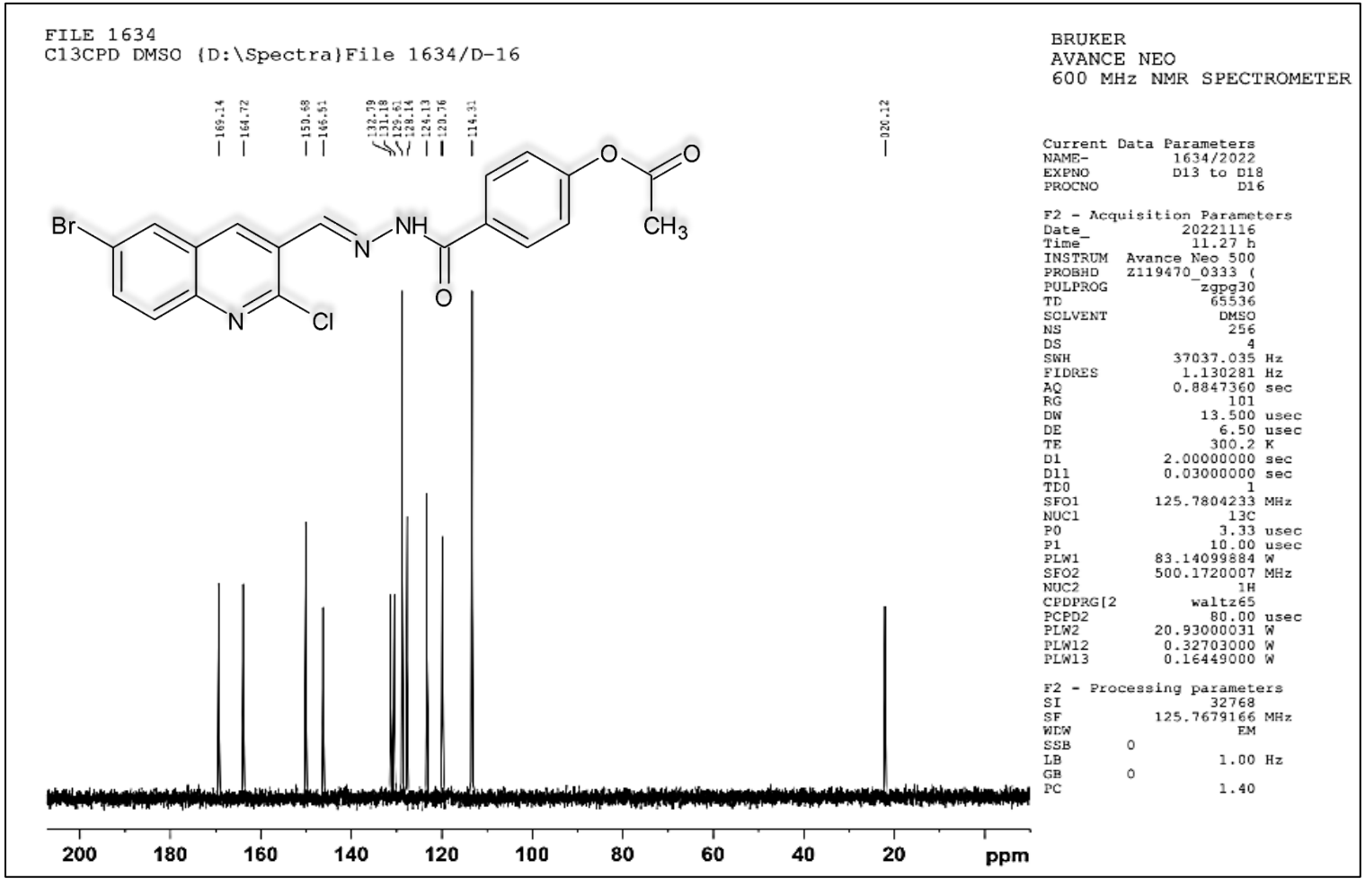

Figure 5.145: ^{13}C NMR spectrum of 4-{2-2-[(6-bromo-2-chloro quinolin-3-yl)methylidene] hydrazine carbonyl} phenyl acetate (Compound 4p)

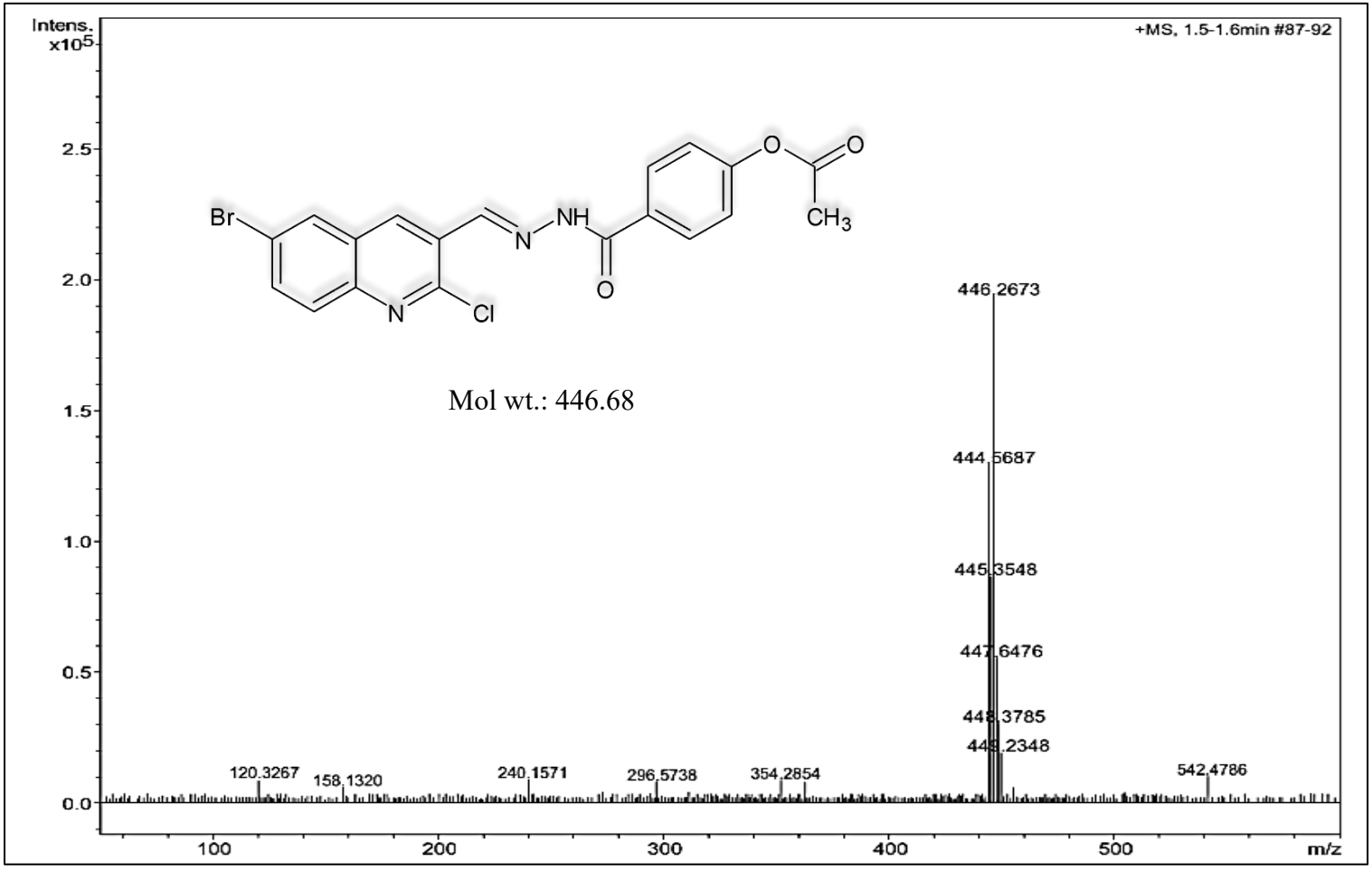

Figure 5.146: Mass spectrum of 4- {2-2- [(6-bromo-2-chloro quinolin-3-yl)methylidene] hydrazine carbonyl} phenyl acetate (Compound 4p)

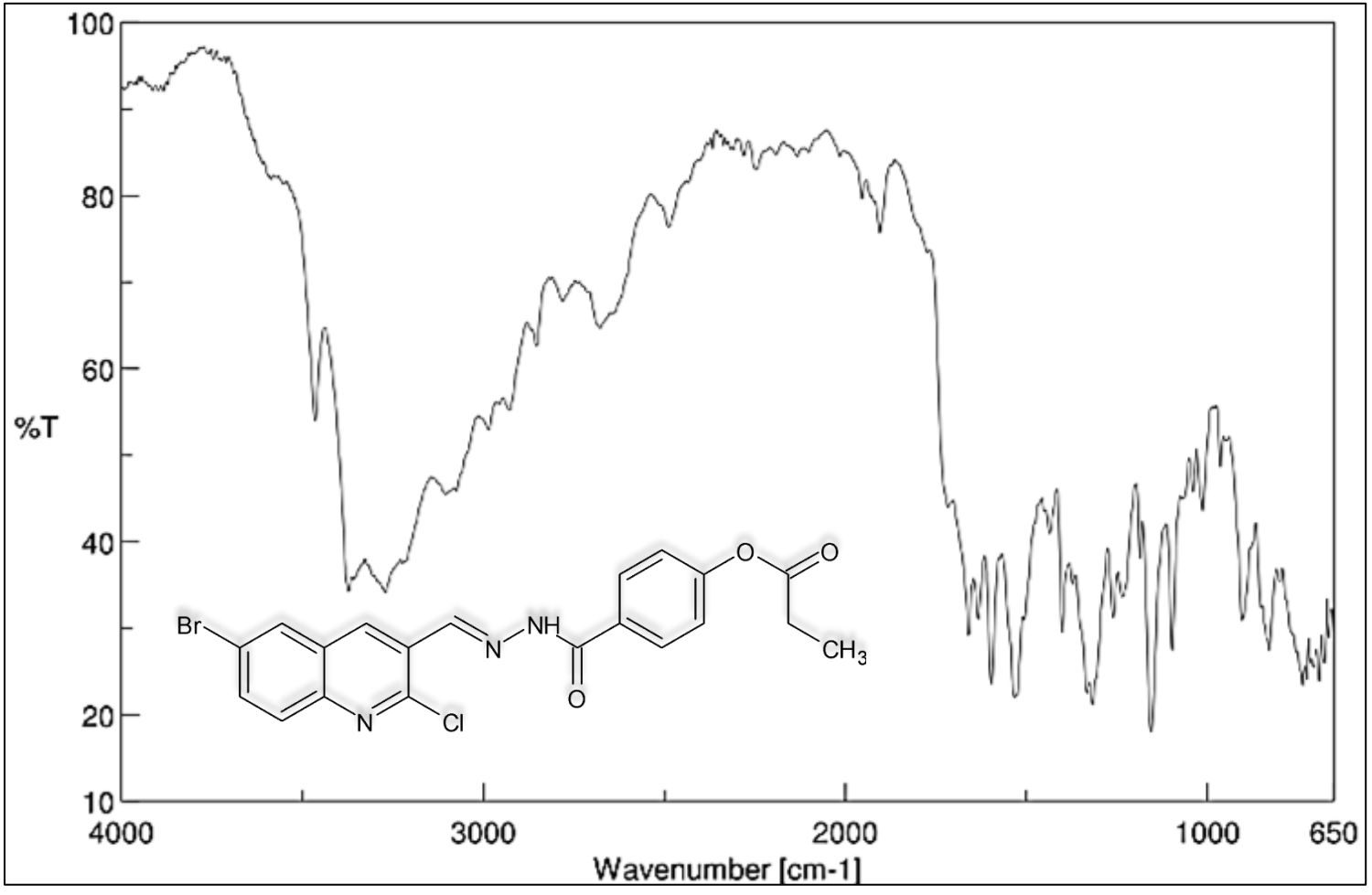

Figure 5.147: IR spectrum of 4- {2-2- [(6-bromo-2-chloro quinolin-3-yl) methylidene] hydrazine carbonyl} phenyl propanoate (Compound 4q)

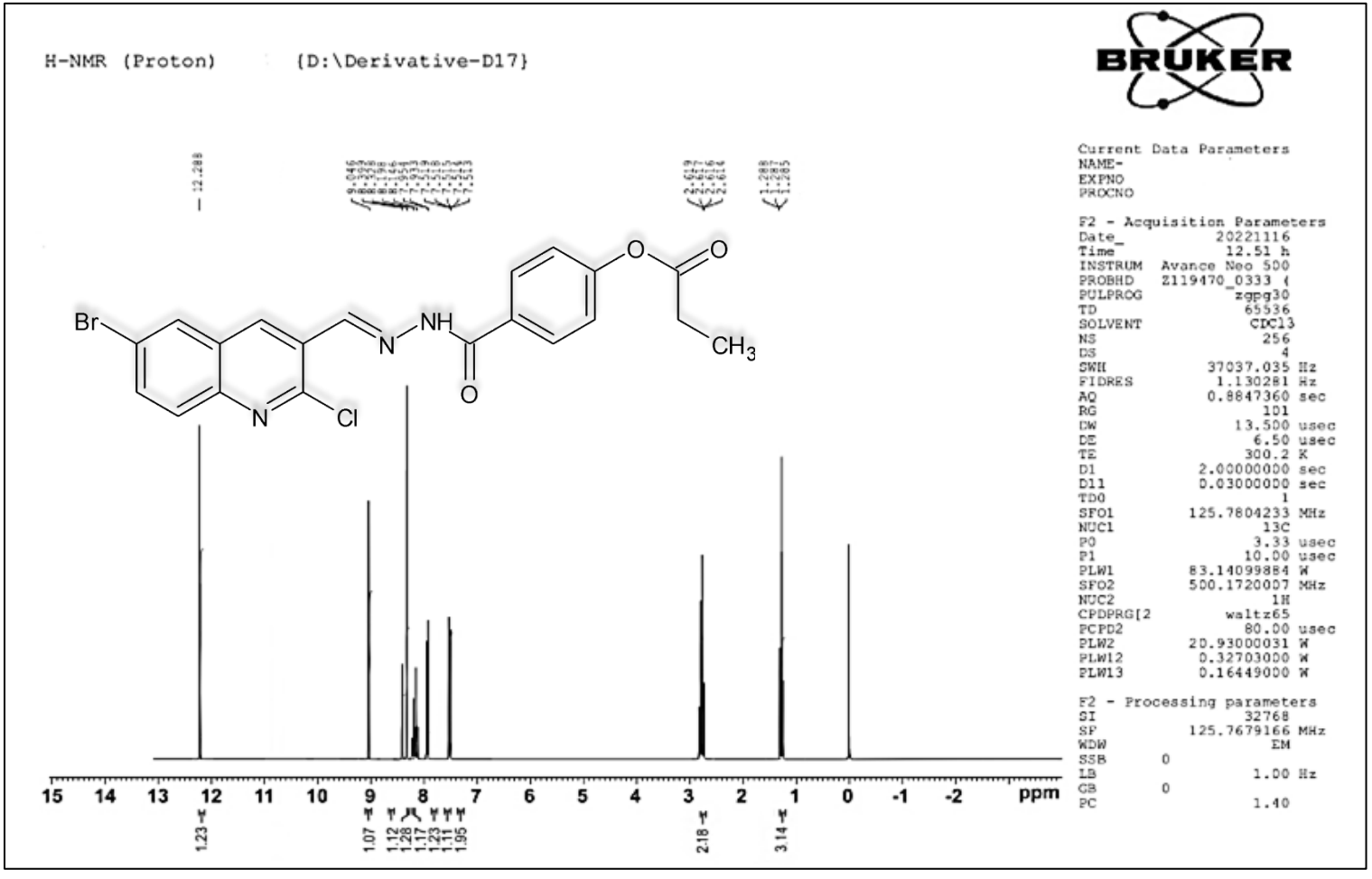

Figure 5.148: ^{1}H NMR spectrum of 4- {2-2- [(6-bromo-2-chloro quinolin-3-yl) methylidene] hydrazine carbonyl} phenyl propanoate (Compound 4q)

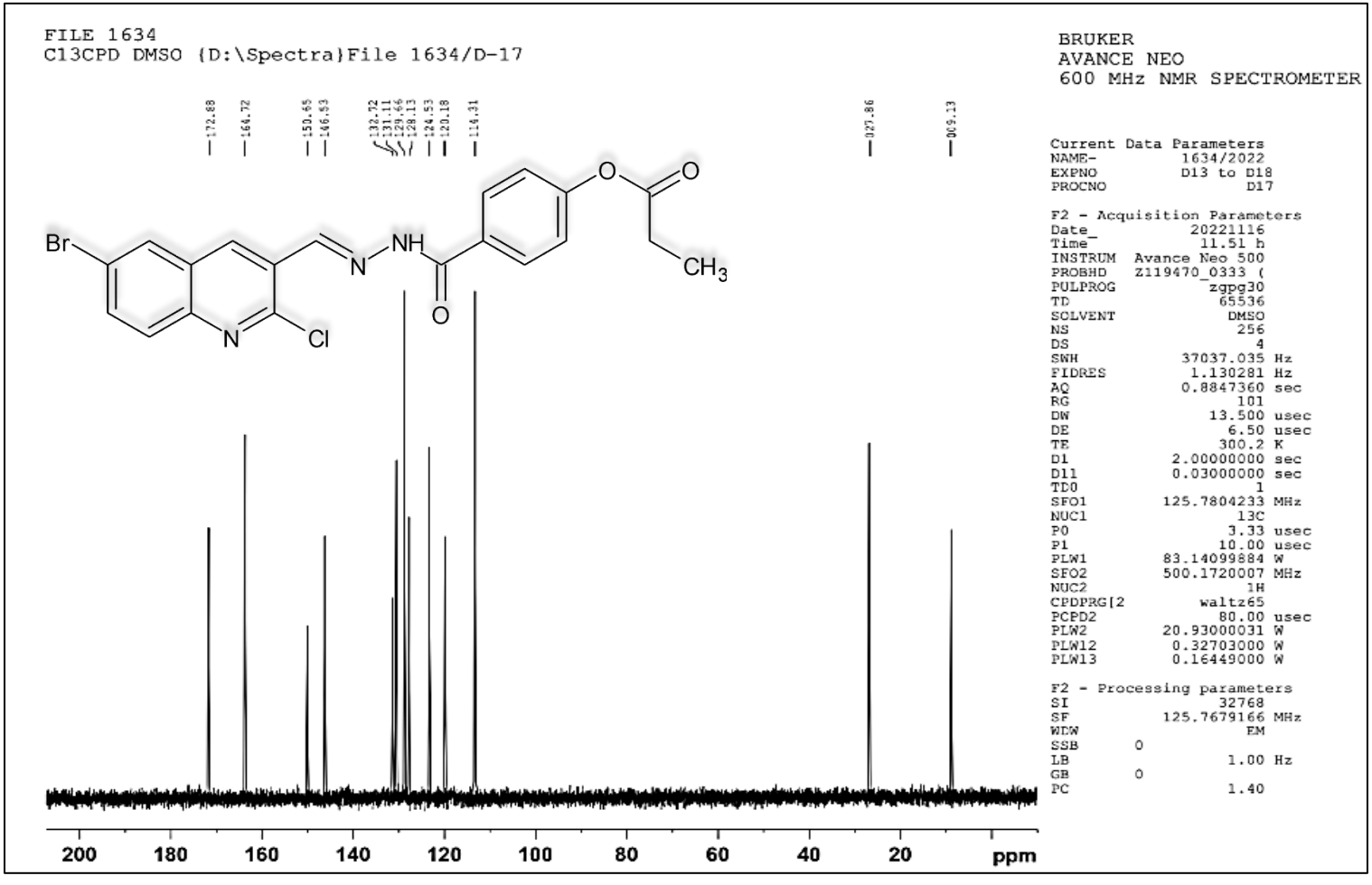

Figure 5.149: ^{13}C NMR spectrum of 4- {2-2- [(6-bromo-2-chloro quinolin-3-yl) methylidene] hydrazine carbonyl} phenyl propanoate (Compound 4q)

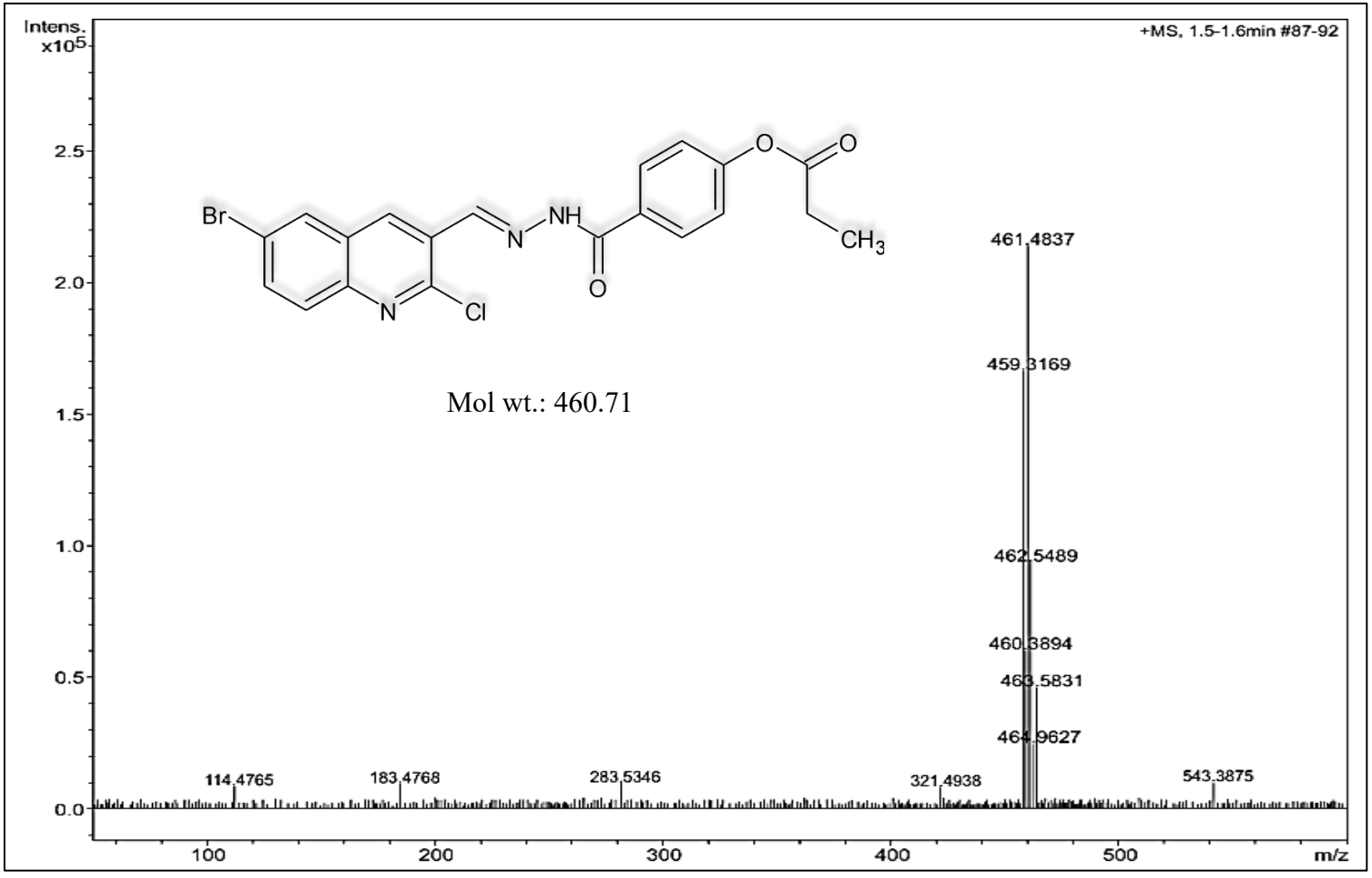

Figure 5.150: Mass spectrum of 4- {2-2- [(6-bromo-2-chloro quinolin-3-yl) methylidene] hydrazine carbonyl} phenyl propanoate (Compound 4q)

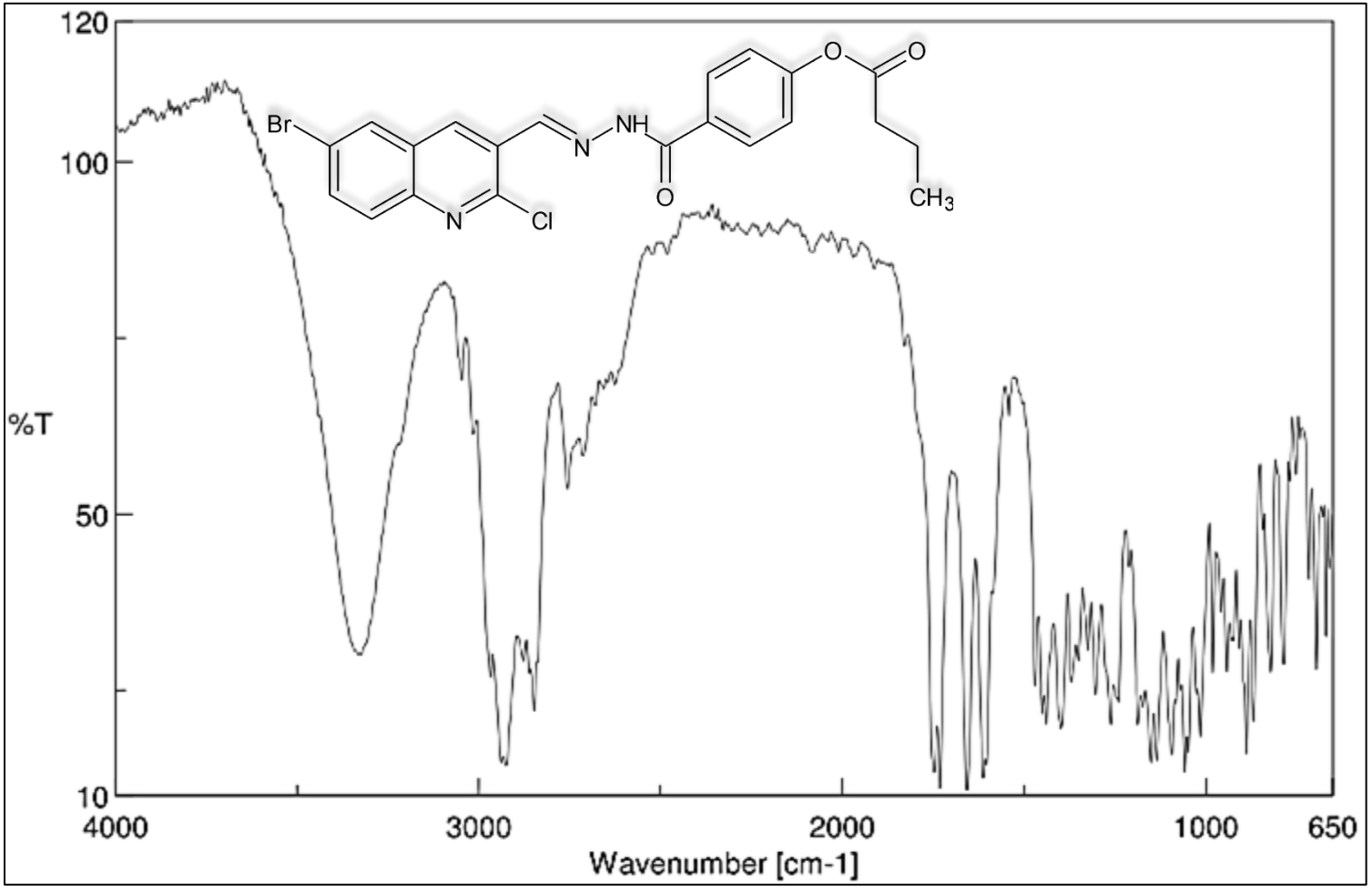

Figure 5.151: IR spectrum of 4- {2-2- [(6-bromo-2-chloro quinolin-3-yl) methylidene] hydrazine carbonyl} phenyl butanoate (Compound 4r)

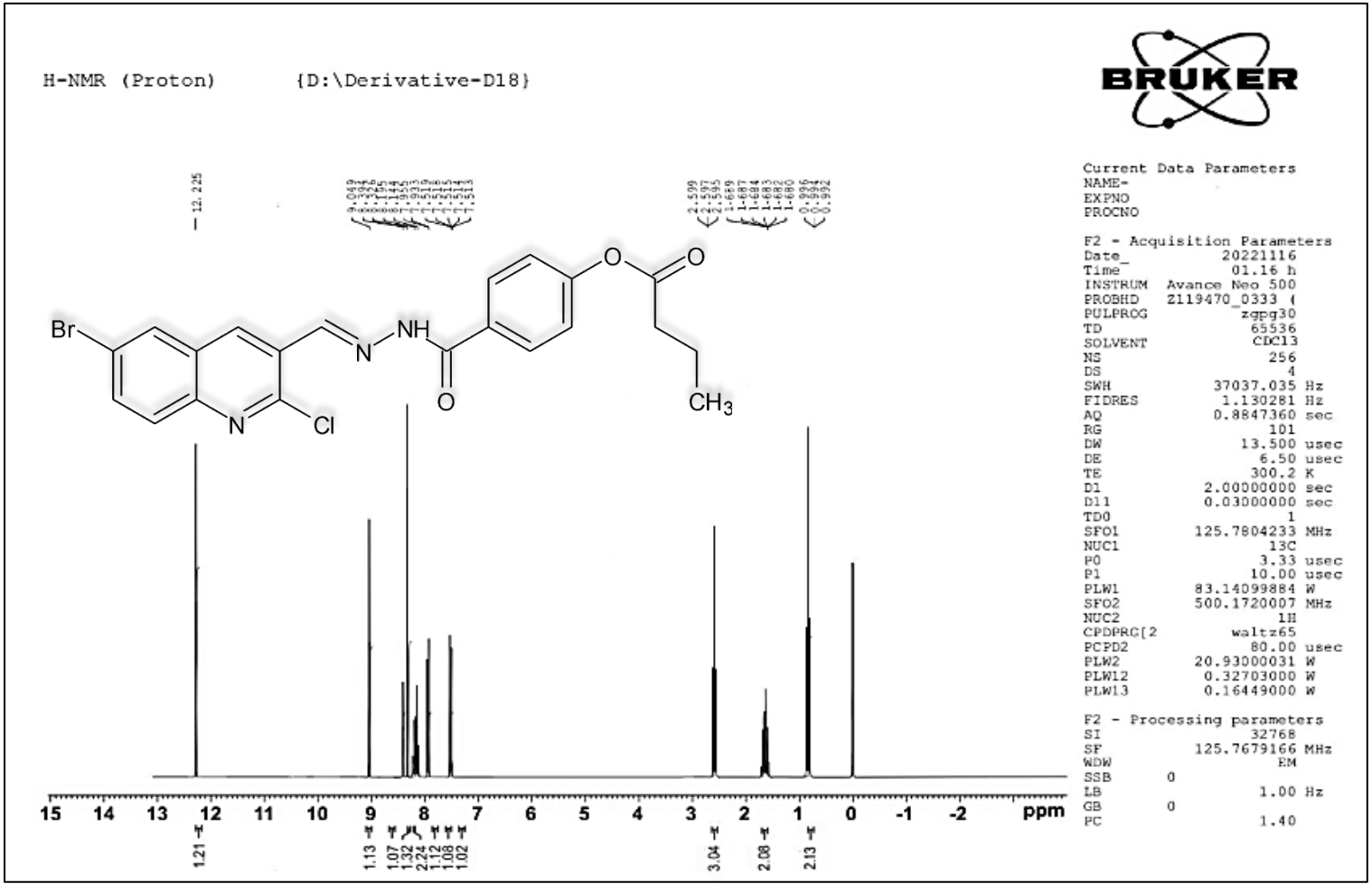

Figure 5.152: ^{1}H NMR spectrum of 4- {2-2- [(6-bromo-2-chloro quinolin-3-yl) methylidene] hydrazine carbonyl} phenyl butanoate (Compound 4r)

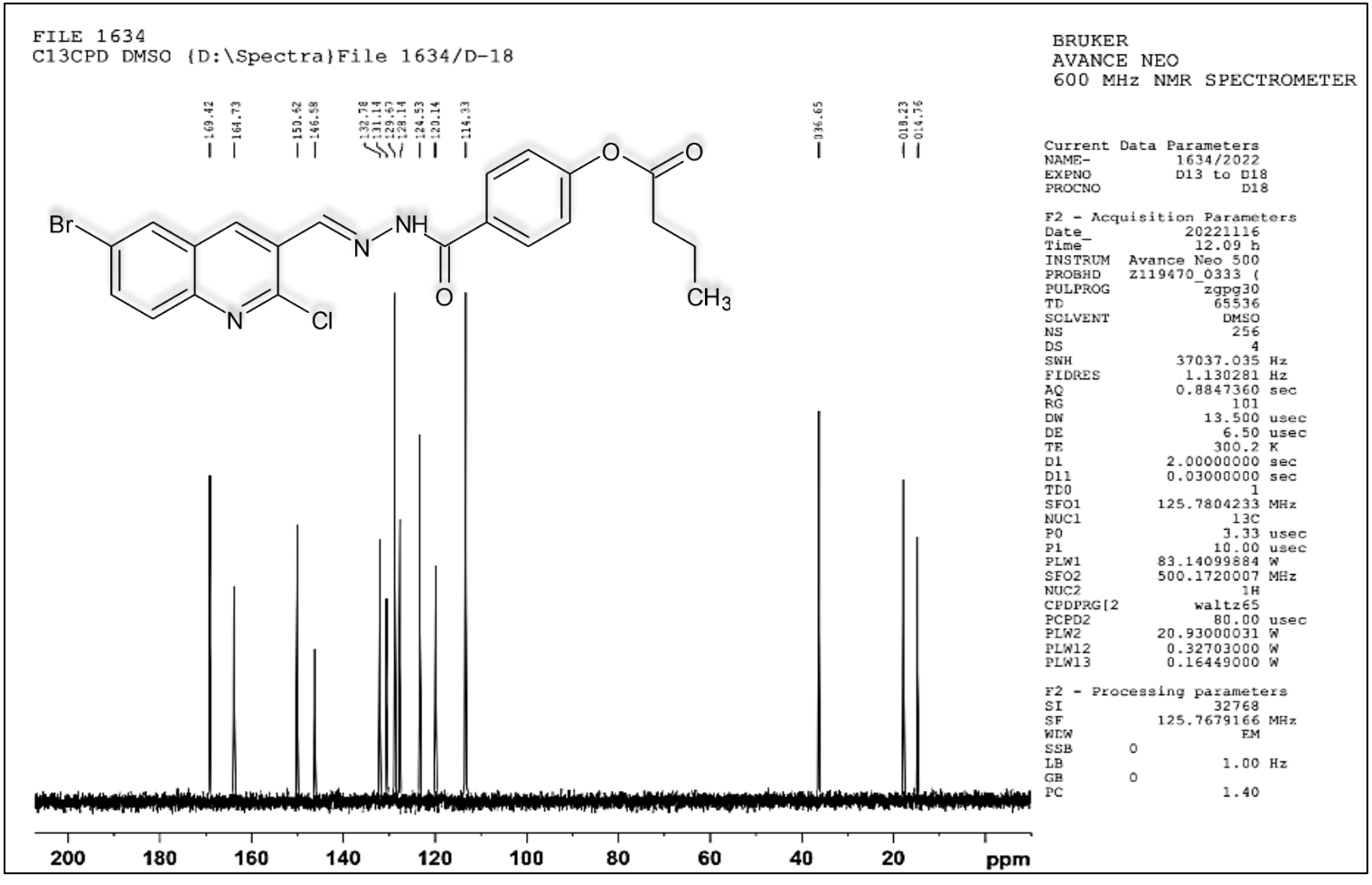

Figure 5.153: ^{13}C NMR spectrum of 4- {2-2- [(6-bromo-2-chloro quinolin-3-yl) methylidene] hydrazine carbonyl} phenyl butanoate (Compound 4r)

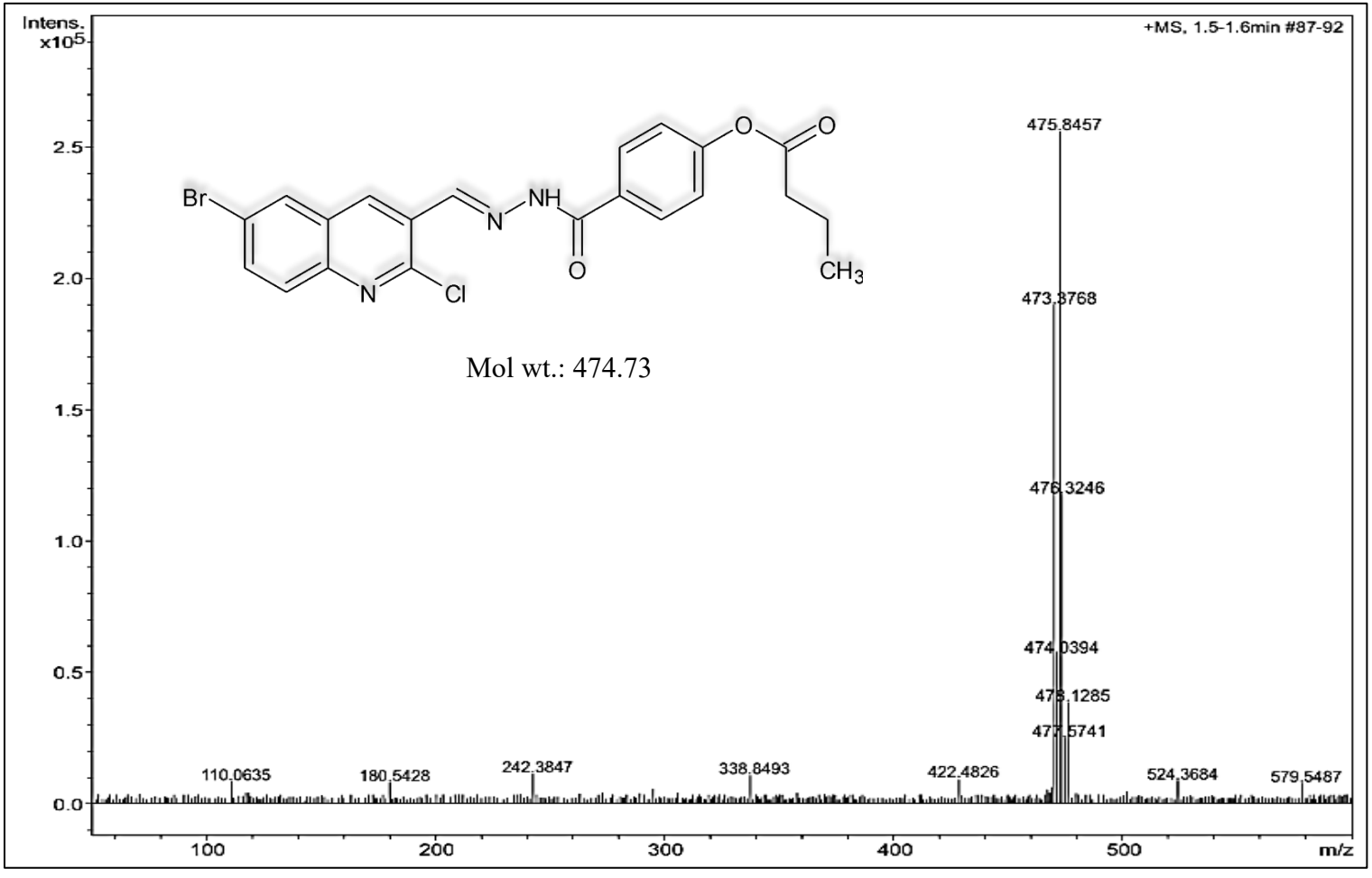

Figure 5.154: Mass spectrum of 4- {2-2- [(6-bromo-2-chloro quinolin-3-yl) methylidene] hydrazine carbonyl} phenyl butanoate (Compound 4r)

CHAPTER-VI

CONCLUSION

6: CONCLUSION

This study involved successful synthesis, biological evaluation, docking studies, and ADME predictions of a series of 6-substituted-2-chloroquinoline-3-carbaldehyde hydrazide ester derivatives.

The synthesis was carried out through a three-step pathway. In the first step, the quinoline core structure was synthesized using the Meth-Cohn reaction using substituted acetanilide with the Vilsmeier-Haack reagent. This step effectively introduced the 6-substituted-2-chloro-3-formyl groups on the quinoline scaffold. In the second step, hydrazide-hydrazone derivatives were formed by reacting 6-substituted-2-chloroquinoline-3-carbaldehyde with 4-hydroxybenzoic acid hydrazide under mild conditions. The third step involved the esterification of the hydrazones with acyl chlorides in the presence of zinc oxide, providing an efficient and eco-friendly route for formation of series of quinoline-based hydrazide esters.

The overall yields of the reactions were favourable, with the percentage yields ranging between 48% and 79%, depending on the specific substituents on the quinoline ring. These yields are consistent with efficient multi-step synthesis and indicate the practicality of scaling up the reactions for further development.

Physiochemical properties such as melting point, solubility, and TLC retention factor (Rf values) were determined for each compound, supporting their structural confirmation and purity. The IR, NMR, and mass spectrometry data further corroborated the successful formation of the intended products.

The anti-TB activity of the synthesized quinoline derivatives was one of the key biological assessments carried out in this study. The compounds were tested for their efficacy against *M. tuberculosis* using the Microplate Alamar Blue assay, which is a widely recognized method for evaluating anti-TB activity. The assay measures the

reduction of the blue dye resazurin to a pink, fluorescent compound by viable bacteria, which provides an indirect quantification of bacterial growth.

The synthesized quinoline derivatives 4a-4r exhibited promising anti-TB activity, with certain compounds showing exceptional potency. Notably, compounds 4m and 4r demonstrated significant anti-TB activity with a MIC of 6.25 µg/ml (comparable to standards) against *M. tuberculosis*. The presence of halogen substituents at specific positions on the quinoline ring showed enhanced activity, suggesting improved interactions with mycobacterial targets. Despite the potent anti-TB activity, compound 4r showed significant cytotoxicity in the MTT assay, limiting its therapeutic potential. Further structural modifications aimed at reducing cytotoxicity without affecting anti-TB activity could be considered for 4r. In addition, compounds 4n, 4o, 4p, and 4q exhibited good anti-TB activity with MIC values of 12.5 µg/ml, making them promising candidates for further development. The observed activity suggests that even slight modifications to the quinoline core, such as variation in chain length or halogen substitutions, can significantly impact biological efficacy.

Furthermore, antibacterial activity was evaluated against Gram-positive bacteria, including *S. aureus* and *B. subtilis* and Gram-negative bacteria including *K. pneumoniae* and *E. coli* using Broth Microdilution assay method. The results demonstrated that several compounds displayed significant antibacterial potency, with distinct activity profiles depending on the structural features and substitutions on the quinoline ring.

Against *S. aureus*, compounds 4f and 4r exhibited the most potent activity, with an MIC of 3.12 µg/ml, underscoring their strong potential as antibacterial agents. Additionally, compounds 4a, 4g, 4i and 4q displayed moderate activity with MIC values of 6.25 µg/ml, further highlighting the quinoline scaffold's versatility in combating bacterial infections.

With *B. subtilis*, compound 4r again showed strong antibacterial activity, with an MIC of 1.6 µg/ml, while compound 4p exhibited even more potent activity with an MIC of 0.8 µg/ml, marking it as one of the most effective compounds in this study. Compounds 4n and 4o also showed good antibacterial activity, with MIC values of 3.12 µg/ml.

For *K. pneumoniae*, compound 4r exhibited the lowest MIC of 12.5 µg/ml, demonstrating good antibacterial activity. This highlights the compound's broad-spectrum potential, as it was effective not only against Gram-positive bacteria but also against *K. pneumoniae*.

In the case of *E. coli*, compound 4o demonstrated the highest potency, with an MIC of 6.25 µg/ml, indicating its strong antibacterial activity against this pathogen. This was followed by compounds 4n, 4q, and 4r, all of which exhibited MIC values of 12.5 µg/ml, confirming their efficacy against *E. coli*.

The presence of halogen substituents (particularly chlorine and bromine) at the 2 and 6 positions of the quinoline ring was a key factor contributing to the enhanced antibacterial activity. Compounds with extended alkyl or ethoxy chains at position 6, as well as hydrazone linkages, showed broad-spectrum activity. These structural modifications likely improved membrane permeability and facilitated stronger interactions with bacterial targets.

- Compound 4r emerged as one of the most promising compounds, demonstrating broad-spectrum antibacterial activity across all four bacterial species, though its cytotoxicity warrants further modification for safety.
- Compounds 4n, 4o, 4p, and 4q also demonstrated a broad spectrum of antibacterial activity against Gram-positive and Gram-negative bacteria.
- Compound 4p showed exceptional activity against *B. subtilis*, while compound 4o was the most potent against *E. coli*.

- Compounds 4n, 4o, 4p, 4q and 4r showed significant antibacterial and anti-TB efficacy which underscores the potential of these quinoline derivatives as promising candidates for the treatment of multi-drug-resistant bacterial and tuberculosis infections, offering versatility in targeting a range of pathogens. Structural modifications of these compounds, particularly in reducing the cytotoxicity, could enhance their therapeutic potential.

The cytotoxicity of the synthesized compounds was assessed using the MTT assay in two cell lines: A549 (lung adenocarcinoma) and Vero cells (non-cancerous). This assay measures cell viability by converting MTT into formazan crystals, which can be quantified by spectrophotometry. Compounds such as 4r and 4m exhibited selective cytotoxicity, showing lower IC_{50} values in cancer cells compared to non-cancerous Vero cells, thereby indicating their potential for selective targeting in therapeutic applications. While compound 4r showed excellent anti-TB activity, it was found to be toxic, with a low IC_{50} value in both cancerous and non-cancerous cell lines, limiting its potential therapeutic application. On the other hand, compounds 4m and 4l exhibited strong anti-TB activity and low cytotoxicity, making them more viable candidates for further development. Microscopic analysis was also carried out to analyse effect of synthesized compounds on cell lines qualitatively.

The correlation between anti-TB activity and cytotoxicity suggests that while halogenated quinoline derivatives like 4r are potent, their toxicity profiles must be carefully managed. For compound 4r, structural modifications to reduce toxicity could include:

- Altering the halogen substitution pattern at the 2 or 6 positions.
- Incorporating more hydrophilic groups to decrease overall cytotoxicity while retaining anti-TB activity.

- Performing SAR studies to identify structural features contributing to both activity and toxicity, allowing for selective optimization.

Docking studies were conducted for the synthesized molecules 4a-4r using two enzymes, PanK and PyrG. Compounds such as 4k, 4o, 4l, and 4b exhibited strong binding affinities for MtPanK, indicated by their high C Scores and favourable D Scores. These compounds showed promising potential as inhibitors of MtPanK, with stable binding conformations and important interactions within the enzyme's active site. The Polar Scores for compounds like 4b and 4q suggest that hydrogen bonding and polar interactions played a significant role in their binding. Additionally, high Chem Scores for compounds such as 4k and 4r indicated strong chemical interactions, which further enhanced the binding stability. Given that PanK is a conserved enzyme across various bacterial species, the strong binding of these compounds suggested the potential for broad-spectrum antibacterial activity. Their inhibition of PanK could impair CoA biosynthesis, leading to bacteriostatic or bactericidal effects. The reference ligand (3AEZ_ligand) consistently showed strong binding affinity, serving as a reliable benchmark. However, compounds like 4k and 4b demonstrated competitive docking scores, making them promising candidates for further investigation.

With enzyme PyrG, the native ligand (4ZDJ_ligand) showed the highest binding affinity with a C Score of 13.17, validating the docking approach. However, synthesized compounds 4b, 4l, and 4o also showed strong binding affinities, suggesting they could act as effective inhibitors of PyrG. Compounds like 4b and 4f displayed strong polar interactions, as indicated by their high Polar Scores, and favourable Chem Scores. This suggests that these compounds form critical hydrogen bonds and other interactions with PyrG, stabilizing their binding within the enzyme's active site. Inhibiting PyrG could disrupt nucleotide biosynthesis, thereby impairing

bacterial RNA and DNA replication. Compounds like 4b and 4l showed promising docking results that could translate into potent inhibition of mycobacterial growth, making them potential candidates for developing antimycobacterial and broad-spectrum antibacterial agents. Structural differences between mycobacterial and human PyrG suggest the potential to design selective inhibitors. The docking results highlighted several synthesized compounds that could specifically target mycobacterial PyrG, reducing the risk of cytotoxicity in human cells.

Compounds 4k, 4o, 4l, and 4b emerged as top candidates for inhibiting both PanK and PyrG, two key enzymes essential for mycobacterial survival. Their strong binding affinities, supported by favourable polar and chemical interactions, suggest significant potential as antimycobacterial agents. These compounds could effectively target multiple mycobacterial pathways, disrupting CoA and nucleotide biosynthesis, thereby impairing mycobacterial growth and survival. Given the conserved nature of these enzymes across various bacterial species, these compounds hold promise for combating drug-resistant strains. While PanK and PyrG are present in humans, its structural differences provide a window for developing selective inhibitors that target bacterial enzymes without significant off-target effects on human cells. Further experimental validation, particularly correlating docking results with biological activity, will help confirm their therapeutic potential and selectivity for bacterial enzymes

ADME predictions conducted through SwissADME revealed several promising pharmacokinetic properties. Most compounds demonstrated high gastrointestinal absorption and lacked BBB permeability, making them suitable candidates for non-CNS-targeting therapies. Furthermore, none of the compounds were P-glycoprotein substrates, reducing the likelihood of efflux-mediated drug resistance. However, several compounds were predicted to inhibit multiple CYP enzymes (CYP1A2,

CYP2C9, CYP2C19, and CYP3A4), which could indicate potential for drug-drug interactions that may need to be managed in further clinical development. The Log S (ESOL) predictions indicated moderate to poor solubility across the series, a limitation that may need to be addressed in future formulations. On the other hand, the favourable Log Po/w values (between 2.89 and 3.73) suggested good membrane permeability, essential for oral bioavailability. The synthetic accessibility scores, ranging between 2.69 and 3.04, reflected the moderate complexity of the molecules, making them feasible for large-scale synthesis.

The quinoline derivatives synthesized in this study represent a promising class of compounds for antimicrobial and antitubercular therapies, with significant potential to combat multi-drug-resistant strains. The observed selective cytotoxicity also positions these molecules as candidates for anticancer therapy, especially for non-CNS cancers where blood-brain barrier penetration is not required. These compounds may offer a dual benefit as antimicrobial agents and anticancer drugs, addressing multiple therapeutic needs.

These findings are encouraging in the context of MDR and XDR TB, where there is an urgent need for new, effective therapies. The quinoline scaffold, already known for its antimicrobial properties, continues to show promise as a versatile structure for anti-TB drug development.

The development of anti-TB drugs with anticancer activity has shown promise, but it has not yet significantly impacted clinical practice. Although certain compounds demonstrate both anti-TB and anticancer properties, there has been limited progress in creating drugs specifically for treating both diseases concurrently. In regions with a high tuberculosis burden, cancer and TB frequently co-exist, particularly among immunocompromised populations (e.g., those with HIV/AIDS), making a dual-purpose drug potentially beneficial. However, most current anti-TB drugs were not

designed with dual activity, and treating co-morbidities requires careful management due to potential drug interactions and overlapping toxicities. The challenge is to balance anti-TB effectiveness with the selective cytotoxicity needed for cancer treatment. While some drugs show dual activity *in vitro*, their efficacy and toxicity *in vivo* require thorough evaluation.

In conclusion, this study successfully synthesized, characterized, and evaluated a new series of quinoline-based hydrazide ester derivatives with potent biological activity. The compounds demonstrated good pharmacokinetic profiles and selective cytotoxicity, making them suitable candidates for further optimization in drug discovery.

CHAPTER-VII

FUTURE SCOPE

7: FUTURE SCOPE

This study has laid a foundation for understanding the anti-TB, antibacterial, and cytotoxic properties of Ester derivatives of 6-substituted-2-chloroquinoline-3-carbaldehyde hydrazide derivatives (4a–4r) in both cancerous and non-cancerous cell lines.

To further develop these compounds as potential therapeutic agents, several avenues of research can be explored –

- **Expansion of Antimicrobial Spectrum**: Future studies should aim to evaluate the effectiveness of these compounds against a wider range of bacterial species, including both Gram-positive and Gram-negative bacteria, as well as drug-resistant strains such as MRSA and multidrug-resistant *M. tuberculosis*. This would help establish the broad-spectrum antibacterial and anti-TB potential of the compounds.
- **Mechanistic Studies on Antibacterial and Anti-TB Activity**: It will be crucial to investigate mechanism of action of synthesized compounds to understand their antibacterial and anti-TB effects. Studies focusing on how these compounds inhibit bacterial growth or interact with key bacterial enzymes and cellular processes will help refine their development as targeted antibacterial or anti-TB drugs.
- ***In vivo* Efficacy and Toxicity**: The *in vitro* results indicate promising activity, but further *in vivo* studies in animal models are essential to confirm the anti-TB, antibacterial, and cytotoxic effects. These studies should assess pharmacokinetics, bioavailability, and systemic toxicity to establish dosing regimens and therapeutic windows.
- **Synergistic Effects**: Investigating the potential synergistic effects of the synthesized compounds when used in combination with existing antibiotics or

anti-TB drugs could provide a pathway to more effective treatments, especially for drug-resistant infections. Combination therapy studies may reveal enhanced efficacy and lower resistance development in bacterial and TB treatments.

- **Structure-Activity Relationship for Optimization**: SAR studies should be conducted to understand structural features that are responsible for the anti-TB, antibacterial, and cytotoxic properties of the compounds. Modifications to these structures could lead to the optimization of the compounds, enhancing their efficacy while minimizing unwanted cytotoxic effects.
- **Cytotoxicity Focus for Selective Therapy**: While the primary focus is on anti-TB and antibacterial activities, compounds exhibiting cytotoxicity in cancerous cells should be further explored for their potential dual applications. Understanding the balance between antimicrobial and cytotoxic effects could open avenues for developing multifunctional compounds that selectively target infections and certain cancer cells, especially in patients with immune-compromising conditions.
- **Formulation Development**: To enhance the solubility, stability and delivery of these compounds, it is essential to develop an appropriate formulation. Drug delivery technologies such as encapsulation in nanoparticles or liposomal formulations could enhance the bioavailability and therapeutic index of these compounds for both antibacterial and anti-TB applications.

Pursuing these research directions, the synthesized compounds (4a–4r) have the potential to contribute to the development of novel anti-TB, antibacterial, and possibly anticancer therapies, addressing the growing challenge of drug-resistant infections and multifaceted disease conditions.

REFERENCES

REFERENCES

1. Minnikin DE. Lipids: Complex lipids, their chemistry, biosynthesis and roles. In: Ratledge C, Stanford J, editors. The biology of the mycobacteria. Vol. 1. Academic Press Inc. Ltd; 1982. p. 95-184.
2. Cole ST, Brosch R, Parkhill J, Garnier T, Churcher C, Harris D, et al. Deciphering the biology of Mycobacterium tuberculosis from the complete genome sequence. Nature. 1998;396(6707):537-44. doi:10.1038/25092.
3. Fitzgerald DW, Sterling TR, Haas DW, Chaisson RE. Tuberculosis. In: Goodman LS, Gilman A, editors. Goodman & Gilman's: The Pharmacological Basis of Therapeutics. 12th ed. McGraw-Hill Education; 2010. p. 1565-605.
4. Hameed HMA, Islam MM, Chhotaray C, Wang C, Liu Y, Tan Y, et al. Molecular targets related to drug resistance mechanisms in MDR-, XDR-, and TDR-Mycobacterium tuberculosis strains. Front Cell Infect Microbiol. 2018;8:114. doi:10.3389/fcimb.2018.00114.
5. World Health Organization. Global tuberculosis report 2020 [Internet]. 2020 [cited 2024 Nov 5]. Available from: https://www.who.int/publications/i/item/9789240013131.
6. World Health Organization (WHO). Global tuberculosis report 2021. World Health Organization; 2021. Available from: https://apps.who.int/iris/handle/10665/346387.
7. Anishetty S, Pulimi M, Pennathur G. Potential drug targets in Mycobacterium tuberculosis through metabolic pathway analysis. Comput Biol Chem. 2005;29(5):368-78. doi:10.1016/j.compbiolchem.2005.09.002.
8. Belete TM. Novel targets to develop new drugs for combating Mycobacterium tuberculosis: A review. Infect Drug Resist. 2022;15:413-29. doi:10.2147/IDR.S351014.

9. Slayden RA, Barry CE. The role of KasA and KasB in the biosynthesis of meromycolic acids and isoniazid resistance in Mycobacterium tuberculosis. Tuberculosis. 2002;82(4):149-60. doi:10.1054/tube.2002.0335.
10. Gualano G, Capone S, Matteelli A, Palmieri F. New antituberculosis drugs: From clinical trial to programmatic use. Infect Dis Rep. 2016;8(2):6569. doi:10.4081/idr.2016.6569.
11. Espinal MA. The global situation of MDR-TB. Tuberculosis. 2003;83(1):44-51. doi:10.1016/S1472-9792(02)00057-6.
12. Amalio T, Michael I. Drug-resistant tuberculosis: What do we do now? Drugs. 2000;59(2):171-9. doi:10.2165/00003495-200059020-00005.
13. Reddy BKK, Rao NVSS, Prasad NS, Kumar PS, Lakshmi N. Anti-tubercular and anti-oxidant activities of novel pyrazole analogues. J Saudi Chem Soc. 2014;18(1):211-8. doi:10.1016/j.jscs.2011.05.015.
14. Shu W, Zhao X, Huang D, Zhang S, Zhang H, Lin Z. Evaluation of novel quinoxaline derivatives as anti-tubercular agents. Bioorg Med Chem Lett. 2019;29(10):1206-11. doi:10.1016/j.bmcl.2019.02.022.
15. Farhat MR, Jacobson KR, Franke MF, Kaur D, Sloutsky A, Murray M, et al. Gyrase mutations are associated with variable levels of fluoroquinolone resistance in Mycobacterium tuberculosis. J Clin Microbiol. 2016;54(3):727-33. doi:10.1128/jcm.02775-15.
16. Nagaraja V, Godbole AA, Henderson SR, Maxwell A. DNA topoisomerase I and DNA gyrase as targets for TB therapy. Drug Discov Today. 2016;21(8):1340-6. doi:10.1016/j.drudis.2016.11.006.
17. Abrahams KA, Besra GS. Mycobacterial cell wall biosynthesis: A multifaceted antibiotic target. Parasitology. 2016;1-18. doi:10.1017/S0031182016002377.
18. Patel S, Sen AK, Dash DK, Kumari M, Baile S, Singh VR, Jain S. A review on tuberculosis and its chemotherapeutic agents. In: Chemotherapeutic Approaches

to Tuberculosis. British Publishing Institute; 2024. p. 145-65. doi:10.9734/bpi/mono/978-81-19315-51-2/CH10.

19. Enarson DA, Chretien J. Epidemiology of respiratory infectious diseases. Curr Opin Pulm Med. 1999;5(2):128-35. doi:10.1097/00063198-199903000-00008.
20. Dony JF, Ahmad J, Khen TY. Epidemiology of tuberculosis and leprosy in Sabah, Malaysia. Tuberculosis. 2004;84(1-2):8-18. doi:10.1016/j.tube.2003.06.002.
21. Walters SB, Dubnau E, Kolesnikova I, Laval F, Daffé M, Smith I. The Mycobacterium tuberculosis PhoPR two-component system regulates genes essential for virulence and complex lipid biosynthesis. Mol Microbiol. 2006;60(2):312-30. doi:10.1111/j.1365-2958.2006.05102.x.
22. Turenne CY, Tschetter L, Wolfe J, Kabani A. Necessity of quality-controlled 16S rRNA gene sequence databases: Identifying nontuberculous Mycobacterium species. J Clin Microbiol. 2001;39(10):3637-48. doi:10.1128/JCM.39.10.3637-3648.2001.
23. Chatterjee D, Khoo KH, McNeil MR, Dell A, Morris HR, Brennan PJ. Structural definition of the non-reducing termini of mannose-capped LAM from Mycobacterium tuberculosis through selective enzymatic degradation and fast atom bombardment-mass spectrometry. Glycobiology. 1993;3(5):497-500. doi:10.1093/glycob/3.5.497.
24. Ahmad S, Mokaddas E. Recent advances in the diagnosis and treatment of multidrug-resistant tuberculosis. Respir Med. 2009;103(12):1777-90. doi:10.1016/j.rmed.2009.07.010.
25. Nahid P, Pai M, Hopewell PC. Advances in the diagnosis and treatment of tuberculosis. Proc Am Thorac Soc. 2006;3(1):103-10. doi:10.1513/pats.200511-119JH.

26. Velayati AA, Farnia P, Masjedi MR. The totally drug-resistant tuberculosis (TDR-TB). Int J Clin Exp Med. 2013;6(4):307-9.
27. Capela R, Félix R, Clariano M, Nunes D, Perry MJ, Lopes F. Target identification in anti-tuberculosis drug discovery. Int J Mol Sci. 2023;24(13):10482. doi:10.3390/ijms241310482.
28. World Health Organization. Global tuberculosis programme: WHO report on the tuberculosis epidemic 1997 [Internet]. 1997 [cited 2024 Nov 5]. Available from: https://apps.who.int/iris/handle/10665/63622.
29. Barry CE. New horizons in the treatment of tuberculosis. Biochem Pharmacol. 1997;54(10):1165-72. doi:10.1016/S0006-2952(97)00319-7.
30. Tomasz A. Multiple-antibiotic-resistant pathogenic bacteria: A report on the Rockefeller University Workshop. N Engl J Med. 1994;330(17):1247-51. doi:10.1056/NEJM199404283301712.
31. World Health Organization (WHO). Global tuberculosis report 2022. World Health Organization; 2022. Available from: https://www.who.int/publications/i/item/9789240061729.
32. Clatworthy AE, Pierson E, Hung DT. Targeting virulence: A new paradigm for antimicrobial therapy. Nat Chem Biol. 2007;3(9):541-8. doi:10.1038/nchembio.2007.24.
33. Koul A, Arnoult E, Lounis N, Guillemont J, Andries K. The challenge of new drug discovery for tuberculosis. Nature. 2011;469(7331):483-90. doi:10.1038/nature09657.
34. Barry CE, Slayden RA, Sampson AE, Lee RE. Use of genomics and combinatorial chemistry in the development of new antimycobacterial drugs. Biochem Pharmacol. 2000;59(3):221-31. doi:10.1016/S0006-2952(99)00279-8.

35. Silva PE, Palomino JC, Ramos DF. New drugs for the treatment of tuberculosis: Hope and reality on the horizon. Rev Inst Med Trop Sao Paulo. 2013;55(Suppl 1):69-83. doi:10.1590/S0036-46652013000700011.
36. Singh R, Manjunatha U, Boshoff HI, Barry CE. Developing new drugs for tuberculosis treatment. Trends Microbiol. 2020;28(12):1027-40. doi:10.1016/j.tim.2020.06.003.
37. Wu S, Zhang Y, Liu X, Zhao Y, Sun Z. Distribution of mutations in the rpoB gene among Mycobacterium tuberculosis isolates with high-level rifampin resistance. J Clin Microbiol. 2011;49(7):2542-4. doi:10.1128/JCM.00112-11.
38. Yan Q, Li X, Zhang Z, Xu X, Wu Y. Exploring potential inhibitors against Mycobacterium tuberculosis DprE1: A molecular docking and molecular dynamics study. J Biomol Struct Dyn. 2022;40(3):1075-87. doi:10.1080/07391102.2020.1840455.
39. Kaneko T, Cooper C, Mdluli K. Challenges and opportunities in developing novel drugs for tuberculosis. Future Med Chem. 2011;3(11):1373-400. doi:10.4155/fmc.11.115.
40. Umumararungu T, Mukazayire MJ, Mpenda M, Mukanyangezi MF, Nkuranga JB, Mukiza J, Olawode EO. A review of recent advances in anti-tubercular drug development. Indian J Tuberc. 2020;67(4):479-86. doi:10.1016/j.ijtb.2020.07.017.
41. Favrot L, Ronning DR, North EJ. Synthesis and biological evaluation of small molecule inhibitors of Mycobacterium tuberculosis MurA. Bioorg Med Chem. 2012;20(11):3254-61. doi:10.1016/j.bmc.2012.03.040.
42. Huszár S, Szádocka S, Chiarelli LR, de Jesus Lopes Ribeiro AL, Orena BS, Esposito M, et al. Mycobacterium tuberculosis DprE1—A vulnerable enzyme with variable susceptibility. J Med Chem. 2020;63(4):1875-91. doi:10.1021/acs.jmedchem.9b01390.

43. Li SY, Zhang SJ, Wang Y, Li XL, Yang LX, Zhang L. In vitro and in vivo activities of the oxazolidinone derivative sutezolid (PNU-100480) against Mycobacterium tuberculosis. Antimicrob Agents Chemother. 2014;58(11):5844-51. doi:10.1128/AAC.02919-14.
44. Mi Y, Zhang Z, Nie Q, Guo X. Novel targets in Mycobacterium tuberculosis identified by genome-based screening and synthetic lethality analysis. J Microbiol Methods. 2022;191:106397. doi:10.1016/j.mimet.2021.106397.
45. Mori G, Degiacomi G, Bellinzoni M, Sorace J, Rajan AJ, Pasca MR, et al. Inhibition of Mycobacterium tuberculosis ATP synthase by bedaquiline: Can we optimize for better selectivity and potency? J Biol Chem. 2016;291(9):4903-12. doi:10.1074/jbc.M115.700120.
46. Villemagne B, Crauste C, Flipo M, Baulard AR, Déprez B, Willand N. Tuberculosis: The drug development pipeline at a glance. Eur J Med Chem. 2012;51:1-16. doi:10.1016/j.ejmech.2012.02.033.
47. Shetye D, Ranjan R, Suresh V. The murE gene as a novel therapeutic target in Mycobacterium tuberculosis. J Mol Biol. 2020;432(9):2966-77. doi:10.1016/j.jmb.2020.01.016.
48. Singh V, Mizrahi V, Warner DF. TB drug discovery in the post-genomic era. EMBO Mol Med. 2016;8(7):739-58. doi:10.15252/emmm.201505981.
49. Borsari C, Ferrari S, Venturelli A, Costi MP. Target-based approaches for the discovery of new antimycobacterial drugs. Drug Discov Today. 2016;22(1):1-15. doi:10.1016/j.drudis.2016.11.014.
50. Dutta NK, Pinn ML, Karakousis PC. Reduced efficacy of Pyrazinamide and other drugs in granulomatous lesions of murine tuberculosis. Antimicrob Agents Chemother. 2016;60(8):4701-9. doi:10.1038/nature09657.

51. Jain A, Mondal R. Extensively drug-resistant tuberculosis: Current challenges and threats. FEMS Immunol Med Microbiol. 2008;53(2):145-50. doi:10.1111/j.1574-695X.2008.00400.x.
52. Islam MM, Hameed HMA, Chhotaray C, Wang C, Tan Y, Liu Z, et al. Drug resistance mechanisms and novel drug targets for tuberculosis therapy. J Genet Genomics. 2016;43(7):371-84. doi:10.1016/j.jgg.2016.05.003.
53. Mdluli K, Kaneko T, Upton A. The tuberculosis drug discovery and development pipeline and emerging drug targets. Cold Spring Harb Perspect Med. 2006;5(6). doi:10.1101/cshperspect.a017947.
54. Manina G, Pasca MR, Buroni S, De Rossi E, Riccardi G. Decaprenylphosphoryl-β-D-ribose 2'-epimerase from Mycobacterium tuberculosis is a magic drug target. Curr Med Chem. 2010;17(27):3099-108. doi:10.2174/092986710793348613.
55. Azam MA, Jayaram U. Inhibitors of alanine racemase enzyme: A review. J Enzyme Inhib Med Chem. 2015;30(6):869-77. doi:10.3109/14756366.2015.1050010.
56. Anthony KG, Strych U, Yeung KR, Shoen CS, Perez O, Krause KL. New classes of alanine racemase inhibitors identified by high-throughput screening show antimicrobial activity against Mycobacterium tuberculosis. PLoS One. 2011;6(5) doi:10.1371/journal.pone.0020374.
57. Koehn EM, Kohen A. Flavin-dependent thymidylate synthase: a novel pathway towards thymine. Arch Biochem Biophys. 2016;493(1):96-102. doi:10.1016/j.abb.2009.07.016.
58. Olaleye O, Raghunand TR, Bhat S, He J, Tyagi S, Lamichhane G, et al. Methionine aminopeptidases from Mycobacterium tuberculosis as novel antimycobacterial targets. Chem Biol. 2010;17(1):86-97. doi:10.1016/j.chembiol.2009.12.014.

59. Novoa-Aponte L, Soto Ospina CY. Mycobacterium tuberculosis P-type ATPases: Possible targets for drug or vaccine development. Biomed Res Int. 2014;2014 ID 296986. doi:10.1155/2014/296986.

60. Sridharan S, Wang L, Brown AK, Dover LG, Kremer L, Besra GS, et al. X-ray crystal structure of Mycobacterium tuberculosis β-ketoacyl acyl carrier protein synthase II (mtKasB). J Mol Biol. 2007;366(2):469-80. doi:10.1016/j.jmb.2006.11.006.

61. Teneva Y, Simeonova R, Valcheva V, Angelova VT. Recent advances in anti-tuberculosis drug discovery based on hydrazide–hydrazone and thiadiazole derivatives targeting InhA. Pharmaceuticals. 2023;16(4):484. doi:10.3390/ph16040484.

62. Hartkoorn RC, Sala C, Neres J, Pojer F, Magnet S, Mukherjee R, et al. Towards a new tuberculosis drug: Pyridomycin – Nature's isoniazid. EMBO Mol Med. 2012;4(9):1032-42. doi:10.1002/emmm.201201689.

63. Wang S, Eisenberg D. Crystal structure of the pantothenate synthetase from Mycobacterium tuberculosis: Snapshots of the enzyme in action. Biochemistry. 2006;45(6):1554-61. doi:10.1021/bi051873e.

64. Parandhaman DK, Hanna LE, Narayanan S. PknE, a serine/threonine protein kinase of Mycobacterium tuberculosis initiates survival crosstalk that also impacts HIV coinfection. PLoS One. 2014;9(1). doi:10.1371/journal.pone.0083541.

65. Prisic S, Husson RN. Mycobacterium tuberculosis serine/threonine protein kinases. Microbiol Spectr. 2014;2(5). doi:10.1128/microbiolspec.MGM2-0006-2013.

66. Soni V, Suryadevara P, Sriram D, Kumar S, Nandicoori VK, Yogeeswari P. Structure-based design of diverse inhibitors of Mycobacterium tuberculosis N-acetylglucosamine-1-phosphate uridyltransferase: Combined molecular

docking, dynamic simulation, and biological activity. J Mol Model. 2015;21(6):174. doi:10.1007/s00894-015-2704-3.

67. Grzegorzewicz AE, Pham H, Gundi VAKB, Scherman MS, North EJ, Hess T, et al. Inhibition of mycolic acid transport across the Mycobacterium tuberculosis plasma membrane. Nat Chem Biol. 2012;8(4):334-41. doi:10.1038/nchembio.794.
68. Pichota A, Duraiswamy J, Yin Z, Keller TH, Alam J, Liung S, et al. Peptide deformylase inhibitors of Mycobacterium tuberculosis: Synthesis, structural investigations, and biological results. Bioorg Med Chem Lett. 2008;18(24):6568-72. doi:10.1016/j.bmcl.2008.10.040.
69. Chiarelli LR, Mori G, Orena BS, Esposito M, Lane T, de Jesus Lopes Ribeiro AL, et al. A multitarget approach to drug discovery inhibiting Mycobacterium tuberculosis PyrG and PanK. Sci Rep. 2018;8:3187. doi:10.1038/s41598-018-21614-4.
70. Ejalonibu MA, Elrashedy AA, Lawal MM, Kumalo HM, Mhlongo NN. Probing the dual inhibitory mechanisms of novel thiophene carboxamide derivatives against Mycobacterium tuberculosis PyrG and PanK: An insight from biomolecular modeling study. J Biomol Struct Dyn. 2020. doi:10.1080/07391102.2020.1844055.
71. Thangadurai R, Nagarajan K, Manjula P, Anand A. A review of anti-tubercular drugs with emphasis on multidrug-resistant Mycobacterium tuberculosis. J Mol Graph Model. 2022;109:108086. doi:10.1016/j.jmgm.2022.108086.
72. Suvvari S, Reddy AS, Venkatraman R. Targeting Mycobacterium tuberculosis growth using host-directed therapies: A new perspective on drug discovery. Infect Drug Resist. 2023;16:4321-33. doi:10.2147/IDR.S377497.
73. Martins LM, Moreno VF, Rosário IS, Graeff CFO, Silva Filho LC. Brønsted acid mediated facile greener multicomponent synthesis of 2,4-diaryl-quinoline

derivatives in water. Orbital Electron J Chem. 2021;14(1):1-9. doi:10.17807/orbital.v14i1.1689.

74. Abdel-Wahab BF, Khidre RE. 2-Chloroquinoline-3-carbaldehyde II: Synthesis, reactions, and applications. J Chem. 2013;2013 ID 851297. doi:10.1155/2013/851297.
75. Joule J, Mills K. Heterocyclic chemistry. 5th ed. Wiley; 2010.
76. Marella A, Tanwar OP, Saha R, Ali MR, Srivastava S, Akhter M, et al. Quinoline: A versatile heterocyclic. Saudi Pharm J. 2013;21(1):1-12. doi:10.1016/j.jsps.2012.03.002.
77. Chinh PT, Tham PT, Tuyen NV, Quynh DH, Van DT, Bang DN, et al. Synthesis of several 2-carbaldehyde derivatives of quinoline and 1,4-dihydroquinoline. Vietnam J Chem. 2020;58(3):309-13. doi:10.1002/vjch.2019000166.
78. Beyzaei H, Moghadam HH, Bagherzade G, Aryan R, Moghaddam-Manesh M. Synthesis and in vitro antibacterial evaluation of Schiff bases derived from 2-chloro-3-quinolinecarboxaldehyde. Avicenna J Med Biochem. 2019;7(1):9-15. doi:10.34172/ajmb.2019.03.
79. Heydari M, Mohammadi AA, Mosleh MR. DABCO-catalyzed highly regioselective synthesis of novel 4H-pyrano[2,3-b]quinoline derivatives: One-pot three-component reaction. J Heterocycl Chem. 2024;61(9):1446-54. doi:10.1002/jhet.4862.
80. Forozan R, Khalili Ghomi M, Iraji A, Montazer MN, Noori M, Dastyafteh N, et al. Synthesis, in vitro inhibitor screening, structure–activity relationship, and molecular dynamic simulation studies of novel thioquinoline derivatives as potent α-glucosidase inhibitors. Sci Rep. 2023;13:7819. doi:10.1038/s41598-023-35140-5.
81. Elkaeed EB, Taghour MS, Mahdy HA, Eldehna WM, El-Deeb NM, Kenawy AM, et al. New quinoline and isatin derivatives as apoptotic VEGFR-2

inhibitors: Design, synthesis, anti-proliferative activity, docking, ADMET, toxicity, and MD simulation studies. J Enzyme Inhib Med Chem. 2022;37(1):2191-205. doi:10.1080/14756366.2022.2110869.

82. Murugan K, Panneerselvam C, Subramaniam J, Paulpandi M, Rajaganesh R, Vasanthakumaran M, et al. Synthesis of new series of quinoline derivatives with insecticidal effects on larval vectors of malaria and dengue diseases. Sci Rep. 2022;12:4765. doi:10.1038/s41598-022-08397-5.
83. Zaib S, Munir R, Younas MT, Kausar N, Ibrar A, Aqsa S, et al. Hybrid Quinoline-Thiosemicarbazone Therapeutics as a New Treatment Opportunity for Alzheimer's Disease-Synthesis, In Vitro Cholinesterase Inhibitory Potential and Computational Modeling Analysis. Molecules. 2021; 26(21):6573. doi:10.3390/molecules26216573.
84. Pokalwar RU. Solvent-free and high-yielding synthesis of new dimethyl 1-(2-chloroquinolin-3-yl)-2,2-dicyanoethylphosphonate from 2-chloroquinoline-3-carbaldehyde. J Emerg Technol Innov Res. 2020;7(3):238-41.
85. Kovalenko SM, Drushlyak OG, Shishkina SV, Konovalova IS, Mariutsa IO, Bunyatyan ND, et al. Methylation of methyl 4-hydroxy-2-thioxo-1,2-dihydroquinoline-3-carboxylate: Synthetic, crystallographic, and molecular docking studies. Molecules. 2020;25(18):4238. doi:10.3390/molecules25184238.
86. Tabassum R, Ashfaq M, Oku H. 7-Hydroxy-4-phenyl-1,2-dihydroquinoline derivatives: Synthesis via one-pot, three-component reaction and structure elucidation. Heliyon. 2020;6(7). doi:10.1016/j.heliyon.2020.e05035.
87. Rocha DHA, Batista VF, Balsa EJF, Pinto DCGA, Silva AMS. Chromene- and quinoline-3-carbaldehydes: Useful intermediates in the synthesis of heterocyclic scaffolds. Molecules. 2020;25(17):3791. doi:10.3390/molecules25173791.

88. Farooq S, Mazhar A, Ghouri A, Ihsan-Ul-Haq, Ullah N. One-pot multicomponent synthesis and bioevaluation of tetrahydroquinoline derivatives as potential antioxidants, α-amylase enzyme inhibitors, anti-cancerous, and anti-inflammatory agents. Molecules. 2020;25(11):2710. doi:10.3390/molecules25112710.
89. Moghaddam FM, Moafi A, Ziadkhani A, Daneshfar M, Razaghdoost N. A facile and efficient route for the synthesis of thiopyranoquinolines-fused indole moiety using 2-chloroquinoline-3-carbaldehydes. ChemistrySelect. 2019;4(40):11683-6. doi:10.1002/slct.201902476.
90. Hackler L Jr, Gyuris M, Huzián O, Alföldi R, Szebeni GJ, Madácsi R, et al. Enantioselective Synthesis of 8-Hydroxyquinoline Derivative, Q134 as a Hypoxic Adaptation Inducing Agent. Molecules. 2019;24(23):4269. doi:10.3390/molecules24234269.
91. Radini IAM, Elsheikh TMY, El-Telbani EM, Khidre RE. New potential antimalarial agents: Design, synthesis and biological evaluation of some novel quinoline derivatives as antimalarial agents. Molecules. 2016;21(7):909. doi:10.3390/molecules21070909.
92. Puskullu MO, Shirinzadeh H, Nenni M, Gurer-Orhan H, Suzen S. Synthesis and evaluation of antioxidant activity of new quinoline-2-carbaldehyde hydrazone derivatives: Bioisosteric melatonin analogues. J Enzyme Inhib Med Chem. 2015;30(3):492-8. doi:10.3109/14756366.2015.1005012.
93. Pereira GR, Brandão GC, Arantes LM, Oliveira Júnior HA, de Paula RC, do Nascimento MFA, et al. 7-Chloroquinolinotriazoles: Synthesis by the azide-alkyne cycloaddition click chemistry, antimalarial activity, cytotoxicity, and SAR studies. Eur J Med Chem. 2013. doi:10.1016/j.ejmech.2013.11.022.
94. Mallandur BK, Rangaiah G, Harohally NV. Synthesis and antimicrobial activity of Schiff bases derived from 2-chloroquinoline-3-carbaldehyde and its

derivatives incorporating 7-methyl-2-propyl-3H-benzimidazole-5-carboxylic acid hydrazide. Synth Commun. 2017;47(9):884-95. doi:10.1080/00397911.2017.1309668.

95. Suryanarayana K, Gangu KK, Kerru N, Khatana K, Satyanarayana B, Maddila S. Synthesis of a novel chloroquinoline, rhodanine encompassed 1,2,3-triazole scaffolds and molecular docking evaluation of their cytotoxicity. J Iran Chem Soc. 2023;20:2643-55. doi:10.1007/s13738-023-02862-2.
96. Shui H, Zhong Y, Luo R, Zhang Z, Huang J, Yang P, Luo N. Cyclometalated iridium complexes-catalyzed acceptorless dehydrogenative coupling reaction: Construction of quinoline derivatives and evaluation of their antimicrobial activities. Beilstein J Org Chem. 2022;18:1507-17. doi:10.3762/bjoc.18.159.
97. Nagamani M, Vishnu T, Jalapathi P, Srinivas M. Molecular docking studies on COVID-19 and antibacterial evaluation of newly synthesized 4-(methoxymethyl)-1,2,3-triazole analogues derived from (E)-1-phenyl-3-(2-(piperidin-1-yl)quinolin-3-yl) prop-2-en-1-one. J Iran Chem Soc. 2022;19(5):1049-60. doi:10.1007/s13738-021-02365-y.
98. Fekadu G, Zeleke D, Abdi B, Guttula A, Eswaramoorthy R, Melaku Y. Synthesis, in silico molecular docking analysis, pharmacokinetic properties, and evaluation of antibacterial and antioxidant activities of fluoroquinolines. BMC Chem. 2022;16(1):1-18. doi:10.1186/s13065-022-00795-0.
99. Lagdhir M, Pandya C, Pandya A, Vekariya RH, Rajani DP. Design and synthesis of new quinoline hybrid derivatives and their antimicrobial, antimalarial, and antitubercular activities. Indian J Chem. 2021;60B:986-98.
100. Zeleke D, Melaku Y, Belay Z, Eswaramoorthy R. Synthesis, molecular docking analysis, and evaluation of antibacterial and antioxidant properties of stilbenes and pinacol of quinolines. Adv Pharmacol Pharm Sci. 2021;2021 ID 6635270. doi:10.1155/2021/6635270.

101. Guje PB, Chidrawar AB, Patwari SB, Madje BR, Rajani DP, Sangshetti JN, et al. Synthesis, molecular docking, antibacterial & antifungal activity study of novel 3-((1H-benzo[d]imidazol-2-ylthio)methyl)-2-chloroquinoline derivatives. Chem Biol Interface. 2020;10(6):149-57.
102. Cieslik W, Szczepaniak J, Krasowska A, Musiol R. Antifungal styryloquinolines as Candida albicans efflux pump inhibitors: Styryloquinolines are ABC transporter inhibitors. Molecules. 2020;25(2):345. doi:10.3390/molecules25020345.
103. Muthukumar K, Velmurugan K, Derin TD, Rajesh P, Rajesh Kannan V, Nandhakumar R. Synthesis, characterization, antibacterial, and antioxidant studies of oxetoquinolines. MOJ Bioorg Org Chem. 2019;3(2):38-43. doi:10.15406/mojboc.2019.03.00096.
104. Krawczyk M, Pastuch-Gawołek G, Hadasik A, Erfurt K. 8-Hydroxyquinoline glycoconjugates containing sulfur at the sugar anomeric position—Synthesis and preliminary evaluation of their cytotoxicity. Molecules. 2019;25(18):4174. doi:10.3390/molecules25184174.
105. Aboelnaga A, EL-Sayed TH. Click synthesis of new 7-chloroquinoline derivatives by using ultrasound irradiation and evaluation of their biological activity. Green Chem Lett Rev. 2018;11(3):254-63. doi:10.1080/17518253.2018.1473505.
106. Korcz A, Maślanka A, Lipka K, Grabarczyk M, Plech T. Synthesis and antimicrobial activity of quinoline derivatives incorporating imidazole rings. Monatsh Chem. 2018;149(12):2395-403. doi:10.1007/s00706-018-2308-0.
107. El-Gamal KMA, Sherbiny FF, El-Morsi AM, Abu-El-khair HE, Eissa IH, El-Sebaei MM. Design, synthesis and antimicrobial evaluation of some novel quinoline derivatives. Pharm Pharmacol Int J. 2015;2(5):165-77. doi:10.15406/ppij.2015.02.00036.

108. Miniyar PB, Barmade MA, Mahajan AA. Synthesis and biological evaluation of 1-(5-(2-chloroquinolin-3-yl)-3-phenyl-1H-pyrazol-1-yl)ethanone derivatives as potential antimicrobial agents. J Saudi Chem Soc. 2015;19(6):655-60. doi:10.1016/j.jscs.2013.12.004.
109. Mathew B, Ross L, Reynolds RC. A novel quinoline derivative that inhibits mycobacterial FtsZ. Tuberculosis. 2013;93(6):1-3. doi:10.1016/j.tube.2013.04.002.
110. Thomas KD, Adhikari AV, Telkar S, Chowdhury IH, Mahmood R, Pal NK, et al. Design, synthesis, and docking studies of new quinoline-3-carbohydrazide derivatives as antitubercular agents. Eur J Med Chem. 2011;46(12):5283-92. doi:10.1016/j.ejmech.2011.07.033.
111. Kumar S, Bawa S, Drabu S, Panda BP. Design and synthesis of 2-chloroquinoline derivatives as non-azole antimycotic agents. Med Chem Res. 2011;20(8):1340-8. doi:10.1007/s00044-010-9463-6.
112. Reddy LV, Nallapati SB, Beevi SS, Mangamoori LN, Mukkanti K, Pal S. A "Green" Synthesis of N-(Quinoline-3-ylmethylene)benzohydrazide Derivatives and their Cytotoxicity Activities. J Braz Chem Soc. 2011;22(9):1742-9. doi:10.1590/S0103-50532011000900018.
113. Eswaran S, Adhikari AV, Chowdhury IH, Pal NK, Thomas KD. New quinoline derivatives: Synthesis and investigation of antibacterial and antituberculosis properties. Eur J Med Chem. 2010;45(9):3374-83. doi:10.1016/j.ejmech.2010.04.022.
114. El-Helw EAE, Asran M, Azab ME, Helal MH, Ramadan SK. Synthesis and in silico studies of certain benzo[f]quinoline-based heterocycles as antitumor agents. Sci Rep. 2024;14(1):15522. doi:10.1038/s41598-024-64785-z.
115. Muthiah GRP, Solomon VR, Hemavathy N, Jeyakanthan J, Kumar D, Mahesh J. Design, synthesis, in silico, and pharmacological evaluation of novel

quinoline derivatives containing substituted piperazine moieties as potential anti-breast cancer agents. Results Chem. 2024;7:101359. doi:10.1016/j.rechem.2024.101359.

116. El-Mernissi R, El Khatabi K, Khaldan A, Bouamrane S, El Mchichi L, Ajana MA, et al. Designing of Novel Quinoline Derivatives as Hepatocellular Carcinoma Inhibitors by Using In silico Approaches. Biointerface Res Appl Chem. 2023;13(3):217. doi:10.33263/BRIAC133.217.
117. Sharma S, Singh S. Molecular docking study for binding affinity of 2H-thiopyrano[2,3-b]quinoline derivatives against CB1a. Interdiscip Perspect Infect Dis. 2023;2023 ID 1618082. doi:10.1155/2023/1618082.
118. Hernández-Ayala LF, Guzmán-López EG, Galano A. Quinoline derivatives: Promising antioxidants with neuroprotective potential. Antioxidants. 2023;12(1853). doi:10.3390/antiox12101853.
119. Samupindi TL, Saravanan V, Narayanan PL, Sumathi DL, Kathiravan MK. Molecular modelling investigation on 4-aminoquinoline derivatives as potent anti-tubercular agents. J Med Pharm Allied Sci. 2022;11(5):5304-11. doi:10.55522/jmpas.V11I5.4167.
120. El-Shershaby MH, El-Gamal KM, Bayoumi AH, El-Adl K, Alswah M, Ahmed HEA, et al. The antimicrobial potential and pharmacokinetic profiles of novel quinoline-based scaffolds: synthesis and in silico mechanistic studies as dual DNA gyrase and DHFR inhibitors. New J Chem. 2021;45(13986):13986-14004. doi:10.1039/d1nj02838c.
121. Celik I, Erol M, Puskullu MO, Uzunhisarcikli E, Ince U, Kuyucuklu G, Suzen S. In vitro and in silico studies of quinoline-2-carbaldehyde hydrazone derivatives as potent antimicrobial agents. Polycycl Aromat Compd. 2020. doi:10.1080/10406638.2020.1821230.

122. Koopaei MN, Assarzadeh MJ, Almasirad A, Ghasemi-Niri SF, Amini M, Kebriaeezadeh A, et al. Synthesis and Analgesic Activity of Novel Hydrazide and Hydrazine Derivatives. Iran J Pharm Res. 2013;12(4):721-7.
123. Tamaddon F, Amrollahi MA, Sharafat L. A green protocol for chemoselective O-acylation in the presence of zinc oxide as a heterogeneous, reusable and eco-friendly catalyst. Tetrahedron Lett. 2005;46(47):7841-4. doi:10.1016/j.tetlet.2005.09.005.
124. Lourenço MCS, de Souza MVN, Pinheiro AC, Ferreira ML, Gonçalves RSB, Nogueira TCM, Peralta MA. Evaluation of anti-tubercular activity of nicotinic and isoniazid analogues. Arkivoc. 2007;(xv):181-91.
125. Franzblau SG, Witzig RS, McLaughlin JC, Torres P, Madico G, Hernandez A, et al. Rapid, low-technology MIC determination with clinical Mycobacterium tuberculosis isolates by using the microplate Alamar Blue assay. J Clin Microbiol. 1998;36(2):362-6. doi:10.1128/jcm.36.2.362-366.1998.
126. Avadhani M, Kukkamalla MA, Bhatt KG. Screening of Punica granatum extract for antimicrobial activity against oral microorganisms. J Ayurvedic Herb Med. 2020;6(2):73-7.
127. Bulbule AM, Mandroli PS, Bhat KG, Bogar CM. In vitro evaluation of cytotoxicity of Emblica officinalis (amla) on cultured human primary dental pulp fibroblasts. J Indian Soc Pedod Prev Dent. 2019;37(3):251-7. doi:10.4103/JISPPD.JISPPD_85_18.
128. Hattarki SA, Bogar C, Bhat K. Triticum aestivum (wheat grass) exhibited anticancer activity on oral cancer (KB) cell line. Int J Pharm Res Health Sci. 2020;8(5):3220-4. doi:10.21276/ijprhs.2020.05.01.
129. Mandroli PS, Prabhakar AR, Bhat K, Krishnamurthy S, Bogar C. An in vitro evaluation of cytotoxicity of curcumin against human periodontal ligament

fibroblasts. AYU Int Q J Res Ayurveda. 2020;40(3):192-5. doi:10.4103/ayu.AYU_294_18.

130. Gasteiger J, Marsili M. Iterative partial equalization of orbital electronegativity: A rapid access to atomic charges. Tetrahedron. 1980;36(22):3219-28. doi:10.1016/0040-4020(80)80168-2.
131. Tripos International. Sybyl-X 2.0. St. Louis (MO): Tripos International; 2012.
132. Degfie T, Endale M, Tafese T, Dekebo A, Shenkute K. In vitro antibacterial, antioxidant activities, molecular docking, and ADMET analysis of phytochemicals from roots of Hydnora johannis. Appl Biol Chem. 2022;65(76). doi:10.1186/s13765-022-00740-8.
133. Daina A, Michielin O, Zoete V. SwissADME: A free web tool to evaluate pharmacokinetics, drug-likeness and medicinal chemistry friendliness of small molecules. Sci Rep. 2017;7:42717. doi:10.1038/srep42717.
134. Meth-Cohn O, Narine B, Tarnowski B. A versatile new synthesis of quinolines and related fused pyridines: Part 5. The synthesis of 2-chloroquinoline-3-carbaldehydes. J Chem Soc Perkin Trans 1. 1981;1520-6. doi:10.1039/P19810001520.
135. Vilsmeier-Haack reaction. SWISwiswift. Available from: https://chemist.swiswiswift.com/reaction/vilsmeier-haack-reaction.
136. Hamama WS, Ibrahim ME, Gooda AA, Zoorob HH. Recent advances in the chemistry of 2-chloroquinoline-3-carbaldehyde and related analogs. RSC Adv. 2018;8(16):8484-8515. doi:10.1039/c7ra11537g.
137. Popiołek Ł. Hydrazide-hydrazones as potential antimicrobial agents: overview of the literature since 2010. Med Chem Res. 2016;25(12):2821-49. doi:10.1007/s00044-016-1756-y.
138. Mitzel T. Interactive Organic Chemistry [Internet]. Chapter 6, pp. 33-34. Hartford (CT): Trinity College; [cited 2024 Nov 5]. Available from:

https://healy.create.stedwards.edu/Chemistry/CHEM30/organicCD(Mitzel)/chapter6/pages33and34/page33and34.htm.

139. Pasha MA, Reddy MB, Manjula K. Zinc dust: an extremely active and reusable catalyst in acylation of phenols, thiophenol, amines and alcohols in a solvent-free system. Eur J Chem. 2010;1(4):385-7. doi:10.5155/eurjchem.1.4.385-387.90.
140. Kamiloglu S, Sari G, Ozdal T, Capanoglu E. Guidelines for cell viability assays. Food Front. 2020;1(3):332-49. doi:10.1002/fft2.44.
141. Çakar B, Çiledağ A. Evaluation of coexistence of cancer and active tuberculosis; 16 case series. Respir Med Case Rep. 2018;23:33-7. doi:10.1016/j.rmcr.2017.11.004.
142. Chen GL, Guo L, Yang S, Ji DM. Cancer risk in tuberculosis patients in a high endemic area. BMC Cancer. 2021;21(1):679. doi:10.1186/s12885-021-08391-6.
143. Malik AA, Sheikh JA, Ehtesham NZ, Hira S, Hasnain SE. Can Mycobacterium tuberculosis infection lead to cancer? Call for a paradigm shift in understanding TB and cancer. Int J Med Microbiol. 2022;312:151558. doi:10.1016/j.ijmm.2022.151558.
144. Mishra G, Pachbhai N. Cancer and tuberculosis: A lethal duo. J Clin Images Med Case Rep. 2021;2(5):1331.
145. Preda M, Tănase BC, Zob DL, Gheorghe AS, Lungulescu CV, Dumitrescu EA, et al. The Bidirectional Relationship between Pulmonary Tuberculosis and Lung Cancer. Int J Environ Res Public Health. 2023;20(2):1282. doi:10.3390/ijerph20021282.
146. Awasthy D, Ambady A, Bhat J, Sheikh G, Ravishankar S, Subbulakshmi V, et al. Essentiality and functional analysis of type I and type III pantothenate kinases of Mycobacterium tuberculosis. Microbiology. 2010;156(9):2691-701.

147. Björkelid C, Bergfors T, Raichurkar AV, Mukherjee K, Malolanarasimhan K, Bandodkar B, Jones TA. Structural and biochemical characterization of compounds inhibiting Mycobacterium tuberculosis pantothenate kinase. J Biol Chem. 2013;288(25):18260-70. doi:10.1074/jbc.M113.476473.
148. Butman HS, Kotzé TJ, Dowd CS, Strauss E. Vitamin in the Crosshairs: Targeting Pantothenate and Coenzyme A Biosynthesis for New Antituberculosis Agents. Front Cell Infect Microbiol. 2020;10:605662. doi:10.3389/f
149. Chetnani B, Kumar P, Surolia A, Vijayan M. M. tuberculosis Pantothenate Kinase: Dual Substrate Specificity and Unusual Changes in Ligand Locations. J Mol Biol. 2010;400(1):171-85. doi:10.1016/j.jmb.2010.04.064.
150. Venkatraman J, Bhat J, Solapure SM, Sandesh J, Sarkar D, Aishwarya S, et al. Screening, Identification, and Characterization of Mechanistically Diverse Inhibitors of the Mycobacterium tuberculosis Enzyme, Pantothenate Kinase (CoaA). J Biomol Screen. 2012;17(3):293-302. doi:10.1177/1087057111423069.
151. Esposito M, Szadocka S, Degiacomi G, Orena BS, Mori G, Piano V, et al. A phenotypic based target screening approach delivers new antitubercular CTP synthetase inhibitors. ACS Infect Dis. 2017;3(7):478-90. doi:10.1021/acsinfecdis.7b00055.
152. Chiarelli LR, Mori G, Orena BS, Esposito M, Lane T, Lopes Ribeiro AL, et al. A multitarget approach to drug discovery inhibiting Mycobacterium tuberculosis PyrG and PanK. Sci Rep. 2018;8:3187. doi:10.1038/s41598-018-21614-4.
153. Ejalonibu MA, Elrashedy AA, Lawal MM, Kumalo HM, Mhlongo NN. Probing the dual inhibitory mechanisms of novel thiophenecarboxamide derivatives against Mycobacterium tuberculosis PyrG and PanK: an insight from biomolecular modeling study. J Biomol Struct Dyn. 2020. doi:10.1080/07391102.2020.1844055.

154. Ejalonibu MA, Elrashedy AA, Lawal MM, Soliman ME, Sosibo SC, Kumalo HM, et al. Dual targeting approach for Mycobacterium tuberculosis drug discovery: insights from DFT calculations and molecular dynamics simulations. Struct Chem. 2019;31(6):2537-52. doi:10.1007/s11224-019-01422-w.

155. Daina A, Michielin O, Zoete V. SwissADME: a free web tool to evaluate pharmacokinetics, drug-likeness and medicinal chemistry friendliness of small molecules. Sci Rep. 2017;7:42717. doi:10.1038/srep42717.

ANNEXURE-I

PUBLICATIONS

Asian Journal of Chemistry; Vol. 36, No. 7 (2024), 1518-1522

ASIAN JOURNAL OF CHEMISTRY

https://doi.org/10.14233/ajchem.2024.31503

Synthesis, Antibacterial Screening and ADME Prediction of Novel Ester Derivatives of 6-Substituted-2-chloroquinoline-3-carbaldehyde

VAIBHAV V. POTDAR[1,*], ARUN B. JOSHI[1] and HIMANSHU JOSHI[2]

[1]Goa College of Pharmacy (Affliated to Goa University), Panaji-403001, India
[2]College of Pharmacy, Graphic Era Hill University, Bhimtal campus, Bhimtal, Nainital-263139, India

*Corresponding author: Tel: +91 832 22226882; E-mail: potdarvaibhavv@gmail.com

Received: 13 March 2024; *Accepted*: 24 April 2024; *Published online*: 29 June 2024; AJC-21669

In this research, a series of novel 2-chloroquinoline-3-carbaldehyde analogues (**4a-f**) were successfully synthesized by employing several acetanilides in combination with hydrazides and acyl chlorides. The methodology yielded compounds with distinct substitutions, thus expanding the chemical diversity of this class of compounds. Characterization through FT-IR, ^{1}H NMR, ^{13}C NMR and mass spectral analysis confirmed the structural integrity of the synthesized derivatives. The ADME study indicates that the synthesized compounds were found to be possessing reliable ADME properties. The antimicrobial properties were tested against bacterial species with ciprofloxacin as standard drug. These newly synthesized compounds hold promise for further exploration of their biological activities and pharmacological profiles, making them valuable candidates for future research in the quest for novel therapeutic agents.

Keywords: Acetanilide, 2-Chloroquinoline-3-carbaldehyde, Vilsmeier-Haack reaction, Acyl chloride, Hydrazide.

INTRODUCTION

Among this heterogeneous class, quinoline, a distinctive heterocyclic compound, serves as an intriguing scaffold, prevalent in various therapeutic agents [1]. This versatile quinoline framework occurs prolifically within the structures of pharmaceutical compounds and is linked to a wide array of therapeutic effects, including analgesic [2], antibacterial [3], antioxidant [4], antimalarial [5], antifungal [6], anti-inflammatory [7,8], anticancer [9], anthelminthic [10], anti-hypertensive [11], antiviral [12,13], cardiovascular [14], central nervous system activity [15], antidiabetic [16] and anti-HIV activities [17]. The manifold pharmacological attributes of heterocyclic compounds bearing the quinoline ring underscore their critical role in medicinal chemistry, sustaining an enduring fascination with their synthesis and exploration.

Based on these observations, there exists a compelling rationale to engage in the synthesis and comprehensive characterization of a series of novel derivatives derived from 2-chloroquinoline-3-carbaldehyde. The chemical attributes of 2-chloroquinoline-3-carbaldehyde have engendered substantial global research interest, owing to its multifaceted applications in both biological and industrial domains. The scientific literature offers an extensive array of methodologies for the synthesis of quinoline compounds [18]. Notably, derivatives stemming from 2-chloroquinoline-3-carbaldehyde play a pivotal role as essential intermediates in the synthesis of crucial heterocyclic compounds [19,20]. These intermediates serve as linchpins in the intricate assembly of various heterocyclic structures, with profound implications for medicinal chemistry and industrial processes. The pursuit of novel derivatives of 2-chloroquinoline-3-carbaldehyde promises to elucidate novel synthetic pathways and expand the repertoire of available comp-ounds, with far-reaching implications for diverse applications.

In this work, a series of quinoline derivatives (**4a-f**) were synthesized, characterized and evaluated for their antimicrobial activity. Furthermore, *in silico* ADME study of the synthesized compounds were also examined and found to comply with the ADME properties, demonstrating their usefulness for drug development.

EXPERIMENTAL

Initially, the synthesis of 2-chloroquinoline-3-carbaldehyde and its derivatives was accomplished *via* Vilsmeier-Haack

reaction [21-23]. Analytically pure chemicals procured from reputable commercial sources such as Alfa Aesar, S.D. Fine Chem. and Spectrochem Ltd. were employed throughout the synthetic process. The determination of melting points was conducted utilizing an open capillary tube and an electrical melting point apparatus and found to be uncorrected. The progress of the chemical reactions, thin-layer chromatography (TLC) was executed on silica gel-G plates having a thickness of 0.5 mm. Visualization of spots was achieved through the application of iodine vapours and ultraviolet light. Infrared (IR) spectra were recorded using the KBr pellet method on an FT/IR-4100 instrument and mass spectra were acquired on a Bruker-ESI-MS model. ^{1}H NMR spectra were obtained in $CDCl_3$ solvent, utilizing a Bruker 500 MHz spectrometer with TMS as internal standard. Similarly, ^{13}C NMR spectra were recorded in DMSO solution on a Bruker Avance Neo 500 MHz NMR spectrometer.

General procedure for the synthesis of substituted 2-chloroquinoline-3-carbaldehyde (2a-d): Dimethylformamide (9.6 mL, 0.125 mol) was cooled to 0 ºC within a flask equipped with a desiccant drying tube. Phosphoryl chloride ($POCl_3$, 32.2 mL, 0.35 mol) was subsequently added dropwise under continuous stirring. To this solution, the acetanilide derivative (0.05 mol) was introduced and after a 5 min interval, the solution was subjected to reflux conditions for an appropriate duration, ranging from 6 to 17 h, at 70-80 ºC. Following the reflux period, the reaction mixture was allowed to cool to room temperature and then carefully poured into ice-cold water (200-300 mL). The resulting crude product was isolated through filtration and subsequently subjected to a drying process. The purification of the compound was achieved by recrystallization, utilizing ethyl acetate as recrystallization solvent.

2-Chloro-6-methylquinoline-3-carbaldehyde (2a): Yellow solid; yield 65%; m.p.: 120-122 ºC. IR (KBr, ν_{max}, cm^{-1}): 3432 (NH *str.*), 2874 (CH aldehyde *str.*), 1690 (C=O *str.*), 1580 (C=N *str.*) 1452-1424 (C-C aromatic *str.*), 820 (C-Cl *str.*). ^{1}H NMR (500 MHz, $CHCl_3$-d_6) δ ppm: 10.30 (s, 1H), 7.2-8.6 (arom. H), 2.38 (s, 3H). ^{13}C NMR (500 MHz, DMSO-d_6) δ ppm: 21.29, 126.69, 126.80, 127.12, 127.48, 130.62, 134.48, 136.38, 147.65, 149.28, 189.28. ESI-MS (*m/z*): 206.13. (M+H)$^+$ (calcd. mass for $C_{11}H_8ClNO$ is 205.64); R_f: 0.61, *n*-hexane:ethyl acetate (2:8).

2-Chloro-6-methoxy-quinoline-3-carbaldehyde (2d): Yellow solid; yield 55%; m.p.: 230-233 ºC. IR (KBr, ν_{max}, cm^{-1}): 2928 (CH aldehyde *str.*), 1681 (C=O *str.*), 1450-1649 (C-C arom. *str.*), 1384 (C=N), 861 (C-Cl *str.*).^{1}H NMR (500 MHz, $CHCl_3$-d_6) δ ppm: 10.38 (s, 1H), 7.32-8.47 (arom. H), 3.84 (s, 3H). ^{13}C NMR (500 MHz, DMSO-d_6) δ ppm: 21.97, 22.33, 25.07, 32.20, 55.34, 106.39, 122.89, 126.34, 127.60, 129.03, 138.23, 145.67, 147.71, 158.53, 189.29. ESI-MS (*m/z*): 222.06 (M+H)$^+$ (calcd. mass for $C_{11}H_8ClNO_2$ is 221.63); R_f: 0.62, *n*-hexane:ethyl acetate (2:8).

General procedure for the synthesis of 2-chloroquinoline-3-carbaldehyde hydrazide derivative (3a-d): A mixture comprising 2-chloroquinoline-3-carbaldehyde (**2**, 1 mmol) and 4-hydroxybenzoic acid hydrazide (1.1 mmol) was stirring in absolute ethanol (20 mL) at room temperature for a period of 1 to 5 h, facilitated by the addition of 2 drops of HCl, which acted as catalyst. The completion of the reaction was monitored using thin-layer chromatography (TLC) and upon reaching the desired endpoint, neutralization was executed by introducing a 10% aqueous solution of Na_2CO_3. The resulting precipitate was isolated *via* filtration, followed by a thorough washing with 20 mL of water. Subsequently, the compound was purified through recrystallization, utilizing ethanol as recrystallization solvent.

***N′*-[(2-Chloro-6-methylquinolin-3-yl)methylidene]-4-hydroxybenzohydrazide (3a):** Yellow solid; yield 32%; m.p.: 167-168 ºC. IR (KBr, ν_{max}, cm^{-1}): 3431 (OH *str.*), 1631 (C=O *str.*), 1515-1458 (C-C arom. *str.*), 1382 (C=N), 847 (C-Cl *str.*). ^{1}H NMR (500 MHz, $CHCl_3$-d_6) δ ppm: 12.10 (s, 1H), 9.63 (s, 1H), 7.4-8.6 (aromatic H), 3.48 (s, 3H). ^{13}C NMR (500 MHz, DMSO-d_6) δ ppm: 21.29, 115.63, 126.42, 126.69, 126.79, 127.03, 127.46, 129.69, 130.20, 130.60, 134.42, 142.24, 146.95, 147.76, 160.46, 162.61. ESI-MS (*m/z*): 340.09 (M+H)$^+$ (calcd. mass for $C_{18}H_{14}ClN_3O_2$ is 339.77). R_f: 0.70, *n*-hexane:ethyl acetate (2:8).

***N′*-[(2-Chloro-6-methoxyquinolin-3-yl)methylidene]-4-hydroxybenzohydrazide (3d):** Yellow solid; yield: 40%; m.p.: 276-278 ºC. IR (KBr, ν_{max}, cm^{-1}): 3432 (OH *str.*), 1627 (C=O *str.*), 1452-1383 (C-C arom. *str.*) 1343 (C=N), 832 (C-Cl *str.*). ^{1}H NMR (500 MHz, $CHCl_3$-d_6) δ ppm: 12.11 (s, 1H), 9.68 (s, 1H), 6.86-8.6 (arom.-H), 2.48 (s, 3H). ^{13}C NMR (500 MHz, DMSO-d_6) δ ppm: 55.34, 107.34, 115.63, 122.90, 126.42, 126.92, 127.53, 129.02, 129.69, 129.87, 142.42, 145.35, 147.22, 158.53, 160.46, 162.61. ESI-MS (*m/z*): *m/z* 356.02 (M+H)$^+$ (calcd. mass for $C_{18}H_{14}ClN_3O_3$ is 355.77). R_f: 0.72, *n*-hexane:ethyl acetate (2:8).

General procedure for the synthesis of ester derivative (4a-f): A mixture containing compound **3** (10 mmol) and 10 mol% of ZnO was prepared. To this mixture, acyl chlorides (12 mmol) were added and the reaction was initiated with stirring at room temperature. The progression of the reaction was tracked using TLC. Once the reaction had reached completion, the resulting mixture was subjected to extraction using ethyl acetate (2 × 5 mL) and ZnO was removed by filtration. The organic layer was subsequently washed with 10% $NaHCO_3$ solution and water, followed by drying using Na_2SO_4. The concentrated organic layer yielded the desired product. Alternatively, the product could also be obtained by adding a 10% $NaHCO_3$ solution and water to the reaction mixture, leading to the separation of the organic layer. This organic layer was then dried with Na_2SO_4 to afford the final product (**Scheme-I**).

4-{2-[(2-Chloro-6-methylquinolin-3-yl)methylidene]-hydrazine carbonyl}phenyl acetate (4a): Yellow solid; yield: 60%; m.p.: 251-254 ºC. IR (KBr, ν_{max}, cm^{-1}): 3250 (NH *str.*), 1620 (C=O *str.*), 1580 (C=N *str.*). ^{1}H NMR (500 MHz, $CHCl_3$-d_6) δ ppm: 12.21 (s, 1H), 8.56 (s, 1H), 7.13-8.28 (arom.-H), 2.38 (s, 3H), 2.37 (s, 3H). ^{13}C NMR (500 MHz, DMSO-d_6) δ ppm: 21.06, 21.29, 122.52, 126.69, 126.76, 126.79, 127.03, 127.46, 129.92, 130.20, 130.60, 134.42, 142.24, 146.95, 147.76, 153.34, 162.61, 169.22. ESI-MS (*m/z*): M+H)$^+$ (calcd. mass for $C_{20}H_{16}ClN_3O_3$ is 381.81). R_f: 0.62, *n*-hexane:ethyl acetate (2:8).

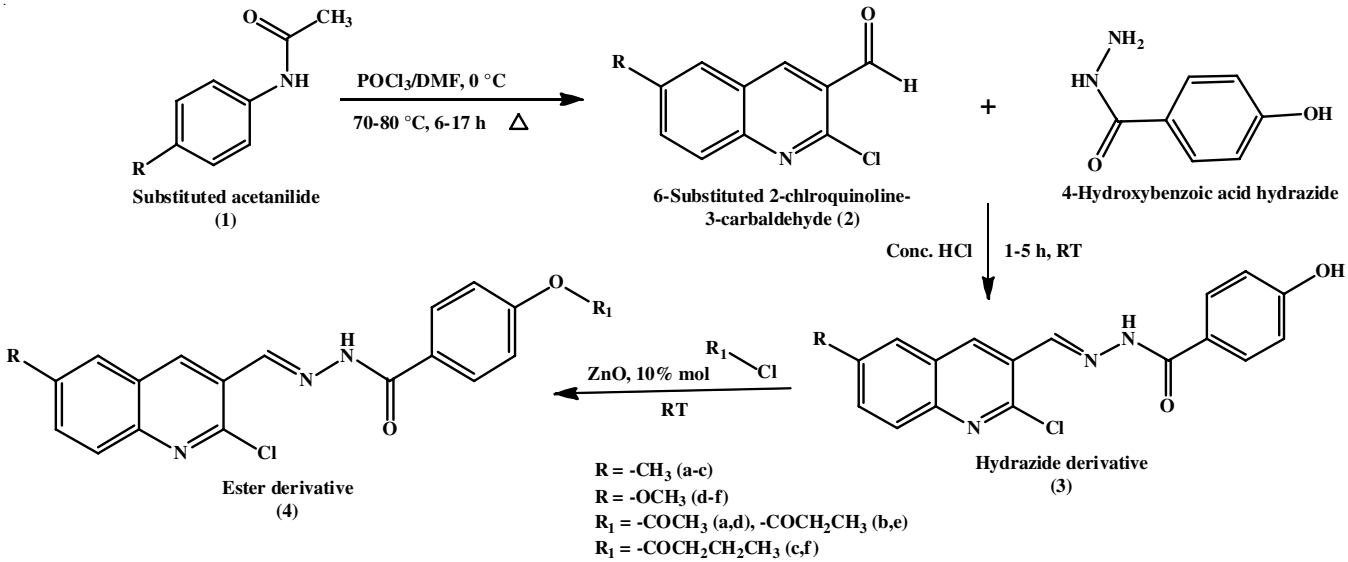

Scheme-I: Synthesis of 2-chloroquinoline-3-carbaldehyde derivatives

4-{2-[(2-Chloro-6-methylquinolin-3-yl)methylidene]-hydrazine carbonyl}phenyl propionate (4b): Yellow solid; yield: 62%; m.p.: 268-270 ºC. IR (KBr, ν_{max}, cm^{-1}): 3260 (NH *str.*), 1620 (C=O *str.*), 1490 (C=N *str.*). ^{1}H NMR (500 MHz, $CHCl_3$-d_6) δ ppm: 12.12 (s, 1H), 8.62 (s, 1H), 7.18 8.55 (arom.-H), 2.72 (s, 3H), 2.52 (q, 2H), 1.38 (s, 3H). ^{13}C NMR (500 MHz, DMSO-d_6) δ ppm: 9.08, 21.29, 27.45, 121.93, 126.69, 126.76, 126.79, 127.03, 127.46, 129.91, 130.20, 130.60, 134.42, 142.24, 146.95, 147.76, 153.85, 162.61, 172.53. ESI-MS (*m/z*): 396.11 $(M+H)^+$ (calcd. mass for $C_{21}H_{18}ClN_3O_3$ is 395.83). R_f: 0.71, *n*-hexane:ethyl acetate (2:8).

4-{2-[(2-Chloro-6-methylquinolin-3-yl)methylidene]-hydrazine carbonyl}phenyl butanoate (4c): Yellow solid; yield: 53%; m.p.: 275-276 ºC. IR (KBr, ν_{max}, cm^{-1}): 3200 (NH *str.*), 1650 (C=O *str.*), 1500 (C=N *str.*). ^{1}H NMR (500 MHz, $CHCl_3$-d_6) δ ppm: 12.01 (s, 1H), 8.68 (s, 1H), 7.15-8.64 (arom.-H), 2.60 (s, 3H), 2.49 (t, 3H), 1.98 (m, 2H), 0.93 (s, 3H). ^{13}C NMR (500 MHz, DMSO-d_6) δ ppm: 13.65, 18.40, 21.29, 39.58, 121.93, 126.69, 126.76, 126.79, 127.03, 127.46, 129.91, 130.20, 130.60, 134.42, 142.24, 146.95, 147.76, 153.21, 162.61, 171.94. ESI-MS (*m/z*): 410.16 $(M+H)^+$ (calcd. mass for $C_{22}H_{20}ClN_3O_3$ is 406.86). R_f: 0.61, *n*-hexane:ethyl acetate (2:8).

4-{2-[(2-Chloro-6-methoxyquinolin-3-yl)methylidene]-hydrazine carbonyl}phenyl acetate (4d): Yellow solid; yield: 70%; m.p.: 280-282 ºC. IR (KBr, ν_{max}, cm^{-1}): 3150 (NH *str.*), 1680 (C=O *str.*), 1520 (C=N *str.*). ^{1}H NMR (500 MHz, $CHCl_3$-d_6) δ ppm: 12.11 (s, 1H), 8.68 (s, 1H), 7.12-5.67 (arom.-H), 3.89 (s, 3H), 2.38 (s, 3H). ^{13}C NMR (75 MHz, DMSO-d_6) δ ppm: 21.06, 55.34, 107.34, 122.52, 122.90, 126.76, 126.92, 127.53, 129.02, 129.86, 129.92, 142.42, 145.35, 147.22, 153.34, 158.53, 162.61, 169.22. ESI-MS (*m/z*): 398.08. $(M+H)^+$ (calcd. mass for $C_{20}H_{16}ClN_3O_4$ is 397.81). R_f: 0.60, *n*-hexane:ethyl acetate (2:8).

4-{2-[(2-Chloro-6-methoxyquinolin-3-yl)methylidene]-hydrazine carbonyl}phenyl propionate (4e): Yellow solid; yield: 65%; m.p.: 235-237 ºC. IR (KBr, ν_{max}, cm^{-1}): 3210 (NH *str.*), 1650 (C=O *str.*), 1550 (C=N *str.*). ^{1}H NMR (500 MHz, $CHCl_3$-d_6) δ ppm: 12.10 (s, 1H), 8.74 (s, 1H), 7.10-8.69 (arom.H), 3.92 (s, 3H), 2.66 (q, 2H), 128 (t, 3H). ^{13}C NMR (75 MHz, DMSO-d_6) δ ppm: 9.08, 27.45, 55.34, 107.34, 121.93, 122.90, 126.76, 126.92, 127.53, 129.02, 129.90, 129.91, 142.42, 145.35, 147.22, 153.85, 158.53, 162.61, 172.53; ESI-MS (*m/z*): 412.07 $(M+H)^+$ (calcd. mass for $C_{21}H_{18}ClN_3O_4$ is 411.83). R_f: 0.70, *n*-hexane: ethyl acetate (2:8).

4-{2-[(2-Chloro-6-methoxyquinolin-3-yl)methylidene]-hydrazine carbonyl}phenyl butanoate (4f): Yellow solid; yield: 70%; m.p.: 270-273 ºC. IR (KBr, ν_{max}, cm^{-1}): 3150 (NH *str.*), 1620 (C=O *str.*), 1480 (C=N *str.*). ^{1}H NMR (500 MHz, $CHCl_3$-d_6) δ ppm: 12.10 (s, 1H), 8.69 (s, 1H), 7.11-8.68 (arom.-H), 3.86 (s, 3H), 2.59 (t, 2H) 1.78 (m, 2H), 1.18 (s, 3H). ^{13}C NMR (75 MHz, DMSO-d_6) δ 13.65, 18.40, 36.20, 55.34, 107.34, 121.93, 122.90, 126.76, 126.92, 127.53, 129.02, 129.86, 129.91, 142.42, 145.35, 147.22, 153.21, 158.53, 162.61, 171.94. ESI-MS (*m/z*): 426.14 $(M+H)^+$ (calcd. mass for $C_{22}H_{20}ClN_3O_4$ is 425.86). R_f: 0.63, *n*-hexane: ethyl acetate (2:8).

Antibacterial activity: The antibacterial activity of synthesized compounds **4a-f** was assessed *in vitro* using the broth microdilution method [24]. Minimum inhibitory concentration (MIC) values were determined to evaluate their antibacterial efficacy. Test microorganisms included Gram-positive strains *Bacillus subtilis* (ATCC 6633) and *Staphylococcus aureus* (ATCC 12598), as well as Gram-negative strains *Klebsiella pneumoniae* (ATCC 29665) and *Escherichia coli* (ATCC 25922). Ciprofloxacin served as the standard drug.

Prediction of ADME properties: The pharmacokinetic parameters of the synthesized compounds were predicted using SwissADME, an online software tool designed for this purpose. The drug likeliness of the compounds was estimated by adhering to Lipinski's rule of five, which serves as a guideline for evaluating the oral bioavailability of chemical entities. The structures of the synthesized compounds **4a-f** were converted into their canonical Simplified Molecular-Input Line-Entry System (SMILES) notation and submitted to SwissADME [25].

RESULTS AND DISCUSSION

Acetanilide derivatives (**1a-d**) were treated with Vilsmeier Haack reagent prepared from DMF and $POCl_3$ resulted in the formation of substituted 2-chloroquinoline-3-carbaldehyde (**2a-d**) showing a proton singlet between δ 10.305-10387 ppm in the NMR spectrum for CHO and the FTIR for C=O absorption of aldehyde appeared between 1690-1680 cm^{-1}. The CH aldehyde absorption band was observed between 2930-2870 cm^{-1} region.

The study involved the synthesis and characterization of ester derivatives of quinoline **4a-f** obtained by treating compounds **3a-d** with acyl chlorides. The characterization of these derivatives revealed significant structural changes and provided insights into their potential biological activities. In the NMR spectra of ester derivatives **4a-f**, the presence of protons in the δ 1-4 ppm range indicated the formation of side chains and substitutions at the C-6 position. The signals at δ 9.639-9.685 ppm corresponding to the -OH group observed in compounds **3a-d** disappeared in the spectra of ester derivatives **4a-f**. These observations confirmed the successful formation of the desired ester derivatives. Additionally, the FTIR spectra displayed a distinctive absorption band at 1680-1620 cm^{-1}, corresponding to the C=O group in the ester functionality. The appearance of an absorption band between 3250-3150 cm^{-1} indicated the presence of -NH groups, while another absorption band in the range of 1580-1480 cm^{-1} confirmed the presence of C=N groups in the compounds. Mass spectral analysis further supported the formation of the ester derivatives as evidenced by the presence of molecular ion peaks M+1 corresponding to the mass of the compounds. This unequivocally demonstrated the successful synthesis of the targeted ester compounds.

Antibacterial activity: The results of the antibacterial activity, presented in Table-1, illustrate the minimum inhibitory concentrations (MIC) for the synthesized compounds. The MIC values represent the lowest concentration of a compound required to inhibit bacterial growth. The findings of this study suggest that the ester derivatives **4a-f** possess antibacterial properties, as evidenced by their MIC values.

Prediction of ADME properties: The ADME properties of synthesized hybrid molecules were predicted using SwissADME software and the representative results are presented in Table-2. All six molecules, **4a-f** adhered to the Lipinski's rule of five, indicating no violations. This rule serves as a fundamental guideline to evaluate drug likeliness, suggesting that these compounds may have favourable pharmacokinetic profiles. The compliance of molecules with this rule underscores their potential suitability for oral administration, given their predicted favourable absorption and distribution characteristics. The number of rotatable bonds (6-9) in these molecules suggests a degree of molecular flexibility that can enhance binding interactions with biological targets without compromising structural integrity or leading to undesirable metabolic instability.

The prediction of high gastrointestinal (GI) absorption for all molecules suggests a promising bioavailability profile, which is critical for oral drug efficacy. Conversely, the absence of blood-brain barrier (BBB) permeation for these compounds indicates specificity in targeting peripheral sites without central nervous system effects. This attribute is particularly advantageous for drugs intended for systemic but not central actions, reducing the risk of central side effects. The analysis revealed that none of the molecules are substrates for P-glycoprotein (pgp), a transporter protein that can lead to drug resistance by effluxing drugs out of cells. This characteristic is beneficial for maintaining therapeutic concentrations at target sites. The consensus log P values, ranging from 3.4 to 4.3, fall within an optimal range that balances solubility and permeability, further affirming the compounds' drug likeliness. Molar refractivity values between 104 and 115, along with 6-9 rotatable bonds, suggest an appropriate balance of molecular flexibility and spatial occupancy, enhancing the likelihood of effective receptor interaction. The synthetic accessibility scores ranged from 2.7

TABLE-1
ANTIMICROBIAL ACTIVITY RESULT

Sample	MIC (μg/mL)			
	Gram-positive		Gram-negative	
	S. aureus	*B. subtilis*	*K. pneumonea*	*E. coil*
a	6.25	6.25	50	100
b	12.50	12.50	50	100
c	6.25	12.50	50	100
d	25.00	12.50	25	100
e	12.5	12.50	25	100
f	25.00	12.50	25	100
Ciprofloxacin	2	2	1	2

Compound **a** demonstrated good activity *S. aureus, B. subtilis, K. pneumonea*, Compound **c** showed good activity against *S. aureus, K. pneumonea*, compounds **d**, **e** and **f** showed very good activity against *K. pneumonea.*

TABLE-2
PHYSICO-CHEMICAL PROPERTIES PREDICTED FOR SYNTHESIZED COMPOUNDS **4a-f** USING SWISSADME

Properties*	**4a**	**4b**	**4c**	**4d**	**4e**	**4f**
Num. rotatable bonds	6	7	8	7	8	9
Num. H-bond acceptors	5	5	5	6	6	6
Num. H-bond donors	1	1	1	1	1	1
Consensus Log Po/w	3.71	4.06	4.36	3.43	3.71	4.04
Molar refractivity	104.39	109.19	114	105.91	110.72	115.53
Bioavailability score	0.55	0.55	0.55	0.55	0.55	0.55
Drug likeliness	Yes	Yes	Yes	Yes	Yes	Yes
Lipinski	0 Violation	0 Violation	0 Violation	0 Violation	0 Violation	0 Violation
Log S (ESOL) (solubility)	-4.88	-5.18	-5.42	-4.65	-4.95	-5.91
Synthetic accessibility	2.79	2.89	3.01	2.83	2.93	3.05s

*Few representative properties are listed in the table.

to 3.0, indicating that these molecules are relatively easy to synthesize, which is favourable for drug development processes. The uniform bioavailability score of 0.55 across all compounds, coupled with their ADME characteristics, predicts a moderate likelihood of success in the preclinical development stages. These findings justify further experimental validation and exploration of these compounds as potential therapeutic agents, laying the groundwork for subsequent *in vitro* and *in vivo* pharmacological studies.

Conclusion

This study successfully synthesized a series of ester derivatives using 6-substituted 2-chloroquinoline-3-carbaldehyde as a pivotal precursor. A thorough characterization spectroscopic techniques affirmed the successful incorporation of ester moieties. Moreover, the evaluation of antibacterial activity against both Gram-positive and Gram-negative bacteria provided valuable insights into the potential pharmaceutical applications. The MIC determination revealed the antibacterial potency of compounds, establishing a foundation for further investigations into their mechanisms of action and therapeutic potential. These ester derivatives represent a valuable expansion of chemical synthesis possibilities, holding implications for medicinal chemistry and drug development.

CONFLICT OF INTEREST

The authors declare that there is no conflict of interests regarding the publication of this article.

REFERENCES

1. O.O. Ajani, K.T. Iyaye and O.T. Ademosun, *RSC Adv.*, **12**, 18594 (2022); https://doi.org/10.1039/d2ra02896d
2. S.K. Gupta and A. Mishra, *Antiinflamm. Antiallergy Agents Med. Chem.*, **15**, 31 (2016); https://doi.org/10.2174/1871523015666160210124545
3. M. Özyanik, S. Demirci, H. Bektas, N. Demirbas, A. Demirbas and S.A. Karaoglu, *Turk. J. Chem.*, **36**, 233 (2012); https://doi.org/10.3906/kim-1109-9
4. S. Maddela, M. Ajitha, M. Venugopal and R. Maddela, *Int. J. Pharm. Pharm. Sci.*, **6**, 254 (2014).
5. I.A. Radini, T.M. Elsheikh, E.M. El-Telbani and R.E. Khidre, *Molecules*, **21**, 909 (2016); https://doi.org/10.3390/molecules21070909
6. S. Kumar, N. Goel, O. Afzal, M.R. Ali and S. Bawa, *J Antibiot. Res.*, **1**, 1 (2015); https://doi.org/10.15744/2574-5980.1.101
7. A.J. Asnani and S. Sahare, *Asian J. Pharm. Clin. Res.*, **6**, 303 (2013).
8. X. Wen, S.B. Wang, D.C. Liu, G.H. Gong and Z.S. Quan, *Med. Chem. Res.*, **24**, 2591 (2015); https://doi.org/10.1007/s00044-015-1323-y
9. U.S. Ramjith, G. Radhika, K.V. Muhammed Shakeel, C.K. Nabeel and A. Cheria, *Int. J. Pharm. Pharm. Sci.*, **5(Suppl 4)**, 521 (2013).
10. S. Rossiter, J.M. Péron, P.J. Whitfield and K. Jones, *Bioorg. Med. Chem. Lett.*, **15**, 4806 (2005); https://doi.org/10.1016/j.bmcl.2005.07.044
11. N. Muruganantham, R. Sivakumar, N. Anbalagan, V. Gunasekaran and J.T. Leonard, *Biol. Pharm. Bull.*, **27**, 1683 (2004); https://doi.org/10.1248/bpb.27.1683
12. M.A. Fakhfakh, A. Fournet, E. Prina, J.F. Mouscadet, X. Franck, R. Hocquemiller and B. Figadère, *Bioorg. Med. Chem.*, **11**, 5013 (2003); https://doi.org/10.1016/j.bmc.2003.09.007
13. J. Ghosh, V. Swarup, A. Saxena, S. Das, A. Hazra, P. Paira, S. Banerjee, N.B. Mondal and A. Basu, *Int. J. Antimicrob. Agents*, **32**, 349 (2008); https://doi.org/10.1016/j.ijantimicag.2008.05.001
14. T.A. Rano, E. Sieber-McMaster, P.D. Pelton, M. Yang, K.T. Demarest and G.H. Kuo, *Bioorg. Med. Chem. Lett.*, **19**, 2456 (2009); https://doi.org/10.1016/j.bmcl.2009.03.051
15. P.W. Smith, P.A. Wyman, P. Lovell, C. Goodacre, H.T. Serafinowska, A. Vong, F. Harrington, S. Flynn, D.M. Bradley, R. Porter, S. Coggon, G. Murkitt, K. Searle, D.R. Thomas, J.M. Watson, W. Martin, Z. Wu and L.A. Dawson, *Bioorg. Med. Chem. Lett.*, **19**, 837 (2009); https://doi.org/10.1016/j.bmcl.2008.12.005
16. D. Edmont, R. Rocher, C. Plisson and J. Chenault, *Bioorg. Med. Chem. Lett.*, **10**, 1831 (2000); https://doi.org/10.1016/S0960-894X(00)00354-1
17. J.F. Mouscadet and D. Desmaële, *Molecules*, **15**, 3048 (2010); https://doi.org/10.3390/molecules15053048
18. O. Meth-Cohn, B. Narine and B. Tarnowski, *J. Chem. Soc., Perkin Trans. 1*, 1520 (1981); https://doi.org/10.1039/p19810001520
19. S. Kumar, S. Bawa, S. Drabu, R. Kumar and L. Machawal, *Acta Poloniae Pharm.-Drug Res.*, **67**, 567 (2010).
20. P.V. Kombarov and M.A. Yurovskaya, *Chem. Heterocycl. Compd.*, **39**, 364 (2003); https://doi.org/10.1023/A:1023975129116
21. S. Kumar, S. Bawa, S. Drabu and B.P. Panda, *Med. Chem. Res.*, **20**, 1340 (2011); https://doi.org/10.1007/s00044-010-9463-6
22. M. Nassiri-Koopaei, M.J. Assarzadeh, A. Almasirad, S.F. Ghasemi-Niri, M. Amini, A. Kebriaeezadeh, N. Nassiri-Koopaei M. Ghadimi and A. Tabei, *Iran. J. Pharm. Res.*, **12**, 721 (2013); https://doi.org/10.22037/ijpr.2013.1366
23. F. Tamaddon, M.A. Amrollahi and L.A. Sharafat, *Tetrahedron Lett.*, **46**, 7841 (2005); https://doi.org/10.1016/j.tetlet.2005.09.005
24. M. Avadhani, M.A. Kukkamalla and K.G. Bhat, *J. Ayur. Herbal Medicine*, **6**, 73 (2020); https://doi.org/10.31254/jahm.2020.6211
25. T. Degfie, M. Endale, T. Tafese, A. Dekebo and K. Shenkute, *Appl. Biol. Chem.*, **65**, 76 (2022); https://doi.org/10.1186/s13765-022-00740-8

Contents lists available at UGC-CARE

International Journal of Pharmaceutical Sciences and Drug Research

[ISSN: 0975-248X; CODEN (USA): IJPSPP]

Available online at www.ijpsdronline.com

Research Article

Innovative Hybrid Compounds Targeting Tuberculosis: Development, Characterization and Bioefficacy Analysis of 6-substituted-2-Chloroquinoline-3-Carbaldehyde Hydrazide Ester Derivatives

Vaibhav V Potdar*, Arun B Joshi

Goa College of Pharmacy, Panaji, Goa University, Goa, India.

ARTICLE INFO

Article history:

Received: 13 March, 2024

Revised: 19 April, 2024

Accepted: 23 April, 2024

Published: 30 May, 2024

Keywords:

2-Chloroquinoline-3-carbaldehyde, Hydrazide, Anit-TB, Hybrid molecules, *Mycobacterium tuberculosis*, ADME

DOI:

10.25004/IJPSDR.2024.160309

ABSTRACT

This study delves into the biological activity of ester compounds obtained from analogs of 6-substituted-2-chloroquinoline-3-carbaldehyde hydrazide, aiming to exploit the combined antitubercular properties of quinoline and hydrazide to create innovative hybrid compounds. The molecules underwent a meticulous multi-step synthesis process, followed by purification through recrystallization. Methodologies such as proton nuclear magnetic resonance (^{1}H-NMR), carbon-13 nuclear magnetic resonance (^{13}C-NMR), fourier-transform infrared (FTIR) and mass spectrometry were used to confirm the molecular structures of developed derivatives. SWISSADME, an online tool, was utilized to predict the ADME properties, shedding light on their pharmacokinetic profiles. Evaluation of *in-vitro* antitubercular activity employing the Alamar blue method highlighted compounds 4a and 4f, exhibiting noteworthy efficacy, achieving threshold concentrations of 6.25 µg/mL for *Mycobacterium tuberculosis* inhibition. These findings suggest the possibility of novel quinoline scaffold as a potential molecule for TB treatment, contributing to ongoing endeavors in TB drug discovery and potentially laying the groundwork to develop effective antitubercular therapies.

Introduction

Tuberculosis (TB) persists because of *Mycobacterium tuberculosis* still exists as a formidable global health threat characterized by high morbidity and mortality rates. Despite the availability of effective treatment protocols, TB control faces obstacles such as the rise of drug-resistant strains, prolonged treatment periods, and its intersection with the human immunodeficiency virus/acquired immunodeficiency syndrome (HIV/AIDS) epidemic. These challenges underscore the pressing need for innovative anti-TB agents that offer improved efficacy, shorter treatment durations, and effectiveness against drug-resistant TB strains.[1-5]

The pursuit of novel anti-TB compounds has been a focal point in the battle against tuberculosis. Among various chemical entities, chloroquinoline-3-carbaldehyde scaffolds have garnered interest because of their potent antimicrobial properties.

Quinoline, a heterocyclic aromatic organic compound, has been a cornerstone in the synthesis of antimalarial, antibacterial, antifungal and many more therapeutic agents, reflecting its versatile therapeutic potential.[6-34] Furthermore, hydrazide analogs have been explored for their pharmacological activities, including anti-TB effects, providing a solid foundation for their use in drug discovery.[35,36]

The integration of chloroquinoline and hydrazide frameworks to develop hybrid molecules represents a novel approach in TB drug discovery. These compounds combine the antimicrobial efficacy of both parent molecules, aiming to enhance activity against *M. tuberculosis* while potentially reducing the likelihood of

***Corresponding Author:** Mr. Vaibhav Potdar

Address: Goa College of Pharmacy, Panaji, Goa University, Goa, India.

Email ✉**:** potdarvaibhavv@gmail.com

Tel.: +91-9420039461

Relevant conflicts of interest/financial disclosures: The authors declare that the research was conducted in the absence of any commercial or financial relationships that could be construed as a potential conflict of interest.

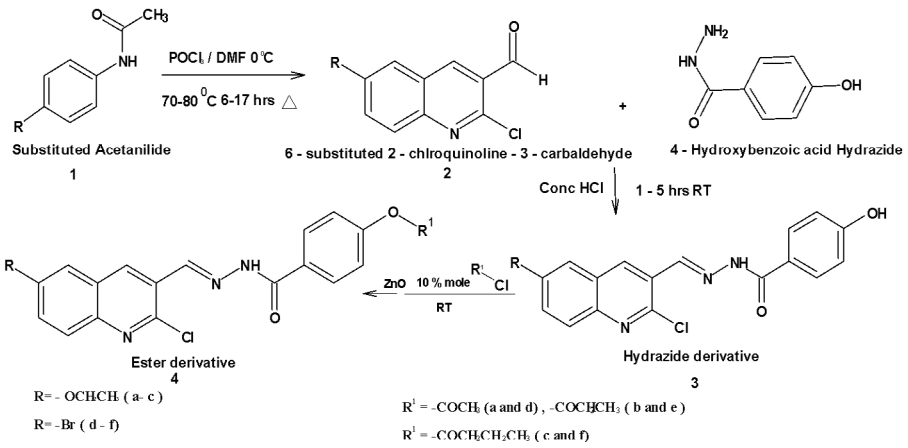

Fig. 1: Scheme for synthesis of ester derivatives of 6-substituted-2-chloroquinoline-3-carbaldehyde hydrazide derivatives

resistance development. Moreover, the synthesis of Schiff base adds to the molecular complexity, possibly offering unique mechanisms of action against TB bacteria.

However, the endeavor to discover new anti-TB agents is fraught with challenges. The process of designing, synthesizing, assessing the biological activity of these substances demands careful consideration of their pharmacokinetic profiles, safety, and effectiveness. The integration of advanced computational tools for predicting ADME properties, alongside traditional assessments like *in-vivo* and *in-vitro* evaluations, plays a crucial role in the early stages of drug development. [37,38]

This study seeks to contribute to the ongoing endeavors in TB drug discovery by exploring the development, characterization, and bioefficacy assessment of ester derivatives of 6-substituted-2-chloroquinoline-3-carbaldehyde hydrazide analogs. The ADME characteristics of the synthesized molecules were predicted by employing SwissADME, a web-based platform. By harnessing the well-established antitubercular properties of quinoline and hydrazide, combined with the innovative design of novel hybrid molecules, we aim to lay the groundwork for the development of fresh and efficacious antitubercular therapies.

Materials And Methods

Chemicals

In the laboratory, 6-substituted-2-chloroquinoline-3-carbaldehyde and its derivatives were synthesized following methods outlined in the literature. Analytical grade chemicals were employed in the synthesis, procured from Alfa Aesar, S.D. Fine chemicals, and Spectrochem Limited. An electrical open-capillary tube equipped melting point apparatus was used to ascertain melting points and are reported without correction. The synthesis progress was tracked using silica gel-G plates, 0.5 mm thick, for thin-layer chromatography (TLC) with spot visualization achieved using iodine vapors and ultraviolet light. Purification of all compounds was carried out via recrystallization using suitable organic solvents. Infrared (IR) spectra were acquired using an FT/IR-4100 instrument employing the KBr pellet technique. Mass spectra were captured using a Bruker ESI-MS device.

The ^{1}H-NMR and ^{13}C-NMR spectra were recorded on a Bruker Avance Neo 500 MHz NMR spectrometer (Bruker, USA), with deuterated chloroform ($CDCl_3$) as the solvent and tetramethyl silane serving as the reference standard.

Synthetic Procedures

A general synthetic protocol for 2-chloroquinoline-3-carbaldehyde analogues (2a, 2d)[39] (Fig. 1)

Drying tube-equipped flask was used to cool 0.125 mol (9.13 g, 9.6 mL) of N, N-dimethylformamide to 0°C. Gradually, through a dropping funnel 0.35 mol (53.7 g, 32.2 mL) of phosphorous oxychloride was added dropwise with constant stirring. Subsequently, 0.05 mol of substituted acetanilide was introduced gradually and the flask was refluxed for an appropriate time duration (6–17 hours) at 70 to 80°C, and the reaction status was tracked using TLC. After the reaction was accomplished and the mixture had reached ambient temperature, it was introduced into ice-cold water (200–300 mL) dropwise. The crude product was filtered, dried, and then recrystallized using ethyl acetate.

Characterization data of 6-substituted-2-chloroquinoline-3-carbaldehyde (2a, 2d)

- *2-Chloro-6-ethoxyquinoline-3-carbaldehyde (2a)*

IR υ (cm^{-1}): 2850 (C-H Aldehyde), 1690 (C=O), 1450–1649 (C-C Aromatic), 1590 (C=N), 720 (C-Cl)

^{1}HNMR (500 MHz, $CDCl_3$: δ 9.73 (s, 1H), 7.24–7.90 (Aromatic, 4H), 4.06 (m, 2H) 1.34(t, 3H)

^{13}C-NMR: δ 14.7, 64.2, 106.4, 121.2, 126.3, 127.6, 130.9, 138.5, 146.5, 147.6, 156.2, 189.3.

2-Chloro-6-bromoquinoline-3-carbaldehyde (2d)

IR υ (cm^{-1}): 2800 (CH Aldehyde), 1590 (C=O), 1350–1480

(C-C Aromatic), 1520 (C=N), 750 (C-Cl), 700 (C-Br)
^{1}H-NMR (500 MHz, $CDCl_3$: δ 9.86 (s, 1H), 8.14-9.04 (Aromatic, 4H)
^{13}C-NMR: δ 120.1, 126.3, 128.1, 129.6, 131.1, 132.7, 138.5, 146.5, 147.6, 189.3.

Synthesis of 6-substituted carbaldehyde hydrazide analog (3a, 3d)[40]

A mixture containing 1-mmol of 6-substituted 2-chloroquinoline-3-carbaldehyde (2a and 2d) and 1.1 mmol of 4-hydroxybenzoic acid hydrazide was prepared in 20 mL of absolute ethanol and stirred at ambient temperature for 1 to 5 hours. Two drops of hydrochloric acid are added to catalyze the process. TLC is used to track the reaction's progress. After the reaction was completed, the mixture is neutralized using a solution of sodium bicarbonate in water (10%). After filtering and washing with 20 mL of water, the resulting precipitate was recrystallized using ethanol.

Characterization data of 6-substituted-2-chloroquinoline-3-carbaldehydehydrazidederivatives (3a & 3d)

- *N'- [(2-chloro-6-ethoxyquinoline -3-yl) methylidene]-4-hydroxybenzohydrazide (3a)*

IR υ (cm^{-1}): 3400 (O-H), 1610 (C=O), 1458–1500 (C-C Aromatic), 1550 (C=N), 780 (C-Cl)
^{1}H-NMR (500 MHz, $CDCl_3$: δ 11.87 (s, 1 H), 9.68(s, 1 H), 8.98 (s, 1 H), 6.88-7.85 (Aromatic, 8 H), 4.06 (m, 2H), 1.34(t, 3H)
^{13}C-NMR: δ 14.2, 64.3, 106.4, 115.7, 121.2, 124.5, 127.6, 128.1, 129.6, 130.9, 131.7, 146.5, 146.5, 150.6, 156.2, 157.4, 164.7.

- *N'-[(2-chloro-6-Bromoquinolin-3-yl) methylidene]-4-hydroxybenzohydrazide (3d)*

IR υ (cm^{-1}): 3470 (O-H), 1690 (C=O), 1458–1515 (C-C Aromatic), 1510 (C=N), 780 (C-Cl), 700 (C-Br)
^{1}H-NMR (500MHz, $CDCl_3$: δ 12.04 (s, 1H), 9.68 (s, 1H), 9.04 (s, 1H), 8.14–8.39 (Aromatic, 8H)
^{13}C-NMR: δ 115.7, 120.1, 124.5, 128.0, 128.1, 129.6, 129.6, 131.1, 132.7, 146.5, 146.5, 150.6, 157.4, 164. 7.

- *Synthesis of ester derivatives of 6-substituted-2-chloroquinoline-3-carbaldehyde hydrazide (4a-f)[41]*

At room temperature, acetyl chloride (12 mmol) was added to a blend of compound 3 (10 mmol) and ZnO (10 mol%), while stirring. The advancement of the reaction was tracked *via* TLC. Following its completion, ethyl acetate (EtOAc) (2×5 mL) was used to extract the reaction mixture. ZnO was removed by filtering. The organic aliquot is subsequently washed with a 10% $NaHCO_3$ solution and water, then dried over Na_2SO_4 to further retrieve the product. An alternative method of isolating the product would be to mix water and 10% $NaHCO_3$ solution, separate the organic layer, and then dry it on Na_2SO_4. The physicochemical properties of these molecules, including percent yield, melting point, and retention factor (Rf) of thin layer chromatography (TLC) analysis, are presented in Table 1.

Characterization data of ester derivatives of 6-substituted-2-chloroquinoline-3-carbaldehyde hydrazine (4a-f)

- *4-{2-[(2-chloro-6-ethoxyquinolin-3-yl) methylidene] hydrazine carbonyl} phenyl acetate (4a)*

IR υ (cm^{-1}): 3500 (N-H), 1620 (C=O), 1550 (C=N)
^{1}H-NMR (500 MHz, $CDCl_3$: δ 11.87 (s, 1H), 8.98 (s, 1H), 7.16–8.51 (Aromatic, 8H), 4.06 (m, 2H), 2.31 (s, 3H), 1.34 (s, 3H)
ESI-MS (m/z): 411.26 (M^+, $C_{21}H_{18}ClN_3O_4$), 412.48 ($M+H^+$, $C_{21}H_{19}Cl\ N_3O_4$), 413.10($M+2H^+$, $C_{21}H_{20}Cl\ N_3O_4$)
^{13}C-NMR: δ 9.1, 14.2, 27.8, 64.3, 106.4, 114.3, 121.2, 127.1, 128.9, 129.6, 130.9, 131.7, 146.5, 146.6, 150.5, 150.6, 156.1. 164.6, 172.8.

- *4-{2-[(2-chloro-6-ethoxyquinolin-3-yl) methylidene] hydrazine carbonyl} phenyl propanoate (4b)*

IR υ (cm^{-1}): 3480 (N-H), 1610 (C=O), 1520 (C=N)
^{1}HNMR (500MHz, $CDCl_3$: δ 12.06 (s,1H), 8.98 (s,1H), 7.16-8.51 (Aromatic,8H), 4.07 (q,2H), 2.61 (q,2H), 1.34 (s,3H),1.08 (s,3H).
ESI-MS (m/z):425.67 (M^+, $C_{22}H_{20}ClN_3O_4$), 426.34 ($M+H^+$, $C_{22}H_{21}ClN_3O_4$), 427.78($M+2H^+$, $C_{22}H_{22}ClN_3O_4$)

Table 1: Physicochemical data of ester derivatives of 6-substituted-2-chloroquinoline-3-carbaldehyde hydrazide

Synthesized compound	*R*	*R^1*	*Molecular formula*	*MW*	*%yield*	*M.P.*	*Rf**
4a	OCH_2CH_3	$COCH_3$	$C_{21}H_{18}ClN_3O_4$	411.84	61	273–274	0.66
4b	OCH_2CH_3	$COCH_2CH_3$	$C_{22}H_{20}ClN_3O_4$	425.67	75	287–289	0.71
4c	OCH_2CH_3	$COCH_2CH_2CH_3$	$C_{23}H_{22}ClN_3O_4$	439.16	78	301–303	0.57
4d	Br	$COCH_3$	$C_{19}H_{13}BrClN_3O_3$	446.26	63	308–310	0.71
4e	Br	$COCH_2CH_3$	$C_{20}H_{15}BrClN_3O_3$	460.38	79	322–324	0.63
4f	Br	$COCH_2CH_2CH_3$	$C_{21}H_{17}BrClN_3O_3$	474.03	69	336–337	0.73

*TLC analysis using mobile phase: n-Hexane: Ethyl Acetate (2:8)

^{13}C NMR: δ 9.3, 14.2, 27.8, 64.3, 106.8, 114.9, 121.1, 127.3, 128.8, 129.2, 130.5, 131.9, 146.5 ,146.6, 150.6,150.8, 156.3, 164.1 ,172.6.

- *4-{2-[(2-chloro-6-ethoxyquinolin-3-yl) methylidene] hydrazine carbonyl} phenyl butanoate (4c)*

IRυ (cm^{-1}): 3350 (N-H), 1590 (C=O), 1520 (C=N)
^{1}H-NMR (500MHz, $CDCl_3$: δ 12.17 (s,1H), 8.98 (s,1H), 7.16–8.50 (Aromatic, 8H), 4.06 (q, 2H), 2.59 (t, 3H) 1.51 (m, 2H), 1.35 (t, 2H), 1.08 (t, 3H)
ESI-MS (m/z): 439.16 (M^+, $C_{23}H_{22}ClN_3O_4$), 440.65 ($M+H^+$, $C_{23}H_{23}ClN_3O_4$), 441.63($M+2H^+$, $C_{23}H_{24}ClN_3O_4$)
^{13}C-NMR: δ 9.1, 14.2, 27.8, 64.3, 106.4, 114.3, 121.2, 124.5, 127.1, 128.9, 129.6, 130.9, 131.7, 146.5, 146.5, 150.6, 150.6, 156.1, 164.6, 172.8.

- *4-{2-[(6-bromo-2-chloroquinolin-3-yl) methylidene] hydrazine carbonyl} phenyl acetate (4d)*

IR υ (cm^{-1}): 3490 (N-H), 1620 (C=O), 1570 (C=N)
^{1}H-NMR (500MHz, $CDCl_3$: δ 12.04 (s, 1H), 9.04 (s, 1H), 7.51–8.39 (Aromatic, 8H), 2.59 (s, 3H)
ESI-MS (m/z): 446.26 (M^+, $C_{19}H_{13}Br\,Cl\,N_3O_3$), 447.64 ($M+H^+$, $C_{19}H_{14}Br\,Cl\,N_3O_3$), 448.37($M+2H^+$, $C_{19}H_{15}Br\,Cl\,N_3O_3$)
^{13}C-NMR: δ 21.0, 114.3, 120.7, 124.1, 128.0-128.1, 129.5-129.7, 131.1, 132.7, 146.4-146.6, 150.5-150.7, 164.7 , 169.1.

- *4-{2-[(6-bromo-2-chloroquinolin-3-yl) methylidene] hydrazine carbonyl} phenyl propanoate (4e)*

IR υ (cm^{-1}): 3500 (N-H), 1690 (C=O), 1540 (C=N)
^{1}H-NMR (500MHz, $CDCl_3$: δ 12.28 (s, 1H), 9.04 (s, 1H), 7.51-8.39 (Aromatic, 8H), 2.61 (q, 2H), 1.28 (t, 3H)
ESI-MS (m/z): 460.38 (M^+, $C_{20}H_{15}Br\,Cl\,N_3O_3$), 461.48 ($M+H^+$, $C_{20}H_{16}Br\,Cl\,N_3O_{33}$), 462.54($M+2H^+$, $C_{20}H_{17}Br\,Cl\,N_3O_3$)
^{13}C-NMR: δ 27.8, 114.3, 120.1, 124.5, 128.0-128.2 ,129.5-129.7, 131.1, 132.7, 146.4-146.6, 150.5-150.7, 164.7, 172.8.

- *4-{2-[(6-bromo-2-chloroquinolin-3-yl) methylidene] hydrazine carbonyl} phenyl butanoate (4f)*

IR (KBR) υ (cm^{-1}): 3350 (N-H), 1650 (C=O), 1490 (C=N)
^{1}H-NMR (500 MHz, Chloroform-d): δ12.22 (s, 1 H), 9.04 (s, 1H), 7.51–8.39 (Aromatic, 8H), 2.59 (t, 3H) 1.68 (m, 2H), 0.99 (t, 2H)
ESI-MS (m/z): 474.03 (M^+, $C_{21}H_{17}BrClN_3O_3$), 475.84 ($M+H^+$, $C_{21}H_{19}BrClN_3O_3$), 476.32($M+2H^+$, $C_{21}H_{20}BrClN_3O_3$)
^{13}C-NMR: δ 20.2, 114.3, 120.1, 124.5, 128.0-128.2, 129.5-129.7,131.1, 132.7, 146.4-146.6, 150.5-150.7, 164.7, 169.4

Antitubercular Activity Screening

Antitubercular action of the compounds towards *M. tuberculosis* was estimated by the microplate Alamar blue assay (MABA)[42] an innocuous method that makes use of a reagent that is stable to heat. This method has demonstrated good correlation with BACTEC radiometric techniques.

Media and Microorganism

The standard strain of *M. tuberculosis* vaccine, ATCC No. 27294 (H37 RV), was employed in the investigation. For the sake of comparison, benchmarks including streptomycin, pyrazinamide, ethambutol, isoniazid, and rifampicin were used.
The Alamar blue solution was made by mixing a 10% solution of Tween 80 in water to enhance dye solubility with the Alamar blue reagent. Additionally, Middlebrook 7H9 broth was supplemented with appropriate additives to support the growth of *M. tuberculosis.*

Assessment of anti-TB activity

To curtail the evaporation loss of the medium from the test wells during the course of incubation, 200 µL of sterile deionized water was initially dispensed into each of the outermost wells of a sterile 96-well plate. Subsequently, Middlebrook 7H9 broth (100 µL) was instilled into each well of the 96-well plate, which was then inoculated with a standardized suspension of *M. tuberculosis* to achieve the desired final inoculum size.
Final concentrations of 100 to 0.2 µg/mL were achieved by serially diluting the compounds directly on the plate. A positive control containing known anti-TB drugs was included for comparison. The plates were covered and concealed by parafilm and then subjected to an incubation for five days at 37°C. 25 µL of freshly prepared blend (1:1, Alamar blue reagent and 10% Tween 80) was added to each well after the incubation period and another 24 hours were spent incubating the plates. In the experimental well, pink and blue coloration is a marker of the presence and absence of bacterial growth, respectively. The minimum inhibitory concentration (MIC) was defined as the minimal drug content required to prevent the conversion from blue to pink coloration in the test well.

Data Analysis

Linear comparison of the MIC values of the experimentally synthesized anti-TB derivatives with reference to the control was employed to confirm the bioefficacies. All procedures involving *M. tuberculosis* were conducted in a biosafety level 3 (BSL-3) laboratory, employing suitable containment equipment and safety protocols to uphold the highest level of safety. Stringent biosafety guidelines were followed to guarantee proper disposal of all infectious materials and mitigate any risk of exposure to hazardous pathogens. These precautions were implemented to maintain a secure laboratory environment and ensure the safety of personnel.

Prediction of ADME characteristics

SwissADME, an online dedicated software program, was employed to forecast the pharmacokinetic aspects of the developed anti-TB derivatives. The drug-likeness of chemical compounds was determined by employing the "Lipinski's Rule of Five for oral bioavailability".

The synthesized compounds (labeled 4a–4f) were forwarded to SwissADME following the conversion of their structure to simplified molecular input line-entry system (SMILES).[43]

Through this process, *in-silico* prediction of pharmacokinetic parameters was conducted, providing valuable insights into the compounds' potential as drug candidates.

Results And Discussion

New ester derivatives of 6-substituted-2-chloroquinoline-3-carbaldehyde hydrazide analogues were synthesized, and their antitubercular action was then assessed.

In the study, our purpose was to explore a better antitubercular treatment strategy by synthesizing hybrid molecules composed with hydrazide and chloroquinoline backbones.

Chemistry

The conversion of substituted acetanilide to 6-substituted-2-chloroquinoline-3-carbaldehyde derivatives (2a, 2d) using phosphoryl chloride ($POCl_3$) in dimethylformamide (DMF) involves a series of chemical reactions involving Vilsmeier-Haack reaction, a form of electrophilic aromatic substitution, and cyclization reaction. The initial reaction involves activation of DMF, the formylating agent by $POCl_3$ to form Vilsmeier-Haack complex (an iminium chloride or chloroiminium ion). The activated complex then interacts with the substituted acetanilide, which acts as the nucleophile. The nucleophilic aromatic ring of the acetanilide attacks the carbon atom of the iminium ion, leading to the introduction of a formyl group (-CHO) into the acetanilide structure. The critical step aromatic rig is formylated to give an intermediate.

Subsequent intramolecular cyclization is facilitated in the presence of $POCl_3$, aiding in the dehydration process. This cyclization results in the closure of the nitrogen-containing ring, ultimately forming the quinoline skeleton. The reaction mixture is then worked up, usually involving hydrolysis to neutralize any remaining reagents and to fully form the derivative.[39]

The presence of aldehyde proton at δ 9.73 (2a) and 9.86 (2d), and aromatic protons in the range of 7.24 to 7.90 (2a) and 8.14 to 9.04 (2d) in proton NMR confirm formation of chloroquinoline carbaldehyde nucleus. FTIR and ^{13}C-NMR further confirm the presence of functional groups and carbon skeleton, respectively, thereby elucidating the structures.

A condensation reaction occurs involving 4-hydroxybenzoic acid hydrazide and 6-substituted -2-chloroquine-3-carbaldehyde in absolute ethanol and hydrochloric acid to yield hydrazide derivatives.[40] The reaction commences with an attack of a hydrazide nitrogen atom on the carbonyl carbon of the 2-chloroquinoline-3-carbaldehyde as a nucleophile. This step is facilitated by the acidic environment, which protonates the carbonyl oxygen, rendering the carbonyl carbon more vulnerable to nucleophilic attack. The nucleophilic attack results in the formation of a tetrahedral intermediate, a common intermediate in reactions involving carbonyl groups. Subsequently, the elimination of water from the tetrahedral intermediate forms a carbon nitrogen double bond to give hydrazide linkage.

The stretching vibration around 3400 cm^{-1} confirms the presence of O-H in FTIR. The ^{1}H-NMR shows characteristic peaks at δ 8.98 (3a) and 9.04 (3d) for methylene protons, hydrazide N-H protons at 9.68, and hydroxy protons at 11.87 (3a) and 12.04 (3d). ^{13}C-NMR helped to confirm the carbon skeleton of the hydrazide compounds.

The hydrazide group is conjugated to the quinoline ring system through the former aldehyde carbon. This introduces a significant degree of structural complexity and potential for biological activity, as both the quinoline and hydrazide moieties are known for their pharmacological properties.

Esterification of quinoline hydrazide derivatives involves the process of acylation followed by esterification as shown in the scheme (Fig. 1). The reaction proceeds with attack of hydrazide nitrogen on the carbonyl carbon of acetyl chloride to give a tetrahedral intermediate. After the nucleophilic attack, the tetrahedral intermediate releases a chloride ion, thus forming the acylated hydrazide.[41]

It undergoes esterification, potentially involving an intramolecular reaction. The introduction of an ester group can affect the solubility, absorption, and distribution of the compound within biological systems, making it a valuable step in drug design and development for the treatment of tuberculosis.

Mass spectrometry with the electrospray ionization method confirmed the molecular weights of synthesized hybrid compounds. ^{13}C-NMR and FTIR verified the presence of carbon backbone and functional groups, respectively. The absence of signal for O-H and the presence of characteristic peaks at δ 8.98 to 9.04 for methylene protons and around 12 for hydrazide protons helped elucidate the structures of compounds 4a-4f.

Antitubercular activity using MABA

The MABA methodology was employed for evaluating the anti-TB action of the prepared analogues. MABA provides a unique combination of sensitivity, specificity, and operational simplicity, making it an efficient framework for rapidly screening potential anti-TB agents.[42] As a significant outcome of this study, the compounds 4a and 4f demonstrated 6.25 µg/mL as MIC, indicating a potent inhibitory effect against *M. tuberculosis*.

In comparison, as exhibited in Table 2 and Fig. 2, MIC values of 12.5 µg/mL for compounds 4b, 4c, 4d, and 4e demonstrate they are moderately active, in contrast to the minimum threshold concentrations of reference anti-TB drugs, e.g., isoniazid and ethambutol at

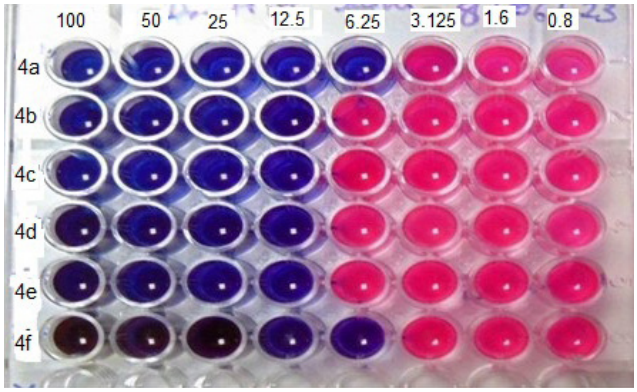

Fig. 2: Micro titer plate showing color change in Alamar blue assay method for synthesized ester derivatives of 6-substituted-2-chloroquinoline-3-carbaldehyde hydrazide 4a-4f depicting MIC values in µg/mL

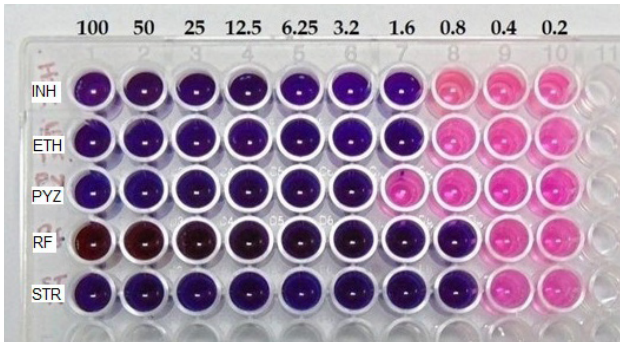

Fig. 3: Micro titer plate showing color change in Alamar blue assay method for standard anti-TB drugs depicting MIC values; INH: Isoniazide (1.6 µg/mL), ETH: Ethambutol (1.6 µg/mL), PYZ: Pyrazinamide (3.125 µg/mL), RF: Rifampicin (0.8 µg/mL), STR: Streptomycin (0.8 µg/mL)

1.6 µg/mL, pyrazinamide at 3.125 µg/mL, rifampicin and streptomycin at 0.8 µg/mL each (Fig. 3).

The MABA method's significance extends beyond its application in this study. Its non-toxic, thermally stable and colorimetric-based approach enables the high-throughput screening of compounds without relying on radioactive markers or biohazardous materials, presenting a safer and more environmentally friendly alternative to traditional methods. Furthermore, the good correlation of MABA with proportional and BACTEC radiometric methods affirms its reliability and reproducibility in assessing the antimicrobial activity of novel compounds.

Prediction of ADME properties

The utilization of SwissADME for prediction provides valuable theoretical attributes related to pharmacokinetic parameters such as ADME of potent drug candidates. This approach is essential for gaining an understanding of how the synthesized compounds may interact within biological systems, thereby offering guidance for subsequent research and development endeavors.[43]

ADME properties of synthesized hybrid molecules were comprehensively predicted using SwissADME and the representative results are presented in Table 3. All six molecules, 4a to 4f adhered to Lipinski's Rule of Five, indicating no violations. This rule serves as a fundamental guideline to evaluate drug likeliness, suggesting that these compounds may have favorable pharmacokinetic profiles. The adherence of molecules to this rule highlights their potential suitability for oral administration, as it indicates predicted favorable absorption and distribution characteristics. The presence of a moderate number of rotatable bonds (6-8) in these molecules suggests a level of molecular flexibility that can potentially improve binding interactions with biological targets while still maintaining structural integrity and avoiding undesirable metabolic instability.

The prediction of high gastrointestinal (GI) absorption for all molecules suggests a promising bioavailability profile, which is critical for oral drug efficacy. Conversely, the absence of blood-brain barrier (BBB) permeation for these compounds indicates specificity in targeting peripheral sites without central nervous system effects. This attribute is particularly advantageous for drugs intended for systemic but not central actions, reducing the risk of central side effects. The analysis revealed that none of the molecules are substrates for P-glycoprotein (Pgp), a transporter protein that can lead to drug resistance by effluxing drugs out of cells. This characteristic is

Table 2: Alamar blue assay results showing MIC values for synthesized derivatives

S. No.	*Synthesized derivatives*	*Concentration of synthesized derivatives (µg/mL) **							
		100	*50*	*25*	*12.5*	*6.25*	*3.125*	*1.6*	*0.8*
01	4a	S	S	S	S	**S**	R	R	R
02	4b	S	S	S	S	R	R	R	R
03	4c	S	S	S	S	R	R	R	R
04	4d	S	S	S	S	R	R	R	R
05	4e	S	S	S	S	R	R	R	R
06	4f	S	S	S	S	**S**	R	R	R

*R- Resistant, S- Sensitive

Table 3: Physicochemical properties predicted for synthesized compounds 4a – 4f using SwissADME

*Compounds properties**	*4a*	*4b*	*4c*	*4d*	*4e*	*4f*
Rotatable bonds no.	7	7	8	6	7	8
H-bond acceptors no	5	5	5	5	5	5
H-bond donors no	1	1	1	1	1	1
Consensus Log Po/w	4.25	3.73	4.04	3.91	4.25	4.54
Molar refractivity	109.24	104.23	109.03	104.43	109.24	114.04
Drug likeliness	Yes	Yes	Yes	Yes	Yes	Yes
Lipinski (violation)	0	0	0	0	0	0
Log S (ESOL) (Solubility)	-5.47	-4.88	-5.11	-5.17	-5.47	-5.71
Synthetic accessibility	2.79	2.78	2.9	2.69	2.79	2.91

*Few representative properties are listed in the table.

beneficial for maintaining therapeutic concentrations at target sites. The consensus log *p-values*, ranging from 3.7 to 4.5, fall within an optimal range that balances solubility and permeability, further affirming the compounds' drug likeliness. Molar refractivity values between 104 and 114, along with 6 to 8 rotatable bonds, suggest an appropriate balance of molecular flexibility and spatial occupancy, enhancing the likelihood of effective receptor interaction. The synthetic accessibility scores fell within the range of 2.7 to 2.9, suggesting that these molecules are relatively straightforward to synthesize. This ease of synthesis is advantageous for drug development processes. The uniform bioavailability score of 0.55 across all compounds, coupled with their ADME characteristics, predicts a moderate likelihood of success in preclinical development stages.

In summary, the ADME predictions for the hybrid molecules 4a to 4f using SwissADME offer promising prospects for their pharmacokinetic profiles. These predictions suggest favorable attributes, such as congruence to the "Lipinski's rule of five", optimal physicochemical properties and high gastrointestinal absorption which is conducive to drug development. Consequently, these findings justify the need for further experimental validation and exploration of these compounds as potential therapeutic agents. This lays the foundation for subsequent pharmacological studies (*in-vitro* and *in-vivo*)

Overall, the results of our investigation represent a significant contribution to the field of antitubercular drug discovery, highlighting the promising antitubercular activity of the synthesized chloroquinoline-hydrazide ester derivatives. It opens new avenues for further research into the optimization and development of these compounds as potential antitubercular therapies. A feasible route for the creation of novel antitubercular drugs that can tackle the problem of drug-resistant TB strains has been suggested by the investigation of chloroquinoline and hydrazide derivatives as the bases for hybrid compounds. Promising preliminary findings have been obtained in this regard.

Conclusion

Pursuing the goal of finding effective antitubercular medicines, this work synthesized and assessed new ester derivatives of 6-substituted-2-chloroquinoline-3-carbaldehyde hydrazide analogs. We succeeded in synthesizing and characterizing the chemicals by means of rigorous purification and precise multi-step synthesis procedures. The derivatives 4a and 4f indicated marked *in-vitro* activity against *M. tuberculosis in-vitro* exhibiting MIC value - 6.25 µg/mL, according to the Alamar blue technique assessment of their antitubercular activity. This finding underscores the therapeutic potential of the chloroquinoline and hydrazide combination, considering their documented antitubercular properties to enhance the efficacy of the novel hybrid molecules. In conclusion, the innovative approach of combining chloroquinoline and hydrazide to create novel antitubercular agents has yielded compounds with significant *in-vitro* efficacy against *M. tuberculosis*. These findings provide a way for future investigations to further understand the mechanisms of action, optimize the lead compounds, and evaluate their *in-vivo* efficacy and safety profiles.

Acknowledgement

The authors are grateful to the Government of Goa, the Principal of Goa College of Pharmacy, for providing facility and support. The authors are thankful to Punjab University's CIL and SAIF for furnishing the instrumental analysis and deeply appreciate Maratha Mandal's central research laboratory, Belgavi, for Biological Screening.

References

1. Nair A, Greeny A, Nandan A. *et al.* Advanced drug delivery and therapeutic strategies for tuberculosis treatment. J. Nanobiotechnol.2023; 21: 414.Available from: doi.org/10.1186/s12951-023-02156-y
2. Singh H, Jindal S, Sing M, Sharma G, Kaur IP. Nano-Formulation of Rifampicin with Enhanced Bioavailability: Development, Characterization, and in-Vivo Safety. Int. J. Pharm. 2015; 485(1-2):138–151.Available from: doi.10.1016/j.ijpharm.2015.02.050.
3. Qi CC, Xu LR, Zhao CJ, Zhang HY, Li QY, Liu MJ, Zhang YX, Tang

Z, Ma XX. Prevalence and Risk Factors of Tuberculosis among People Living with HIV/AIDS in China: A Systematic Review and Meta-Analysis. BMC Infect. Dis. 2023; 23: 584. Available from: doi.10.1186/s12879-023-08575-4
4. Dheda K, Barry III CE, Maartens G. Tuberculosis. The Lancet.2016; 387(10024) :1211-1226. Available from:doi. 10.1016/S0140-6736(15)00151-5
5. Uplekar M, Weil D, Lonnroth K, Jaramillo E, Lienhardt C, Dias HM, at al for WHO's Global TB Programme. WHO's new end TB strategy. Lancet. 2015;385(9979):1799-1801. Available from: doi.10.1016/S0140-6736(15)60570-0
6. Ajani OO, Iyaye KT, Ademosun OT. Recent advances in chemistry and therapeutic potential of functionalized quinoline motifs – A Review. RSC Advances. 2022;12(29):18594–614.Available from: doi.10.1039/d2ra02896d
7. Elebiju OF, Ajani OO, Oduselu GO, Ogunnupebi TA, Adebiyi E. Recent advances in functionalized quinoline scaffolds and hybrids—exceptional pharmacophore in therapeutic medicine. Frontiers in Chemistry. 2023; 6:10. Available from: doi.10.3389/fchem.2022.1074331
8. Mandhane PG, Joshi RS, Mahajan PS, Nikam MD, Nagargoje DR, Gill CH. Synthesis, characterization and antimicrobial screening of substituted Quiazolinones derivatives. Arabian Journal of Chemistry. 2015 ;8(4):474–9.Available from : doi.10.1016/j.arabjc.2011.01.025
9. Korcz M, Sączewski F, Bednarski P, Kornicka A. Synthesis, structure, chemical stability, and *in-vitro* cytotoxic properties of novel quinoline-3-carbaldehyde hydrazones bearing a 1,2,4-triazole or benzotriazole moiety. Molecules. 2018 ;23(6):1497. Available from: doi.10.3390/molecules23061497
10. Kumar R, Pathak D.Synthesis and biological evaluation of some novel quinoline derivatives bearing pyrazole moiety. Int J Pharm Sci Drug Res. 2023; 15(2):139-143.
11. Patel AJ, Dholakia AB, Patel VC. A green perspective: Synthesis of 2-chloro-3-formylquinolines and its derivatives. Synthetic Communications. 2020; 51(2):163–90. Available from: doi.10.1080/00397911.2020.1824277
12. Zeleke D, Eswaramoorthy R, Belay Z, Melaku Y. Synthesis and antibacterial, antioxidant, and molecular docking analysis of some novel quinoline derivatives. Journal of Chemistry. 2020:1–16. Available from: doi.10.1155/2020/1324096
13. Abdel-Wahab BF, Khidre RE, Farahat AA, El-Ahl A-AS. 2-chloroquinoline-3-carbaldehydes: Synthesis, reactions and applications. Arkivoc. 2012 ;2012(1):211–76. Available from: doi.10.3998/ark.5550190.0013.107
14. El-Samahy FA, Ibrahim NM, Mahran MR. The behavior of 2-chloroquinoline-3-carbaldehyde and 2-oxoquinoline-3-carbaldehyde toward stabilized methylene triphenyl phosphoranes and secondary amines. Phosphorus, Sulfur, and Silicon Related Elements. 2016; 191(1):59–64. Available from: doi.10.1080/10426507.2015.1085042
15. Mhaske GS, Sen A, Shah A, Sen D, Phadtare GR, Awate SS, Sakpal PH, Khiste RH, Neharkar VS.Synthesis, cytotoxicity, PDGFR inhibitory activity and docking study of novel 2-aminoquinoline-3-carboxamide derivatives as potential anticancer agents.EurChem Bull. 2023;12(Special Issue 1):292-305.
16. Subashini R, Roopan SM, Khan FN. Synthesis and free radical scavenging property of some quinoline derivatives. Journal of the Chilean Chemical Society. 2010;55(3):317–9. Available from: doi.10.4067/s0717-97072010000300008
17. Bahadur V, Mastronicola D, Singh AK, Tiwari HK, Pucillo LP, Sarti P, et al. Antigiardial activity of novel triazolyl-quinolone-based chalcone derivatives: When oxygen makes the difference. Frontiers in Microbiology. 2015;6. Available from: doi.10.3389/fmicb.2015.00256
18. Hamama WS, Ibrahim ME, Gooda AA, Zoorob HH. Recent advances in the chemistry of 2-chloroquinoline-3-carbaldehyde and related analogs. RSC Advances. 2018;8(16):8484–515.Available from: doi.10.1039/c7ra11537g
19. Zadsirjan V, Mahdizadeh SJ, Heravi MM, Heydari M. Synthesis of novel *n*-functionalized 4-aryl-tetrahydrobiquinoline-2,5-(1*h*,3*h*)-diones via one-pot three-component reaction: A joint experimental and computational study. Canadian Journal of Chemistry. 2018;96(12):1071–8.Available from :doi.10.1139/cjc-2017-0564
20. Gbe GD, Sagne JA, Doumade Z, Ané A. Synthesis of N-alkyl-3-(1H-benzimidazolyl) -2-chloroquinoline derivatives potential candidates against infectious organisms. African Journal of Pure and Applied Chemistry. 2021;15(2):8–12. Available from: doi.10.5897/ajpac2020.0857
21. Yasaei Z, Mohammadpour Z, Shiri M, Tanbakouchian Z, Fazelzadeh S. Isocyanide reactions toward the synthesis of 3-(oxazol-5-yl) quinoline-2-carboxamides and 5-(2-tosylquinolin-3-yl)oxazole. Frontiers in Chemistry. 2019;7: 433. Availablefrom: doi.10.3389/fchem.2019.00433
22. Sangwan K, Singh B. Antiproliferative activity of novel imatinib analogue as potential anticancer agents, synthesis and *in-vitro* screening. Indian Journal of Pharmaceutical Education and Research. 2023;57(2s): s453-s458.Available from: doi.10.5530/ijper.57.2s.53
23. Insuasty D, Abonia R, Insuasty B, Quiroga J, Laali KK, Nogueras M, et al. Microwave-assisted synthesis of diversely substituted quinoline-based dihydropyridopyrimidine and dihydropyrazolopyridine hybrids. ACS Combinatorial Science. 2017; 19(8):555–63. Available from: doi.10.1021/acscombsci.7b00091
24. Saral A, Sudha P, Muthu S, Sevvanthi S, Sangeetha P, Selvakumari S. Vibrational spectroscopy, Quantum Computational and Molecular Docking Studies on 2-chloroquinoline-3-carboxaldehyde. Heliyon. 2021;7(7): e07529.Available from: doi.10.1016/j.heliyon. 2021. e07529
25. Govender H, Mocktar C, Koorbanally NA. Synthesis and bioactivity of quinoline-3-carboxamide derivatives. Journal of Heterocyclic Chemistry. 2018;55(4):1002–9. Available from: doi.10.1002/jhet.3132
26. Maigali SS, Abd-El-Maksoud MA, El-Hussieny M, Soliman FM, Abdel-Aziz MS, Shalaby E-SM. Chemistry of phosphorus ylides: Part 41 synthesis of antimicrobial agents from the reaction of amino antipyrine, coumarin- and quinoline-carbaldehyde with phosphacumulene and phosphaallene ylides. Journal of Chemical Research. 2014; 38(12):754–61. Available from: doi.10.3184/174751914x14179446629855
27. Guje PB, Chidrawar AB, Patwari SB, Madje BR, Rajani DP, Sangshetti JN, Damale M, PokalwarRU.Synthesis, molecular docking, antibacterial and antifungal activity study of novel-3-((1H-benzo[d] imidazole-2-ylthio)methyl)-2-chloroquinoline derivatives. Chem Biol Interface. 2020; 10(6):149-157.
28. Volovnenko TA, Tarasov AV, Zubatyuk RI, Shishkin OV, Turov AV, VolovenkoYuM. Interaction of 2-chloroquinoline- 3-carbaldehydes with 2-hetaryl- acetonitriles. Chemistry of Heterocyclic Compounds. 2009;45(12):1489–502.Available from: doi.10.1007/s10593-010-0456-7
29. Fekadu M, Zeleke D, Abdi B, Guttula A, Eswaramoorthy R, Melaku Y. Synthesis, in silico molecular docking analysis, pharmacokinetic properties and evaluation of antibacterial and antioxidant activities of fluoroquinolines. BMC Chemistry. 2022;16(1). Available from: doi.10.1186/s13065-022-00795-0
30. Suryanarayana K, Gangu KK, Kerru N, Khatana K, Satyanarayana B, Maddila S. Synthesis of a novel chloroquinoline, rhodanine encompassed 1,2,3-triazole scaffolds and molecular docking evaluation of their cytotoxicity. Journal of the Iranian Chemical Society. 2023;20(10):2643–55. Available from: doi.10.1007/s13738-023-02862-2
31. Noori M, Davoodi A, Iraji A, Dastyafteh N, Khalili M, Asadi M, et al. Design, synthesis, and in silico studies of quinoline-based-benzo[d] imidazole bearing different acetamide derivatives as potent α-glucosidase inhibitors. Scientific Reports. 2022 ;12(1): 14019. Available from: doi.10.1038/s41598-022-18455-7
32. Forozan R, Ghomi MK, Iraji A, Montazer MN, Noori M, Dastyafteh N, et al. Synthesis, *in-vitro* inhibitor screening, structure–activity

relationship, and Molecular Dynamic Simulation Studies of novel thioquinoline derivatives as potent α-glucosidase inhibitors. Scientific Reports. 2023;13(1). Available from :doi.10.1038/s41598-023-35140-5
33. Moghaddam FM, Moafi A, Ziadkhani A, Daneshfar M, Razaghdoost N. A facile and efficient route for the synthesis of thiopyran quinolines-fused indole moiety using 2-chloroquinoline-3-carbaldehydes. Chemistry Select. 2019;4(40):11683–6. Available from :doi.10.1002/slct.201902476
34. Bhardwaj N, Choudhary D, Pathania A, Baranwal S, Kumar P. Synthesis and molecular docking studies of quinoline derivatives as HIV non-nucleoside reverse transcriptase inhibitors. Turkish Journal of Chemistry. 2020;44(6):1623–41. Available from :doi.10.3906/kim-2004-14
35. Mandewale MC, Patil UC, Shedge SV, Dappadwad UR, Yamgar RS. A review on quinoline hydrazone derivatives as a new class of potent antitubercular and Anticancer Agents. Beni-Suef University Journal of Basic and Applied Sciences. 2017;6(4):354–61. Available from :doi.10.1016/j.bjbas.2017.07.005
36. Popiołek Ł. Hydrazide–Hydrazones as potential antimicrobial agents: Overview of the literature since 2010. Medicinal Chemistry Research. 2016;26(2):287–301. Available from :doi.10.1007/s00044-016-1756-y
37. Mahantheshappa SS, Shivanna H, Satyanarayan ND. Synthesis, antimicrobial, antioxidant, and ADMET studies of quinoline derivatives. European Journal of Chemistry. 2021; 12(1):37–44. Available from :doi.10.5155/eurjchem.12.1.37-44.2038
38. Golea L, Chebaki R, Laabassi M, Mosset P. Synthesis, characterization of some substituted Quinolines derivatives: DFT, computational, in silico ADME, molecular docking and biological activities. Chemical Data Collections. 2023; 43:100977. Available from :doi.10.1016/j.cdc.2022.100977
39. Kumar S, Bawa S, Drabu S, Panda BP. Design and synthesis of 2-chloroquinoline derivatives as non-azoles antimycotic agents. Medicinal Chemistry Research. 2010;20(8):1340–8. Available from :doi.10.1007/s00044-010-9463-6
40. Koopaei MN, Assarzadeh MJ, Almasirad A, Ghasemi-Niri SF, Amini M, Kebriaeezadeh A, et al. Synthesis and Analgesic Activity of Novel Hydrazide and Hydrazine Derivatives.Iran J Pharm Res. 2013;12(4):721–7.
41. Tamaddon F, Amrollahi MA, Sharafat L. A green protocol for chemoselective O-acylation in the presence of zinc oxide as a heterogeneous, reusable and eco-friendly catalyst. Tetrahedron Letters. 2005; 46(45):7841–4. Available from :doi.10.1016/j.tetlet.2005.09.005
42. Lourenço MC, Souza MV, Pinheiro AC, Ferreira M de, Gonçalves RS, Nogueira TC, et al. Evaluation of antitubercular activity of Nicotinic and isoniazid analogues. Arkivoc. 2007 ;(15):181–91. Available from:doi.10.3998/ark.5550190.0008.f18
43. Degfie T, Endale M, Tafese T, Dekebo A, Shenkute K. In-vitro antibacterial, antioxidant activities, molecular docking, and ADMET analysis of phytochemicals from roots of Hydnora Johannis. Applied Biological Chemistry. 2022; 65(1).Available from: doi.10.1186/s13765-022-00740-8.sm. 2022; 65(1):76

HOW TO CITE THIS ARTICLE: Potdar VV, Joshi AB. Innovative Hybrid Compounds Targeting Tuberculosis: Development, Characterization and Bioefficacy Analysis of 6-substituted-2-Chloroquinoline-3-Carbaldehyde Hydrazide Ester Derivatives. Int. J. Pharm. Sci. Drug Res. 2024;16(3):378-386.
DOI: 10.25004/IJPSDR.2024.160309

ANNEXURE-II

PRESENTATIONS

G-CEIP

Certificate of Participation

Presented to

VAIBHAV POTDAR

in recognition of your participation in the

"Research Showcase Presentation (RSP)" titled

Synthesis, characterization and Antimycobacterial Activity of Novel Quinoline Derivatives

from

7th Annual International Conference on IPR

Current Global Trends in IPR:

What we do/should know !!

held on November 15-16, 2022 at Goa College of Pharmacy, Panaji-Goa

Umesh Banakar, Ph.D.
Professor

Dr. Gopal Krishna Rao
Principal

G-CEIP

Certificate of Participation

Presented to

VAIBHAV V. POTDAR

in recognition of your participation in the

"Research Showcase Presentation (RSP)" at the

6th Annual International Conference on IPR

Global Trends in IPR: Patenting & Beyond !!

held on December 1-2, 2021 at Goa College of Pharmacy, Panaji-Goa

Umesh Banakar, Ph.D.
Professor

Dr. Gopal Krishna Rao
Principal